

2013-09-24

Phase Partitioning and Thermo-physical Properties of Athabasca Bitumen / Solvent Mixtures

Nourozieh, Hossein

Nourozieh, H. (2013). Phase Partitioning and Thermo-physical Properties of Athabasca Bitumen / Solvent Mixtures (Doctoral thesis, University of Calgary, Calgary, Canada). Retrieved from <https://prism.ucalgary.ca>. doi:10.11575/PRISM/27329

<http://hdl.handle.net/11023/1022>

Downloaded from PRISM Repository, University of Calgary

UNIVERSITY OF CALGARY

Phase Partitioning and Thermo-physical Properties of Athabasca Bitumen / Solvent
Mixtures

by

Hossein Nourozieh

A THESIS

SUBMITTED TO THE FACULTY OF GRADUATE STUDIES
IN PARTIAL FULFILMENT OF THE REQUIREMENTS FOR THE
DEGREE OF DOCTOR OF PHILOSOPHY

DEPARTMENT OF CHEMICAL AND PETROLEUM ENGINEERING

CALGARY, ALBERTA

SEPTEMBER, 2013

© Hossein Nourozieh 2013

Abstract

The phase behaviour and thermo-physical properties of bitumen/solvent systems are of crucial importance for heavy oil and bitumen *in-situ* recovery methods as well as pipeline transportation, surface upgrading, and refining. The equilibrium properties of mixtures containing heavy oil are also important for the development of numerical simulators, the application of various thermal and non-thermal recovery processes, and the application of fluid extraction processes.

The main objective of this study was the development of a comprehensive understanding of the phase behaviour of bitumen/solvent mixtures. A new pressure-volume-temperature (PVT) apparatus was designed and constructed to acquire experimental data for the phase behaviour of bitumen/solvent mixtures and their thermo-physical properties. A new methodology for phase detection and accurate volume measurements was proposed for obtaining single liquid, vapour-liquid, and liquid-liquid equilibrium properties as well as the extraction yield for bitumen/solvent systems.

New vapour-liquid and liquid-liquid equilibrium data for Athabasca bitumen / ethane and Athabasca bitumen / propane mixtures were experimentally acquired and corresponding phase diagrams were generated over wide ranges of temperatures and pressures. The effect of different parameters, such as the solvent-to-oil ratio, pressure, and temperature, on equilibrium phase compositions, saturated phase properties (density and viscosity), and the distribution of fractions in different phases were studied. The optimal solvent for bitumen viscosity reduction was identified at different operating conditions. The potential applications of ethane and propane for the supercritical and subcritical extraction of valuable components from bitumen were also experimentally evaluated. The generated data were then modelled with the Peng-Robinson equation of state to accurately predict the phase boundaries and phase compositions.

New measurements for thermo-physical properties of Athabasca bitumen / *n*-hexane and Athabasca bitumen / condensate mixtures were conducted at different temperatures,

pressures, and solvent weight fractions. The mixture density and viscosity data were evaluated with predictive schemes as well as with correlation models representing certain mixing rules proposed in the literature. The influences of pressure, temperature, and solvent weight fraction on the density and viscosity of mixtures were considered in the models and evaluated from the experimental results.

Acknowledgments

This thesis would not have been possible without the contributions of many people through their academic advice and mentoring, research guidance, and the usual moral support so indispensable for the focus and resilience of all graduate students.

I would like to express my profound gratitude to my supervisor, Dr. Jalal Abedi, for his guidance, encouragement, and support throughout the course of this project. He taught me the art of creative thinking and systematic research. I have learnt a lot from his great personality as well as his scientific knowledge and experience.

I wish to thank the members of my advisory committee, Dr. Robert A. Heidemann, Dr. Brij B. Maini, and Dr. Gordon R. Moore for their helpful discussions, technical input, and suggestions. I appreciate my examining committee, Dr. Laurence Lines and Dr. G. Ali Mansoori, for their time and comments. Dr. Tadahiro Okazawa is acknowledged for the original design of the experimental apparatus. The constructive comments and support provided by Dr. Hassan Hassanzadeh are also highly appreciated.

Special thanks go to my best friend and colleague in the Solvent-Heat Assisted Recovery Processes (SHARP) research group, Mohammad Kariznovi, for his friendship and valuable discussions on technical issues and PVT modelling. Together we achieved many incredible accomplishments on the topics of phase behaviour of bitumen/solvent mixtures and heavy oil recovery techniques, which will always remind me of those sweet days of working together.

I am thankful to Mr. K. Van Fraassen for fruitful technical discussions. The cooperation of Drs. Gordon R. Moore and Raj Mehta in providing their laboratory facilities is also appreciated.

I sincerely appreciate the help I have received from the people in the Department of Chemical and Petroleum Engineering at the University of Calgary. I am very grateful for the great efforts of the machine-shop people in fabricating the experimental apparatus. My special thanks go to Mr. Rob Scorey and Larry Trudeau for their kind help and

support. My thanks are also extended to helpful people in engineering stores at the University of Calgary. I wish to express my appreciation for all the administrative support offered by the Department of Chemical and Petroleum Engineering staff and for their kind and friendly attitude.

I would also like to acknowledge the assistance and moral support of all my friends and fellow graduate students, in particular: Mehdi Bahonar, Bitā Bayestehparvin, S. Reza Etminan, S. Ali Feizabadi, Amir Ghaderi, Mohsen Ghanavati, Rohallah Hashemi, Moslem Hosseininejad, Mehdi Majdi Yazdi, Maryam Moghadasi, S. Javad Paitakhti, Moosa Rabiei, Mohammad Reza Rahmanian, Hashem Salari, Saeed Shad, Sadeq Shahamat, Fakhry Seyedeyn-Azad, S. Hamed Tabatabaie, and Saeed Taheri for their continued friendship and support through my undergraduate to Ph.D. studies. Our friendships are one of the most important treasures of my life.

I wish to express my appreciation for the financial support of all member companies of the SHARP Research Consortium: Alberta Innovates Energy and Environment Solutions, Chevron Energy Technology Co., Computer Modelling Group Ltd., ConocoPhillips Canada, Devon Canada Co., Foundation CMG, Husky Energy, Japan Canada Oil Sands Ltd., Laricina Energy, Brion Energy Corp., Nexen Inc., Natural Sciences and Engineering Research Council of Canada (NSERC), OSUM Oil Sands Co., Penn West Energy, Statoil Canada Ltd., Suncor Energy, and Total E&P Canada.

Finally, but importantly, I would like to thank my family for their continuous moral support during all stages of my studies. I deeply express my true love to my wonderful wife, Saina. I truly appreciate her understanding, cooperation, and patience throughout the years of my studies.

To

My Beloved Parents

and

My Lovely Wife, Saina

Table of Contents

Approval Page.....	i
Abstract.....	ii
Acknowledgements.....	iv
Dedication.....	vi
Table of Contents.....	vii
List of Tables.....	xi
List of Figures.....	xvii
List of Symbols, Abbreviations and Nomenclature.....	xxxviii
Chapter 1: Introduction.....	1
Chapter 2: Apparatus and Verification.....	7
2.1. Designed Apparatus.....	9
2.1.1. Equilibrium Cell.....	13
2.1.2. Sampling and Feeding Cells.....	15
2.1.3. Density Measurements.....	16
2.1.4. Viscosity Measurements.....	19
2.1.5. Charging and Discharging of Fluids.....	20
2.1.6. Pressure Measurements.....	21
2.1.7. Temperature Measurements.....	21
2.1.8. Data Acquisition System.....	22
2.1.9. Fluid Sampling for Further Analysis.....	23
2.1.10. Solubility Measurements.....	24
2.1.11. Volume Corrections.....	25
2.1.12. Gas and Liquid Analysis.....	25
2.2. Experimental Procedure.....	26
2.3. Apparatus Verification.....	28
2.3.1. Materials.....	29
2.3.2. Saturation Pressure of Pure Component.....	29
2.3.3. Phase Detection.....	30
2.3.4. Equilibrium Criteria.....	32
2.3.5. Phase Properties.....	33
2.3.6. Solubility and Saturated Liquid Viscosities.....	34
2.3.7. Comparison of Two Designed Apparatuses.....	36
Chapter 3: Bitumen Properties.....	39
3.1. Bitumen Samples.....	39
3.2. Density and Viscosity.....	39
3.2.1. Density of Bitumens.....	43
3.2.2. Viscosity of Bitumens.....	51

3.3. Compositional Analysis	56
3.4. SARA Analysis	59
3.5. Molecular Weight.....	60
3.5.1. Cryoscopy Method.....	61
3.5.2. Accuracy of Measurements.....	62
3.5.3. Molecular Weight of Bitumen Samples.....	63
Chapter 4: Phase Behaviour of Bitumen/Ethane Mixtures	65
4.1. Introduction	65
4.2. Literature Background.....	68
4.3. Vapour-Liquid Equilibrium for Surmont Bitumen / Ethane Systems	70
4.3.1. Saturated Phase Properties	74
4.3.2. Equilibrium K-values and GOR.....	78
4.4. Vapour-Liquid Equilibrium for JACOS Bitumen / Ethane Mixtures	81
4.5. Vapour-Liquid Equilibrium for MacKay River Bitumen / Ethane Mixtures...	87
4.6. Comparison of Solubility of Ethane and Saturated Liquid Density and Viscosity for Different Bitumen Samples	94
4.7. Liquid-Liquid Equilibrium for Bitumen/Ethane Mixtures	98
4.7.1. Bitumen Extraction	103
4.7.2. Effect of Pressure	105
4.7.3. Effect of Overall Ethane Concentration.....	110
4.7.4. Phase Properties	113
4.7.5. Effect of Solvent Type	116
4.7.6. Compositional Analyses of Extracts and Residues.....	118
4.7.6.1. Bitumen and Equilibrium Phases	119
4.7.6.2. Effect of Pressure	122
4.7.6.3. Effect of Overall Ethane Concentration	126
4.7.7. SARA Analysis of Extracts and Residues	130
4.7.8. Equilibrium K-values and Molecular Weight.....	135
4.7.9. Phase Diagrams for MacKay River Bitumen / Ethane Systems	138
Chapter 5: Phase Behaviour of Bitumen/Propane Mixtures	145
5.1. Introduction	145
5.2. Literature Background.....	148
5.3. Vapour-Liquid Equilibrium.....	153
5.3.1. Saturated Phase Properties	156
5.3.2. Equilibrium K-values and GOR.....	159
5.4. Liquid-Liquid Equilibrium	161
5.4.1. Physical Properties.....	164
5.4.1.1. Volume Change on Mixing	164
5.4.1.2. Phase Compositions.....	167
5.4.1.3. Density and Viscosity of Phases.....	169
5.4.2. Extraction Yield	173

5.4.2.1. Effect of Pressure	175
5.4.2.2. Effect of Temperature.....	177
5.4.2.3. Effect of Overall Propane Concentration	179
5.4.2.4. Effect of Propane Density	180
5.4.3. Compositional Analysis of Extracts and Residues	181
5.4.3.1. Effect of Pressure	187
5.4.3.2. Effect of Temperature.....	196
5.4.3.3. Effect of Overall Propane Concentration	201
5.4.4. SARA Analysis of Extracts and Residues	205
5.4.4.1. Effect of Pressure	207
5.4.4.2. Effect of Temperature.....	212
5.4.4.3. Effect of Overall Propane Concentration	214
5.5. Phase Diagrams	218
5.6. Comparison of Saturated Liquid Properties for Light Hydrocarbons / Bitumen Systems.....	227
5.6.1. Constant Pressure and Constant Temperature	228
5.6.2. Constant Solvent Weight Fraction and Constant Temperature.....	231
Chapter 6: Thermo-physical Properties of Bitumen/Hexane Mixtures	235
6.1. Introduction	235
6.2. Literature Background.....	237
6.3. Density of Mixtures.....	239
6.3.1. Prediction of Mixture Density	243
6.3.2. Volume Change on Mixing.....	249
6.3.3. Improvement in Calculation of Mixture Density.....	257
6.3.3.1. Excess Volume Mixing Rule.....	257
6.3.3.2. Effective Liquid Densities.....	257
6.4. Viscosity of Mixtures	262
6.4.1. Correlation and Prediction of Mixture Viscosity.....	266
Chapter 7: Thermo-physical Properties of Bitumen/Condensate Mixture.....	282
7.1. Introduction	282
7.2. Literature Background.....	285
7.3. Condensate Properties	286
7.3.1. Compositional Analysis	287
7.3.2. Molecular Weight	287
7.3.3. Density and Viscosity	291
7.4. Density of Mixture	293
7.4.1. Prediction of Mixture Density	298
7.4.2. Volume Change on Mixing.....	305
7.4.3. Improvement in Calculation of Mixture Density.....	310
7.5. Viscosity of Mixtures	314
7.5.1. Correlation and Prediction of Mixture Viscosity.....	318

7.6. Repeatability of Data.....	330
7.7. Asphaltene Precipitation.....	332
Chapter 8: Equation of State Modelling.....	334
8.1. Introduction	334
8.2. Equilibrium Calculation	339
8.3. Characterization.....	342
8.4. MacKay River Bitumen / Ethane Mixtures	344
8.5. Surmont Bitumen / Ethane Mixtures.....	349
8.6. Surmont Bitumen / Propane Mixtures.....	350
Chapter 9: Conclusions and Recommendations	356
9.1. Conclusions	356
9.2. Recommendations	358
References	360
Appendix A: Copyrights and Permissions	381

List of Tables

Table 2–1: Equipment installed in the original designed apparatus and modified apparatus (Nourozieh et al. 2012a).	12
Table 2–2: Specifications of o-rings used in equilibrium cell.	14
Table 2–3: Specifications of cells.	15
Table 2–4: Calculate coefficient for equation 2-4.	19
Table 2–5: Viscosity range for viscometer.	20
Table 2–6: Standard gas and its composition.	26
Table 2–7: Chemical sample specifications.	29
Table 2–8: Experimental vapour-liquid and liquid-liquid equilibrium properties for simple binary systems; T , temperature; P , pressure; w_s , composition; ρ , density.	34
Table 2–9: Initial propane/bitumen ratio and corresponding equilibrium properties of propane/bitumen systems for the two designed experimental apparatuses (Nourozieh et al. 2012a).	37
Table 2–10: The deviations for reported experimental data using two proposed apparatus (Nourozieh et al. 2012a).	38
Table 3–1: UNITAR definition of heavy oils and bitumen at reservoir temperature (Gray 1994).	40
Table 3–2: Coefficients of the correlation equation for the density of Surmont bitumen (equation 3-1).	46
Table 3–3: Coefficients of the correlation equation for the density of MacKay River bitumen (equation 3-1).	47
Table 3–4: Coefficients of the correlation equation for the density of JACOS bitumen (equation 3-1).	48
Table 3–5: Coefficients of the correlation equation for calculation of ρ_o (equation 3-2).	49
Table 3–6: Coefficients of the correlation equation for calculation of α (equations 3-3 and 3-5).	49
Table 3–7: Average absolute deviation (AARD) and maximum deviation (MAD) of calculated densities.	50
Table 3–8: Coefficients of the correlation equations for the viscosity of different bitumens (equations 3-6 and 3-7).	52
Table 3–9: Compositional analysis of bitumen samples.	57

Table 3–10: SARA analysis for bitumen samples.....	60
Table 3–11: Molecular weight of 1-propanol using freezing point depression method... ..	62
Table 3–12: Molecular weight of <i>n</i> -tetradecane using freezing point depression method.	63
Table 3–13: Repeated measurements for the molecular weight of bitumen samples.....	63
Table 3–14: Molecular weight of bitumen samples.....	64
Table 4–1: Experimental design and feeding information for Surmont bitumen / ethane systems at temperature, T and pressure P	71
Table 4–2: Experimental vapour-liquid equilibrium properties for Surmont bitumen / ethane systems at $T = (50, 100, 150, \text{ and } 190)^\circ\text{C}$; P , pressure; ρ_s , saturated liquid density; μ_s , saturated liquid viscosity; w_s , weight fraction of ethane in saturated liquid phase.	72
Table 4–3: Experimental vapour-liquid equilibrium properties of repeated experiments at $T = (50, 150, \text{ and } 190)^\circ\text{C}$ for Surmont bitumen / ethane systems; P , pressure; ρ_s , saturated liquid density; μ_s , saturated liquid viscosity; w_s , weight fraction of ethane in saturated liquid phase.....	74
Table 4–4: Experimental vapour-liquid equilibrium properties for JACOS bitumen / ethane mixtures at $T = (50, 100 \text{ and } 150)^\circ\text{C}$; P , pressure; ρ_s , saturated liquid density; μ , saturated liquid viscosity; w_s , weight fraction of ethane in saturated liquid phase.....	82
Table 4–5: Experimental vapour-liquid equilibrium properties of repeated experiments at $T = (50, 150, \text{ and } 190)^\circ\text{C}$ for JACOS bitumen / ethane mixtures; P , pressure; ρ_s , saturated liquid density; μ_s , saturated liquid viscosity; w_s , weight fraction of ethane in saturated liquid phase.....	82
Table 4–6: Experimental vapour-liquid equilibrium properties for MacKay River bitumen / ethane mixtures at $T = (50, 100, 150 \text{ and } 190)^\circ\text{C}$; P , pressure; ρ_s , saturated liquid density; μ , saturated liquid viscosity; w_s , weight fraction of ethane in saturated liquid phase.	88
Table 4–7: Experimental vapour-liquid equilibrium properties of repeated experiments at $T = (50, 150, \text{ and } 190)^\circ\text{C}$ for MacKay River bitumen / ethane mixtures; P , pressure; ρ_s , saturated liquid density; μ_s , saturated liquid viscosity; w_s , weight fraction of ethane in saturated liquid phase.....	89
Table 4–8: Experimental design for MacKay River bitumen / ethane systems at ambient temperature; P , pressure; S/B; solvent-to-bitumen ratio; w_f , weight fraction of ethane in feed (overall ethane concentration); V_t , total mixture volume before equilibrium; $m_{\text{C}_2\text{H}_6}$, total mass of ethane in equilibrium cell; m_{bit} , total mass of bitumen in equilibrium cell.	101

Table 4–9: Liquid-liquid equilibrium properties for MacKay River bitumen/ethane systems at ambient temperatures; P , pressure; T , temperature; w , overall ethane weight fraction; ρ , densities; μ , L_2 viscosity (Nourozieh et al. 2011a).	102
Table 4–10: Composition and volume ratio of phases for MacKay River bitumen / ethane systems at ambient temperature; P , pressure; T , temperature; w , weight fraction of ethane; $V_1 \cdot V_2^{-1}$, L_1 to L_2 volume ratio (Nourozieh et al. 2011a).	103
Table 4–11: Extraction Yield EY for MacKay River bitumen / ethane systems at ambient temperatures; P , pressure; T , temperature; w , overall ethane weight fraction (Kariznovi et al. 2013c).	105
Table 4–12: Equilibrium phase properties for MacKay River bitumen / solvent mixtures at ambient temperature and at a pressure of 5 MPa with an overall solvent concentration of 0.4 weight fraction; w , weight fraction of solvent; ρ , densities; μ , L_2 viscosity (Nourozieh et al. 2011a).	117
Table 4–13: SARA analysis (in weight percent) of flashed-off liquid samples taken from two equilibrium phases in the liquid-liquid equilibrium study of MacKay River bitumen / ethane mixtures; P , pressure; T , temperature; w , overall ethane concentration in weight fraction.	130
Table 4–14: SARA analysis (in weight percent) of residues taken from two equilibrium phases in the liquid-liquid equilibrium study of MacKay River bitumen / ethane mixtures; P , pressure; T , temperature; w , overall ethane concentration in weight fraction.	131
Table 4–15: Correlated molecular weight and calculated K-values of components at equilibrium conditions for MacKay River bitumen / ethane mixtures at ambient temperature; w , overall ethane weight fraction (Kariznovi et al. 2013c).	136
Table 4–16: Calculated molecular weight of flashed-off phase samples taken from liquid-liquid equilibrium study of MacKay River bitumen / ethane mixtures at ambient temperature; w , overall ethane weight fraction (Kariznovi et al. 2013c).	138
Table 5–1: Experimental design and feeding information for Surmont bitumen / propane systems at temperature T and pressure P	154
Table 5–2: Experimental vapour-liquid equilibrium properties for Surmont bitumen / propane mixtures at $T = (50, 100, 150, 175 \text{ and } 190)^\circ\text{C}$; P , pressure; ρ_s , saturated liquid density; μ_s , saturated liquid viscosity; w_s , weight percent of propane in saturated liquid phase.	155
Table 5–3: Experimental vapour-liquid equilibrium properties of repeated experiments at $T = (150 \text{ and } 175)^\circ\text{C}$ for Surmont bitumen / propane systems; P , pressure; ρ_s , saturated liquid density; μ_s , saturated liquid viscosity; w_s , weight fraction of propane in saturated liquid phase.	155

Table 5–4: Liquid-liquid equilibrium properties for Surmont bitumen / propane mixtures at a constant overall propane concentration of 40 weight percent; P , pressure; T , temperature; w , weight fraction of propane; ρ , densities; μ , viscosity.....	163
Table 5–5: Liquid-liquid equilibrium properties for Surmont bitumen / propane mixtures at a constant overall propane concentration of 60 weight percent; P , pressure; T , temperature; w , weight fraction of propane; ρ , densities; μ , viscosity.....	163
Table 5–6: Liquid-liquid equilibrium properties for Surmont bitumen / propane mixtures at a constant overall propane concentration of 80 weight percent; P , pressure; T , temperature; w , weight fraction of propane; ρ , densities; μ , viscosity.....	163
Table 5–7: The volume change on the mixing and volume ratio of phases in liquid-liquid equilibrium of Surmont bitumen / propane mixtures; P , pressure; T , temperature; w , weight fraction of propane; V_t , total volume of mixtures; V_L , volume of each phase at equilibrium condition.....	165
Table 5–8: The calculated extraction yield EY in liquid-liquid equilibrium of Surmont bitumen / propane mixtures; P , pressure; T , temperature; w , weight fraction of propane in mixture.....	174
Table 5–9: SARA analysis (in weight percent) of extracts and residues taken from liquid-liquid equilibrium study of Surmont bitumen / propane mixtures; P , pressure; T , temperature; w , overall propane concentration in weight fraction.....	205
Table 5–10: Operational conditions for constant temperature and constant solvent weight fraction experiments; T , temperature; w_s , solvent weight fraction.....	232
Table 5–11: Experimental saturated liquid densities for Surmont bitumen saturated with different solvents; T , temperature; ρ_s , saturated liquid density; w_s , weight percent of solvent in saturated liquid phase.	233
Table 5–12: Experimental saturated liquid viscosities for Surmont bitumen saturated with different solvents; T , temperature; μ_s , saturated liquid viscosity; w_s , weight percent of solvent in saturated liquid phase.	233
Table 6–1: Experimental liquid densities of Surmont bitumen / n -hexane mixtures at 0.05 and 0.1 weight fractions of hexane; T , temperature; P , pressure; ρ_m , density of mixture.....	240
Table 6–2: Experimental liquid densities of Surmont bitumen / n -hexane mixtures at 0.2 and 0.3 weight fractions of hexane; T , temperature; P , pressure; ρ_m , density of mixture.....	241
Table 6–3: Experimental liquid densities of Surmont bitumen / n -hexane mixtures at 0.4 and 0.5 weight fractions of hexane; T , temperature; P , pressure; ρ_m , density of mixture.....	242

Table 6–4: The deviations of different models for the calculation of Surmont bitumen / <i>n</i> -hexane mixture densities.	258
Table 6–5: Experimental liquid viscosities of Surmont bitumen / <i>n</i> -hexane mixtures at 0.05 and 0.1 weight fractions of hexane; <i>T</i> , temperature; <i>P</i> , pressure; μ_m , viscosity of mixture.	263
Table 6–6: Experimental liquid viscosities of Surmont bitumen / <i>n</i> -hexane mixtures at 0.2 and 0.3 weight fractions of hexane; <i>T</i> , temperature; <i>P</i> , pressure; μ_m , viscosity of mixture.	264
Table 6–7: Experimental liquid viscosities of Surmont bitumen / <i>n</i> -hexane mixtures at 0.4 and 0.5 weight fractions of hexane; <i>T</i> , temperature; <i>P</i> , pressure; μ_m , viscosity of mixture.	265
Table 6–8: Calculated AARDs of different models for the correlation and prediction of the viscosity for Surmont bitumen / <i>n</i> -hexane mixtures.	268
Table 7–1: Boiling point distribution of condensate.	288
Table 7–2: Component distribution of condensate.	290
Table 7–3: Measured ρ_{exp} and correlated ρ_{corr} density of condensate at different temperatures <i>T</i> and pressures <i>P</i> ; AD, absolute deviation.	292
Table 7–4: Measured μ_{exp} and correlated μ_{corr} viscosity of condensate at different temperatures <i>T</i> and pressures <i>P</i> ; ARD, absolute relative deviation.	294
Table 7–5: Experimental liquid densities of the pseudo-binary mixtures of Surmont bitumen / condensate at 0.05 and 0.1 weight fractions of condensate; <i>w</i> , weight fraction of condensate in the mixture; <i>T</i> , temperature; <i>P</i> , pressure; ρ_m , density of mixture.	295
Table 7–6: Experimental liquid densities of the pseudo-binary mixtures of Surmont bitumen / condensate at 0.2 and 0.3 weight fractions of condensate; <i>w</i> , weight fraction of condensate in the mixture; <i>T</i> , temperature; <i>P</i> , pressure; ρ_m , density of mixture.	296
Table 7–7: Experimental liquid densities of the pseudo-binary mixtures of Surmont bitumen / condensate at 0.4 and 0.5 weight fractions of condensate; <i>w</i> , weight fraction of condensate in the mixture; <i>T</i> , temperature; <i>P</i> , pressure; ρ_m , density of mixture.	297
Table 7–8: Deviations of different models for calculation of Surmont bitumen / condensate mixture density.	311
Table 7–9: Experimental liquid viscosities of the pseudo-binary mixtures of Surmont bitumen / condensate at 0.05 and 0.1 weight fractions of condensate; <i>w</i> , weight fraction of condensate in the mixture; <i>T</i> , temperature; <i>P</i> , pressure; μ_m , density of mixture.	315

Table 7–10: Experimental liquid viscosities of the pseudo-binary mixtures of Surmont bitumen / condensate at 0.2 and 0.3 weight fractions of condensate; w , weight fraction of condensate in the mixture; T , temperature; P , pressure; μ_m , density of mixture.	316
Table 7–11: Experimental liquid viscosities of the pseudo-binary mixtures of Surmont bitumen / condensate at 0.4 and 0.5 weight fractions of condensate; w , weight fraction of condensate in the mixture; T , temperature; P , pressure; μ_m , density of mixture.	317
Table 7–12: Calculated AARDs of different models for the correlation and prediction of the viscosity for Surmont bitumen / condensate mixtures.	319
Table 7–13: Repeated experiments for density and viscosity of Surmont bitumen / condensate mixtures at temperature T ; P , pressure; ρ_s , saturated liquid density; μ_s , saturated liquid viscosity; w_s , weight fraction of condensate in mixture. .	331
Table 8–1: Coefficient of the correlation equation for the binary interaction parameters and calculated AARDs of ethane solubilities in MacKay River bitumen using two approaches.	346

List of Figures

Figure 2–1: The schematic diagram of the designed apparatus for the phase behaviour study of bitumen/ solvent systems (Nourozieh et al. 2012a).	11
Figure 2–2: The experimental apparatuses: the original designed apparatus and the modified apparatus (Nourozieh et al. 2012a).	12
Figure 2–3: Schematic diagram of equilibrium cell.	14
Figure 2–4: Density measuring cell (mPDS 2000 V3) from Anton Paar website.	16
Figure 2–5: Viscometer (ViscoPro 2000 system 4, Cambridge Viscosity) from Cambridge Viscosity website.....	20
Figure 2–6: Small piston-cylinder cell for liquid phase sampling.	23
Figure 2–7: Varian 3900 gas chromatograph (from http://www.asap4u.nl/pdf/varian/3900.PDF).	26
Figure 2–8: Saturation pressure of <i>n</i> -pentane versus temperature (Nourozieh et al. 2012a).	30
Figure 2–9: Phase detection on the basis of density measurements for vapour-liquid equilibria of methane/ <i>n</i> -octadecane system at 125°C and 2034 kPa.....	31
Figure 2–10: Phase detection on the basis of density measurements for liquid-liquid equilibria of ethane/methanol system at 22°C and 4891 kPa.	32
Figure 2–11: Volume change on mixing (equilibrium criteria) for simple binary systems; ♦, ethane/ethanol at 40°C and 1103 kPa; ■, methane/ <i>n</i> -propanol at 22°C and 4000 kPa; ▲, ethane/ <i>n</i> -tetradecane at 50°C and 1055 kPa; ●, methane/ <i>n</i> -octadecane at 125°C and 2034 kPa.	33
Figure 2–12: Comparison of measured solubility data and literature values for carbon dioxide / ethanol system at different pressures; ■, this study at 303.2 K; ♦, Chiu et al. (2008) at 303.12 K; Δ, Secuianu et al. (2008) at 303.2 K; +, Day et al. (1996) at 303.12 K; ×, Stievano and Elvassore (2005) at 303.15 K; ■, this study at 323.2 K; ●, Mehl et al. (2011) at 323.2 K; ▲, Dalmolin et al. (2006) at 323 K; ×, Stievano and Elvassore (2005) at 323.15 K; ♦, Gao et al. (2002) at 323 K; ○, Joung et al. (2001) at 322.5 K; Δ, Chen et al. (2000) at 323 K; +, Jennings et al. (1991) at 325 K (Kariznovi et al. 2013a).	35
Figure 2–13: Comparison of measured saturated liquid viscosities and literature data for carbon dioxide / alcohol systems at different pressures; ●,+●, carbon dioxide / methanol; ■,×,■, carbon dioxide / ethanol; ●,■, this study at 303.2 K; ●,■, this study at 323.2 K; +, Sih et al. (2007) at 323.15 K; ×, Sih et al. (2008) at 323.15 K (Kariznovi et al. 2013a).	36

Figure 3–1: Density of Surmont bitumen as a function of pressure at different isotherms; □, 23°C; ◇, 50°C; Δ, 60°C; ○, 70°C; +, 80°C; ●, 90°C; *, 100°C; ×, 125°C; ▲, 150°C; ■, 175°C; ◆, 190°C.....	45
Figure 3–2: Density of MacKay River bitumen as a function of pressure at different isotherms; ■, 50°C; ▲, 60°C; □, 70°C; ◇, 80°C; Δ, 90°C; ○, 100°C; +, 110°C; ●, 120°C; *, 130°C; ×, 140°C; ▲, 150°C; ■, 160°C; ◆, 170°C.....	45
Figure 3–3: Density of MacKay River bitumen as a function of pressure at different isotherms; ◆, 50°C; ■, 60°C; ▲, 70°C; ×, 80°C; *, 90°C; ●, 100°C; +, 110°C; ○, 120°C; Δ, 130°C; ◇, 140°C; □, 150°C; ▲, 160°C; ■, 170°C.	46
Figure 3–4: Coefficient ρ_0 of equation 3-1 as a function of temperature for three different bitumens; ◆, Surmont; ■, MacKay River; ▲, JACOS.	48
Figure 3–5: Coefficient α of equation 3-1 as a function of temperature for three different bitumens; ◆, Surmont; ■, MacKay River; ▲, JACOS.	50
Figure 3–6: Viscosity of Surmont bitumen as a function of temperature at two different pressures; ◆, 2 MPa; ▲, 10 MPa; solid lines, equation 3-6; dashed lines, equation 3-7.....	53
Figure 3–7: Viscosity of MacKay River bitumen as a function of temperature at two different pressures; ◆, 1 MPa; ▲, 14 MPa; solid lines, equation 3-6; dashed lines, equation 3-7.	54
Figure 3–8: Viscosity of JACOS bitumen as a function of temperature at two different pressures; ◆, 1 MPa; ▲, 14 MPa; solid lines, equation 3-6; dashed lines, equation 3-7.....	54
Figure 3–9: Viscosity of different bitumens as a function of temperature at two different pressures; ----, 0.1 MPa; —, 10 MPa; blue color, Surmont; black color, MacKay River; red color, JACOS; green color, Athabasca bitumen reported by Mehrotra and Svrcak (1986).....	55
Figure 3–10: Viscosity ratio of different bitumens as a function of pressure at two different pressures; ----, 150°; —, 25°C; blue color, Surmont; black color, MacKay River; red color, JACOS; green color, Athabasca bitumen reported by Mehrotra and Svrcak (1986).....	56
Figure 3–11: Step-wise procedure for SARA analysis (Speight 2007).	59
Figure 4–1: Phase transitions for vapour-liquid equilibrium study of Surmont bitumen / ethane mixtures; ◆, 50°C and 2 MPa; ◆, 100°C and 4 MPa; ◆, 150°C and 6 MPa; ◆, 190°C and 8 MPa.....	73
Figure 4–2: Measured solubility of ethane in Surmont bitumen as a function of pressure at different temperatures.....	75

Figure 4–3: Viscosity of ethane-saturated Surmont bitumen as a function of pressure at different temperatures.....	76
Figure 4–4: Density of ethane-saturated Surmont bitumen as a function of pressure at different temperatures.....	77
Figure 4–5: Measured K-value for Surmont bitumen / ethane systems as a function of pressure at different temperatures.	79
Figure 4–6: Measured GOR for Surmont bitumen / ethane systems as a function of pressure at different temperatures.	80
Figure 4–7: Measured solubility of ethane in JACOS bitumen as a function of pressure at different temperatures.....	83
Figure 4–8: Viscosity of ethane-saturated JACOS bitumen as a function of pressure at different temperatures.....	84
Figure 4–9: Density of ethane-saturated JACOS bitumen as a function of pressure at different temperatures.....	86
Figure 4–10: Measured K-values for JACOS bitumen / ethane systems at different temperatures and pressures.....	86
Figure 4–11: Measured GOR for JACOS bitumen / ethane systems as a function of pressure at different temperatures.	87
Figure 4–12: Measured solubility of ethane in MacKay River bitumen as a function of pressure at different temperatures.	90
Figure 4–13: Viscosity of ethane-saturated MacKay River bitumen as a function of pressure at different temperatures.	91
Figure 4–14: Density of ethane-saturated MacKay River bitumen as a function of pressure at different temperatures.	91
Figure 4–15: Measured K-values for MacKay River bitumen / ethane systems as a function of pressure at different temperatures.....	93
Figure 4–16: Measured GOR for MacKay River bitumen / ethane systems as a function of pressure at different temperatures.	93
Figure 4–17: Comparison of the measured solubility of ethane in different bitumen samples from Athabasca field as a function of pressure at different temperatures; black symbols, 50°C; blue symbols, 100°C; green symbols, 150°C; red symbols, 190°C; solid symbols, JACOS bitumen; open symbols, Surmont bitumen; +, MacKay River bitumen; ×, Mehrotra and Svrcek (1985a).	95
Figure 4–18: Comparison of the measured viscosity of ethane-saturated bitumen for different bitumen samples from Athabasca Field as a function of pressure at	

different temperatures; black symbols, 50°C; blue symbols, 100°C; green symbols, 150°C; red symbols, 190°C; solid symbols, JACOS bitumen; open symbols, Surmont bitumen; +, MacKay River bitumen; ×, Mehrotra and Svrcek (1985a).....	96
Figure 4–19: Comparison of the measured density of ethane-saturated bitumen for different bitumen samples from Athabasca field as a function of pressure at different temperatures; black symbols, 50°C; blue symbols, 100°C; green symbols, 150°C; red symbols, 190°C; solid symbols, JACOS bitumen; open symbols, Surmont bitumen; +, MacKay River bitumen; ×, Mehrotra and Svrcek (1985a).....	97
Figure 4–20: Liquid-liquid phase transition: saturated phase density ρ and saturated phase viscosity μ versus volume V ; a) saturated phase density; b) saturated phase viscosity (Nourozieh et al. 2011a).....	102
Figure 4–21: Effect of pressure on the extraction yield of components from MacKay River bitumen at two different overall ethane weight fractions w_f and at ambient temperature; —, $w_f = 0.6$; - - - -, $w_f = 0.4$; ●, method 1, ●, method 2, ●, method 3 (Nourozieh et al. 2011a).....	106
Figure 4–22: The extraction yield of MacKay River bitumen as a function of ethane density at two different overall ethane weight fractions w_f and at ambient temperature; —, $w_f = 0.6$; ⋯, $w_f = 0.4$; ●, method 1, ●, method 2, ●, method 3 (Kariznovi et al. 2012b).....	108
Figure 4–23: Effect of overall ethane concentration on the extraction yield of components from MacKay River bitumen at different pressures P and at ambient temperature; —, $P = 9$ MPa; - - - -, $P = 5$ MPa; ●, method 1, ●, method 2, ●, method 3 (Nourozieh et al. 2011a).....	111
Figure 4–24: The extraction yield of MacKay River with respect to the volume ratio of ethane and bitumen at different pressures P and ambient temperature; —, $P = 9$ MPa; ⋯, $P = 5$ MPa; ●, method 1, ●, method 2, ●, method 3 (Kariznovi et al. 2012b).....	112
Figure 4–25: Effect of overall ethane concentration on the composition of equilibrium phases in liquid-liquid equilibrium study of MacKay River bitumen / ethane mixtures at ambient temperature and a constant pressure of 9 MPa; ▲, solvent-enriched phase; ■, asphaltene-enriched phase (Nourozieh et al. 2011a).	114
Figure 4–26: Effect of overall ethane concentration on the density of equilibrium phases in liquid-liquid equilibrium study of MacKay River bitumen / ethane mixtures at ambient temperature and a constant pressure of 9 MPa; ▲, solvent-enriched phase; ■, asphaltene-enriched phase; the density of pure ethane at the same condition is 390 kg/m ³ (Nourozieh et al. 2011a).....	115

- Figure 4–27: Effect of overall ethane concentration on the viscosity of asphaltene-enriched phase in the liquid-liquid equilibrium study of MacKay River bitumen / ethane mixtures at ambient temperature and at different pressures P ; — — —, 9 MPa; —, 5 MPa (Nourozieh et al. 2011a)..... 116
- Figure 4–28: Effect of different solvents on the composition of equilibrium phases and on the extraction of light components from MacKay River bitumen at a constant pressure of 5 MPa and at ambient temperature, with an overall solvent concentration of 0.4 weight fraction; ■, propane; ■, ethane (Nourozieh et al. 2011a)..... 117
- Figure 4–29: Boiling point curves (temperature versus weight percent distilled) for raw MacKay River bitumen (▲) and two flashed-off phase samples (extract ● and residue □) taken from liquid-liquid equilibrium of MacKay River bitumen / ethane mixtures at a constant pressure of 5 MPa and at a constant overall ethane concentration of 0.4 weight fraction (Nourozieh et al. 2012b)..... 120
- Figure 4–30: Compositional analysis (component weight percent) for raw bitumen (black) and two flashed-off phase samples (extract, red, and residue, blue) taken from liquid-liquid equilibrium of MacKay River bitumen / ethane mixtures at a constant pressure of 5 MPa and at a constant overall ethane concentration of 0.4 weight fraction (Nourozieh et al. 2012b; Kariznovi et al. 2013c)..... 121
- Figure 4–31: Carbon number distribution for raw bitumen (▲) and two flashed-off phase samples (extract ● and residue □) taken from liquid-liquid equilibrium study of MacKay River bitumen / ethane mixtures at a constant pressure of 5 MPa and at a constant overall ethane concentration of 0.4 weight fraction. 121
- Figure 4–32: Boiling point curves (temperature versus weight percent distilled) for raw MacKay River bitumen (▲) and two extracts taken from liquid-liquid equilibrium study of MacKay River bitumen / ethane mixtures at different pressures and at a constant overall ethane concentration of 0.4 weight fraction; ○, 5 MPa; □, 9 MPa (Nourozieh et al. 2012b)..... 123
- Figure 4–33: Compositional analysis (component weight percent) for raw bitumen (black) and two extracts taken from liquid-liquid equilibrium study of MacKay River bitumen / ethane mixtures at different pressures and at a constant overall ethane concentration of 0.4 weight fraction; blue, 5 MPa; red, 9 MPa (Nourozieh et al. 2012b)..... 124
- Figure 4–34: Carbon number distribution for raw bitumen (▲) and two extracts taken from liquid-liquid equilibrium study of MacKay River bitumen / ethane mixtures at different pressures and at a constant overall ethane concentration of 0.4 weight fraction; ○, 5 MPa; □, 9 MPa..... 124

- Figure 4–35: Carbon number distribution for raw bitumen (▲) and two residues taken from liquid-liquid equilibrium study of MacKay River bitumen / ethane mixtures at different pressures and at a constant overall ethane concentration of 0.4 weight fraction; ○, 5 MPa; □, 9 MPa..... 125
- Figure 4–36: Compositional analysis (component weight percent) for raw bitumen (black) and two residues taken from liquid-liquid equilibrium study of MacKay River bitumen / ethane mixtures at different pressures and at a constant overall ethane concentration of 0.4 weight fraction; blue, 5 MPa; red, 9 MPa..... 126
- Figure 4–37: Boiling point curves (temperature versus weight percent distilled) for raw MacKay River bitumen (▲) and two extracts taken from liquid-liquid equilibrium study of MacKay River bitumen / ethane mixtures at different overall ethane concentrations and at a constant pressure of 9 MPa; ○, overall ethane weight fraction of 0.4; □, overall ethane weight fraction of 0.9 (Nourozieh et al. 2012b)..... 127
- Figure 4–38: Compositional analysis (component weight percent) for raw bitumen (black) and two extracts taken from liquid-liquid equilibrium study of MacKay River bitumen / ethane mixtures at different overall ethane concentrations and at a constant pressure of 9 MPa; blue, overall ethane weight fraction of 0.4; red, overall ethane weight fraction of 0.9 (Nourozieh et al. 2012b). 127
- Figure 4–39: Carbon number distribution for raw MacKay River bitumen (▲) and two extracts taken from liquid-liquid equilibrium study of MacKay River bitumen / ethane mixtures at different overall ethane concentrations and at a constant pressure of 9 MPa; ○, overall ethane weight fraction of 0.4; □, overall ethane weight fraction of 0.9. 128
- Figure 4–40: Carbon number distribution for raw MacKay River bitumen (▲) and two residues taken from liquid-liquid equilibrium study of MacKay River bitumen / ethane mixtures at different overall ethane concentrations and at a constant pressure of 9 MPa; ○, overall ethane weight fraction of 0.4; □, overall ethane weight fraction of 0.9. 129
- Figure 4–41: Compositional analysis (component weight percent) for raw bitumen (black) and two residues taken from liquid-liquid equilibrium study of MacKay River bitumen / ethane mixtures at different overall ethane concentrations and at a constant pressure of 9 MPa; blue, overall ethane weight fraction of 0.4; red, overall ethane weight fraction of 0.9 (Nourozieh et al. 2012b). 129
- Figure 4–42: SARA compositional analysis of raw bitumen and two flashed-off liquid phases taken from liquid-liquid equilibrium study of MacKay River bitumen / ethane mixtures at ambient temperature and at 9 MPa with an overall ethane concentration of 0.6 weight fraction; black, raw bitumen; red, extract; blue, residue. 132

Figure 4–43: Effect of overall ethane concentration and pressure on the SARA compositional analysis of extracts taken from liquid-liquid equilibrium study of MacKay River bitumen / ethane mixtures at ambient temperatures; black, raw bitumen; red, 5 MPa and overall ethane concentration of 0.6 weight fraction; blue, 9 MPa and overall ethane concentration of 0.6 weight fraction; green, 9 MPa and overall ethane concentration of 0.8 weight fraction.....	133
Figure 4–44: Effect of overall ethane concentration on the SARA compositional analysis of residues taken from liquid-liquid equilibrium study of MacKay River bitumen / ethane mixtures at ambient temperatures and at a constant pressure of 9 MPa; black, raw bitumen; red, overall ethane concentration of 0.4 weight fraction; blue, overall ethane concentration of 0.6 weight fraction; green, overall ethane concentration of 0.8 weight fraction.	134
Figure 4–45: Pressure-Temperature (P - T) diagram for Mackay River bitumen / ethane systems; ●, vapour-liquid experimental data; ●, the experimental data of Athabasca bitumen / ethane systems by Mehrotra and Svrcek (1985a); ■, liquid-liquid experimental data.	139
Figure 4–46: Pressure-Composition (P - x) diagram for Mackay River bitumen / ethane systems at ambient temperature; ●, the experimental data of Athabasca bitumen / ethane systems by Mehrotra and Svrcek (1985a); ■, liquid-liquid experimental data.	140
Figure 4–47: Coexisting phase compositions for Mackay River bitumen / ethane systems at ambient temperature and at a constant overall ethane concentration of 0.4 weight fraction; ●, the experimental data of Athabasca bitumen / ethane systems by Mehrotra and Svrcek (1985a); ■, liquid-liquid experimental data.	142
Figure 4–48: Coexisting phase densities for Mackay River bitumen / ethane systems at ambient temperature and at a constant overall ethane concentration of 0.4 weight fraction; ●, the experimental data of Athabasca bitumen / ethane systems by Mehrotra and Svrcek (1985a); ■, liquid-liquid experimental data.	143
Figure 5–1: Measured solubility of propane in Surmont bitumen as a function of pressure at different temperatures.....	156
Figure 5–2: Viscosity of propane-saturated Surmont bitumen as a function of pressure at different temperatures.....	157
Figure 5–3: Density of propane-saturated Surmont bitumen as a function of pressure at different temperatures.....	158
Figure 5–4: Measured K-values for Surmont bitumen / propane systems as a function of pressure at different temperatures.	160

Figure 5–5: Measured GOR for Surmont bitumen / propane systems as a function of pressure at different temperatures.	161
Figure 5–6: Digital photographs of gas-free bitumen (left) and flashed-off liquid samples (middle and right) taken from liquid-liquid equilibrium study of Surmont bitumen / propane mixtures.	162
Figure 5–7: Liquid-liquid phase equilibria for Surmont bitumen / propane systems at the temperature of 50°C; the concentration of propane in liquid phases as a function of overall propane concentration at different pressures.	167
Figure 5–8: Liquid-liquid phase equilibria for Surmont bitumen / propane systems at the temperature of 100°C; the concentration of propane in liquid phases as a function of overall propane concentration at different pressures.	168
Figure 5–9: Liquid-liquid phase equilibria for Surmont bitumen / propane systems at the temperature of 50°C; density of equilibrium phases as a function of overall propane concentration at different pressures.	170
Figure 5–10: Liquid-liquid phase equilibria for Surmont bitumen / propane systems at the temperature of 100°C; density of equilibrium phases as a function of overall propane concentration at different pressures.	170
Figure 5–11: Liquid-liquid phase equilibria for Surmont bitumen / propane systems at the temperature of 50°C; the viscosity of asphaltene-enriched phase as a function of overall propane concentration at different pressures.	172
Figure 5–12: Liquid-liquid phase equilibria for Surmont bitumen / propane systems at the temperature of 100°C; the viscosity of asphaltene-enriched phase as a function of overall propane concentration at different pressures.	173
Figure 5–13: Effect of pressure and overall propane concentration on the extraction yield of Surmont bitumen using propane at the temperature of 50°C (Nourozieh et al. 2012c).	176
Figure 5–14: Effect of pressure and overall propane concentration on the extraction yield of Surmont bitumen using propane at 100°C.	177
Figure 5–15: Effect of temperature and overall propane concentration on the extraction yield of Surmont bitumen using propane at a constant pressure of 8 MPa.	178
Figure 5–16: Effect of propane density and overall propane concentration on the extraction yield of Surmont bitumen.	180
Figure 5–17: Boiling point curves (temperature versus weight fraction distilled) for raw Surmont bitumen (▲) and two extracts taken from liquid-liquid equilibrium of Surmont bitumen / propane mixtures; □, the solvent-enriched phase at the temperature of 50°C and at a constant pressure of 2 MPa with a constant overall concentration of 0.4 weight fraction; ●, the solvent-enriched phase at	

- the temperature of 100°C and at a constant pressure of 6 MPa with a constant overall propane concentration of 0.8 weight fraction..... 183
- Figure 5–18: Compositional analysis (component weight percent) for raw bitumen (black) and two flashed-off phase samples (extract, red, and residue, blue) taken from liquid-liquid equilibrium of Surmont bitumen / propane mixtures at the temperature of 50°C and at a constant pressure of 2 MPa with a constant overall propane concentration of 0.4 weight fraction..... 184
- Figure 5–19: Carbon number distribution for raw bitumen (▲) and two flashed-off phase samples (extract ● and residue □) taken from liquid-liquid equilibrium of Surmont bitumen / propane mixtures at 50°C and at a constant pressure of 2 MPa with a constant overall propane concentration of 0.4 weight fraction... 185
- Figure 5–20: Compositional analysis (component weight percent) for raw bitumen (black) and two flashed-off phase samples (extract, red, and residue, blue) taken from liquid-liquid equilibrium of Surmont bitumen / propane mixtures at the temperature of 100°C and at a constant pressure of 6 MPa with a constant overall propane concentration of 0.8 weight fraction..... 186
- Figure 5–21: Carbon number distribution for raw bitumen (▲) and two flashed-off phase samples (extract ● and residue □) taken from liquid-liquid equilibrium of Surmont bitumen / propane mixtures at 100°C and at a constant pressure of 6 MPa with a constant overall propane concentration of 0.8 weight fraction... 187
- Figure 5–22: Boiling point curves (temperature versus weight percent distilled) for raw bitumen (▲) and extracts taken from liquid-liquid equilibrium of Surmont bitumen / propane mixtures at different pressures, temperatures, and overall propane concentrations; ■, 50°C, 2 MPa, and overall propane concentration of 0.4 weight fraction; ○, 50°C, 8 MPa, and overall propane concentration of 0.4 weight fraction; +, 50°C, 2 MPa, and overall propane concentration of 0.8 weight fraction; ×, 50°C, 8 MPa, and overall propane concentration of 0.8 weight fraction; ●, 100°C, 8 MPa, and overall propane concentration of 0.4 weight fraction; Δ, 100°C, 6 MPa, and overall propane concentration of 0.8 weight fraction; *, 100°C, 8 MPa, and overall propane concentration of 0.8 weight fraction..... 189
- Figure 5–23: Compositional analysis (component weight percent) for raw bitumen (black) and extracts taken from liquid-liquid equilibrium of Surmont bitumen / propane mixtures at a constant temperature of 50°C and at different pressures and overall propane concentrations; red, 2 MPa, and overall propane concentration of 0.4 weight fraction; blue, 8 MPa, and overall propane concentration of 0.4 weight fraction; green, 2 MPa, and overall propane concentration of 0.8 weight fraction..... 190
- Figure 5–24: Compositional analysis (component weight percent) for raw bitumen (black) and residues taken from liquid-liquid equilibrium of Surmont bitumen /

propane mixtures at a constant temperature of 50°C and at different pressures and overall propane concentrations; red, 2 MPa, and overall propane concentration of 0.4 weight fraction; blue, 8 MPa, and overall propane concentration of 0.4 weight fraction; green, 2 MPa, and overall propane concentration of 0.8 weight fraction..... 190

Figure 5–25: Compositional analysis (component weight percent) for raw bitumen (black) and extracts taken from liquid-liquid equilibrium of Surmont bitumen / propane mixtures at a constant temperature of 100°C and at different pressures and overall propane concentrations; red, 6 MPa, and overall propane concentration of 0.8 weight fraction; blue, 8 MPa, and overall propane concentration of 0.4 weight fraction; green, 8 MPa, and overall propane concentration of 0.8 weight fraction..... 192

Figure 5–26: Compositional analysis (component weight percent) for raw bitumen (black) and residues taken from liquid-liquid equilibrium of Surmont bitumen / propane mixtures at a constant temperature of 100°C and at different pressures and overall propane concentrations; red, 6 MPa, and overall propane concentration of 0.8 weight fraction; blue, 8 MPa, and overall propane concentration of 0.4 weight fraction; green, 8 MPa, and overall propane concentration of 0.8 weight fraction..... 192

Figure 5–27: Carbon number distribution for raw bitumen (▲) and flashed-off solvent enriched phases (extracts) taken from liquid-liquid equilibrium of Surmont bitumen / propane mixtures at different pressures, temperatures, and overall propane concentrations; ■, 50°C, 2 MPa, and overall propane concentration of 0.4 weight fraction; ○, 50°C, 8 MPa, and overall propane concentration of 0.4 weight fraction; +, 50°C, 2 MPa, and overall propane concentration of 0.8 weight fraction; ×, 50°C, 8 MPa, and overall propane concentration of 0.8 weight fraction; ●, 100°C, 8 MPa, and overall propane concentration of 0.4 weight fraction; Δ, 100°C, 6 MPa, and overall propane concentration of 0.8 weight fraction; *, 100°C, 8 MPa, and overall propane concentration of 0.8 weight fraction..... 194

Figure 5–28: Carbon number distribution for raw bitumen (▲) and flashed-off asphaltene-enriched phases (residues) taken from liquid-liquid equilibrium of Surmont bitumen / propane mixtures at different pressures, temperatures, and overall propane concentrations; ■, 50°C, 2 MPa, and overall propane concentration of 0.4 weight fraction; ○, 50°C, 8 MPa, and overall propane concentration of 0.4 weight fraction; +, 50°C, 2 MPa, and overall propane concentration of 0.8 weight fraction; ×, 50°C, 8 MPa, and overall propane concentration of 0.8 weight fraction; ●, 100°C, 8 MPa, and overall propane concentration of 0.4 weight fraction; Δ, 100°C, 6 MPa, and overall propane concentration of 0.8 weight fraction; *, 100°C, 8 MPa, and overall propane concentration of 0.8 weight fraction..... 195

- Figure 5–29: Compositional analysis (component weight percent) for extracts taken from liquid-liquid equilibrium of Surmont bitumen / propane mixtures at a constant pressure of 8 MPa and at different temperatures and overall propane concentrations; red, 100°C and overall propane concentration of 0.4 weight fraction; green, 100°C and overall propane concentration of 0.8 weight fraction; blue, 50°C and overall propane concentration of 0.4 weight fraction; black, 50°C and overall propane concentration of 0.8 weight fraction. 198
- Figure 5–30: Compositional analysis (component weight percent) for residues taken from liquid-liquid equilibrium of Surmont bitumen / propane mixtures at a constant pressure of 8 MPa and at different temperatures and overall propane concentrations; red, 100°C and overall propane concentration of 0.4 weight fraction; green, 100°C and overall propane concentration of 0.8 weight fraction; blue, 50°C and overall propane concentration of 0.4 weight fraction; black, 50°C and overall propane concentration of 0.8 weight fraction. 199
- Figure 5–31: SARA compositional analysis of raw bitumen (black) and two flashed-off phase samples (extract, red, and residue, blue) taken from liquid-liquid equilibrium of Surmont bitumen / propane mixtures at 50°C and 2 MPa with an overall propane concentration of 0.4 weight fraction. 206
- Figure 5–32: SARA compositional analysis of raw bitumen (black) and two flashed-off phase samples (extract, red, and residue, blue) taken from liquid-liquid equilibrium of Surmont bitumen / propane mixtures at 100°C and 8 MPa with an overall propane concentration of 0.4 weight fraction. 207
- Figure 5–33: SARA compositional analysis of raw bitumen (black) and two extracts taken from liquid-liquid equilibrium of Surmont bitumen / propane mixtures at different pressures and at 100°C with an overall propane concentration of 0.8 weight fraction; red, 6 MPa; blue, 8 MPa. 209
- Figure 5–34: SARA compositional analysis of raw bitumen (black) and two residues taken from liquid-liquid equilibrium of Surmont bitumen / propane mixtures at different pressures and at 100°C with an overall propane concentration of 0.8 weight fraction; red, 6 MPa; blue, 8 MPa. 209
- Figure 5–35: SARA compositional analysis of raw bitumen (black) and two extracts taken from liquid-liquid equilibrium of Surmont bitumen / propane mixtures at different pressures and at 50°C with an overall propane concentration of 0.4 weight fraction; red, 2 MPa; blue, 8 MPa. 210
- Figure 5–36: SARA compositional analysis of raw bitumen (black) and two residues taken from liquid-liquid equilibrium of Surmont bitumen / propane mixtures at different pressures and at 50°C with an overall propane concentration of 0.4 weight fraction; red, 2 MPa; blue, 8 MPa. 210

Figure 5–37: SARA compositional analysis of raw bitumen (black) and two extracts taken from liquid-liquid equilibrium of Surmont bitumen / propane mixtures at different pressures and at 50°C with an overall propane concentration of 0.8 weight fraction; red, 2 MPa; blue, 8 MPa. 211

Figure 5–38: SARA compositional analysis of raw bitumen (black) and two residues taken from liquid-liquid equilibrium of Surmont bitumen / propane mixtures at different pressures and at 50°C with an overall propane concentration of 0.8 weight fraction; black, raw bitumen; red, 2 MPa; blue, 8 MPa. 211

Figure 5–39: SARA compositional analysis of raw bitumen (black) and two extracts taken from liquid-liquid equilibrium of Surmont bitumen / propane mixtures at different temperatures and at 8 MPa with an overall propane concentration of 0.4 weight fraction; red, 50°C; blue, 100°C..... 212

Figure 5–40: SARA compositional analysis of raw bitumen (black) and two residues taken from liquid-liquid equilibrium of Surmont bitumen / propane mixtures at different temperatures and at 8 MPa with an overall propane concentration of 0.4 weight fraction; red, 50°C; blue, 100°C..... 213

Figure 5–41: SARA compositional analysis of raw bitumen (black) and two extracts taken from liquid-liquid equilibrium of Surmont bitumen / propane mixtures at different temperatures and at 8 MPa with an overall propane concentration of 0.8 weight fraction; red, 50°C; blue, 100°C..... 213

Figure 5–42: SARA compositional analysis of raw bitumen (black) and two residues taken from liquid-liquid equilibrium of Surmont bitumen / propane mixtures at different temperatures and at 8 MPa with an overall propane concentration of 0.8 weight fraction; red, 50°C; blue, 100°C..... 214

Figure 5–43: SARA compositional analysis of raw bitumen (black) and two extracts taken from liquid-liquid equilibrium of Surmont bitumen / propane mixtures with different overall propane concentrations at 100°C and 8 MPa; red, 0.4 weight fraction; blue, 0.8 weight fraction. 215

Figure 5–44: SARA compositional analysis of raw bitumen (black) and two residues taken from liquid-liquid equilibrium of Surmont bitumen / propane mixtures with different overall propane concentrations at 100°C and 8 MPa; red, 0.4 weight fraction; blue, 0.8 weight fraction. 216

Figure 5–45: SARA compositional analysis of raw bitumen (black) and two extracts taken from liquid-liquid equilibrium of Surmont bitumen / propane mixtures with different overall propane concentrations at 50°C and 2 MPa; red, 0.4 weight fraction; blue, 0.8 weight fraction. 216

Figure 5–46: SARA compositional analysis of raw bitumen (black) and two residues taken from liquid-liquid equilibrium of Surmont bitumen / propane mixtures

with different overall propane concentrations at 50°C and 2 MPa; red, 0.4 weight fraction; blue, 0.8 weight fraction.	217
Figure 5–47: SARA compositional analysis of raw bitumen (black) and three extracts taken from liquid-liquid equilibrium of Surmont bitumen / propane mixtures with different overall propane concentrations at 50°C and 8 MPa; red, 0.4 weight fraction; blue, 0.6 weight fraction; green, 0.8 weight fraction.	217
Figure 5–48: SARA compositional analysis of raw bitumen (black) and three residues taken from liquid-liquid equilibrium of Surmont bitumen / propane mixtures with different overall propane concentrations at 50°C and 8 MPa; red, 0.4 weight fraction; blue, 0.6 weight fraction; green, 0.8 weight fraction.	218
Figure 5–49: Pressure-temperature (P - T) diagram for Surmont bitumen / propane systems; ●, vapour-liquid experimental data; ●, vapour-liquid experimental data for Athabasca bitumen / propane systems taken from Badamchi-Zadeh et al. (2009a); ■, liquid-liquid experimental data.	219
Figure 5–50: Pressure-composition (P - x) diagram for Surmont bitumen / propane systems at 50°C; ●, vapour-liquid experimental data; ●, vapour-liquid experimental data for Athabasca bitumen / propane systems taken from Badamchi-Zadeh et al. (2009a); ■, liquid-liquid experimental data.	220
Figure 5–51: Pressure-composition (P - x) diagram for Surmont bitumen / propane systems at 100°C; ●, vapour-liquid experimental data; ■, liquid-liquid experimental data.	221
Figure 5–52: Coexisting phase compositions for Surmont bitumen /propane systems at 50°C and at a constant overall propane concentration of 0.4 weight fraction; ●, vapour-liquid experimental data; ●, vapour-liquid experimental data for propane / Athabasca bitumen systems taken from Badamchi-Zadeh et al. (2009a); ■, liquid-liquid experimental data.	223
Figure 5–53: Coexisting phase compositions for Surmont bitumen / propane systems at 100°C and at a constant overall propane concentration of 0.6 weight fraction; ●, vapour-liquid experimental data; ■, liquid-liquid experimental data.....	224
Figure 5–54: Coexisting phase densities for Surmont bitumen / propane systems at 50°C and at a constant overall propane concentration of 0.4 weight fraction; ●, vapour-liquid experimental data; ●, vapour-liquid experimental data for propane / Athabasca bitumen systems taken from Badamchi-Zadeh et al. (2009a); ■, liquid-liquid experimental data.	225
Figure 5–55: Coexisting phase densities for Surmont bitumen / propane systems at 100°C and at a constant overall propane concentration of 0.6 weight fraction; ●, vapour-liquid experimental data; ■, liquid-liquid experimental data.....	226

Figure 5–56: The maximum solubility of light hydrocarbon gases in Surmont bitumen at the temperatures of 150 and 190°C; blue, butane; black, propane; red, ethane; green, methane.....	229
Figure 5–57: Comparison of the measured saturated bitumen density of Surmont bitumen and different light hydrocarbon gases at the temperatures of 150 and 190°C; blue, butane; black, propane; red, ethane; green, methane.....	229
Figure 5–58: Comparison of the measured saturated bitumen viscosity of Surmont bitumen and different light hydrocarbon gases at the temperatures of 150 and 190°C; blue, butane; black, propane; red, ethane; green, methane.	230
Figure 5–59: The comparison of the saturated liquid densities for Surmont bitumen saturated with different solvents at different temperatures and a constant solvent weight fraction.	233
Figure 5–60: The comparison of the saturated liquid viscosities for Surmont bitumen saturated with different solvents at different temperatures and a constant solvent weight fraction.	234
Figure 6–1: Digital photographs of the precipitated asphaltene from the mixture of Surmont bitumen / <i>n</i> -hexane at the temperature of 100°C and at a concentration of 0.6 <i>n</i> -hexane weight fraction; a) immediately after experiment; b) after evaporation of <i>n</i> -hexane.	239
Figure 6–2: Density of Surmont bitumen / <i>n</i> -hexane mixtures as a function of the weight fraction of <i>n</i> -hexane at different temperatures and at a constant pressure of 2 MPa; ■,▲,○,◆,×, experimental data; ----, predicted values.	244
Figure 6–3: Density of Surmont bitumen / <i>n</i> -hexane mixtures as a function of the weight fraction of <i>n</i> -hexane at different temperatures and at a constant pressure of 10 MPa; ■,▲,○,◆,×, experimental data; ----, predicted values.	245
Figure 6–4: Density of Surmont bitumen / <i>n</i> -hexane mixtures as a function of pressure at different <i>n</i> -hexane weight fractions and at the lowest temperature (23°C); ○, ×, ▲, ■, ◆, +, experimental data; ----, predicted values.	245
Figure 6–5: Density of Surmont bitumen / <i>n</i> -hexane mixtures as a function of pressure at different <i>n</i> -hexane weight fractions and at the highest temperature (190°C); ○, ×, ▲, ■, ◆, +, experimental data; ----, predicted values.	246
Figure 6–6: Density of Surmont bitumen / <i>n</i> -hexane mixtures as a function of pressure at different temperatures and at the lowest solvent weight fraction (0.05); ○, ×, ▲, ■, ◆, experimental data; ----, predicted values.	247
Figure 6–7: Density of Surmont bitumen / <i>n</i> -hexane mixtures as a function of pressure at different temperatures and at the highest solvent weight fraction (0.5); ○, ×, ▲, ■, ◆, experimental data; ----, predicted values.	247

Figure 6–8: Density of Surmont bitumen / <i>n</i> -hexane mixtures as a function of temperature at different <i>n</i> -hexane weight fractions and at the lowest pressure (2 MPa); ○, ×, ▲, ■, ◆, experimental data; ----, predicted values.	248
Figure 6–9: Density of Surmont bitumen / <i>n</i> -hexane mixtures as a function of temperature at different <i>n</i> -hexane weight fractions and at the highest pressure (10 MPa); ○, ×, ▲, ■, ◆, +, experimental data; ----, predicted values.	249
Figure 6–10: Effect of temperature on the volume change on mixing for Surmont bitumen / <i>n</i> -hexane mixtures with different solvent weight fractions at a constant pressure of 2 MPa.	251
Figure 6–11: Effect of temperature on the volume change on mixing for Surmont bitumen / <i>n</i> -hexane mixtures with different solvent weight fractions at a constant pressure of 10 MPa.	252
Figure 6–12: Effect of pressure on the volume change on mixing for Surmont bitumen / <i>n</i> -hexane mixtures with different solvent weight fractions at 190°C.	253
Figure 6–13: Effect of pressure on the volume change on mixing for Surmont bitumen / <i>n</i> -hexane mixtures at a constant solvent weight fraction of 0.5 and at different temperatures.	254
Figure 6–14: Volume change on mixing for Surmont bitumen / <i>n</i> -hexane mixtures as a function of the weight fraction of hexane at different temperatures and at a constant pressure of 2 MPa.	256
Figure 6–15: Volume change on mixing for Surmont bitumen / <i>n</i> -hexane mixtures as a function of the weight fraction of hexane at different temperatures and at a constant pressure of 10 MPa.	256
Figure 6–16: Calculated densities of Surmont bitumen / <i>n</i> -hexane mixtures using no volume change on mixing assumption versus the measured values.	259
Figure 6–17: Calculated densities of Surmont bitumen / <i>n</i> -hexane mixtures using excess volume mixing rule versus the measured values.	260
Figure 6–18: Calculated densities of Surmont bitumen / <i>n</i> -hexane mixtures using effective liquid densities versus the measured values.	260
Figure 6–19: Density of Surmont bitumen / <i>n</i> -hexane mixtures as a function of the weight fraction of <i>n</i> -hexane at different temperatures and at a constant pressure of 2 MPa; ■, ▲, ○, ◆, ×, experimental data; —, no volume change on mixing; ----, excess volume mixing rule; — — —, effective liquid densities.	261
Figure 6–20: Density of Surmont bitumen / <i>n</i> -hexane mixtures as a function of pressure at different <i>n</i> -hexane weight fractions and at the highest temperature (190°C); ○, ×, ▲, ■, ◆, +, experimental data; —, no volume change on mixing; ----, excess volume mixing rule; — — —, effective liquid densities.	261

Figure 6–21: The comparison between the calculated viscosities with Arrhenius’ model and experimental data for Surmont bitumen / <i>n</i> -hexane mixtures.	269
Figure 6–22: The comparison between the calculated viscosities with power law model and experimental data for Surmont bitumen / <i>n</i> -hexane mixtures.	270
Figure 6–23: The comparison between the calculated viscosities with Cragoe’s model and experimental data for Surmont bitumen / <i>n</i> -hexane mixtures.	271
Figure 6–24: The comparison between the calculated viscosities with Lederer’s model and experimental data for Surmont bitumen / <i>n</i> -hexane mixtures.	272
Figure 6–25: The comparison between the calculated viscosities with Shu’s model and experimental data for Surmont bitumen / <i>n</i> -hexane mixtures.	273
Figure 6–26: The comparison between the calculated viscosities with Lobe’s model and experimental data for Surmont bitumen / <i>n</i> -hexane mixtures.	273
Figure 6–27: Viscosity of Surmont bitumen / <i>n</i> -hexane mixtures as a function of the weight fraction of <i>n</i> -hexane at different temperatures and at a constant pressure of 2 MPa; ○, ×, ▲, ■, ◆, measured viscosities; calculated values: —, power law model; - - -, Cragoe’s model.	275
Figure 6–28: Viscosity of Surmont bitumen / <i>n</i> -hexane mixtures as a function of the weight fraction of <i>n</i> -hexane at different temperatures and at a constant pressure of 10 MPa; ○, ×, ▲, ■, ◆, measured viscosities; calculated values: —, power law model; - - -, Cragoe’s model.	275
Figure 6–29: Viscosity of Surmont bitumen / <i>n</i> -hexane mixtures as a function of temperature at different weight fractions of <i>n</i> -hexane and at a constant pressure of 2 MPa; ○, ×, ▲, ■, ◆, +, measured viscosities; calculated values: —, power law model; - - -, Cragoe’s model.	276
Figure 6–30: Viscosity of Surmont bitumen / <i>n</i> -hexane mixtures as a function of temperature at different weight fractions of <i>n</i> -hexane and at a constant pressure of 10 MPa; ○, ×, ▲, ■, ◆, +, measured viscosities; calculated values: —, power law model; - - -, Cragoe’s model.	277
Figure 6–31: Effect of <i>n</i> -hexane concentration w_s and pressure P on the viscosity of Surmont bitumen / <i>n</i> -hexane mixtures at the lowest temperature (28°C); ○, ×, ▲, ■, ◆, +, measured viscosities; calculated values: —, power law model; - - -, Cragoe’s model.	278
Figure 6–32: Effect of <i>n</i> -hexane concentration w_s and pressure P on the viscosity of Surmont bitumen / <i>n</i> -hexane mixtures at the highest temperature (190°C); ○, ×, ▲, ■, ◆, +, measured viscosities; calculated values: —, power law model; - - -, Cragoe’s model.	279
Figure 6–33: Effect of pressure P on the viscosity of Surmont bitumen / <i>n</i> -hexane mixtures at the lowest <i>n</i> -hexane weight fraction (0.05); ○, ×, ▲, ■, ◆, +,	

measured viscosities; calculated values: —, power law model; - - -, Cragoe's model.....	280
Figure 6–34: Effect of pressure P on the viscosity of Surmont bitumen / n -hexane mixtures at the highest n -hexane weight fraction (0.5); \circ , \times , \blacktriangle , \blacksquare , \blacklozenge , $+$, measured viscosities; calculated values: —, power law model; - - -, Cragoe's model.....	280
Figure 7–1: Density of Surmont bitumen / condensate mixtures as a function of the weight fraction of condensate at different temperatures and at a constant pressure of 2 MPa; \blacksquare , \blacktriangle , \circ , \blacklozenge , \times , experimental data; ----, predicted values.	299
Figure 7–2: Density of Surmont bitumen / condensate mixtures as a function of the weight fraction of condensate at different temperatures and at a constant pressure of 10 MPa; \blacksquare , \blacktriangle , \circ , \blacklozenge , \times , experimental data; ----, predicted values. ..	300
Figure 7–3: Density of Surmont bitumen / condensate mixtures as a function of pressure at different condensate weight fractions and at the lowest temperature (23°C); \circ , \times , \blacktriangle , \blacksquare , \blacklozenge , $+$, experimental data; ----, predicted values.....	300
Figure 7–4: Density of Surmont bitumen / condensate mixtures as a function of pressure at different condensate weight fractions and at the highest temperature (190°C); \circ , \times , \blacktriangle , \blacksquare , \blacklozenge , $+$, experimental data; ----, predicted values.	301
Figure 7–5: Density of Surmont bitumen / condensate mixtures as a function of pressure at different temperatures and at the lowest solvent weight fraction (0.05); \circ , \times , \blacktriangle , \blacksquare , \blacklozenge , experimental data; ----, predicted values.	302
Figure 7–6: Density of Surmont bitumen / condensate mixtures as a function of pressure at different temperatures and at the highest solvent weight fraction (0.5); \circ , \times , \blacktriangle , \blacksquare , \blacklozenge , experimental data; ----, predicted values.	303
Figure 7–7: Density of Surmont bitumen / condensate mixtures as a function of temperature at different condensate weight fractions and at the lowest pressure (2 MPa); \circ , \times , \blacktriangle , \blacksquare , \blacklozenge , experimental data; ----, predicted values.	304
Figure 7–8: Density of Surmont bitumen / condensate mixtures as a function of temperature at different condensate weight fractions and at the highest pressure (10 MPa); \circ , \times , \blacktriangle , \blacksquare , \blacklozenge , $+$, experimental data; ----, predicted values.	304
Figure 7–9: Effect of temperature on the volume change on mixing for Surmont bitumen / condensate mixtures with different solvent weight fractions at a constant pressure of 2 MPa.....	306
Figure 7–10: Effect of temperature on the volume change on mixing for Surmont bitumen / condensate mixtures with different solvent weight fractions at a constant pressure of 10 MPa.....	306
Figure 7–11: Effect of pressure on the volume change on mixing for Surmont bitumen / condensate mixtures with different solvent weight fractions at 190°C.....	307

Figure 7–12: Effect of pressure on the volume change on mixing for Surmont bitumen / condensate mixtures at a constant solvent weight fraction of 0.5 and at different temperatures.	308
Figure 7–13: Volume change on mixing for Surmont bitumen / condensate mixtures as a function of the weight fraction of pentane at different temperatures and at a constant pressure of 2 MPa.	309
Figure 7–14: Volume change on mixing for Surmont bitumen / condensate mixtures as a function of the weight fraction of pentane at different temperatures and at a constant pressure of 10 MPa.	310
Figure 7–15: Calculated densities of Surmont bitumen / condensate mixtures using no volume change on mixing assumption versus the measured values.	312
Figure 7–16: Calculated densities of Surmont bitumen / condensate mixtures using excess volume mixing rule versus the measured values.	312
Figure 7–17: Density of Surmont bitumen / condensate mixtures as a function of the weight fraction of condensate at different temperatures and at a constant pressure of 2 MPa; ■,▲,○,◆,×, experimental data; —, no volume change on mixing; ----, excess volume mixing rule.	313
Figure 7–18: Density of Surmont bitumen / condensate mixtures as a function of pressure at different condensate weight fractions and at the highest temperature (190°C); ○, ×, ▲, ■, ◆, +, experimental data; —, no volume change on mixing; ----, excess volume mixing rule.	313
Figure 7–19: The comparison between the calculated viscosities with Arrhenius’ model and experimental data for Surmont bitumen / condensate mixtures.	319
Figure 7–20: The comparison between the calculated viscosities with power law model and experimental data for Surmont bitumen / condensate mixtures.	320
Figure 7–21: The comparison between the calculated viscosities with Cragoe’s model and experimental data for Surmont bitumen / condensate mixtures.	321
Figure 7–22: The comparison between the calculated viscosities with Lederer’s model and experimental data for Surmont bitumen / condensate mixtures.	322
Figure 7–23: The comparison between the calculated viscosities with Shu’s model and experimental data for Surmont bitumen / condensate mixtures.	323
Figure 7–24: The comparison between the calculated viscosities with Lobe’s model and experimental data for Surmont bitumen / condensate mixtures.	323
Figure 7–25: Viscosity of Surmont bitumen / condensate mixtures as a function of the weight fraction of condensate at different temperatures and at a constant pressure of 2 MPa; ○, ×, ▲, ■, ◆, measured viscosities; calculated values: —, power law model; - - -, Cragoe’s model.	325

- Figure 7–26: Viscosity of Surmont bitumen / condensate mixtures as a function of the weight fraction of condensate at different temperatures and at a constant pressure of 10 MPa; \circ , \times , \blacktriangle , \blacksquare , \blacklozenge , measured viscosities; calculated values: —, power law model; - - -, Cragoe’s model..... 325
- Figure 7–27: Viscosity of Surmont bitumen / condensate mixtures as a function of temperature at different weight fractions of condensate and at a constant pressure of 2 MPa; \circ , \times , \blacktriangle , \blacksquare , \blacklozenge , $+$, measured viscosities; calculated values: —, power law model; - - -, Cragoe’s model..... 327
- Figure 7–28: Viscosity of Surmont bitumen / condensate mixtures as a function of temperature at different weight fractions of condensate and at a constant pressure of 10 MPa; \circ , \times , \blacktriangle , \blacksquare , \blacklozenge , $+$, measured viscosities; calculated values: —, power law model; - - -, Cragoe’s model..... 327
- Figure 7–29: Effect of condensate concentration w_s and pressure P on the viscosity of Surmont bitumen / condensate mixtures at the lowest temperature (28°C); \circ , \times , \blacktriangle , \blacksquare , \blacklozenge , $+$, measured viscosities; calculated values: —, power law model; - - -, Cragoe’s model..... 328
- Figure 7–30: Effect of condensate concentration w_s and pressure P on the viscosity of Surmont bitumen / condensate mixtures at the highest temperature (190°C); \circ , \times , \blacktriangle , \blacksquare , \blacklozenge , $+$, measured viscosities; calculated values: —, power law model; - - -, Cragoe’s model. 328
- Figure 7–31: Effect of pressure P on the viscosity of Surmont bitumen / condensate mixtures at the lowest condensate weight fraction (0.05); \circ , \times , \blacktriangle , \blacksquare , \blacklozenge , $+$, measured viscosities; calculated values: —, power law model; - - -, Cragoe’s model..... 329
- Figure 7–32: Effect of pressure P on the viscosity of Surmont bitumen / condensate mixtures at the highest condensate weight fraction (0.5); \circ , \times , \blacktriangle , \blacksquare , \blacklozenge , $+$, measured viscosities; calculated values: —, power law model; - - -, Cragoe’s model..... 330
- Figure 7–33: Digital photographs of the precipitated asphaltene for the mixture of Surmont bitumen / condensate at different temperatures and at concentrations higher than 0.5 condensate weight fractions. 332
- Figure 8–1: Boiling point curves (temperature versus weight percent distilled) for raw MacKay River bitumen (\blacktriangle) and developed characterization method (\square).... 344
- Figure 8–2: Comparison of measured (symbols) and predicted solubilities of ethane in MacKay River bitumen as a function of equilibrium pressure at different temperatures; —, first approach;— —, second approach. 345
- Figure 8–3: Comparison of experimental and modelling results for pressure-composition (P-x) diagram for the mixture of Mackay River bitumen / ethane at ambient

temperature; ●, the experimental data of Athabasca bitumen / ethane systems by Mehrotra and Svrcek (1985a); ■, liquid-liquid experimental data; lines, predictions by Peng-Robinson equation of state using second approach..... 346

Figure 8–4: Comparison of experimental and modelling results for coexisting phase compositions for the mixture of Mackay River bitumen / ethane at ambient temperature and at a constant overall ethane concentration of 0.4 weight fraction; ●, the experimental data of Athabasca bitumen / ethane systems by Mehrotra and Svrcek (1985a); ■, liquid-liquid experimental data; lines, predictions by Peng-Robinson equation of state using second approach..... 347

Figure 8–5: A comparison of measured and predicted composition of equilibrium phases in liquid-liquid equilibrium study of MacKay River bitumen / ethane mixtures at ambient temperature and a constant pressure of 9 MPa; ▲, solvent-enriched phase; ■, asphaltene-enriched phase; lines, predictions by Peng-Robinson equation of state using second approach. 348

Figure 8–6: A comparison of measured and predicted compositional analysis (component weight percent) for extract (blue and red) and residue (black and green) taken from liquid-liquid equilibrium of MacKay River / ethane mixtures at a constant temperature of 22°C, a constant pressure of 9 MPa, and an overall ethane concentration of 0.4 weight fraction; blue and black, experimental data; red and green, predictions by Peng-Robinson equation of state using second approach. 348

Figure 8–7: Boiling point curves (temperature versus weight percent distilled) for raw Surmont bitumen (▲) and developed characterization method (□)..... 349

Figure 8–8: Comparison of measured (symbols) and predicted solubilities of ethane in Surmont bitumen as a function of equilibrium pressure at different temperatures; —, predictions by Peng-Robinson equation of state. 350

Figure 8–9: Comparison of measured (symbols) and predicted solubilities of propane in Surmont bitumen as a function of equilibrium pressure at different temperatures; —, predictions by Peng-Robinson equation of state (case 1)... 351

Figure 8–10: Comparison of experimental (symbols) and equation of state modelling results (lines) for pressure-composition ($P-x$) diagram for Surmont bitumen / propane systems at 50°C; ●, vapour-liquid experimental data; ●, vapour-liquid experimental data for propane / Athabasca bitumen systems taken from Badamchi-Zadeh et al. (2009a); ■, liquid-liquid experimental data; blue line, case 1; black line, case 2; red line, case 3. 352

Figure 8–11: Comparison of experimental (symbols) and equation of state modelling results (lines) for pressure-composition ($P-x$) diagram for the mixture of Surmont bitumen / propane at 100°C; ●, vapour-liquid experimental data; ■,

liquid-liquid experimental data; blue line, case 1; black line, case 2; red line, case 3. 353

Figure 8–12: Comparison of experimental and modelling results for coexisting phase compositions for Surmont bitumen /propane systems at 50°C and at a constant overall propane concentration of 0.4 weight fraction; ●, vapour-liquid experimental data; ●, vapour-liquid experimental data for propane / Athabasca bitumen systems taken from Badamchi-Zadeh et al. (2009a); ■, liquid-liquid experimental data; lines, predictions by Peng-Robinson equation of state (case 3)..... 354

Figure 8–13: Comparison of experimental and modelling results for coexisting phase compositions for Surmont bitumen / propane systems at 100°C and at a constant overall propane concentration of 0.6 weight fraction; ●, vapour-liquid experimental data; ■, liquid-liquid experimental data; lines, predictions by Peng-Robinson equation of state (case 3). 355

List of Symbols, Abbreviations, and Nomenclature

Uppercase

<i>A</i>	density measuring cell calibration constant
<i>AA</i>	density measuring cell calibration constant
<i>AB</i>	density measuring cell calibration constant
<i>AC</i>	density measuring cell calibration constant
<i>AD</i>	density measuring cell calibration constant
<i>AE</i>	density measuring cell calibration constant
<i>AF</i>	density measuring cell calibration constant
<i>AG</i>	density measuring cell calibration constant
<i>AH</i>	density measuring cell calibration constant
<i>AI</i>	density measuring cell calibration constant
<i>AI</i>	density measuring cell calibration constant
<i>AK</i>	density measuring cell calibration constant
<i>B</i>	density measuring cell calibration constant
<i>K</i>	equilibrium K-value
<i>K_f</i>	molal freezing point depression constant
<i>L₁</i>	solvent-enriched phase
<i>L₂</i>	asphaltene-enriched phase
<i>MW</i>	molecular weight
<i>N_c</i>	carbon number
<i>P</i>	pressure
<i>R</i>	gas constant
<i>R²</i>	coefficient of determination
<i>SG</i>	specific gravity
<i>T</i>	temperature
<i>T_b</i>	boiling point temperature

T_{br}	reduced boiling point temperature
T_f	freezing point temperature
V	volume
Z	compressibility factor

Lowercase

a	van der Waals attractive term
b	covolume
dd	period of oscillation
f	fugacity
v	molar volume
w	weight fraction
x	mole fraction
y	mole fraction

Scripts

B	bitumen
c	critical
cal	calculated
corr	correlation
exp	experiment
g	gas
m	mixture
s	solvent
sc	standard condition
t	total

Greek

α	coefficient of bitumen density correlation
β	binary interaction coefficient in mixture density correlation
δ	Peng-Robinson binary interaction coefficient
ε	molality
η	exponent in Lobe mixing rule
θ	adjustable parameter in Lederer correlation
κ	acentric factor vapour pressure function for Peng-Robinson
λ	function to match vapour pressures for Peng-Robinson equation of state
μ	dynamic viscosity
ν	kinematic viscosity
ξ	modelled value
ρ	density
ϕ	fugacity coefficient
φ	volume fraction
ω	acentric factor

Abbreviation

AAD	average absolute deviation
AARD	average absolute relative deviation
AD	absolute deviation
API	American Petroleum Institute
CMG	Computer Modelling Group
CT	computed tomography
ES-SAGD	expanding solvent SAGD
EY	extraction yield
GC	gas chromatography
GCOS	Great Canadian Oil Sand

GHG	green house gas
GOR	gas-oil ratio
IBP	initial boiling point
MAD	maximum absolute deviation
MW	molecular weight
NMR	nuclear magnetic resonance
NAGD	naphtha-assisted gravity drainage
PVT	pressure-volume-temperature
SAGD	steam assisted gravity drainage
SARA	saturate-aromatic-resin-asphaltene
SCM	standard cubic meter
SCN	single carbon number
SG	specific gravity
SimDis	simulated distillation
SOR	steam-oil ratio
SSR	sum of squared residual
VAPEX	vapour extraction
UNITAR	United Nations Institute for Training and Research

Chapter 1: Introduction

Heavy oil and bitumen reserves as an alternative to conventional oil reserves have attracted increasing attention in recent years. The world's total estimated reserves of conventional oil are one trillion barrels, whereas heavy oil, tar sands and bitumen reserves amount to six trillion barrels of oil in place (Das and Butler 1998). The majority of heavy crude resources are in Canada (~36%) and Venezuela (~27%) (Janish 1979).

Unconventional oils are very viscous and immobile at reservoir conditions; hence, recovery techniques that are used in conventional reserves are not applicable and practical for heavy oil and bitumen resources. Production of these oils requires specialized extraction techniques. Different technologies, both surface-mining and *in-situ* processes, have been developed for extracting these resources which may supply the fuel demand for the next few centuries. Open pit mining is applied for unconsolidated oil sands at shallow depths (depth less than 100 meters). In this technique, the bitumen mixed with sand is extracted and the bitumen is then separated from the sand using hot water and solvent (Tipman et al. 2001). The open pit mining is not applicable for oil sands that are deposited hundreds of meters deep. *In-situ* bitumen recovery from oil sand formations has become economically successful in Canada in the past two decades. Inventions and developments of recovery processes utilizing steam injection, such as cyclic steam stimulation (CSS) and steam-assisted-gravity-drainage (SAGD) have contributed to this success (Butler and Stephens 1981; Butler 1985).

The current steam-based processes are not optimal: 1) high energy is required to generate steam makes the processes economically vulnerable to high fuel costs; 2) the product quality is poor (subject to substantial differentials in selling price); 3) the product requires dilution with expensive solvents in order to be transported by pipeline and accepted by heavy oil refineries; and, 4) significant emissions of greenhouse gases, large consumption of fresh water for steam generation, high costs of the produced water

treatments for reuse, and environmental concerns over the waste water disposal make the current steam-based processes not only economically vulnerable, but also very environmentally unfriendly.

Solvent-assisted processes potentially provide remedies to the limitations outlined above. When bitumen is heated during the SAGD process, the heat provided by steam is consumed by the bitumen and the surrounding reservoir formations. Large portions of energy are lost and unrecoverable. In a solvent injection process, the solvent injected into the reservoir is largely recoverable with the produced bitumen. Solvents can also contribute to *in-situ* upgrading of bitumen to produce higher grades of heavy oil than the original bitumen. The compounded effects of solvent and heat on the bitumen viscosity can provide bitumen production rates that could be equivalent to or higher than those from injection of steam alone. This improved recovery product is complimented by a process that uses less fresh water and has lower greenhouse gas emissions. Improving the knowledge around the use of solvents for recovery processes supports the goals of developing recovery methods that have a reduced environmental footprint.

Numerous schemes to utilize solvent and heat have been invented and patented, e.g. N-Solv (heated solvent vapour injection), ES-SAGD (expanding solvent-SAGD), SAVEX (vapour extraction initiated by SAGD) and LASER (liquid addition to steam for enhanced recovery). Each method appears to have shown promising results in laboratory-scale tests (Fraunfeld et al. 2005; Orr 2009). However, there is a distinct lack of basic data and mechanistic knowledge relevant to the solvent/heat-assisted-recovery processes. Even the most fundamental experimental data, such as solubility of commonly used solvents in bitumen are not available. Quantitative effects of solvent on bitumen viscosity and phase behaviours are also not well understood. Despite the importance of experimental data for developing a good understanding of solvent-assisted bitumen recovery processes, there are few studies that have considered low operating temperatures (<120°C) and/or light hydrocarbon gases (i.e. methane and ethane).

In addition to their application for the recovery and production of bitumen, solvents are also utilized for transportation and processing of bitumen. The recovered bitumen is highly viscous at ambient temperature and its viscosity should be lower for economical transportation. There are several techniques for reducing heavy oil and bitumen viscosity: heating, dilution, and oil in water emulsion (Escojido et al. 1991). The heating method is not really practical in Canada, due to atmospheric conditions. In the winter months, heat lost is high due to very low temperatures.

In Canada, USA, and Venezuela, dilution is the most practical method and has been extensively used by industry. The heavy oil viscosity is reduced by blending it with a less viscous hydrocarbon, such as condensate, natural gasoline or naphtha (Escojido et al. 1991). There is an optimal viscosity for bitumen/condensate blends which can be obtained based on the size of pipeline and pump requirement. This optimal viscosity occurs at an optimal diluent concentration and corresponds to economical transportation of bitumen (Escojido et al. 1991). To obtain this ideal concentration, accurate viscosity data for the mixture of bitumen and diluent at different diluent concentrations are required. An appropriate model that can represent the viscosity and density of bitumen diluted with solvent is also very important and essential. Such a model will help in the accurate prediction of the thermo-physical properties of bitumen/solvent mixtures and improvement in the design and optimization of the process.

Bitumen is a mixture of valuable components (e.g. light and medium hydrocarbon components) and undesirable components (e.g. asphaltene). To remove unwanted components and improve the quality of the produced oil, upgrading techniques and extraction processes have been considered by the oil industry. Light hydrocarbon solvents, such as ethane and propane, can be used for bitumen upgrading and supercritical extraction (Pang and McLaughlin 1985; Deo et al. 1992; Subramanian and Hanson 1998; Rose 1999).

Supercritical extraction increases the amount of components extracted and has a high solvent recovery. At supercritical conditions, the solvent behaves like a liquid and its

solubility increases significantly; therefore, it can extract more components from bitumen. Another main advantage of supercritical extraction is high solvent recovery. The solubility of solvent can be dramatically changed by adjusting the temperature and pressure, and its value can decrease significantly. Ethane is one of the best candidates for the supercritical extraction of valuable components from bitumen. Ethane and carbon dioxide have favourable critical properties and can be used in the supercritical extraction process at relatively low temperatures (close to ambient temperature) (Yu et al. 1989; Rose 1999). Propane can also be considered for supercritical extraction, but at slightly higher temperatures (temperature more than 100°C) (Deo et al. 1992).

Supercritical extraction has been a well-known technique for more than a century with wide applications in the food industry (Zosel 1978). However, it is a new technique for heavy oil and bitumen recovery, and a significant gap exists in the literature regarding the supercritical extraction of heavy oil and bitumen. The field and commercial applications of supercritical extraction require phase behaviour data of the bitumen/solvent systems.

In conclusion, hydrocarbon solvents can be used for recovering, transportation, and processing of heavy oil and bitumen. Hydrocarbon solvents can be used as additives to steam-based *in-situ* recovery processes to improve the performance of the process and reduce its environmental impact. They are widely used for viscosity reduction in bitumen transportation, and they are used for surface upgrading or supercritical extraction to improve the quality of the produced oil. Apart from the process type, the phase behaviour and thermo-physical properties of bitumen, hydrocarbon solvents, and their mixtures are required to design and optimize these processes.

This study is aimed at providing a good understanding of the phase behaviour of bitumen/solvent mixtures applicable for *in-situ* recovery processes, surface upgrading methods, and pipeline transportation. Thus, a PVT apparatus was designed and constructed to conduct the phase behaviour experiments for different bitumen samples from Athabasca field diluted with different solvents (ethane, propane, hexane, and

condensate). The generated results include the composition, density, and viscosity of phases at equilibrium condition as well as the extraction yield and phase partitioning occurs in bitumen/solvent mixtures. The measured density and viscosity data for bitumen, solvent, and their mixtures were evaluated with predictive schemes as well as with correlation models representing certain mixing rules proposed in the literature. The influence of pressure, temperature, and solvent weight fraction on the density and viscosity of mixtures was considered in the models and evaluated from the experimental results. The vapour-liquid and liquid-liquid equilibrium compositions were modelled with Peng-Robinson equation of state. The simulated distillation (SimDis) data were used to characterize the bitumen and the component properties (boiling point, molecular weight, and specific gravity) were calculated from the extrapolation of existing correlations.

This dissertation is organized into eight chapters. Chapter 1 provides a general description of the application of hydrocarbon solvents in the production and processing of heavy oil and bitumen. It also lists research objectives followed in this study and the organization of the text in different chapters. Chapter 2 provides an extensive description of the designed experimental apparatus and procedures. It includes the design, fabrication and quality check of the apparatus. The experimental procedure and methodology used during the course of this study are explained in full detail in this chapter.

The measurements of bitumen properties, such as density, viscosity, compositional measurements, molecular weight and saturate-aromatic-resin-asphaltene (SARA) analysis, are presented in Chapter 3. The density and viscosity were measured over a wide range of temperatures and pressures. These measurements were used for the interpretation of the solvent effect on bitumen properties and also used for a modelling study, as detailed in the remaining chapters.

Chapters 4 and 5 present the vapour-liquid and liquid-liquid phase equilibria for bitumen/ethane and bitumen/propane mixtures. The results of vapour-liquid equilibria cover the solubility, density, and viscosity measurements of the saturated liquid, K-values, and gas-oil ratio (GOR) for the temperature range of 50 to 190°C and the pressure

range of 1 to 8 MPa. For liquid-liquid equilibrium conditions, the properties of equilibrium phases as well as component extraction using ethane and propane were investigated. The effects of pressure, temperature, and overall solvent concentration on the phases' composition, density, viscosity, and compositional analysis have been studied.

Chapter 5 ends up with the results of a series of phase behaviour experiments at constant solvent concentration for ethane, propane, and butane. In these experiments, the effect of dissolution of different solvents on the thermo-physical properties of the saturated bitumen was investigated. Along with gaseous solvents (ethane and propane), two liquid solvents (*n*-hexane and condensate) were considered in the phase behaviour studies in Chapters 6 and 7. A different approach was considered for these experiments. A specific amount of liquid solvent was dissolved in bitumen, and the viscosity and density of the liquid were then measured. At high concentrations, possibilities of liquid-liquid equilibrium or formation of solid asphaltene were considered and investigated.

Chapter 8 presents the phase behaviour modelling study of bitumen/solvent systems using the Peng-Robinson equation of state. The modelling study starts with bitumen characterization using the compositional analysis, density and molecular weight of the bitumen. The characterized bitumen was then introduced into the equation of state model. Finally, the equation of state was tuned to match the vapour-liquid and liquid-liquid data.

Chapter 2: Apparatus and Verification¹

This chapter provides an extensive description of the designed experimental apparatus and procedures. It includes the design, fabrication and quality check of the apparatus. The experimental procedure and methodology used during the course of this study are explained in full detail in this chapter. The validation of generated experimental data is also presented in this chapter. The designed experimental apparatus was used for all phase behaviour measurements reported in this thesis.

One of the major challenges in the phase behaviour experimental study of heavy crudes, such as bitumen and solvent systems, is the long equilibration time that is dependent on the experimental conditions. These conditions include pressure, temperature, and the unique properties of the solvent and oil. Oil viscosity is the key factor that determines the equilibration time, especially at low temperatures found in reservoirs where the oil viscosity (e.g. Athabasca bitumen) is in the order of million centipoises.

Previous researches into the phase behaviour of bitumen/solvent systems show that equilibration is the most time-consuming part of the experiments. Effective mixing, through agitation by rocking, results in a reduction in the time required to reach equilibrium. At low temperatures, around room temperature, the experiments still require a long time to reach equilibrium even when the equilibrium cell is agitated.

In our previous study (Kariznovi et al. 2011a), we reviewed experimental setups that have been used for the phase behaviour study of bitumen/solvent systems and highlighted their shortcomings and limitations. A new apparatus that can cover a wide range of temperatures (up to 200°) and pressures (up to 40 MPa) was proposed to overcome these

¹ Some portions of this chapter are reprinted from “Fuel Processing Technology, 102, H. Nourozieh, M. Kariznovi, J. Abedi, Development and evaluation of a modified experimental apparatus for phase behavior study of solvent–heavy crude systems, 116-123, Copyright (2012), with permission from Elsevier.” and “Fuel, 90, M. Kariznovi, H. Nourozieh, J. Abedi, Experimental apparatus for phase behavior study of solvent–bitumen systems: a critical review and design of a new apparatus, 536-546, Copyright (2011), with permission from Elsevier.”

shortcomings. The proposed experimental setup was verified using simple binary and ternary systems. The apparatus was validated using data from the literature for three different systems: vapour-liquid, liquid-liquid, and vapour-liquid-liquid. The results for these systems were compared with published data and good agreement was obtained.

In this chapter, the proposed apparatus and its modifications are explained in detail. The rocking mechanism in the proposed apparatus accelerated the experiments and reduced the equilibration time; however, it still takes a few days to run an experiment for the phase behaviour study of bitumen/solvent mixtures at low temperature conditions. Thus, it is necessary to conduct parallel experiments either using two apparatuses or using a new approach. Conducting parallel experiments in phase equilibrium can significantly reduce the time required and provide the opportunity to undertake two, three, or even more experiments simultaneously. The experimental results of Luo et al. (2007a) indicate that the equilibration time for a Lloydminster heavy oil and propane system at constant temperature and different pressures were almost the same. Accordingly, the design of an experimental apparatus with two or more equilibrium cells installed in an oven could significantly increase the number of experiments that can be conducted in a certain period of time.

The experimental results by Luo et al. (2007b), Zou et al. (2007), Jossy et al. (2009) and Nourozieh et al. (2010) indicate that solvent-to-bitumen ratio affects equilibrium phase properties, such as density, viscosity, volume, and phase composition. The solvent-to-solute ratio is also a significant parameter in supercritical fluid extraction processes, where the low volatility materials are extracted from various mixtures. Generally, two different techniques have been applied for cases where the bitumen-to-solvent ratio was constant. The first technique uses flow-cell apparatus, in which both the solvent and bitumen were continuously injected into a mixing cell (Yu et al. 1989). The equilibrium fluids were then transferred into a visual cell separator, where the phases were segregated by density difference. The second technique, proposed by Han et al. (1992), was used to collect solubility data for solvents in heavy hydrocarbons. The bitumen was fed into a cell

and the solvent was added to keep the pressure constant. Thus, an apparatus with two or more equilibrium cells in a temperature-controlled oven could be used to conduct multiple simultaneous experiments with different solvent-to-bitumen ratios at constant temperature and pressure.

Following this discovery, an apparatus capable of conducting two parallel experiments at the same time was designed. The apparatus is capable of conducting experiments related to phase behaviour study of bitumen/solvent mixtures which are applicable for both *in-situ* recovery methods and fluid extraction processes. In addition to the phase behaviour study of heavy oil systems, the apparatus can be used for the experimental investigation of phase partitioning, phase separation, and component extraction using different solvents. This modification can be expanded to more equilibrium cells.

2.1. Designed Apparatus

The experimental apparatus was designed to acquire the following experimental data for various bitumen/solvent systems at a wide range of temperatures and pressures:

1. The solubility of solvents in bitumen
2. The number of phases, volume ratios, and the composition of each phase at equilibrium
3. The viscosity and density of the saturated phases
4. The extent of extraction
5. Asphaltene precipitation and flocculation

The schematic diagram of the apparatus is shown in Figure 2–1. It consists of two feeding cells, two equilibrium cells, four sampling cells, an auxiliary cell, a density measuring cell, a viscometer, and three Quizix automated pressure-activated pumps. The equilibrium and sampling cells, density measuring cell, and viscometer are placed in a temperature-controlled Blue M oven. The Quizix pumps charge and discharge water to

displace the fluids or keep the pressure constant. The equilibrium, sampling, feeding, and auxiliary cells are equipped with pistons to prevent the contamination of the mixture with water. The pistons are sealed with Viton o-rings supported by Teflon® backup rings.

The density measuring cell and viscometer are used for phase detection, showing a clear phase separation, and allowing for accurate phase volume measurements. The density measuring cell can detect any phase that passes through it allowing for the detection of the phases with very small volume. While commercial PVT systems require a subjective visual observation for phase detection, this apparatus does not. Data are produced directly without a subjective evaluation.

The rocking equilibrium cells have a maximum volume of about 900 cm³ providing sufficient saturated phase volume for the measurement of physical properties, such as density and viscosity. The Quizix pumps charge and discharge the fluids with an accuracy of ± 0.001 cm³. The density measuring cell and viscometer are installed in series to improve phase detection. Their in-line measurements provide higher accuracy data than sending very small samples to the viscometer and density measuring cell.

Figure 2–2 shows a comparison of the two apparatuses (original designed and modified). Adding an equilibrium cell to the original apparatus enables the performance of two simultaneous experiments without any additional equipment. As a result, the total cost remains almost the same, but the advantage of conducting two experiments at once is achieved. The density measuring cell, viscometer, and pumps are the most expensive components of the PVT apparatus. Only one density measuring cell and one viscometer are installed in the modified apparatus, which is the same as the single equilibrium cell apparatus.

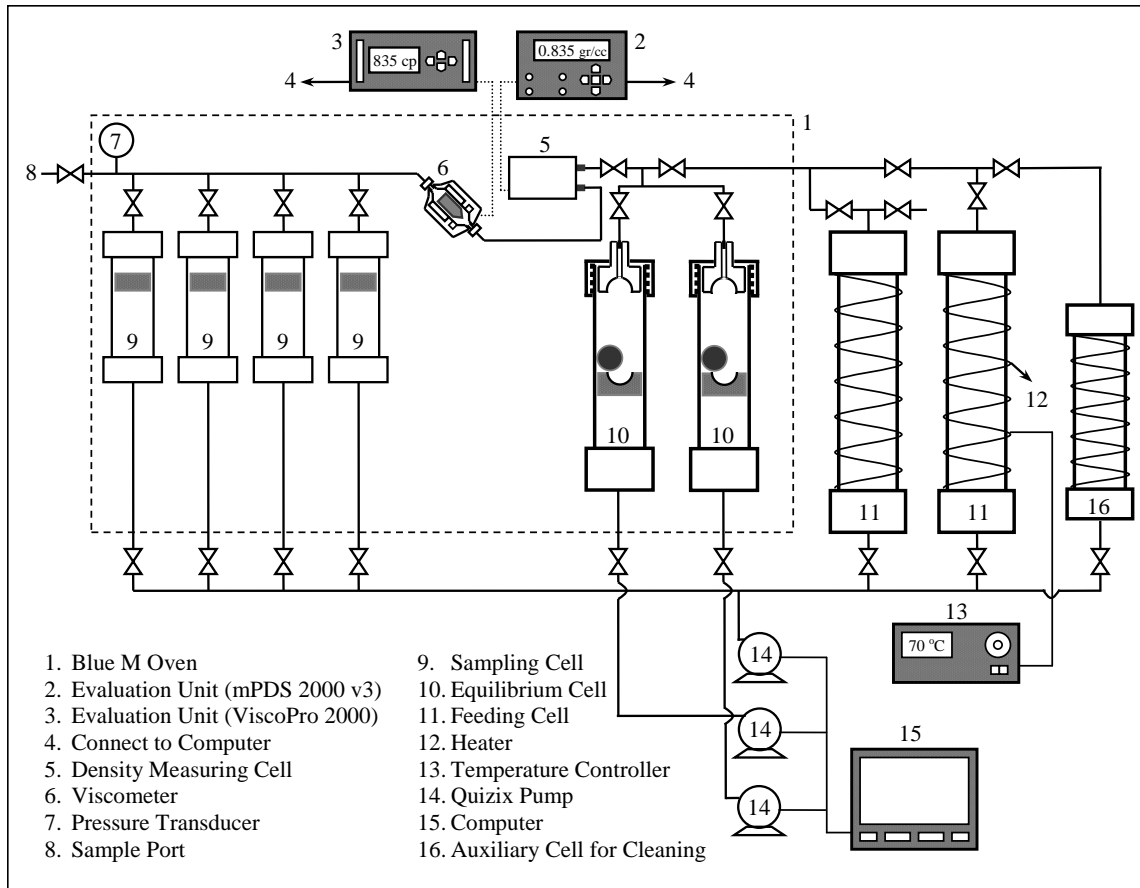


Figure 2–1: The schematic diagram of the designed apparatus for the phase behaviour study of bitumen/solvent systems (Nourozieh et al. 2012a).

This new apparatus has no limitation on the number of phases and has the capability of measuring the mole or weight fraction of the feeding fluids. It can handle temperatures up to 200°C, which is the maximum operating temperature for the density measuring cell, and pressures up to 40 MPa.

In this design, two equilibrium cells are installed in a Blue M oven to speed up the experiments. Two cells are maintained at the same temperature but equilibrated at different pressures or different solvent-to-bitumen ratios. Effective mixing, through agitation by rocking, results in a reduction in the time required to reach equilibrium. Table 2–1 summarizes the components required for the original designed and modified apparatuses. The addition of an extra equilibrium cell almost doubles the rate of data generation without significantly changing the total cost.

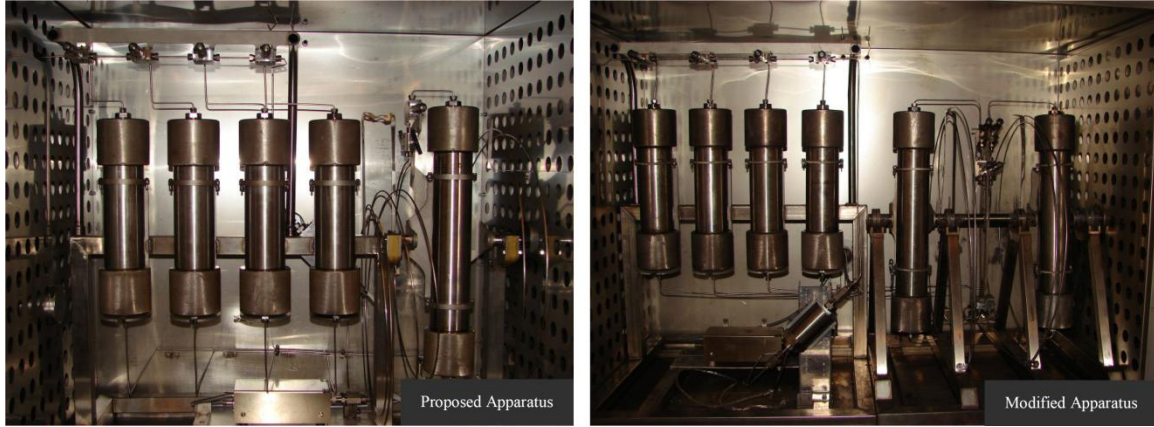


Figure 2–2: The experimental apparatuses: the original designed apparatus and the modified apparatus (Nourozieh et al. 2012a).

Two equilibrium cells are placed in the same oven with only one density measuring cell and one viscometer installed to measure the equilibrium fluid properties of both equilibrium cells. It is worth mentioning that with this design, the repeatability of experimental data can also be easily verified. Two experiments with the same operation conditions can be conducted at the same time to check the results.

Table 2–1: Equipment installed in the original designed apparatus and modified apparatus (Nourozieh et al. 2012a).

Equipment	Original Designed Apparatus	Modified Apparatus
Feeding Cell	2	2
Equilibrium Cell	1	2
Sampling Cell	4	4
Density Measuring Cell	1	1
Viscometer	1	1
Quizix Pump	2	2 or 3*
Blue M Oven	1	1
Pressure Transducer	1	1
Computer	1	1

* depends on the experimental procedure for conducting the experiments

In the modified apparatus, two or three pumps can be used, depending on the experimental procedure. Two pumps can be connected to the equilibrium cells; and, when the system reaches equilibrium, one pump is disconnected and diverted to the sampling

cells for displacing the fluid at a constant pressure. In this case, the system works with two pumps and the cost for an extra pump is saved. Alternatively, a separate pump can be connected to the sampling and feeding cells.

2.1.1. Equilibrium Cell

As previously described, a rocking equilibrium cell was used for effective mixing of bitumen and solvent mixtures. A more detailed schematic diagram of the equilibrium cell is presented in Figure 2–3. The cell was constructed in the Machine Shop in the Department of Chemical and Petroleum Engineering at the University of Calgary. The cylindrical shaped cell has a two-inch inside diameter with 0.5 inch thickness made of 316 stainless steel Schedule 170 pipe. It was designed for a maximum pressure of 5000 psi, respectively. The cell has a maximum volume of about 900 cm³, which provides sufficient saturated phase volume for the measurement of physical properties, such as density and viscosity. In addition, it provides ease of phase detection and enough phase volumes for further analyses. At each end of the equilibrium cell, a threaded cap with plug was used to provide complete sealing and ensure that there is no fluid leakage. The plug is equipped with an o-ring which is further supported by a back-up split o-ring. The specifications of the o-rings are summarized in Table 2–2.

A rolling ball inside the equilibrium cell expedites the mixing of solvent and bitumen to reach an equilibrium condition. The ball has one and half inch outside diameter made of 316 stainless steel Schedule 170 and a completely smooth surface. To prevent contamination of the bitumen/solvent mixture with water, an isolated brass moving piston was installed inside the equilibrium cell. To guard against o-ring failure and possible contamination, the brass piston was equipped with two Viton o-rings, each supported by a back-up split Teflon o-ring.

To reduce the dead volume in the equilibrium cell and complete discharge of equilibrium fluids, both plug and the moving piston were constructed with a semi-spherical hole on one side. The outside diameter of the ball is the same as inner diameter

of the holes in plug and moving piston. This way, when the piston is moved upwards, the ball, which is sitting on the piston, completely displaces the equilibrium fluids inside the equilibrium cell. The plug at the bottom of equilibrium cell was built with a very smooth cone shaped surface. This feature creates a very small volume and enough surface contact for water to push the piston upward if the piston reaches to the end of the equilibrium cell. The equilibrium cell (the ends with plugs) is connected to the apparatus using 1/8” line and HiP Taper Seal fittings.

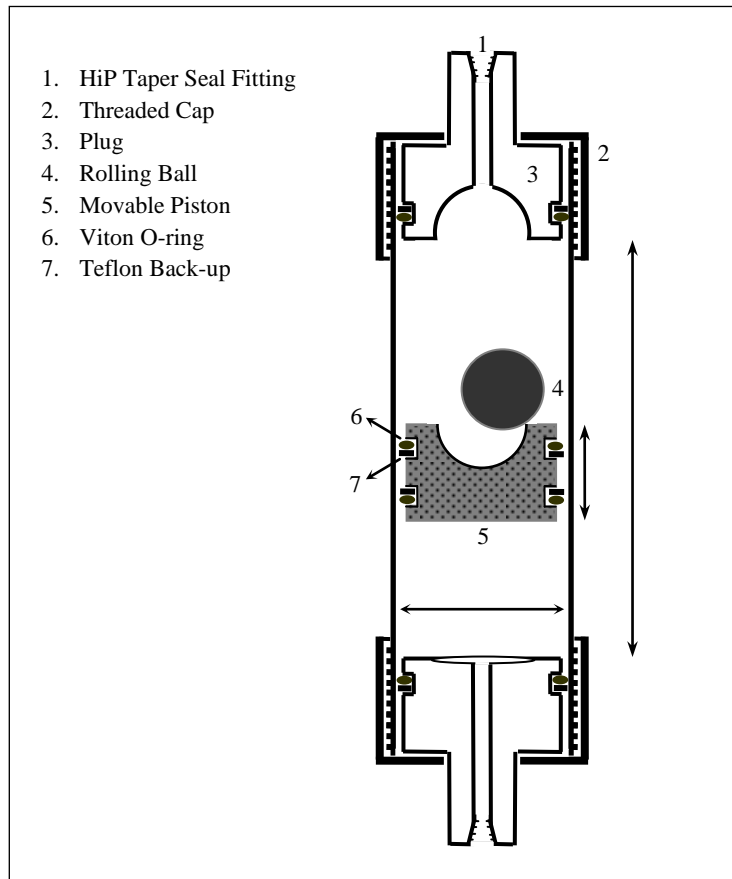


Figure 2–3: Schematic diagram of equilibrium cell.

Table 2–2: Specifications of o-rings used in equilibrium cell.

O-ring	Provider	Size	Temp. Range (°C)	Compatible Fluids
Viton	The o-ring Store	1-3/4 ID×2 OD×1/8 W	– 26 to 200	Halogenated Hydrocarbons, Di-Ester Lubricants,
Teflon Back-up	Hose and Fittings	1-3/4 ID×2 OD×1/8 W	– 54 to 260	Petroleum Oils, Fuels, Silicone Oils

2.1.2. Sampling and Feeding Cells

Four sampling and two feeding cells were also constructed in the Machine Shop at the University of Calgary. The specifications of the cells, such as length, volume, and diameter, are summarized in Table 2–3. The cylindrical shaped cells are made of 316 stainless steel Schedule 170 pipe. The operating conditions of the cells are the same as the equilibrium cells. The cells are also equipped with two threaded caps with plugs to provide complete sealing. The o-ring specifications are similar to those of the equilibrium cell but are different sizes. All cells are connected to the apparatus using 1/8” line and HiP Taper Seal fittings.

Table 2–3: Specifications of cells.

Cells	Size (inch)	Piston Size (inch)	Volume (cm ³)
Sampling	2 ID (3 OD) × 14 (length)	2 OD	500
Feeding	3 ID (4 OD) × 25 (length)	3 OD	2000

Four sampling cells were designed with a maximum volume of 500 cm³, which is a sufficient volume for each phase at equilibrium condition to be completely collected. One of the sampling cells is used to purge the phase boundary portion and clean the transition between the phases and other three cells are used to collect the sample from each phase.

Two feeding cells with the volume of 2000 cm³ are filled with the bitumen and solvent and used to accurately measure the fluids injected into the equilibrium cell. The cells, which were installed outside the oven, can pressurize the gaseous solvent and also displace the fluids at liquid or vapour state. To ensure accurate volume measurements, the feeding cells are heated to the experimental temperature. For high temperature phase behaviour experiments, the solvent and bitumen are usually charged at the maximum temperature of 100°C to avoid vaporizing the light components of the bitumen.

2.1.3. Density Measurements

The Anton Paar densitometer was used in this apparatus to measure the density of fluids. It can measure the fluid density in the range of 0-3 g/cm³ with an error of 0.001-0.0001 g/cm³ (dependent on the measuring conditions) in the temperature and pressure ranges of -10 to +200°C and 0 to 70 MPa (0-10,000 psi), respectively. The densitometer consists of two parts: an external measuring cell and an evaluation unit (Figure 2–4). The external measuring cell (DMA HPM) was placed on the downstream side of the equilibrium cell to measure the density of equilibrium fluids at high pressure and high temperature conditions. The measuring cell is equipped with a U-shaped Hastelloy tube that the fluid is transferred into. The tube is electronically vibrated at its characteristic frequency, which is dictated by the density of the fluid. The characteristic frequency is precisely determined and converted into the period of oscillation, which is displayed on the evaluation unit. The evaluation unit (mPDS 2000) indicates the period of oscillation as well as the temperature and pressure of the fluid in the measuring cell. The density of the fluid is calculated on the basis of the readings and the calibration constants are determined in the calibration step.

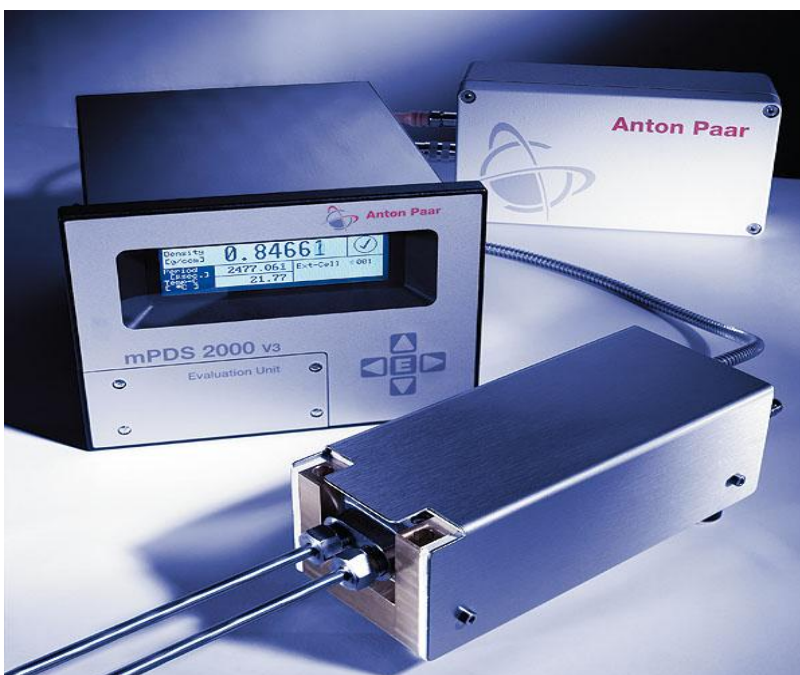


Figure 2–4: Density measuring cell (mPDS 2000 V3) from Anton Paar website.

There are two methods used to calibrate the density measuring cell. The first method is an adjustment for a single temperature and pressure and the development of a specific two-parameter equation for each point. This method requires introducing two parameters for each temperature and pressure into the density measuring cell and gives an accurate result only at that specific temperature and pressure. Consequently, for a wide range of pressures and temperatures, few hundred calibration points are required to be introduced into the density measuring cell. For single point calibration, a specific equation is developed for each temperature and pressure which is only a function of the density measuring cell frequency. The following equation is used to determine density from the period of oscillation of the measuring cell,

$$\rho = A \times dd^2 - B \quad 2-1$$

where dd is the period of oscillation of the sample, A and B are apparatus constants obtained from,

$$A = \frac{\rho_1 - \rho_2}{dd_1^2 - dd_2^2} \quad 2-2$$

$$B = \frac{dd_2^2 \times \rho_1 - dd_1^2 \times \rho_2}{dd_1^2 - dd_2^2} \quad 2-3$$

Subscripts 1 and 2 denote the standard fluids or the known fluid properties. The apparatus constants A and B are determined by measuring the periods of oscillation with two known fluid densities at the specific temperature and pressure. This method is applicable when the system pressure and temperature do not change and all experiments are performed at fixed temperature and pressure conditions. As wide ranges of pressure and temperature were considered during phase behaviour studies, this method is not applicable and it is necessary to look for another method of calibration that can accommodate a wide range of temperature and pressure conditions.

In the second method, the density measuring cell is adjusted over wide temperature and pressure ranges. The final calibration equation is a function of temperature, pressure

and density measuring cell frequency. This approach works for a range of calibration temperatures and pressures and is more applicable for our experiments. As a result, this method was used for calibration.

To calibrate the density measuring cell using wide-range calibration, the following procedure was applied:

1. The U-shaped Hastelloy tube in the density measuring cell was cleaned with toluene and acetone. The tube was purged with nitrogen and helium to remove and evaporate the cleaning liquids. Then, the tube was evacuated and flushed with the calibration fluids (nitrogen and water).
2. Two calibration fluids were selected: gaseous nitrogen and liquid water. The nitrogen and water were selected for two main reasons. First, density data for the fluids are accurately available over a wide range of pressures and temperatures. Second, the densities of bitumen, solvent, and their mixtures would be a value between those of nitrogen and water at desired conditions.
3. Density data of nitrogen and water were gathered from the National Institute of Standards and Technology (NIST) database at different temperatures and pressures.
4. The density measuring periods of two samples were recorded at different temperatures and pressures. In total, 756 measurements were performed, and the data were used to develop the calibration curve (378 points for each fluid). The temperature range was from ambient temperature to 190°C with a 10°C interval. Pressure was from 0 to 2000 psig with an increment of 100 psig.
5. The NIST data and density measuring cell frequency were used to generate the calibration curve as a function of temperature, pressure, and measuring cell frequency. A regression method was used to find the coefficients of calibration, using recorded frequencies, temperatures, and pressures based on the following equation:

$$\rho = AA + AB \times T + AC \times dd + AD \times T^2 + AE \times dd^2 + (AF + AG \times T + AH \times dd + AI \times T^2 + AJ \times dd^2) \times P^2 + AK \times P^4 \quad 2-4$$

where,

T: Temperature, °C

P: Pressure, psig

dd: Density Measuring Cell Frequency

6. The calibration parameters were introduced into the density measuring cell.

Equation 2-4 is a function of temperature, pressure and density measuring cell frequency. The density measuring cell can measure temperature and frequency, and a pressure transducer is connected to measure pressure. The calculated coefficients for the wide range calibration method are listed in Table 2-4. The accuracy of density measurements was examined using pure hydrocarbons and standard fluids. The density measurements are accurate within $\pm 0.0002 \text{ g/cm}^3$.

Table 2-4: Calculate coefficient for equation 2-4.

AA	-2.717016E+00	AG	-2.477566E-09
AB	1.291192E-02	AH	-4.507972E-12
AC	3.202436E-05	AI	3.391586E-12
AD	-2.379853E-05	AJ	-1.389845E-15
AE	1.013911E-08	AK	2.915026E-13
AF	-1.550838E-06		

2.1.4. Viscosity Measurements

The Cambridge viscometer was used to measure viscosity in the range of 0.2 to 10,000 mPa.s with an accuracy of $\pm 1.0\%$ of full scale and at the temperatures and pressures up to 315°C and 140.6 MPa (20,000 psi), respectively. The in-line piston-style viscometer (Figure 2-5) uses two magnetic coils within a stainless steel sensor and a magnetic piston inside the pipeline. The piston is forced magnetically back and forth within a predetermined distance. The fluid sample surrounds the piston and depending on the viscosity, the piston's round trip travel time is measured under the exertion of a

constant force. The time required to complete a two-way cycle is an accurate measure of viscosity. A specific piston is required for each viscosity range. The viscosity ranges are summarized in Table 2–5. The viscometer is equipped with a sensor (SPL-440) and is factory calibrated. The accuracy of the measurements was tested using pure hydrocarbons and standard fluids. The average error for the measurements was less than 5%.

Table 2–5: Viscosity range for viscometer.

Piston Size (inch)	0.310	0.3085	0.3055	0.297	0.274	0.225
Viscosity Range (mPa.s)	0.2-2	0.25-5	1-20	10-200	100-2000	500-10000



Figure 2–5: Viscometer (ViscoPro 2000 system 4, Cambridge Viscosity) from Cambridge Viscosity website.

2.1.5. Charging and Discharging of Fluids

Two Quizix automated pressure-activated pumps (QX-6000) were used to charge and discharge water to displace the fluids or keep the pressure constant within the system. The Quizix pump is a precision metering pump with two piston-cylinders, with the total volume of 16.7 cm³ equipped with an electric motor. When both cylinders are engaged, the pump provides a continuous flow of fluid at the minimum and maximum flow rates of 0.001 and 50 cm³/min, respectively. The maximum operating pressure of the pump is 41.3 MPa (6000 psi).

Water was selected as the working fluid for the pumps. It is a non-corrosive and readily available fluid that causes less damage to the cylinders. The direct injection of bitumen and solvent into the phase behaviour apparatus using the pump could cause corrosion or o-ring swelling problems. High viscous fluids, such as bitumen, cannot be

easily sucked into the pump. In addition, cleaning and evacuating the pump requires significant maintenances. For this reason, all cells (equilibrium, sampling, and feeding cells) were designed with the piston and o-rings to displace the bitumen and solvent.

Each Quizix pump has two safety features to avoid any damage to the apparatus and equipment. First, there is a safety pressure set point at which any running pump cylinders will be automatically stopped. This safety pressure is manually specified by the user. Second, the maximum operating pressure of the pump is 41.3 MPa (6000 psi). The pump will be stopped automatically if the pressure exceeds the maximum operating pressure.

2.1.6. Pressure Measurements

The pressure inside the apparatus was measured and controlled by three different pressure transducers. An inline pressure transducer was installed as shown in Figure 2–1 (equipment#7). The transducer is a Rosemount 3051CG5A capable of measuring the pressure from -0.1 to 13.8 MPa (-14.2 to 2000 psi) with an accuracy of 0.04%. The Quizix pumps are also equipped with pressure transducers. Each Quizix pump has two cylinders, each with a transducer. The pressure within the system can be manually controlled by the pumps. Thus, during the charging and discharging of the fluid, three pressure transducers control and measure the pressure inside the system. The reported pressure is the reading from the pressure transducer.

2.1.7. Temperature Measurements

A Blue M oven was used to maintain a constant temperature during the experiments. The equilibrium and sampling cells, density measuring cell, and viscometer were placed inside the oven. The oven (DCW-1406-E-PM-GOP) is equipped with a temperature controller capable of maintaining the temperature within $\pm 0.1^{\circ}\text{C}$. The temperature range of oven is 15°C above ambient to 350°C . The oven is equipped with a safety switch so that if the temperature exceeds the maximum set temperature, the oven automatically shut

down. The safety temperature for the oven was set to 200°C, which is the maximum operating temperature for the density measuring cell.

In addition to the oven, two built-in temperature sensors also report the temperature inside the system. The built-in sensor in the density measuring cell measures the temperature of fluid during the density measurements. The error in the temperature measurements was less than 0.1°C. A built-in temperature sensor installed in the viscometer can also measure the temperature of fluid during the viscosity measurements.

2.1.8. Data Acquisition System

All of the measurements for the temperature, pressure, density, viscosity, and volume were recorded using a Dell personal computer and data acquisition software. The Anton Paar densitometer was connected to the computer using RS-232 serial port. The period of oscillations, density, and temperature measurements were continuously recorded in an excel file using the DMA HPM Excel tool provided by the Anton Paar Company. The Rosemount transducer with a 4–20 mA transmitter output (Digital Signal Based on HART Protocol) was directly connected to the Anton Paar evaluation units and pressure measurements were also recorded by DMA HPM Excel file.

The Cambridge viscometer was connected to the computer using a RS-232 serial port and the viscosity and temperature measurements were recorded using Windows HyperTerminal software. The Quizix pumps were connected to the computer using the serial expander/isolator provided by Chandler Engineering. The pump was connected into the expander using a phone-type communication cable and the expander was directly connected through a RS-232 serial port. Up to four pumps can be connected with an expander/isolator to the computer. The pumps were controlled and operated with the PumpWorks software. This software is an easy-to-use windows-based program. The program allows viewing all of the system data to be viewed at a glance and recorded all operating data (flow rate, pressure, etc.) directly to the hard disk of the computer, where it was immediately available for review, analysis, and graphing. The pump can also be

programmed to deliver a specified amount of fluid or to operate for a specified period of time and then stop automatically.

During the course of the experiments, the density, viscosity, temperature, pressure, flow rate, and volume measurements were graphically displaced on the monitor. The pressure within the system was controlled with the Quizix pumps. The fluid volumes and flow rates were measured and controlled by the pumps. The temperature was changed and controlled by the temperature controller installed in the front panel of Blue M oven.

2.1.9. Fluid Sampling for Further Analysis

As mentioned previously, the samples from each phase can be collected through the sampling port shown in Figure 2–1 for further analysis. To collect the samples, two small high pressure piston-cylinder cells (Figure 2–6) were constructed in the Machine Shop, each with a total volume of 20 cm³. The cells were equipped with a moving piston; one side of the piston for sampling and the other side connected to a screw with an adjustable handle to control the movement of the piston. To start collecting the sample, the piston was pushed completely to the end using the handle and the cell was evacuated. Then, the cell, which was connected to the sampling port and the valves, was opened. The Quizix pump was set to constant pressure mode to control the pressure during the sampling. The diluted oil was transferred into the cell by turning the handle slowly and letting the piston move backwards. The weight of cell before and after sampling was measured using a Sartorius balance (Model: LP4200S) with a measurement uncertainty of ±0.01 g. This method allowed the weight of fluid in the sampling cell to be determined exactly.

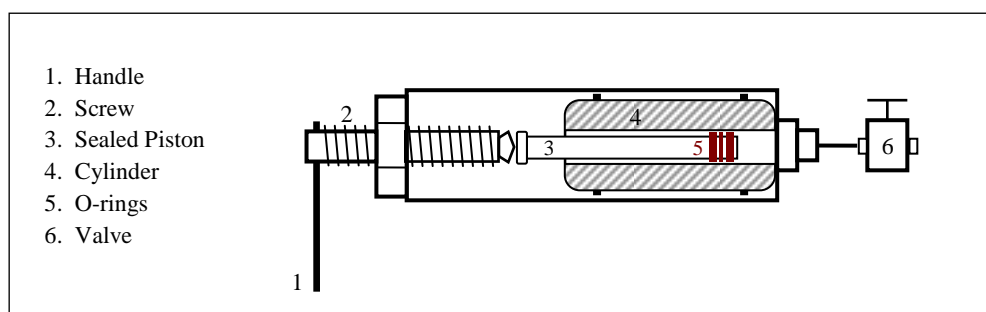


Figure 2–6: Small piston-cylinder cell for liquid phase sampling.

2.1.10. Solubility Measurements

To measure the composition of the gas-saturated liquid(s), the collected samples were analyzed with two different methods. The first method, which is applicable for light hydrocarbon gases (C_1 to C_4), is to flash the collected samples at atmospheric pressure. The second method, applicable for heavy hydrocarbon gases ($>C_5$), is based on volume measurements during the phase behaviour experiments (the second method is not explained here).

For light hydrocarbon gases (gas at ambient temperature and pressure), the collected saturated-liquid samples were flashed at atmospheric condition and the volume of the evolved gas was measured by the Chandler Engineering Gasometer (Model 2331). To ensure that all dissolved gas was evolved from the oil, the liquid sample was heated. The gasometer measured the volume of gas with 0.2% accuracy and reported the corresponding gas temperature.

The solubility was calculated using two methods: volumetric and mass conservation. The former method is based on the volume measured by the Gasometer. With the density of the gas at atmospheric condition, the mass of solvent (evolved gas) was calculated and solubility was obtained as,

$$w = \frac{V_g(T, P^{sc}) \rho_g(T, P^{sc})}{m_m} \quad 2-5$$

where V_g and ρ_g are the volume and the density of the evolved gas at atmospheric condition, respectively. The weight of the saturated liquid was obtained by weighing the small sample cell before ($m_{2,cell}$) and after sampling ($m_{1,cell}$),

$$m_m = m_{1,cell} - m_{2,cell} \quad 2-6$$

The latter method is based on the weight of the sample before and after evolving the solvent. The solubility was calculated as,

$$w = \frac{m_{1,cell} - (m_{2,cell} + m_{residu\text{ oil}})}{m_{1,cell} - m_{2,cell}} \quad 2-7$$

The maximum deviation for solubility measurements using these two different methods is 2%.

2.1.11. Volume Corrections

The bitumen and solvent are charged into the equilibrium cell using the Quizix pumps. By measuring the volume and density of fluid at constant temperature and pressure, the mass of the fluid inside the equilibrium cell is obtained. As previously mentioned, the Quizix pumps are working with water at ambient temperature. During the displacement steps, the water is injected to or discharged from the equilibrium cell at experimental condition. When the experiments are conducted at ambient temperature, there is no change in the volume of water during the displacing of the fluids because the pump injected the water from ambient condition. When the oven temperature is different from the ambient temperature, the volume expansion or shrinkage occurs for water. Thus, the volume correction is required for the experiments at temperatures different than ambient condition. It was found that the following volume correction should be considered during the volume measurements,

$$V_{True} = V_{inj} \frac{\rho_{water}(T^{sc}, P)}{\rho_{water}(T, P)} \quad 2-8$$

For example, it was found that 100 cm³ injected water at 4 MPa and ambient temperature (20°C) would displace 108.8 cm³ fluids at 4 MPa and 150°C. The volume correction is considerable at large volumes or high temperature variations.

2.1.12. Gas and Liquid Analysis

The gas and liquid samples were also analyzed during the phase behaviour experiments. The vapour phase at equilibrium condition and the evolved gas from flashed-off saturated liquids were analyzed with a gas chromatograph GC-3900 (Varian) equipped with a flame ionization detector (FID) (Figure 2–7). The GC column is a wall

coated open tubular (WCOT) column type (CP-Sil 5 CB: 10 m × 0.15 mm × 2 μm), which was provided by Agilent Technologies. Ultra high-purity helium (99.999%) is used as the carrier gas. The column was designed to detect the hydrocarbon components and the GC was calibrated with a standard gas mixture provided with the Praxair (Table 2–6). Bitumen is not volatile; therefore, the composition of the vapour phase is almost equal to the composition of the solvent. To acquire more reliable results, ultra high purity gases C₁ to C₄ were also used as calibration standards. This GC was used for vapour phase compositional analysis.

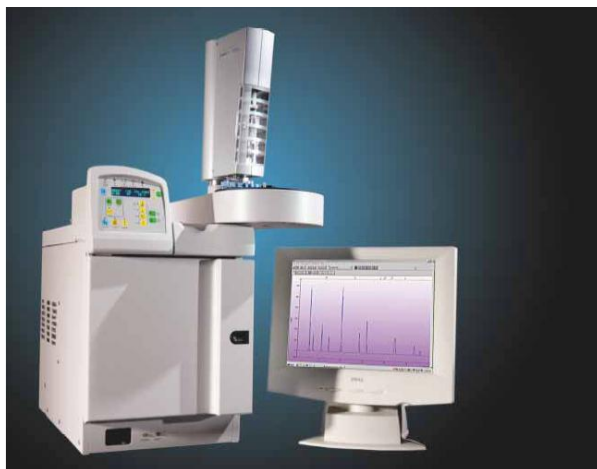


Figure 2–7: Varian 3900 gas chromatograph (from <http://www.asap4u.nl/pdf/varian/3900.PDF>).

Table 2–6: Standard gas and its composition.

Standard Gas	C ₁	C ₂	C ₃	n-C ₄	CO	CO ₂	H ₂	N ₂
Composition (mole percent)	0.9740	1.0000	0.976	0.9670	2.5300	7.5400	0.0202	85.9928

The flashed-off liquid samples were also analyzed with a SimDis unit explained in Section 3.3.

2.2. Experimental Procedure

Prior to each experiment, the entire system is thoroughly cleaned using toluene to remove any contaminants, including oil and solid particles. To ensure no contaminants were left inside the system, cells and lines are successively evacuated and flushed with

helium and pure solvent. After cleaning, bitumen is charged into the equilibrium cells using two Quizix pumps. By measuring the volume and density of bitumen at constant temperature and pressure, the mass of the bitumen inside each equilibrium cell is obtained.

A benefit of the new design (two equilibrium cells) versus an apparatus with a single equilibrium cell is that the lines need only be cleaned once when both equilibrium cells are charged, i.e. both equilibrium cells are filled with predetermined volumes of bitumen and the lines are then cleaned. The solvent is then charged into the cells with the same procedure. With this procedure, the mass fraction of the injected fluids is known.

To measure the equilibrium properties at a specific temperature and pressure, the experimental pressure and temperature are fixed for each equilibrium cell. The equilibrium cells are placed inside the same oven. Therefore, they both have the same temperature but can be at different pressures and/or different solvent-to-bitumen ratios. The equilibrium time is a function of the bitumen viscosity while the viscosity is temperature-dependent. The pressure does not have a significant effect on the viscosity, thus, both equilibrium cells will reach equilibrium at almost the same time (Luo et al. 2007a).

After charging the equilibrium cells, they are rocked to achieve effective mixing and reach equilibrium for the bitumen/solvent system. During the mixing period, the volume of water, which is charged or discharged to maintain a constant pressure in each equilibrium cell, is recorded. Equilibrium is achieved when there is no change in the cumulative volume of water in both cells as the volume change on the mixing is the criteria for the equilibrium condition.

When equilibrium is achieved, both cells are kept in a vertical position for phase separation. The equilibrium fluids in the first equilibrium cell are then discharged through the density measuring cell and viscometer, while constant temperature and pressure are maintained. The pressure is measured by both the in-line and Quizix pump pressure transducers. The phase samples are collected with steady readings of the viscometer and

the density measuring cell with any change in density and viscosity indicating the passage of a phase boundary through the measuring instruments.

Liquid and vapour phases are transferred into sampling cells 1 to 3, and the last sampling cell is used to purge the phase boundary portion and clean the transition between the phases. The denser phase can completely displace the lighter phases which are vertically segregated in the order of phase density, resulting in clean samples with sharp density variation. The volume of each phase is measured by monitoring the volume of water charged into the equilibrium cell. The phase samples can be collected through the sampling port for compositional analysis and further study.

During the discharging of equilibrium fluids, if a sharp transition of phase boundary is not observed using density and viscosity measurements, the equilibrium phases are not properly segregated. In this case, the experiment is repeated and the phase separation period is increased.

When the equilibrium fluids in the first cell are discharged, all lines, the density measuring cell, and the viscometer are cleaned to remove any contaminant using toluene or similar solvents. To ensure that no contaminants were left inside the system, the lines are successively evacuated and flushed with helium and pure solvent. The second equilibrium cell will then be discharged with the same procedure as the first equilibrium cell. In the case of liquid-liquid equilibrium, it is necessary to empty and clean the sampling cells for the discharging of the second equilibrium cell.

2.3. Apparatus Verification

Several different binary and ternary systems were selected to evaluate the designed apparatus. The experiments for the systems of methane/*n*-propanol, ethane/ethanol, 1-butanol/water, ethane/methanol, carbon dioxide/ethanol, carbon dioxide/methanol, methane/*n*-octadecane, ethane/*n*-tetradecane, and propane/*n*-decane were conducted at different temperatures and pressures. For some systems, the phase compositions and

phase densities were compared with the available literature data. The purpose of these experiments was to check the validity and accuracy of the experimental results produced from the proposed apparatus. A variety of binary systems was selected to evaluate the apparatus for the systems, hydrocarbon/hydrocarbon, non-hydrocarbon/hydrocarbon, and hydrocarbon/alcohol. This also verified the success of the apparatus for a vapour-liquid and liquid-liquid equilibrium conditions.

2.3.1. Materials

All gases were supplied by Praxair. *n*-pentane, *n*-decane, *n*-tetradecane, and *n*-octadecane were obtained from the Alfa Aesar Company. All the chemicals were used without any further purification. Table 2–7 summarizes the chemical sample specifications.

Table 2–7: Chemical sample specifications.

Chemical Name	Source	Initial Purity (fraction)	Purification Method
Methane	Praxair (3.7 ultra high purity)	0.9997 mole	none
Ethane	Praxair	0.99 mole	none
Propane	Praxair	0.995 mole	none
Carbon Dioxide	Praxair (4.8 research)	0.9999 mole	none
Methanol	EMD Chemicals	0.998 mass	none
Ethanol	Commercial Alcohols	0.997 mass	none
1-butanol	Sigma-Aldrich	0.997 mass	none
<i>n</i> -propanol	Mallinckrodt Baker Inc	0.999 mass	none
<i>n</i> -pentane	Alfa Aesar	0.99 mass	none
<i>n</i> -decane	Alfa Aesar	0.99 mass	none
<i>n</i> -tetradecane	Spectrum Chemical Mfg. Corp	0.99 mass	none
<i>n</i> -octadecane	Alfa Aesar	0.99 mass	none

2.3.2. Saturation Pressure of Pure Component

To investigate the reproducibility of the apparatus for phase behaviour studies, the saturation pressure of a pure component (*n*-pentane) was measured over the temperature range of 50 to 100°C and the results were compared with the NIST data in Figure 2–8.

The figure illustrates the accuracy of the pressure measurements. The average absolute deviation for saturation pressure measurements is less than 2.4%.

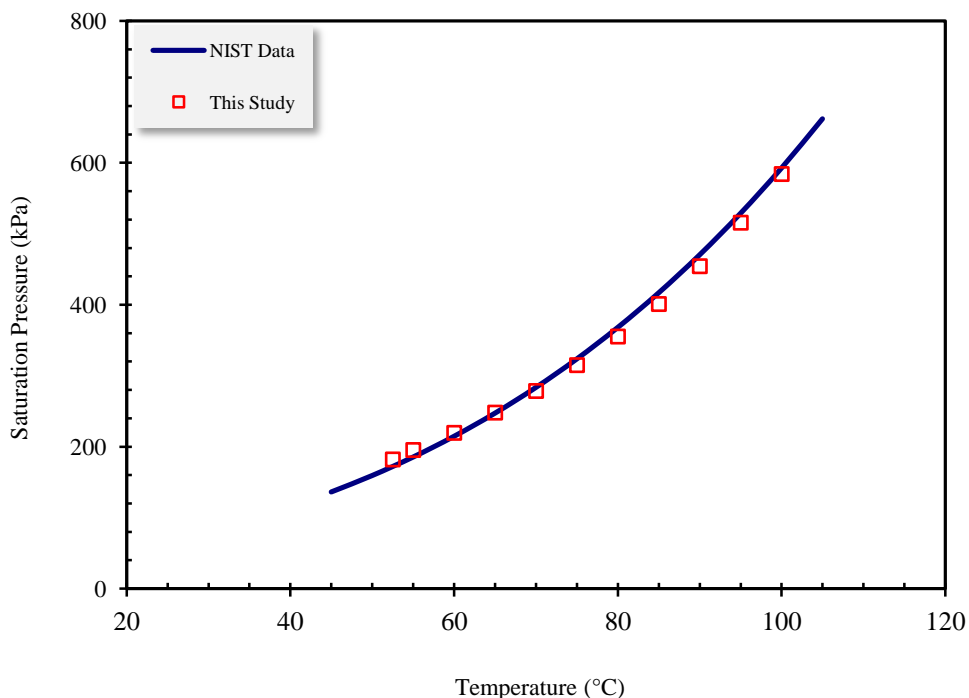


Figure 2–8: Saturation pressure of *n*-pentane versus temperature (Nourozieh et al. 2012a).

2.3.3. Phase Detection

Vapour-Liquid. The vapour-liquid equilibrium experiments were conducted for methane/*n*-octadecane binary systems based on the experimental procedure previously outlined. When equilibrium was achieved, the equilibrium cell was placed in a vertical position for phase separation. The density of the equilibrium fluid was continuously measured as it was discharged from the equilibrium cell. Figure 2–9 shows the density measurement during the sampling. The density towards the beginning of the experiment was about 2 kg/m³, which shows the density of helium inside the lines. The flow rate to push the fluids was too low (0.1–3 cm³/min) to keep the system at equilibrium and was the maximum rate at which the fluids could be displaced at constant pressure. The flow rate is dependent on the equilibrium fluid properties and apparatus specifications such as the o-rings and line diameter.

After about 10 cm³ of volume displacement, the gas phase was detected at the density measuring cell. There was a sharp change in density from ~ 2 to ~ 10 kg/m³ which shows the density of a vapour mixture containing mostly methane. The density measuring cell detected two different gases with a small density difference. Discharging was continued to detect the final phase, which was liquid. The sharp increase in density from ~ 10 to ~ 700 kg/m³ confirmed the liquid phase.

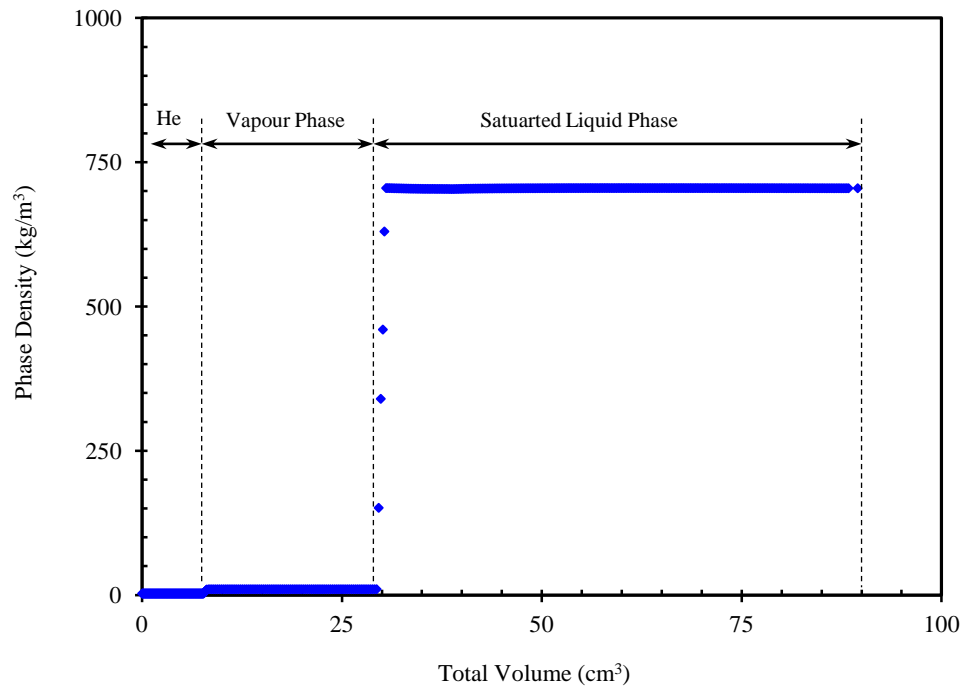


Figure 2–9: Phase detection on the basis of density measurements for vapour-liquid equilibria of methane/n-octadecane system at 125°C and 2034 kPa.

Liquid-Liquid. The liquid-liquid mixing experiment was performed to investigate the capability of the experimental setup to identify the phase boundary between two liquids. Figure 2–10 illustrates the phase detection experimental results for the sampling of ethane/methanol binary system at the temperature of 22°C and the pressure of 4891 kPa. The overall ethane composition in the mixture was around 70 percent by weight. As depicted in the figure, at the start of the phase sampling, helium flowed though the density measuring cell, and its density was close to zero. There was a sharp change in

density when the lighter liquid phase passed through the density measuring cell. There was a second jump that indicated the second liquid phase. In some experiments for alcohol/hydrocarbon mixtures, the sharp change in density from liquid 1 to liquid 2 was not observed. This is an indication that the vertical segregation between them was not complete. The data suggested that fine droplets of the lighter liquid were still suspended in the densest lower liquid. This situation could be alleviated by leaving the equilibrium cell in the vertical position for a longer period of time.

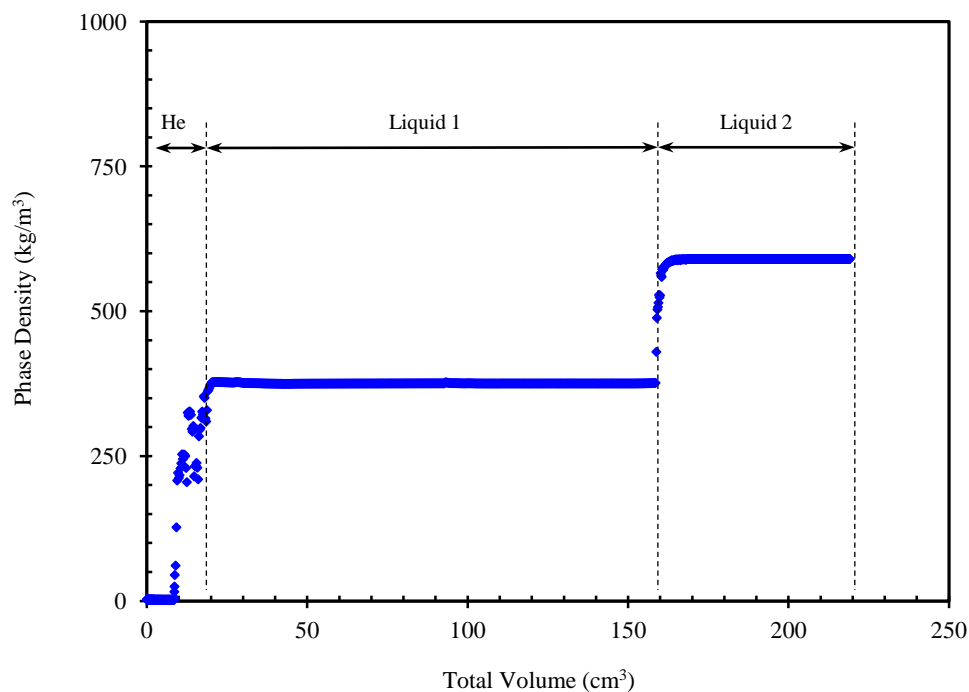


Figure 2–10: Phase detection on the basis of density measurements for liquid-liquid equilibria of ethane/methanol system at 22°C and 4891 kPa.

2.3.4. Equilibrium Criteria

As mentioned previously, stabilized volume was the criteria for equilibrium. Thus, the binary systems under study were determined to have reached equilibrium condition when the volume of each mixture at constant pressure and temperature did not change for at least 12 hours. Figure 2–11 illustrates the volume of each mixture versus equilibration time for some binary systems under different conditions. As depicted in the figures, after

about one hour, the total injected volume of water in each binary system to maintain the desired pressure became constant. Further mixing and agitation using the rocking mechanism would not change the state of system.

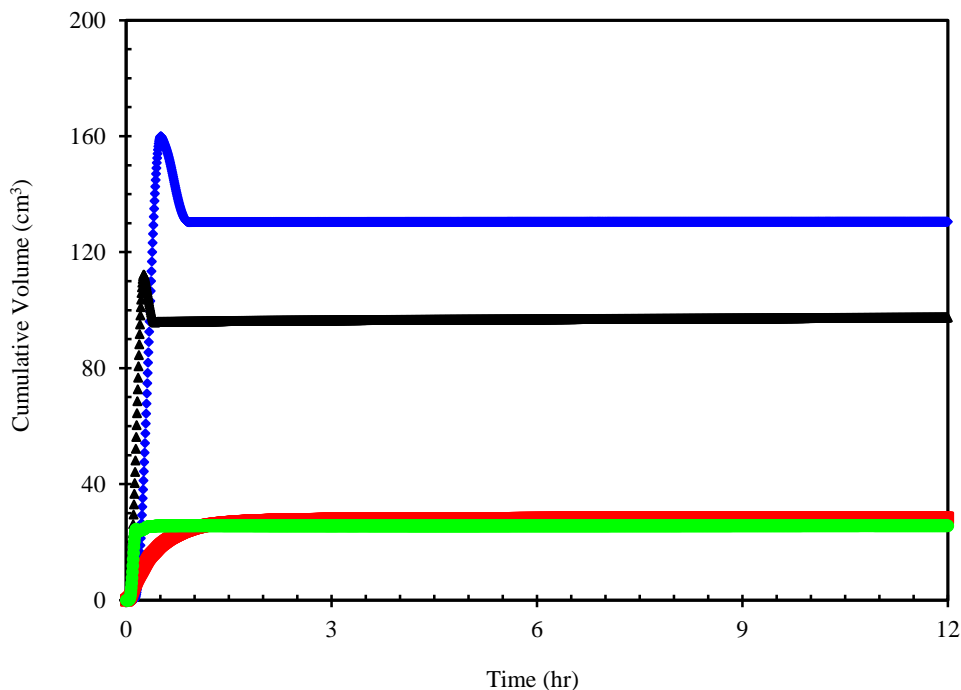


Figure 2–11: Volume change on mixing (equilibrium criteria) for simple binary systems; \blacklozenge , ethane/ethanol at 40°C and 1103 kPa; \blacksquare , methane/*n*-propanol at 22°C and 4000 kPa; \blacktriangle , ethane/*n*-tetradecane at 50°C and 1055 kPa; \bullet , methane/*n*-octadecane at 125°C and 2034 kPa.

To confirm the equilibrium state of the system, experiments were conducted with different rocking rates and mixing times. The resulting phase properties showed no difference in composition, density, and viscosity during these different experiments.

2.3.5. Phase Properties

The experimental results (saturated phase properties such as composition and density) for the simple binary systems, along with the literature values, are presented in Table 2–8. Both liquid phase compositions and saturated liquid phase densities were compared to the available data.

The experimental results agree well with the literature data indicating that the quality of the generated data is good and is comparable to that of the data reported by other researchers. Although a direct comparison of experimental data for some binary pairs is not possible due to a difference in the isotherms or isobars in two studies, the data are reasonably consistent with present measurements.

Table 2–8: Experimental vapour-liquid and liquid-liquid equilibrium properties for simple binary systems; T , temperature; P , pressure; w_s , composition; ρ , density.

System	Source	T (°C)	P (MPa)	$10^2 w_s$ (wt%)		ρ (kg/m ³)	
				Phase 1	Phase 2	Phase 1	Phase 2
Ethane + Methanol	This study*	21.8	1.20	5.6	----	750	----
	Ishihara et al. (1998)	25	0.963	5.0	----	762.0	----
	This study*	21.8	3.13	22.5	----	671	----
	Ishihara et al. (1998)	25	3.410	23.0	----	674.0	----
	This study**	21.8	4.89	42.2	97.1	590	375
	Ishihara et al. (1998)	25	4.859	40.8	93.7	592.2	374.7
Ethane + Ethanol	This study*	40.3	5.13	38.7	----	577	----
	Suzuki et al. (1990)	40.3	5.117	36.9	----	----	----
Propane + <i>n</i> -Decane	This Study*	71.2	1.479	30.0	----	----	----
	Reamer and Sage (1966)			30.84	99.01	----	----
	This Study*	104.5	2.758	41.9	----	----	----
	Reamer and Sage (1966)			42.00	97.56	----	----
	This Study*	137.8	4.137	42.8	----	----	----
Reamer and Sage (1966)	42.24			92.94	----	----	
1-Butanol + Water	This Study**	21.9	0.10	----	----	835	981
	Hill and Malisoff (1926)	25	0.101	----	----	845.0	986.5

* vapour-liquid equilibrium

** liquid-liquid equilibrium

2.3.6. Solubility and Saturated Liquid Viscosities

The apparatus and the experimental procedure presented in Sections 2.1 and 2.2 were also checked for carbon dioxide / ethanol binary systems at the temperatures of 30 and 50°C and at different pressures. Figure 2–12 illustrates the experimental solubility and saturated liquid density of carbon dioxide / ethanol systems at different pressures which are in good agreement with the literature data. Previous studies (Mehl et al. 2011; Chiu et

al. 2008; Secuianu et al. 2008; Dalmolin et al. 2006; Stievano and Elvassore 2005; Gao et al. 2002; Joung et al. 2001; Chen et al. 2000; Chang et al. 1998; Day et al. 1996; Jennings et al. 1991) have reported the saturated liquid phase composition at the temperatures of 30 and 50°C. There are significant deviations in the data from different authors. The experimental solubility data found in this study are consistent with the data of Secuianu et al. (2008), Chiu et al. (2008), and Stievano and Elvassore (2005) at the temperature of 30°C. At the temperature of 50°C, our solubility data seem to agree with the measurements of Joung et al. (2001) and Mehl et al. (2011).

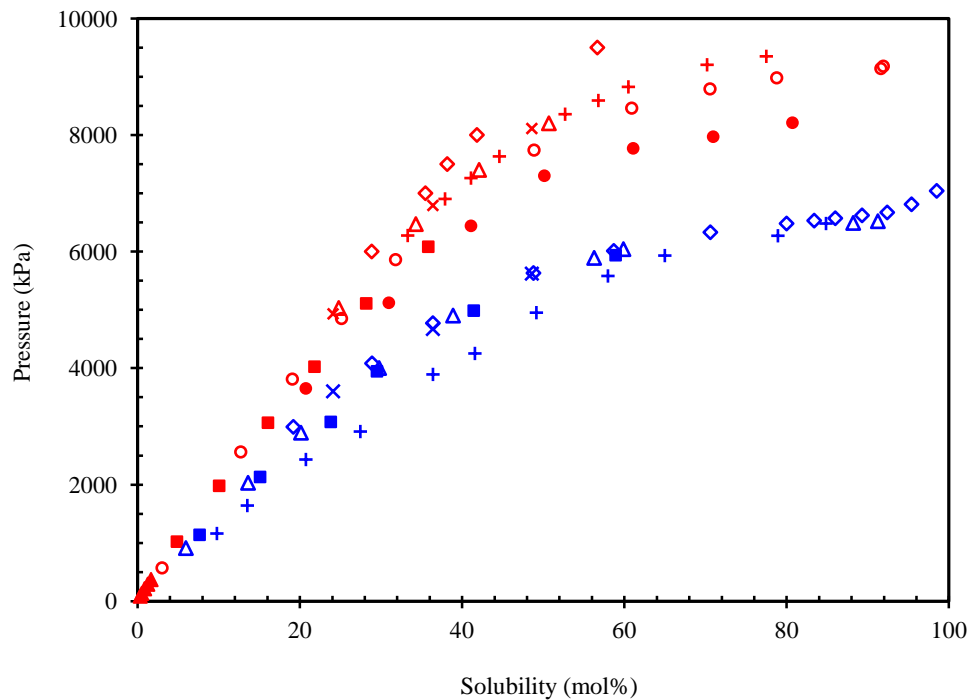


Figure 2–12: Comparison of measured solubility data and literature values for carbon dioxide / ethanol system at different pressures; ■, this study at 303.2 K; ◇, Chiu et al. (2008) at 303.12 K; △, Secuianu et al. (2008) at 303.2 K; +, Day et al. (1996) at 303.12 K; ×, Stievano and Elvassore (2005) at 303.15 K; ■, this study at 323.2 K; ●, Mehl et al. (2011) at 323.2 K; ▲, Dalmolin et al. (2006) at 323 K; ×, Stievano and Elvassore (2005) at 323.15 K; ◇, Gao et al. (2002) at 323 K; ○, Joung et al. (2001) at 322.5 K; △, Chen et al. (2000) at 323 K; +, Jenning et al. (1991) at 325 K (Kariznovi et al. 2013a).

As plotted in Figure 2–13, the viscosity of carbon dioxide / alcohol systems decreases with increasing pressure. The impact of pressure on viscosity reduction is more pronounced at lower temperatures due to higher dissolution of carbon dioxide in alcohol

at lower temperatures. Sih et al. (2007, 2008) also measured the gas-expanded liquid viscosity for carbon dioxide / methanol and carbon dioxide / ethanol systems at the temperature of 30°C using a customized falling-weight viscometer. These data are also presented in the figure. Our measured viscosity data are consistent with Sih et al. (2007, 2008) measurements.

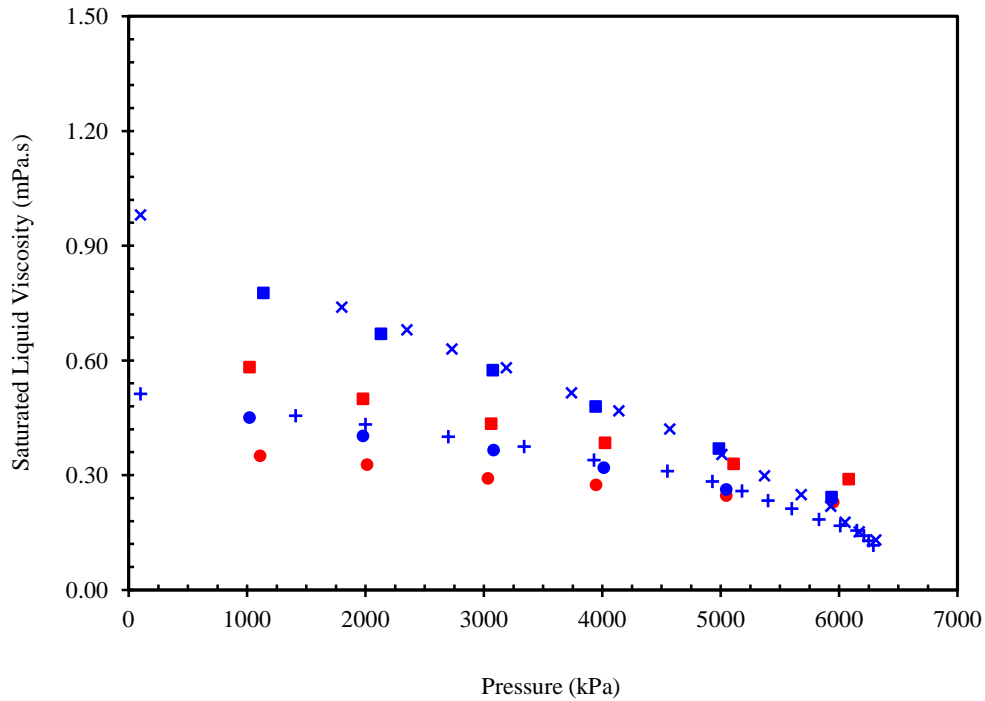


Figure 2–13: Comparison of measured saturated liquid viscosities and literature data for carbon dioxide / alcohol systems at different pressures; ●,+,●, carbon dioxide / methanol; ■,×,■, carbon dioxide / ethanol; ●,■, this study at 303.2 K; ●,■, this study at 323.2 K; +, Sih et al. (2007) at 323.15 K; ×, Sih et al. (2008) at 323.15 K (Kariznovi et al. 2013a).

2.3.7. Comparison of Two Designed Apparatuses

Bitumen/solvent mixtures can form different equilibrium conditions, such as vapour-liquid, liquid-liquid, and vapour-liquid-liquid, depending on the type of solvent, the initial mass fraction of the solvent-to-bitumen, the pressure, and the temperature. To validate the modified apparatus and the experimental results, three experiments for Athabasca bitumen / propane systems were conducted at different conditions. The results were

compared with the data generated by another PVT apparatus. The experiments at the pressure of 4 MPa and three different temperatures, 50, 100 and 150°C, were conducted.

The procedures to charge the equilibrium cell, reach equilibrium and discharge the equilibrium fluids were described in Section 2.2. At 100 and 150°C, vapour-liquid equilibrium exists while at 50°C, liquid-liquid equilibrium is observed. Phase detection during the displacement of the equilibrium phases was based on the density measurements. The properties of the saturated phases and their compositions are summarized in Table 2–9. For comparison, the results of original apparatus are also listed in Table 2–9.

Table 2–9: Initial propane/bitumen ratio and corresponding equilibrium properties of propane/bitumen systems for the two designed experimental apparatuses (Nourozieh et al. 2012a).

Run No.	Apparatus	P(MPa)	T(°C)	S/B Ratio*	10 ² w _s (wt%)		Saturated Phase Properties		
					Phase 1	Phase 2	μ (mPa.s)	ρ (kg/m ³)	
							Phase 2	Phase 1	Phase 2
1	Original	4.08	50.9	1/1	62.5	21.5	127.0	586	860
	Modified	4.08	50.2	1/1	60.7	21.5	129.2	604	864
2	Original	4.04	100.4	2/3	Pure C ₃	22.9	2.7	105	775
	Modified	4.00	99.9	2/3	Pure C ₃	22.0	3.6	105	784
3	Original	4.12	149.8	1/4	Pure C ₃	8.7	5.4	65	849
	Modified	3.94	148.9	1/4	Pure C ₃	8.4	4.7	65	856

*S/B Ratio: solvent-to-bitumen ratio wt/wt

As the results indicate, the equilibrium fluid properties for three experiments are in good agreement with those obtained using original apparatus. The viscosity data are still comparable and the difference in measurements can be explained by apparatus specifications. The Cambridge viscometer used for these measurements was equipped with sensor SPC-372 while the one used in first apparatus was equipped with SPL-440. The former, which is a flow-through viscosity sensor, is capable of measuring the viscosity in the range of 0.25 to 20,000 mPa.s and pressure up to 14 MPa. The latter, a high-pressure research viscosity sensor, can measure the viscosity in the range of 0.2 to 10,000 mPa.s and pressure up to 140 MPa. The deviations of measurements with two

developed apparatuses are summarized in Table 2–10. The viscosity data are the ones with high deviations, as a result of different sensors installed in the Cambridge viscometers. The deviation is even higher at lower viscosities, which is also due to the difference in the viscometer sensors.

Table 2–10: The deviations for reported experimental data using two proposed apparatus (Nourozieh et al. 2012a).

Run No.	P (%)	T (%)	w_s (%)		Saturated Phase Properties		
			Phase 1	Phase 2	μ (%)	ρ (%)	
					Bitumen-enriched (Phase 2)	Phase 1	Phase 2
1	0.0	0.2	2.9	0.0	1.7	3.1	0.5
2	1.0	0.1	----	3.9	33.3	0.0	1.2
3	4.4	0.2	----	3.4	13.0	0.0	0.8

Chapter 3: Bitumen Properties

This chapter presents the measurements of bitumen properties, density, viscosity, compositional measurements, molecular weight and SARA analysis. The density and viscosity of raw bitumen were reported over a wide range of temperatures and pressures. These properties were used for the interpretation of the solvent effect on bitumen properties and also used for the modelling studies, as detailed in the remaining chapters.

3.1. Bitumen Samples

Athabasca bitumen samples for this study were provided by three different oil companies in Canada. One bitumen sample was received from Japan Canada Oil Sands Limited (JACOS) operated a SAGD project in the Hangingstone area. One sample from Suncor operated a SAGD project at MacKay River and one sample from ConocoPhillips operated a SAGD project (Surmont project) in southeast of Fort McMurray. The samples have been processed by companies to remove sand and water. During this study, three samples are referred as JACOS, MacKay River, and Surmont bitumens.

3.2. Density and Viscosity

Density, a thermodynamic property of hydrocarbon fluid, plays a key role in the material balance calculation involved in chemical and petroleum processes. Viscosity is a transport property defined as the resistance of a fluid to shearing force. The viscosity of a liquid is a function of intermolecular forces that limit the motion of adjacent molecules. Density and viscosity are particularly important for both reservoir and production engineers because they determine the fluid flow properties and are essential to the estimation of the total mass of reserves. Tremendous amounts of accurate viscosity and density data are required to design an efficient chemical process for the reduction of oil viscosity in enhanced oil recovery or pipeline transportation. Viscosity data are more

critical for highly viscous fluids, such as bitumen, in which the viscosity is in the order of million centipoises under reservoir conditions. Nearly all recovery processes aim at reducing the bitumen viscosity; therefore, the production and pipeline transportation of such viscous fluids require specific data on the viscosity and density of raw bitumen as well as oil mixed with different diluents.

Petroleum crudes are categorized based on their density and viscosity. Crudes can be classified as either conventional or unconventional. Conventional oil has low density and viscosity at reservoir conditions thus can be recovered using conventional recovery techniques, such as water flooding. Unconventional crudes (heavy oils, extra heavy oils, or bitumen) have very high viscosity at reservoir conditions rendering it immobile or only partially mobile fluid in reservoir. The production of unconventional oils is more difficult due to their high viscosity. They must be heated or diluted first in order to become mobile and be produced. United Nations Institute for Training and Research (UNITAR) categorized petroleum fluids based on their viscosity and density. Table 3–1 presents the density and viscosity range for conventional oil, heavy oil, and bitumen.

Table 3–1: UNITAR definition of heavy oils and bitumen at reservoir temperature (Gray 1994).

	Viscosity (mPa.s)	Density (kg.m ⁻³)	API Gravity
Conventional Oil	< 10 ²	< 934	> 20
Heavy Oil	10 ² -10 ⁵	934-1000	10-20
Bitumen	> 10 ⁵	> 1000	< 10

Numerous studies measuring bitumen viscosity and density have been reported in the literature. Mehrotra and Svrcek (1984, 1985a, 1985b, 1985c, 1988a) and Svrcek and Mehrotra (1989) reported the density and viscosity of different Alberta bitumens at atmospheric pressure. Mehrotra and Svrcek (1986, 1987a) also measured the viscosity of the Athabasca and Cold Lake bitumens over the temperature range of 40 to 120°C and at pressures up to 10 MPa.

Mehrotra et al. (1989a) measured the effect of temperature on the viscosity of Cold Lake bitumen fractions. The fractions were obtained using vacuum distillation of a large

Cold Lake bitumen sample and the effect of temperature on the viscosity of each bitumen fraction was modelled using a two-parameter correlation. Eastick and Mehrotra (1990) generated the viscosity data for a number of reconstituted mixtures of the Cold Lake bitumen fractions. The binary blend viscosity data were modelled with a two-parameter viscosity correlation. Recently, Badamchizadeh et al. (2009a, 2009b) reported the viscosity and density data for Athabasca bitumen at different temperatures and pressures (Nourozieh et al. 2013).

Alongside the experimental measurements, correlations for the density and viscosity of bitumen have also been developed. Khan et al. (1984) modified the Eyring and Hildebrand theories to predict the viscosity of Athabasca bitumen for the temperature range of 20 to 130°C. Mehrotra and Svrcek (1986) developed a correlation for viscosity of gas-free Athabasca bitumen as a function of temperature and pressure. They did the same study for Cold Lake bitumen (Mehrotra and Svrcek 1987a).

Mehrotra and Svrcek (1987b) have proposed a method based on the extended principle of corresponding states for calculating the viscosity of Alberta bitumens. Svrcek and Mehrotra (1988) tested eight empirical viscosity-temperature correlations for bitumens and found that the models provided a satisfactory representation of the viscosity of seven Alberta bitumens over the temperature range of 10 to 130°C with an average deviation of less than 10%. A one-parameter generalized correlation was finally developed (Nourozieh et al. 2013).

Mehrotra (1991) developed a correlation for predicting the viscosity of pure heavy hydrocarbons. In a subsequent study, Mehrotra (1992a) proposed a one-parameter equation for predicting the viscosity of pure hydrocarbons, bitumen fractions, and gases. The author predicted the viscosity of oil-sand bitumens diluted with light gases and liquid diluents. Mehrotra (1992b) also developed a model for predicting the mixture viscosity of bitumen or bitumen cuts blended with liquid diluents such as toluene. Mehrotra (1992c) developed a mixing rule for predicting the viscosity of Alberta bitumens saturated with

pure gases (nitrogen, carbon monoxide, methane, carbon dioxide, and ethane) (Nourozieh et al. 2013).

Puttagunta et al. (1993) proposed a correlation that predicted the combined effect of temperature and pressure on the viscosity of Canadian bitumens and heavy oils. Miadonye et al. (1994) proposed a correlation for predicting bitumen viscosity that only requires a single viscosity measurement. Miadonye et al. (1995) have also developed a viscosity correlation to predict the viscosity-temperature relationship of bitumen mixed with various proportions of diluents (Great Canadian Oil Sands (GCOS) synthetic crude, mobile solvent, and naphtha). Miadonye et al. (2000) proposed an equation for predicting the kinematic viscosity of bitumens and heavy oils mixed with diluents. The correlation they defined is applicable for wide range of data and requires viscosity information for raw bitumen and pure solvent at any given temperature. In 2001, Miadonye et al. (2001) extended the correlation to predict the viscosity of bitumen-diluent mixtures, as well as the mass fraction required to reduce bitumen viscosity to pumping viscosity. Oyekunle (2000) developed a two-parameter correlation for calculating the bitumen viscosity. The author included the softening point in the model and validated the model using bitumen samples obtained from Russian crudes. Both average absolute deviation and standard error were less than 8% over a wide range of softening points (Nourozieh et al. 2013).

Badamchi-Zadeh et al. (2009a) measured and correlated the density and viscosity of Athabasca bitumen. In addition, they correlated the density and viscosity of propane-saturated bitumen at different temperatures and pressures. For the density prediction, they assumed that no volume change occurred upon mixing. The viscosity of the liquid phase was predicted using the Lobe mixing rule. Motahhari et al. (2011) correlated the viscosity of a condensate, two bitumen samples from Peace River field, and bitumen/condensate mixtures using expanded fluid viscosity model (Nourozieh et al. 2013).

The development of reliable correlations for the viscosity and density of bitumen is essential and requires extensive experimental data over wide ranges of pressure and temperature. The resulting correlations can directly be applied in a reservoir simulator to

calculate the viscosity at the desired temperature and pressure. If a comprehensive set of data is available, not only can correlations be easily developed, but the comparison of saturated bitumen density and viscosity with raw data can be made. Although some experimental data have been measured to study the viscosity of bitumen as a function of temperature, few measurements for the pressure dependence of bitumen viscosity have been reported. Thus, this section reports the physical properties of Athabasca bitumen samples, density and viscosity, for a wide range of temperatures and pressures prior to determining the solubility measurements for any bitumen.

To measure the viscosity and density of bitumen, the setup was cleaned; and, the appropriate piston for the viscosity measurement was installed. The system was then evacuated and the bitumen was charged into the system filling the line that connects the density measuring cell and the viscometer with bitumen. The oven temperature was kept constant, and the system pressure was set to the desired pressure to measure the viscosity and density. The pressure was monitored by the pressure transducer connected to the line. The temperature was simultaneously monitored by the oven, viscometer, and density measuring cell thermocouples. The viscosity and density of the bitumen were then measured at fixed temperature and pressure.

3.2.1. Density of Bitumens

The density of the bitumen samples was measured over wide range of temperatures by the Anton Paar density measuring cell. The temperature was varied within $\pm 0.1^\circ\text{C}$ and the pressure was controlled by the Quizix pump within 0.01 MPa. The uncertainty of density measurements was 0.1 kg/m^3 . The density of bitumen samples at different temperatures (23 to 190°C) over the pressure range, atmospheric pressure to 14 MPa, was measured. As expected, the density of bitumen reduced with increasing temperature at a constant pressure. This behaviour was observed for all pressures. At a constant temperature, however, the bitumen density increased with increasing pressure.

The measured density values were correlated with the following equation that takes into account the impact of pressure and temperature,

$$\rho = \rho_0 \exp\{\alpha P\} \quad 3-1$$

$$\rho_0 = a_1 + a_2 T + a_3 T^2 \quad 3-2$$

$$\alpha = a_4 \exp(a_5 T) \quad 3-3$$

where T represents temperature in Celsius, P is the pressure in MPa, and ρ is the density in kg/m^3 . In order to obtain the coefficients of the equations, a minimization algorithm was applied. The regression of the experimental data with the minimization algorithm usually suffers from the convergence problem or from the existence or uniqueness of the solution. This study developed a procedure to obtain the coefficients of equations 3-1 to 3-3 where the solution is unique and no convergence problem is observed. The proposed model is applicable for cases where the density measurements at different pressures are conducted at an isothermal condition.

Assume that at a constant temperature, the density of bitumen is measured at different pressures, as is the case here. In equation 3-1, the terms α and ρ_0 would be constant at the isothermal condition and the density is an exponential function of pressure. Thus, at each temperature, a value for α and a value for ρ_0 can be obtained.

The relationship between bitumen density and pressure can be understood by plotting the density as a function of pressure at a constant temperature. Figures 3–1 to 3–3 illustrate the variation of bitumen density with pressure at different isothermal conditions for three different bitumens. The symbols are the experimental data and solid lines are the correlations of the exponential functions. As expected, the density of bitumen increases with pressure at a constant temperature. This behaviour is observed for all temperatures and a linear trend for the variation of density with pressure at each isotherm condition is obtained.

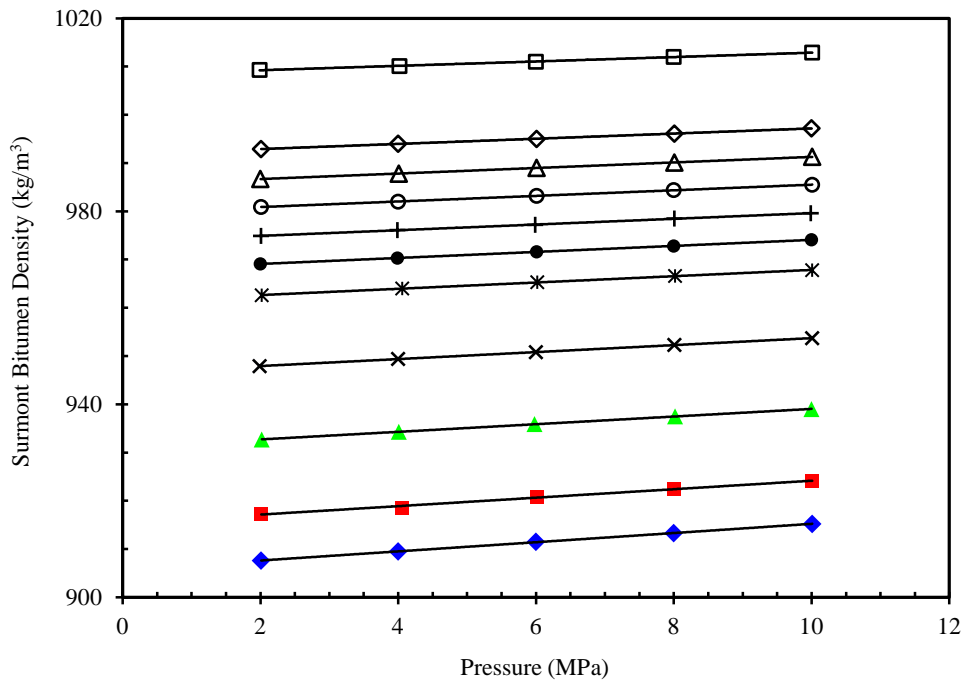


Figure 3-1: Density of Surmont bitumen as a function of pressure at different isotherms; □, 23°C; ◇, 50°C; Δ, 60°C; ○, 70°C; +, 80°C; ●, 90°C; *, 100°C; ×, 125°C; ▲, 150°C; ■, 175°C; ◆, 190°C.

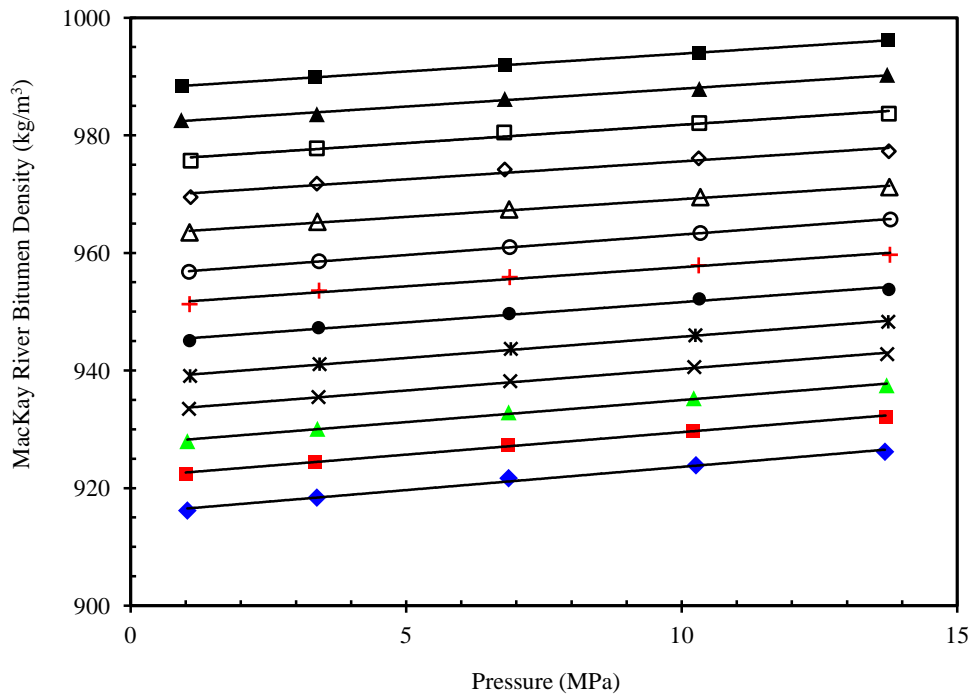


Figure 3-2: Density of MacKay River bitumen as a function of pressure at different isotherms; ■, 50°C; ▲, 60°C; □, 70°C; ◇, 80°C; Δ, 90°C; ○, 100°C; +, 110°C; ●, 120°C; *, 130°C; ×, 140°C; ▲, 150°C; ■, 160°C; ◆, 170°C.

The coefficients α and ρ_0 for each temperature and bitumen are listed in Tables 3–2 to 3–4. As the tables show, the value of α increases with the temperature resulting in an increase in the pressure dependency of the density as the temperature increases.

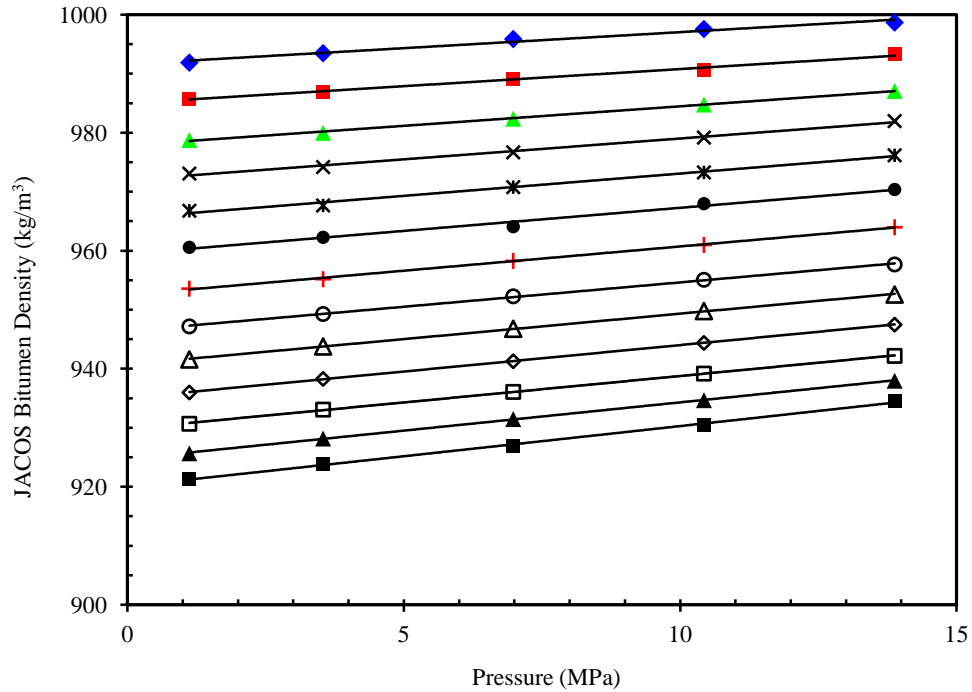


Figure 3–3: Density of MacKay River bitumen as a function of pressure at different isotherms; \blacklozenge , 50°C; \blacksquare , 60°C; \blacktriangle , 70°C; \times , 80°C; $*$, 90°C; \bullet , 100°C; $+$, 110°C; \circ , 120°C; \triangle , 130°C; \diamond , 140°C; \square , 150°C; \blacktriangle , 160°C; \blacksquare , 170°C.

Table 3–2: Coefficients of the correlation equation for the density of Surmont bitumen (equation 3-1).

T (°C)	ρ_0 (kg/m ³)	α (1/MPa)
23.0	1008.33	4.495×10^{-4}
49.9	991.83	5.379×10^{-4}
60.1	985.53	5.808×10^{-4}
69.9	979.72	5.899×10^{-4}
79.9	973.72	6.044×10^{-4}
89.8	967.84	6.430×10^{-4}
100.6	961.34	6.755×10^{-4}
125.0	946.49	7.606×10^{-4}
150.3	931.14	8.454×10^{-4}
174.6	915.39	9.528×10^{-4}
190.0	905.73	10.423×10^{-4}

Table 3–3: Coefficients of the correlation equation for the density of MacKay River bitumen (equation 3-1).

T (°C)	ρ_0 (kg/m ³)	α (1/MPa)
50	987.84	6.094×10^{-4}
60	981.86	6.149×10^{-4}
70	975.56	6.357×10^{-4}
80	969.48	6.263×10^{-4}
90	963.11	6.237×10^{-4}
100	956.16	7.252×10^{-4}
110	951.09	6.785×10^{-4}
120	944.76	7.233×10^{-4}
130	938.53	7.656×10^{-4}
140	932.94	7.833×10^{-4}
150	927.49	8.027×10^{-4}
160	921.89	8.234×10^{-4}
170	915.73	8.563×10^{-4}

In order to obtain the coefficients of equation 3-2, the values of ρ_0 were plotted as a function of temperature (Figure 3–4). This figure shows a linear variation of ρ_0 with temperature where a_3 is too small and ρ_0 can be considered a linear function of temperature. Table 3–5 summarizes the coefficients of equation 3-2 for three different bitumens along with the coefficients of determination. The coefficient of determination is calculated from,

$$R^2 = 1 - \frac{\sum_i (y_i - \xi_i)^2}{\sum_i (y_i - \bar{y})^2} \quad 3-4$$

where y_i represents the measured data and ξ_i represents the modelled values. Both a linear function and a second order function for the variation of ρ_0 with temperature were considered. Although the second order function shows better correlation of ρ_0 , the results using the linear function are acceptable. Overall, at a constant pressure, the bitumen density showed a linear reduction with temperature and the linear trend was observed for all pressures.

Table 3-4: Coefficients of the correlation equation for the density of JACOS bitumen (equation 3-1).

T (°C)	ρ_0 (kg/m ³)	α (1/MPa)
50	991.62	5.456×10^{-4}
60	984.99	5.869×10^{-4}
70	977.87	6.737×10^{-4}
80	971.97	7.231×10^{-4}
90	965.53	7.792×10^{-4}
100	959.46	8.112×10^{-4}
110	952.52	8.577×10^{-4}
120	946.39	8.671×10^{-4}
130	940.73	9.114×10^{-4}
140	935.06	9.529×10^{-4}
150	929.83	9.577×10^{-4}
160	924.74	10.288×10^{-4}
170	920.09	11.016×10^{-4}

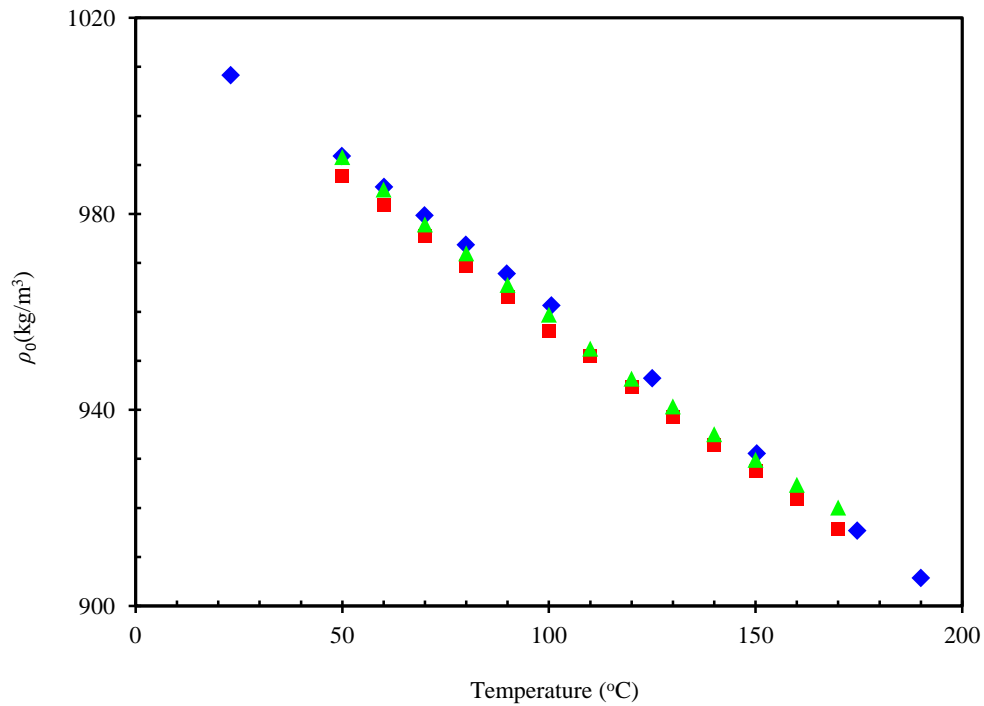


Figure 3-4: Coefficient ρ_0 of equation 3-1 as a function of temperature for three different bitumens; \blacklozenge , Surmont; \blacksquare , MacKay River; \blacktriangle , JACOS.

Table 3–5: Coefficients of the correlation equation for calculation of ρ_o (equation 3-2).

Bitumen	a_1 (kg.m ⁻³)	a_2 (kg.m ⁻³ .[°C] ⁻¹)	a_3 (kg.m ⁻³ .[°C] ⁻²)	R^2
Surmont	1022.59	-0.61215	0	0.99989
	1021.62	-0.58976	-1.017×10 ⁻⁴	0.99995
MacKay River	1017.44	-0.60163	0	0.99945
	1021.19	-0.67874	3.505×10 ⁻⁴	0.99983
JACOS	1020.15	-0.60219	0	0.99756
	1029.29	-0.79007	8.540×10 ⁻⁴	0.99976

To obtain the coefficients of equation 3-3, the values of α were also plotted as a function of temperature in Figure 3–5. For Surmont bitumen, a non-linear trend for the variation of α with temperature is observed while for MacKay River and JACOS bitumens, a linear variation was obtained. The exponential term in equation 3-3 can be replaced with the simple linear function,

$$\alpha = a_4 + a_5 T \quad 3-5$$

This equation has been considered by Badamchi-Zadeh et al. (2009a), Guan et al. (2013), Kariznovi et al. (2013b), and Nourozieh et al. (2013) in the correlation of Athabasca bitumen density with acceptable results. Both exponential and linear functions for the variation of α with temperature were considered, and the fitted coefficients with the coefficient of determination α are summarized in Table 3–6.

Table 3–6: Coefficients of the correlation equation for calculation of α (equations 3-3 and 3-5).

Bitumen	Equation	a_4 (MPa ⁻¹)	a_5 ([°C] ⁻¹)	R^2
Surmont	Linear	3.528×10 ⁻⁴	3.416×10 ⁻⁶	0.98599
	Exponential	4.187×10 ⁻⁴	4.762×10 ⁻³	0.99390
MacKay River	Linear	4.745×10 ⁻⁴	2.167×10 ⁻⁶	0.93194
	Exponential	5.074×10 ⁻⁴	3.029×10 ⁻³	0.93277
JACOS	Linear	3.657×10 ⁻⁴	4.226×10 ⁻⁶	0.97829
	Exponential	4.548×10 ⁻⁴	5.295×10 ⁻³	0.95220

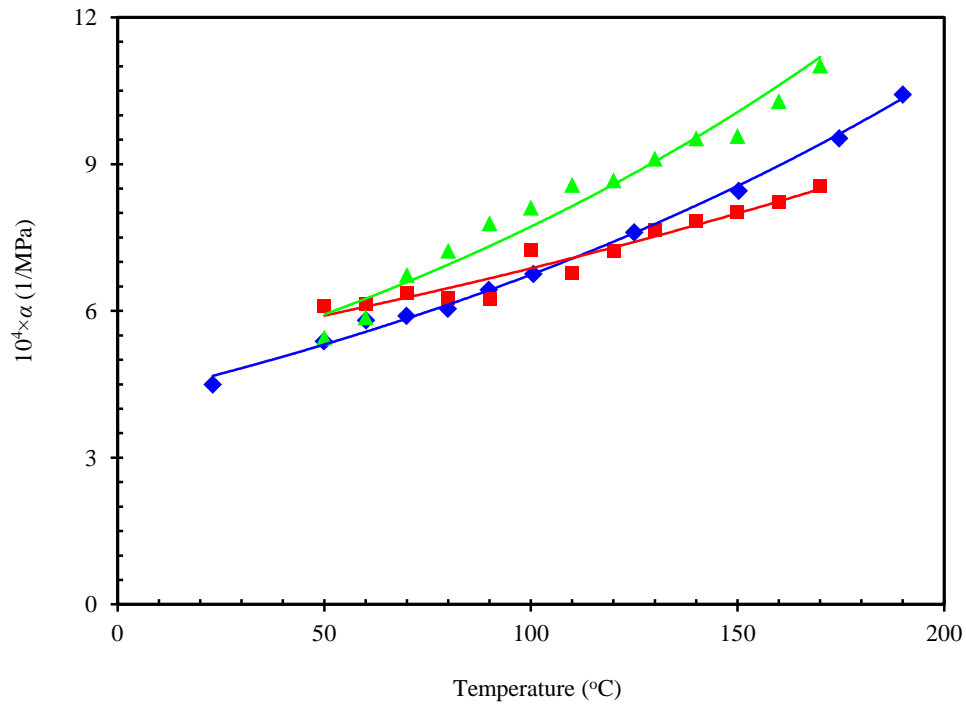


Figure 3–5: Coefficient α of equation 3-1 as a function of temperature for three different bitumens; ♦, Surmont; ■, MacKay River; ▲, JACOS.

Table 3–7 summarizes the average absolute relative deviation (AARD) and maximum absolute deviation (MAD) for the cases considered. The correlated values show a maximum absolute deviation of $\pm 1.7 \text{ kg/m}^3$ from the measured values. As expected, the best results are obtained with the second order function for ρ_0 and an exponential function for α .

Table 3–7: Average absolute deviation (AARD) and maximum deviation (MAD) of calculated densities.

Bitumen	ρ_0	Linear		Second Order		
		α	AARD (%)	MAD	AARD (%)	MAD
Surmont	Linear		0.021	0.6	0.017	0.5
	Exponential		0.029	0.7	0.016	0.5
MacKay River	Linear		0.058	1.2	0.032	1.0
	Exponential		0.055	1.2	0.032	0.9
JACOS	Linear		0.097	2.8	0.046	1.7
	Exponential		0.091	2.4	0.050	1.7

3.2.2. Viscosity of Bitumens

The viscosity of the bitumen samples was also measured using the Cambridge viscometer equipped with sensor SPC-372 at temperatures up to 200°C over the pressure range atmospheric pressure to 14 MPa. The viscometer was factory calibrated, requiring only the use of appropriate piston for the viscosity measurement. Three different pistons corresponding to different temperature ranges were used for viscosity measurements.

The measured data show that the viscosity of bitumen increases with increasing pressure and decreases with increasing temperature. The viscosity of a pure and simple component is not highly sensitive to pressure and is not affected by a moderate pressure increase. However, at the same temperature and over similar pressure increments, the bitumen viscosity increases significantly (near 50% increase in the viscosity from the lowest pressure to the highest pressure). This is explained by the structure of bitumen. Bitumen is composed of a variety of components including asphaltenes. Asphaltenes are a fraction of bitumen made up of complex molecules with a high ratio of carbon to hydrogen that are insoluble in normal alkanes. Changes in pressure affect the viscosity of complex molecules more than molecules with a simple structure (Reid et al. 1977; Mehrotra and Svrcek 1986). The impact of temperature change on bitumen viscosity is more pronounced than the effect of pressure.

The viscosity data were fitted with the two correlations proposed by Mehrotra and Svrcek (1986). The correlations take into account the impact of pressure and temperature on the bitumen viscosity and the authors examined the developed correlations for their viscosity measurements over the temperature and pressure ranges of 43 to 120°C and 0 to 10 MPa. Mehrotra and Svrcek (1986) presented the following two empirical correlations for the viscosity of solvent-free bitumen,

$$\ln(\mu_B) = \exp[b_1 + b_2 \ln(T)] + b_3 P_g \quad 3-6$$

$$\ln(\ln(\mu_B)) = [b_1 + b_2 \ln(T)] + b_3 P_g \quad 3-7$$

in which μ_B is the bitumen viscosity in mPa.s, T is the temperature in K, and P_g is the gauge pressure in MPa. Equation 3-6 represents a linear variation for the logarithm of viscosity as a function of pressure while in equation 3-7, a linear relationship between the pressure and double logarithm of viscosity is considered. The constants for equations 3-6 and 3-7 are summarized in Table 3–8 along with the coefficients fitted by other authors for Athabasca bitumen. The regression of the coefficients was performed using a MATLAB subroutine. The AARDs of the correlated results from the experimental values are also summarized in Table 3–8. A comparison of AARDs reveals that two models show large deviations when they are applied to our viscosity measurements. This could be due to the wider temperature range (50 to 190°C) considered in this study compared to the Mehrotra and Svrcek (1986) study.

A closer examination of the best fitted coefficients presented in Table 3–8 reveals that the regression of the experimental data results in almost the same coefficients for Surmont and MacKay River bitumens. As will be presented later, the correlated viscosity of Surmont and MacKay River bitumens are nearly identical. JACOS bitumen also has similar viscosity values to those reported for Athabasca bitumen by Mehrotra and Svrcek (1986). This can be observed by comparing the best fitted coefficients of two bitumen samples.

Table 3–8: Coefficients of the correlation equations for the viscosity of different bitumens (equations 3-6 and 3-7).

Coefficients	equation	b_1	b_2	b_3 (MPa ⁻¹)	AARD (%)
Surmont Bitumen	3-6	25.65193	-4.04208	0.031101	8.4
	3-7	24.84525	-3.90450	0.004723	9.2
MacKay River Bitumen	3-6	25.42828	-4.00814	0.031285	8.2
	3-7	24.56448	-3.86113	0.005137	7.1
JACOS Bitumen	3-6	23.94318	-3.76445	0.040273	8.4
	3-7	22.92858	-3.59230	0.007243	3.4
Athabasca Bitumen	3-6	23.42920	-3.67720	0.0345755	2.8
Mehrotra and Svrcek (1986)	3-7	22.85150	-3.57840	0.00511938	1.8

A comparison of the magnitude of coefficient b_3 in three bitumens demonstrates that JACOS bitumen has a larger b_3 value than Surmont and MacKay River bitumens. This shows that the viscosity of JACOS bitumen is more pressure dependent than the other two bitumens. For example, at the temperature of 50°C, an increase in pressure from 1 to 10 MPa results in a 75% increase in the JACOS bitumen viscosity while for the MacKay River bitumen, viscosity increases only 50%.

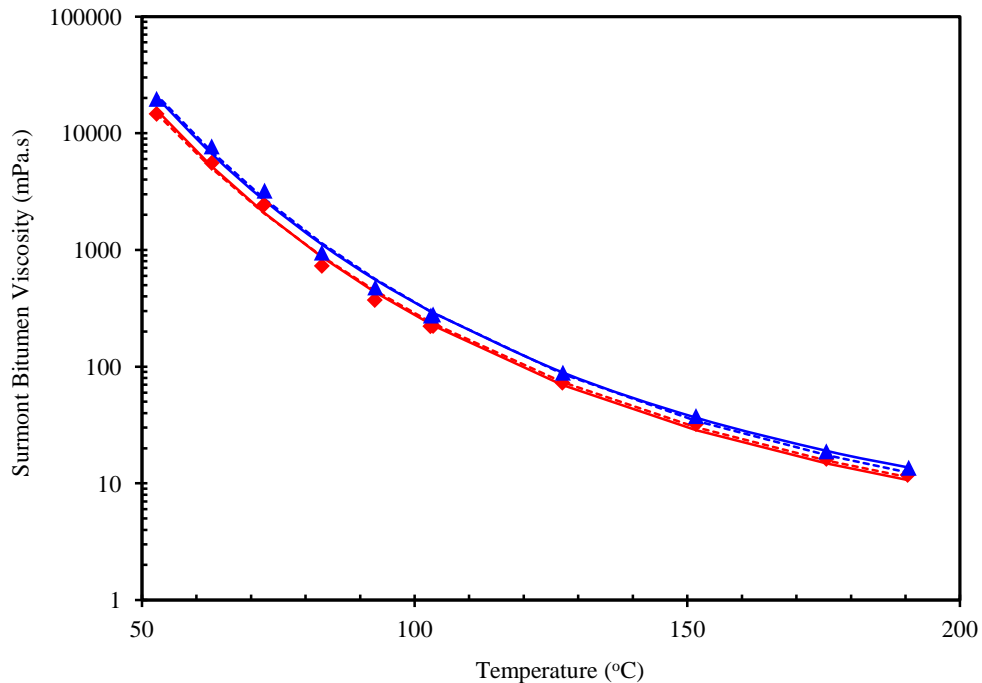


Figure 3-6: Viscosity of Surmont bitumen as a function of temperature at two different pressures; \blacklozenge , 2 MPa; \blacktriangle , 10 MPa; solid lines, equation 3-6; dashed lines, equation 3-7.

The correlated data for two viscosity correlations using the coefficients listed in Table 3-8 are presented in Figures 3-6 to 3-8. Figure 3-6 shows the measured and correlated viscosity data versus temperature at different pressures for Surmont bitumen. Figures 3-7 and 3-8 illustrate the same results for MacKay River and JACOS bitumens, respectively. In these plots, the solid and dashed lines denote the results correlated by equations 3-6 and 3-7, respectively, and the symbols show the experimental data. The figures illustrate that the viscosity of bitumens increases with pressure and decreases with

temperature. The impact of temperature on the bitumen viscosity is more pronounced than the effect of pressure.

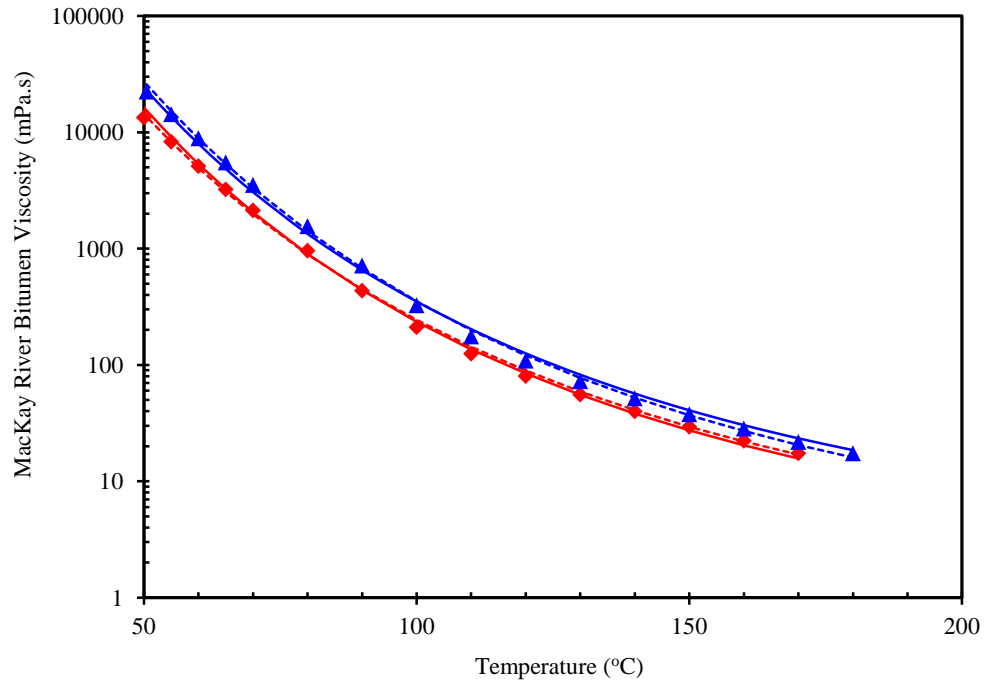


Figure 3-7: Viscosity of MacKay River bitumen as a function of temperature at two different pressures; \blacklozenge , 1 MPa; \blacktriangle , 14 MPa; solid lines, equation 3-6; dashed lines, equation 3-7.

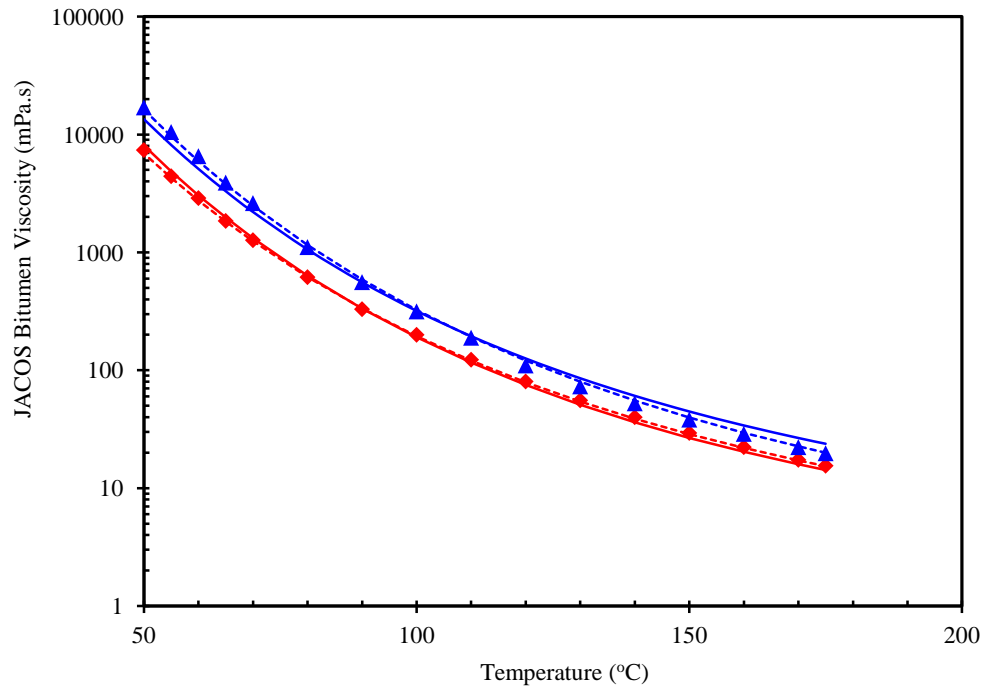


Figure 3-8: Viscosity of JACOS bitumen as a function of temperature at two different pressures; \blacklozenge , 1 MPa; \blacktriangle , 14 MPa; solid lines, equation 3-6; dashed lines, equation 3-7.

As depicted in Figures 3–6 to 3–8, the viscosity data are well fitted with two empirical correlations. The results of two models at low temperatures are the same. However, as the temperature increases, the deviation of two models from each other becomes more pronounced. Overall, two models correlate the viscosity data well over the studied pressure and temperature ranges. Nevertheless, on the basis of AARDs, equation 3-7 results in lower deviations.

Figure 3–9 presents a comparison of the viscosity of different bitumens over the temperature range of 25 to 200°C at two pressures (0.1 and 10 MPa). The results show that the viscosity of Surmont bitumen is higher than that of other bitumens. JACOS bitumen has the lowest viscosity and the viscosity data of JACOS bitumen are almost identical to the data of Athabasca bitumen reported by Mehrotra and Svrcek (1986) at atmospheric pressure. At 10 MPa, JACOS bitumen shows higher viscosity than Athabasca bitumen.

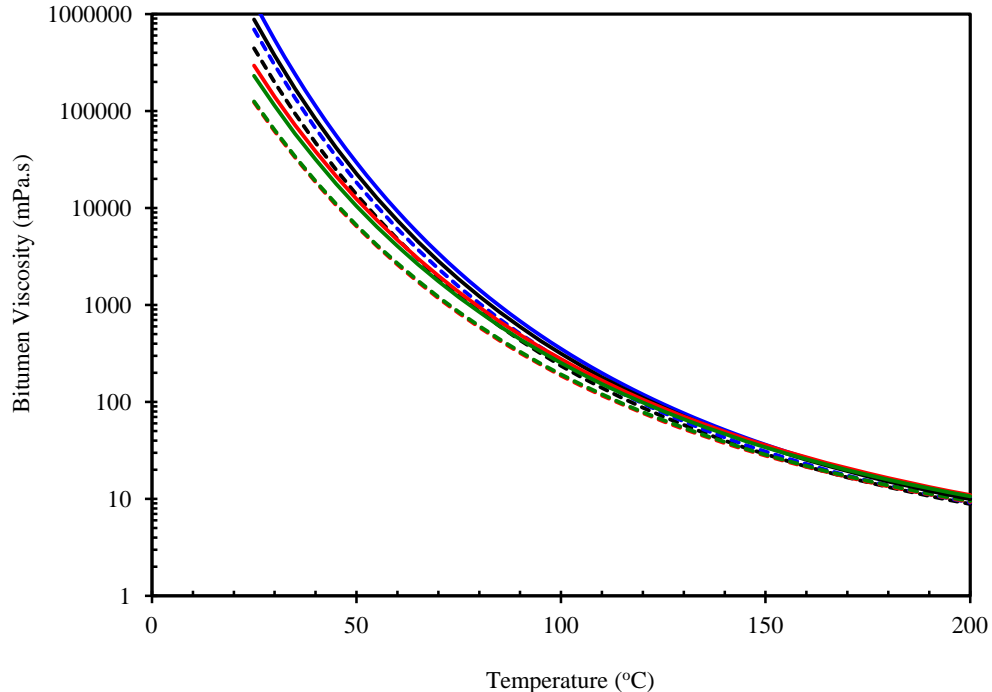


Figure 3–9: Viscosity of different bitumens as a function of temperature at two different pressures; ----, 0.1 MPa; —, 10 MPa; blue color, Surmont; black color, MacKay River; red color, JACOS; green color, Athabasca bitumen reported by Mehrotra and Svrcek (1986).

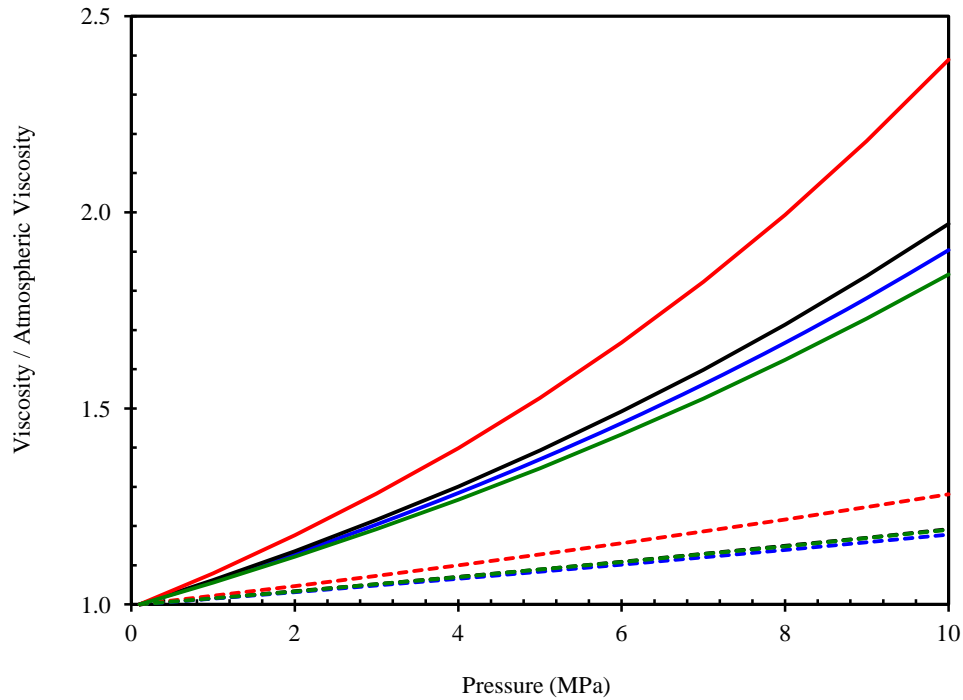


Figure 3–10: Viscosity ratio of different bitumens as a function of pressure at two different pressures; ----, 150°; —, 25°C; blue color, Surmont; black color, MacKay River; red color, JACOS; green color, Athabasca bitumen reported by Mehrotra and Svrcek (1986).

Figure 3–10 shows the pressure dependency of different bitumens calculated from equation 3-7 at two different temperatures. As depicted in the figure, the viscosity of JACOS bitumen is more pressure dependent than that of other bitumens. As the temperature increases, the pressure dependence of viscosity is reduced. At the temperature of 150°C, the viscosity ratios of Surmont, MacKay River, and Athabasca bitumens overlies each other. This indicates that these three bitumens have a similar viscosity increase under the pressure increment.

3.3. Compositional Analysis

Before the phase behaviour experiments, the bitumen samples were subjected to compositional analysis to obtain carbon number distributions up to C_{100} . The compositional analysis was done using the standard test method, ASTM D7169. This method provides useful information and analyzes the amount of residue by the

determination of the distribution of boiling points in petroleum fractions, vacuum residues, and crude oils. The distribution of the boiling points and the intervals of cut points in residues and crude oils are determined using a high-temperature gas chromatography. An external standard method is used to determine the amount of residue (or sample recovery). This method relies on the applicability of SimDis for the oil samples that cannot be completely distilled using the chromatographic system. With this standard method, the elution of components and their boiling point distribution at temperatures up to 720°C is determined. At this temperature, the component $n\text{-C}_{100}$ is eluted. The boiling point distributions for three bitumen samples are given in Table 3–9.

Table 3–9: Compositional analysis of bitumen samples.

%Off	MacKay River	JACOS*	Surmont
IBP	200.3	221.7	192.4
1	218.5	238.1	213.2
2	242.2	256.3	236.1
3	258.5	268.2	252.7
4	271.4	278.6	265.7
5	283.4	287.6	277.6
6	293.2	294.9	288.4
7	301.7	301.4	297.1
8	309.6	307.6	305.2
9	316.9	313.5	312.8
10	324.2	319.2	320.1
11	331.0	324.9	327.2
12	337.8	330.2	334.1
13	344.3	335.5	341.0
14	350.4	340.8	347.5
15	356.4	345.9	353.8
16	362.4	350.7	360.1
17	368.2	355.5	366.3
18	374.1	360.4	372.5
19	379.9	365.2	378.8
20	385.7	369.8	385.1
21	391.6	374.7	391.3
22	397.4	379.5	397.5
23	403.1	384.3	403.5
24	408.6	389.1	409.4
25	413.9	394.0	415.0
26	419.1	398.7	420.3
27	424.1	403.5	425.6
28	429.2	408.0	431.0
29	434.3	412.5	436.4
30	439.6	416.8	441.9
31	444.8	420.9	447.7
32	450.4	424.9	453.2
33	455.6	429.1	458.8

34	461.0	433.2	464.6
35	466.6	437.4	470.3
36	472.1	441.7	476.1
37	477.7	446.1	482.0
38	483.5	450.6	488.2
39	489.6	454.8	494.6
40	495.7	459.2	500.4
41	501.3	463.8	506.2
42	507.0	468.4	512.1
43	512.7	472.9	518.1
44	518.5	477.5	524.4
45	524.7	482.2	531.2
46	531.4	487.1	537.7
47	537.8	492.1	544.1
48	544.2	497.1	550.9
49	550.9	501.6	557.8
50	557.8	506.3	564.7
51	564.7	511.0	571.2
52	571.2	515.8	577.7
53	577.6	520.7	584.2
54	584.2	526.0	590.4
55	590.5	531.4	596.3
56	596.5	536.7	602.1
57	602.4	541.9	607.8
58	608.3	547.2	613.2
59	613.8	552.8	618.5
60	619.3	558.3	623.7
61	624.7	563.7	628.5
62	629.6	569.0	633.0
63	634.2	574.2	637.3
64	638.7	579.5	641.7
65	643.2	584.8	645.9
66	647.6	590.1	649.9
67	651.6	595.2	653.7
68	655.4	600.2	657.1
69	659.3	605.4	661.4
70	664.0	610.5	665.9
71	668.9	615.5	670.5
72	673.4	620.7	674.6
73	678.5	625.6	679.9
74	683.7	630.4	684.7
75	688.7	635.0	689.5
76	693.3	639.7	693.8
77	698.2	644.5	698.8
78	703.1	649.3	703.5
79	707.8	653.8	708.0
80	713.3	658.2	713.3
81	718.5	663.9	718.4
82	723.9	669.8	723.8
83	729.6	675.0	729.5
84	735.6	681.4	735.4

* de-asphaltened bitumen

3.4. SARA Analysis

The SARA analysis is based on the separation of different fractions (saturates, aromatics, resins, and asphaltenes) using a *n*-paraffin solvent and the adsorption of fractions on clay or silica gel. The saturate fraction contains the lightest components and non-polar hydrocarbons. This includes *n*-paraffins, iso-paraffins and naphthenic groups. The aromatic fraction is composed of the components that have benzene rings. The resin fraction includes polynuclear aromatics with higher molecular weight and density. This fraction is more polar and has higher heteroatom content compared to the aromatic fraction. The last fraction is asphaltene that is defined as the materials insoluble in *n*-paraffins but soluble in aromatic solvents. The asphaltene has particularly high molecular weight and is responsible for considerably increasing the viscosity of bitumen.

The asphaltene fraction of bitumen is precipitated with a paraffinic solvent such as pentane or heptane. The resin fraction is adsorbed on attapulgus clay while the aromatic fraction is adsorbed on silica gel. Figure 3–11 shows the procedure for differentiating the fractions.

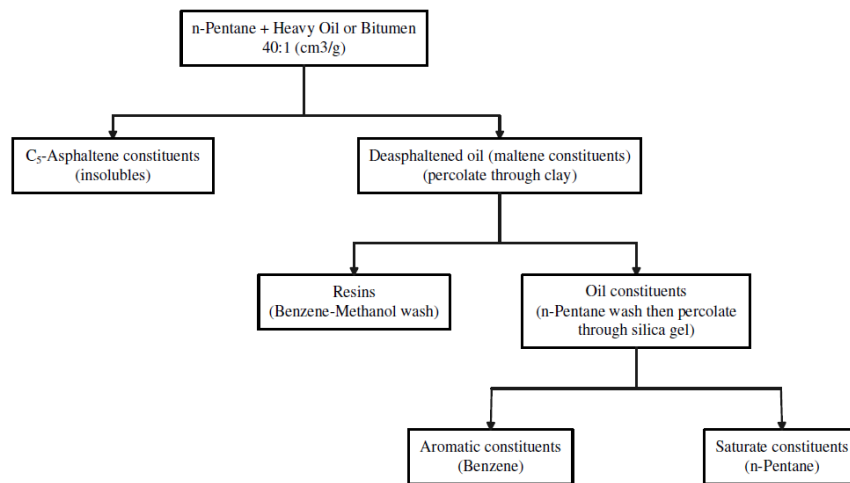


Figure 3–11: Step-wise procedure for SARA analysis (Speight 2007).

The SARA analysis was performed on the samples to determine the different fractions (saturate, aromatic, resin, and asphaltene) in bitumen samples. The asphaltene

fraction of bitumen was precipitated using heptane as the precipitant. The SARA compositional analysis of different bitumens was completed using the ASTM D2007 method and the results are presented in Table 3–10.

Table 3–10: SARA analysis for bitumen samples.

Fraction	JACOS*	MacKay River	Surmont
Saturates	18.72	11.76	12.26
Aromatics	33.20	57.00	40.08
Resins	28.27	21.61	36.53
Asphaltenes	17.35	9.62	11.13

* *n*-pentane as precipitant

3.5. Molecular Weight

The molecular weight of a compound can be measured by two different methods: vapour pressure osmometry and cryoscopy method. The vapour pressure osmometry is based on the change in the boiling point of a solvent when a solute is added (Chung et al. 1979). The osmometer has a column filled with the pure solvent and a column with the solvent/solute solution. Thermistors produced the electrical signal of differential heating to achieve vapour equilibrium in each column. A plot of concentration as a function of electrical differential can be made with the measurement of the solutions of different concentrations of solute with a known molecular weight.

The cryoscopy method is based on freezing point depression. Freezing point depression is the change in the freezing point of a solvent by dissolving a solute because the solution has a lower freezing point than a pure solvent (Cryette 1994). The change in the freezing point can be used to determine the molecular weight of the solute.

When a solute is dissolved in a solvent, the freezing temperature is lowered in proportion to the number of moles of solute added to solution. This property, known as the freezing-point depression, is a colligative property dependent on the ratio of solute and solvent particles, not on the nature of the solute. The properties of a solution differ from those of a pure solvent due to interactions that take place between the solute and

solvent molecules. These properties are dependent only upon the number of particles (ions or molecules) that are dissolved in the solvent and not on the identity of the particles.

3.5.1. Cryoscopy Method

The freezing points of different solution concentrations with a known solute and a known solvent can be used to generate the calibration curves. Thus, the molal freezing point depression constant of the solvent is determined, which, together with the known molecular weight of the solvent can be used to determine the molecular weight of a given compound. When a particular solute is dissolved in a solvent, the following expression holds true:

$$\Delta T = T_f^\circ - T_f = K_f \varepsilon \quad 3-8$$

The terms T_f° and T_f refer to the freezing-point temperatures of the pure solvent and solution, respectively. The term “ ε ” indicates the molality of the solution, which is defined as the number of moles of solute per 1000 g of solvent. This quantity is used, rather than molarity, because it is not temperature dependent. The constant, K_f , is referred to as the freezing-point-depression constant and is dependent only upon the solvent. This value is obtained for a prepared mixture and can be converted to molecular weight.

Before any molecular weight measurements, the instrument should be calibrated to find the freezing-point-depression constant for the solvents. Generally, two solutions (depending on the solute) can be considered, aqueous and non-aqueous. For the aqueous solution, water is used as the solvent. Benzene is selected as the solvent for non-aqueous solutions. The calibration of the instrument was done with the prepared solutions provided by the factory.

3.5.2. Accuracy of Measurements

Following the calibration of the instrument that is utilized for the freezing-point depression measurement using solutions provided by the factory, the accuracy of measurements for different solutes was examined. An alcohol, 1-propanol, and an organic compound, *n*-tetradecane, were selected. To determine the effect of the molality of the solution on the accuracy of the measurements, varieties of solutions were considered.

The molecular weight of 1-propanol is 60.1 g/g-mol. Distilled water was used as the solvent and the molecular weight of 1-propanol was measured at two different molal solutions. Table 3–11 summarizes the measured molecular weight and the percentage error. The data show that the measurements are accurate within 1% and the measurements are not affected when the solutions are prepared at different molal concentrations.

Table 3–11: Molecular weight of 1-propanol using freezing point depression method.

Solution (molal)	Test No.	Cryette Reading (ΔT)	MW (g/mol)	Error (%)
0.3022	1	560	60.3173	0.362
	2	561	60.2098	0.183
	3	560	60.3173	0.362
0.1561	4	293	59.5532	0.910
	5	294	59.3507	1.247
	6	293	59.5532	0.910

For non-aqueous solutions, it is necessary to calibrate the instrument using benzene as the solvent. The calibration procedure explained in the manual was followed, and the molecular weight of *n*-tetradecane was measured using the benzene as the solvent. Table 3–12 presents the measured values for the molecular weight and the percentage error. In this case, the measurements are accurate within 2% compared to the molecular weight of *n*-tetradecane, which is 198.39 g/g-mol.

Table 3–12: Molecular weight of *n*-tetradecane using freezing point depression method.

Test No.	Cryette Reading (ΔT)	MW (g/mol)	Error (%)
1	536	201.29	1.5
2	535	201.67	1.7
3	537	200.92	1.3

3.5.3. Molecular Weight of Bitumen Samples

After the instrument was calibrated and the accuracy of the measurements was examined, the molecular weight of three bitumen samples was measured. Benzene was used as solvent for the measurements. The solutions were prepared with 0.15 molal concentrations. This value is within the range recommended by the factory for molecular weight measurements. Table 3–13 summarizes the measured molecular weights of JACOS, Surmont, and MacKay River bitumens for four different measurements.

Table 3–13: Repeated measurements for the molecular weight of bitumen samples.

Test No.	Bitumen	m_{Benzene} (g)	m_{Bitumen} (g)	ΔT	MW (g/mol)
1	JACOS	32.0180	2.8015	837	535.23
2	JACOS	32.0180	2.8015	849	527.67
3	JACOS	32.0180	2.8015	849	527.67
4	JACOS	32.0180	2.8015	841	532.68
5	Surmont	32.0440	2.7350	811	538.84
6	Surmont	32.0440	2.7350	804	543.53
7	Surmont	32.0440	2.7350	806	542.18
8	Surmont	32.0440	2.7350	821	532.28
9	MacKay River	32.0120	2.5710	797	515.94
10	MacKay River	32.0120	2.5710	794	517.89
11	MacKay River	32.0120	2.5710	804	511.45
12	MacKay River	32.0120	2.5710	815	504.55

Table 3–14 lists the average molecular weights of JACOS, Surmont and MacKay River bitumens. The measured values are precise within $\pm 1.5\%$. Based on the measurements, Surmont bitumen is heavier than JACOS and MacKay River bitumens.

Table 3–14: Molecular weight of bitumen samples.

Bitumen	MW (g/mol)
JACOS	530.8 ± 4.4
MacKay River	512.5 ± 6.9
Surmont	539.2 ± 7.9

Chapter 4: Phase Behaviour of Bitumen/Ethane Mixtures

This chapter presents the vapour-liquid and liquid-liquid phase equilibria for bitumen/ethane mixtures and their applications for bitumen recovery processes. The results of vapour-liquid equilibria cover the solubility, density, and viscosity measurements of the saturated liquid phase, K-values, and GOR. For liquid-liquid equilibrium conditions, the properties of equilibrium phases as well as extraction yield were studied. The effects of pressure, temperature, and overall solvent concentration on the phases' composition, density, viscosity, and compositional analysis have been evaluated. The generated vapour-liquid and liquid-liquid equilibrium data in this chapter are applied for equation of state modelling in Chapter 8.

4.1. Introduction

Ethane is one of the simplest hydrocarbons and organic components with a chemical formula of C_2H_6 and is comprised of two carbon atoms and six hydrogen atoms with a molecular weight of 30.07 g/mol. Ethane is one of the constituents of natural gas produced from gas reservoirs. Ethane's boiling point, critical temperature and pressure are $-88.6^\circ C$, $32.27^\circ C$ and 4.88 MPa, respectively (Yaws 1999). The critical temperature of ethane is close to ambient temperature which makes it a potential candidate for supercritical extraction process in the petrochemical industry. Ethane can also be used for conventional oil recovery in miscible and immiscible displacement processes. However, its application for heavy oil and bitumen recovery has been limited to laboratory experiments, and no field-scale project has been reported yet. Lim et al. (1995) did a bench-scale sand pack flood test with Cold Lake bitumen using both subcritical and supercritical ethane. The results showed that, by using supercritical ethane, the bitumen production rate can be increased by an average of 25% with the rate being almost twice that of subcritical ethane in the first cycle. In addition, the supercritical ethane

experiments had a 25% higher solvent recovery when the apparatus was depressurized at the end of the experiment. The experimental data indicated that supercritical ethane performs better than subcritical ethane for *in-situ* bitumen recovery.

Ethane can also be considered as a gaseous additive to steam-based bitumen recovery processes. Using the gaseous additive for steam-based recovery processes is not a new idea; experimental and modelling studies have shown that, in steam-based process such as SAGD, a gaseous solvent can be co-injected with steam to improve the process performance. Field results by Sperry (1981) and modelling and simulation results by Weinstein (1974) indicated encouraging results from the application of a gas additive to steam in thermal processes for heavy oil and bitumen recovery methods.

The results of field trials in the Paris Valley field reported by Meldau et al. (1981) confirmed the applicability of a gas additive in steam-based processes. Experimental studies by Pursley (1975) confirmed the field and simulation results. Redford and McKay (1980) conducted three-dimensional (3-D) physical model experiments with the co-injection of methane, ethane, propane, butane, pentane, natural gasoline, and naphtha with steam. The results showed improvement in the oil recovery rate with the co-injection of the additives with steam.

Overall, additives can improve the performance of the steam-based recovery processes. As a result, Butler (1999) proposed a process called Steam and Gas Push (SAGP) which can improve the performance of the SAGD process. In this process, non-condensable gases are co-injected with steam. Physical model experiments (Butler et al. 1999, 2000; Jiang et al. 2000) confirmed the beneficial effect of non-condensable gas additives. The experiments showed that the non-condensable gas can form insulation at the edge of the chamber and reduce the heat loss. The effect of non-condensable gas co-injection on the SAGD process has been also investigated by several authors (Edmund et al. 1994; Goite et al. 2001; Bagci and Gumrah 2004; Al-Murayri et al. 2011).

During the SAGP process, ethane is in vapour form in the steam chamber for a given steam temperature and pressure. It moves to the edge of the chamber and forms an

insulative layer at the edge of the chamber which reduces the heat loss. In addition, ethane has a considerable solubility in bitumen compared to methane and nitrogen. Thus, it diffuses and dissolves in bitumen and reduces the bitumen viscosity. The viscosity reduction by ethane dissolution increases the production rate and ultimate oil recovery. Even if diffusion and dispersion play an important role in the process, the understanding of the bitumen/ethane interaction is critical for the understanding and optimization of the process. The equilibrium concentration and the solubility of ethane are governed by the complex interaction between bitumen and ethane.

In addition to the oil recovery processes, ethane is a potential candidate for bitumen upgrading and supercritical extraction processes (Rose et al. 2001). Ethane has favourable critical properties; and, at supercritical condition, it behaves as a liquid-like solvent and its solubility increases significantly. The main advantage of supercritical extraction is the high solvent recovery. That is, the solubility of solvent can dramatically change with the adjustment of the operating conditions and thus most of solvent can be recovered. The critical temperature of ethane is quite low; therefore, the extraction process can be operated at a lower temperature than that of the distillation process and, as result, requires lower energy (Parkinson and Johnson 1989).

Supercritical extraction has been a well known technique for more than a century with a wide range of applications in the food industry (Zosel 1978); however, its application for heavy oil and bitumen extraction is relatively new; and, a significant gap exists in the literature. Field and commercial applications of supercritical extraction for bitumen using ethane require phase behaviour data. Phase behaviour studies using supercritical fluids and bitumen are limited and can be categorized into those with constant solvent-to-bitumen ratios and those with semi-batch extractors. In the second category, the extractor is fed with a fixed amount of bitumen or heavy oil. The solvent then flows through the extractor and withdraws the lighter components. The first category has wider applications for modelling and thermodynamic studies of bitumen/ethane systems while the semi-batch method is more practical for field application.

In summary, ethane can be used for the recovery and processing of heavy oil and bitumen, as a gas additive to steam-based recovery processes or in supercritical extraction processes for surface upgrading. The phase behaviour and thermodynamic properties of bitumen/ethane mixtures are extremely important to the design and optimization of these processes.

4.2. Literature Background

There are a number of experimental investigations that focus on the phase behaviour of bitumen/ethane systems available in literature; however, these studies are confined to conditions where the bitumen and ethane form vapour and liquid phases at equilibrium condition. Mehrotra and Svrcek (1985a, 1985b, 1985c, 1988a), Fu et al. (1988) and Frauenfeld et al. (2002) measured the solubility of ethane in bitumen and its corresponding saturated liquid properties.

Mehrotra and Svrcek (1985a, 1985b, 1985c, 1988a) reported the experimental data on the solubility and saturated phase density and viscosity for bitumen/ethane mixtures at temperatures up to 115°C and at the pressures up to 10 MPa. The authors measured the experimental data for four different bitumens: Athabasca, Peace River, Cold Lake, and Wabasca.

Fu et al. (1988) measured the vapour-liquid equilibrium properties of Cold Lake bitumen / ethane mixture using a modified Ruska rocking cell apparatus at temperatures up to 150°C and the pressures up to 12 MPa. The authors only reported the composition of phases at equilibrium condition during the phase behaviour studies. More recently, Frauenfeld et al. (2002) measured the solubility of ethane in a Cold Lake blend oil at a temperature of 15°C and in Lloydminster Aberfeldy oil at a temperature of 19°C and at the pressures up to 3 MPa.

The study of liquid-liquid separation and partitioning of components in the bitumen/solvent systems can provide valuable information for surface upgrading methods

and also the performance of solvent-based recovery processes. In addition to the vapour-liquid equilibrium studies, the liquid-liquid separation and extraction of light components from heavy crudes using ethane has been studied by Rose (1999) and Rose et al. (2001). They presented the supercritical extraction data for Peace River bitumen / ethane systems and found that extraction yields increased by both increasing the extraction pressure and decreasing the operating temperature. As temperature is reduced and pressure rises, the extracted oil becomes heavier. At higher temperatures or lower pressures, the extracted oil is lighter and has lower viscosities.

Lim et al. (1995) also evaluated the differences in the production rate of a sand pack saturated with Cold Lake bitumen using subcritical and supercritical ethane. No experimental data for liquid-liquid equilibrium, extraction of bitumen with ethane at ambient temperature, and partitioning of components within phases have been reported.

The available experimental data in the literature indicate that the data are limited to a temperature range of 22 to 114°C and the pressures up to 10 MPa. Few data for a high temperature condition (150°C) and liquid-liquid extraction have been reported. No experimental data for a wide range of temperatures (i.e. ambient to 200°C) including both vapour-liquid and liquid-liquid phases has been reported in the literature. In addition, no experimental data for physical and chemical properties of equilibrium phases as well as phase diagrams for bitumen/ethane mixtures have been reported.

In this research, phase behaviour experiments for the bitumen/ethane system have been conducted to consider both vapour-liquid and liquid-liquid equilibrium conditions. The liquid-liquid equilibrium was detected at the temperatures less than 30°C. In the case of the liquid-liquid equilibrium, two phases, solvent-enriched and asphaltene-enriched, exist at equilibrium condition. The former is mostly composed of solvent and some light components extracted from the bitumen phase. The latter mainly consists of the heavy components of bitumen, such as asphaltenes and resins, which cannot be extracted by solvent. The extraction yield depends on the temperature, pressure and solvent-to-bitumen ratio.

In this chapter, the phase behaviour study including phase partitioning and component distribution within the phases at equilibrium condition for Athabasca bitumen / ethane system has been considered over a temperature range of ambient to 200°C and at pressures up to 10 MPa. The experimental data are presented in three different sections: vapour-liquid equilibrium, liquid-liquid equilibrium, and phase diagrams.

4.3. Vapour-Liquid Equilibrium for Surmont Bitumen / Ethane Systems

Vapour-liquid experiments were conducted to determine the influence of pressure and temperature on the phase equilibrium properties of bitumen/ethane mixtures. The experiments were carried out at 20 different operating conditions; combination of four different temperatures (50, 100, 150, and 190°C) and five different pressures (1, 2, 4, 6, and 8 MPa). The details of each experiment, such as the amount of bitumen and solvent charged into the equilibrium cell, are presented in Table 4–1. The amounts of solvent and bitumen in each experiment are the required mass of each species to have both vapour and liquid phases at equilibrium condition and to obtain enough phase samples for solubility measurements. As expected, the weight fraction of ethane in the equilibrium cell increased with pressure and reduced with temperature due to variation of solubilities with temperature and pressure.

The results of the vapour-liquid experiments for Surmont bitumen / ethane systems are summarized in Table 4–2. The repeatability of the generated data was examined by repeating one experiment each at 50, 150, and 190°C: these data are presented in Table 4–3. As the data presented in the table show, the measurements of the solubilities in two experiments at similar conditions were in good agreement and the saturated phase densities were precise to less than 0.5 kg/m³. The deviation for the saturated liquid viscosities was less than 5%.

Table 4–1: Experimental design and feeding information for Surmont bitumen / ethane systems at temperature, T and pressure P .

T (°C)	P (MPa)	Equilibrium Cell		$P_{Equilibrium}$ (MPa)
		C ₂ H ₆ (g)	Bitumen (g)	
50	1	4	46	1.103
	2	7.5	42.5	2.103
	4	10	40	4.109
	6	11.25	45	6.101
	8	12.5	37.5	8.073
100	1	2.5	47.5	1.013
	2	5	45	1.958
	4	6	44	3.978
	6	7.5	42.5	6.025
	8	11.25	45	8.076
150	1	2.5	47.5	1.138
	2	5	45	1.999
	4	6	44	4.040
	6	7.5	42.5	6.025
	8	11.25	45	8.204
190	1.25	5	45	1.455
	2	5	45	2.185
	4	6	44	4.019
	6	7.5	42.5	6.039
	8	11.25	45	8.073

As Table 4–2 indicates, the dissolution of ethane in bitumen reduced the density and viscosity of the saturated liquid phase. Depending on the temperature, the decreasing trends of density and viscosity with the solubility of ethane were different. At a constant temperature, the solubility of ethane in bitumen increased with increasing pressure. Thus, the density and viscosity of saturated liquid phase showed a decreasing trend with the equilibrium pressure. Although pressure increases the density and viscosity of gas-free bitumen at a constant temperature, the dissolution of ethane in bitumen compensated for this effect and reversed the impact of pressure on the density and viscosity (reduction of density and viscosity with pressure).

For Surmont bitumen / ethane mixtures, a clear phase transition between two phases of vapour and liquid was observed for all experiments during the phase sampling at equilibrium condition. Figure 4–1 illustrates the density measurements and phase transitions for Surmont bitumen / ethane mixtures at different temperatures. As depicted in the figure, the volume of each phase and the saturated phase densities were measured during the course of experiments.

Table 4–2: Experimental vapour-liquid equilibrium properties for Surmont bitumen / ethane systems at $T = (50, 100, 150, \text{ and } 190)^\circ\text{C}$; P , pressure; ρ_s , saturated liquid density; μ_s , saturated liquid viscosity; w_s , weight fraction of ethane in saturated liquid phase.

T ($^\circ\text{C}$)	P (MPa)	$10^2 w_s$	ρ_s (kg/m^3)	μ_s (mPa.s)
51.3	1.103	1.76	974.7	1822
50.7	2.103	3.64	957.0	652
50.8	4.109	7.75	916.5	118
50.9	6.101	12.2	874.2	35.8
50.9	8.090	14.2	856.7	26.7
100.5	1.013	0.91	949.6	138
100.3	1.958	1.90	940.4	102
100.6	3.978	3.71	919.1	49.2
100.7	6.025	6.15	897.2	25.6
100.6	8.076	8.45	876.0	16.2
149.9	1.200	0.67	921.6	27.4
149.7	1.999	1.33	915.9	23.4
149.3	4.040	2.65	900.9	16.2
149.9	6.025	4.33	885.9	11.0
149.9	8.204	5.55	869.3	8.14
189.4	1.455	0.72	900.8	10.6
189.4	2.096	1.18	897.1	9.68
189.7	4.019	2.10	884.8	7.69
189.9	6.039	3.18	872.1	6.13
189.4	8.073	4.40	859.1	5.07

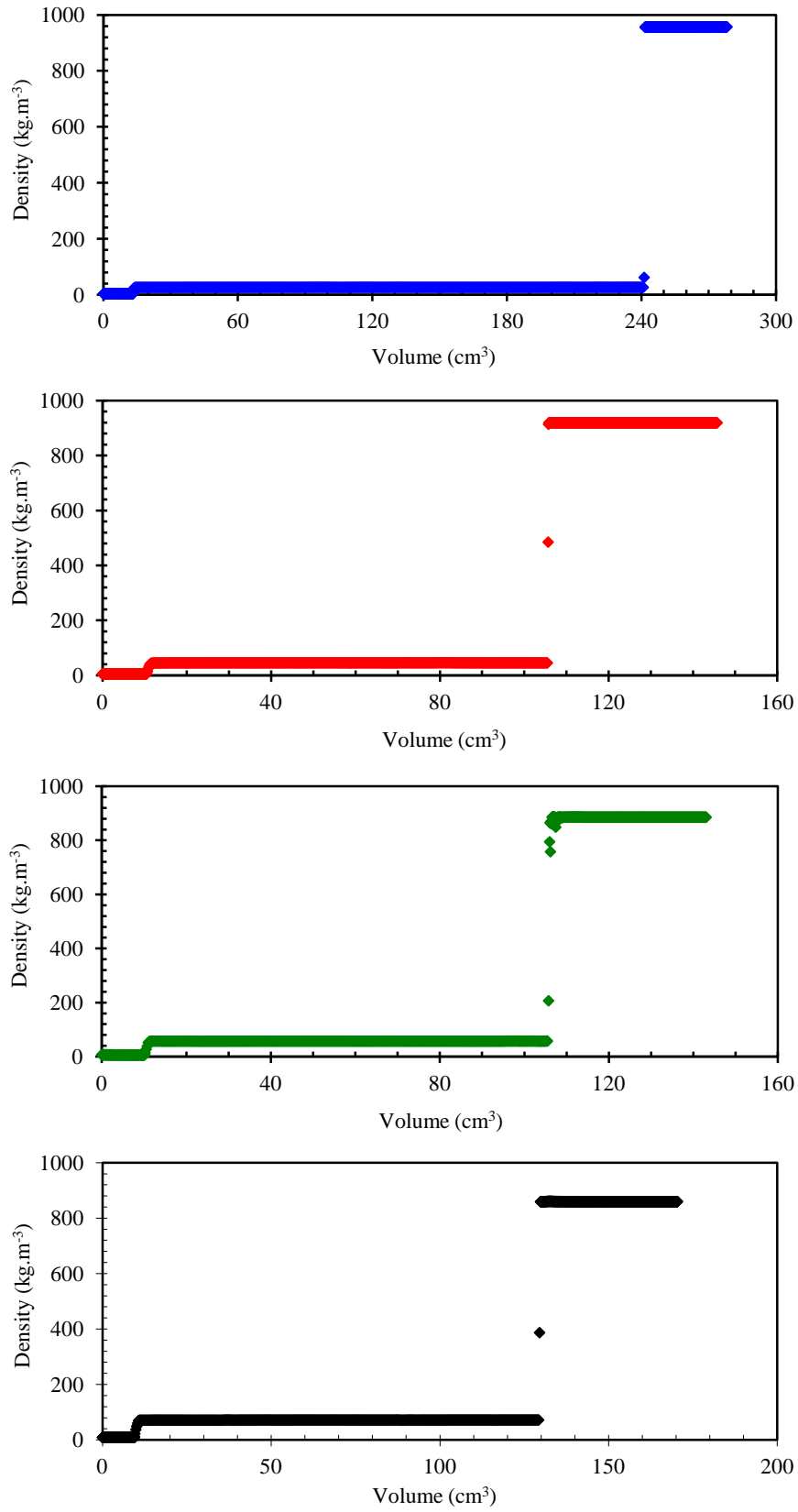


Figure 4-1: Phase transitions for vapour-liquid equilibrium study of Surmont bitumen / ethane mixtures; \blacklozenge , 50°C and 2 MPa; \blacklozenge , 100°C and 4 MPa; \blacklozenge , 150°C and 6 MPa; \blacklozenge , 190°C and 8 MPa.

Table 4–3: Experimental vapour-liquid equilibrium properties of repeated experiments at $T = (50, 150, \text{ and } 190)^\circ\text{C}$ for Surmont bitumen / ethane systems; P , pressure; ρ_s , saturated liquid density; μ_s , saturated liquid viscosity; w_s , weight fraction of ethane in saturated liquid phase.

T ($^\circ\text{C}$)	P (MPa)	$10^2 w_s$	ρ_s (kg/m^3)	μ_s (mPa.s)
50.9	8.073	14.2	854.1	24.2
	8.107	14.1	859.2	29.1
149.7	1.138	0.65	921.5	28.7
	1.241	----	921.5	26.7
	1.179	0.69	921.9	26.7
189.4	2.185	1.19	896.5	9.68
	2.006	1.17	897.6	----

4.3.1. Saturated Phase Properties

Figures 4–2 to 4–4 illustrate the experimental results for the Surmont bitumen / ethane systems for the temperatures greater than 50°C , in which the vapour-liquid equilibrium exists in equilibrium condition. The solubility measurements are shown in Figure 4–2, and Figures 4–3 and 4–4 demonstrate the ethane-saturated bitumen density and viscosity as a function of equilibrium pressure.

In Figure 4–2, the x -axis shows the equilibrium pressure and the y -axis indicates the measured solubilities of ethane in bitumen. The isotherms corresponding to each temperature are shown by different colours. The solubility of ethane in bitumen increases with pressure at a constant temperature and reduces with temperature at a constant pressure. The solubility of ethane varies with pressure more significantly at the lowest temperature (50°C) compared to the highest temperature (190°C). Generally, ethane has a much higher solubility in bitumen than methane at equal operating conditions and this behaviour is more significant at low temperatures. In this section, the temperature of 50°C is the lowest temperature considered, and the vapour-liquid equilibrium exists in the studied pressure range (< 8 MPa).

As depicted in Figure 4–2, the difference between the isotherms becomes more considerable as the temperature decreases from 190 to 50°C. The solubility curves demonstrate almost linear trends for the temperatures 100, 150, and 190°C. The linear increasing trend of solubility with pressure changes to a non-linear variation as the temperature decreases to 50°C. At this temperature, the solubility values flatten beyond a pressure of about 6 MPa. This behaviour was also observed by Mehrotra and Svrcek (1985a) for Athabasca bitumen / ethane mixtures. The authors found that, at three temperatures of 49, 80, and 107°C, the solubility of ethane in bitumen became flat beyond about 7-8 MPa. This indicated a formation of second liquid phase at equilibrium condition.

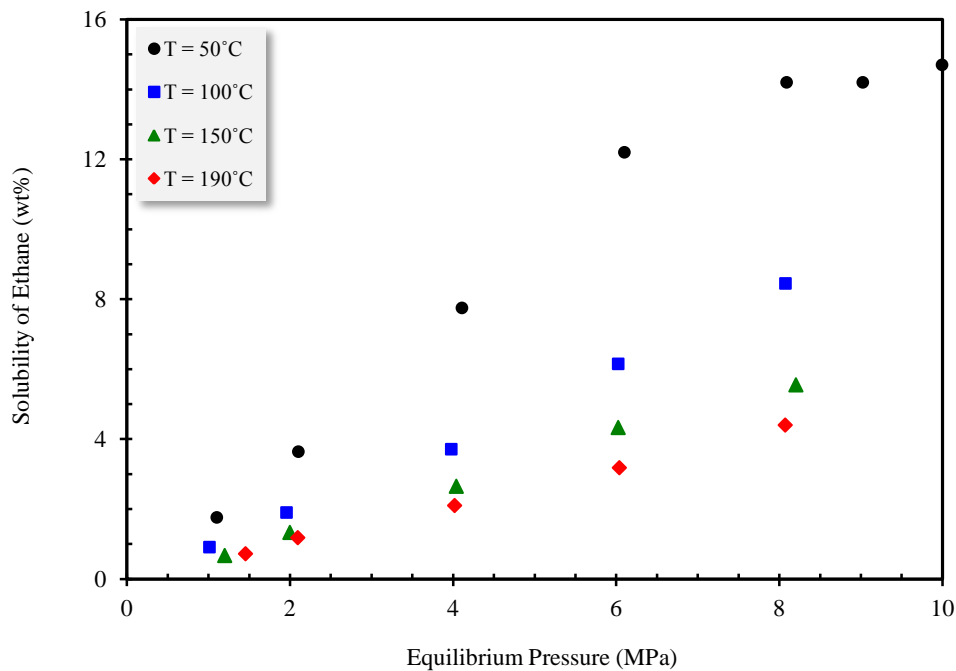


Figure 4–2: Measured solubility of ethane in Surmont bitumen as a function of pressure at different temperatures.

Figures 4–3 and 4–4 display the saturated bitumen density and viscosity as a function of pressure. The symbols on the y-axis are the density and viscosity of raw bitumen at the desired temperature without any dissolved ethane. These values are presented in these

figures to determine the impact of dissolved ethane on the density and viscosity of bitumen.

As anticipated from Figure 4–3, when ethane is dissolved into the bitumen sample, the viscosity of the ethane-saturated bitumen is significantly reduced, even at low equilibrium pressures. For instance, at the equilibrium pressure of 1.103 MPa and the temperature of 50.9°C, the viscosity of the mixture is 1822 mPa.s, which is about one tenth of the viscosity of the raw bitumen (18429 mPa.s) with no dissolved solvent. When the equilibrium pressure is increased to 8.073 MPa, the viscosity of the mixture is only 24.2 mPa.s, which is low enough for oil to be recovered from the reservoir.

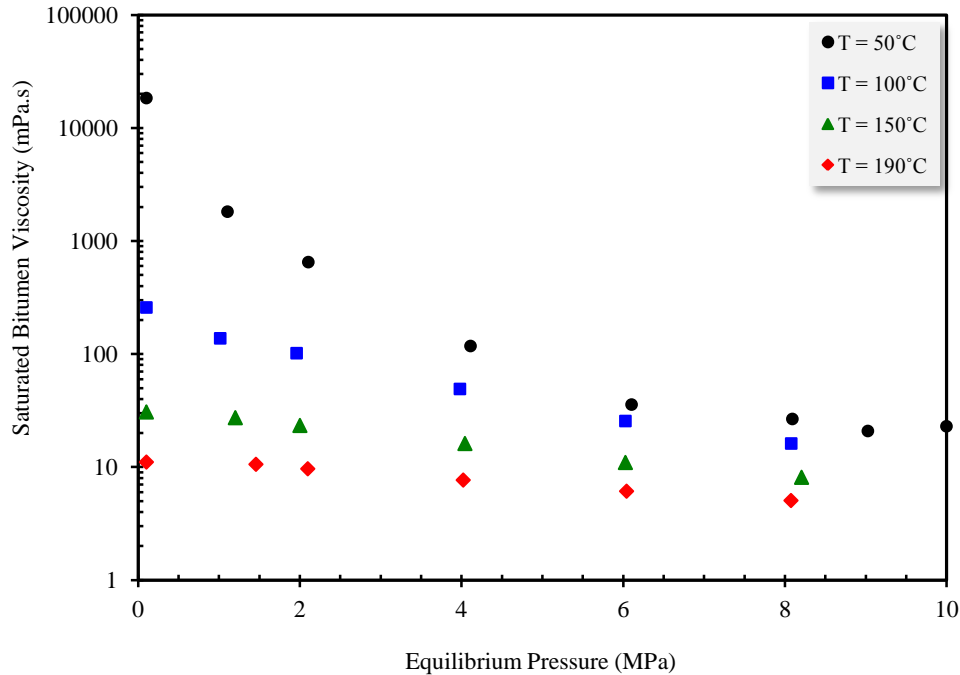


Figure 4–3: Viscosity of ethane-saturated Surmont bitumen as a function of pressure at different temperatures.

The viscosity of ethane-saturated bitumen significantly reduces with pressure at all temperatures. The variation of saturated bitumen viscosity with the equilibrium pressure has a linear trend for the temperatures of 100, 150, and 190°C. The same trend was observed for bitumen/methane system (Kariznovi et al. 2012a; Kariznovi 2013). However, at a temperature of 50°C, the viscosity shows a non-linear variation and the

viscosity reduction is considerable. This behaviour, as presented in Figure 4–4, is much more significant for density in which the ethane-saturated bitumen density at the temperature of 50°C crosses over other temperatures and reaches a value even lower than the one at 190°C. The solubility of ethane at the temperature of 50°C is much higher than those at 100, 150 and 190°C, particularly at the highest pressure (e.g. 8 MPa), causing a greater reduction in density. A noticeable behaviour in the saturated density and viscosity curves is observed at the temperature of 50°C and the pressures higher than 8 MPa in which the density and viscosity is not further decreased with the equilibrium pressure. The analysis of the vapour phase at these conditions shows the existence of light hydrocarbons. That is, some light hydrocarbon components are extracted from the bitumen phase into vapour phase.

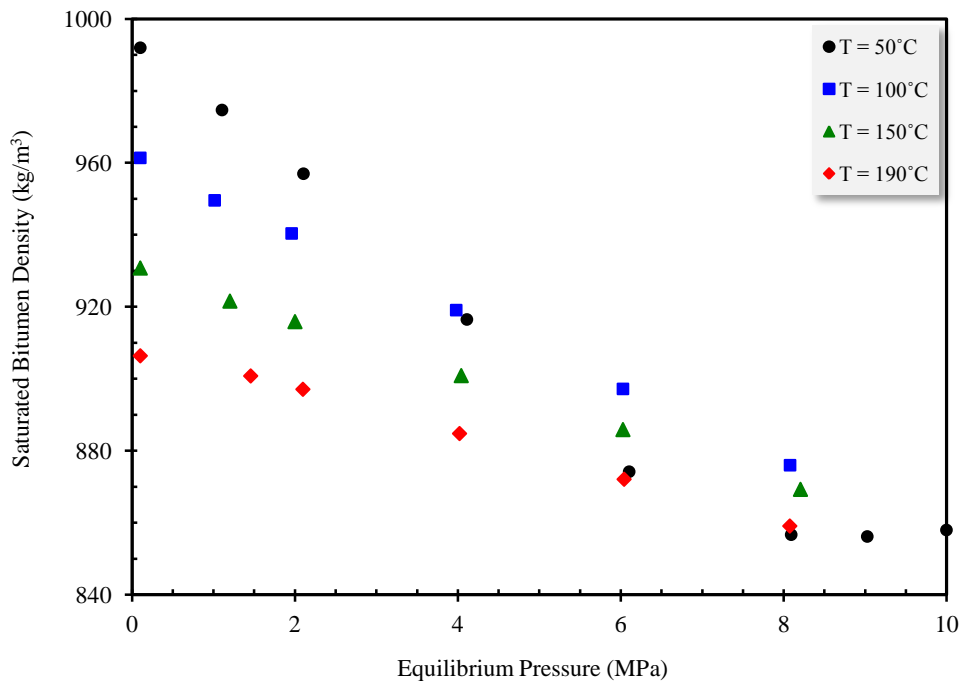


Figure 4–4: Density of ethane-saturated Surmont bitumen as a function of pressure at different temperatures.

As indicated in Figure 4–4, the variation of the saturated bitumen density with the equilibrium pressure is linear. Although the slope of variation changes with temperature,

the linear trend is observed for all temperatures. As previously mentioned, the linear decreasing trend of density with pressure reduces as the temperature increases.

A closer examination of the saturated viscosity data reveals that the impact of ethane dissolution in bitumen viscosity reduces as the temperature increases. For example, at the temperature of 50.9°C and a pressure of 8.073 MPa, the viscosity of the saturated liquid phase is 24.2 mPa.s, which is much less than 18429 mPa.s for the gas-free bitumen while the viscosity reduction for 150°C is from 30.8 (raw bitumen) to 8.1 mPa.s (at 8 MPa). This may occur due to lower dissolution of ethane at higher temperatures and/or the rapid reduction of bitumen viscosity with temperature, i.e. the bitumen viscosity is quit low at higher temperatures and the viscosity reduction is not significant due to lower solubility of ethane. Hence, the impact of pressure on the reduction of bitumen viscosity is more pronounced at lower temperatures.

4.3.2. Equilibrium K-values and GOR

Experimental solubility and density data for pseudo-binary systems of bitumen/solvent are commonly used in reservoir simulation software to build appropriate thermodynamic and phase behaviour models. An approach for the thermodynamic modelling and equilibrium calculation rather than equation of state tuning is using experimental K-values. Thus, on the basis of experiments, the equilibrium K-values for different components present in mixtures are obtained and directly applied into reservoir simulation software, such as Computer Modelling Group's STARS (Advanced Process & Thermal Reservoir Simulator). Moreover, K-values are usually used to tune equation of state parameters. The K-values for Surmont bitumen / ethane mixtures were calculated using the following equation:

$$k = \frac{y_{C2H6}}{x_{C2H6}} \quad 4-1$$

where y_{C2H6} and x_{C2H6} are the mole fractions of ethane in equilibrium vapour and liquid phases, respectively.

The equilibrium vapour phase for all experiments was analyzed with a Varian GC 3900 gas chromatography system, and the results confirmed pure ethane as the vapour phase (except at the temperature 50°C and pressures higher than 6 MPa). Thus, a value of 1 for $y_{C_2H_6}$ was considered for all temperatures and pressures; and, the values for $x_{C_2H_6}$ were obtained using the data presented in Table 4–2 along with the molecular weight measurements for the bitumen. The measured K-values for the Surmont bitumen / ethane systems were plotted as a function of equilibrium pressure in Figure 4–5. The K-values are in the range (1 to 10) for Surmont bitumen / ethane mixtures, with the values determined by the composition of ethane in the liquid phase because $y_{C_2H_6} = 1$: a higher solubility results in a lower K-value. As depicted in Figure 4–5, the increase in pressure or the decrease in temperature leads to lower K-values.

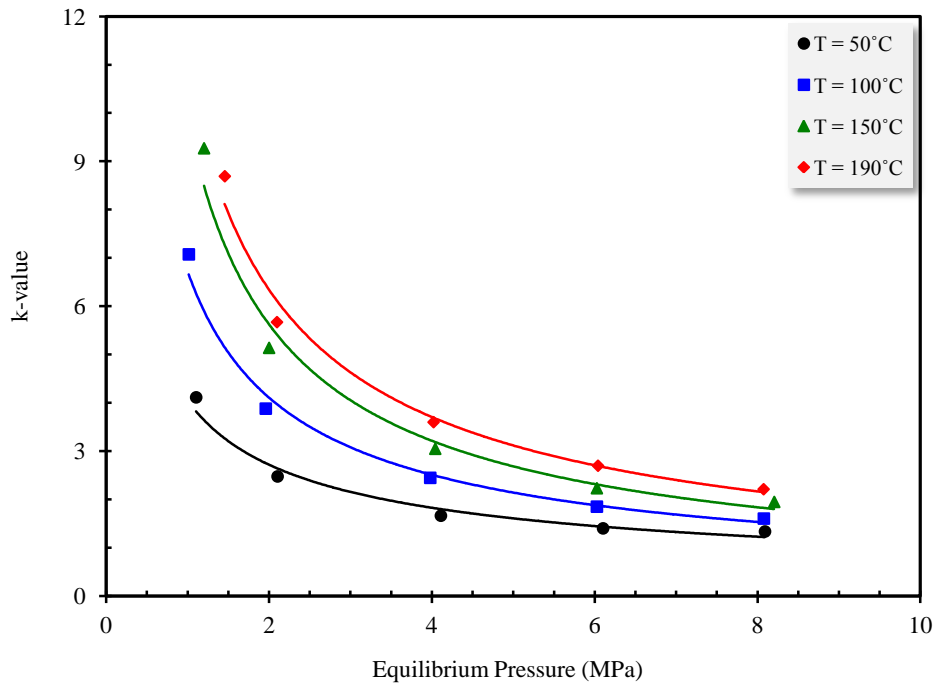


Figure 4–5: Measured K-value for Surmont bitumen / ethane systems as a function of pressure at different temperatures.

The solubility of ethane in bitumen was found to be significant and more than the solubility of methane at the same conditions. A comparison with the data reported by Kariznovi et al. (2012a) and Kariznovi (2013) for bitumen/methane mixtures shows that

the isotherms for bitumen/ethane mixtures are more separated from each other than those for bitumen/methane systems. This is more pronounced when the GOR plots are compared. GOR is defined as the ratio of the volume of gas that comes out of solution to the volume of oil at standard conditions. The standard conditions considered throughout this thesis were a pressure of 1 atm and a temperature of 20°C. The solubility data along with the bitumen and hydrocarbon gas properties were used to obtain the GORs at different pressures and temperatures. The following equation was applied to obtain GOR,

$$GOR = \frac{\frac{w_{C_2H_6}}{\rho_{C_2H_6}(T^{sc}, P^{sc})}}{(100 - w_{C_2H_6})}}{\rho_B(T^{sc}, P^{sc})} \quad 4-2$$

Figure 4–6 illustrates the experimentally measured GORs using equation 4-2 for Surmont bitumen saturated with ethane. This figure is somehow similar to the solubility plot and reveals that the equilibrium properties of bitumen / ethane mixtures are much more dependent on the temperature than those of bitumen/methane mixtures.

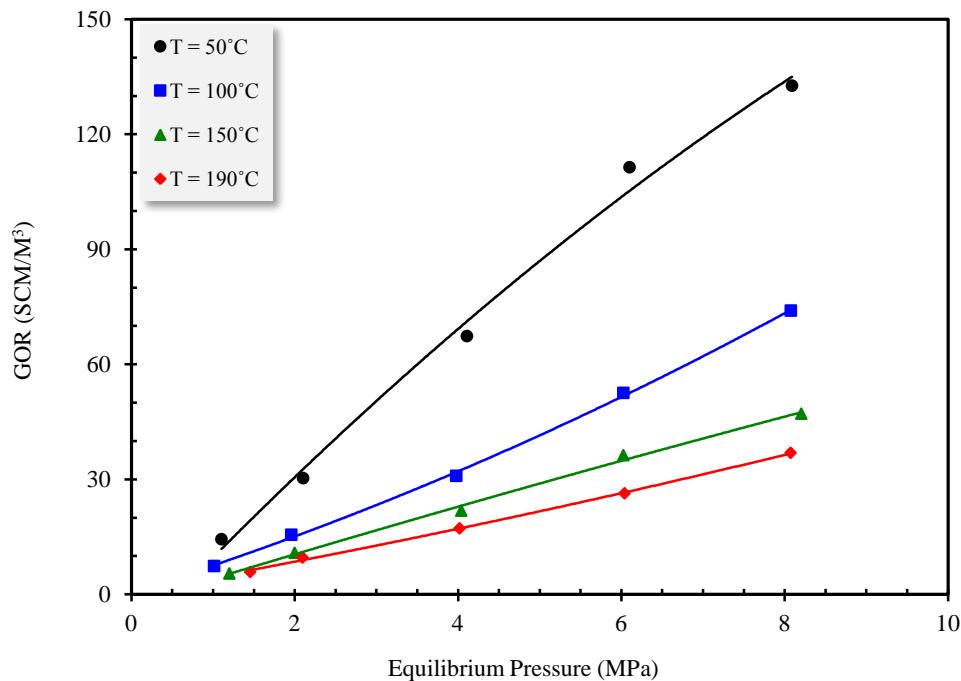


Figure 4–6: Measured GOR for Surmont bitumen / ethane systems as a function of pressure at different temperatures.

4.4. Vapour-Liquid Equilibrium for JACOS Bitumen / Ethane Mixtures

Vapour-liquid equilibrium experiments were conducted to determine the influence of pressure and temperature on the phase equilibrium properties of JACOS bitumen / ethane mixtures. Experiments at three different temperatures (50, 100 and 150°C) and four different pressures (2, 4, 6 and 8 MPa) were conducted. The results of the vapour-liquid experiments for JACOS bitumen / ethane systems are summarized in Table 4–4. As with Surmont bitumen / ethane mixtures, the repeatability of the generated data was examined by repeating one experiment each at temperatures of 50, 100, and 150°C; the data are presented in Table 4–5. As the table shows, the measurements for the solubilities are within ± 0.5 weight percent of ethane at a temperature of 50°C. This may be due to the high solubility values at low temperatures. The saturated phase densities are precise to less than 0.5 kg/m^3 . The deviation for the saturated liquid viscosities is less than 5%.

As Table 4–4 shows, the variations of solubility, saturated liquid density and viscosity with pressure for JACOS bitumen follow the same trend as those of Surmont bitumen. The dissolution of ethane in bitumen reduces the density and viscosity of saturated liquid phase. Depending on the temperature, the decreasing trends of density and viscosity with the solubility of ethane are different. At a constant temperature, the solubility of ethane in bitumen increases with pressure. Thus, the density and viscosity of the saturated liquid phase shows a decreasing trend with the equilibrium pressure. Although pressure increases the density and viscosity of gas-free bitumen at a constant temperature, the dissolution of ethane in bitumen compensates for this pressure effect and even leads to the reduction of density and viscosity with pressure.

Figures 4–7 to 4–9 illustrate the experimental results for JACOS bitumen / ethane systems for temperatures greater than 50°C in which the vapour-liquid equilibrium exists. The solubility measurements are plotted as a function of equilibrium pressure in Figure 4–7, and the saturated phase properties are presented with respect to equilibrium pressure in Figures 4–8 and 4–9.

Table 4–4: Experimental vapour-liquid equilibrium properties for JACOS bitumen / ethane mixtures at $T = (50, 100 \text{ and } 150)^\circ\text{C}$; P , pressure; ρ_s , saturated liquid density; μ , saturated liquid viscosity; w_s , weight fraction of ethane in saturated liquid phase.

T ($^\circ\text{C}$)	P (MPa)	$10^2 w_s$	ρ_s (kg/m^3)	μ_s (mPa.s)
50.6	2.082	4.16	954.9	566
50.7	4.123	9.00	912.9	94.4
49.3	6.060	13.4	869.2	29.6
50.3	8.080	14.5	851.7	21.0
100.3	2.013	2.16	937.4	81.4
100.3	4.072	4.91	914.7	39.5
100.2	6.074	6.25	893.8	21.9
100.2	8.080	8.50	872.0	13.7
149.7	2.227	1.68	911.3	18.6
150.0	4.067	2.86	897.7	13.7
149.9	6.167	4.79	879.7	9.62
149.7	8.169	5.79	865.9	7.19

Table 4–5: Experimental vapour-liquid equilibrium properties of repeated experiments at $T = (50, 150, \text{ and } 190)^\circ\text{C}$ for JACOS bitumen / ethane mixtures; P , pressure; ρ_s , saturated liquid density; μ_s , saturated liquid viscosity; w_s , weight fraction of ethane in saturated liquid phase.

T ($^\circ\text{C}$)	P (MPa)	$100 w_s$	ρ_s (kg/m^3)	μ_s (mPa.s)
	2.082	4.66	954.5	573
	2.082	3.66	955.3	559
50.5	4.123	8.57	912.7	95.2
	4.123	9.41	913.0	93.6
	8.100	14.5	849.4	---
	8.059	14.4	854.0	21.0
	4.081	4.64	914.5	39.7
100.3	4.067	4.47	915.0	39.2
	4.067	5.61	914.5	39.7
	6.163	5.06	878.9	9.78
149.9	6.170	4.53	880.5	9.45

The solubility of ethane (Figure 4–7) in JACOS bitumen increases with pressure and reduces with temperature. The solubility of ethane significantly changes with pressure at low temperatures (e.g. 50°C). In this section, a temperature of 50°C is the lowest temperature considered, and the vapour-liquid equilibrium exists in the studied pressure range (< 8 MPa).

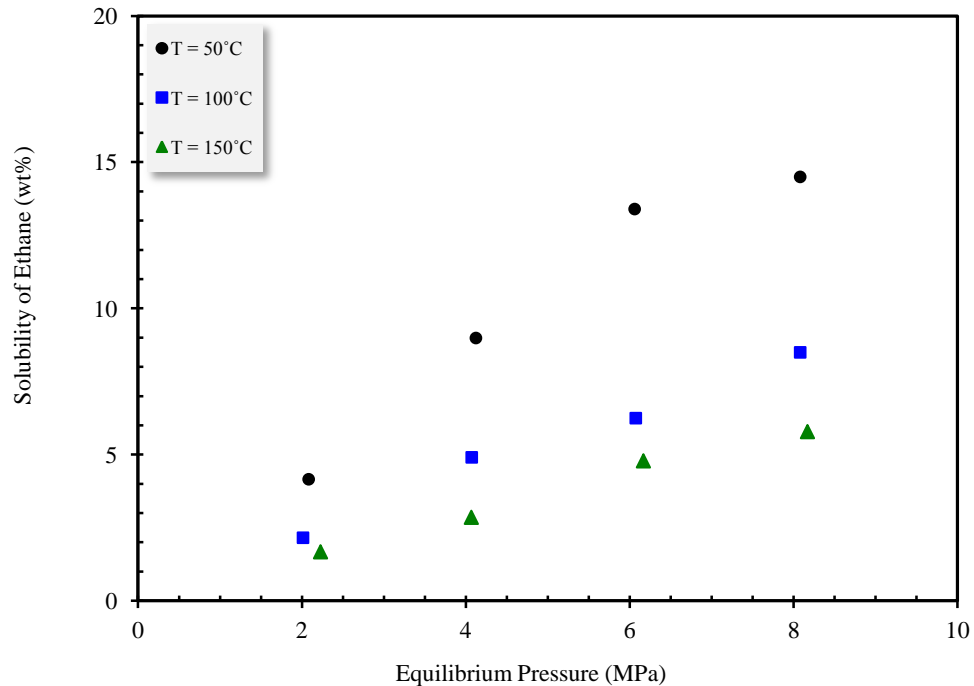


Figure 4–7: Measured solubility of ethane in JACOS bitumen as a function of pressure at different temperatures.

As depicted in Figure 4–7, the difference between the isotherms becomes more significant as temperature decreases from 150 to 50°C. The solubility curves demonstrate an almost linear variation with pressure at the temperatures of 100 and 150°C and a non-linear variation at 50°C. At 50°C, the solubility values flatten beyond a pressure of about 6 MPa. This behaviour was also observed for Surmont bitumen / ethane mixtures and by Mehrotra and Svrcek (1985a) for Athabasca bitumen / ethane mixtures.

Figure 4–8 displays the saturated bitumen viscosity versus pressure. The symbols on the y-axis are the viscosity of gas-free bitumen at given temperature. They allow evaluating the impact of dissolved ethane in the viscosity of bitumen. As anticipated from

Figure 4–8, when ethane is dissolved into the bitumen sample, the viscosity of ethane-saturated bitumen is significantly reduced, even at low equilibrium pressures. For instance, at an equilibrium pressure of 2.082 MPa and temperature of 50.6°C, the viscosity of the mixture is 566 mPa.s, which is about one tenth of the viscosity of the raw bitumen (6467 mPa.s) with no dissolved solvent. When the equilibrium pressure is increased to 8.080 MPa, the viscosity of the mixture is only 21.0 mPa.s, which is low enough for oil to be recovered from the reservoir. The viscosity of ethane-saturated bitumen reduces significantly with pressure at three studied temperatures. The viscosity behaviour has a linear trend with pressure at the temperatures of 100 and 150°C and a non-linear trend at the temperature of 50°C, with considerable viscosity reduction.

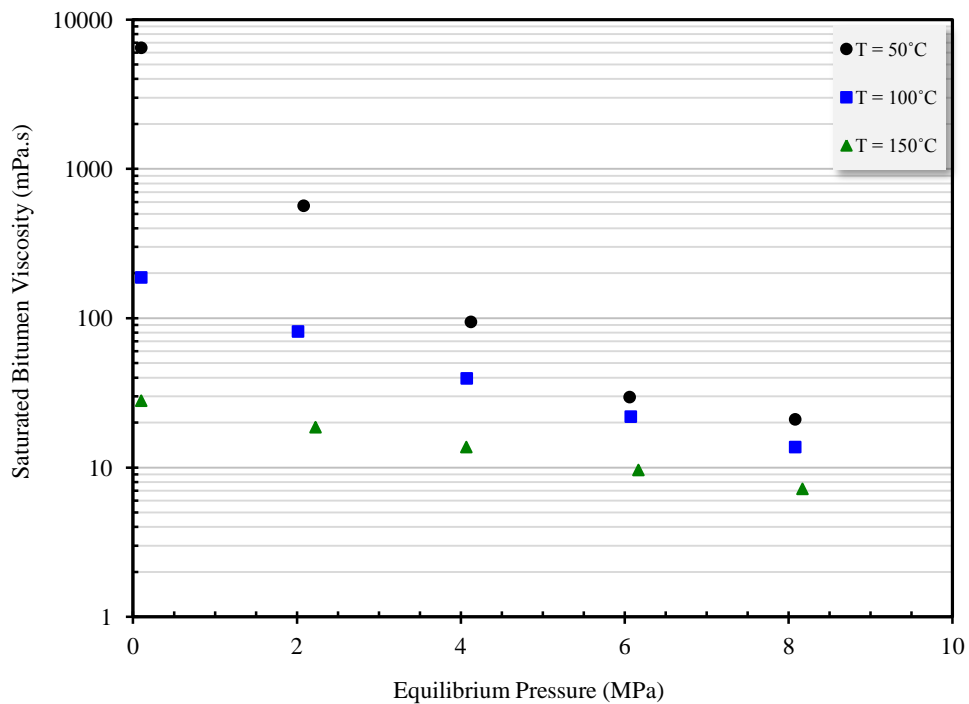


Figure 4–8: Viscosity of ethane-saturated JACOS bitumen as a function of pressure at different temperatures.

A closer examination of the saturated viscosity data reveals that the impact of ethane dissolution in bitumen viscosity reduces as temperature increases. For example, at 50.6°C and a pressure of 8.080 MPa, the viscosity of saturated liquid phase is 21.0 mPa.s which

is much less than 6467 mPa.s for the gas-free bitumen whereas the viscosity at 150°C is reduced from 28.0 (raw bitumen) to 7.19 mPa.s (at 8 MPa). This may occur due to the lower dissolution of ethane at higher temperatures and/or the rapid reduction of bitumen viscosity with temperature, i.e. the bitumen viscosity is quit low at high temperatures; and, due to the low solubility of ethane at these temperatures, the viscosity reduction is not significant. Hence, the impact of pressure (ethane solubility) on the reduction of bitumen viscosity is more pronounced at lower temperatures.

Figure 4–9 presents the gas-saturated bitumen density as a function of equilibrium pressure for JACOS bitumen / ethane mixtures. This figure clearly shows a significant reduction in the saturated bitumen density with pressure at 50°C where the density crossovers other temperatures and reaches a value even lower than the one at 150°C. The solubility of ethane at a temperature of 50°C is much higher than at 100 and 150°C, particularly at higher pressures, thereby, causing a greater reduction in density. For all temperatures, a linear decreasing trend for the saturated bitumen density with the equilibrium pressure is observed.

The K-values for JACOS bitumen / ethane mixtures were calculated using Equation 4-1. The equilibrium gases for all experiments were analyzed with Varian GC 3900 system and the results confirmed pure ethane as the vapour phase. Thus, as with Surmont bitumen / ethane systems, a value of 1 for $y_{C_2H_6}$ was considered for all temperatures and pressures; and, the values of $x_{C_2H_6}$ were obtained using the data presented in Table 4–4, along with the molecular weight measurements for the bitumen.

The measured K-values for JACOS bitumen / ethane systems were plotted as a function of equilibrium pressure in Figure 4–10. The K-values are in the range of 1 to 5 for JACOS bitumen / ethane mixtures, because the temperature 190°C was not considered in the experiments. Considering Equation 4-1, a higher solubility results in a lower K-value, thus, as depicted in Figure 4–10, an increase in pressure or a decrease in temperature leads to lower K-values.

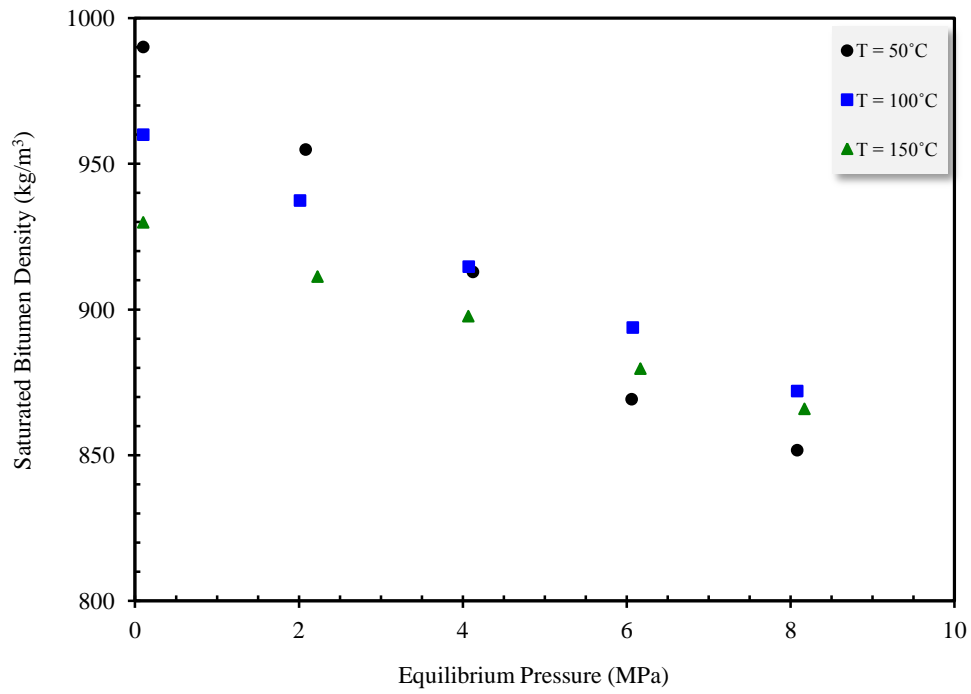


Figure 4-9: Density of ethane-saturated JACOS bitumen as a function of pressure at different temperatures.

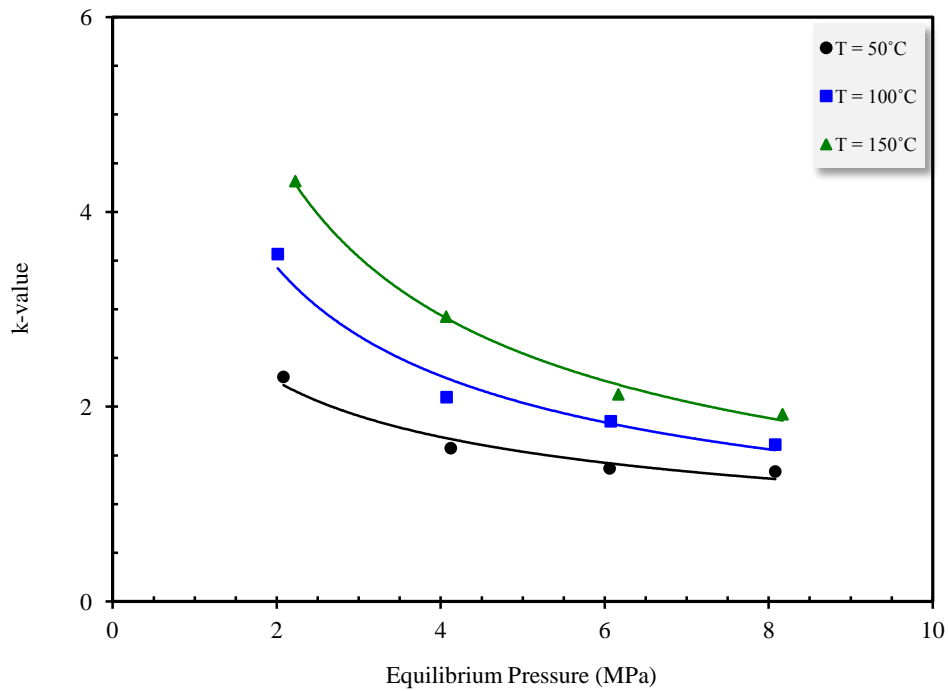


Figure 4-10: Measured K-values for JACOS bitumen / ethane systems at different temperatures and pressures.

Figure 4–11 illustrates the measured GORs for JACOS bitumen saturated with ethane calculated with equation 4-2. The solubility of ethane in JACOS bitumen is greater than that of methane at the same conditions (Kariznovi 2013). The solubility data along with the bitumen and hydrocarbon gas properties were used to obtain GOR at different pressures and temperatures.

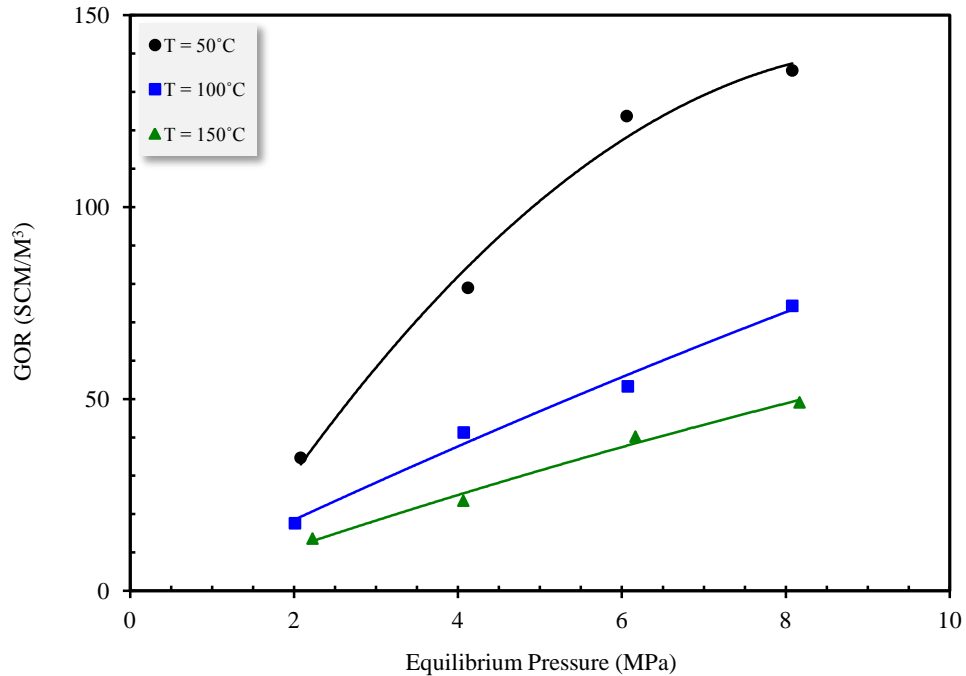


Figure 4–11: Measured GOR for JACOS bitumen / ethane systems as a function of pressure at different temperatures.

4.5. Vapour-Liquid Equilibrium for MacKay River Bitumen / Ethane Mixtures

Vapour-liquid experiments for MacKay River bitumen / ethane mixtures were also conducted at four temperatures (50, 100, 150 and 190)°C, and five different pressures (1, 2, 4, 6 and 8 MPa). The results of the vapour-liquid experiments for these systems are summarized in Table 4–6. As with Surmont bitumen / ethane mixtures, the repeatability of the generated data was examined by repeating one experiment in each isotherm; and, the data are presented in Table 4–7. The solubility measurements were precise within

± 0.2 weight fraction of ethane, and the saturated phase densities were precise within ± 2 kg/m^3 . The deviation for the saturated liquid viscosities was less than 5%.

Table 4–6: Experimental vapour-liquid equilibrium properties for MacKay River bitumen / ethane mixtures at $T = (50, 100, 150$ and $190)^\circ\text{C}$; P , pressure; ρ_s , saturated liquid density; μ , saturated liquid viscosity; w_s , weight fraction of ethane in saturated liquid phase.

T ($^\circ\text{C}$)	P (MPa)	$10^2 w_s$	ρ_s (kg/m^3)	μ_s (mPa.s)
51.0	1.069	1.79	967.9	1225
53.3	1.951	3.14	951.6	404
51.0	4.012	7.36	910.3	86.3
50.7	6.001	11.9	868.5	28.1
53.7	8.066	14.0	846.8	17.1
100.3	1.079	1.06	942.7	112
99.9	2.054	2.10	932.8	80.4
100.4	4.109	3.99	911.2	38.1
100.7	6.101	6.19	889.8	21.3
101.0	8.100	8.18	868.8	13.0
149.5	1.138	0.75	915.7	22.2
149.9	1.979	1.40	909.8	20.4
149.8	4.082	2.65	894.8	13.6
150.6	6.032	4.07	879.1	9.68
149.6	8.052	5.62	863.8	7.31
190.5	1.399	0.82	894.5	9.10
189.4	2.065	1.22	890.7	8.42
189.8	4.067	2.45	877.4	6.66
190.1	6.046	3.58	864.9	5.43
190.1	8.052	4.64	851.5	4.44

As the data reveal, the density and viscosity of saturated liquid phase were reduced with the dissolution of ethane in MacKay River bitumen. The decreasing trend of density and viscosity with the solubility of ethane is a function of temperature. Generally, the solubility of ethane in bitumen increases with pressure at a constant temperature and as a result, the density and viscosity of saturated liquid phase reduce with the equilibrium

pressure. Even if pressure increases the density and viscosity of gas-free bitumen at a constant temperature, the dissolution of ethane in bitumen with increasing pressure compensates for this pressure effect and it reverses the pressure effect on the density and viscosity.

Table 4–7: Experimental vapour-liquid equilibrium properties of repeated experiments at $T = (50, 150, \text{ and } 190)^\circ\text{C}$ for MacKay River bitumen / ethane mixtures; P , pressure; ρ_s , saturated liquid density; μ_s , saturated liquid viscosity; w_s , weight fraction of ethane in saturated liquid phase.

T ($^\circ\text{C}$)	P (MPa)	$10^2 w_s$	ρ_s (kg/m^3)	μ_s (mPa.s)
50.7	5.991	11.8	868.0	27.2
	6.012	12.0	868.9	28.9
99.9	2.068	2.44	933.1	79.0
	2.075	1.93	931.6	77.3
	2.020	1.93	933.7	85.1
149.8	4.054	2.30	897.7	14.0
	4.078	2.88	893.7	13.5
	4.116	2.77	892.9	13.1
189.4	2.096	1.24	890.7	8.50
	2.034	1.20	890.6	8.34

Figure 4–12 illustrates the solubility of ethane in MacKay River bitumen with respect to pressure. The solubility of ethane in bitumen increases with pressure and reduces with temperature. The solubility of ethane changes with pressure more significantly at low temperatures (e.g. 50°C). As depicted in Figure 4–12, the difference between the isotherms becomes more considerable as temperature decreases from 190 to 50°C .

The solubility increases linearly with the equilibrium pressure at the temperatures of 100 , 150 , and 190°C whereas a non-linear trend for solubility with pressure is observed at the temperature of 50°C . At this temperature, the solubility values flatten beyond a pressure of about 6 MPa. This behaviour was also observed for Surmont and JACOS bitumens and by Mehrotra and Svrcek (1985a) for Athabasca bitumen / ethane mixtures.

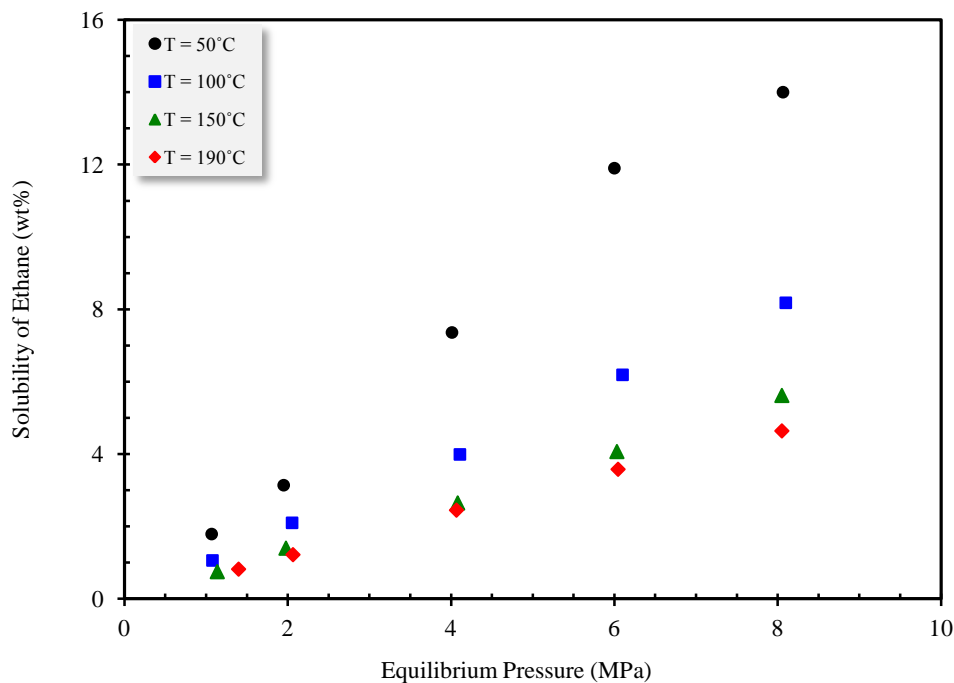


Figure 4–12: Measured solubility of ethane in MacKay River bitumen as a function of pressure at different temperatures.

Figures 4–13 and 4–14 display the saturated bitumen density and viscosity as a function of pressure. The symbols on the y-axis are the density and viscosity of gas-free MacKay River bitumen at atmospheric pressure. As indicated in Figure 4–13, when the bitumen is saturated with ethane, the viscosity of the saturated liquid phase is significantly reduced, even at low equilibrium pressures. For instance, at an equilibrium pressure of 1.069 MPa and a temperature of 51°C, the viscosity of the mixture is 1225 mPa.s, which is about one tenth of the viscosity of the raw bitumen (13763 mPa.s) with no dissolved solvent. When the equilibrium pressure is increased to 8.066 MPa, the viscosity of the mixture is only 17.1 mPa.s. The viscosity of ethane-saturated bitumen also reduces significantly with pressure for all temperatures. The viscosity, when presented in a semi-log plot, varies linearly with the equilibrium pressure at the temperatures of 100, 150, and 190°C. However, a non-linear decreasing trend with considerable viscosity reduction is observed at the temperature of 50°C.

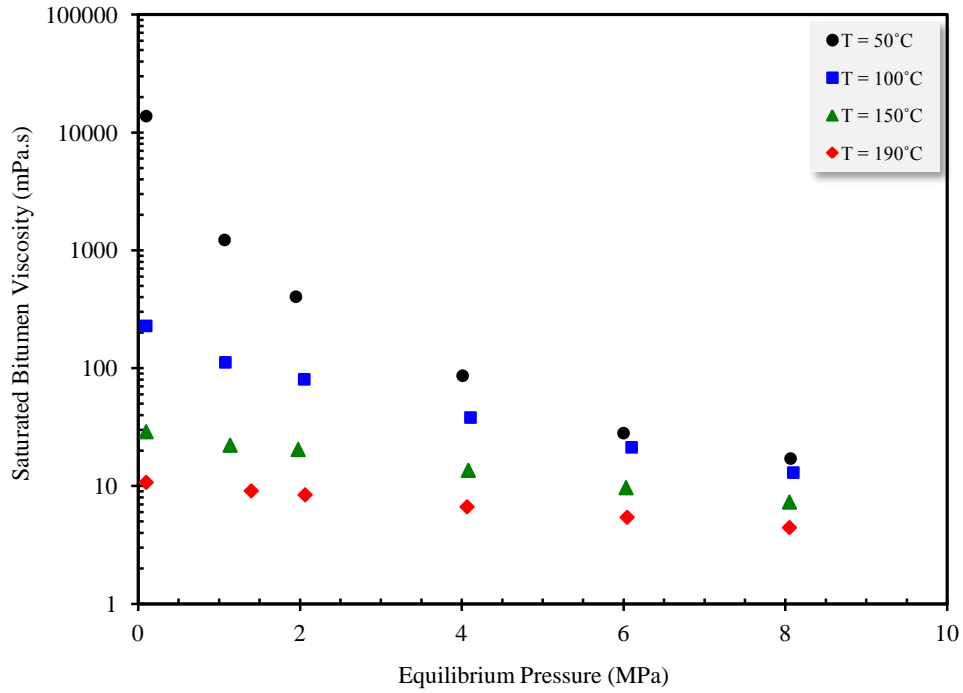


Figure 4-13: Viscosity of ethane-saturated MacKay River bitumen as a function of pressure at different temperatures.

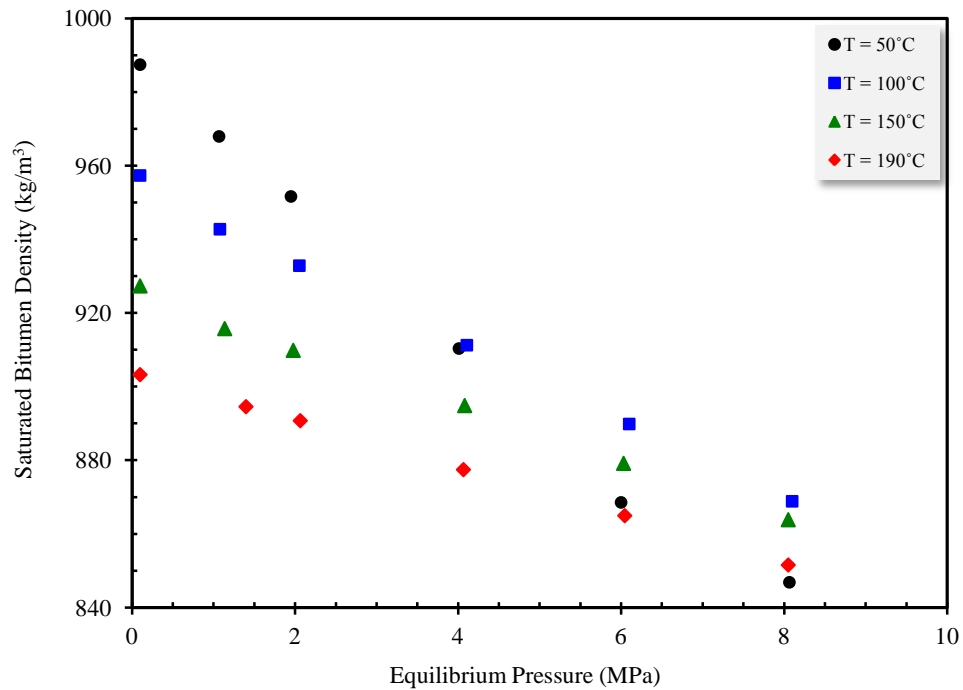


Figure 4-14: Density of ethane-saturated MacKay River bitumen as a function of pressure at different temperatures.

A closer examination of the saturated viscosity data reveals that the impact of dissolution of ethane in bitumen viscosity reduces as temperature increases. For example, at the temperature of 51°C and a pressure of 8.066 MPa, the viscosity of saturated liquid phase is 17.1 mPa.s which is much less than 13764 mPa.s for the gas-free bitumen whereas the viscosity reduction for the temperature of 190°C is from 10.74 (raw bitumen) to 4.44 mPa.s (at 8 MPa). This may occur due to the lower dissolution of ethane at higher temperatures and/or the rapid reduction of bitumen viscosity with temperature.

Figure 4–14 shows a linear decreasing trend for the saturated bitumen density with the equilibrium pressure in four isotherms. The ethane-saturated bitumen density is more significantly reduced at a temperature of 50°C than at other temperatures, i.e. it intersects other isotherms and reaches a value even lower than the one at the temperature of 190°C. The solubility of ethane at the temperature of 50°C is much higher than at 100, 150 and 190°C, particularly at higher pressures, thereby causing a greater reduction in density.

Figures 4–15 and 4–16 demonstrate the K-values and GORs for MacKay River bitumen / ethane mixtures as a function of pressure, respectively. The K-values were calculated using Equation 4-1 considering value of 1 for $y_{C_2H_6}$ for all temperatures and pressures and the values of $x_{C_2H_6}$ were calculated from the data presented in Table 4–6 along with the molecular weight measurements for the bitumen. The GORs were calculated with equation 4-2 which requires solubility data as well as the bitumen and ethane properties at different pressures and temperatures.

As anticipated from Figure 4–15, K-values are determined by the composition of ethane in the liquid phase because $y_{C_2H_6} = 1$, i.e. a larger value for the solubility results in a lower K-value. Thus, an increase in pressure or a decrease in temperature leads to lower K-values.

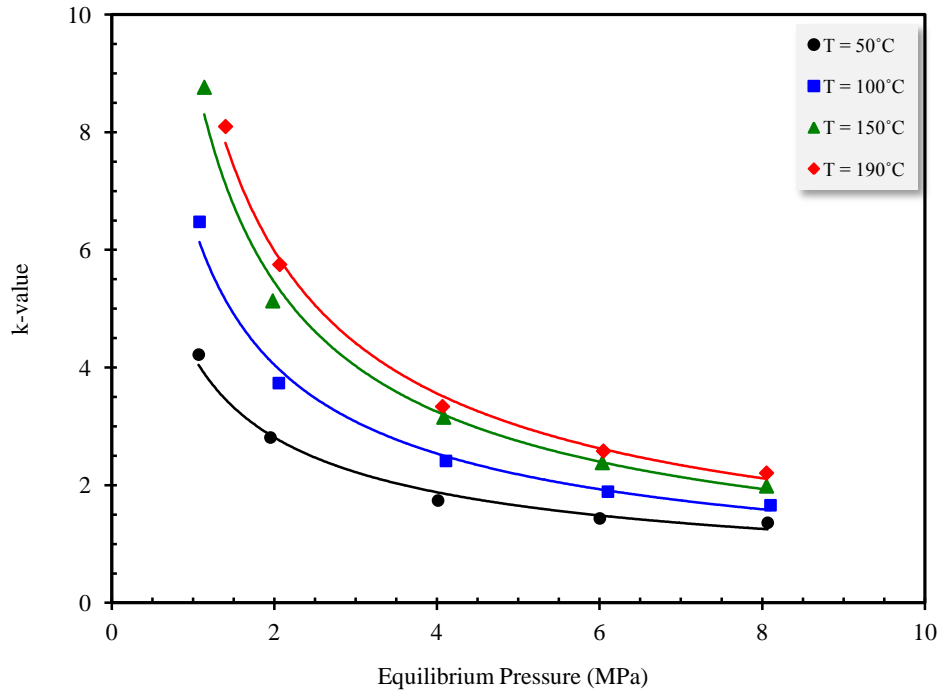


Figure 4-15: Measured K-values for MacKay River bitumen / ethane systems as a function of pressure at different temperatures.

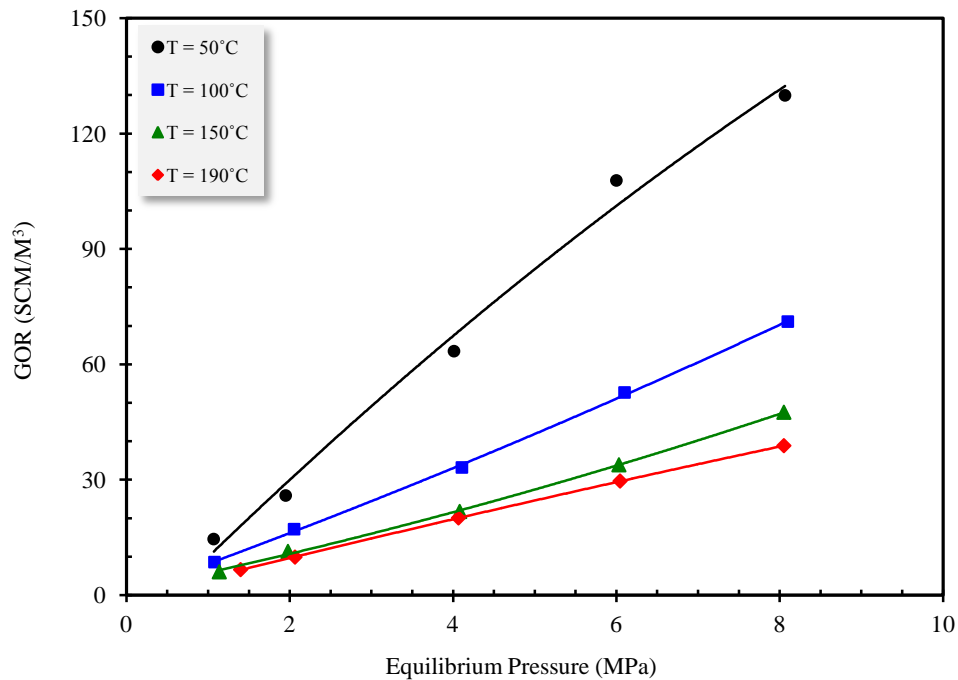


Figure 4-16: Measured GOR for MacKay River bitumen / ethane systems as a function of pressure at different temperatures.

Figure 4–16 reveals that the GOR plot follows the same trend as the solubility because both show the amount of solvent dissolved in the bitumen. At the lowest temperature (50°C) and the highest pressure (8 MPa), the maximum volume of ethane dissolved in the bitumen is 131 SCM/M³, while this value reduces to 40 at the temperature of 190°C at a similar pressure. For bitumen/methane mixtures, GORs vary from 20 to 15 in the above-mentioned conditions (Kariznovi 2013). This clearly indicates that the equilibrium properties of bitumen/ethane mixtures are much more dependant on the temperature than those of methane.

4.6. Comparison of Solubility of Ethane and Saturated Liquid Density and Viscosity for Different Bitumen Samples

In solvent-based recovery processes, the dissolution of solvent into the bitumen determines the oil recovery rates. Indeed, the solubility of a solvent in the bitumen quantifies the amount of solvent dissolved into the bitumen, and it strongly depends on the properties of the bitumen and the operating pressure and temperature. The solubility and saturated bitumen properties for bitumen/ethane systems were reported in Sections 4.3 to 4.5. Mehrotra and Svrcek (1985a) also conducted the same measurements with a bitumen sample provided from Athabasca field. All the bitumen samples were provided from Athabasca field but their locations would not have been the same. In this section, the solubility measurements and corresponding density and viscosity values are compared for different bitumen samples from Athabasca field.

Figure 4–17 illustrates the solubility measurements for bitumen/ethane mixtures. In this figure, the measured solubilities are plotted as a function of pressure for JACOS, MacKay River, and Surmont bitumens. The data by Mehrotra and Svrcek (1985a) at 50°C are also shown in this figure. The measured data indicate a negligible difference between the solubility of ethane in different bitumens. Although the solubility data at 50°C demonstrate a slightly discrepancy, the measurements are close at other

temperatures. The deviations may be caused by the experimental uncertainty in the solubility measurements. The solubility data by Mehrotra and Svrcek (1985a) show lower values than the measured data in this study; however, the trends are the same and can be considered for comparison.

It is expected that Mehrotra and Svrcek (1985a) used a bitumen sample that was originally heavier than the samples of this study. The solubility of ethane in the heavier bitumen sample is lower at the same temperature and pressure. To confirm this claim, the saturated bitumen density and viscosity are shown in Figures 4–18 and 4–19 as a function of equilibrium pressure.

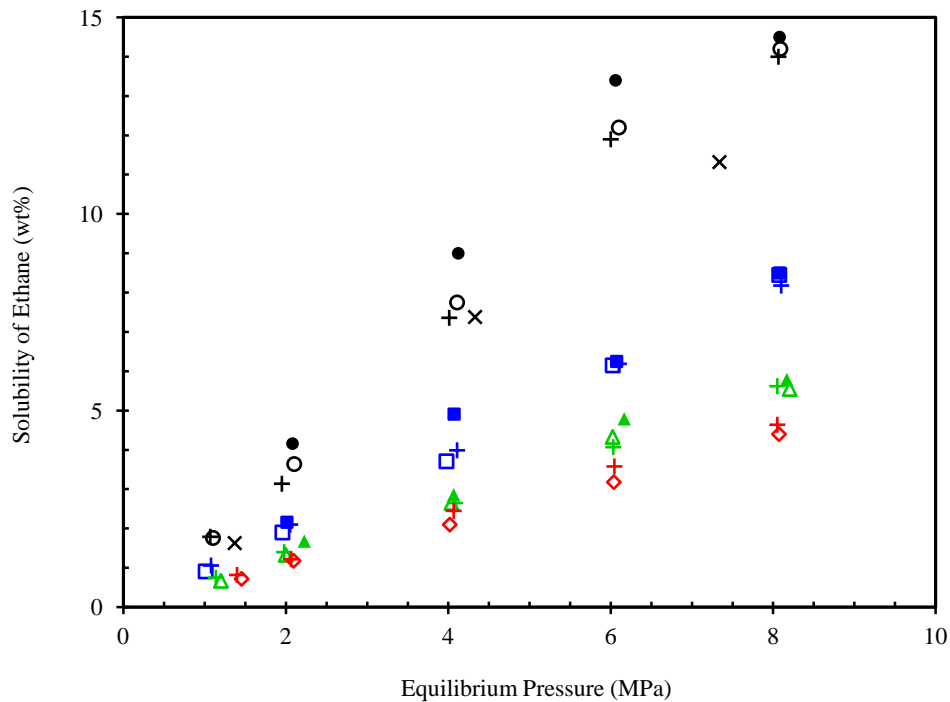


Figure 4–17: Comparison of the measured solubility of ethane in different bitumen samples from Athabasca field as a function of pressure at different temperatures; black symbols, 50°C; blue symbols, 100°C; green symbols, 150°C; red symbols, 190°C; solid symbols, JACOS bitumen; open symbols, Surmont bitumen; +, MacKay River bitumen; ×, Mehrotra and Svrcek (1985a).

Figure 4–18 illustrates the viscosity of ethane-saturated bitumen as a function of equilibrium pressure. The data for four different bitumens are compared in this figure and no significant difference in the viscosities can be observed. The data indicate that the

viscosity of saturated Athabasca bitumen used in Mehrotra and Svrcek (1985a) study is higher than that of other bitumens; and, MacKay River bitumen has the lowest saturated phase viscosities.

A comparison of the viscosity data of different bitumens saturated with ethane shows that the measured data in this study are consistent and they follow the same trend as the measurements by Mehrotra and Svrcek (1985a). The gas-free bitumen viscosity data are shown in Figure 4–18 for comparison. The viscosity of gas-free Surmont bitumen is higher than that of JACOS and MacKay River bitumens; and, as previously shown, the solubility values are almost identical at the same temperature and pressure. Thus, at identical ethane weight fractions, the heavier bitumen (Surmont) would have a higher viscosity. As depicted in Figure 4–18, the viscosity of ethane-saturated Surmont bitumen is greater than those of JACOS and MacKay River bitumens over the temperature and pressure ranges.

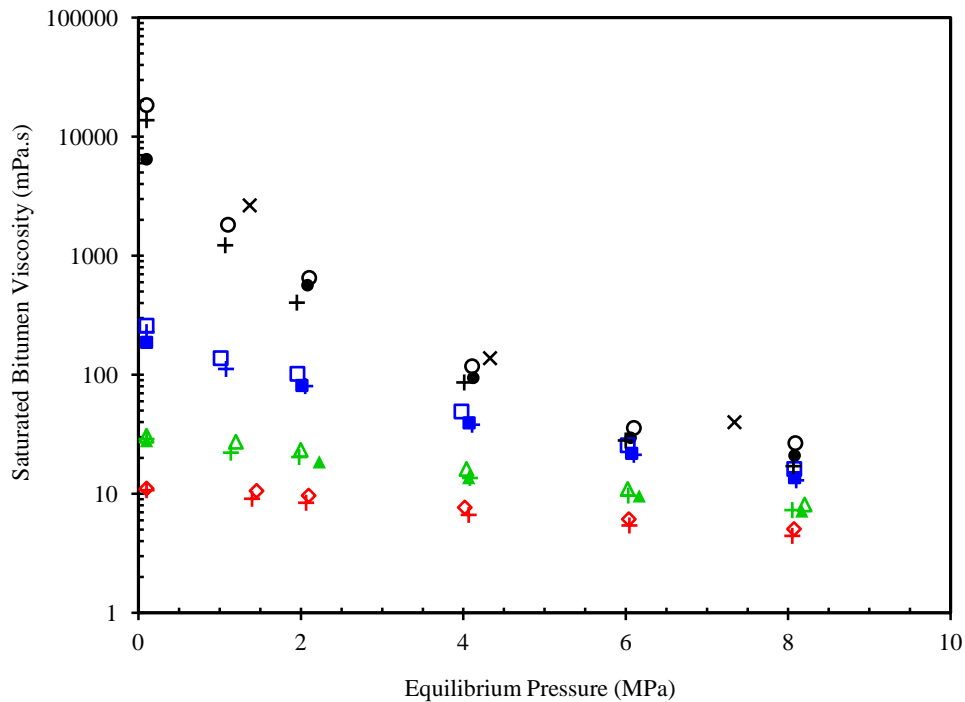


Figure 4–18: Comparison of the measured viscosity of ethane-saturated bitumen for different bitumen samples from Athabasca Field as a function of pressure at different temperatures; black symbols, 50°C; blue symbols, 100°C; green symbols, 150°C; red symbols, 190°C; solid symbols, JACOS bitumen; open symbols, Surmont bitumen; +, MacKay River bitumen; ×, Mehrotra and Svrcek (1985a).

Figure 4–19 demonstrates the density of ethane-saturated bitumen for four different mixtures. The gas-free bitumen density data are also shown in y-axis for comparison. The density of gas-free Surmont bitumen is higher than those of JACOS and MacKay River bitumens, but the solubility values are almost identical at the same temperature and pressure. Thus, at identical ethane weight fractions, the denser bitumen (Surmont) would have higher saturated bitumen densities. The saturated liquid density data reported by Mehrotra and Svrcek (1985a) are higher than those of Surmont, JACOS, and MacKay River bitumens at the same conditions. This can be attributed to lower solubilities of ethane in bitumen (shown in Figure 4–17) and/or higher gas-free bitumen densities.

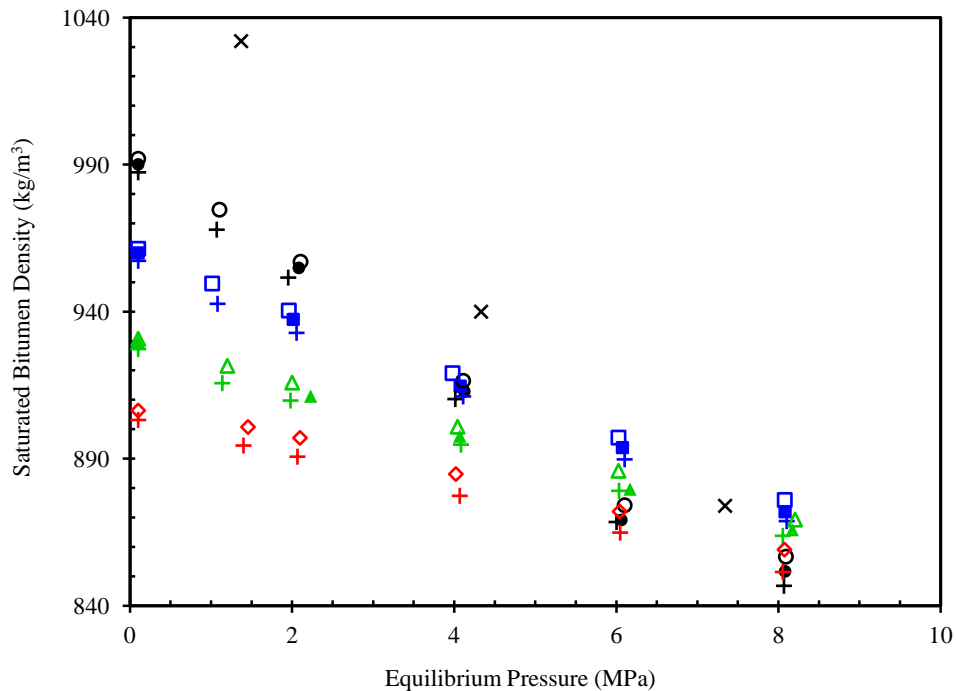


Figure 4–19: Comparison of the measured density of ethane-saturated bitumen for different bitumen samples from Athabasca field as a function of pressure at different temperatures; black symbols, 50°C; blue symbols, 100°C; green symbols, 150°C; red symbols, 190°C; solid symbols, JACOS bitumen; open symbols, Surmont bitumen; +, MacKay River bitumen; ×, Mehrotra and Svrcek (1985a).

For bitumen samples saturated with ethane, a linear relationship exists between the saturated liquid viscosity and equilibrium pressure at three temperatures (100, 150, and 190°C). At the temperature of 50°C, the saturated liquid viscosity data show a sharp non-linear variation with pressure. A linear decreasing trend for the saturated liquid density as

a function of pressure at all isotherms is observed. A noticeable behaviour for the saturated liquid density at the temperature of 50°C occurs at the pressures higher than 6 MPa, where the variation of density with pressure deviates from the linear decreasing trend. That is, the measured saturated liquid density data show higher values than expected. This is due to the extraction of some light components into the vapour phase at higher pressures (> 6 MPa).

4.7. Liquid-Liquid Equilibrium for Bitumen/Ethane Mixtures²

As previously mentioned, liquid-liquid separation and extraction of light components from heavy crudes using ethane were studied by Rose (1999) and Rose et al. (2001). Mehrotra et al. (1985) also modelled the liquid-liquid equilibrium for bitumen/ethane systems at ambient temperature using Peng-Robinson equation of state. The authors predicted the effect of solvent-to-bitumen ratio on the composition of equilibrium phases; and, they found that the solubility of ethane in the solvent-enriched phase increases linearly with increasing solvent-to-bitumen ratio while ethane solubility in the asphaltene-enriched phase reduces.

Mehrotra and Svrcek (1985b, 1988a) observed a notable behaviour in their solubility measurements for Peace River and Cold Lake bitumens saturated with ethane. The viscosity of ethane-saturated bitumen levelled off at 16.1°C with the increase in pressure. In addition, the repetition of measurement at 23°C and 4.1 MPa with different amounts of ethane to Peace River bitumen at equilibrium resulted in different solubility values and saturated phase properties. For Cold Lake bitumen / ethane systems, the viscosity of gas-saturated bitumen differs slightly for pressure greater than 6 MPa at three temperatures higher than the critical temperature. The authors argued that these behaviours were due to

² Some portions of this section are reprinted with permission from “Journal of Chemical and Engineering Data, 56 (11), H. Nourozieh, M. Kariznovi, J. Abedi, Physical properties and extraction measurements for Athabasca bitumen + light hydrocarbon system: Evaluation of pressure effect, solvent-to-bitumen ratio, and solvent type, 4261-4267, Copyright (2011) American Chemical Society” and “Journal of Chemical and Engineering Data, 58 (6), M. Kariznovi, H. Nourozieh, J. Abedi, Experimental determination of k-values and compositional analysis of liquid phases in the liquid-liquid equilibrium study of (Athabasca bitumen + ethane) systems, 1772-1780, Copyright (2013) American Chemical Society”.

the upgrading of bitumen or the extraction of light components into the solvent-enriched phase. No experimental data for the liquid-liquid equilibrium or for the extraction of bitumen with ethane at ambient temperature and the partitioning of components within the phases have been reported.

The liquid-liquid equilibrium for MacKay River bitumen / ethane systems formed at the temperatures less than 30°C. In this case, two phases, solvent-enriched and asphaltene-enriched, exist at equilibrium condition. The solvent-enriched phase is mostly composed of ethane and some light components extracted from the bitumen phase. The asphaltene-enriched phase mainly consists of the heavy components of bitumen, such as asphaltenes, which cannot be extracted by ethane. The liquid-liquid equilibrium can also be considered as an extraction process in which the light components are separated from undesirable constituents, such as asphaltene. The extraction yield depends on the temperature, pressure and solvent-to-bitumen ratio.

The experimental data for the liquid-liquid equilibrium, saturated phase properties, and extraction yield of MacKay River bitumen using ethane are studied at ambient temperature in this section. In addition, phase partitioning and component distribution within phases at equilibrium conditions are evaluated. The flashed-off liquid samples taken from the phases (solvent- and asphaltene-enriched phases) in liquid-liquid equilibrium experiments were subjected to compositional analyses to obtain carbon number distributions up to C₁₀₀. The K-value for each component present in the mixture at equilibrium condition was calculated on the basis of compositional analysis of liquid phases and available correlations for the molecular weight of heavy components. The impact of pressure and solvent-to-bitumen ratio on the boiling point curves and compositional analysis of flashed-off liquids as well as equilibrium K-values were evaluated. Finally, the molecular weight of flashed-off liquid phases was estimated on the basis of molecular weight and compositional analysis of liquids.

The liquid-liquid equilibrium of MacKay River bitumen / ethane systems at the average temperature of 21.6°C was achieved at three pressures (5 to 9 MPa) and four

different overall ethane concentrations (In this study, the terms of overall ethane concentration, solvent-to-bitumen ratio and feed concentration are used interchangeably; and, they refer to overall composition of ethane in equilibrium cell). The solubility, viscosity, density and volume of each liquid phase were measured during experiments.

The procedure to charge the equilibrium cell was described in Section 2.2. The bitumen was transferred directly to the density measuring cell and viscometer. The density and volume of the bitumen were measured to calculate the mass of the bitumen charged into the equilibrium cell. Table 4–8 summarizes the amount of bitumen and ethane that was used for each experiment to observe two liquid phases at the desired pressure and solvent-to-bitumen ratio. These values are the minimum amounts of components for each experiment to achieve the liquid-liquid equilibrium and possibility of phase sampling for further analysis.

The minimum solvent-to-bitumen ratio was estimated on the basis of Mehrotra and Svrcek (1985a) experiments for Athabasca bitumen / ethane mixtures. The authors reported a maximum ethane solubility of 11.85 wt% at 22.7°C and a pressure of 4.11 MPa. It should be noted that the saturation pressure of ethane is 3.931 MPa at the temperature of 22°C. Thus, the minimum pressure and solvent-to-bitumen ratio considered here to have liquid-liquid equilibrium are 5 MPa and 1:4, respectively.

To obtain the desired solvent-to-bitumen ratio, the volumes of charged components into equilibrium cell were evaluated and determined considering the maximum volume of the equilibrium cell (900 cm³). For example, at the solvent-to-bitumen ratio of 9:1, the maximum amount of bitumen to reach this ratio was 30 g. This can be determined from the third column of Table 4–8 which shows the total volume of mixture before mixing.

As previously mentioned, after equilibrium is achieved, the changes in viscosity and density while transferring equilibrium fluids indicate a passage of a phase boundary through the measuring instruments. Figure 4–20 illustrates the density and viscosity profile for an experiment at the pressure of 9 MPa and an overall ethane concentration of 0.8 weight fractions. The density and viscosity of equilibrium phases, as well as the

volume of each phase at equilibrium condition were measured for each experiment. For all experiments, a transition profile was obtained. As discussed, the volume of phases at equilibrium condition was used to calculate the extraction yield of the components.

Table 4–8: Experimental design for MacKay River bitumen / ethane systems at ambient temperature; P , pressure; S/B; solvent-to-bitumen ratio; w_f , weight fraction of ethane in feed (overall ethane concentration); V_i , total mixture volume before equilibrium; $m_{C_2H_6}$, total mass of ethane in equilibrium cell; m_{bit} , total mass of bitumen in equilibrium cell.

P /MPa	Solvent Loading		V_i (cm ³)	Equilibrium Cell	
	S/B	$10^2 w_f$		$m_{C_2H_6}$ (g)	m_B (g)
5.09	1:4	20	~170	25	100
5.08	2:3	40	~120	28	42
5.05	3:2	60	~189	54	36
7.08	2:3	40	~117	28	42
9.08	2:3	40	~114	28	42
9.08	3:2	60	~205	63	42
9.04	4:1	80	~340	120	30
9.05	9:1	90	~728	270	30

Tables 4–9 and 4–10 summarize the experimental results of the liquid-liquid equilibrium study of MacKay River bitumen / ethane mixtures. Table 4–9 summarizes the densities of the pure ethane, the solvent-enriched phase (liquid 1, L_1) and the asphaltene-enriched phase (liquid 2, L_2). The viscosities of the asphaltene-enriched phase were also measured and are given in Table 4–9. The solvent-enriched phase had a low viscosity that was not measured during the experiments. Table 4–10 summarizes ethane concentration in both liquid phases and the volume ratio of the phases at equilibrium conditions. This table shows that the solvent-enriched phase (L_1) has a much higher ethane concentration than the asphaltene-enriched phase. This can be attributed to the solvent-enriched phase being mainly comprised of liquid ethane and light components, while the asphaltene-enriched phase mainly contains heavy components, in which the solubilities of ethane are much lower than those of ethane in the light components.

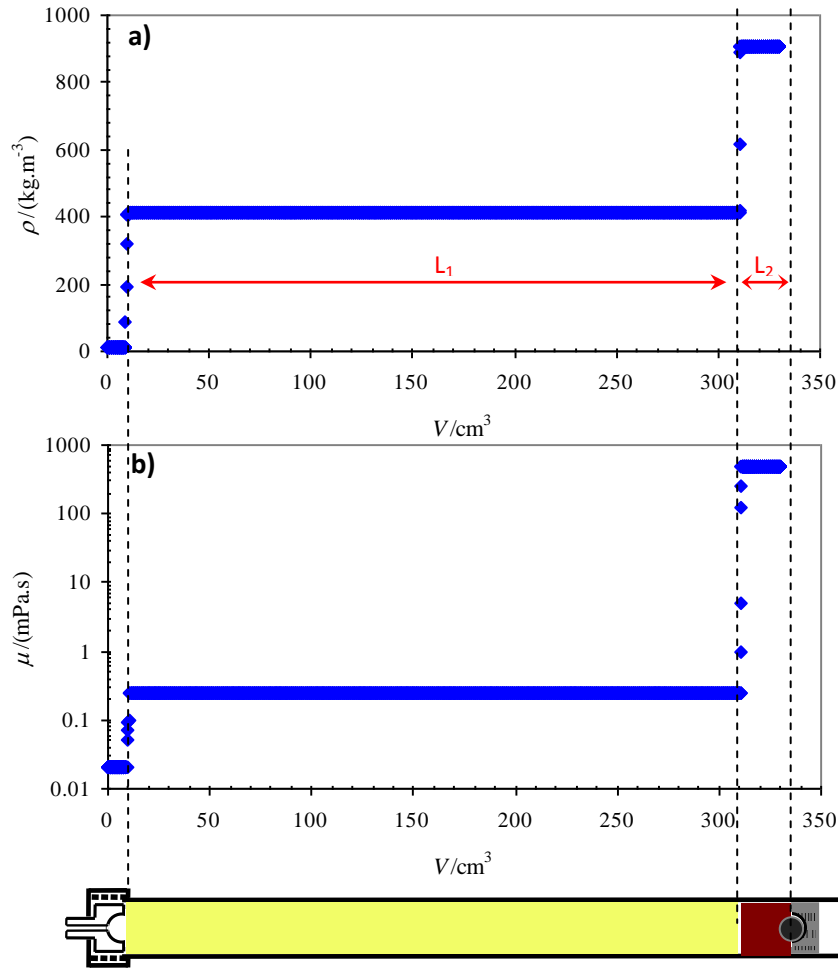


Figure 4–20: Liquid-liquid phase transition: saturated phase density ρ and saturated phase viscosity μ versus volume V ; a) saturated phase density; b) saturated phase viscosity (Nourozieh et al. 2011a).

Table 4–9: Liquid-liquid equilibrium properties for MacKay River bitumen/ethane systems at ambient temperatures; P , pressure; T , temperature; w , overall ethane weight fraction; ρ , densities; μ , L_2 viscosity (Nourozieh et al. 2011a).

P (MPa)	T (°C)	$10^2 w$	ρ (kg/m ³)			μ (mPa·s)
			Pure Ethane	L_1	L_2	
5.09	22.7	20	350	399	854	45.5
5.08	21.6	40	355	397	864	64.8
5.05	21.5	60	355	385	878	115
7.08	21.5	40	376	425	862	67.2
9.08	21.4	40	390	448	859	64.4
9.08	21.1	60	390	431	881	146
9.04	21.5	80	389	414	906	491
9.05	21.1	90	390	404	931	1908

Table 4–10: Composition and volume ratio of phases for MacKay River bitumen / ethane systems at ambient temperature; P , pressure; T , temperature; w , weight fraction of ethane; $V_1 \cdot V_2^{-1}$, L_1 to L_2 volume ratio (Nourozieh et al. 2011a).

P (MPa)	T (°C)	$10^2 w$			$(V_1 \cdot V_2^{-1}) / (m^3/m^3)$
		Feed	L_1	L_2	
5.09	22.7	20	----	17.9	0.150
5.08	21.6	40	91.4	15.7	1.112
5.05	21.5	60	92.9	14.5	3.322
7.08	21.5	40	87.7	16.6	1.113
9.08	21.4	40	84.5	16.6	1.112
9.08	21.1	60	89.0	15.5	3.072
9.04	21.5	80	93.1	13.1	10.779
9.05	21.1	90	96.0	11.6	32.019

As the results show, with increasing overall ethane concentration at a constant pressure, the density of the solvent-enriched phase decreases; whereas, the density of the asphaltene-enriched phase increases. The viscosity of the asphaltene-enriched phase increases with increasing pressure and overall ethane concentration. Thus, an increase in pressure or overall ethane concentration results in the higher extraction of light components from the bitumen. This leads to an increase in the fraction of heavier components in the asphaltene-enriched phase than raw bitumen. More details about the experimental results and their trends with pressure and solvent-to-bitumen ratio are discussed in the following sections.

4.7.1. Bitumen Extraction

The experimental results in Tables 4–9 and 4–10 indicate that the pressure and overall solvent concentration affect the physical properties of the liquid phases at equilibrium conditions. To find out how these parameters impact the extraction of the light component from the bitumen at a desired condition, a mass balance equation was set up to calculate the fraction of bitumen that is extracted into the solvent-enriched phase (L_1). The extraction yield is of particular importance for supercritical fluid extraction processes where the low volatility materials are extracted from various mixtures. The

calculation is based on the solubility of ethane in each liquid phase, and the volume and density of liquid phases. The general equation for the calculation of extraction yield is:

$$\text{Extracted Bitumen (\%)} = 100 \times \left(\frac{m_{B,L_1}}{m_{B,t}} \right) \quad 4-3$$

where m_{B,L_1} represents the amount of bitumen partitioned in the solvent-enriched phase (L_1), and $m_{B,t}$ is the total amount of bitumen charged into the equilibrium cell.

To calculate m_{B,L_1} , two methods are considered:

$$\text{Method 1: } m_{B,L_1} = \rho_{L_1} V_{L_1} (1 - w_{C_2,L_1}) \quad 4-4$$

and

$$\text{Method 2: } m_{B,L_1} = m_{B,t} - \rho_{L_2} V_{L_2} (1 - w_{C_2,L_2}) \quad 4-5$$

where ρ_{L_i} and V_{L_i} are the density and volume of saturated liquid i at equilibrium condition, w_{C_2,L_i} represents the weight fraction of ethane in saturated liquid i , and $m_{B,t}$ is the total amount of bitumen calculated from the density and the volume of bitumen charged into the equilibrium cell.

Finally, the extraction can also be calculated on the basis of all equilibrium fluid properties as:

$$\text{Method 3: Extracted Bitumen (\%)} = 100 \times \left(\frac{\rho_{L_1} V_{L_1} (1 - w_{C_2,L_1})}{\rho_{L_1} V_{L_1} (1 - w_{C_2,L_1}) + \rho_{L_2} V_{L_2} (1 - w_{C_2,L_2})} \right) \quad 4-6$$

All these methods for the calculation of the extraction of bitumen were considered in this study for comparison of the different approaches. The required measured parameters in each approach indicate that the extraction measurements can be calculated even with limited experimental measurements. Table 4–11 summarizes the average values for extraction yields obtained from three methods at different pressures and solvent-to-bitumen ratios.

The apparatus used for this study was batch for the bitumen and solvent. Solvent contacted the whole bitumen and extracted light fractions. As the table shows, the

extraction yields increase with pressure at constant temperature and overall ethane concentration. For example, at a constant overall ethane weight fraction of 0.6, the extraction yields increase from an average of 0.110 weight fraction to 0.155 with increasing the pressure from 5 to 9 MPa.

Table 4–11: Extraction Yield EY for MacKay River bitumen / ethane systems at ambient temperatures; P , pressure; T , temperature; w , overall ethane weight fraction (Kariznovi et al. 2013c).

P (MPa)	T (°C)	10^2w	10^2EY
5.09	22.7	20	2.9
5.08	21.6	40	4.8
5.05	21.5	60	11.0
7.08	21.5	40	7.9
9.08	21.4	40	10.1
9.08	21.1	60	15.5
9.04	21.5	80	27.7
9.05	21.1	90	38.4

The experimental results also indicate that the extraction yield increases with increasing overall ethane concentration. The maximum extraction yield was obtained at the highest overall ethane concentration for two pressures (5 and 9 MPa). For example, at the pressure of 9 MPa, the extraction yield increases from 0.101 weight fraction to 0.384 when the overall ethane concentration is increased from 0.4 to 0.9 weight fraction. The effect of overall ethane concentration on the extraction yield is more significant at low pressure (5 MPa) compared to high pressure (9 MPa). The increase in the overall ethane concentration from (0.4 to 0.6) weight fraction leads to an increase in the extraction yield that is more than double at the pressure of 5 MPa, while the increase is 1.5 times for a pressure of 9 MPa.

4.7.2. Effect of Pressure

The effect of pressure on the extraction of light components from bitumen is discussed in this section. The overall ethane concentration was kept constant (weight

fraction of 0.4), which corresponds to 0.654, 0.641, and 0.633 initial ethane volume fractions at the pressures of 5, 7 and 9 MPa, respectively. The extraction yields calculated from three different above-mentioned methods are shown in Figure 4–21. In general, the extraction yields increases with equilibrium pressure at constant temperature and overall ethane concentration. The increase in the amount of the extracted components is expected based on the results of binary systems reported in the literature. Moradinia and Teja (1987) and Schemitt and Reid (1985) reported the increase in the solubility of heavy hydrocarbon in solvents with increase in pressure. Rose (1999) also confirmed this behaviour for Peace River bitumen / ethane mixture at 47°C.

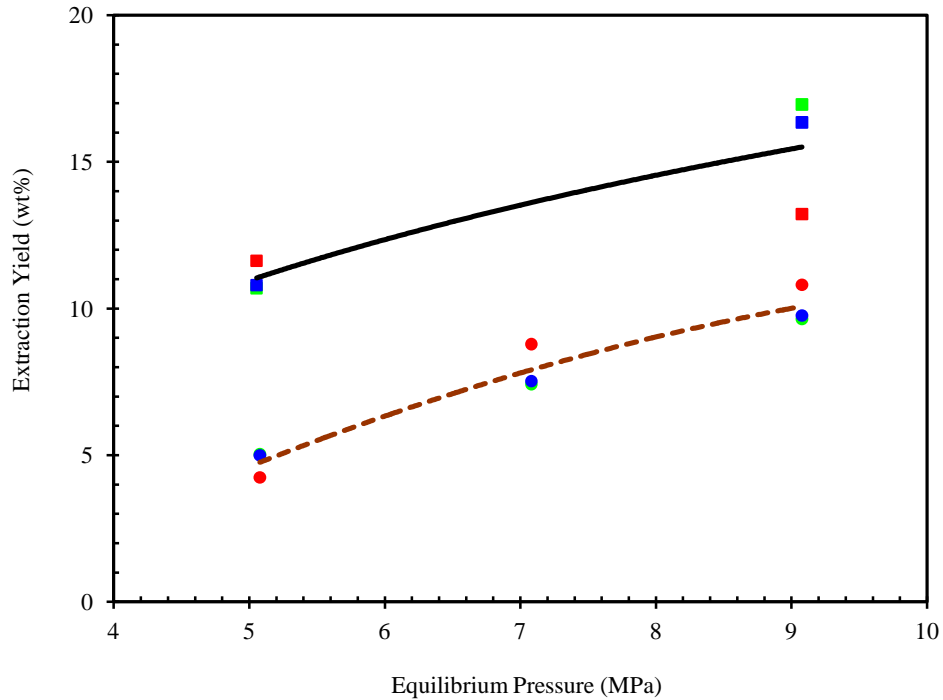


Figure 4–21: Effect of pressure on the extraction yield of components from MacKay River bitumen at two different overall ethane weight fractions w_f and at ambient temperature; —, $w_f = 0.6$; - - - -, $w_f = 0.4$; ●, method 1, ●, method 2, ●, method 3 (Nourozieh et al. 2011a).

As anticipated from Figure 4–21, at the overall ethane concentration of 0.6 weight fraction, the extraction yields increase from an average of 0.11 to 0.155 weight fraction with increasing the pressure from 5 to 9 MPa. This confirms that the extent of the extraction yield reduces as the overall ethane concentration increases. Thus, at the overall

ethane concentration of 0.4 weight fraction, the increase in pressure from (5 to 9) MPa almost doubles the extraction yield, whereas this amount is increased 1.5 times for the overall ethane concentration of 0.6 weight fraction. These results can be explained by the fact that at higher pressures, ethane has a stronger ability to extract the light components from bitumen.

The increase in the extraction yield with pressure was also observed at supercritical conditions, where the pressure variation results in a dramatic change in density of supercritical fluid. The results by Rose (1999) indicated that, as the pressure was increased from 7.3 to 15 MPa, the extraction yield increased by almost four times. The author attributed this observation to the liquid-like behaviour of ethane at high pressure conditions, i.e. at 7.3 MPa, the bitumen/ethane system is similar to vapour-liquid extraction process while at 15 MPa, the system behaves like liquid-liquid extraction.

The results for the liquid-liquid separation of the studied MacKay River bitumen / ethane system also confirm the increase in the solvent's ability to extract more components with increased pressure. In the case considered here, where ethane was liquid in the studied pressure range, the pressure also increases the attractive forces between the solute and solvent that may not be as high as supercritical condition. In fact, in the supercritical condition, the variation of solvent density with pressure at a constant temperature is considerably more than the density variation in subcritical conditions. Nevertheless, the pressure increases the extraction yield in the liquid-liquid separation.

The study of extraction yield on the basis of solvent density instead of the pressure could enable the comparison of different solvents. As plotted in Figure 4-22, the bitumen extraction yield shows a linear variation with ethane density at two different overall ethane weight fractions. From this figure, it can be concluded that the extraction yield is higher at higher solvent densities. Thus, it is expected that the hydrocarbon components heavier than ethane would have a higher extraction yield. This will be discussed in more detail in Section 4.7.5.

Figure 4–21 also illustrates that, as the pressure increases, the extraction yield for all overall ethane concentrations increases. However, the increase in the extraction of light components is levelled off and vanished at high pressures. This trend can be attributed to the initial extraction of light hydrocarbons and that at higher pressures, the bitumen is depleted in light hydrocarbons. Thus, as the pressure is increased, the remaining components in bitumen become heavier; and, the lower affinity of ethane for heavier components results in a change in the slope of extraction curve. Furthermore, the enrichment of solvent with light hydrocarbons results in lower extraction yield at higher pressures. This phenomenon is also observed by Rose (1999) for Peace River bitumen / ethane mixtures at the temperature of 47°C. Subramanian (1996) also obtained the same behaviour for bitumen/propane mixtures. The author explained the decrease in the extraction yield due to the cosolubilizing nature of light hydrocarbons, i.e. the light hydrocarbons act as cosolubilizing agents for heavier species; thus, as bitumen becomes leaner in light hydrocarbons, the residual phase becomes less soluble in the solvent.

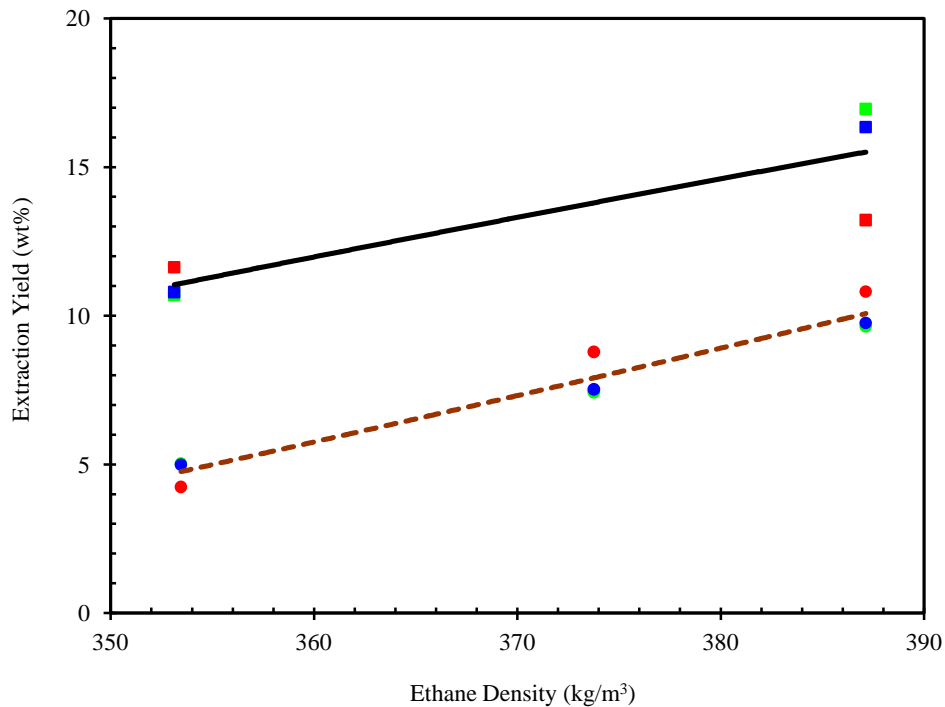


Figure 4–22: The extraction yield of MacKay River bitumen as a function of ethane density at two different overall ethane weight fractions w_f and at ambient temperature; —, $w_f = 0.6$; ----, $w_f = 0.4$; ●, method 1, ●, method 2, ●, method 3 (Kariznovi et al. 2012b).

The viscosity data in Table 4–9 indicate that the viscosity of the asphaltene-enriched phase (L_2) remains almost constant with increasing pressure, while the extraction yields favour a heavier asphaltene-enriched phase (L_2). Increasing the pressure, indeed, increases the light component extraction from the asphaltene-enriched phase, resulting in higher viscosity for the asphaltene-enriched phase. In contrast, the solubility of ethane increases with pressure and leads to a lower viscosity for the asphaltene-enriched phase. These two phenomena offset each other, and the viscosity of the asphaltene-enriched phase remains almost constant.

In general, the pressure affects the viscosity of asphaltene-enriched phase in three ways.

- At a constant temperature, the increase in pressure results in the increase in the viscosity of gas-free bitumen.
- The components in the asphaltene-enriched phase become heavier with increasing the equilibrium pressure, due to the higher extraction of light components into solvent-enriched phase at higher pressures.
- The viscosity of a liquid decreases with increasing solubility of ethane at higher pressures.

The first listed factor has a small effect on the viscosity; however, the other two factors can result in significant changes in the viscosity. The effects of the first and second factors cancel that of the third. Thus, the viscosity of the asphaltene-enriched phase remains almost constant.

This result is an indirect indication of component distribution within the phases. As the pressure increases, there is a balance between the light components that are separating from the bitumen and ethane that dissolves in the bitumen. This can be seen from the composition of equilibrium liquids summarized in Table 4–10. At a constant overall ethane concentration of 0.4 weight fraction, the concentration of ethane in the solvent-enriched phase reduces with equilibrium pressure, due to the higher extraction of

components. However, the concentration of ethane in the asphaltene-enriched phase increases due to the higher pressure within the system.

The composition of equilibrium liquids is also affected by pressure with a behaviour similar to that explained for the viscosity of the asphaltene-enriched phase. The components in the asphaltene-enriched phase become heavier with increasing pressure, due to the higher extraction of light components at higher pressures; thus, a reduction in the concentration of ethane in this phase is expected (lower solubility of ethane in heavier component at fixed temperature and pressure). However, the solubility of ethane in the liquid generally increases with pressure. The first factor compensates the second one. Further investigations on the component distribution within the phases are presented in Section 4.7.6.

The viscosity of the asphaltene-enriched phase provides information about the fluid flow properties of undesirable constituents separated from the original bitumen at experimental conditions. It should be noted that the above-mentioned behaviour for viscosity is observed for the asphaltene-enriched phase at equilibrium conditions. That is, the liquid phase contains the heavier components of bitumen that were saturated with ethane. If the viscosity for flashed-off liquid samples is to be analyzed, an increase in the viscosity of residue with pressure is expected. This is due to greater extraction of light components from bitumen at higher pressures resulting in a heavier flashed-off liquid phase. Rose (1999) measured the viscosity of the extracted oil for Peace River bitumen / ethane system and determined the effect of pressure: the extracted oil at higher equilibrium pressure had a higher viscosity.

4.7.3. Effect of Overall Ethane Concentration

To evaluate the effect of increasing the amount of solvent in the equilibrium cell on the physical properties and extraction yields, ethane-to-bitumen ratio (equivalently, the overall ethane concentration) was increased at constant pressures (5 and 9 MPa). The cumulative extraction yields at two pressures are plotted versus the overall ethane

concentration in Figure 4–23. The maximum extraction yield is obtained at the highest overall ethane concentration for both pressures. As depicted in this figure, the extraction yield increases with increasing the overall ethane concentration. For example, at 9 MPa, the extraction yield increases from 0.101 to 0.384 weight fraction when the overall ethane concentration is increased from 0.4 to 0.9 weight fraction. The effect of the overall ethane concentration is less pronounced at higher pressures.

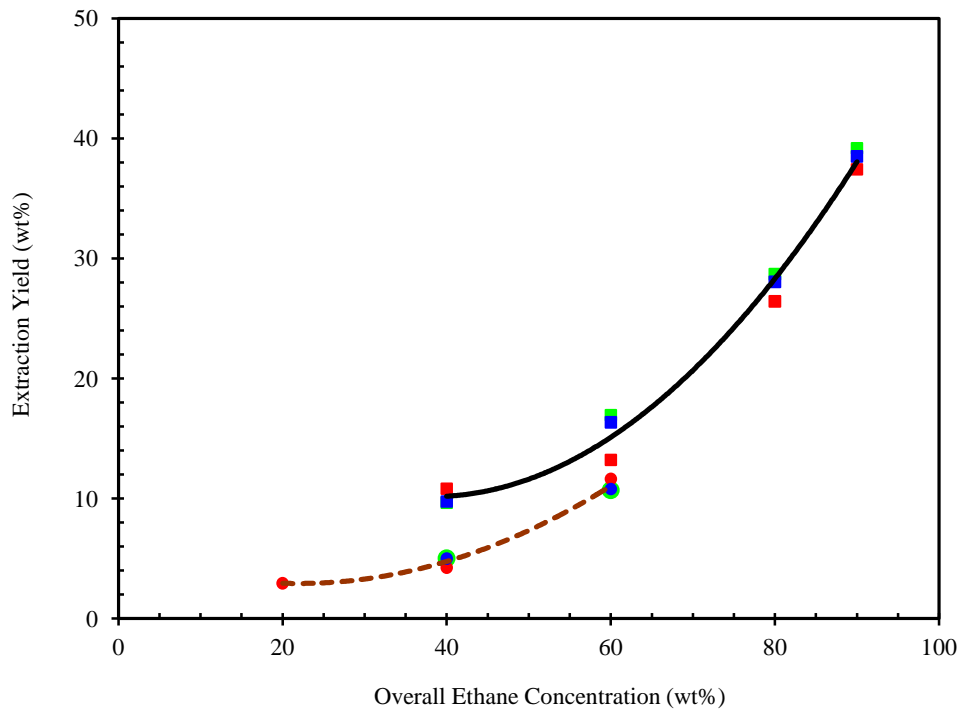


Figure 4–23: Effect of overall ethane concentration on the extraction yield of components from MacKay River bitumen at different pressures P and at ambient temperature; —, $P = 9$ MPa; - - -, $P = 5$ MPa; ●, method 1, ●, method 2, ●, method 3 (Nourozieh et al. 2011a).

The increase in extraction yield with the overall ethane concentration can be explained by the available ethane molecules for extracting the components from bitumen that increase as the amount of ethane in contact with bitumen is increased. Consequently, the extraction yield should increase with the overall ethane concentration. However, the rate is expected to change as the volume of ethane increases.

In low ethane volumes, the extraction yield is significantly affected by the overall ethane concentration. As the volume of ethane in contact with the bitumen increases, the

content of the light components and constitutes, such as saturates, in bitumen is depleted. Consequently, a further increase in the volume of ethane does not significantly change the extraction yield. This behaviour can be clearly investigated if the extraction yield is plotted as a function of the amount of ethane (in g) in contact with bitumen. Figure 4–24 shows such a plot for MacKay River bitumen / ethane mixture. As depicted in the figure, the increase in the extraction yield levelled off and vanished at higher amounts of ethane. This indicates that the components left in the asphaltene-enriched phase become heavier as ethane extracted light components and subsequently the lower affinity of ethane for heavier components results in the change in the slope of extraction curve.

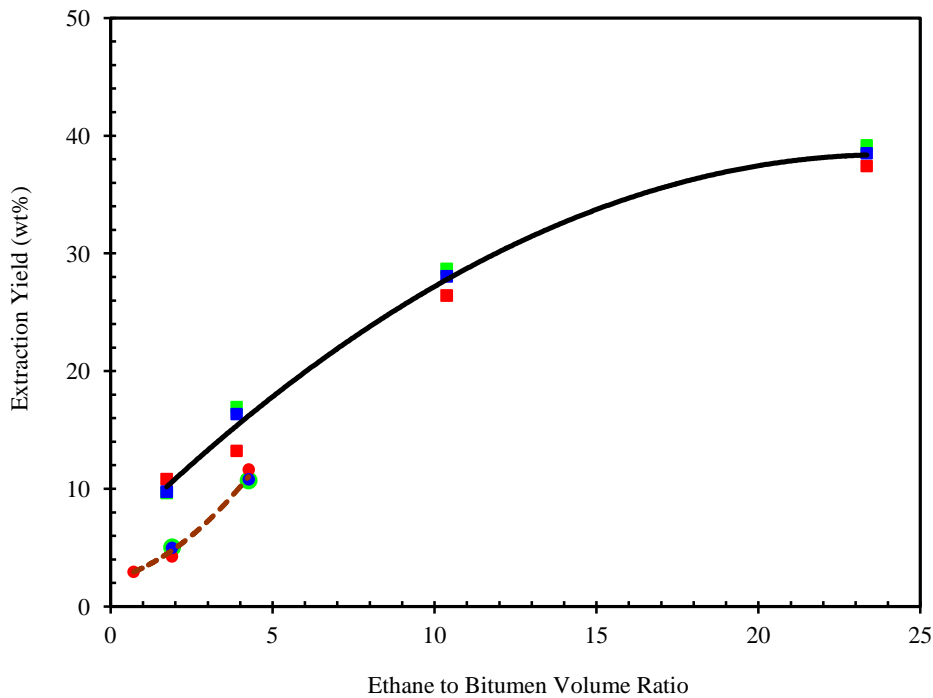


Figure 4–24: The extraction yield of MacKay River with respect to the volume ratio of ethane and bitumen at different pressures P and ambient temperature; —, $P = 9$ MPa; ---, $P = 5$ MPa; ●, method 1, ●, method 2, ●, method 3 (Kariznovi et al. 2012b).

In Figure 4–24, the extraction yield is plotted versus the volume of ethane in contact with bitumen. As indicated in this figure, the variation of extraction yield with the volume of ethane is not linear for MacKay River bitumen / ethane mixtures. If this figure is generated for a pure solute instead of bitumen, a linear increasing trend is expected.

Deo et al. (1992) reported a linear variation of the cumulative extracted hexadecane in weight percent with carbon dioxide volume. The reason is the constant solubility of hexadecane in carbon dioxide at fixed temperature and pressure. As more solvent be in contact with solute, more solute will be dissolved and extracted. In the case of MacKay River bitumen / ethane mixtures, the extracted fluid is a mixture in which the composition changes with the overall ethane concentration. Thus, the extraction plot is concave down and its trend levels off at high overall ethane concentrations. The slope of the curve decreases with increasing the overall ethane concentration. This is due to the extraction of light components at low overall ethane concentrations. Since no more light components are available in the asphaltene-enriched phase to be extracted with ethane, the extraction curve becomes flat at higher overall ethane concentrations.

4.7.4. Phase Properties

Figure 4–25 illustrates the concentration of ethane in both liquid phases at a pressure of 9 MPa and four different overall ethane concentrations (0.4, 0.6, 0.8, and 0.9 weight fraction). As depicted in the figure, the concentration of ethane in solvent-enriched phase increases with increasing overall ethane concentration at a constant pressure. This is expected, because when more ethane is added to the system, it propagates into the solvent-enriched phase (L_1). In contrast, ethane concentration in the asphaltene-enriched phase reduces, as shown in Figure 4–25. This is due to a greater extraction yield at higher overall ethane concentrations, which results in a heavy liquid phase with a lower solubility of ethane.

As expected, a heavier hydrocarbon has a lower solubility at a constant temperature and pressure. Mehrotra et al. (1985) predicted this behaviour with equation of state modelling of bitumen/ethane mixtures. The concentration of ethane in the solvent-enriched phase linearly increases with overall ethane concentration, whereas the asphaltene-enriched phase shows a non-linear decreasing trend.

Figure 4–26 demonstrates the density of equilibrium liquid phases as a function of overall ethane concentration. As the figure shows, with increasing the overall ethane concentration, the density of ethane-enriched phase decreases; whereas, the density of asphaltene-enriched phase increases. As ethane concentration increases, more light components are extracted into the solvent-enriched phase; thus, the density of asphaltene-enriched phase increases. However, the density of the solvent-enriched phase decreases and approaches the density of pure ethane at the experimental conditions of 21.6°C, 9 MPa, and overall ethane concentration of 0.9 weight fraction, which is 390 kg/m³. This is caused by the large volume of ethane in contact with the bitumen at higher overall concentrations.

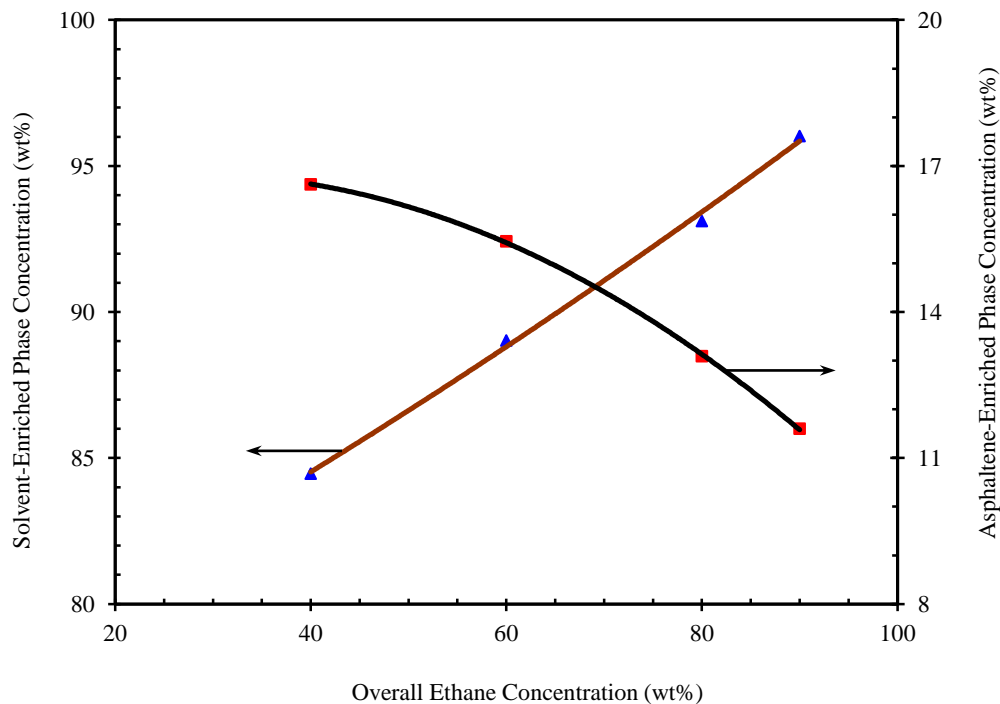


Figure 4–25: Effect of overall ethane concentration on the composition of equilibrium phases in liquid-liquid equilibrium study of MacKay River bitumen / ethane mixtures at ambient temperature and a constant pressure of 9 MPa; ▲, solvent-enriched phase; ■, asphaltene-enriched phase (Nourozieh et al. 2011a).

The composition and density data of equilibrium phases have opposite trends. Increasing ethane concentration leads to the reduction of density. Comparatively, the composition data presented in Figure 4–25 and the density measurements shown in

Figure 4–26 indicate that the composition of ethane in the solvent-enriched phase linearly increases with the overall ethane concentration, while the density decreases. For the asphaltene-enriched phase, both the composition and density have non-linear trend with overall ethane concentration.

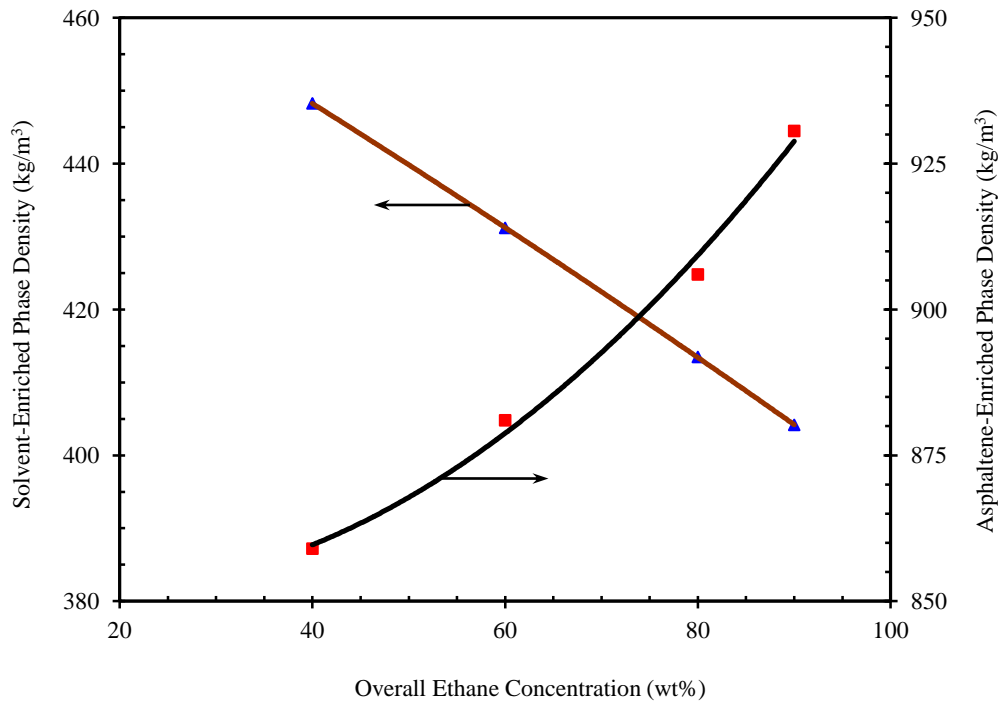


Figure 4–26: Effect of overall ethane concentration on the density of equilibrium phases in liquid-liquid equilibrium study of MacKay River bitumen / ethane mixtures at ambient temperature and a constant pressure of 9 MPa; ▲, solvent-enriched phase; ■, asphaltene-enriched phase; the density of pure ethane at the same condition is 390 kg/m³ (Nourozieh et al. 2011a).

To notify how the asphaltene-enriched phase becomes heavier with increasing overall ethane concentration and pressure, the viscosity of this phase (L_2) was plotted with respect to the overall ethane concentration in Figure 4–27 at two different pressures. The blue symbols represent the data at the pressure of 5 MPa, while the red ones denote the values at the pressure of 9 MPa. The viscosity of the asphaltene-enriched phase increases with equilibrium pressure and overall ethane concentration. Thus, as stated before, increases in pressure and overall ethane concentration result in the increase in the extraction of light components from the bitumen. This leads to an increase in the fraction of heavy components in the asphaltene-enriched phase compared to the raw bitumen.

Comparatively, at higher pressures, the overall ethane concentration has a more pronounced effect on the viscosity of asphaltene-enriched phase.

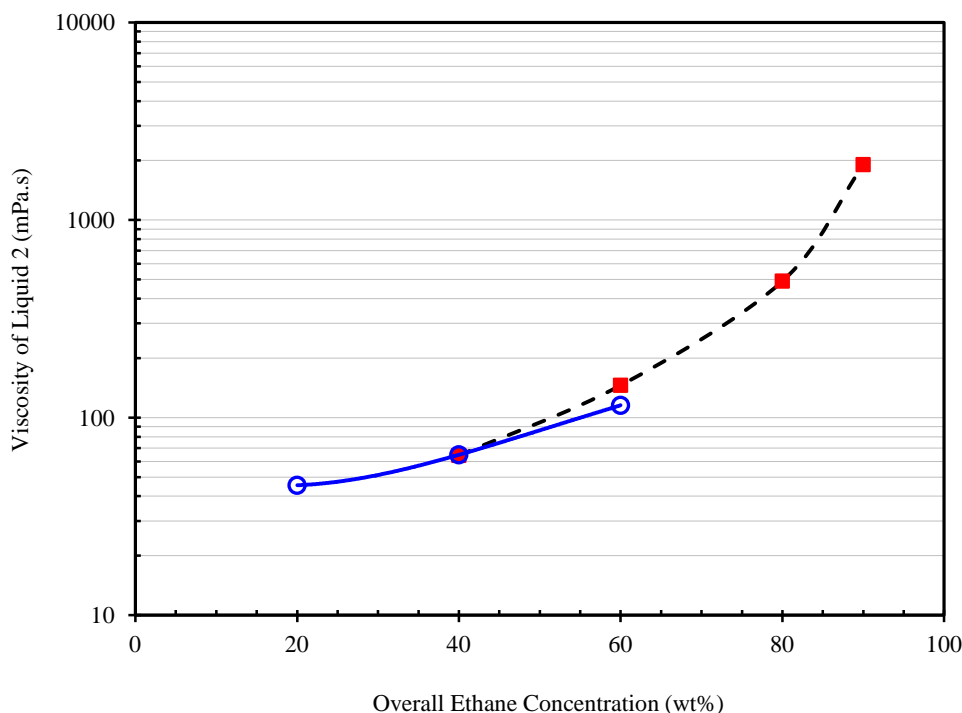


Figure 4–27: Effect of overall ethane concentration on the viscosity of asphaltene-enriched phase in the liquid-liquid equilibrium study of MacKay River bitumen / ethane mixtures at ambient temperature and at different pressures P ; ---, 9 MPa; —, 5 MPa (Nourozieh et al. 2011a).

4.7.5. Effect of Solvent Type

To evaluate the effect of the solvent type on extraction yield and phase compositions, an experiment at a pressure of 5 MPa and an overall solvent concentration of 0.4 weight fraction for MacKay River bitumen / propane system was conducted. The experimental results obtained for the bitumen/propane system were compared with those of the bitumen/ethane system at the same conditions. Figure 4–28 illustrates the extraction yields and the solvent composition in the equilibrium phases for two systems (bitumen/ethane and bitumen/propane). For comparison, the equilibrium phase properties for two solvents are also summarized in Table 4–12.

The generated experimental results for bitumen/ethane and bitumen/propane systems indicate that the extraction yield using propane is much greater than that of ethane at the

same conditions. This is due to the nature of propane, which extracts more components into the solvent-enriched phase (L_1) than ethane. The composition data for both phases confirm that propane extracts more components from the bitumen than ethane and has a higher solubility in the remaining heavy liquid phase. The weight fraction of propane in the solvent-enriched phase is less than that of ethane. This is due to greater extraction of bitumen by propane than ethane. As expected, the higher extraction yield, the heavier asphaltene-enriched phase. However, even at these conditions, the solubility of propane in this phase is much higher than that of ethane with its lower extent of extraction.

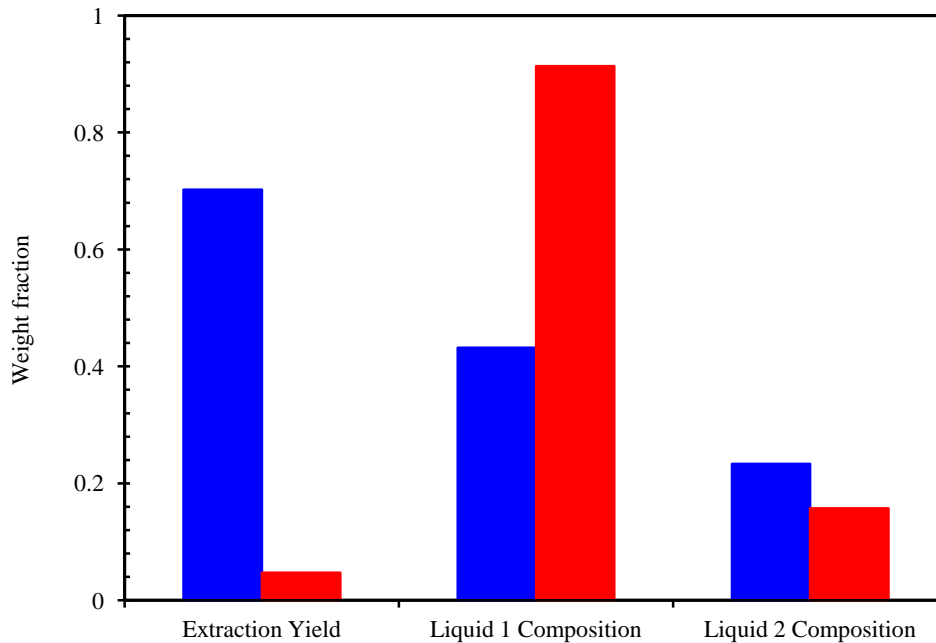


Figure 4–28: Effect of different solvents on the composition of equilibrium phases and on the extraction of light components from MacKay River bitumen at a constant pressure of 5 MPa and at ambient temperature, with an overall solvent concentration of 0.4 weight fraction; ■, propane; ■, ethane (Nourozieh et al. 2011a).

Table 4–12: Equilibrium phase properties for MacKay River bitumen / solvent mixtures at ambient temperature and at a pressure of 5 MPa with an overall solvent concentration of 0.4 weight fraction; w , weight fraction of solvent; ρ , densities; μ , L_2 viscosity (Nourozieh et al. 2011a).

Solvent	$10^2 w$		ρ (kg·m ⁻³)			μ (mPa.s)
	L_1	L_2	Pure Solvent	L_1	L_2	
Ethane	91.4	15.7	355	397	864	64.8
Propane	43.2	23.3	510	715	873	393

4.7.6. Compositional Analyses of Extracts and Residues

In previous sections, the liquid-liquid equilibrium of MacKay River bitumen / ethane mixtures at the average temperature of 21.6°C was conducted at three pressures (5 to 9 MPa) and four different overall ethane concentrations. The physical properties, such as composition, viscosity, density and volume, of each liquid phase were measured during the experiments and the impact of pressure and solvent-to-bitumen ratio on these properties was evaluated. The measured physical properties indicated that, in the case of the liquid-liquid equilibrium of MacKay River bitumen / ethane mixtures, two phases, solvent-enriched and asphaltene-enriched, exist at equilibrium conditions. The former is mostly composed of solvent and some light components extracted from the bitumen phase. The latter mainly consists of the heavy components of bitumen, such as asphaltene, which cannot be extracted by ethane. The results also denoted that the increase in both pressure and solvent-to-bitumen ratio raises the extraction yield and the separation of light components from the asphaltene-enriched phase. These analyses were concluded based on the measurement of physical properties. However, no compositional analysis in terms of component distribution and partitioning between two phases has been reported.

In this section, the phase partitioning and component distribution within the phases at equilibrium conditions for MacKay River bitumen / ethane mixtures are discussed. The K-value for each component present in the mixture at equilibrium condition is calculated based on compositional analysis of the liquid phases and the available correlations for the molecular weight of heavy components. The impacts of pressure and solvent-to-bitumen ratio on the boiling point curves and compositional analysis of flashed-off liquids are investigated. Finally, the molecular weight of flashed-off liquid phases is estimated on the basis of molecular weight and compositional analysis of liquids. The terms extract and residue refer to the flashed-off liquid samples taken from each liquid phase at equilibrium condition (extract is the flashed-off liquid sample taken from the solvent-

enriched phase and residue is the flashed-off liquid sample taken from the asphaltene-enriched phase).

The bitumen and flashed-off liquid samples taken from the liquid-liquid equilibrium experiments were subjected to compositional analyses to obtain carbon number distributions up to C_{100} . The compositional analysis of raw bitumen and flashed-off liquid samples provide the distribution of components at equilibrium conditions. In addition, the impacts of pressure and solvent-to-bitumen ratio on the phase partitioning can also be evaluated in more detail. The compositional analysis was done on the basis of the standard test method, ASTM D7169 explained in Section 3.3.

4.7.6.1. Bitumen and Equilibrium Phases

Based on extraction yield results, no conclusions can be drawn about the distribution of components. For example, the experimental results in Section 4.7.1 show that at an overall ethane concentration of 0.4 weight fraction and a constant pressure of 5 MPa, 0.048 weight fraction of bitumen was extracted into the solvent-enriched phase. However, the type and composition of components in the extracted phase (L_1) are not known.

Figure 4–29 illustrates the boiling point curve and the composition analyses for two flashed-off phase samples and raw bitumen. As depicted in this figure, there is a significant difference in the boiling point curve of extract (flashed-off liquid phase taken from solvent-enriched phase) and the raw bitumen. If two flashed-off liquid samples, extract and residue, at equilibrium pressure of 5 MPa and the overall ethane concentration of 0.4 weight fraction are compared on the basis of boiling point curves, it can be concluded that residue has a much higher boiling point curve than extract. That is, ethane has extracted light components from bitumen. In addition, if the boiling point curves of raw bitumen and residue are compared, no significant difference is observed. Thus, it can be concluded that the boiling point curve of bitumen is a function of heavy components rather than light fractions.

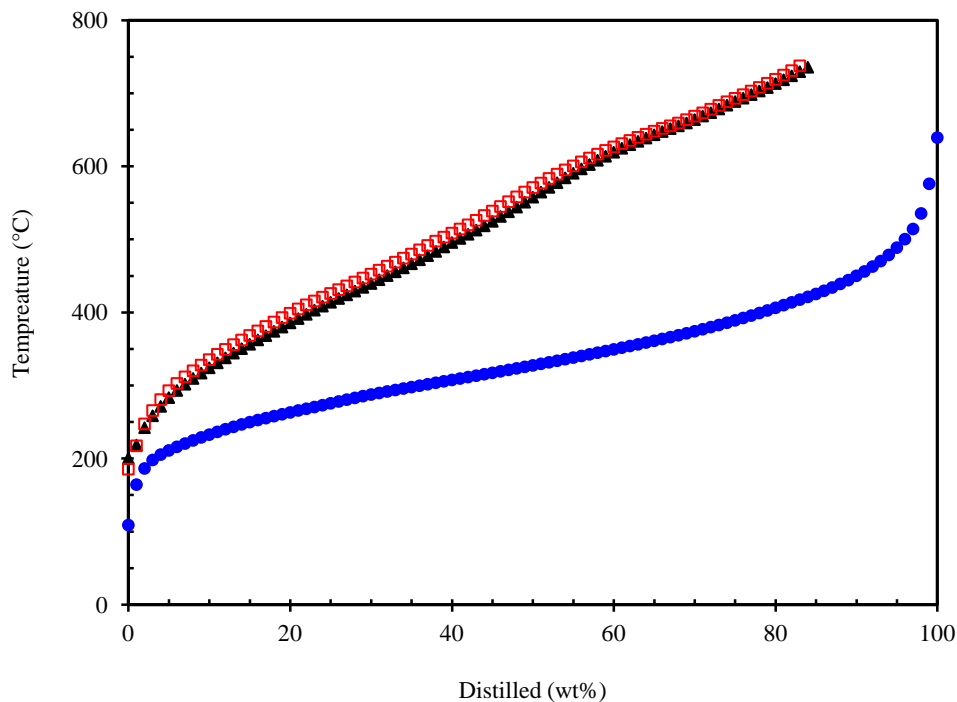


Figure 4–29: Boiling point curves (temperature versus weight percent distilled) for raw MacKay River bitumen (▲) and two flashed-off phase samples (extract ● and residue □) taken from liquid-liquid equilibrium of MacKay River bitumen / ethane mixtures at a constant pressure of 5 MPa and at a constant overall ethane concentration of 0.4 weight fraction (Nourozieh et al. 2012b).

Generally, heavier molecular weight hydrocarbons have higher boiling points. The residue is mainly composed of heavy components such as asphaltene; thus, it is heavier than the extract which contains light hydrocarbons. The differences in the boiling point curves and compositions of residue and raw bitumen are not significant. The C_{100+} fraction for raw bitumen is 0.188 while the C_{100+} fraction is 0.199 for the residue taken from the experiment at 5 MPa and an overall ethane concentration of 0.4 weight fraction. The difference in C_{100+} fractions is due to the nature of the solvent (i.e. ethane), which is more selective towards the saturate fraction than either the resin or aromatic fractions. Studies by Schmitt and Reid (1985) and Moradinia and Teja (1987) showed that *n*-paraffins have higher solubilities in supercritical fluids, such as ethane, compared to other classes of hydrocarbons, such as aromatics.

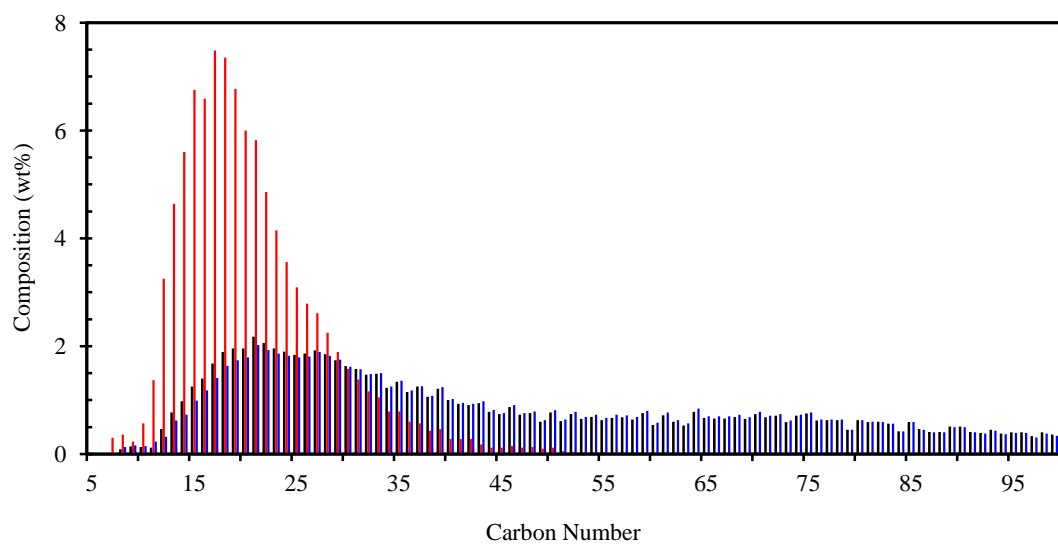


Figure 4-30: Compositional analysis (component weight percent) for raw bitumen (black) and two flashed-off phase samples (extract, red, and residue, blue) taken from liquid-liquid equilibrium of MacKay River bitumen / ethane mixtures at a constant pressure of 5 MPa and at a constant overall ethane concentration of 0.4 weight fraction (Nourozieh et al. 2012b; Kariznovi et al. 2013c).

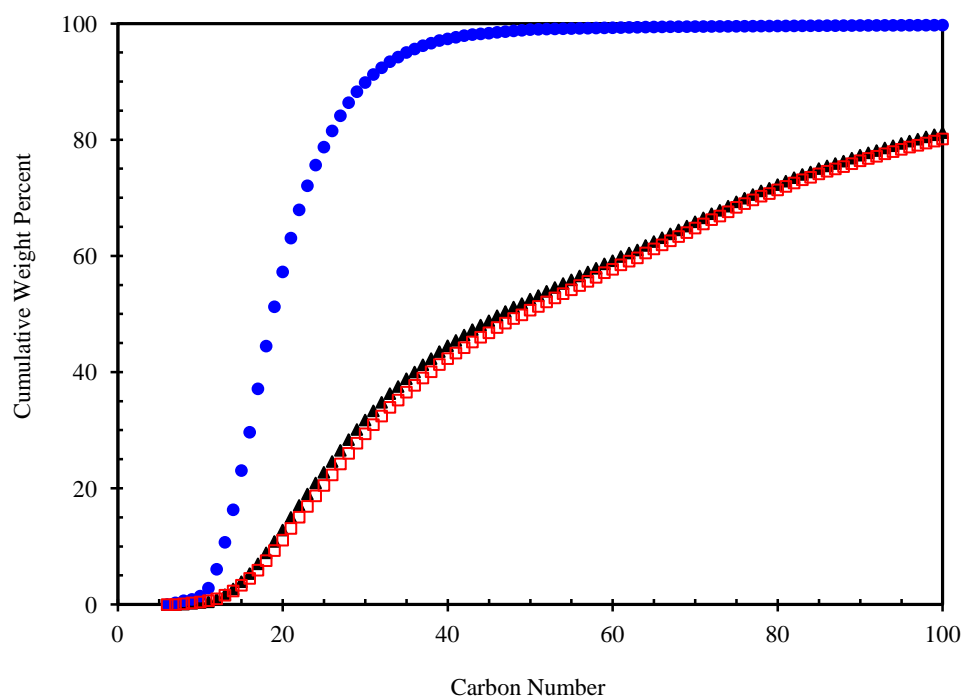


Figure 4-31: Carbon number distribution for raw bitumen (▲) and two flashed-off phase samples (extract ● and residue □) taken from liquid-liquid equilibrium study of MacKay River bitumen / ethane mixtures at a constant pressure of 5 MPa and at a constant overall ethane concentration of 0.4 weight fraction.

Figure 4–30 illustrates the weight fraction of each carbon number in raw bitumen, extract, and residue. As the figure indicates, the extract is composed of components with carbon numbers of C₈–C₅₀, mainly containing components between C₁₂ and C₃₅. The compositions of raw bitumen and residue are really similar. However, the raw bitumen has higher light components than the residue. Figure 4–31 shows the carbon number distribution for three liquid samples. Both Figure 4–30 and Figure 4–31 clearly demonstrate the component distribution of each phase.

4.7.6.2. Effect of Pressure

The impact of pressure on the extraction of MacKay River bitumen using ethane was examined by conducting a number of extractions at a constant overall ethane concentration of 0.4 weight fraction and three pressures, ranging from 5 to 9 MPa. Table 4–11 clearly demonstrates that as the pressure increases, the fraction of bitumen extracted into the solvent-enriched phase increases. The ability of ethane to extract the components increases with increasing the pressure, due to the increased attractive forces between the solute and solvent that resulted from higher solvent densities (Johnston et al. 1982). In other words, with stronger attractive forces, the solvent is capable of holding more of the solute.

The composition of the flashed-off liquid samples taken from liquid-liquid equilibrium in each experiment was measured to determine how the pressure affects the composition of the extracted oil. Generally, the higher the temperature in the boiling point curves is corresponded to heavier sample. Varying the pressure affects the composition of the extracted oil at a constant overall ethane concentration.

The boiling point curves of two extracts taken at two different pressures (5 and 9 MPa) are shown in Figure 4–32. The extracts at the different pressures have the same initial boiling points but the final boiling points differ depending on the pressure at which the experiment was performed. The difference between the end points of the boiling point curves indicates that a greater amount of heavy hydrocarbons are extracted at the higher

pressures. This is clearly shown by Figures 4–33 and 4–34, in which the component weight fraction and the carbon number distribution of each liquid sample are compared. At lower pressures, fewer compounds are soluble in ethane, i.e. the amount of the extracted oil is less and the extracted oil is composed of lighter constituents.

As the pressure increases, the extracted oil becomes significantly heavier. Hence, by manipulating the pressure, the characteristics of the extracted oil can be controlled. A low operating pressure produces an extracted oil that is relatively light; and, by gradually increasing the pressure, the product becomes heavier. It is worth noting that, at the elevated pressure, the extraction yield is higher; consequently, the amount of light components in the extracted oil is higher, but the fraction of light components decreases with equilibrium pressure due to increase in the fraction of heavy components.

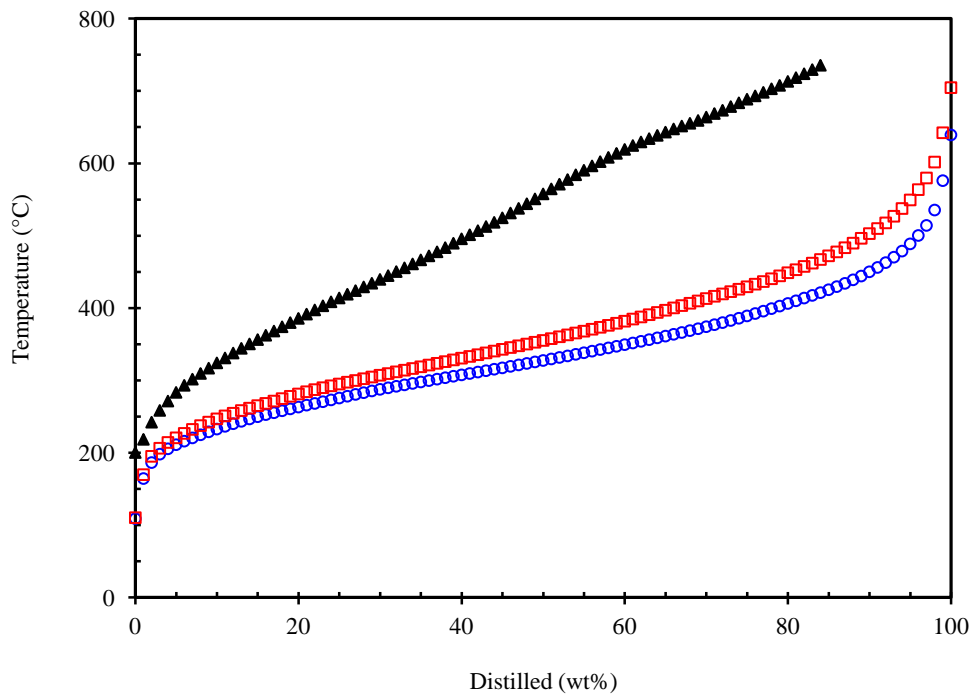


Figure 4–32: Boiling point curves (temperature versus weight percent distilled) for raw MacKay River bitumen (▲) and two extracts taken from liquid-liquid equilibrium study of MacKay River bitumen / ethane mixtures at different pressures and at a constant overall ethane concentration of 0.4 weight fraction; ○, 5 MPa; □, 9 MPa (Nourozieh et al. 2012b).

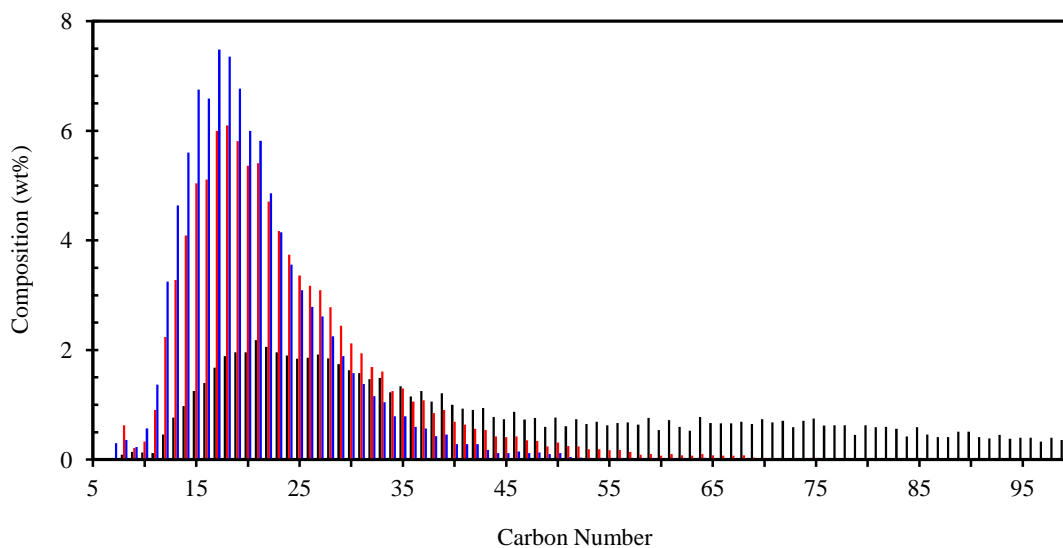


Figure 4-33: Compositional analysis (component weight percent) for raw bitumen (black) and two extracts taken from liquid-liquid equilibrium study of MacKay River bitumen / ethane mixtures at different pressures and at a constant overall ethane concentration of 0.4 weight fraction; blue, 5 MPa; red, 9 MPa (Nourozieh et al. 2012b).

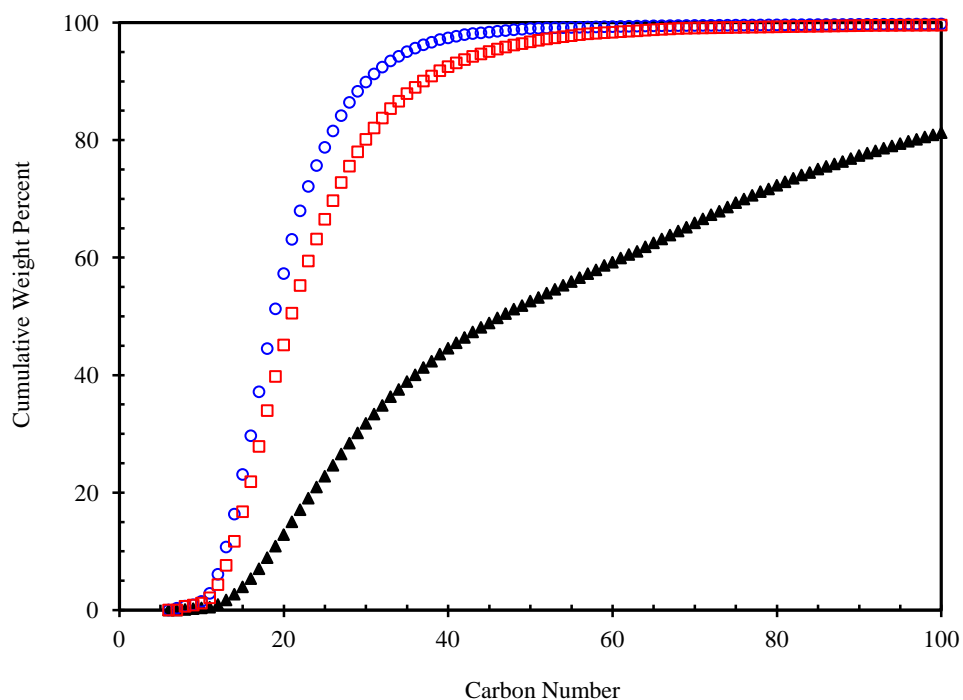


Figure 4-34: Carbon number distribution for raw bitumen (▲) and two extracts taken from liquid-liquid equilibrium study of MacKay River bitumen / ethane mixtures at different pressures and at a constant overall ethane concentration of 0.4 weight fraction; ○, 5 MPa; □, 9 MPa.

To have a better understanding about the component distribution, the fraction of components and carbon number distribution in residues (flashed-off phase samples taken from asphaltene-enriched phases) were plotted in Figures 4–35 and 4–36, respectively. The composition of raw bitumen is also shown for comparison in the figures. The chemical analysis of the residues at equilibrium conditions also verifies the impact of pressure on the extraction. As depicted in Figures 4–35 and 4–36, the residue becomes heavier with increasing pressure, indicating the depletion of light components in this phase. The C_{100+} fraction of residues taken from the liquid-liquid equilibrium at 5 and 9 MPa and a constant overall ethane concentration of 0.4 weight fraction are 0.199 and 0.207, respectively.

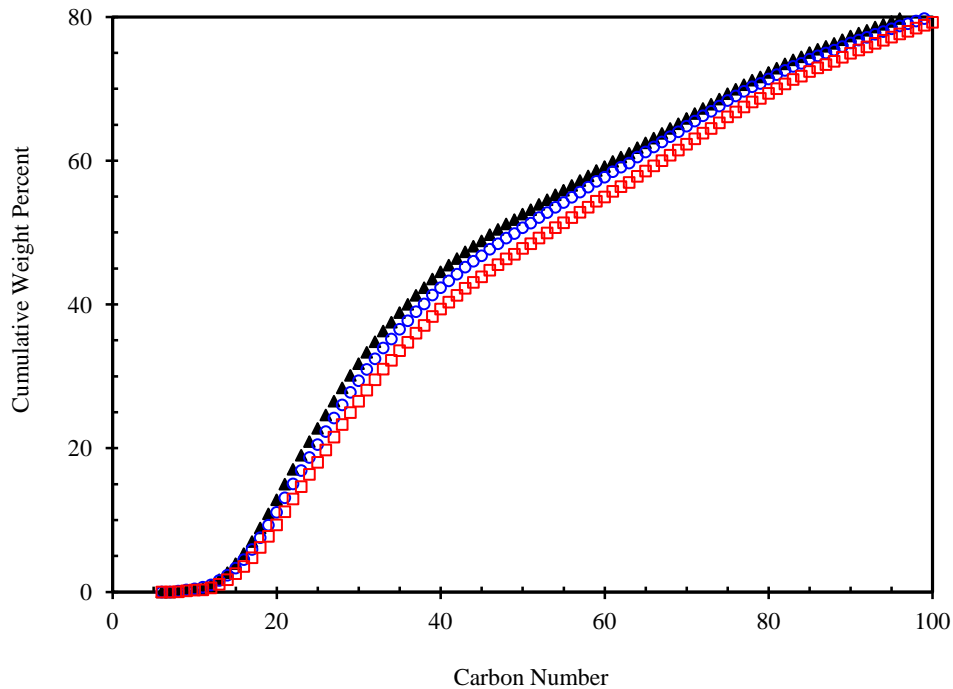


Figure 4–35: Carbon number distribution for raw bitumen (\blacktriangle) and two residues taken from liquid-liquid equilibrium study of MacKay River bitumen / ethane mixtures at different pressures and at a constant overall ethane concentration of 0.4 weight fraction; \circ , 5 MPa; \square , 9 MPa.

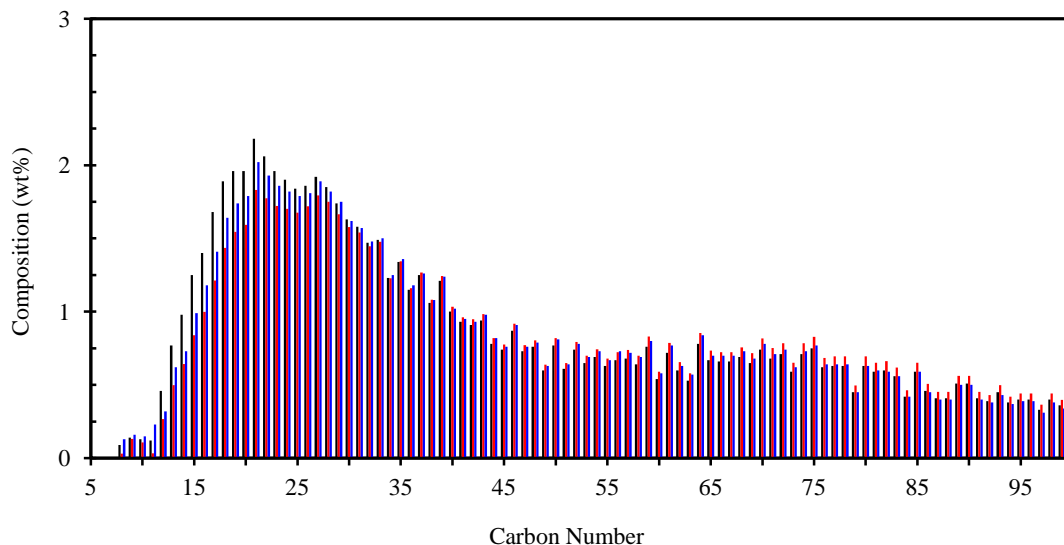


Figure 4–36: Compositional analysis (component weight percent) for raw bitumen (black) and two residues taken from liquid-liquid equilibrium study of MacKay River bitumen / ethane mixtures at different pressures and at a constant overall ethane concentration of 0.4 weight fraction; blue, 5 MPa; red, 9 MPa.

4.7.6.3. Effect of Overall Ethane Concentration

To evaluate the effect of the overall ethane concentration on the distribution of components in two liquid phases, ethane-to-bitumen ratio was increased at two constant pressures of 5 and 9 MPa. The maximum extraction yield was obtained at the highest overall ethane concentration at both pressures. The boiling point curves of the extracts taken from liquid-liquid equilibrium study at the overall ethane concentrations of 0.4 and 0.9 weight fractions and a constant pressure of 9 MPa were plotted in Figure 4–37. As depicted in the figure, the components in the extracts at higher overall ethane concentrations are heavier. This is more pronounced when the weight fraction of components in the extracts are examined (Figures 4–38 and 4–39).

Figure 4–38 shows the increase in the overall ethane concentration shifts the distribution of components toward the intermediate hydrocarbons. Thus, a higher fraction of intermediate components are extracted at overall ethane concentration of 0.9 weight fraction compared to that of 0.4 weight fraction at a constant pressure of 9 MPa. This occurs due to complete depletion of asphaltene-enriched phase from light components.

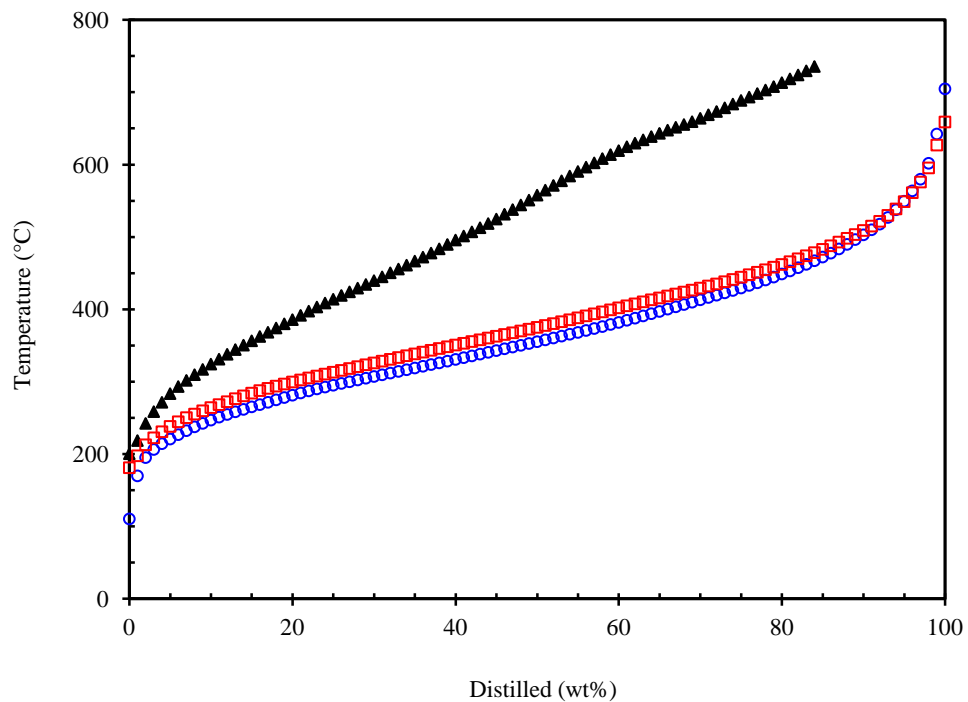


Figure 4-37: Boiling point curves (temperature versus weight percent distilled) for raw MacKay River bitumen (\blacktriangle) and two extracts taken from liquid-liquid equilibrium study of MacKay River bitumen / ethane mixtures at different overall ethane concentrations and at a constant pressure of 9 MPa; \circ , overall ethane weight fraction of 0.4; \square , overall ethane weight fraction of 0.9 (Nourozieh et al. 2012b).

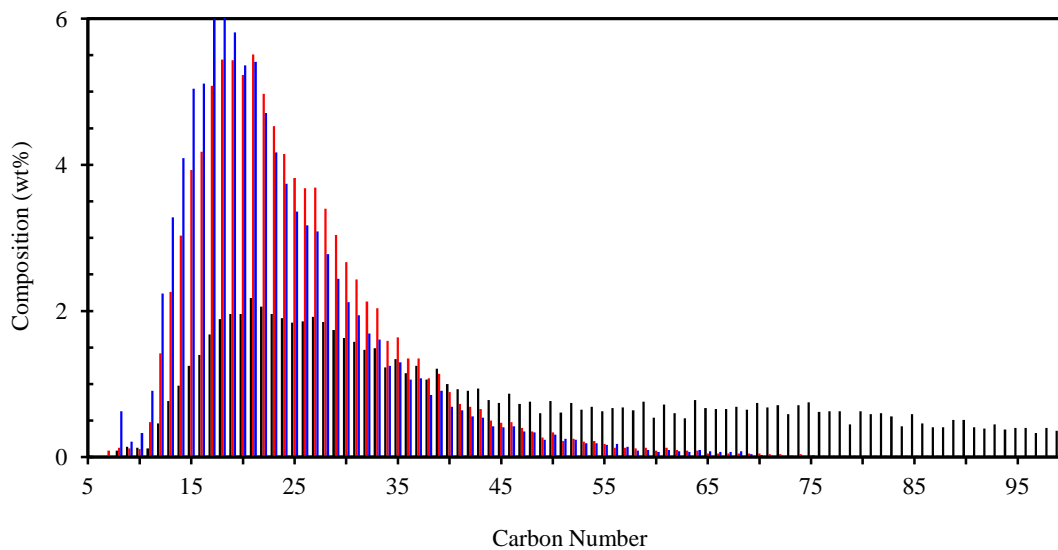


Figure 4-38: Compositional analysis (component weight percent) for raw bitumen (black) and two extracts taken from liquid-liquid equilibrium study of MacKay River bitumen / ethane mixtures at different overall ethane concentrations and at a constant pressure of 9 MPa; blue, overall ethane weight fraction of 0.4; red, overall ethane weight fraction of 0.9 (Nourozieh et al. 2012b).

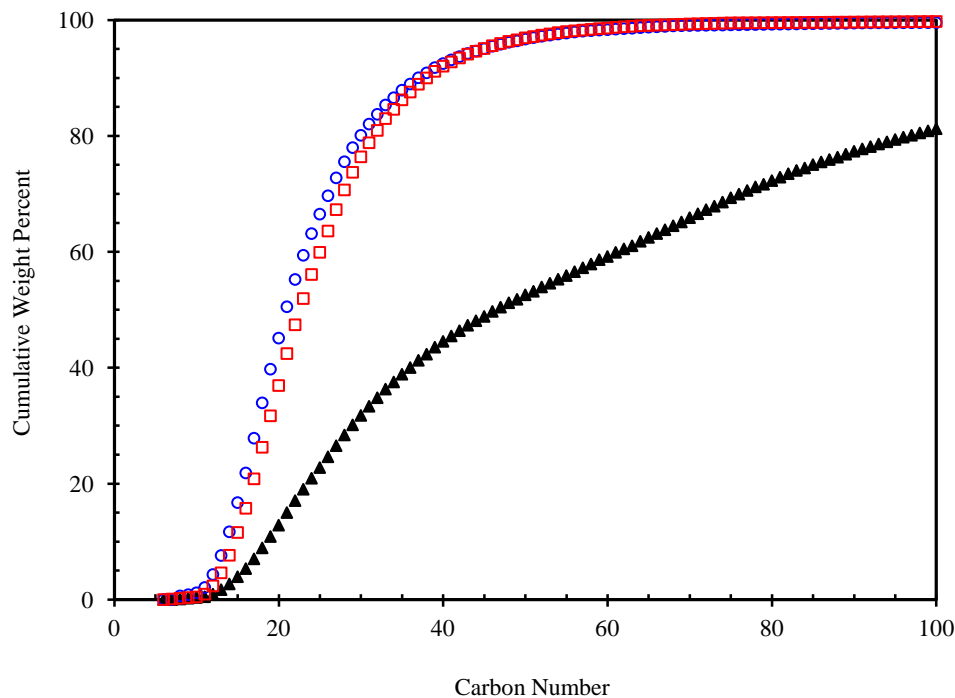


Figure 4–39: Carbon number distribution for raw MacKay River bitumen (▲) and two extracts taken from liquid-liquid equilibrium study of MacKay River bitumen / ethane mixtures at different overall ethane concentrations and at a constant pressure of 9 MPa; ○, overall ethane weight fraction of 0.4; ◻, overall ethane weight fraction of 0.9.

The cumulative extraction yields in Table 4–11 show that 0.384 weight fraction of bitumen is extracted into the solvent-enriched phase at the overall ethane concentration of 0.9 weight fraction and a constant pressure of 9 MPa. The compositional analyses and boiling point curves of the extracts do not clearly demonstrate the component distribution and extractions. Thus, the compositional analyses of residues are also presented in Figures 4–40 and 4–41.

Figure 4–41 shows that how the asphaltene-enriched phase becomes heavier with increasing overall ethane concentration. Indeed, the asphaltene-enriched phase (L_2) at the overall ethane concentration of 0.9 weight fraction contains no components lighter than C_{22} . Thus, it can be concluded that the overall ethane concentration controls the cumulative extraction. The complete extraction of components C_8 - C_{21} can be attained by increasing the overall ethane concentration in the mixture. The C_{100+} fractions of two

residues taken from liquid-liquid equilibrium study at the overall ethane concentrations of 0.4 and 0.9 weight fractions are 0.207 and 0.297, respectively.

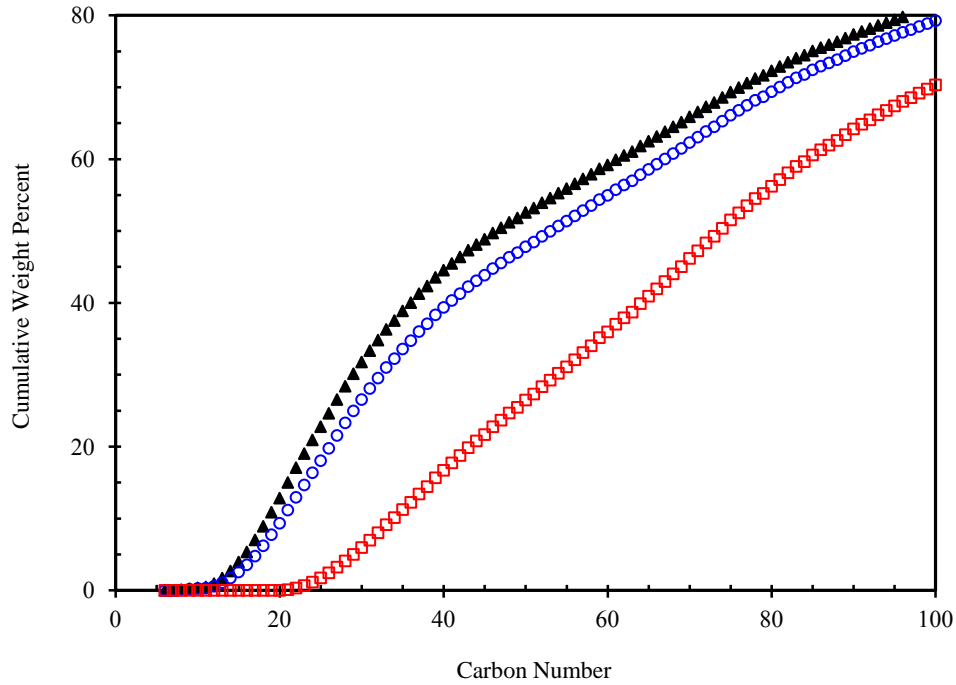


Figure 4-40: Carbon number distribution for raw MacKay River bitumen (\blacktriangle) and two residues taken from liquid-liquid equilibrium study of MacKay River bitumen / ethane mixtures at different overall ethane concentrations and at a constant pressure of 9 MPa; \circ , overall ethane weight fraction of 0.4; \square , overall ethane weight fraction of 0.9.

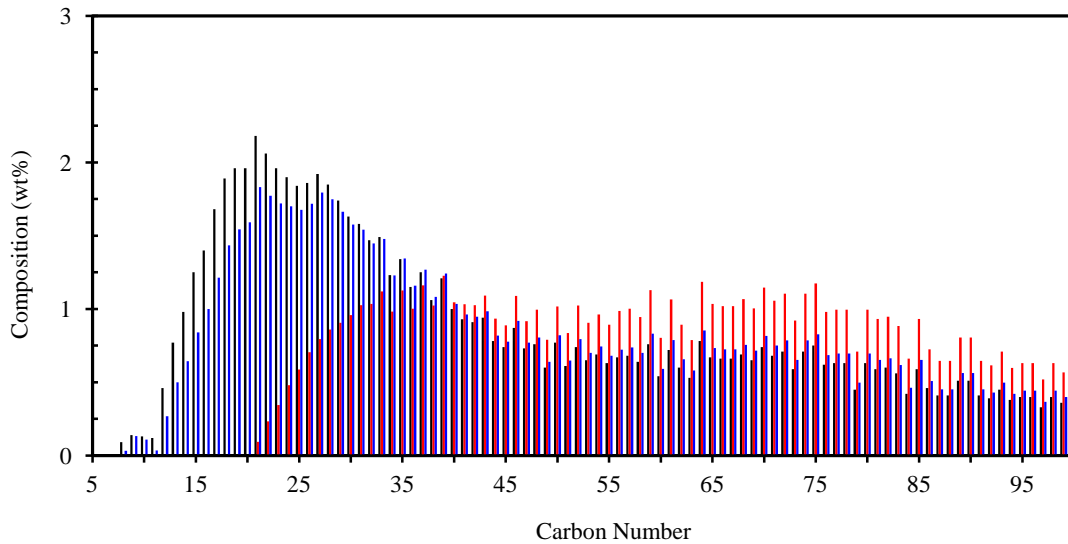


Figure 4-41: Compositional analysis (component weight percent) for raw bitumen (black) and two residues taken from liquid-liquid equilibrium study of MacKay River bitumen / ethane mixtures at different overall ethane concentrations and at a constant pressure of 9 MPa; blue, overall ethane weight fraction of 0.4; red, overall ethane weight fraction of 0.9 (Nourozieh et al. 2012b).

4.7.7. SARA Analysis of Extracts and Residues

The SARA analyses were conducted on the flashed-off liquid samples taken from two equilibrium liquid phases at different operating conditions. Table 4–13 summarizes the SARA analysis results for extracts and residues.

Table 4–13: SARA analysis (in weight percent) of flashed-off liquid samples taken from two equilibrium phases in the liquid-liquid equilibrium study of MacKay River bitumen / ethane mixtures; *P*, pressure; *T*, temperature; *w*, overall ethane concentration in weight fraction.

<i>T</i> (°C)	<i>P</i> (MPa)	10 ² <i>w</i>	Phase	Saturates	Aromatics	Resins	Asphaltenes
21.5	5.05	60	L ₁	58.56	37.36	4.08	0.00
			L ₂	8.76	42.49	37.06	11.69
21.4	9.08	40	L ₁	----	----	----	----
			L ₂	10.49	48.30	29.29	11.92
21.1	9.08	60	L ₁	52.80	36.63	10.57	0.00
			L ₂	7.55	40.57	38.79	13.09
21.5	9.04	80	L ₁	48.13	51.18	0.69	0.00
			L ₂	5.22	38.01	41.25	15.52

The results show that the solvent-enriched phases are mostly composed of saturates with a considerable amount of aromatics. No asphaltenes were detected in the samples, and the resin content is small and is a function of the operating conditions. The absence of asphaltenes in the solvent-enriched phases is due to the nature of ethane. The asphaltene fraction of bitumen is less soluble in light hydrocarbon components, such as ethane, propane, and butane. Ethane precipitates the resins and asphaltenes from the bitumen. The resin content of extracts and their comparison with that of bitumen confirms that the samples have also much lower resin contents than the bitumen (less than 10 wt%). The asphaltenes and resins are structurally different from ethane, due to their large, polar, and highly aromatic molecules (Rose 1999; Mansoori 2009). The pressure and overall ethane concentrations affects the distribution of fractions in two liquid phases.

The mutual solubility of compounds in petroleum crudes can generally be devoted to two factors: the ratio of high to low molecular weight compounds and the ratio of polar to nonpolar compounds (Kawanaka et al. 1989). Change in these ratios affect the asphaltene content of extract and residue compared to the raw bitumen (Deo et al. 1993). Thus, the material balance on the asphaltene fractions of raw bitumen and that of a residue or an extract to obtain the fractions of the other liquid phase is misleading. Table 4–14 presents the measured asphaltene content of residues and the calculated values based on the material balance on the bitumen charged into the equilibrium cell and the asphaltene content of extracts. The measured asphaltene contents are much higher than the calculated values on the basis of material balance. This indicates that the asphaltenes are a collection of components specific to a given mixture, not a definite class of compounds (Deo et al. 1993). Indeed, the lighter components in the mixtures keep the asphaltenes in the solution (Mansoori 1996, 2002). According to Nellensteyn (1938), the resins (cosolubilizing agents) and other hydrocarbons help the asphaltenes micelles to be covered in the oil. In the liquid-liquid equilibrium experiments, the light hydrocarbons are stripped from the asphaltene-enriched phase; thus, the tendency of asphaltene molecules to stay in the solution reduces.

Table 4–14: SARA analysis (in weight percent) of residues taken from two equilibrium phases in the liquid-liquid equilibrium study of MacKay River bitumen / ethane mixtures; *P*, pressure; *T*, temperature; *w*, overall ethane concentration in weight fraction.

<i>T</i> (°C)	<i>P</i> (MPa)	10 ² <i>w</i>	Phase	Saturates	Aromatics	Resins	Asphaltenes
21.5	5.05	60	L ₂ (experiment)	8.76	42.49	37.06	11.69
			L ₂ (mass balance)	5.88	59.47	23.81	10.83
21.1	9.08	60	L ₂ (experiment)	7.55	40.57	38.79	13.09
			L ₂ (mass balance)	4.44	60.64	23.58	11.34
21.5	9.04	80	L ₂ (experiment)	5.22	38.01	41.25	15.52
			L ₂ (mass balance)	0	58.00	28.99	13.02

Figure 4–42 illustrates a comparison of the SARA fractions in raw bitumen and those of two liquid phases at the temperature of 21.6°C and the pressure of 9 MPa with an

overall ethane concentration of 0.6 weight fraction. As depicted in the figure, the saturate and aromatic contents of the residue are lower than those of raw bitumen. The extract is mostly composed of saturates with a considerable amount of aromatics. No asphaltenes were detected in the extract. The resin content of extract compared to that of bitumen confirms that the samples have also much lower resin contents than bitumen. The asphaltene fraction of bitumen is insoluble in ethane. Therefore, the resin and asphaltene contents of residue are much higher than those of extracts and raw bitumen. This indicates that ethane substantially precipitates the resin and asphaltene contents of the bitumen and that the contribution of resins to the extract is much less than that of saturate and aromatic fractions.

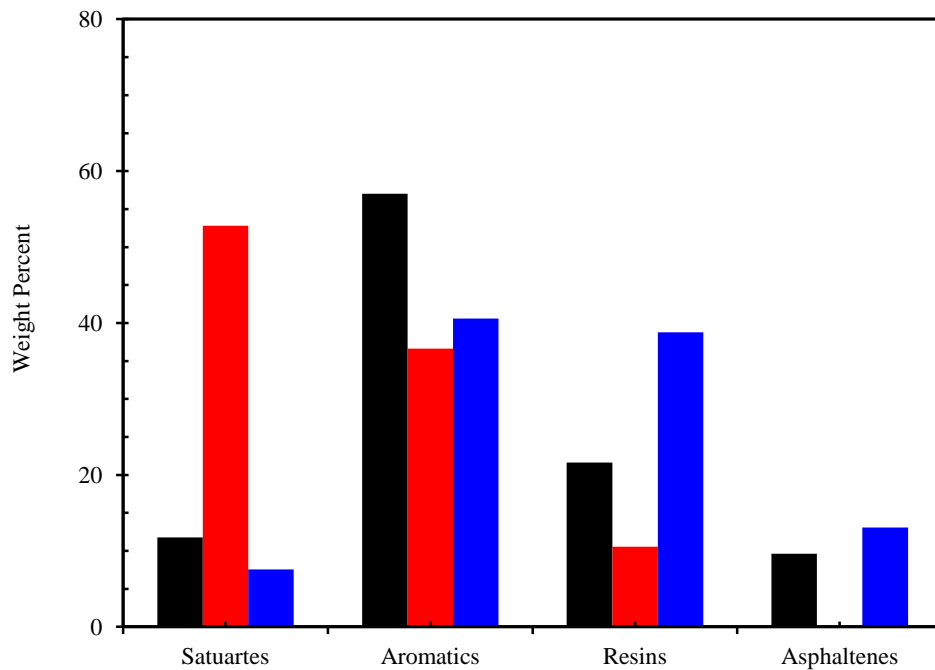


Figure 4–42: SARA compositional analysis of raw bitumen and two flashed-off liquid phases taken from liquid-liquid equilibrium study of MacKay River bitumen / ethane mixtures at ambient temperature and at 9 MPa with an overall ethane concentration of 0.6 weight fraction; black, raw bitumen; red, extract; blue, residue.

The excess volume of ethane in the mixture enhances the precipitation of asphaltene and resin fractions. This is evident through the comparison of the SARA fractions of extracts presented in Figure 4–43 at different overall ethane concentrations. The increase

in overall ethane concentration increases the saturate and aromatic contents of extract, consequently reducing the asphaltene and resin fractions. An opposite trend in the SARA fractions of residues is evident in Figure 4–44.

The analysis of the residues points out the presence of saturate and aromatic fractions in the flashed-off samples taken from the asphaltene-enriched phase. However, the addition of ethane as a non-polar solvent in excess amounts produces a residue free from saturate and aromatic fractions. At the same time, the extracts become free from the asphaltene and resin fractions.

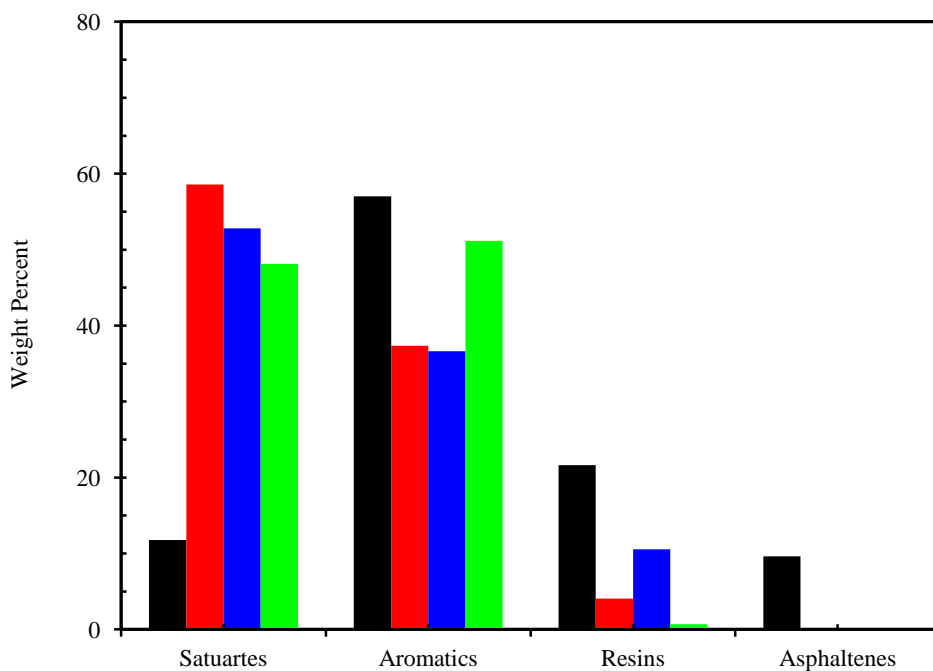


Figure 4–43: Effect of overall ethane concentration and pressure on the SARA compositional analysis of extracts taken from liquid-liquid equilibrium study of MacKay River bitumen / ethane mixtures at ambient temperatures; black, raw bitumen; red, 5 MPa and overall ethane concentration of 0.6 weight fraction; blue, 9 MPa and overall ethane concentration of 0.6 weight fraction; green, 9 MPa and overall ethane concentration of 0.8 weight fraction.

Increases in the pressure at a constant temperature and overall ethane concentration result in an extract with a higher resin fraction and a residue with lower saturate and aromatic contents. Figure 4–43 shows the impact of pressure on the variation of different fractions in extracts. As anticipated from the figure, the impact of pressure on the

distribution of fractions within the phase is highly dependent on the overall ethane concentrations. Figure 4–43 also shows an increase in the resin content of extract with the pressure at a constant overall ethane concentration of 0.6 weight fraction. However, when the overall ethane concentration is increased to 0.8 weight fraction, the resin content of extract reduces and instead the aromatic fraction increases. Hence, the resin fraction of bitumen is more readily extracted with the increase in the pressure, and the aromatic content of the extract reduces at low overall ethane concentrations (e.g. 0.4 weight fraction).

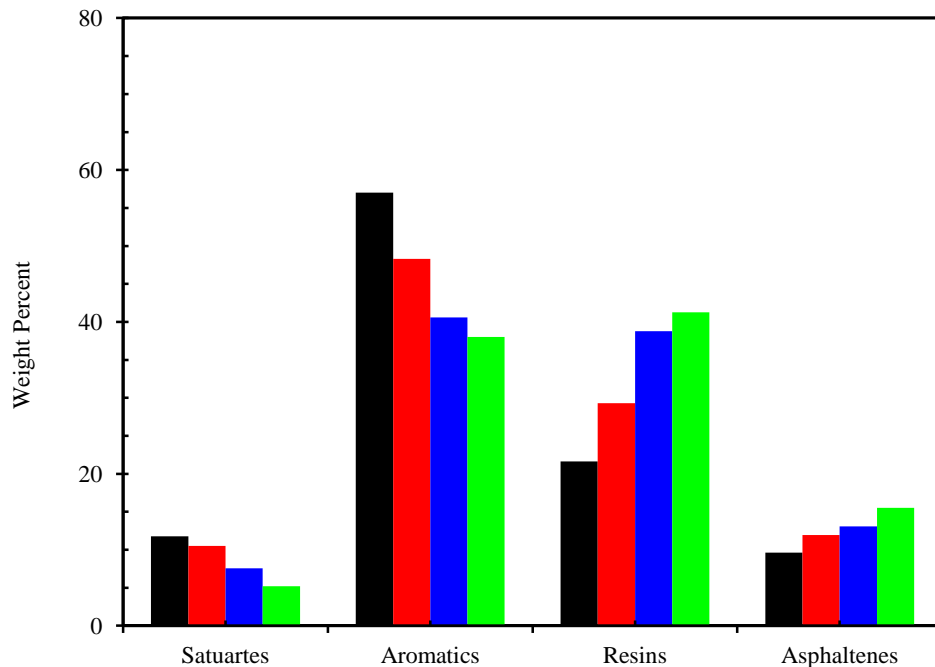


Figure 4–44: Effect of overall ethane concentration on the SARA compositional analysis of residues taken from liquid-liquid equilibrium study of MacKay River bitumen / ethane mixtures at ambient temperatures and at a constant pressure of 9 MPa; black, raw bitumen; red, overall ethane concentration of 0.4 weight fraction; blue, overall ethane concentration of 0.6 weight fraction; green, overall ethane concentration of 0.8 weight fraction.

Thus, it can be concluded that pressure enhances the extraction of saturates and aromatic fractions into the solvent-enriched phase at higher overall ethane concentrations while it increases the extraction of the resin fraction at lower overall ethane concentrations.

4.7.8. Equilibrium K-values and Molecular Weight

The experimental solubility and density data for binary systems of bitumen/solvent systems can provide an appropriate thermodynamic and phase behaviour model for reservoir simulation software. An approach for the thermodynamic modelling and equilibrium calculation rather than equation of state is using experimental k -values. Thus, on the basis of experiments, the equilibrium k -values for different components present in a mixture can be obtained and directly applied into reservoir simulation software. There are some experimental equilibrium K-values reported in the literature for the mixtures of bitumen and light hydrocarbon gases at vapour-liquid equilibrium condition (Frauenfeld et al. 2002). However, no data for liquid-liquid equilibrium K-values or distribution of components in different phases using generated K-values have been reported. The compositional analysis of liquid phases combined with the available correlations for molecular weight distribution enable the determination of equilibrium K-values for all components present in a mixture. The following correlation for the molecular weight of components (C_n , where $n \geq 10$) was applied to calculate equilibrium K-values,

$$MW = \left[\frac{6.97996 - \ln(1080 - T_b)}{0.01964} \right]^{\frac{3}{2}} \quad 4-7$$

where T_b is in K. For components with $n \leq 10$, the molecular weight was taken from Riazi (2005). The calculated K-values for different components are summarized in Table 4–15. As the table shows the trends discussed in previous sections are also observed in the equilibrium K-value. As pressure or overall ethane concentration increases, the extraction yield increases and lighter components are largely partitioned into the solvent-enriched phase (L_1) and results in an infinity value for the equilibrium K-value. The infinity value for specific component indicates that the component is completely extracted by solvent into the solvent-enriched phase. Therefore, the component does not exist in the asphaltene-enriched phase (L_2). On the other hand, the K-value equal to zero means that ethane cannot extract the component and it remains in the asphaltene-enriched phase (L_2).

Table 4–15: Correlated molecular weight and calculated K-values of components at equilibrium conditions for MacKay River bitumen / ethane mixtures at ambient temperature; w , overall ethane weight fraction (Kariznovi et al. 2013c).

Component	MW	$w = 0.4$ and $P = 5$ MPa	$w = 0.4$ and $P = 9$ MPa	$w = 0.9$ and $P = 9$ MPa
C ₂	30.07	1.284	1.240	1.258
C ₆	84	∞	∞	∞
C ₇	95	∞	∞	∞
C ₈	107	0.062	0.902	∞
C ₉	121	0.032	0.072	∞
C ₁₀	136	0.086	0.138	∞
C ₁₁	149	0.134	1.192	∞
C ₁₂	163	0.229	0.379	∞
C ₁₃	176	0.168	0.298	∞
C ₁₄	191	0.173	0.288	∞
C ₁₅	207	0.153	0.272	∞
C ₁₆	221	0.126	0.232	∞
C ₁₇	237	0.119	0.224	∞
C ₁₈	249	0.101	0.193	∞
C ₁₉	261	0.088	0.170	∞
C ₂₀	275	0.075	0.152	∞
C ₂₁	289	0.065	0.134	0.407
C ₂₂	303	0.057	0.120	0.147
C ₂₃	317	0.050	0.110	0.091
C ₂₄	331	0.044	0.100	0.059
C ₂₅	345	0.039	0.091	0.045
C ₂₆	359	0.035	0.084	0.036
C ₂₇	373	0.031	0.078	0.032
C ₂₈	387	0.028	0.072	0.027
C ₂₉	400	0.024	0.066	0.023
C ₃₀	415	0.022	0.061	0.019
C ₃₁	429	0.020	0.057	0.016
C ₃₂	443	0.018	0.053	0.014
C ₃₃	457	0.016	0.049	0.013
C ₃₄	471	0.014	0.046	0.011
C ₃₅	485	0.013	0.044	0.010
C ₃₆	499	0.011	0.041	0.009
C ₃₇	513	0.010	0.039	0.008
C ₃₈	528	0.009	0.036	0.007
C ₃₉	542	0.008	0.033	0.006
C ₄₀	556	0.006	0.030	0.006
C ₄₁	570	0.007	0.030	0.005
C ₄₂	584	0.007	0.027	0.005
C ₄₃	599	0.004	0.025	0.004
C ₄₄	614	0.003	0.023	0.004
C ₄₅	629	0.004	0.024	0.004
C ₄₆	641	0.004	0.021	0.003
C ₄₇	656	0.004	0.021	0.003
C ₄₈	670	0.004	0.019	0.002
C ₄₉	684	0.004	0.017	0.002
C ₅₀	698	0.003	0.017	0.002

C ₅₁	713	0.002	0.017	0.002
C ₅₂	727	0.001	0.014	0.002
C ₅₃	742	0.001	0.012	0.002
C ₅₄	756	0.001	0.012	0.002
C ₅₅	770	0.001	0.011	0.001
C ₅₆	785	0.001	0.011	0.001
C ₅₇	799	0.001	0.009	0.001
C ₅₈	814	0.001	0.006	0.001
C ₅₉	828	0.001	0.005	0.001
C ₆₀	843	0.001	0.005	0.001
C ₆₁	857	0.001	0.006	0.001
C ₆₂	872	0.001	0.006	0.001
C ₆₃	886	0.001	0.005	0.001
C ₆₄	901	0.001	0.005	0.001
C ₆₅	915	0.001	0.005	0.000
C ₆₆	930	0.001	0.004	0.000
C ₆₇	945	0.001	0.004	0.000
C ₆₈	959	0.000	0.005	0.000
C ₆₉	974	0.000	0.003	0.000
C ₇₀	988	0.000	0.002	0.000
C ₇₁	1003	0.000	0.001	0.000
C ₇₂	1018	0.000	0.001	0.000
C ₇₃	1033	0.000	0.001	0.000
C ₇₄	1047	0.000	0.001	0.000
C ₇₅	1062	0.000	0.000	0.000
C ₇₆	1077	0.000	0.000	0.000
C ₇₇	1092	0.000	0.000	0.000
C ₇₈	1107	0.000	0.000	0.000
C ₇₉	1121	0.000	0.000	0.000
C ₈₀	1136	0.000	0.000	0.000
C ₈₁	1151	0.000	0.000	0.000
C ₈₂	1166	0.000	0.000	0.000
C ₈₃	1181	0.000	0.000	0.000
C ₈₄	1196	0.000	0.000	0.000
C ₈₅	1211	0.000	0.000	0.000
C ₈₆	1226	0.000	0.000	0.000
C ₈₇	1241	0.000	0.000	0.000
C ₈₈	1256	0.000	0.000	0.000
C ₈₉	1271	0.000	0.000	0.000
C ₉₀	1286	0.000	0.000	0.000
C ₉₁	1302	0.000	0.000	0.000
C ₉₂	1317	0.000	0.000	0.000
C ₉₃	1332	0.000	0.000	0.000
C ₉₄	1347	0.000	0.000	0.000
C ₉₅	1362	0.000	0.000	0.000
C ₉₆	1378	0.000	0.000	0.000
C ₉₇	1393	0.000	0.000	0.000
C ₉₈	1408	0.000	0.000	0.000
C ₉₉	1424	0.000	0.000	0.000
C ₁₀₀	1439	0.000	0.000	0.000

The molecular weights of the flashed-off liquid samples were calculated based on component mole fraction and its molecular weight and the results are summarized in Table 4–16. As the table shows, the molecular weight of the extract (L_1) as well as the residue increases with the pressure and overall ethane concentration. This is an indirect indication of component distribution within the phases. The overall ethane concentration significantly changes the molecular weight of the samples, which may be due to the complete extraction of light components from the asphaltene-enriched phase (L_2) at high overall concentrations resulting in a high molecular weight value for the asphaltene-enriched phase.

Table 4–16: Calculated molecular weight of flashed-off phase samples taken from liquid-liquid equilibrium study of MacKay River bitumen / ethane mixtures at ambient temperature; w , overall ethane weight fraction (Kariznovi et al. 2013c).

Equilibrium Condition	L_1	L_2
$w = 0.4$ and $P = 5$ MPa	259	541
$w = 0.4$ and $P = 9$ MPa	286	572
$w = 0.9$ and $P = 9$ MPa	370	870

4.7.9. Phase Diagrams for MacKay River Bitumen / Ethane Systems

The presentation of phase diagrams, such as pressure-temperature (P - T) at a constant composition or pressure-composition (P - x) at a constant temperature, for the bitumen/solvent systems is beyond the scope of this study. Many experimental data and higher resolution near the boundary, where the phase transition occurs, are required to develop a quantitative phase diagrams. Consequently, the phase behaviour of these mixtures is investigated with qualitative phase diagrams. These diagrams were drawn based on all of the generated experimental data in this research. Thus, the regions were defined on the basis of the experimental data; and, the transition zones and the regions between the experimental points may subject to further experimental analysis.

As previously mentioned, the mixture of MacKay River bitumen and ethane exhibits the liquid-liquid partitioning at the temperatures less than 30°C. The experiments were

designed to analyze the important parameters and their impacts on the physical properties. Based on the experimental observations, the qualitative pressure-temperature diagram for Mackay River bitumen / ethane systems is presented in Figure 4–45. The blue symbols correspond to the experiments in which the vapour-liquid equilibrium exists. The red symbols are the experimental conditions which lead to liquid-liquid equilibrium. Finally, the green symbols are the experimental data reported in the literature.

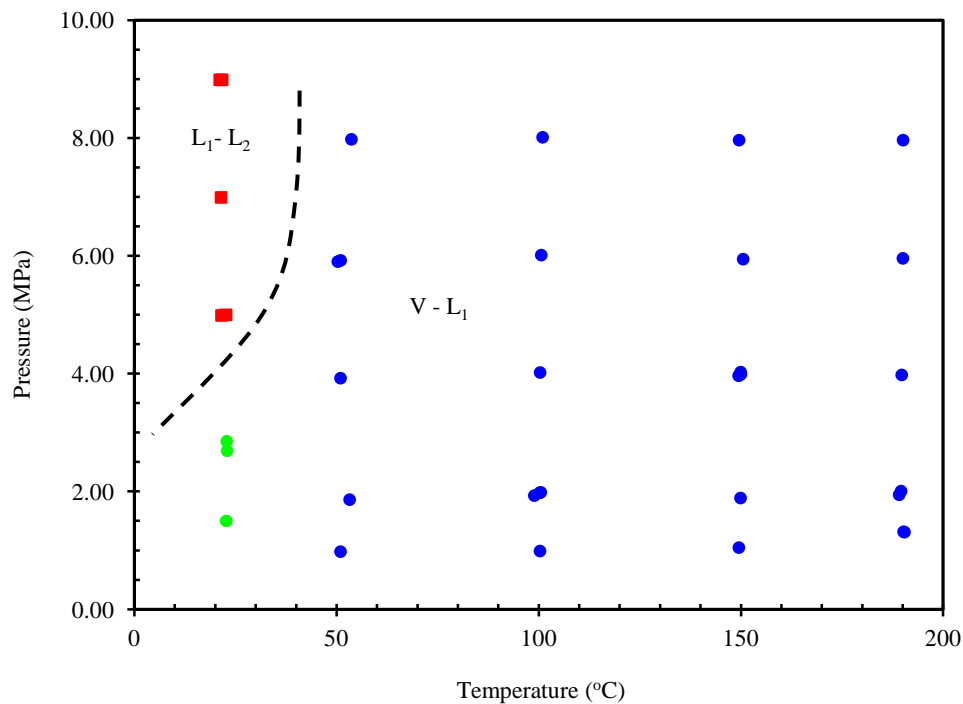


Figure 4–45: Pressure-Temperature (P - T) diagram for Mackay River bitumen / ethane systems; •, vapour-liquid experimental data; •, the experimental data of Athabasca bitumen / ethane systems by Mehrotra and Svrcek (1985a); ■, liquid-liquid experimental data.

As Figure 4–45 indicates, there is a narrow range in which more than two phases can form. The transition between the regions is presented by a dashed line, and no experimental data have confirmed the three-phase region yet. The boundary between the vapour-liquid and liquid-liquid regions is clearly determined at ambient temperature, where the transition occurs at the pressure around 4 MPa. At the temperatures higher than

30°C where ethane is at supercritical conditions, the vapour phase contains the light hydrocarbons extracted from bitumen at high pressures (> 6 MPa). In this case, the liquid-liquid behaviour is also observed for bitumen/ethane mixtures.

In addition to the pressure-temperature diagram, the phase behaviour of MacKay River bitumen / ethane mixtures is presented as pressure-composition diagram in Figure 4-46 at a constant temperature of 21.6°C. Three regions, depending on the pressure and overall ethane concentration, L_1 , L_1 - L_2 , and L_1 -V, were observed during the experiments.

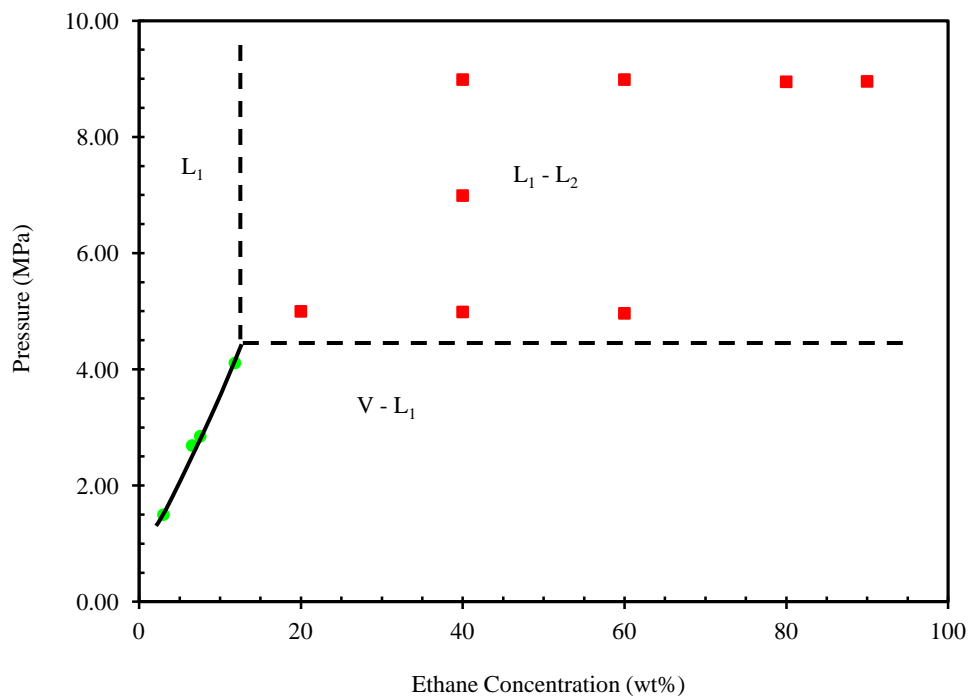


Figure 4-46: Pressure-Composition (P - x) diagram for Mackay River bitumen / ethane systems at ambient temperature; ●, the experimental data of Athabasca bitumen / ethane systems by Mehrotra and Svrcek (1985a); ■, liquid-liquid experimental data.

At 21.6°C, the vapour phase is pure ethane in the V- L_1 region, and the composition of liquid phase varies with the pressure. In the L_1 - L_2 region, as more ethane is added to the mixture at this temperature, the physical properties of phases change. As anticipated from Figure 4-46 and the results in Section 4.7.7, if two liquids are present at equilibrium conditions, the less dense phase (i.e. solvent-enriched phase, L_1) is rich in saturates and/or

aromatics while the more dense phase (i.e. asphaltene-enriched phase, L_2) is rich in resins and asphaltenes. The selectivity of the component distribution is clearly a function of the overall ethane concentration and pressure.

The pressure-composition diagram presented in Figure 4-46 indicates that, for pressures greater than 4 MPa, the increase in the overall ethane concentration converts the state of the system from single phase into a L_1 - L_2 equilibrium condition. However, for pressures less than 4 MPa, the single phase region changes to a V - L_1 equilibrium by which the vapour phase is virtually pure ethane. The pressure of 4 MPa is the saturation pressure of ethane at ambient temperature. The dashed lines in Figure 4-46 are the qualitative transition boundaries between the L_1 - L_2 and V - L_1 regions and between L_1 - L_2 and L_1 regions. The boundary between L_1 and V - L_1 regions were experimentally confirmed and are shown by a solid line.

By combining the phase behaviour observations and the physical property measurements at constant overall ethane concentration and temperature, a diagram for the compositions of the coexisting phases versus equilibrium pressure and a diagram for the densities of coexisting phases versus equilibrium pressure were constructed. Figures 4-47 and 4-48 show these diagrams for Mackay River bitumen / ethane mixtures at a constant overall ethane concentration of 0.4 weight fraction and at a constant temperature of 21.6°C.

Figure 4-47 shows the compositions of the coexisting phases at different equilibrium pressures. The plot is shown for the cases where there is excess ethane in the system (overall ethane concentration is 0.4 weight fraction). In other words, no single phase region can be detected at constant temperature and pressure. As anticipated from the figure, the composition of ethane in L_1 within V - L_1 region increases with the pressure. This behaviour is expected, because the solubility of hydrocarbon gases in bitumen increases with the pressure. As the pressure further increases to 4 MPa, the V - L_1 region is still observed, and the vapour phase is pure ethane. However, at pressures higher than 4 MPa, the vapour phase (i.e. solvent-enriched phase) composition dramatically changes

and reduces with the pressure. The V-L₁ equilibrium changes to L₁-L₂ equilibrium condition.

In L₁-L₂ region, the composition of the solvent-enriched phase (L₁) reduces with the pressure, due to the extraction of light hydrocarbons into this phase. On the other hand, the composition of ethane in the asphaltene-enriched phase (L₂) remains constant with pressure. The slope of curve for the composition of ethane in L₂ is not the same as that of V-L₁ region, i.e. ethane composition in L₂ does not increase with pressure as in L₁ within V-L₁ region. The bitumen components in L₂ become heavier with increasing pressure, due to higher extraction of light components into L₁ at higher pressures; thus, a reduction in the composition of ethane in L₂ is expected (the heavier hydrocarbon component, the lower solubility of ethane at fixed temperature and pressure). In contrast, the solubility of ethane in the heavy hydrocarbons increases with pressure. The first factor compensates for the second one and no change in the composition is observed.

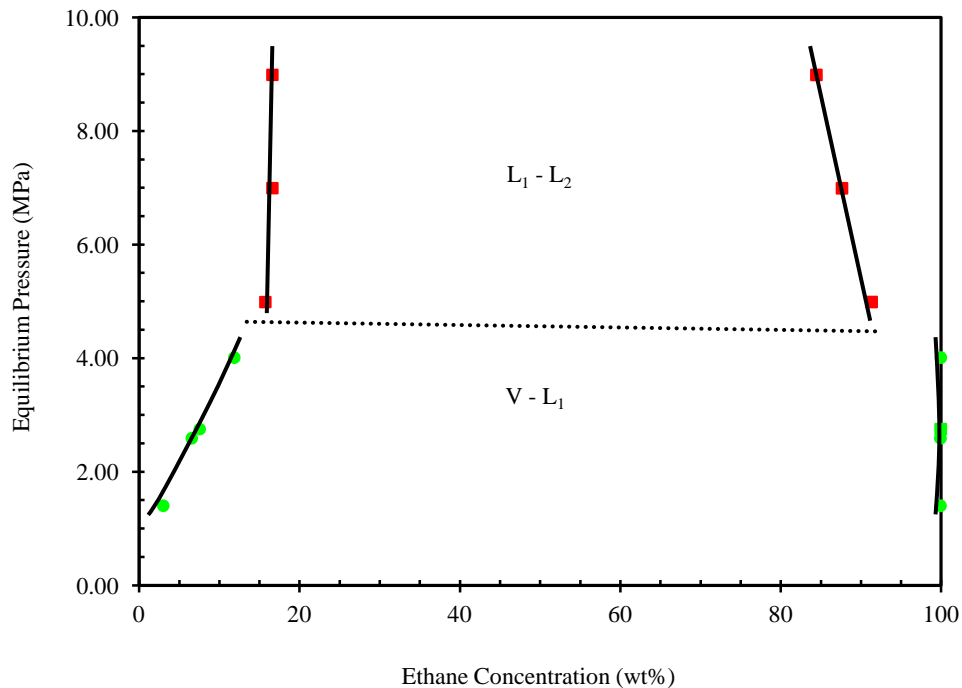


Figure 4–47: Coexisting phase compositions for Mackay River bitumen / ethane systems at ambient temperature and at a constant overall ethane concentration of 0.4 weight fraction; ●, the experimental data of Athabasca bitumen / ethane systems by Mehrotra and Srceek (1985a); ■, liquid-liquid experimental data.

Figure 4–48 shows the densities of the coexisting phases at different equilibrium pressures. Similar to the compositions of the coexisting phases, there is an excess volume of ethane in the mixture (overall ethane concentration is 0.4 weight fraction). That is, no single phase region is detected at the studied pressure range. As anticipated from the figure, the density of L_1 within $V-L_1$ region reduces with the pressure, due to higher dissolution of ethane in the saturated bitumen with the increase in pressure. Nevertheless, further increases in the pressure result in a change in the state of system from $V-L_1$ equilibrium to L_1-L_2 equilibrium. The dramatic variation in the density of the solvent-enriched phase indicates the phase transition from vapour into L_1 . The experimental results in the liquid-liquid equilibrium study indicate that the density of L_1 in L_1-L_2 region is higher than the density of pure ethane at a specified pressure. This confirms that the light hydrocarbon components are extracted into the solvent-enriched phase (L_1).

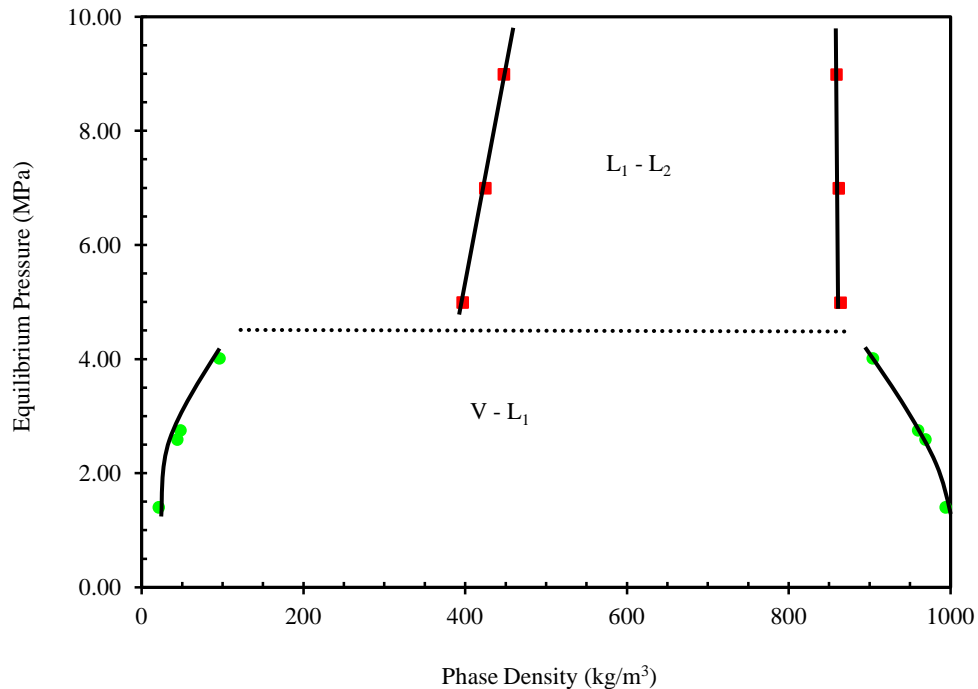


Figure 4–48: Coexisting phase densities for Mackay River bitumen / ethane systems at ambient temperature and at a constant overall ethane concentration of 0.4 weight fraction; ●, the experimental data of Athabasca bitumen / ethane systems by Mehrotra and Svrcek (1985a); ■, liquid-liquid experimental data.

Further investigation of coexisting phase densities reveals that pressure affects the densities of both liquid phases at equilibrium conditions. The influence of pressure on the density of the phases is an indirect indication of the pressure effect on the extraction yield, which causes an increase in the densities of L_1 and L_2 in L_1 - L_2 region. The variation in the density of L_2 is not as significant as that of L_1 . This is due to three main factors,

- The increase in ethane composition in L_2 with pressure
- The direct impact of pressure on the density of liquid, i.e. the increase in density with pressure
- L_2 becomes leaner in light hydrocarbons with the increase in pressure

The density results in Figure 4–48 for L_2 reveal that the first factor is balanced with other two factors; and, a slight increase in the density of L_2 is observed.

Although the density of L_2 remains almost constant with pressure, the density of L_1 is considerably increased with pressure. In this case, the greater extraction of bitumen components and the influence of pressure on the density of liquid result in an increase in the density of L_1 . Thus, as the pressure increases, more components are transferred into L_1 making this phase much heavier. The compositional analysis presented in Section 4.7.6 confirms the above-mentioned behaviours.

Chapter 5: Phase Behaviour of Bitumen/Propane Mixtures

This chapter provides the vapour-liquid and liquid-liquid equilibrium data for bitumen/propane mixtures and their applications for bitumen recovery processes. Similar to bitumen/ethane mixtures, the results of vapour-liquid equilibria cover the solubility, density, and viscosity measurements of the saturated liquid, K-values, and GOR. For liquid-liquid equilibrium conditions, the properties of equilibrium phases as well as extraction yield were studied. The effect of different parameters on the phases' composition, density, viscosity, and compositional analysis has been investigated. The vapour-liquid and liquid-liquid equilibrium data were then combined to generate phase diagrams. In this chapter, the effect of dissolution of different solvents on the thermo-physical properties of the saturated bitumen was also investigated. The reported data in this chapter are used for the tuning of equation of state.

5.1. Introduction

Vapour extraction (Vapex) process was described and patented by Butler and Mokrys in 1991 (Butler and Mokrys 1991). It is a new oil recovery process with the same analogy as the SAGD process using solvent instead of steam. It has application in thin reservoirs, where SAGD cannot be applied due to high heat loss. A series of experimental studies by Butler and Mokrys (Mokrys and Butler 1993; Butler and Mokrys 1993a, 1993b) show that this technique can be economically applied for heavy oil recovery. Propane is one of the best solvents which can be considered for Vapex process in Alberta reservoirs. Low dew point pressure makes propane a favourable solvent for Vapex process. Its mixtures with non-condensable gases such as methane and nitrogen enable to adjust the dew point pressure of the mixture.

Propane has high solubility in heavy oil and bitumen compared to methane, ethane, and nitrogen and leads to significant viscosity reduction. The diluted oil is mobile at

reservoir condition with an economical production rate. In addition, propane can also contribute to an *in-situ* upgrading process which leads to the production of higher oil quality by deasphalting (Nourozieh et al. 2011b). *In-situ* upgrading improves the oil quality and reduces the processing cost of the produced oil. In addition to solvent-based recovery processes such as Vapex, propane can be considered as an additive to steam-based processes. As previously mentioned, in steam-based processes such as cyclic steam injection and SAGD, a small amount of additive solvent can be co-injected with steam to improve the process performance.

The application of propane for the *in-situ* heavy oil recovery has widely been evaluated. Mokrys and Butler (1993) investigated the de-asphaltening phenomena and oil upgrading during propane injection into a physical model. They used Lloydminster heavy oil with API gravity of 13 and the asphaltene content of 16 weight percent. They considered two different cases, the injection of pure propane and the co-injection of propane with steam. The results indicated that the recovery for both cases are comparable while the steam-propane co-injection is more energy efficient compared to pure steam injection. The viscosity of oil produced from steam-propane co-injection was lowered by a factor of as much as 50 times. In another study, Jiang (1997) came up with a similar finding as Mokrys and Butler (1993) and found out that, propane concentration in the oil must exceed a certain value (critical concentration) to have oil upgrading (asphaltene precipitation) in the reservoir. This value is in the range of 20-30 weight percent propane. The higher initial injection rate can lead to higher oil recovery by using less solvent.

Goite et al. (2001) conducted a series of lab experiments for heavy oil recovery (API gravity of 13.5) from the Morichal field, Venezuela. They determined the influence of the use of propane and its optimum concentration as an additive during steam injection. The results show that the optimal concentration of propane appears about 5:100 propane to steam mass ratio. In subsequent study, Ferguson et al. (2001) used the same oil and apparatus as Goite et al. and found out that oil production rate is accelerated when

propane was used as an additive to steam compared to pure steam. They obtained almost the same optimum propane concentration as Goite et al. (2001).

Tinns (2001) conducted the co-injection experiments with propane to steam mass ratio of 5:100 using an oil with API gravity of 21. Tinns observed an acceleration in the oil production rate. By measuring the density and viscosity of produced oil, the author found out that an increase in the API gravity and the decrease in the viscosity of produced oil which is corresponded to oil upgrading. Rivero and Mamora (2002) conducted a feasibility study experiments using propane as a steam additive to improve injectivity and oil production rate. They used an extra-heavy oil from Hamaca field, Venezuela which had the AIP gravity of 8 and a viscosity of 25,000 mPa.s at the temperature of 50°C. They considered four different propane to steam mass ratios, and the experimental results show that, with steam-propane co-injection, the oil production accelerated by 17% compared to pure steam injection. In addition, the steam injectivity can be three times higher in the case of propane-steam co-injection compared to pure steam injection.

Venturini and Mamora (2003) performed a simulation study to evaluate the steam-propane co-injection, for the production of Hamaca heavy crude oil. They considered a 1-D model to describe the physical model and characterized the oil with ten pseudo-components. The simulation results matched the experimental data and confirmed the experimental finding. Both experimental and simulation studies showed that oil production is accelerated by 20% when steam-propane was co-injected compared to pure steam injection. Venturini and Mamora (2003) came up with a general conclusion considering their research and previous results in this area as “Small concentrations of gaseous additives can alter and improve both early and ultimate recovery of heavy oil, on the order of 10-20% under favorable conditions. However, the addition of too large amount of additive again reduces the efficiency”.

Deng (2005) did a numerical study of hybrid process with propane and steam co-injection and simulated the process under different operating strategies and investigated the effect of the use of propane as additive in the hybrid process. The author ran a cost

model to evaluate the economical performance of the process. The results show the cost of propane-steam co-injection is in the same order of pure steam injection. Deng (2005) concluded that there is an optimum value for propane to steam ratio in the injection gas, and the co-injection of propane in large amount has a negative effect on the process.

Apart from the application of propane for *in-situ* oil recovery, supercritical propane has been tested for its capability to extract bitumen from oil sands. Jacoby (1987) performed experimental studies on the extraction of Athabasca oil sands using solvents such as ethane, propane, butane, and pentane in the supercritical and liquid states. Hwang [39] and Subramanian (1996) conducted supercritical fluid extraction of Whiterock and PR Spring bitumens using propane as the solvent.

Based on the above-mentioned applications and research studies, the bitumen/propane interaction and its phase behaviour and thermodynamic properties are extremely important to design and optimize the recovery and extraction processes. It is critical to specify the number of phases which are formed for heavy oil / propane systems at different temperatures and pressures, and determine the density and viscosity of the equilibrium phases. For the extraction processes, the component distribution and the extraction yield should be identified.

5.2. Literature Background

There are limited data in the literature for the phase behaviour study of bitumen/propane systems, and the data have been limited to the low temperatures (< 100°C) and to pressures less than the vapour pressure of propane.

Radoz et al. (1987) reported the experimental phase equilibrium compositions for two systems containing propane and petroleum derived oil mixtures near the temperature of 126.9°C and at the pressures (3 to 5.5) MPa. Two oil samples with different chemical compositions, one was rich in saturates (paraffines and naphthenes) and the other was rich in aromatics, were used for the experiments. The experimental results confirmed that

the solubility of propane in the propane-saturates-rich-oil mixture is greater than in the propane-aromatics-rich-oil mixture. The same observation for the solubility of heavy components in the vapour phase was found. In addition, the increase in pressure was favored the extraction of more components from the oil phase in both samples.

Deo et al. (1992) conducted the extraction of a paraffinic crude oil, bitumen-derived liquid and native Whiterocks bitumen with carbon dioxide and propane. For the paraffinic crude oil, the analysis of the extraction data with carbon dioxide revealed that at constant temperature of 37.85°C, the extraction yields increased as the pressure was increased from (7.6 to 17.2) MPa. However, the extraction yields for a constant pressure (10.3 MPa) were practically identical at the three temperatures (23.85, 30.85, and 37.85°C) near critical condition, while the yields decreased at the higher temperatures (65.85°C).

For bitumen-derived liquid, extractions with propane were conducted at a temperature of 48.85°C and three pressures (5.5, 10.3, and 17.2 MPa) and at a constant pressure of 10.3 MPa and three different temperatures, (37.85, 106.85, and 134.85)°C. In general, as the pressure was increased at constant temperature, the extraction yields increased. Furthermore, the highest yields were obtained near propane critical temperature. The extraction yield at the temperature of 106.85°C is higher than 37.85°C demonstrating the enhanced solubility in propane phase near critical point. Generally, the extraction yields for propane were considerably higher than for carbon dioxide, due to the stronger affinity of propane for hydrocarbon components of the feedstocks.

For native Whiterocks bitumen, the extraction yields were lower than those of the bitumen derived liquid; however, the trends were similar. The same as before, the extraction yields increased as a function of pressure and is most effective near critical temperature of propane. In addition, the carbon-number distributions indicated that heavier compounds are extracted at higher pressures. For carbon dioxide extractions, a total of 2 wt% of material was extracted at the highest pressure (30.9 MPa) and at a constant temperature of 93.85°C while the lower pressure results in no oil extraction.

Han et al. (1998) studied the phase behaviour of Fengcheng bitumen with supercritical propane at temperatures (108, 115, and 125)°C and at the pressures (4.4 to 8.6) MPa. The authors conducted the experiments for a constant mass ratio of propane to bitumen (1:1.3). The authors reported the propane concentration, density, and viscosity of two phases at equilibrium conditions. The results showed that, at a constant temperature, supercritical propane had stronger ability to extract Fengcheng bitumen at higher pressures.

Frauenfeld et al. (2002) measured the solubility of ethane and propane in Cold Lake blend oil and the solubility of methane, ethane, propane and carbon dioxide in Lloydminster Aberfeldy oil at temperatures less than 20°C. Freitag et al. (2005) measured the solubility, density and viscosity of a Winter (Lloydminster) oil / propane system at the temperatures, (15 and 28)°C, and at the pressures lower than vapour pressure of propane. The authors examined the measured solubility of propane in Winter (Lloydminster) oil system with two different experimental procedures and they found that the amount of propane dissolved in the oil increased by 5 to 20% if the sample has already been exposed to higher propane concentrations.

Luo et al. (2007a) measured the solubility of propane in three Lloydminster heavy oil samples with different asphaltene contents at the temperature of 23°C and at the pressures less than 800 kPa. The experimental pressure was less than the vapour pressure of propane. The results showed that propane solubility is strongly affected by the asphaltene content of heavy oil. The oil sample with lowest asphaltene content had the highest solubility. In a subsequent study, Luo et al. (2007b) also measured the phase equilibrium properties for Lloydminster heavy oil / propane system and for Lloydminster heavy oil / solvent (gas mixture: methane, propane, *n*-butane, and *i*-butane) mixture at the temperature of 23.9°C in the pressure range of (0.5 to 5) MPa using a PVT system from D. B. Robinson Design & Manufacturing Ltd. For all experiments, the volume ratio of solvent to heavy oil was about 1.

For heavy oil / propane mixture, they found out that the heavy oil / propane mixture divided into three layers at the pressures of (1.965, 2.979, and 5.019) MPa. The top layer was a solvent-enriched oil which contains some light components extracted from the heavy oil. The middle layer was the heavy oil with the dissolved solvent and the bottom layer contained heavy components (the asphaltene precipitates from middle layer). Increase in the pressure resulted in the extraction of more light components from heavy oil into top layer and the accumulation of heavy components in bottom layer. The authors also measured the viscosity of degassed liquid from each phase and the results confirms that higher pressure results in higher viscosity of bottom layer liquid and lower viscosity for top and middle layers.

For heavy oil / solvent mixture (solvent was a mixture of methane, propane, *n*-butane, and *i*-butane), the authors found out that the mixture divided into two layers, solvent-enriched and asphaltene-enriched, at the pressures (3.202 and 5.048) MPa while only one phase for (0.551 and 2.068) MPa pressures. The authors also compared the compositions of the solvent mixture dissolved into the heavy oil for four pressures. The major component dissolved in was methane at the pressures (0.551 and 2.068) MPa while at the pressures (3.202 and 5.048) MPa, the major component of the dissolved solvent mixture was butane. In these experiments, the same trends as heavy oil / propane mixture for the behaviour of carbon number distribution with pressure were observed.

Jossy et al. (2009) conducted phase partitioning measurements for a UTF bitumen / propane system at the temperatures (10 and 40)°C near the vapour pressure of propane using computed tomography (CT) scans on the visual cell. They evaluated different solvent-to-bitumen volume ratios (0.35, 1, 1.5, and 2) to find out how the solvent/oil loading affect the phase volume, phase composition and phase density and viscosity. The authors concluded that the onset of liquid phase portioning is likely to be around a ratio of one (volume). In addition, the behaviour of phase partitioning at two temperatures was not the same. The chemical analysis of degassed saturated liquids showed the heavier liquid has much higher asphaltene content (35.2 and 34.3 wt% at the temperatures of 10

and 40°C, respectively) than raw bitumen (15.7) whereas the lighter liquid is much lower (1.6 and 1.7 wt% at the same temperatures).

Badamchi-Zadeh et al. (2009a) measured the solubility and saturated phase density and viscosity for Athabasca bitumen diluted with propane for the temperatures (10 to 50)°C. For all experiments, they only considered vapour-liquid equilibrium and propane concentration of less than 23 wt% to prevent asphaltene precipitation or second liquid formation. In subsequent study, Badamchi-Zadeh et al. (2009b) measured the solubility of carbon dioxide and mixtures of carbon dioxide and propane in Athabasca bitumen. Multiple-liquid phases were observed at pure carbon dioxide contents above approximately 12 wt%. The authors reported volume of each phases for multiple phase equilibrium. Multiple-liquid phases were also observed in a ternary mixture of 13.1% propane, 19.2 wt% carbon dioxide, and bitumen.

To date, no wide temperature range phase behaviour study has been reported for bitumen/propane mixtures that includes both vapour-liquid and liquid-liquid equilibria. The generated experimental data in this research show that bitumen/propane mixtures can have liquid-liquid separation for the temperatures less than 120°C. The lighter liquid (liquid 1, i.e. the solvent-enriched phase) contains light components extracted from the bitumen. The heavier liquid (liquid 2, i.e. the asphaltene-enriched phase) is mostly composed of heavy fractions of bitumen. The extraction yield changes with the pressure, temperature, and the amount of solvent (overall propane concentration). The chemical analysis of the degassed saturated liquids showed the heavier liquid had much higher asphaltene content than raw bitumen, whereas the lighter liquid had much lower asphaltene content than raw bitumen.

The experimental results for Surmont bitumen / propane systems are presented in this chapter. As with bitumen/ethane mixtures, this section considers both vapour-liquid and liquid-liquid equilibria. For the vapour-liquid equilibrium condition, the reported data are the solubility of propane in bitumen, the density and viscosity of the saturated bitumen, K-values and GOR. Liquid-liquid experiments at two temperatures (50 and 100)°C are

then presented. The results include the measurements of physical properties (density and viscosity) and propane concentrations in both liquid phases. In addition, the light component extraction is investigated; and, the impacts of pressure, temperature and solvent (propane) loading on the distribution of components are presented. Finally, the phase diagrams for bitumen/propane mixtures on the basis of measured data have been developed and presented.

5.3. Vapour-Liquid Equilibrium

The experimental results for Surmont bitumen / propane systems indicate that, for all pressures less than 10 MPa, the vapour-liquid equilibrium exists at the temperatures of (150, 175 and 190)°C. At 100°C, the phase transition occurs at the pressures around 4.5 MPa; and, the vapour-liquid equilibrium exists for the pressures of 2 and 4 MPa. The vapour-liquid experiments were carried out at 17 different operating conditions; a combination of five different temperatures, 50, 100, 150, 175, and 190°C, and five different pressures, 1, 2, 4, 6, and 8 MPa. The details of each experiment including the amount of bitumen and solvent charged into the equilibrium cell are presented in Table 5–1. The amount of solvent and bitumen in each experiment is the required mass of each species to have both vapour and liquid phases at equilibrium condition and to obtain enough phase samples for solubility calculations. As expected, the weight fraction of propane in the equilibrium cell increases with pressure and reduces with temperature.

The experimental results of vapour-liquid equilibrium for Surmont bitumen / propane mixtures at five temperatures (50, 100, 150, 175, and 190)°C are summarized in Table 5–2. The repeatability of generated data was examined by repeating some experiments at the temperatures of (150 and 175)°C; these data are presented in Table 5–3. As the data presented in Table 5–3 show, the measurements of the solubilities in two experiments at similar conditions are quite well in agreement and the saturated phase densities are precise within 0.5 kg/m³. The deviation for the saturated liquid viscosities is less than 5%.

Table 5–1: Experimental design and feeding information for Surmont bitumen / propane systems at temperature T and pressure P .

T (°C)	P (MPa)	Equilibrium Cell		$P_{\text{Equilibrium}}$ (MPa)
		C_3H_{10} (g)	Bitumen (g)	
50	1	18	54	1.082
100	2	13	52	1.965
	4	32	48	3.992
150	1	4	46	1.172
	2	6	44	2.096
	4	10.8	49.2	4.012
	6	15	45	6.046
	8	40	40	8.080
175	1.25	5	45	1.496
	2	6	44	2.216
	4	5.75	42.5	4.243
	6	10	40	6.136
	8	12.5	37.5	8.118
190	1.25	6	44	1.379
	4	10.8	49.2	4.026
	6	12.5	50	6.039
	8	15	45	7.990

For the vapour-liquid experiments of Surmont bitumen / propane mixtures, a clear phase transition between two phases, vapour and liquid, was observed for all experiments during the phase sampling at equilibrium condition. As Table 5–2 indicates, the dissolution of propane in bitumen reduces the density and viscosity of saturated liquid phase. Depending on the temperature, the decreasing trend of density and viscosity with the solubility of propane is different. At a constant temperature, the solubility of propane in bitumen increases with pressure. Thus, the density and viscosity of saturated liquid phase shows a decreasing trend with the equilibrium pressure. Although pressure increases the density and viscosity of gas-free bitumen at a constant temperature, the dissolution of propane in bitumen compensates this effect and also changes its effect (reduction of density and viscosity with increasing pressure).

Table 5–2: Experimental vapour-liquid equilibrium properties for Surmont bitumen / propane mixtures at $T = (50, 100, 150, 175 \text{ and } 190)^\circ\text{C}$; P , pressure; ρ_s , saturated liquid density; μ_s , saturated liquid viscosity; w_s , weight percent of propane in saturated liquid phase.

T ($^\circ\text{C}$)	P (MPa)	w_s	ρ_s (kg/m^3)	μ_s (mPa.s)
50.2	1.082	10.1	914.1	71.7
100.2	1.965	7.03	902.5	23.9
100.2	3.992	23.9	780.5	2.07
149.5	1.172	1.51	912.5	21.2
150.0	2.096	3.53	896.0	14.2
149.9	4.012	8.34	858.5	6.86
150.4	6.046	13.1	814.1	3.38
150.0	8.080	19.4	768.0	1.96
174.2	1.496	1.98	896.4	10.0
175.0	2.216	3.18	887.0	7.70
174.5	4.243	6.30	856.8	----
176.0	6.136	10.3	822.7	2.61
175.5	8.118	14.2	791.7	1.93
189.4	1.379	1.37	893.0	9.22
188.9	4.026	5.48	856.9	4.94
189.2	6.039	8.61	828.2	3.20
189.7	7.990	12.4	798.7	2.20

Table 5–3: Experimental vapour-liquid equilibrium properties of repeated experiments at $T = (150 \text{ and } 175)^\circ\text{C}$ for Surmont bitumen / propane systems; P , pressure; ρ_s , saturated liquid density; μ_s , saturated liquid viscosity; w_s , weight fraction of propane in saturated liquid phase.

T ($^\circ\text{C}$)	P (MPa)	$10^2 w_s$	ρ_s (kg/m^3)	μ_s (mPa.s)
150	8.052	19.5	766.9	1.91
	8.107	19.3	769.0	2.00
175	4.267	6.43	856.8	----
	4.219	6.17	856.8	----
	8.107	14.2	791.5	----
	8.128	14.2	791.9	1.93

5.3.1. Saturated Phase Properties

The solubility measurements for Surmont bitumen / propane systems at five temperatures, (50, 100, 150, 175 and 190)°C, are shown in Figure 5–1. The x -axis shows the equilibrium pressure and the y -axis is the measured solubility of propane in bitumen. The isotherms corresponding to each temperature are shown by different colors. The solubility increases with increasing equilibrium pressure at a constant temperature and decreases with increasing temperature at a constant pressure. The variation of solubility with equilibrium pressure is more significant at low temperatures. Generally, propane has much higher solubility in bitumen compared to ethane and methane at the same operating conditions; and, this behaviour is more considerable at low temperatures.

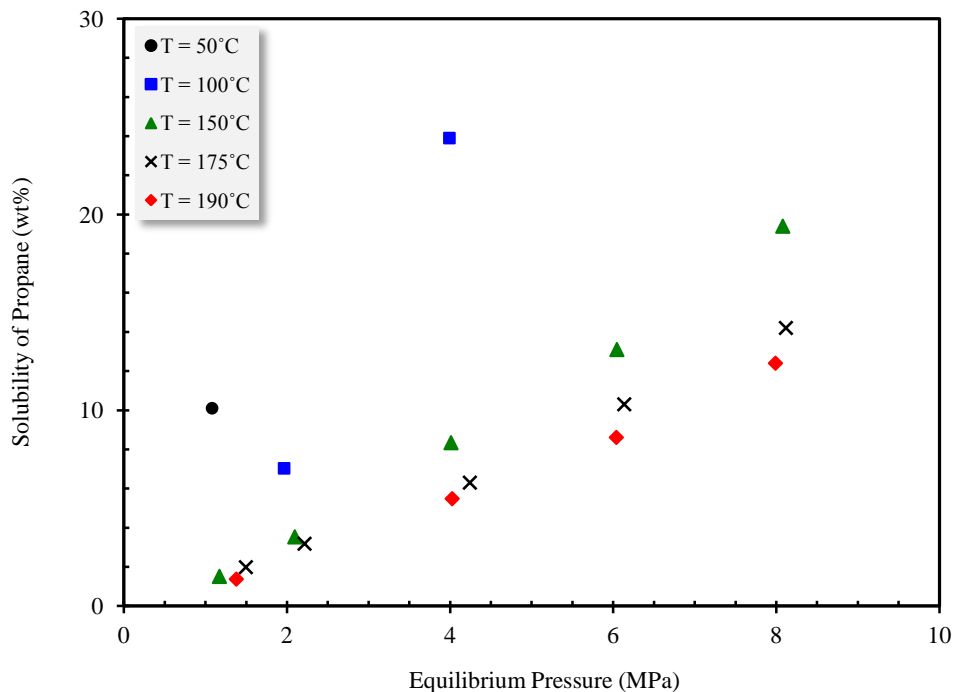


Figure 5–1: Measured solubility of propane in Surmont bitumen as a function of pressure at different temperatures.

The difference between the isotherms becomes more significant as the temperature decreases from (190 to 100)°C. This behaviour was also observed for bitumen/ethane systems. As it is not presented here, the solubility values flatten beyond the pressures (1.5 and 4) MPa at the temperatures (50 and 100)°C, respectively. The vapour-liquid

equilibrium no longer exists at these pressures and temperatures. Thus, the solubility is not increased with equilibrium pressure due to depletion of bitumen from light components.

Figures 5–2 and 5–3 illustrate the propane-saturated viscosity and density for Surmont bitumen at different temperatures and pressures. When propane is dissolved into the bitumen, the viscosity of the saturated bitumen is significantly reduced, even at low equilibrium pressures. This makes propane a good candidate for solvent injection processes in which the reservoir cannot be operated at high pressure condition. For example, at the equilibrium pressure of 1.082 MPa and at the temperature of 50.2°C, the viscosity of the mixture is 71.2 mPa.s, which is much lower than the viscosity of the raw bitumen (18429 mPa.s) with no dissolved propane. The viscosity in this condition is low enough for oil to be recovered from the reservoir.

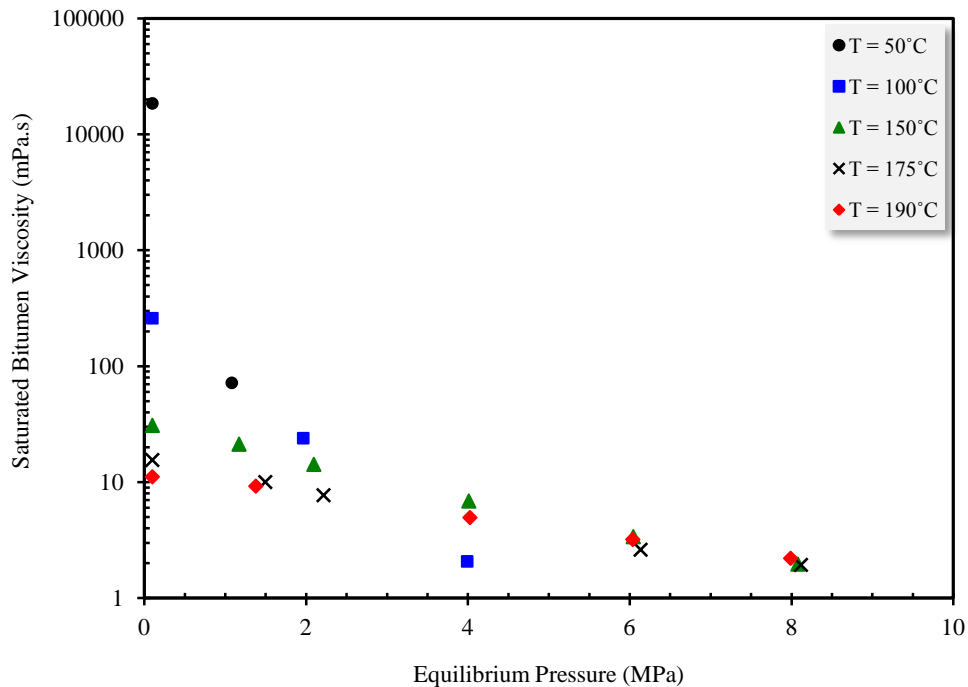


Figure 5–2: Viscosity of propane-saturated Surmont bitumen as a function of pressure at different temperatures.

The viscosity of propane-saturated bitumen also significantly reduces with equilibrium pressure at all temperatures. The variations of saturated viscosity and density with equilibrium pressure are linear for all temperatures. There are crossovers for gas-saturated bitumen viscosity and density. It seems that the effect of solubility at low temperatures is more significant than the effect of temperature on the bitumen viscosity. Thus, lower saturated density and viscosity are obtained at low temperatures and high pressures. It can be concluded that, at low temperatures, the solvent has the same or even greater effect on the viscosity reduction, compared to that at high temperatures.

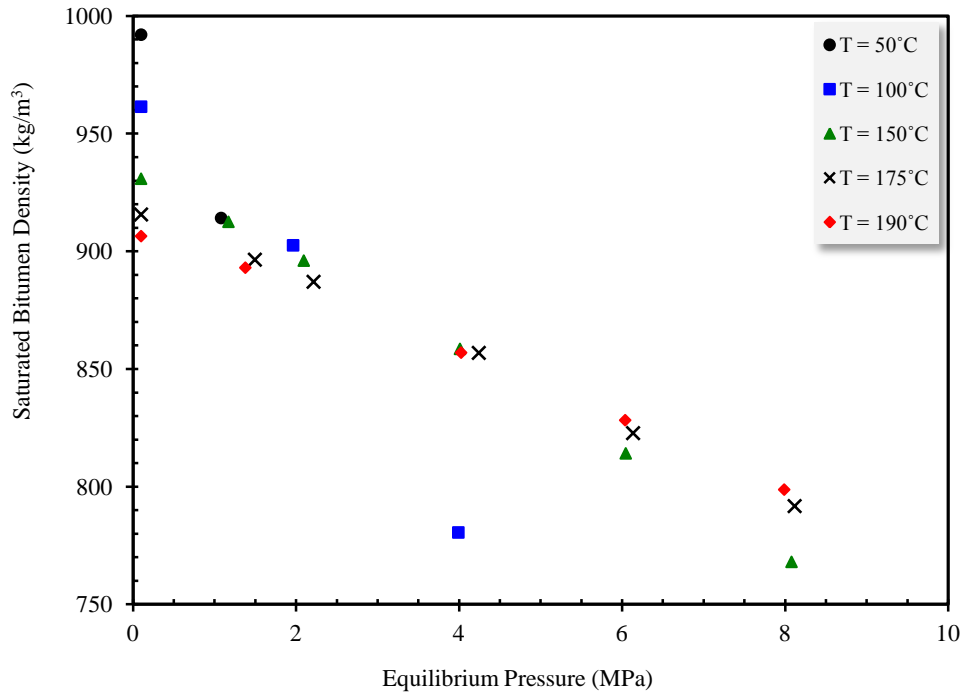


Figure 5-3: Density of propane-saturated Surmont bitumen as a function of pressure at different temperatures.

A closer examination of the saturated viscosity data reveals that the saturated bitumen has a viscosity less than 100 mPa.s over the studied temperature and pressure ranges. The viscosity reduction is a major recover mechanism considered in the solvent-based recovery processes. Although the decrease in temperature significantly increases the viscosity of raw bitumen, the greater solubility of propane at low temperatures offset

this effect. For example, at 100.2°C and a pressure of 3.992 MPa, the viscosity of saturated liquid phase is 2.07 mPa.s while the viscosity at 189.7°C and a constant pressure of 7.990 MPa is 2.2. This shows that manipulating the pressure and temperature, the viscosity of liquid phase can be controlled.

5.3.2. Equilibrium K-values and GOR

The experimental solubility and density data for the pseudo-binary systems of bitumen/solvent systems are commonly used in reservoir simulation software to build appropriate thermodynamic and phase behaviour models. On the basis of experiments, the equilibrium K-values for propane present in mixture are obtained and directly applied into reservoir simulation software such as CMG-STARs. Furthermore, K-values are usually used to tune equation of state parameters. The K-values for Surmont bitumen / propane mixtures were calculated using Equation 4-1 in which the mole fractions of propane in equilibrium vapour and liquid phases are used instead. $y_{C_3H_8} = 1$ was considered for all temperatures and pressures; the values for $x_{C_3H_{10}}$ were obtained using the data presented in Table 5–2 along with the molecular weight measurements for the bitumen. The measured K-values for Surmont bitumen / propane system are plotted as a function of equilibrium pressure in Figure 5–4. The K-values are in the range (1 to 10) for Surmont bitumen / propane mixtures and its value is determined by the composition of propane in the liquid phase because $y_{C_3H_8} = 1$. Higher solubility resulted in lower K-value. As depicted in Figure 5–4, the increase in pressure or the decrease in temperature leads to lower K-values. The solubility of propane in bitumen was found to be significant and more than the solubility of methane and ethane at the same condition. As anticipated from Figure 5–1, for bitumen/propane mixtures, the solubility of propane is considerable and as a result, the viscosity reduction is also significant.

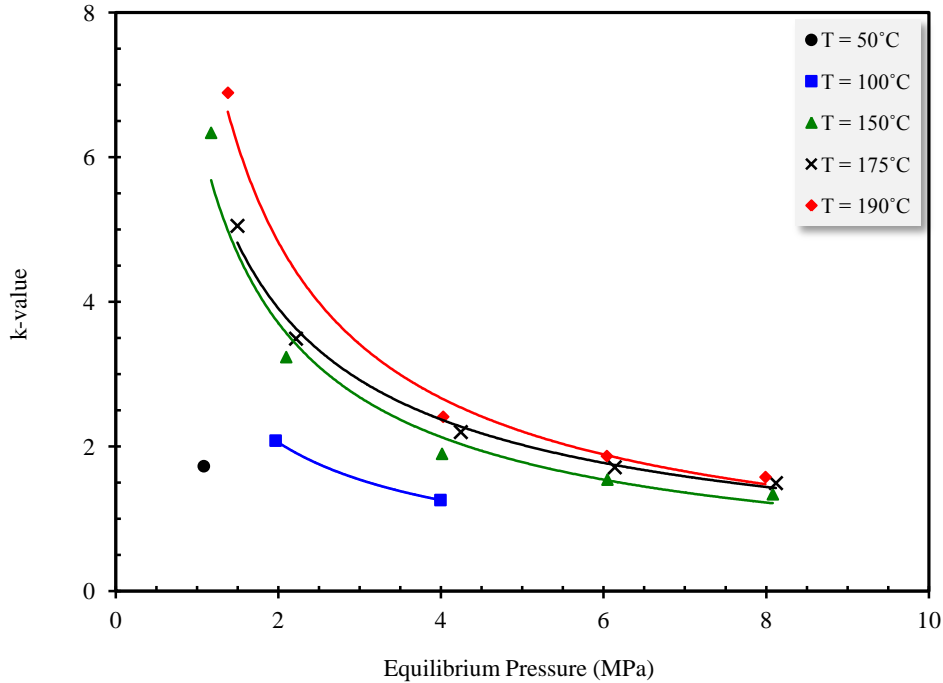


Figure 5-4: Measured K-values for Surmont bitumen / propane systems as a function of pressure at different temperatures.

GOR is an indirect indication of solvent solubility in bitumen. Indeed, the GOR is the ratio of the volume of gas that comes out of solution, to the volume of oil at standard conditions. The solubility data along with the bitumen and hydrocarbon gas properties were used to obtain GOR at different pressures and temperatures. Equation 4-2 was applied to obtain GOR for Surmont bitumen saturated with propane and the results are presented in Figure 5-5. This figure follows the same trend as the solubility plot and it reveals that the equilibrium properties of bitumen/propane mixtures are much more dependant on the temperature than those of ethane and methane. The experimental results indicate higher GOR values were obtained at lower temperatures, considering an isobar condition. This was due to the higher solubility of propane in the mixture. As depicted in Figure 5-5, a sharp increase in the GOR is observed at 100°C. The pressure of 4 MPa was an upper limit for the vapour-liquid equilibrium of the mixture.

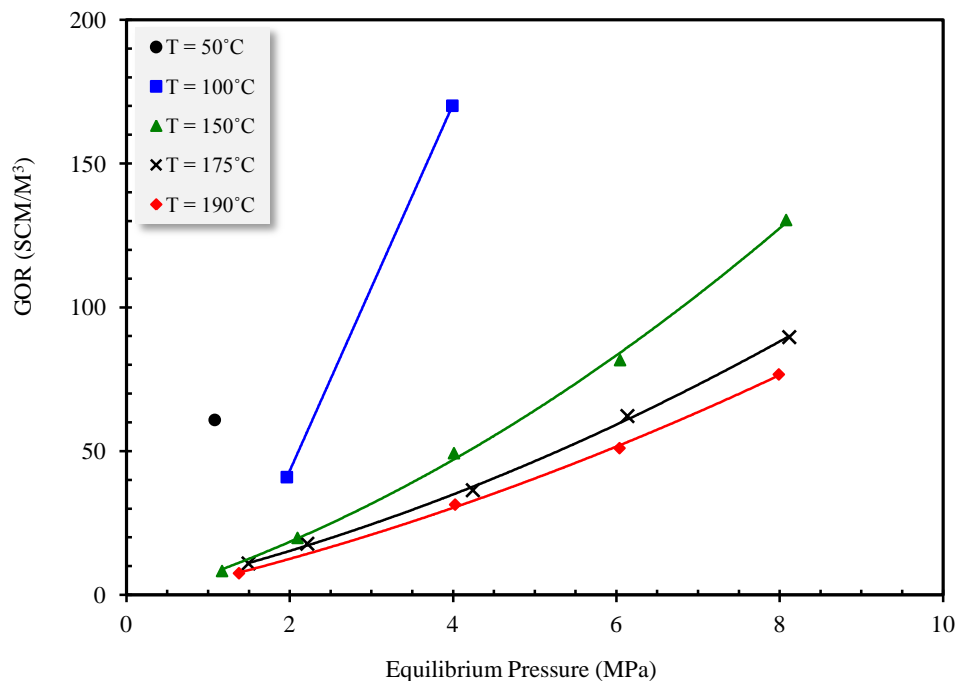


Figure 5–5: Measured GOR for Surmont bitumen / propane systems as a function of pressure at different temperatures.

5.4. Liquid-Liquid Equilibrium

The liquid-liquid phase separation for the bitumen/propane mixtures was initially observed at the temperature of 100°C. At this temperature, the measured solubility of propane in bitumen was increased from (1 to 4) MPa. When the pressure was further increased to 6 MPa, the solubility of propane was dramatically increased from 23.9 weight percent to a value higher than 65 depending on the overall propane concentration. Further experimental investigations on the mixtures showed that the separation of heavy constituents from the bitumen occurs at this pressure and a new liquid phase was formed at equilibrium condition. It was found that the upper liquid phase contains light components in which the composition of propane is considerably higher than the lower liquid phase.

Thus, further analysis on the bitumen/propane mixtures indicated that the mixtures of bitumen and propane formed two liquids at the temperature of 100°C and the pressures greater than 4.5 MPa and at the temperature of 50°C and the pressures greater than 2

MPa. The solvent-enriched phase contained light components extracted from the bitumen while asphaltene-enriched phase was mostly heavy fractions of bitumen. The chemical analysis of the degassed saturated liquids shows the asphaltene-enriched phase has much higher asphaltene content than raw bitumen, whereas the solvent-enriched phase has much lower asphaltene content than raw bitumen. Figure 5–6 illustrates the digital photographs of flashed-off liquid samples and raw bitumen at ambient condition. As anticipated from the figure, the solvent-enriched phase contain no asphaltenes as it has a light brown color.



Figure 5–6: Digital photographs of gas-free bitumen (left) and flashed-off liquid samples (middle and right) taken from liquid-liquid equilibrium study of Surmont bitumen / propane mixtures.

Indeed, the partitioning of the bitumen/propane mixtures into two liquid phases can be considered as a asphaltene precipitation process in which the properties of the precipitated asphaltene is different from those of pentane or heptane. That is, the precipitation appears as a heavy liquid phase at equilibrium condition. It was found that the yield of precipitation for propane is much higher than pentane and heptane, and generally, the precipitation yield reduces with the carbon number of normal alkanes. As it will be presented in Section 5.4.4, propane as a precipitant separates a large fraction of resins with the asphaltene.

To evaluate all the important parameters and their impact on the physical properties, as well as the component distribution, a series of experiments at two temperatures (50 and 100°C), at different pressures, and at a variety of overall propane concentrations were

conducted. The experimental results are summarized in Tables 5–4 to 5–6. Each table corresponds to a specific overall propane concentration.

Table 5–4: Liquid-liquid equilibrium properties for Surmont bitumen / propane mixtures at a constant overall propane concentration of 40 weight percent; P , pressure; T , temperature; w , weight fraction of propane; ρ , densities; μ , viscosity.

T (°C)	P (MPa)	10^2w		ρ (kg/m ³)		μ (mPa·s)	
		L ₁	L ₂	L ₁	L ₂	L ₁	L ₂
50.3	2.096	47.5	22.7	660.7	853.2	----	115
50.3	5.046	46.0	22.9	678.4	858.2	----	218
50.3	8.018	44.6	22.7	691.9	861.4	----	154
100.1	6.060	65.5	26.5	512.9	768.9	0.22	4.33
100.1	8.066	49.5	25.1	600.4	786.8	0.56	7.43

Table 5–5: Liquid-liquid equilibrium properties for Surmont bitumen / propane mixtures at a constant overall propane concentration of 60 weight percent; P , pressure; T , temperature; w , weight fraction of propane; ρ , densities; μ , viscosity.

T (°C)	P (MPa)	10^2w		ρ (kg/m ³)		μ (mPa·s)	
		L ₁	L ₂	L ₁	L ₂	L ₁	L ₂
50.2	2.082	73.0	20.0	542.4	877.4	----	68.4
50.3	5.046	71.4	20.1	559.7	883.3	----	484
50.3	8.052	70.4	19.9	572.1	888.6	----	156
100.2	6.039	80.9	22.3	437.5	808.5	0.07	9.29
100.1	8.045	76.4	22.2	472.8	820.9	----	8.90

Table 5–6: Liquid-liquid equilibrium properties for Surmont bitumen / propane mixtures at a constant overall propane concentration of 80 weight percent; P , pressure; T , temperature; w , weight fraction of propane; ρ , densities; μ , viscosity.

T (°C)	P (MPa)	10^2w		ρ (kg/m ³)		μ (mPa·s)	
		L ₁	L ₂	L ₁	L ₂	L ₁	L ₂
50.3	2.054	87.9	17.4	493.2	911.9	----	388
50.3	5.026	86.3	17.1	506.2	917.8	----	548
50.2	7.969	86.1	17.8	519.3	920.9	----	1666
100.1	6.149	89.5	20.9	402.5	848.3	----	17.3
100.0	7.976	88.4	18.2	425.0	860.4	----	24.7

Tables 5–4 to 5–6 list the measurements at overall propane concentrations of 40, 60 and 80 weight percentages, respectively. In each table, the operating conditions, concentration of propane in the solvent-enriched phase (L₁) and in the asphaltenes-

enriched phase (L_2), densities and viscosities of each liquid phase are presented. The viscosity of the solvent-enriched phase was too low and close to the viscosity of pure propane; therefore, it was only measured for the experiments that the extraction of components into the solvent-enriched phase was significant. Further discussions of the measured liquid-liquid equilibrium data are presented in the following sections.

5.4.1. Physical Properties

The performances of the solvent-based recovery processes depend on the viscosity and density of the phases that form at *in-situ* condition. These properties are directly affected by the solubility of the solvent, the temperature and the pressure. In this section, physical properties of phases at equilibrium conditions are evaluated.

5.4.1.1. Volume Change on Mixing

The vapour-liquid equilibrium data of Surmont bitumen / propane mixtures presented in Section 5.3 indicated that the dissolution of propane in gaseous state into the bitumen results in the variation of the total volume of the mixture. The measured volume of the mixture from the initial state and its value during the mixing process at fixed pressure and temperature determined the equilibrium condition. For the vapour-liquid equilibrium condition, the change in the total volume of the mixture from the initial state up to the equilibrium condition is significant. Because the gaseous solvent is condensed into the liquid phase, and the equivalent amount of solvent dissolved into the bitumen in gaseous state occupies a large volume (at equilibrium temperature and pressure). However, for the liquid-liquid equilibrium condition, the volume change on the mixing is not as significant as vapour-liquid equilibrium because solvent is not condensed during the mixing process.

The mixtures of bitumen and propane in the liquid-liquid equilibrium condition were subjected to the volume change on the mixing. Although the volume change on the mixing is not significant as the vapour-liquid cases, its value is changed with the operating parameters. Table 5–7 summarizes the ratio of equilibrium total volume to the

initial total volume for the mixtures of propane and Surmont bitumen. In this table, the volume ratio of phases at equilibrium condition is also listed.

Table 5–7: The volume change on the mixing and volume ratio of phases in liquid-liquid equilibrium of Surmont bitumen / propane mixtures; P , pressure; T , temperature; w , weight fraction of propane; V_t , total volume of mixtures; V_L , volume of each phase at equilibrium condition.

T (°C)	P (MPa)	$10^2 w$	$V_{t, \text{equil}} / V_{t, \text{initial}}$	V_{L1} / V_{L2}
50.3	2.096	40	0.944	2.15
50.2	2.082	60	0.951	3.93
50.3	2.054	80	0.969	13.94
50.3	5.046	40	0.959	2.74
50.3	5.046	60	0.958	4.36
50.3	5.026	80	0.977	14.31
50.3	8.018	40	0.967	3.36
50.3	8.052	60	0.958	4.98
50.2	7.969	80	0.986	14.54
100.1	6.060	40	0.870	0.73
100.2	6.039	60	0.887	2.98
100.1	6.149	80	0.920	11.90
100.1	8.066	40	0.908	1.45
100.1	8.045	60	0.930	3.53
100.0	7.976	80	0.939	12.71

As the data in Table 5–7 shows, the mixtures of Surmont bitumen / propane undergo a negative volume change on the mixing. That is, the mixture total volume reduces during the mixing process and reaching to the equilibrium state. The negative volume change on the mixing is observed for all measured data at different temperatures, pressures, and overall propane concentrations.

As presented earlier, the value of volume change on the mixing is varied with the operating parameters. The measured data (Table 5–7) show that at constant temperature and pressure, the volume change on the mixing reduces with the increase in the overall propane concentration. This trend is expected because the mixture of two components reaches to lower values of the volume change on the mixing at infinite dilution of each component. Thus, the measured ratio for the total volumes presented in Table 5–7 reach

to a value of 1 at higher overall propane concentrations. This trend might not be correct for some mixtures such as (toluene + *n*-octane) in which the volume change on mixing shows a zero value around 0.2 mole fraction of toluene (Asfour et al., 1990). The increasing trend of the measured ratio for the total volume toward a value of 1 is observed at two different temperatures and at three studied pressures. It should be noticed here that the mixtures under study are not in the single phase region, and the impact of the component distribution should also be taken into the account when the volume change upon mixing is studied.

The density of raw bitumen and pure propane is a function of temperature and pressure. Thus, the volume of the components and its molecular behaviour is changed with the change in the operating conditions. The measured ratio of total volume presented in Table 5–7 during the mixing process reduces with the increase in pressure at a constant temperature. This is due to a better arrangement of propane molecules in the bitumen molecules. As pressure increases at a constant temperature, the density of raw bitumen as well as pure propane are increased. The molecules of each component are made to come closer together with the increase in the pressure and consequently reduction in the occupied volume. In the pseudo-binary mixtures, the same behaviour occurs with a considerable difference. The molecules of different sizes are forced to come closer together. The decreasing trend of the measured ratio for the total volume with the pressure is observed at two different temperatures and at three studied overall propane concentrations.

The effect of temperature on the volume change on the mixing is also noticeable from Table 5–7. The increase in the temperature enhances the volume change on the mixing for the mixtures. It is due to the arrangement of the molecules in the mixtures. From Table 5–7, it can be concluded that the effect of pressure on the volume change on mixing is more considerable at high temperatures. Once again, it is noticeable that the mixtures under study are in the liquid-liquid equilibrium condition and the impact of the component distribution on the volume change on mixing is also significant.

5.4.1.2. Phase Compositions

The concentration of propane in two co-existing phases was measured (Tables 5–4 to 5–6), and the results are shown in Figures 5–7 and 5–8 for the temperatures (50 and 100)°C, respectively. As depicted in the figures, the concentration of propane in the solvent-enriched phase is much higher than that of the asphaltene-enriched phase. This is because the solvent-enriched phase composes of propane and light components extracted from the bitumen. The asphaltene-enriched phase, however, is mainly composed of the heavy constituents such as asphaltene and resin in which the concentration of propane in this phase is much less than in the solvent-enriched phase.

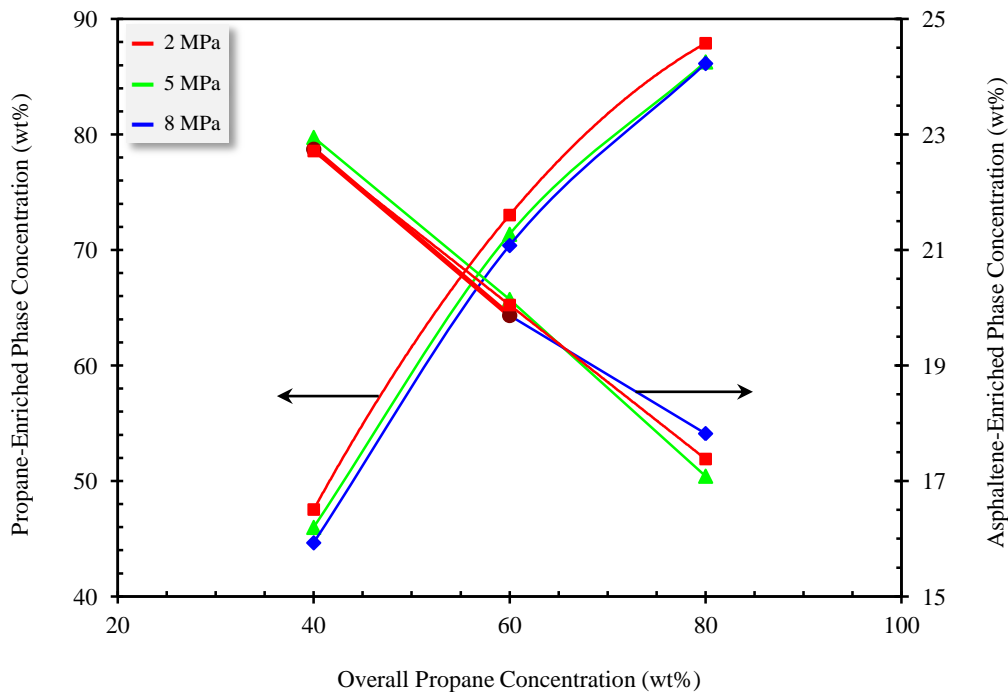


Figure 5–7: Liquid-liquid phase equilibria for Surmont bitumen / propane systems at the temperature of 50°C; the concentration of propane in liquid phases as a function of overall propane concentration at different pressures.

As anticipated from Figures 5–7 and 5–8, the pressure and overall propane concentration affect the composition of the equilibrium phases. The overall propane concentration has a much greater effect on the composition of phases at equilibrium condition as does the pressure. The concentration of propane in the solvent-enriched

phase increases at higher overall propane concentrations. This is expected, because when more propane is added to the system, it goes into the solvent-enriched phase (L_1). However, propane concentration in the asphaltene-enriched phase is reduced: this is due to the higher extraction yield at higher overall propane concentrations, which results in a heavier liquid phase and a corresponding lower propane concentration. As expected, the heavier hydrocarbon has lower propane solubility at a constant pressure and temperature. This behaviour is the same for two temperatures (50 and 100)°C.

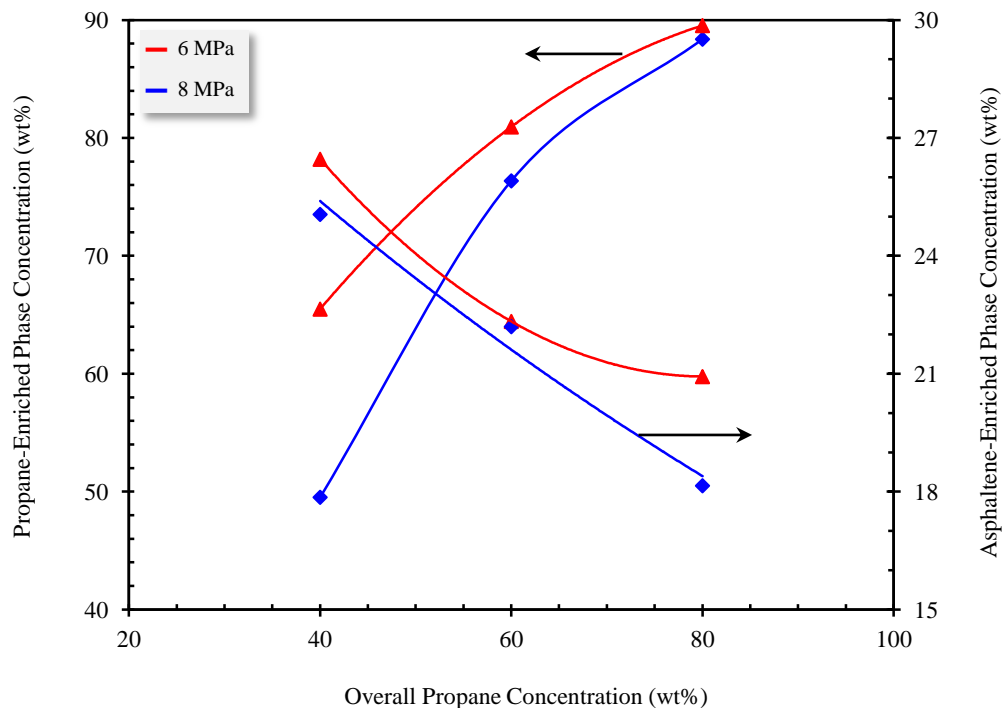


Figure 5-8: Liquid-liquid phase equilibria for Surmont bitumen / propane systems at the temperature of 100°C; the concentration of propane in liquid phases as a function of overall propane concentration at different pressures.

Although the impact of pressure on the concentration of propane in two liquid phases is not significant, the increase in the pressure reduces the concentration of propane in two phases. This is due to the extraction of light component into the solvent-enriched phase and corresponding reduction in propane concentration. Furthermore, the extraction of light components from the asphaltene-enriched phase results in a heavier liquid phase and consequently lower propane solubility. The impact of pressure on the concentration of

propane in two liquid phases is more pronounced at the temperature of 100°C compared to 50°C. The distribution of components within the phase is considerably changed with the pressure at high temperatures. This might be the reason that the impact of pressure at high temperatures is more significant.

5.4.1.3. Density and Viscosity of Phases

Figures 5–9 and 5–10 demonstrate the densities of equilibrium phases as a function of overall propane concentration at different pressures. For both temperatures (50 and 100°C), the increase in the overall propane concentration results in a lower density for the solvent-enriched phase and a higher density for the asphaltene-enriched phase. As the overall propane concentration increases, more light components are extracted into the solvent-enriched phase; thus, the density of the asphaltene-enriched phase increases. The density of the solvent-enriched phase decreases and approaches the density of pure propane at the experimental conditions because even with the higher extraction of light component from the bitumen, the concentration of propane in the solvent-enriched phase increases with increasing overall propane concentration. A comparison of Figure 5–7 for the phase compositions and Figure 5–9 for the phase densities provides a good understanding about the behaviour of the solvent-enriched phase.

The effect of the pressure on the equilibrium phase densities is clearly demonstrated in Figures 5–9 and 5–10, and the increase in phase densities with pressure is expected. Generally speaking, the pressure affects the density of the asphaltene-enriched phase in the three ways. Firstly, at a constant temperature, an increase in pressure results in an increase in the viscosity of raw bitumen. Secondly, the bitumen components in the asphaltene-enriched phase become heavier with increasing pressure, due to higher extraction of light components from the asphaltene-enriched phase at higher pressures. Finally, the density of propane-saturated bitumen decreases with the increasing propane concentration at higher pressures. The first factor has a small effect on the density; however, the other two factors result in significant changes in the density. The effect of

the first and second factors compensates that of the third. Thus, the density of the asphaltene-enriched phase increases.

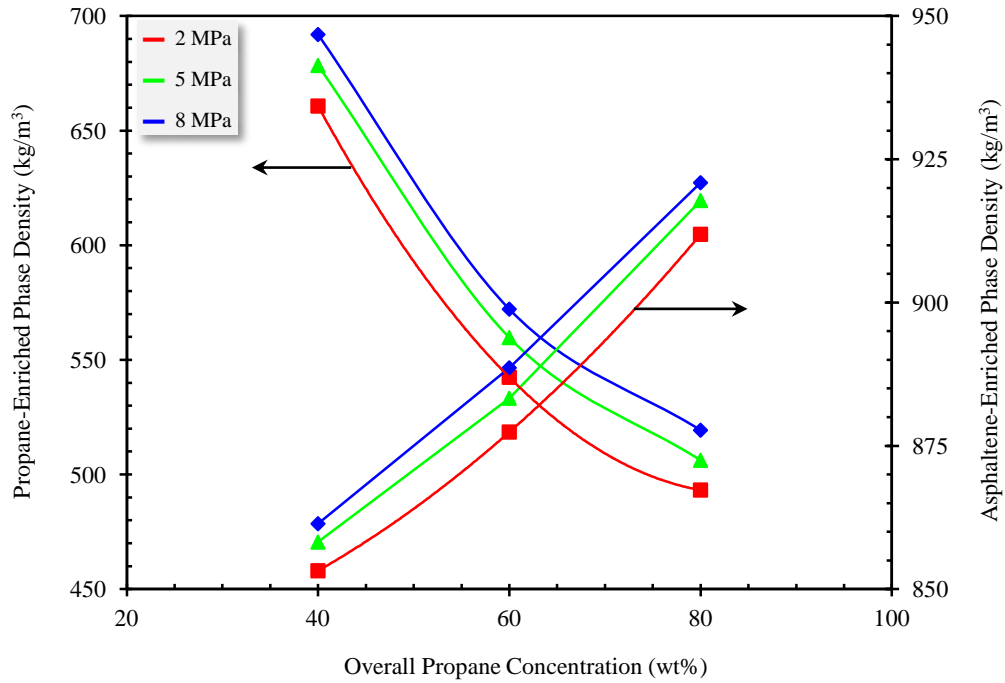


Figure 5-9: Liquid-liquid phase equilibria for Surmont bitumen / propane systems at the temperature of 50°C; density of equilibrium phases as a function of overall propane concentration at different pressures.

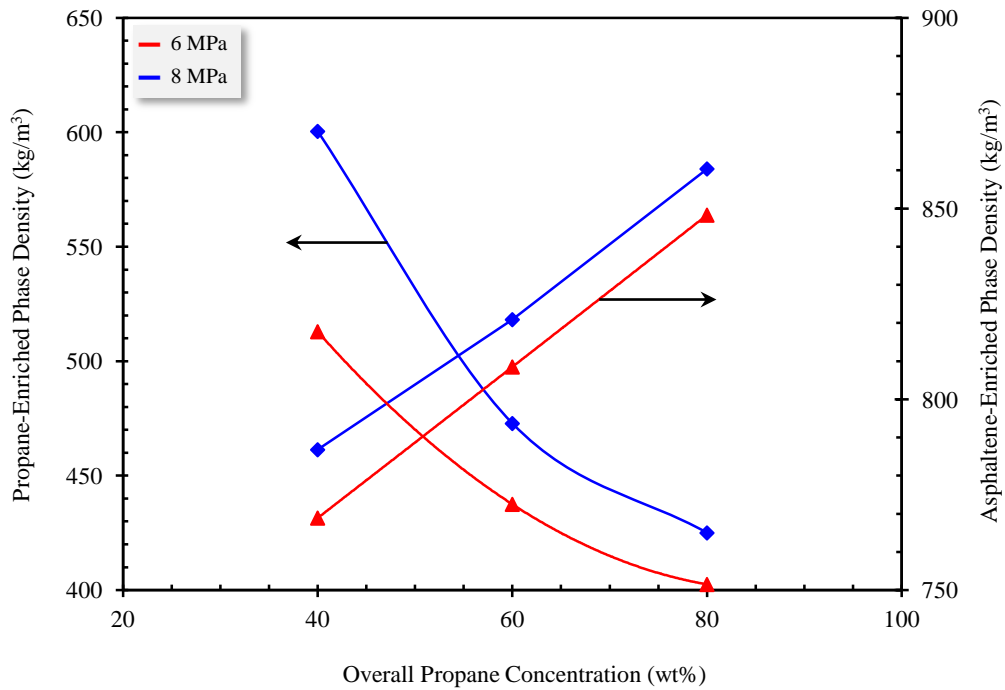


Figure 5-10: Liquid-liquid phase equilibria for Surmont bitumen / propane systems at the temperature of 100°C; density of equilibrium phases as a function of overall propane concentration at different pressures.

These results are an indirect indication of component distribution within the phases. As the pressure increases, there is a balance between the light components that are separating from the bitumen and propane that dissolves in the bitumen. This can be seen from the composition of equilibrium liquids summarized in Tables 5–4 to 5–6. As anticipated from these tables, at a constant overall propane concentration of 40 weight percent, the composition of propane in the solvent-enriched phase reduces due to higher extraction of components and, the composition of propane in the asphaltene-enriched phase decreases because of a produced heavier phase. The bitumen components in the asphaltene-enriched phase become heavier with increasing pressure, due to higher extraction of light components at higher pressures; thus, a reduction in the composition of propane in this phase is expected (a heavier hydrocarbon component, lower the solubility of propane at fixed temperature and pressure). However, the solubility of propane in hydrocarbons increases with pressure. The first factor cancels the second one and the concentration of propane in both phases reduces. Further investigations about the component distribution within the phases are presented in Section 5.4.3.

To illustrate how the viscosity of the asphaltene-enriched phase changes with increasing the overall propane concentration and pressure, the viscosity of this phase is plotted as a function of overall propane concentration in Figures 5–11 and 5–12. Generally, the increase in pressure and overall propane concentration results in higher extraction of light components from the bitumen, leading to the increase in the viscosity of the asphaltene-enriched phase.

From the vapour-liquid equilibrium data, it was found that the dissolution of propane in bitumen significantly reduces the viscosity of saturated liquid phase especially at low temperature. For example, at 3.992 MPa and at 100.2°C, the measured viscosity of saturated phase is 2.07 mPa which is much lower than 258.7 mPa of the raw bitumen without any propane dissolution. When the pressure increased to 6.060 MPa, the respective viscosities of the solvent-enriched and asphaltene-enriched phases are 0.22 and 4.33 mPa, which again both are lower than the viscosity of the raw bitumen. Although the

viscosity of the asphaltene-enriched phase, if compared to pressure 3.992 MPa, increases with the pressure (2.07 to 4.33 mPa.s), both equilibrium phases have a viscosity in the same magnitude of conventional crude oil and can be easily produced from the reservoir.

It is worth to point out that when pressure increases at a constant overall propane concentration, the viscosity of asphaltene-enriched phase increases. For example, at the temperature of 50°C and at a constant overall propane concentration of 80 weight percent, the viscosity of the asphaltene-enriched phase is 388 mPa.s at 2 MPa, while the viscosity is increased to 1666 mPa.s when pressure increases to 8 MPa. Even with this increase in the viscosity, the asphaltene-enriched phase has a viscosity lower than raw bitumen. It is noticeable that the impact of pressure on the viscosity of the asphaltene-enriched phase is more pronounced at higher overall propane concentrations.

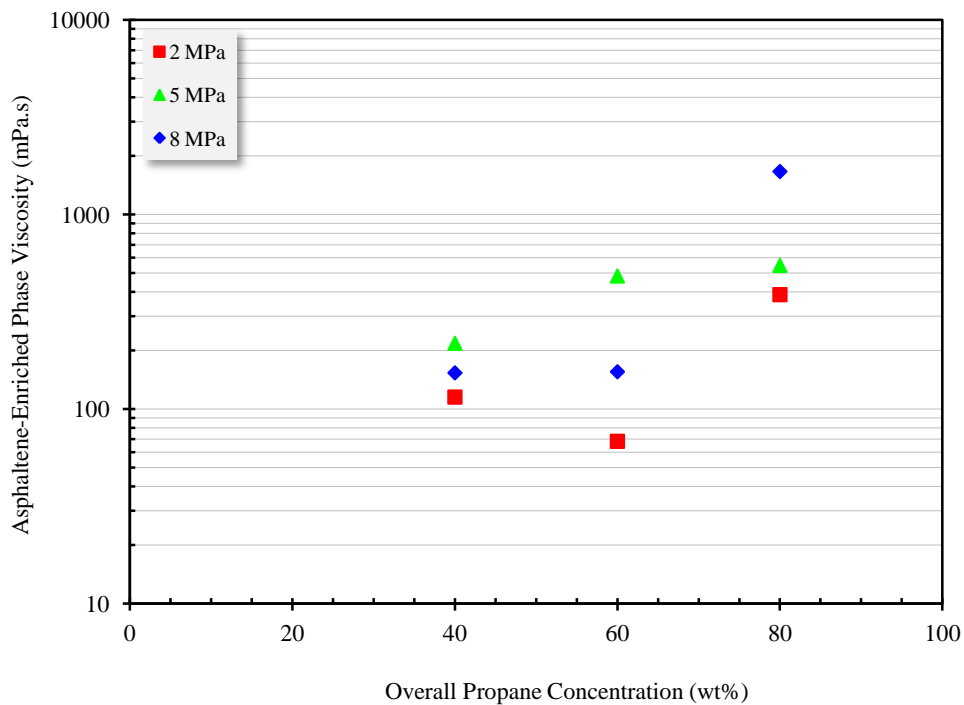


Figure 5–11: Liquid-liquid phase equilibria for Surmont bitumen / propane systems at the temperature of 50°C; the viscosity of asphaltene-enriched phase as a function of overall propane concentration at different pressures.

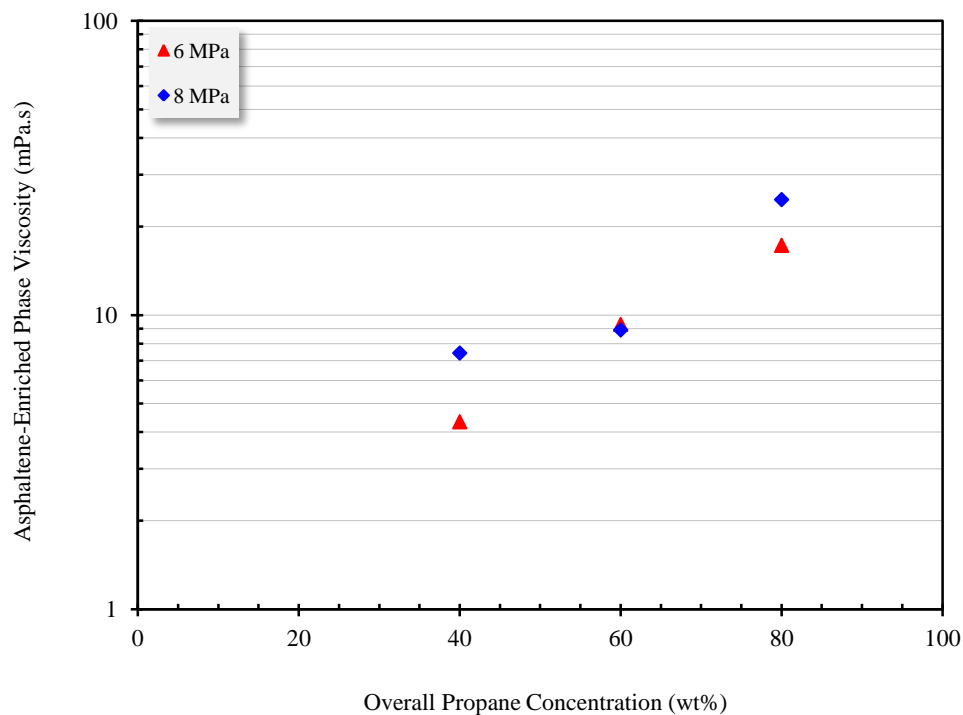


Figure 5-12: Liquid-liquid phase equilibria for Surmont bitumen / propane systems at the temperature of 100°C; the viscosity of asphaltene-enriched phase as a function of overall propane concentration at different pressures.

The impact of overall propane concentration on the viscosity of the asphaltene-enriched phase is also evident from Figures 5-11 and 5-12 at different pressures. As anticipated from these figures, the viscosity of the asphaltene-enriched phase increases with the overall propane concentration at a constant pressure. The increase in the viscosity is attributed to the depletion of the asphaltene-enriched phase from the light components and consequently lower propane solubility.

5.4.2. Extraction Yield

The generated experimental results in Tables 5-4 to 5-6 demonstrate that temperature, pressure, and overall propane concentration affect the physical properties of the two liquid phases at equilibrium condition. In fact, the distribution of the components within the phases is changed with process variables (i.e. temperature, pressure and overall propane concentration). In the fluid extraction processes, the properties of the solvent-

enriched phase are considerably important. Because, it determines the extend of the extraction process. The extraction yield is defined as the fraction of bitumen that was extracted into the solvent-enriched phase. The extraction yield is of particular importance for fluid extraction process where the low volatility materials are extracted from various mixtures and the undesirable components are left as residues.

The extraction yield is calculated based on the solubility of propane in each liquid phase, and the volume and density of liquid phases. The general equation for the calculation was presented in Section 4.7.1. The proposed calculation methods account the error introduced in the volume measurements during the experiments. The required measured parameters in each approach indicate that the extraction measurements can be calculated even with limited experimental measurements. Table 5–8 summarizes the average value for extraction yields obtained from three different methods. A maximum deviation of 4 % is observed using different methods for extraction yield calculation.

Table 5–8: The calculated extraction yield EY in liquid-liquid equilibrium of Surmont bitumen / propane mixtures; P , pressure; T , temperature; w , weight fraction of propane in mixture.

T (°C)	P (MPa)	10^2w	10^2EY	<i>Deviation</i>
50.3	2.096	40	53.17	± 2.40
50.2	2.082	60	44.79	± 3.55
50.3	2.054	80	52.50	± 0.86
50.3	5.046	40	60.58	± 2.26
50.3	5.046	60	49.78	± 3.16
50.3	5.026	80	56.98	± 4.01
50.3	8.018	40	66.34	± 2.33
50.3	8.052	60	54.31	± 1.89
50.2	7.969	80	58.44	± 4.10
100.1	6.060	40	18.07	± 1.48
100.2	6.039	60	27.82	± 2.10
100.1	6.149	80	42.61	± 1.67
100.1	8.066	40	42.34	± 3.31
100.1	8.045	60	37.77	± 2.93
100.0	7.976	80	47.01	± 2.71

The apparatus used for this study is batch for the bitumen and solvent. Solvent contacts the whole bitumen and extracts light fractions. In general, the extraction yields increases with the increase in pressure at a constant temperature and at a constant overall propane concentration. The experimental results also indicate that the extraction yield reduces with increasing temperature.

5.4.2.1. Effect of Pressure

The impact of pressure on the extraction yield of bitumen was evaluated at two temperatures (50 and 100°C). Three different pressures (2, 5, and 8 MPa) were considered for the temperature of 50°C, and at 100°C, two pressures (6 and 8 MPa) resulted in liquid-liquid separation.

As the data in Table 5–8 show, the extraction yield generally increases with the pressure at a constant temperature and a constant overall propane concentration. The maximum extraction yield, 66 wt%, is obtained at the highest pressure (8 MPa) and the lowest temperature (50°C). This is in agreement with the results obtained by Deo et al. (1992) for a bitumen-derived liquid and by Subramanian and Hanson (1998) for Uinta Basin Utah oil sand deposits. The change in extraction yield with pressure is due to the variation of solvent density with the pressure. Higher the density for propane, higher extraction yield is achieved.

To evaluate the effect of increasing pressure on extraction yields, the pressure was increased at a constant overall propane concentration. The extraction yields at three pressures are plotted against the overall propane concentration in Figure 5–13. As depicted in the figure, at the temperature of 50°C, the extraction yield increases with increasing pressure, regardless of the overall propane concentration. To compare the results and to investigate the temperature effect, the extraction yields at the two pressures (6 and 8) MPa and at a constant temperature of 100°C are plotted as a function of the overall propane concentration in Figure 5–14. In this case, the extend of extraction is also increased with the pressure.

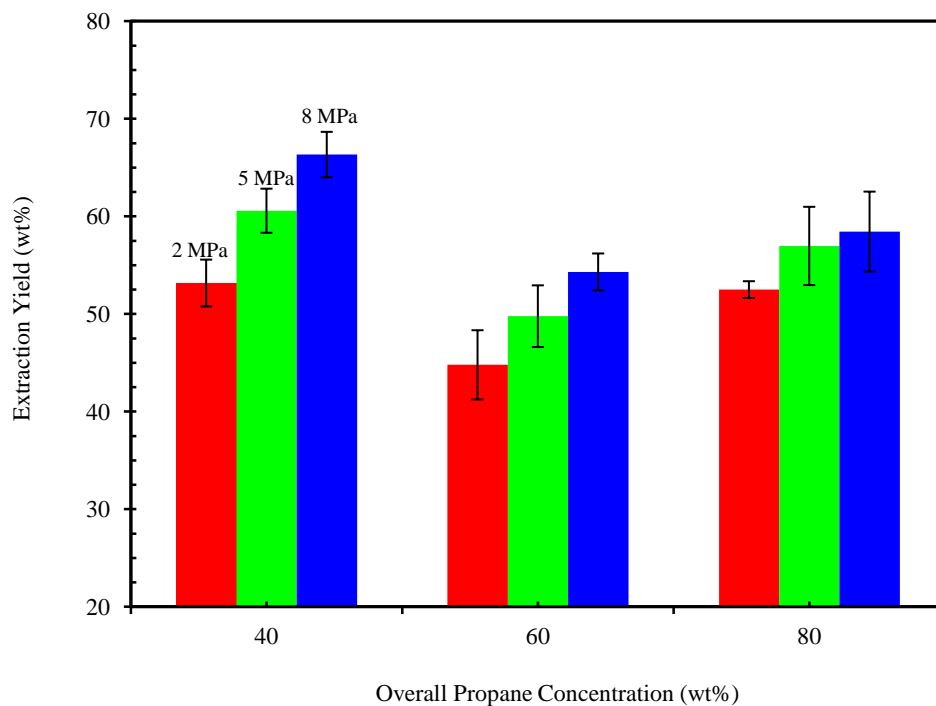


Figure 5–13: Effect of pressure and overall propane concentration on the extraction yield of Surmont bitumen using propane at the temperature of 50°C (Nourozieh et al. 2012c).

It can be concluded that the increasing trend for the variation of extraction yield with the pressure is observed at two different temperatures and at three different overall propane concentrations. The effect of pressure on extraction yield is more significant at high temperatures. This might be due the nature of propane at high temperatures which behaves like supercritical fluid close to the critical condition. Although the extraction capability at high temperatures is less than that of low temperatures, the impact of pressure is more pronounced at higher temperatures as presented in Figure 5–14. For instance, at the temperature of 50°C, an increase in the pressure from 5 to 8 MPa at a constant overall propane concentration of 40 weight percent increases the extraction yield about 10 percent (60.58 to 66.34) while the increase in the pressure (6 to 8) MPa at the temperature of 100°C, doubles the extraction yield (18.07 to 42.34). The higher variations of extraction yield with the pressure are also observed at other two overall propane concentrations.

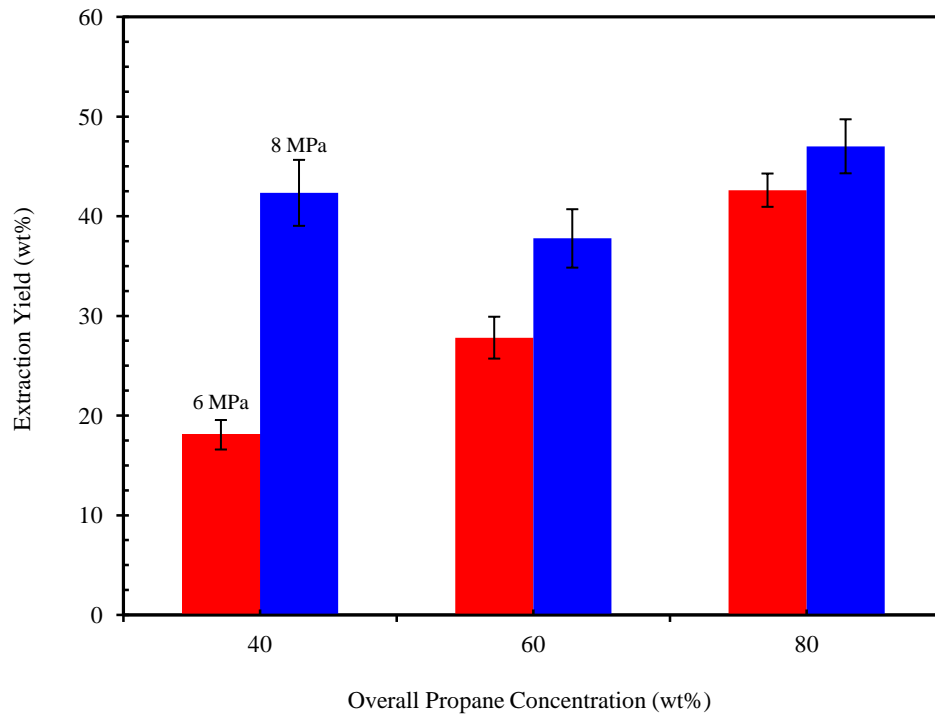


Figure 5–14: Effect of pressure and overall propane concentration on the extraction yield of Surmont bitumen using propane at 100°C.

The extraction yield can be converted into precipitation yield (the separation of heavy constituents from the bitumen) through the following equation,

$$\text{Precipitation Yield (\%)} = 100 - EY \quad 5-1$$

On the basis of the above equation, the precipitation of undesirable components from the bitumen using propane can be controlled. The experimental study by Akbarzadeh et al. (2004) for Athabasca bitumen diluted with propane indicated that the yield of precipitate decreases with the pressure. The measured data here is also confirmed this behaviour, because the extraction yield increases with pressure and accordingly the precipitation yield reduces with pressure. This behaviour was observed at two different temperatures (50 and 100°C).

5.4.2.2. Effect of Temperature

As presented in Table 5–8, the extraction yield reduces with the increase in the temperature at a constant pressure and overall propane concentration. That is, the yields

of 66.34 and 42.34 weight percent are obtained for two temperatures of 50 and 100°C at a constant pressure of 8 MPa and at a constant overall propane concentration of 40 weight percent. The decreasing trend of extraction yield with temperature is also observed at other overall propane concentrations and is plotted in Figure 5–15. The variation of extraction yield with temperature at a constant pressure is attributed to the change in the density of propane with the temperature. The density of propane at a constant pressure is higher at lower temperatures and reduces with increasing temperature. Thus, on the basis of the measured extraction yields, it can be concluded that the increase in the temperature reduces the density of propane and consequently decreases the extraction yield, regardless of the overall propane concentration.

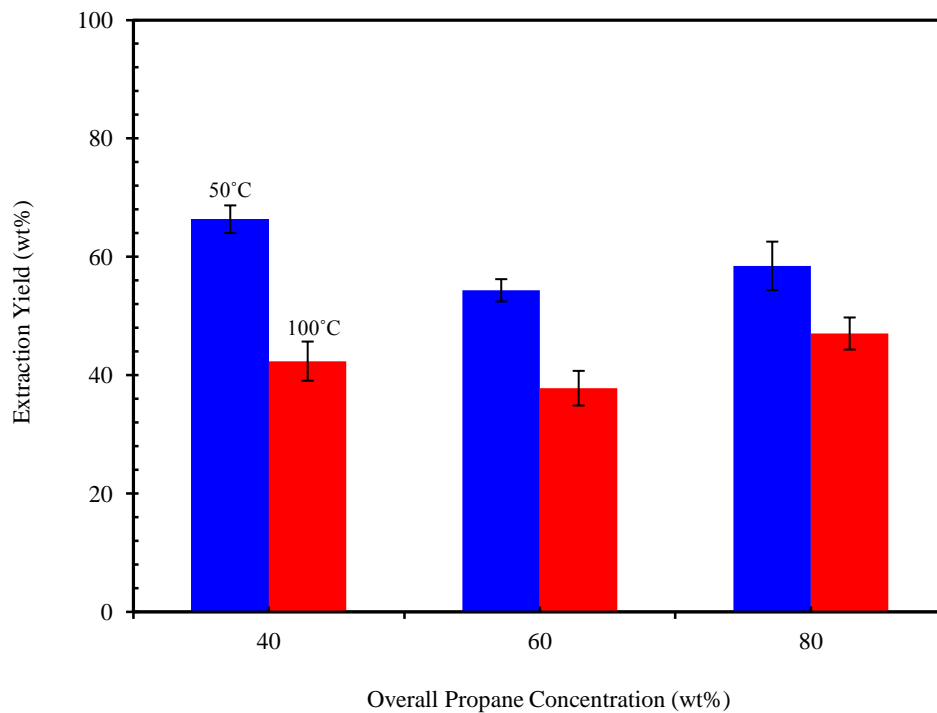


Figure 5–15: Effect of temperature and overall propane concentration on the extraction yield of Surmont bitumen using propane at a constant pressure of 8 MPa.

The significant variations in the extraction yield with temperature are mainly due to the change in the nature of the system by adjusting the operating pressure and temperature. At a low temperature (e.g. 50°C) and a pressure (e.g. 2 MPa) higher than

saturation pressure, propane is in the liquid state and under this condition, the liquid-liquid extraction occurs in the mixtures. Thus, the extraction yield is much higher than that of a high temperature condition (e.g. 100°C). This is because of the higher attractive forces in the liquid state compared to the vapour condition. In contrast, at a high temperature (e.g. 100°C) and even at a relatively high pressure (e.g. 6 MPa), propane density is much lower than the liquid propane. Thus, the system shows a behaviour similar to vapour-liquid extraction process in which the capacity of propane for the extraction is much less than that of liquid state.

5.4.2.3. Effect of Overall Propane Concentration

The experimental data presented in Tables 5-4 to 5-6 indicates that the overall propane concentration affects the extraction yield and the properties of equilibrium phases. The variation of extraction yield with the solvent overall concentration is presented in Figures 5-13 and 5-14. No increasing or decreasing trend for the variation of extraction yield with the overall propane concentration is observed. However, the results show that the extraction yield reduces with the overall propane concentration and reaches to a minimum value at the overall propane concentration of 60 weight percent. Then, the extraction yield increases with further increase in the overall propane concentration.

If the extraction yield is converted into the separation of heavy constituents from the bitumen using Equation 5-2, it is found that the precipitation yield is not increased with the solvent overall concentrations. As it is expected on the basis of asphaltene precipitation by pentane or heptanes, the yield of asphaltene precipitation increases with the dilution of bitumen with excess volume of pentane or heptane. However, the experimental results obtained here for the propane does not show any continuous increasing trend for the precipitation yield with the overall propane concentration. It might be due to change in the distribution of different fractions (saturate, aromatic, resin, and asphaltene) at different overall propane concentrations. As it will be discussed in

Sections 5.4.3 and 5.4.4, the distribution of components on the basis of the SimDis analysis and the partitioning of different fractions on the basis of SARA analysis are significantly changed with the variation of overall propane concentration. The asphaltene and resin fractions of bitumen play an important role in the observed behaviours.

5.4.2.4. Effect of Propane Density

The impact of temperature and pressure on the extraction yield is attributed to the change in propane density. The analysis of the data presented in Sections 5.4.2.1 and 5.4.2.2 confirmed that the extraction yield increases with the increase in pressure or the decrease in the temperature. The density of propane rises with an increase in the pressure at a constant temperature or a decrease in temperature at a constant pressure. Thus, if the measured extraction yields at different operating conditions are plotted against propane density, the extraction capacity of solvent can be evaluated. Figure 5–16 demonstrates the extraction yields obtained for the bitumen as a function of propane density at different solvent overall concentrations.

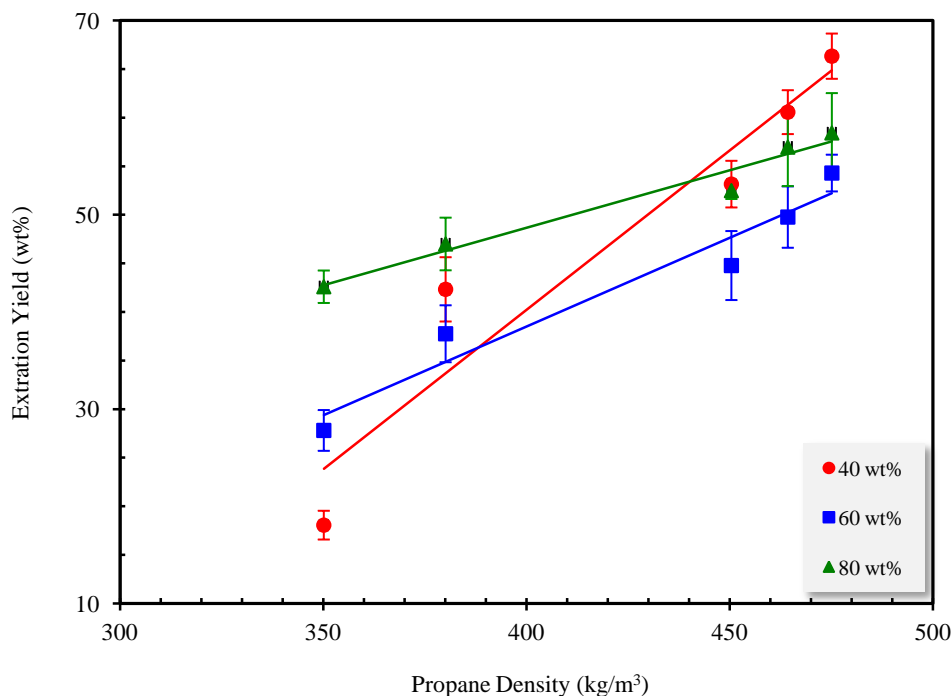


Figure 5–16: Effect of propane density and overall propane concentration on the extraction yield of Surrmont bitumen.

As depicted in Figure 5–16, the extraction yield increases as the density of pure propane increases. Although the density of propane at the temperature of 50°C over the studied pressures is much higher than its corresponding values at the temperature of 100°C, the plot of extraction yield as a function of propane density follows a linear increasing trend. The increasing trend of extraction yield with propane density is observed at two other overall propane concentrations. This confirms that propane density at a constant overall propane concentration determines the separation of undesirable constituents. This indicates that the extraction yield is a strong function of propane density.

The densities of pure propane at a constant pressure of 8 MPa and at two different temperatures (50 and 100)°C are 475.1 kg/m³ and 380.1 kg/m³, respectively. The corresponding extraction yields are 66.34 and 42.34 weight percent at a constant overall propane concentration of 40 weight percent, 54.31 and 37.77 at a constant overall propane concentration of 60 weight percent, and 58.44 and 47.01 at a constant overall propane concentration of 80 weight percent. The values indicate that at higher pure propane density, higher extraction yields are obtained. The propane density is changed by adjusting the temperature and pressure.

Although no experimental data are reported at a constant density of pure propane with different combinations of pressures and temperatures, it is expected that the extraction yield would be the same if the density of propane kept constant by adjusting the operating conditions. The study by the Subramanian (1996) indicated that the similar extraction yields are obtained if the same propane density is maintained with a combination of temperature and pressure, and the extraction yield is mainly controlled by the density of propane. However, Deo et al. (1992) concluded the enhanced solubility of bitumen in propane near critical point.

5.4.3. Compositional Analysis of Extracts and Residues

The phase samples taken from two equilibrium phases were first flashed at the atmospheric condition to measure the volume of evolved gas for solubility calculation.

Then, the flashed-off phase samples produced after each experiment were subjected to compositional analysis using the ASTM 7169 method. The compositional analysis of raw bitumen and flashed-off liquid samples give the distribution of components at equilibrium conditions. In addition, the impact of pressure, temperature, and solvent-to-bitumen ratio on the phase partitioning can also be evaluated in more detail.

The terms extract and residue, used throughout this chapter, refer to the flashed-off liquid samples taken from each liquid phase at equilibrium condition (extract is the flashed-off liquid sample taken from solvent-enriched phase and residue is the flashed-off liquid sample taken from asphaltene-enriched phase).

The experimental results indicated that two liquids, the solvent-enriched and the asphaltene-enriched, exist at equilibrium condition for Surmont bitumen / propane mixtures at the temperature of 50°C and at the pressures greater than 2 MPa and at the temperature of 100°C and at the pressures higher than 4.5 MPa. Figure 5–17 shows the boiling point curve of the extracts obtained at two temperatures with the lowest equilibrium pressure. For the comparison, the boiling point curve of raw Surmont bitumen is also indicated.

As depicted in this figure, the extract produced at the temperature of 50°C is consistently heavier than the extract at the temperature of 100°C. This is clearly verified by the higher boiling point curves for the extracted oil taken at the temperature of 50°C. Higher boiling point curves are generally corresponded to the heavier molecular weight hydrocarbons. The raw bitumen sample is heavier than two extracts. This indicates that the light components of bitumen are extracted into the solvent-enriched phase, and depending on the condition of the experiment, the distribution of components is different. The initial boiling points for two extracts as well as raw bitumen are close to each other. In contrast, the weight fraction of distilled raw bitumen (0.813) is much lower than those of two extracts (0.853 and 0.994) indicating that the separation of undesirable and heavy constituents from bitumen significantly changed the composition of the solvent-enriched phases.

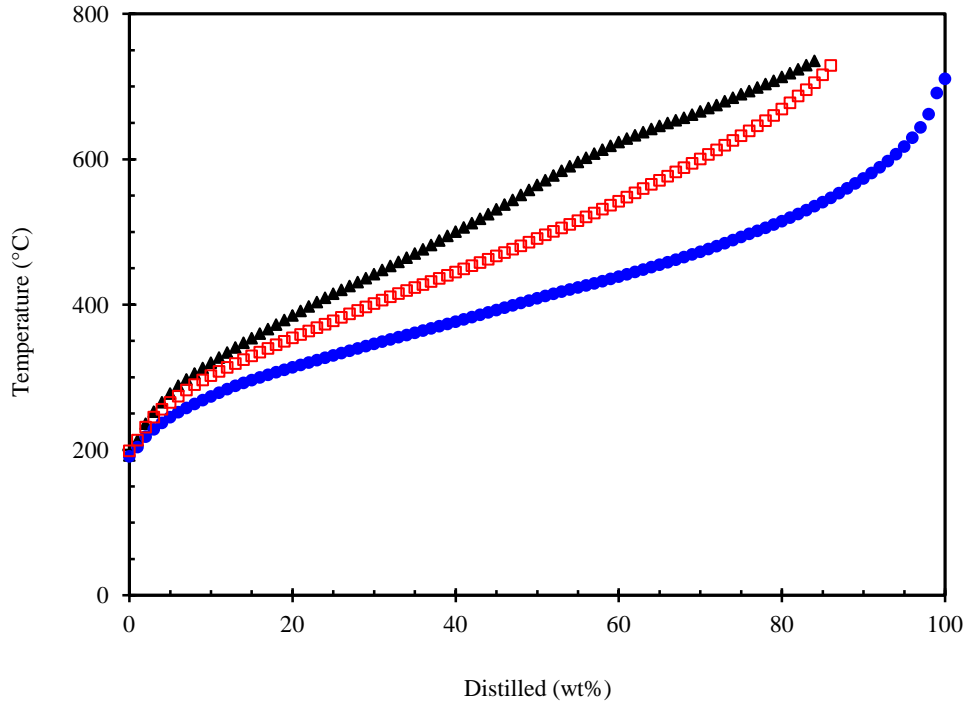


Figure 5–17: Boiling point curves (temperature versus weight fraction distilled) for raw Surmont bitumen (▲) and two extracts taken from liquid-liquid equilibrium of Surmont bitumen / propane mixtures; □, the solvent-enriched phase at the temperature of 50°C and at a constant pressure of 2 MPa with a constant overall concentration of 0.4 weight fraction; ●, the solvent-enriched phase at the temperature of 100°C and at a constant pressure of 6 MPa with a constant overall propane concentration of 0.8 weight fraction.

The evaluation of component distribution on the basis of the carbon number in extracts gives better understanding of liquid-liquid upgrading in the bitumen/propane mixtures. Thus, the boiling point curve of the samples and raw bitumen is usually converted into the carbon number distribution with the built-in software installed in the SimDis apparatus. As the residues contain much higher heavy constituents, these samples were not analyzed in this study. Thus, the boiling point curve for these samples is not presented. However, the carbon number distribution of residues is back calculated from the corresponding physical properties of the phases and the carbon number distributions of extracts and raw bitumen by the following equation,

$$w_{L2,i} = \frac{m_B w_{B,i} - \rho_{L1} V_{L1} (1 - w_{S,L1}) w_{L1,i}}{\sum [m_B w_{B,i} - \rho_{L1} V_{L1} (1 - w_{S,L1}) w_{L1,i}]} \quad 5-2$$

where $w_{L,i}$ is the weight fraction components in extract (1) or residue (2), m_B is the mass of bitumen charged into the equilibrium cell, w_B is the weight fraction of components in bitumen, ρ_L is the density of equilibrium phase, w_S is the weight fraction of solvent in the solvent enriched phase, and V_L is the volume of equilibrium phase.

Figure 5–18 presents the compositional analysis for extract and residue produced at the temperature of 50°C and a constant pressure of 2 MPa as well as that of raw bitumen. As depicted in the figure, the extract contains lighter components compared to the raw bitumen and the residue. This indicates that the separation of heavy constituents such as asphaltene from the bitumen significantly changes the composition of the solvent-enriched phase toward a lighter phase. As it also anticipated from Figure 5–18, the distribution of components is balanced at carbon number C₅₅. The extract is composed of a higher fraction of components with carbon number less than 55 while the residue contains a higher fraction of components with carbon number larger than 55. Thus, the light components (C₅₅-) partitioned into the solvent-enriched phase and heavy components (C₅₅₊) precipitated into the asphaltene-enriched phase. The carbon number C₅₅ can be considered as an inflection point in which the distribution of components changes for liquid phases.

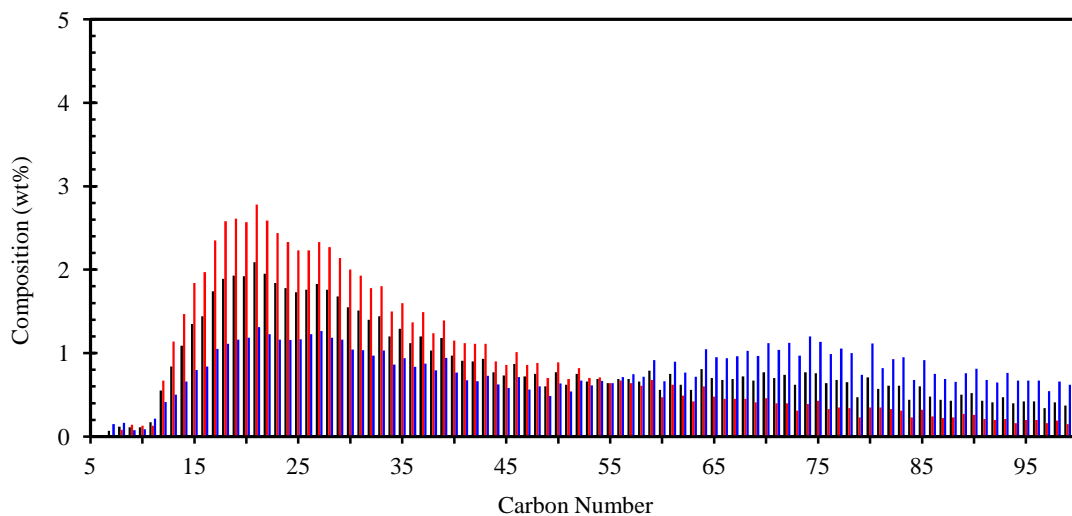


Figure 5–18: Compositional analysis (component weight percent) for raw bitumen (black) and two flashed-off phase samples (extract, red, and residue, blue) taken from liquid-liquid equilibrium of Surmont bitumen / propane mixtures at the temperature of 50°C and at a constant pressure of 2 MPa with a constant overall propane concentration of 0.4 weight fraction.

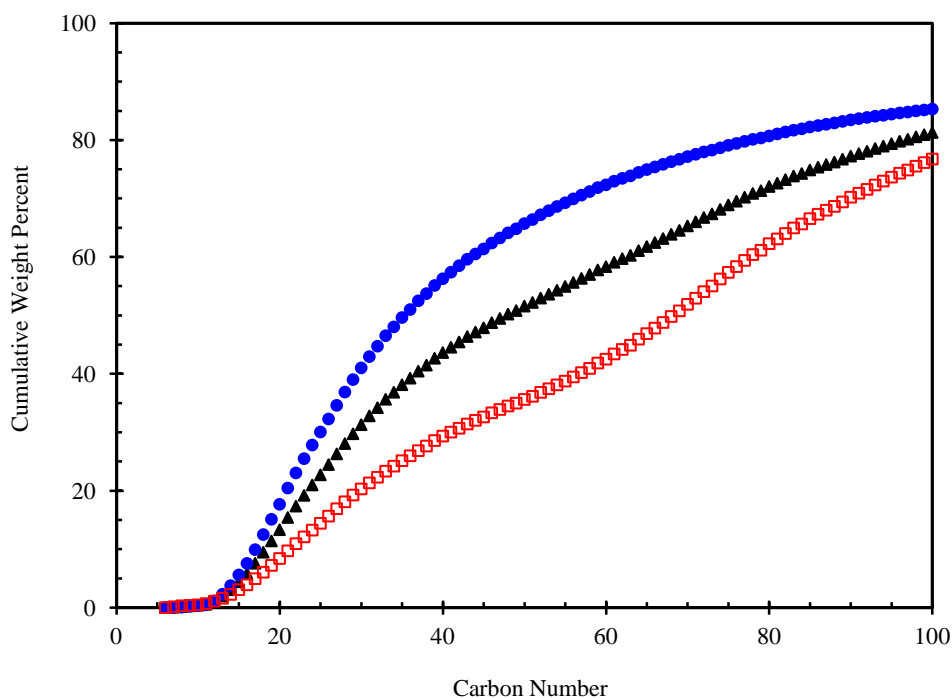


Figure 5–19: Carbon number distribution for raw bitumen (▲) and two flashed-off phase samples (extract ● and residue □) taken from liquid-liquid equilibrium of Surmont bitumen / propane mixtures at 50°C and at a constant pressure of 2 MPa with a constant overall propane concentration of 0.4 weight fraction.

A comparison of three samples (extract, residue, and raw bitumen) based on cumulative carbon number presented in Figure 5–19 shows that the weight fraction of un-distilled components (C_{100+}) is significantly different. This is clearly shown by the configuration of cumulative carbon number curves. That is, the end point of the curve for the extract is higher than raw bitumen and residue. The weight fraction of un-distilled components in extract, residue, and bitumen are 0.147, 0.232, and 0.187, respectively.

In Figures 5–17 to 5–19, the compositional analysis of extract and residue produced at the temperature of 50°C as well as raw was compared. The same analysis but at the temperature of 100°C and a constant pressure of 6 MPa is also conducted to evaluate two equilibrium phases at supercritical condition. In this case, it was observed that the extract was light brown in color, whereas the sample produced at the temperature of 50°C and constant pressure of 2 MPa is dark. Figure 5–20 presents the compositional analysis for extract and residue produced at the temperature of 100°C and a constant pressure of 6

MPa. As expected in this case, the distribution of components in two equilibrium phases are completely different than the temperature of 50°C. The inflection point for the distribution of component in two equilibrium liquid phases was moved toward the C₄₅. At the temperature of 100°C, the asphaltene-enriched phase is considerably depleted from the light components (C₂₀-) while the solvent-enriched phase contains no components heavier than C₇₀. This might be due to the operating condition of process which is close the critical point of propane. The experimental data in the literature confirmed that the extracted phase with propane near the critical condition contains light components of the oil (Deo et al. 1992).

Figure 5–21 shows a comparison of three samples (extract, residue, and raw bitumen) based on cumulative carbon number. The end point of the curves for three samples is considerably different. The extract is completely distilled while a large fraction of residue was remained as un-distilled fraction. The weight fraction of un-distilled components (C₁₀₀₊) in extract, residue, and raw bitumen are 0.04, 0.324, and 0.187, respectively. This indicates that the two equilibrium liquid phases at the temperature of 100°C contains components with largely different boiling points.

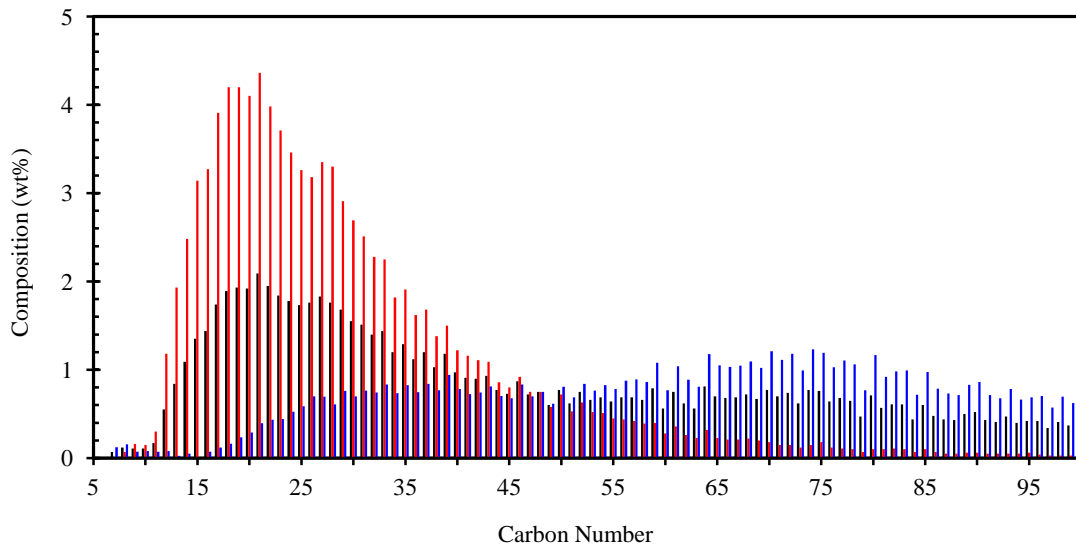


Figure 5–20: Compositional analysis (component weight percent) for raw bitumen (black) and two flashed-off phase samples (extract, red, and residue, blue) taken from liquid-liquid equilibrium of Surmont bitumen / propane mixtures at the temperature of 100°C and at a constant pressure of 6 MPa with a constant overall propane concentration of 0.8 weight fraction.

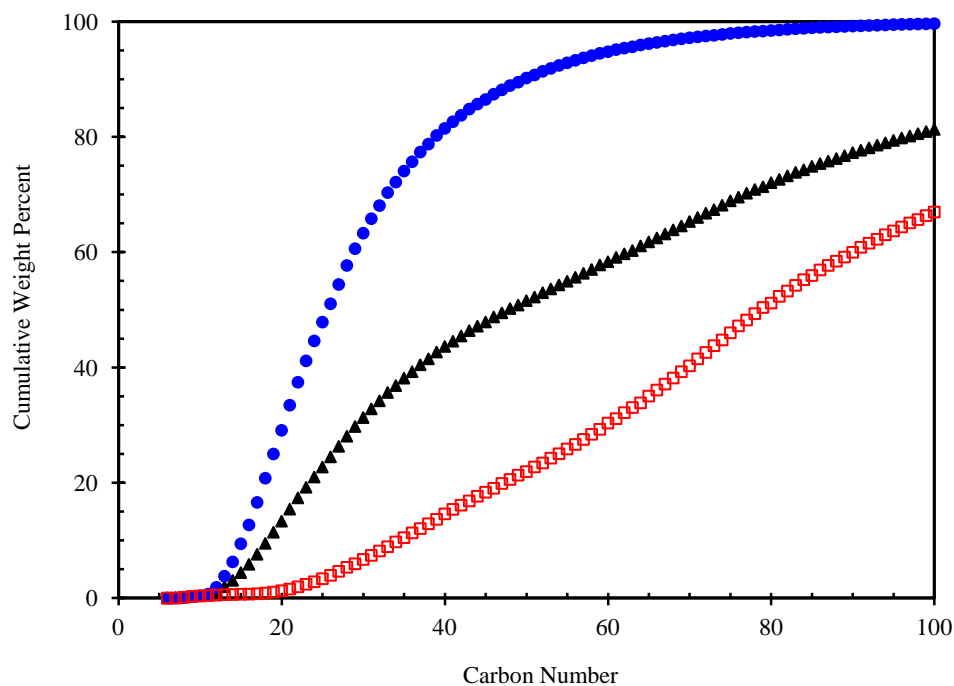


Figure 5–21: Carbon number distribution for raw bitumen (▲) and two flashed-off phase samples (extract ● and residue □) taken from liquid-liquid equilibrium of Surmont bitumen / propane mixtures at 100°C and at a constant pressure of 6 MPa with a constant overall propane concentration of 0.8 weight fraction.

5.4.3.1. Effect of Pressure

The measured experimental data presented in Sections 5.4.1 and 5.4.2, show that pressure affects the physical properties of two equilibrium liquid phases and the extraction yield. Generally, it was observed that the extraction yield is increased with the pressure. The impact of pressure is explained with the extraction power of the solvent to extract the components from the asphaltene-enriched phase. In this section, the impact of pressure is evaluated from the compositional analysis results. The analysis was conducted at three different cases: a constant temperature of 50°C and a constant overall propane concentration of 0.4 weight fraction, a constant temperature of 50°C and a constant overall propane concentration of 0.8 weight fraction, and a constant temperature of 100°C and a constant overall concentration of 0.8 weight fraction. Figure 5–22 demonstrates the boiling point curve of extracts produced at different operating conditions.

Considering a constant temperature of 50°C and a constant overall propane concentration of 0.4 weight fraction, the initial boiling points for the samples at two different pressures are close to each other. However, the weight fraction of distilled raw bitumen is much lower than those of the extracts, and as the pressure reduces, the weight fraction of distilled samples increases. In fact, increasing the pressure results in an extract that contains higher boiling point components. A comparison shows that the weight fraction of distilled raw bitumen is 0.813 that is lower than those of extracts, 0.853 and 0.825 at the pressures of (2 and 8) MPa, respectively. This also indicates that the pressure enhances the extraction of undesirable and heavy constituents into the solvent-enriched phase resulting to a lower fraction of distilled sample.

If a constant overall propane concentration of 0.8 weight fraction was considered at the temperature of 50°C, again it was observed that the extract produced at the pressure of 8 MPa is consistently heavier than the extract produced at the pressure of 2 MPa. The raw bitumen sample is heavier than two extracts. This is clearly verified by the higher boiling point curves for the raw bitumen compared to two extracts. The initial boiling points for two extracts as well as raw bitumen are close to each other. In contrast, the weight fraction of distilled raw bitumen (0.813) is much lower than those of two extracts (0.979 and 0.932). As the pressure increases, the weight fraction of distilled samples reduces.

The previous studies on the supercritical extraction processes have shown that the impact of pressure on the behaviour of the process would change with temperature (Deo et al. 1992; Rose et al. 2001). Thus, in the current study, the effect of pressure on the boiling point curve at the temperature of 100°C is also evaluated. In this case, the overall propane concentration was fixed at 0.8 weight fraction and the pressures were (6 and 8) MPa. The liquid-liquid separation is not observed at pressures less than 4.5 MPa. As shown in Figure 5–22, the extract produced at the pressure of 8 MPa is consistently heavier than the extract produced at the pressure of 6 MPa. The raw bitumen sample is much heavier than two extracts. This is distinctly observed by the higher boiling point

curves for the raw bitumen compared to two extracts. A large difference in the boiling point curves and the weight fraction of distilled samples is evident. The weight fraction of distilled raw bitumen is 0.813 that is much lower than those of two extracts, 0.996 and 0.994 at (6 and 8) MPa, respectively, indicating that the solvent-enriched phases are completely distilled and thus, the separation of undesirable and heavy constituents from bitumen significantly changes the composition of solvent-enriched phases.

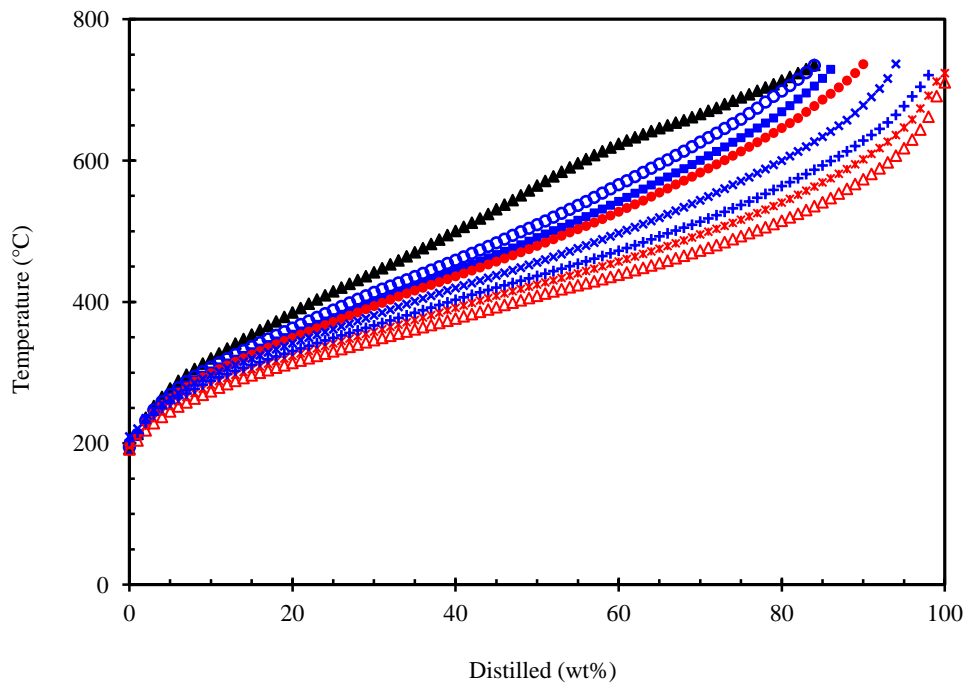


Figure 5–22: Boiling point curves (temperature versus weight percent distilled) for raw bitumen (\blacktriangle) and extracts taken from liquid-liquid equilibrium of Surmont bitumen / propane mixtures at different pressures, temperatures, and overall propane concentrations; \blacksquare , 50°C, 2 MPa, and overall propane concentration of 0.4 weight fraction; \circ , 50°C, 8 MPa, and overall propane concentration of 0.4 weight fraction; $+$, 50°C, 2 MPa, and overall propane concentration of 0.8 weight fraction; \times , 50°C, 8 MPa, and overall propane concentration of 0.8 weight fraction; \bullet , 100°C, 8 MPa, and overall propane concentration of 0.4 weight fraction; \triangle , 100°C, 6 MPa, and overall propane concentration of 0.8 weight fraction; $*$, 100°C, 8 MPa, and overall propane concentration of 0.8 weight fraction.

The impact of pressure on the component distribution of extracts and residues at the temperature of 50°C is presented in Figures 5–23 and 5–24, respectively. In these figures, the component distribution of raw bitumen is also plotted.

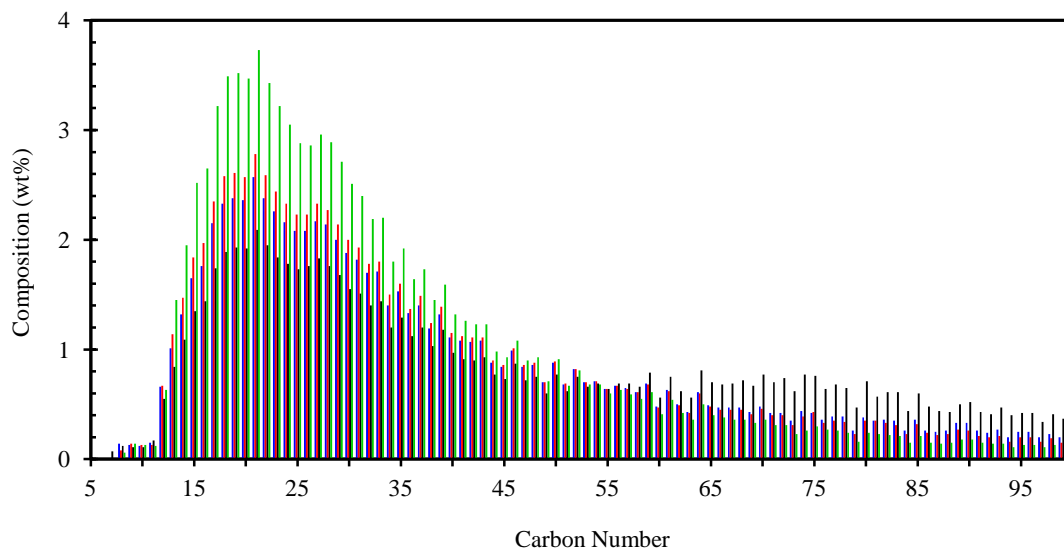


Figure 5–23: Compositional analysis (component weight percent) for raw bitumen (black) and extracts taken from liquid-liquid equilibrium of Surmont bitumen / propane mixtures at a constant temperature of 50°C and at different pressures and overall propane concentrations; red, 2 MPa, and overall propane concentration of 0.4 weight fraction; blue, 8 MPa, and overall propane concentration of 0.4 weight fraction; green, 2 MPa, and overall propane concentration of 0.8 weight fraction.

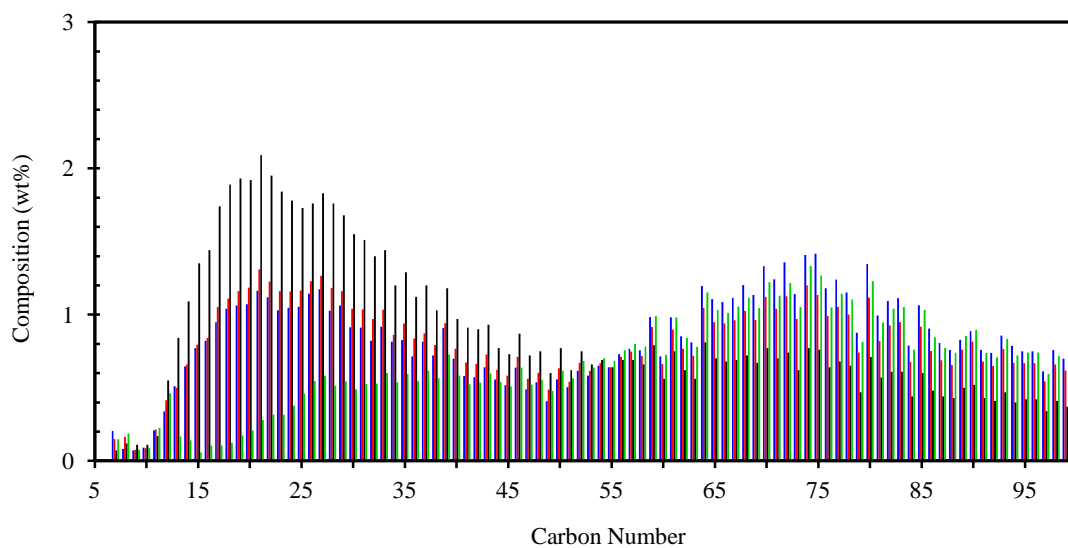


Figure 5–24: Compositional analysis (component weight percent) for raw bitumen (black) and residues taken from liquid-liquid equilibrium of Surmont bitumen / propane mixtures at a constant temperature of 50°C and at different pressures and overall propane concentrations; red, 2 MPa, and overall propane concentration of 0.4 weight fraction; blue, 8 MPa, and overall propane concentration of 0.4 weight fraction; green, 2 MPa, and overall propane concentration of 0.8 weight fraction.

As depicted in Figure 5–23, the extract produced at the pressure of 2 MPa is composed of higher fraction of light components than the extract produced at the pressure

of 8 MPa. This clearly shows the extraction of heavier components at high pressures (e.g. 8 MPa) which resulting in an overall lower fraction of light components compared to 2 MPa. From Figure 5–23, it can also be concluded that a large increase in the pressure leads to an extract which has a similar component distribution to raw bitumen. In other words, the pressure significantly changes the composition of the solvent-enriched phase toward raw bitumen.

The variation of component fractions in the solvent-enriched phases with the pressure can also be evaluated and analyzed from its corresponding fraction in the asphaltene-enriched phase. Figure 5–24 illustrates the component distribution of the residues produced at two pressures, (2 and 8) MPa, and at a constant temperature of 50°C with a constant overall propane concentration of 0.4 weight fraction. From the figure, it can be clearly observed that the residues have the lower weight fraction of light components compared to raw bitumen. A comparison of two residues indicates that the residue produced at 8 MPa is much heavier than that produced at the pressure of 2 MPa. This shows that the extracted phase (solvent-enriched phase) becomes heavier with increasing the pressure and consequently, an equilibrium phase (asphaltene-enriched phase) with a larger fraction of the heavy constitutes is remained. The higher fraction of light components in residue produced at the pressure of 2 MPa compared to residue produced at the pressure of 8 MPa is consistent with the data presented here for liquid phases.

Figures 5–25 and 5–26 present the compositional analysis for the extracts and residues produced at pressures (6 and 8) MPa and at a constant temperature of 100°C. As depicted in the figure, the extract produced at the pressure of 6 MPa is composed of higher fraction of light components than the extract produced at the pressure of 8 MPa. This is evidence that the extraction of heavier components occurs at higher pressures (e.g. 8 MPa). Thus, the extracted phase (solvent-enriched phase) contains heavier hydrocarbon components compared to the pressure of 6 MPa. As anticipated from Figure 5–25, the increase in the pressure at the temperature of 100°C results in an increase in hydrocarbon

components with equivalent carbon number less than 30 (e.g. C₃₀). This might be due to the operating condition of process which is close the critical point of propane.

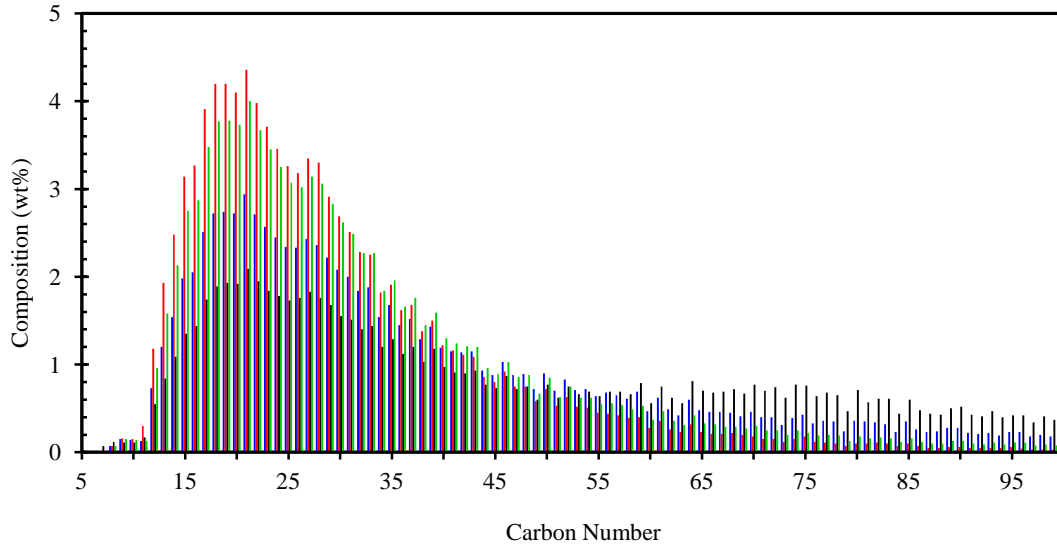


Figure 5-25: Compositional analysis (component weight percent) for raw bitumen (black) and extracts taken from liquid-liquid equilibrium of Surmont bitumen / propane mixtures at a constant temperature of 100°C and at different pressures and overall propane concentrations; red, 6 MPa, and overall propane concentration of 0.8 weight fraction; blue, 8 MPa, and overall propane concentration of 0.4 weight fraction; green, 8 MPa, and overall propane concentration of 0.8 weight fraction.

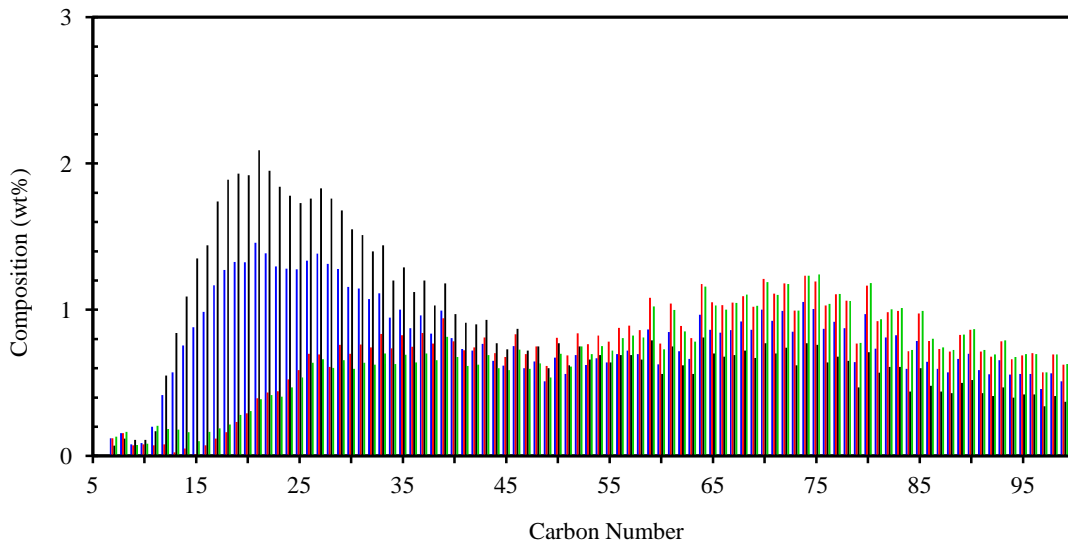


Figure 5-26: Compositional analysis (component weight percent) for raw bitumen (black) and residues taken from liquid-liquid equilibrium of Surmont bitumen / propane mixtures at a constant temperature of 100°C and at different pressures and overall propane concentrations; red, 6 MPa, and overall propane concentration of 0.8 weight fraction; blue, 8 MPa, and overall propane concentration of 0.4 weight fraction; green, 8 MPa, and overall propane concentration of 0.8 weight fraction.

The comparison of two residues is difficult in Figure 5–26; because no large difference in the composition of extracts was observed. However, by plotting the cumulative carbon number of three samples (residues and raw bitumen), it can be seen that the residue produced at the pressure of 8 MPa is slightly heavier than the residue produced at the pressure of 6 MPa. In fact, the higher extraction of light components into upper liquid phase at the pressure of 8 MPa cause a heavier asphaltene-enriched phase at equilibrium condition.

Figure 5–27 presents a comparison of samples (extracts and raw bitumen) based on cumulative carbon number. At a constant temperature of 50°C and overall propane concentration of 0.4 weight fraction, the end point of the curve for the extract produced at the pressure of 2 MPa is higher than that produced at the pressure of 8 MPa and that of raw bitumen. Although a large fraction of extracts is remained un-distillable for two pressures, the extract produced at the pressure of 2 MPa contains much higher content of light components compared to the extract produced at the pressure of 8 MPa. The weight fraction of un-distilled components (C_{100+}) in two extracts and raw bitumen are 0.147, 0.175, and 0.187, respectively. This confirms that the pressure changes the composition of the solvent-enriched phase toward raw bitumen.

A similar behaviour at the temperature of 50°C and overall propane concentration of 0.8 weight fraction was also observed. The weight fractions of un-distilled components (C_{100+}) in two exactas produced at the pressures of 2 and 8 MPa and in raw bitumen are 0.021, 0.069, and 0.187, respectively. As the pressure increases, the weight fraction of un-distilled components (C_{100+}) in the extracts increases toward its corresponding value for the bitumen, and the curve for the cumulative carbon number starts to overlies the bitumen curve.

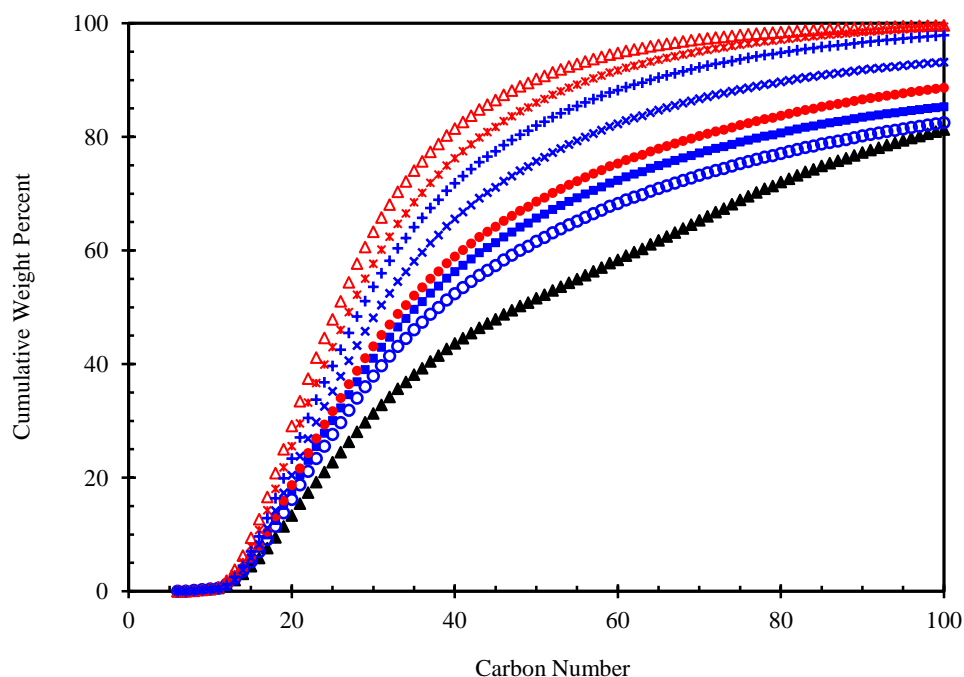


Figure 5–27: Carbon number distribution for raw bitumen (▲) and flashed-off solvent enriched phases (extracts) taken from liquid-liquid equilibrium of Surmont bitumen / propane mixtures at different pressures, temperatures, and overall propane concentrations; ■, 50°C, 2 MPa, and overall propane concentration of 0.4 weight fraction; ○, 50°C, 8 MPa, and overall propane concentration of 0.4 weight fraction; +, 50°C, 2 MPa, and overall propane concentration of 0.8 weight fraction; ×, 50°C, 8 MPa, and overall propane concentration of 0.8 weight fraction; ●, 100°C, 8 MPa, and overall propane concentration of 0.4 weight fraction; △, 100°C, 6 MPa, and overall propane concentration of 0.8 weight fraction; *, 100°C, 8 MPa, and overall propane concentration of 0.8 weight fraction.

If the cumulative carbon number of extracts produced at the temperature of 100°C and overall propane concentration of 0.8 weight fraction is compared, no significant difference in two extracts is detected. From Figure 5–27, it is found that the end point of the curve for two extracts is almost the same and higher than that of raw bitumen. Although both extracts are completely distilled, the extract produced at the pressure of 6 MPa contains higher content of light components compared to the extract produced at the pressure of 8 MPa. The weight fraction of un-distilled components (C_{100+}) in two extracts at the pressures of (6 and 8) MPa and in raw bitumen are 0.004, 0.006, and 0.187, respectively. This reveals that the extract produced at the pressure of 8 MPa is heavier than the one produced at the pressure of 6 MPa.

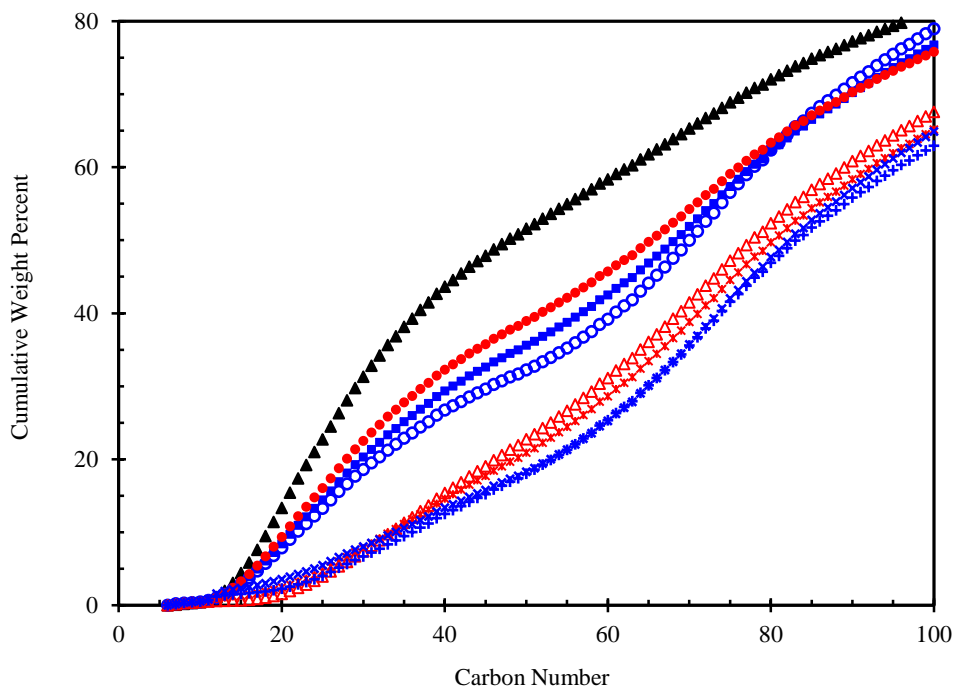


Figure 5–28: Carbon number distribution for raw bitumen (\blacktriangle) and flashed-off asphaltene-enriched phases (residues) taken from liquid-liquid equilibrium of Surmont bitumen / propane mixtures at different pressures, temperatures, and overall propane concentrations; \blacksquare , 50°C, 2 MPa, and overall propane concentration of 0.4 weight fraction; \circ , 50°C, 8 MPa, and overall propane concentration of 0.4 weight fraction; $+$, 50°C, 2 MPa, and overall propane concentration of 0.8 weight fraction; \times , 50°C, 8 MPa, and overall propane concentration of 0.8 weight fraction; \bullet , 100°C, 8 MPa, and overall propane concentration of 0.4 weight fraction; \triangle , 100°C, 6 MPa, and overall propane concentration of 0.8 weight fraction; $*$, 100°C, 8 MPa, and overall propane concentration of 0.8 weight fraction.

Figure 5–28 displays the cumulative carbon number of residues and raw bitumen. The end point of the curve for the residues is lower than that of raw bitumen. The weight fraction of un-distilled components (C_{100+}) in two residues produced at the pressures of 2 and 8 MPa (50°C and 0.4 overall propane weight fraction) and in raw bitumen are 0.232, 0.210, and 0.187, respectively. When the pressure increases at the temperature of 50°C and a constant overall propane concentration of 0.4 weight fraction, the cumulative carbon number presented in Figure 5–28 does not show any variation. As expected, the end point of the curve for the residues is lower than that of raw bitumen. The weight fractions of un-distilled components (C_{100+}) in two residues produced at the pressures of 2 and 8 MPa and in raw bitumen are 0.371, 0.351, and 0.187, respectively.

Figure 5–28 also shows that the end point of the curve for the residues produced at the temperature of 100°C and a constant overall propane concentration of 0.8 weight fraction is much lower than that of raw bitumen. The end point of the curve for the residue produced at the pressure of 6 MPa is slightly higher than that of the residue produced at the pressure of 8 MPa. The weight fraction of un-distilled components (C_{100+}) in two residues produced at the pressures of (6 and 8) MPa and in raw bitumen are 0.324, 0.349, and 0.187, respectively.

5.4.3.2. Effect of Temperature

In Section 5.4.1, it was found that temperature affects the physical properties of two equilibrium liquid phases and the extraction yield. The significant variations in the extraction yield with temperature are mainly due to the change in the nature of the system. At a low temperature (e.g. 50°C) and a relatively low pressure (e.g. 2 MPa), propane is in the liquid state and under this condition, the liquid-liquid extraction occurs in the mixtures. However, at a high temperature condition (e.g. 100°C) and even at a high pressure (e.g. 6 MPa), propane density is much lower than liquid propane. Thus, the system shows a behaviour similar to vapour-liquid extraction process in which the capacity of propane for the extraction is much less than that of liquid state.

In this section, the impact of temperature is evaluated from the compositional analysis results. The analysis was conducted at two different cases: a constant overall propane concentration of 0.4 weight fraction and a constant pressure of 8 MPa, and a constant overall propane concentration of 0.8 weight fraction and a constant pressure of 8 MPa. This enables an appropriate evaluation of the temperature effect.

The boiling point curve of the extracts presented in Figure 5–22 shows that at a constant pressure of 8 MPa with a constant overall propane concentration of 0.4 weight fraction, the weight fraction of distilled raw bitumen and that of extract at the temperature of 50°C is much lower than the extract produced at 100°C. Indeed, the extract produced at the temperature of 50°C is substantially similar to the raw bitumen due the combined

effects of low temperature, high pressure, and low overall propane concentration. Increasing the temperature, however, results in an extract that contains lower boiling point components. A comparison shows that the weight fraction of distilled raw bitumen is 0.813 that is lower than those of two extracts, 0.825 and 0.887 at the temperatures of (50 and 100)°C, respectively. This also indicates that the decrease in the temperature enhances the extraction of undesirable and heavy constituents into the solvent-enriched phase resulting to a lower fraction of distilled sample.

A similar behaviour at a constant pressure of 8 MPa with a constant overall propane concentration of 0.8 weight fraction was obtained. The extract produced at the temperature of 50°C is consistently heavier than the one produced at the temperature of 100°C. The raw bitumen sample is heavier than two extracts and this is not similar to the results obtained at an overall propane concentration of 0.4 weight fraction in which the end points of the curve for the raw bitumen and that of extract at the temperature of 50°C was identical (a larger difference in the boiling curves of bitumen and two extracts was observed at the overall propane concentration of 0.8 weight fraction). Increasing the temperature results in an extract that contains lower boiling point components. A comparison shows that the weight fraction of distilled raw bitumen is 0.813 that is lower than those of two extracts, 0.932 and 0.994, produced at the temperatures of 50 and 100°C, respectively.

The impact of temperature on the component distribution of extracts and residues is presented in Figures 5–29 and 5–30. In these figures, the component distribution of raw bitumen is also plotted. As depicted in Figure 5–29, the extract produced at the temperature of 100°C is composed of higher fraction of light components than the one produced at the temperature of 50°C. This clearly shows the extraction of heavier components at low temperatures (e.g. 50°C) in which the extracted phase contains heavier hydrocarbon components resulting in a lower fraction of light components compared to the temperature of 100°C. In fact, at low temperatures, the system behaves similar to the liquid-liquid extraction and as the temperature increases, the behaviour of

system is changed into the vapour-liquid extraction. It is worth to mention that the component distribution in a higher overall propane concentration shows a larger difference in the fraction of components in the samples compared to the overall propane concentration of 0.4 weight fraction. This might be because of the impact of the overall propane concentration that changes the partitioning of the components.

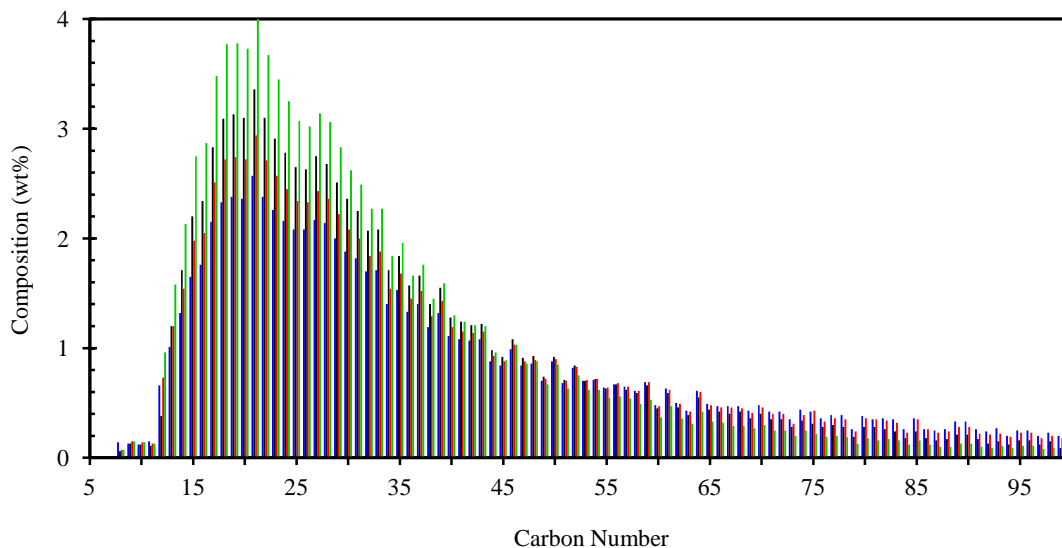


Figure 5–29: Compositional analysis (component weight percent) for extracts taken from liquid-liquid equilibrium of Surmont bitumen / propane mixtures at a constant pressure of 8 MPa and at different temperatures and overall propane concentrations; red, 100°C and overall propane concentration of 0.4 weight fraction; green, 100°C and overall propane concentration of 0.8 weight fraction; blue, 50°C and overall propane concentration of 0.4 weight fraction; black, 50°C and overall propane concentration of 0.8 weight fraction.

Figure 5–30 illustrates the component distribution of the residues produced at two temperatures, (50 and 100)°C, and at a constant pressure of 8 MPa with constant overall propane concentrations of 0.4 and 0.8 weight fractions. From the figure, it can clearly be observed that the residues have the lower weight fraction of light components compared to raw bitumen. It is worth to mentioned that the fraction of components with carbon number less than 55 in raw bitumen is larger than two residues, whereas the corresponding values for carbon number bigger than 55 is greater in two residues. A comparison of two residues indicates that the residue produced at the temperature of 50°C is composed of much heavier components than the one produced at the temperature

of 100°C. This shows that the extracted phase (the solvent-enriched phase) becomes heavier with decreasing the temperature and consequently, an equilibrium phase (the asphaltene-enriched phase) with a larger fraction of the heavy constituents is remained.

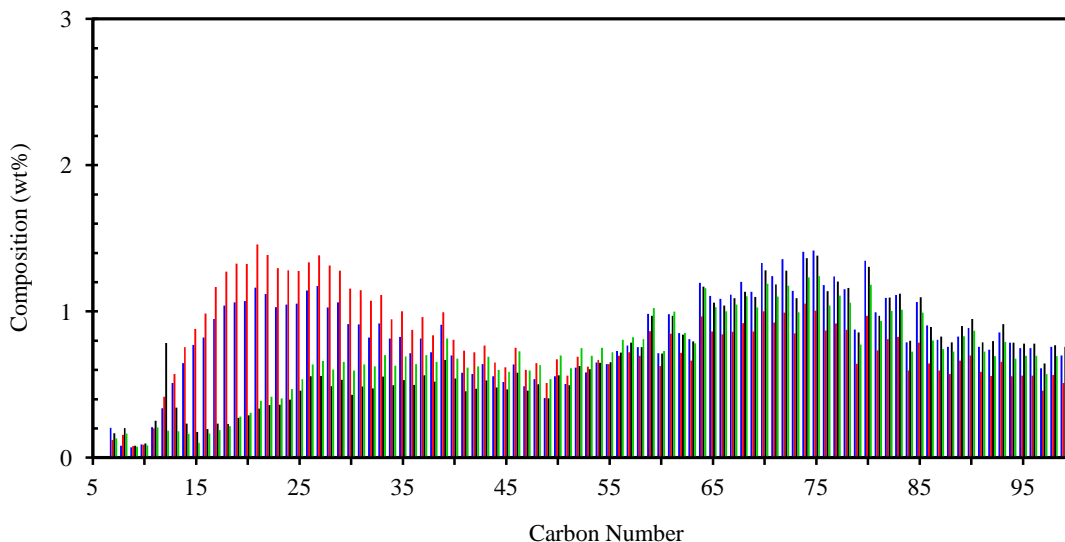


Figure 5–30: Compositional analysis (component weight percent) for residues taken from liquid-liquid equilibrium of Surmont bitumen / propane mixtures at a constant pressure of 8 MPa and at different temperatures and overall propane concentrations; red, 100°C and overall propane concentration of 0.4 weight fraction; green, 100°C and overall propane concentration of 0.8 weight fraction; blue, 50°C and overall propane concentration of 0.4 weight fraction; black, 50°C and overall propane concentration of 0.8 weight fraction.

A comparison of extracts based on cumulative carbon number (Figure 5–27) shows that the end point of the curve for the extract produced at the temperature of 50°C with a constant overall propane concentration of 0.4 weight fraction is close to that of raw bitumen and both are lower than that of 100°C. Although the end points of the curve for the extract produced at the temperature of 50°C and raw bitumen are close, the extract contains much higher content of light components compared to the raw bitumen. This is clearly noticeable in the cumulative carbon number range of C_{20} - C_{80} . At the same carbon number, higher fraction of distilled components is obtained for the extract produced at 50°C compared to raw bitumen. The comparison of the cumulative carbon number of two extracts indicates that the temperature change the composition of solvent-enriched phase toward lighter components. The weight fraction of un-distilled components (C_{100+}) in two

extracts produced at the temperatures of (50 and 100)°C and in raw bitumen are 0.175, 0.114, and 0.187, respectively. Figure 5–28 displays the cumulative carbon number of residues and raw bitumen. The end point of the curve for the residues is lower than that of raw bitumen. An unexpected behaviour for the cumulative carbon number is observed at the temperature of 50°C. The residue produced at the temperature of 50°C, which is depleted from lighter components, shows a lower weight fraction of un-distilled components (C_{100+}), 0.210, compared to its corresponding value, 0.242, at the temperature of 100°C. It is expected from the results that the weight fraction of un-distilled components in the residue produced at the temperature of 50°C would be higher than its corresponding value at the temperature of 100°C. This behaviour might be due to the extraction of hydrocarbon components in the range (C_{20} to C_{80}) into the solvent-enriched phase and the precipitation of heavy constituents such as asphaltene into the asphaltene-enriched phase.

Considering a higher overall propane concentration (0.8 weight fraction), the end point of the curve for the extract produced at the temperature of 100°C is higher than the one produced at the temperature of 50°C and that of raw bitumen (Figure 5–27). The extract produced at the temperature of 100°C is completely distilled whereas a large fraction of bitumen and the extract produced at the temperature of 50°C is remained as un-distillable. This reveals that the solvent-enriched phase at the temperature of 100°C contains much higher content of light components compared to the solvent-enriched phase at the temperature of 50°C. The weight fraction of un-distilled components (C_{100+}) in two extracts at (50 and 100)°C and in raw bitumen are 0.069, 0.006, and 0.187, respectively. The cumulative carbon number of residues presented in Figure 5–28 does not show any substantial variation. As expected, the end point of the curve for the residues is lower than that of raw bitumen. The weight fraction of un-distilled components (C_{100+}) in two residues produced at the temperatures of (50 and 100)°C and in raw bitumen are 0.351, 0.349, and 0.187, respectively.

5.4.3.3. Effect of Overall Propane Concentration

The precipitation of asphaltene from the bitumen using the light hydrocarbon solvents is mainly due to the solubility of asphaltene fraction (Mannistu et al. 1997). Pentane precipitates the asphaltene from the bitumen and it is expected that the lighter hydrocarbon solvents extract the oil that is free from the asphaltene. Depending on the hydrocarbon solvent, other fractions of bitumen such as resin can also be precipitated from the bitumen. The precipitation and separation of heavy constituents from the bitumen is directly affected by the concentration of solvent. That is, the extent of precipitation is greater at higher solvent concentrations. The impact of change in the overall propane concentration on the physical properties of two equilibrium liquid phases and the extraction yield was explained in Sections 5.4.1 and 5.4.2. As it is expected on the basis of asphaltene precipitation using pentane or heptanes, the yield of asphaltene precipitation increases with the dilution of bitumen with excess pentane or heptane. However, it is not a true statement for the extent of precipitation using propane.

In this section, the compositional analysis results for the extracts and residues produced at different overall propane concentrations are presented. The analysis was conducted at two different cases: at a constant temperature of 100°C and at a constant pressure of 8 MPa and at a constant temperature of 50°C and at a constant pressure of 8 MPa. This enables an appropriate evaluation of solvent concentration effect.

Figure 5–22 demonstrates the boiling point curve of the extracts produced at two overall propane concentrations, (0.4 and 0.8) weight fractions, at a constant pressure (8 MPa), and a constant temperature (50 or 100°C). The initial boiling points for the samples are close to each other. However, the weight fraction of distilled raw bitumen and that of extracts are different. The raw bitumen is much heavier than the two extracts. The extract produced at an overall propane concentration of 0.4 weight fraction is substantially heavier than the extract produced at an overall propane concentration of 0.8 weight fraction. This is due to the nature of propane that precipitates undesirable

constitutes from the bitumen resulting in an extract with lower boiling point components. A comparison shows that the weight fraction of distilled raw bitumen is 0.813 that is lower than those of two extracts (produced at 100°C and 8 MPa), 0.887 and 0.994 at (0.4 and 0.8) weight fractions of propane, respectively. This also indicates that the volume of solvent in excess enhances the precipitation of undesirable and heavy constituents such as asphaltene from the solvent-enriched phase.

Comparing the results obtained at the temperature of 50°C with those explained for 100°C, it can be concluded that the decrease in the temperature enhances the precipitation of asphaltene molecules from the bitumen. A comparison shows that the weight fraction of distilled raw bitumen is 0.813 that is lower than those of two extracts, 0.825 and 0.932 at (0.4 and 0.8) overall propane concentrations, respectively. This also indicates that the volume of solvent in excess enhances the precipitation of undesirable and heavy constituents such as asphaltene from the solvent-enriched phase.

The impact of overall propane concentration on the component distribution of extracts and residues is also presented in Figures 5–29 and 5–30. As anticipated from Figure 5–29, the extract produced at an overall propane concentration of 0.4 weight fraction is composed of lighter components than the one produced at an overall propane concentration of 0.8 weight fraction considering a constant temperature of 100°C. This clearly shows the precipitation of asphaltene fractions at higher overall propane concentrations in which the extracted phase contains low boiling point hydrocarbons. At the temperature of 50°C, the extract produced at a high propane concentration (0.8 weight fraction) is composed of higher fraction of light components than the one produced at a low propane concentration (0.4 weight fraction). This is evidence that the separation of heavier components occurs at higher propane concentrations (e.g. 0.8 weight fraction). Thus, the extracted phase (the solvent-enriched phase) contains lighter hydrocarbon components compared to an overall propane concentration of 0.4 weight fraction. A large increase in the overall propane concentration likely precipitates much heavier components (e.g. C₅₅₊) and leads to an extract free of asphaltene molecules.

A similar comparison on the component distribution of residues produced at the temperature of 100°C indicates that the distribution in the residues is completely different (Figure 5–30). At an overall propane concentration of 0.4 weight fraction, the light hydrocarbon components ($<C_{50}$) are still presents in the residue and its distribution is somehow similar to that of raw bitumen. However, by increasing the overall propane concentration to 0.8 weight fraction, the residue is depleted from the light hydrocarbon components ($<C_{50}$) and its distribution is substantially changed. It can be concluded that the excess volume of propane forces the heavy constitutes such as asphaltene to precipitate into the asphaltene-enriched phase and consequently attracts the light hydrocarbon components into the solvent-enriched phase. Thus, the overall propane concentration determines the extend of complete separation of components within the phases. The impact of overall propane concentration on the component distribution of residues produced at the temperature of 50°C is somehow similar to 100°C.

Figures 5–27 and 5–28 present a comparison of extracts and residues based on cumulative carbon number in terms of variation in concentration. The end point of the curve for the extract produced at an overall propane concentration of 0.8 weight fraction is higher than the one produced at an overall propane concentration of 0.4 weight fraction at the temperature of 100°C and both are greater than that of raw bitumen. The comparison of the cumulative carbon number of two extracts indicates that the excess volume of solvent provides a solvent-enriched phase with lighter components free of heavy constitutes. The weight fraction of un-distilled components (C_{100+}) in two extracts at an overall propane concentrations of 0.4 and 0.8 weight fractions and in raw bitumen are 0.114, 0.006, and 0.187, respectively.

An examination of the cumulative carbon number of residues presented in Figure 5–28 confirms the direct impact of overall propane concentration on the distribution of components in residues. As expected, the end point of the curve for the residues is lower than that of raw bitumen. However, two residues reveal a large difference in the end points of the curve. This verifies the existence of heavy constitutes and lack of light

components in the residue produced at an overall propane concentration of 0.8 weight fraction. The weight fraction of un-distilled components (C_{100+}) in two residues at the overall propane concentration of (0.4 and 0.8) weight fractions and in raw bitumen are 0.242, 0.349, and 0.187, respectively.

The above-noted trend was also observed at the temperature of 50°C from a comparison of cumulative carbon number for the raw bitumen and the extracts. The weight fraction of un-distilled components (C_{100+}) in two extracts produced at (0.4 and 0.8) weight fractions of overall propane concentration and in raw bitumen are 0.175, 0.069, and 0.187, respectively. As the overall propane concentration increases, the weight fraction of un-distilled components (C_{100+}) in the extracts reduces. Figure 5–28 also illustrates the cumulative carbon number of residues produced at the temperature of 50°C which confirms the direct impact of overall propane concentration on the distribution of components in the asphaltene-enriched phases. As expected, the end point of the curve for the raw bitumen is higher than that of residues. However, two residues reveal a large difference in the end points of the curve. The weight fraction of un-distilled components (C_{100+}) in two residues produced at the overall propane concentration of (0.4 and 0.8) weight fractions and in raw bitumen are 0.210, 0.351, and 0.187, respectively. A comparison of the fraction of un-distilled components in two residues and their corresponding value for the extracts indicates that at higher propane concentrations, the solvent-enriched phase extracts low boiling point hydrocarbons ($C_{100+} = 0.069$) and consequently, its respective asphaltene-enriched phase contains much greater high boiling point hydrocarbons ($C_{100+} = 0.351$). At low propane concentrations (e.g. 0.4 weight fraction), however, the solvent-enriched phase contains a wide range of hydrocarbons ($C_{100+} = 0.175$) and consequently, its respective asphaltene-enriched phase is also composed of all hydrocarbons ($C_{100+} = 0.210$).

5.4.4. SARA Analysis of Extracts and Residues

The SARA analysis was performed on the extracts and residues produced at different operating conditions. Table 5–9 summarizes the SARA analysis results for extracts and residues. The weight percentage of the four fractions for the residues was calculated from the equilibrium information and SARA analysis of the extracts.

Table 5–9: SARA analysis (in weight percent) of extracts and residues taken from liquid-liquid equilibrium study of Surmont bitumen / propane mixtures; P , pressure; T , temperature; w , overall propane concentration in weight fraction.

T (°C)	P (MPa)	10^2w	Phase	Saturates	Aromatics	Resins	Asphaltenes
50.3	2.096	40	L ₁	17.25	56.52	25.17	1.06
			L ₂	6.62	21.49	49.38	22.52
50.3	2.054	80	L ₁	27.01	58.05	14.94	0.00
			L ₂	0.00	19.45	58.03	22.51
50.3	8.018	40	L ₁	13.15	51.97	26.65	8.23
			L ₂	10.54	17.12	55.61	16.73
50.3	8.052	60	L ₁	23.58	52.86	23.57	0.00
			L ₂	0.00	24.67	51.29	24.03
50.2	7.969	80	L ₁	22.09	67.03	10.88	0.00
			L ₂	0.00	2.79	71.04	26.17
100.1	6.149	80	L ₁	33.40	60.99	5.61	0.00
			L ₂	0.00	23.62	57.60	18.78
100.1	8.066	40	L ₁	21.57	47.94	29.96	0.53
			L ₂	5.34	34.23	41.42	19.01
100.0	7.976	80	L ₁	31.32	55.93	12.75	0.00
			L ₂	0.00	24.79	55.12	20.10

The results show that the extracts mostly composed of the saturates with a considerable amount of aromatics. No asphaltene is detected in the samples and the resin content is varied depending on the operating conditions. The asphaltene fraction of bitumen is less soluble in the light hydrocarbon components such as ethane, propane, and butane. Pentane precipitates the asphaltene from the bitumen and it is expected that the lighter hydrocarbon solvents extract the oil that is free from the asphaltene. The resin content of extracts and comparison with that of bitumen confirms that the samples have

also lower resin contents compared to the bitumen. The pressure, temperature, and overall propane concentrations affects the distribution of fractions in extracts and residues.

Figures 5–31 and 5–32 illustrate a comparison of the SARA fractions in raw bitumen and those of extracts and residues produced at two different operating conditions. Figure 5–31 shows the SARA compositional analysis for extract and residue produced at the temperature of 50°C and the pressure of 2 MPa with an overall propane concentration of 0.4 weight fraction. Figure 5–32 demonstrates the same results for the temperature of 100°C and the pressure of 8 MPa with the same overall propane concentration of 0.4 weight fraction.

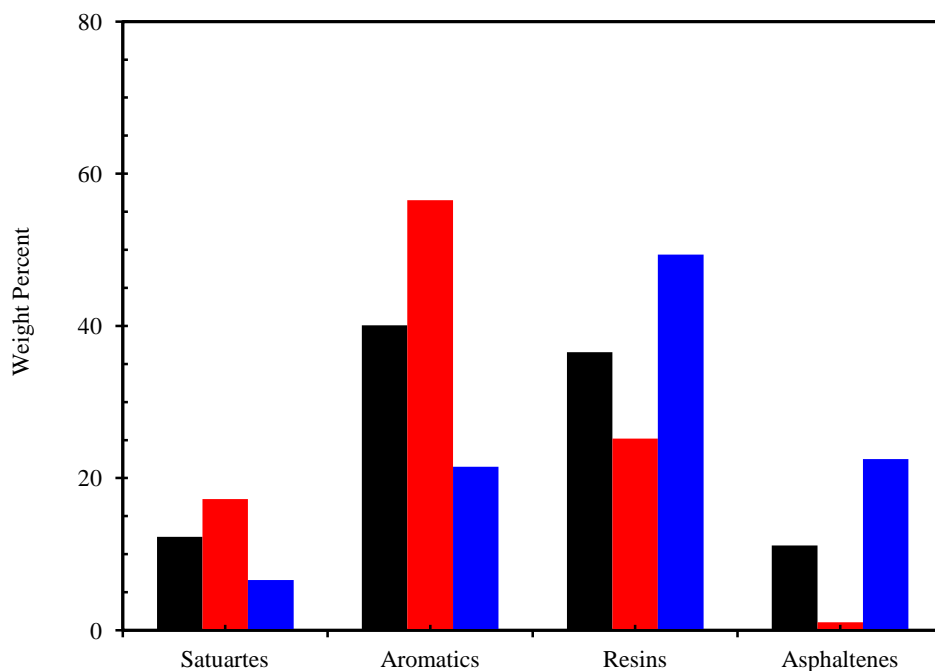


Figure 5–31: SARA compositional analysis of raw bitumen (black) and two flashed-off phase samples (extract, red, and residue, blue) taken from liquid-liquid equilibrium of Surmont bitumen / propane mixtures at 50°C and 2 MPa with an overall propane concentration of 0.4 weight fraction.

As depicted in the figures, the saturate and aromatic contents of the residues are lower than the saturate and aromatic contents of raw bitumen while the extracts mostly composed of the saturate with a considerable amount of aromatic. No asphaltene is detected in the extracts. The resin content of the extracts and comparison with that of

bitumen confirms that the samples have also lower resin contents compared to the bitumen. The asphaltene fraction of bitumen is less soluble in propane. Therefore, the resin and asphaltene contents of residues are much higher than those of the extracts and those of raw bitumen. This indicates that propane substantially precipitates the resin and asphaltene content of the bitumen and the contribution of resins to the solvent-enriched phases is less than that of saturate and aromatic fractions.

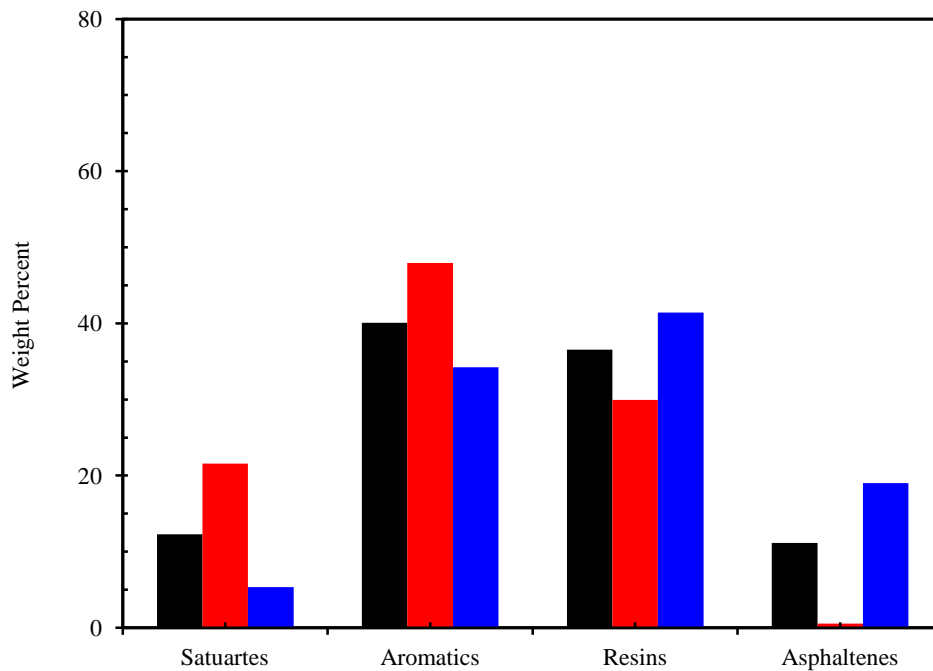


Figure 5-32: SARA compositional analysis of raw bitumen (black) and two flashed-off phase samples (extract, red, and residue, blue) taken from liquid-liquid equilibrium of Surmont bitumen / propane mixtures at 100°C and 8 MPa with an overall propane concentration of 0.4 weight fraction.

5.4.4.1. Effect of Pressure

The increase in the pressure at a constant temperature and at a constant overall propane concentration results in an extract with higher resin fraction and a residue with lower saturate and aromatic contents. Figures 5-33, 5-35, and 5-37 shows the impact of pressure on the variation of different fractions in the extracts and Figures 5-34, 5-36, and 5-38 demonstrates the same effect on the variation of different fractions in the residues.

As anticipated from Figures 5–35 and 5–36, at the temperature of 50°C, the impact of pressure on the distribution of fractions within the phase is highly depend on the overall propane concentrations. Figure 5–35 shows that an increase in the asphaltene and resin content of the extracts with the pressure and Figure 5–36 illustrates the decrease in the corresponding values in the residues. This behaviour is expected because the increase in the pressure enhances the extraction of high boiling point components into the solvent-enriched phase.

The extend of asphaltene precipitation is found to decrease with an increase in the pressure for pentane and heptane solvents (Akbarzadeh et al. 2005). The results presented here is in agreement with the behaviour observed for pentane and heptanes. The asphaltene content of liquid phase increases with the pressure and this confirmed the lower extend of precipitation at higher pressures.

On the other hand, at high overall propane concentrations (e.g. 0.8 weight fraction), Figure 5–37, the pressure results in the depletion of saturates and aromatic contents of the residues and consequently an increase in the aromatic content of the extracts. This increase occurs because of higher solubility of bitumen components in propane at higher pressures and due to the fact that the saturate fraction of bitumen is preferentially extracted. Hence, the aromatic fraction of bitumen is extracted more with the increase in the pressure and the saturate content of the solvent-enriched phase reduces. Thus, it can be concluded that the pressure enhances the extraction of saturates and aromatic fractions into the solvent-enriched phase at higher propane concentrations while it increases the extraction of resin and asphaltene content at lower propane concentrations. The SARA analysis results show that propane is more selective towards the saturate and aromatic fractions of the bitumen.

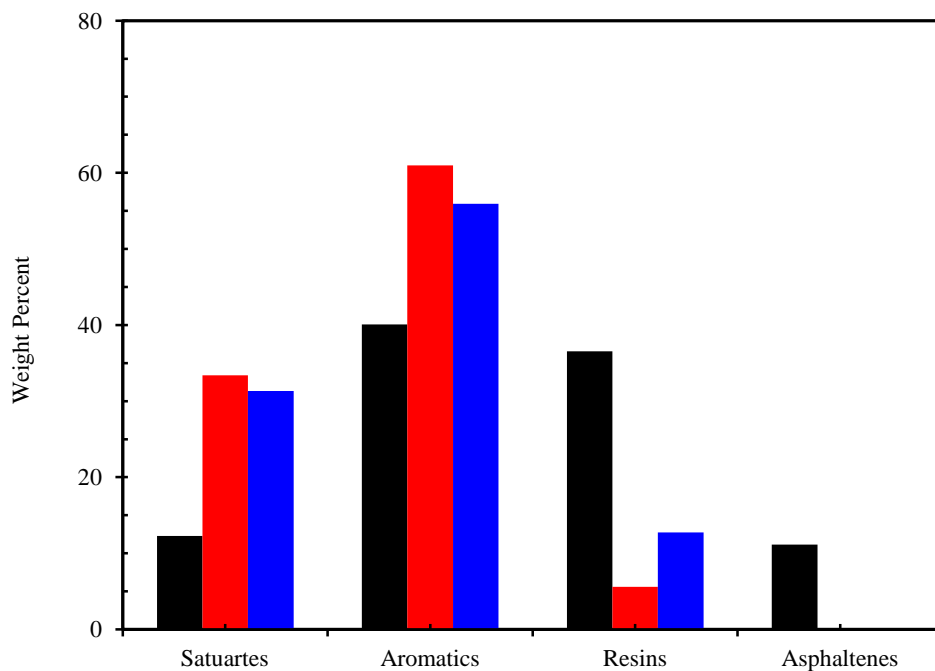


Figure 5-33: SARA compositional analysis of raw bitumen (black) and two extracts taken from liquid-liquid equilibrium of Surmont bitumen / propane mixtures at different pressures and at 100°C with an overall propane concentration of 0.8 weight fraction; red, 6 MPa; blue, 8 MPa.

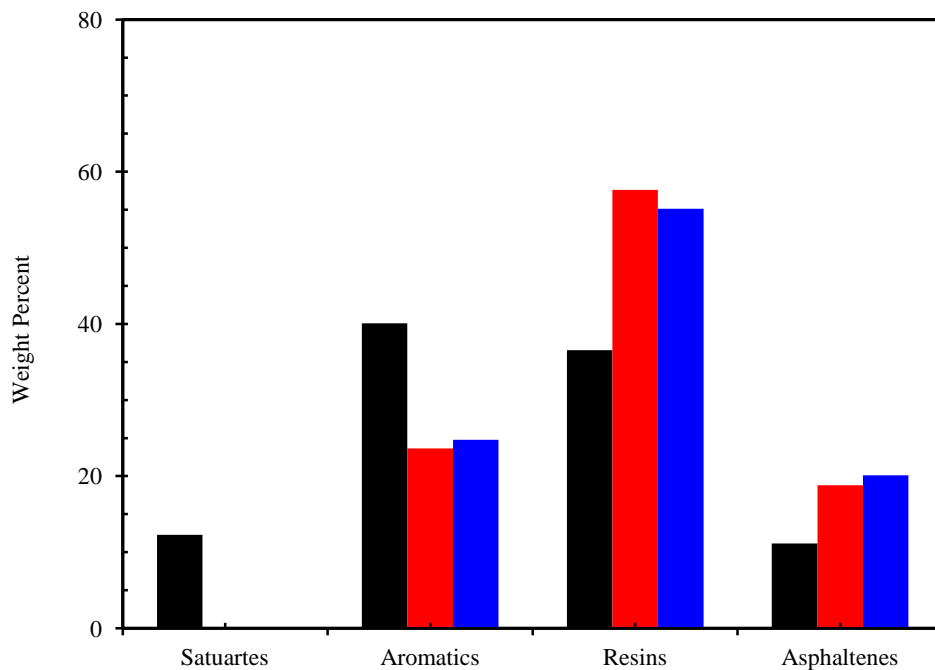


Figure 5-34: SARA compositional analysis of raw bitumen (black) and two residues taken from liquid-liquid equilibrium of Surmont bitumen / propane mixtures at different pressures and at 100°C with an overall propane concentration of 0.8 weight fraction; red, 6 MPa; blue, 8 MPa.

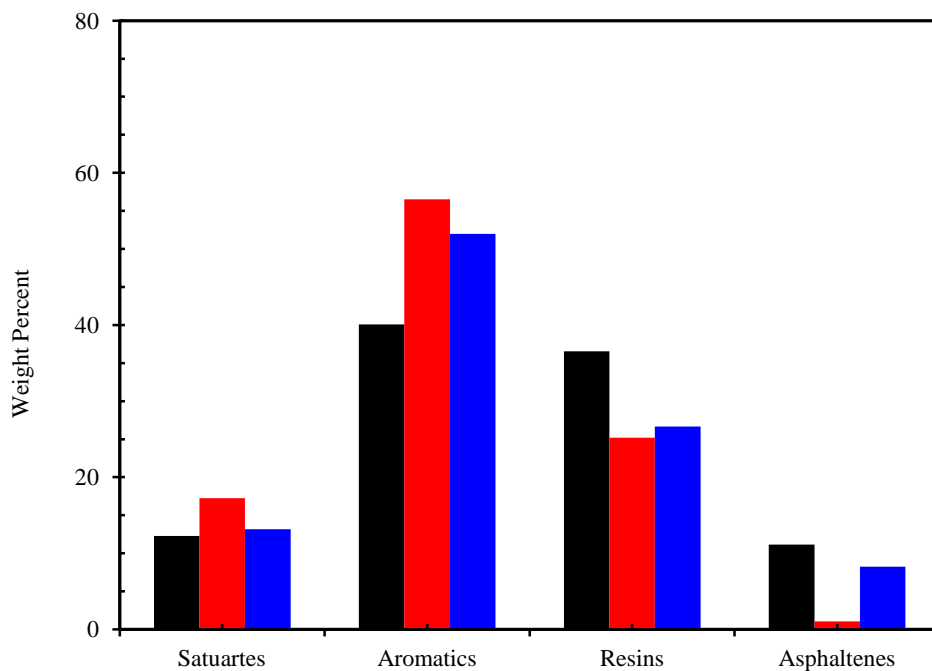


Figure 5-35: SARA compositional analysis of raw bitumen (black) and two extracts taken from liquid-liquid equilibrium of Surmont bitumen / propane mixtures at different pressures and at 50°C with an overall propane concentration of 0.4 weight fraction; red, 2 MPa; blue, 8 MPa.

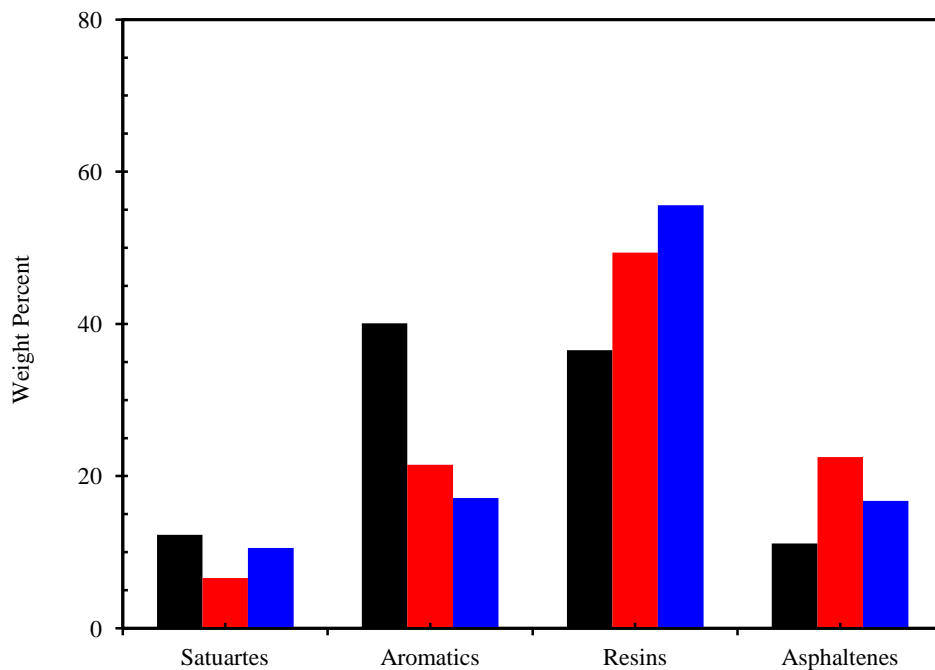


Figure 5-36: SARA compositional analysis of raw bitumen (black) and two residues taken from liquid-liquid equilibrium of Surmont bitumen / propane mixtures at different pressures and at 50°C with an overall propane concentration of 0.4 weight fraction; red, 2 MPa; blue, 8 MPa.

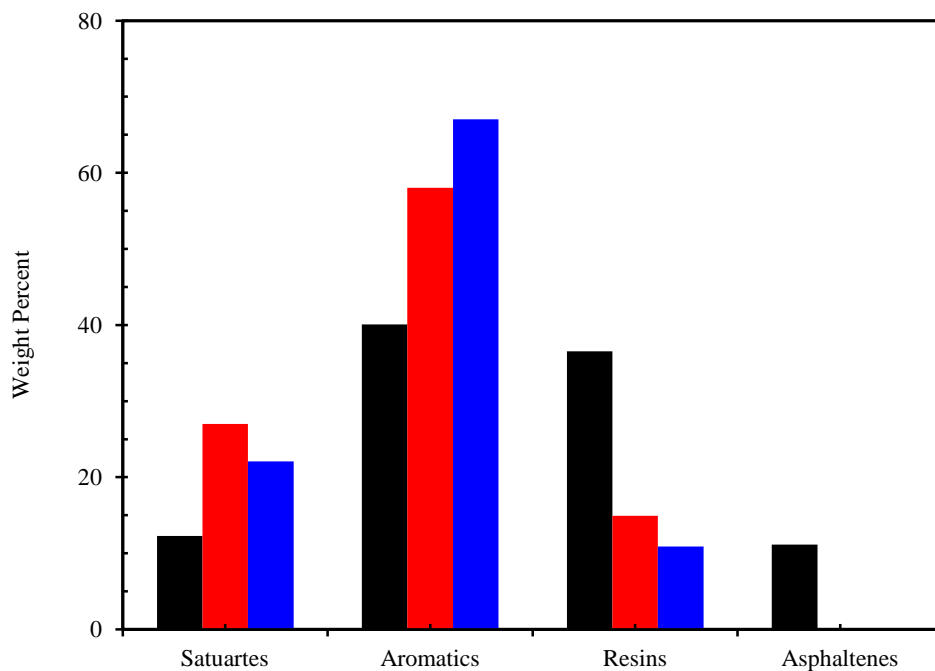


Figure 5–37: SARA compositional analysis of raw bitumen (black) and two extracts taken from liquid-liquid equilibrium of Surmont bitumen / propane mixtures at different pressures and at 50°C with an overall propane concentration of 0.8 weight fraction; red, 2 MPa; blue, 8 MPa.

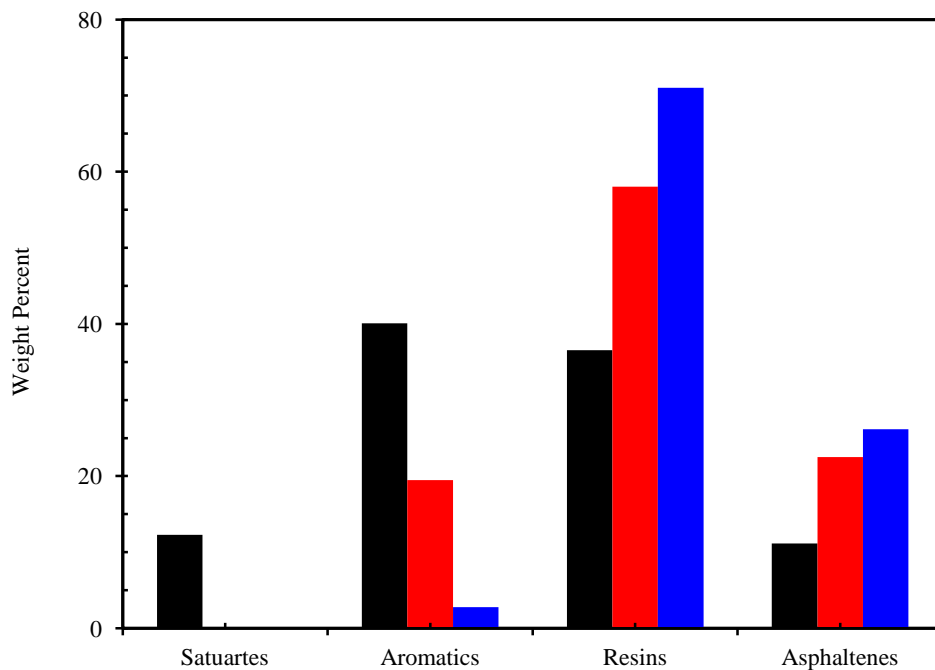


Figure 5–38: SARA compositional analysis of raw bitumen (black) and two residues taken from liquid-liquid equilibrium of Surmont bitumen / propane mixtures at different pressures and at 50°C with an overall propane concentration of 0.8 weight fraction; black, raw bitumen; red, 2 MPa; blue, 8 MPa.

5.4.4.2. Effect of Temperature

The impact of temperature on the distribution of fractions within the phases was also investigated at a constant pressure of 8 MPa and at two overall propane concentrations of (0.4 and 0.8) weight fractions. The SARA compositional analysis of the extracts and residues are presented in Figures 5–39 and 5–40 for a constant overall propane concentration of 0.4 weight fraction and in Figures 5–41 and 5–42 for a constant overall propane concentration of 0.8 weight fraction.

As depicted from Figures 5–39 and 5–40, the increase in the temperature enhances the saturates content and lowers the asphaltene fraction of extracts. In fact, at high temperatures, the solvent-enriched phase contains considerably saturates and aromatic fractions. The resin content of extracts slightly increases, and the existence of resins in the extracts is due to low overall propane concentration (e.g. 0.4 weight fraction). An examination of SARA analysis for residues presented in Figure 5–40 shows that the asphaltene and aromatic contents of the asphaltene-enriched phase rise with temperature.

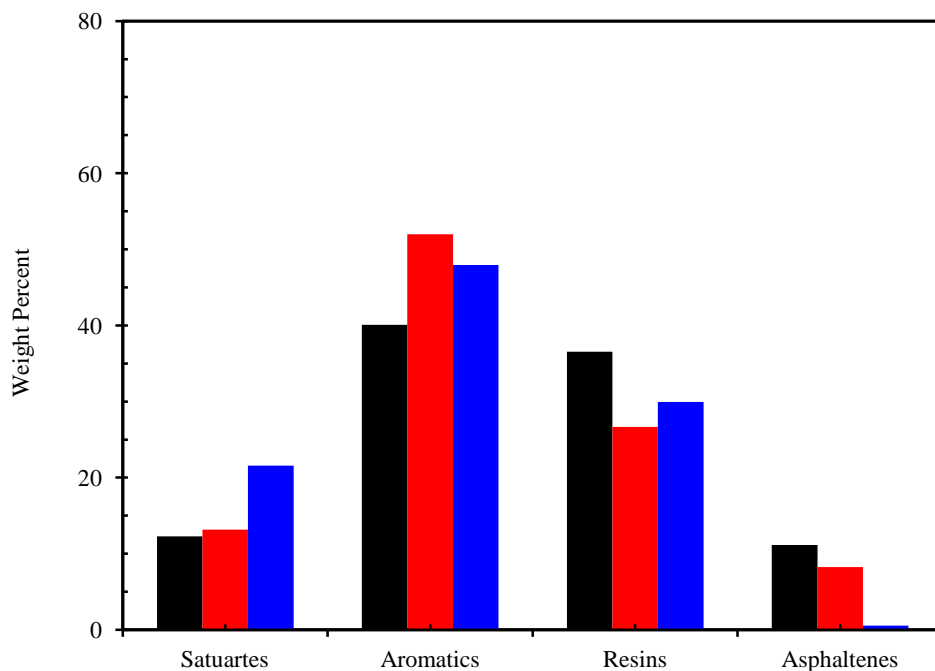


Figure 5–39: SARA compositional analysis of raw bitumen (black) and two extracts taken from liquid-liquid equilibrium of Surmont bitumen / propane mixtures at different temperatures and at 8 MPa with an overall propane concentration of 0.4 weight fraction; red, 50°C; blue, 100°C.

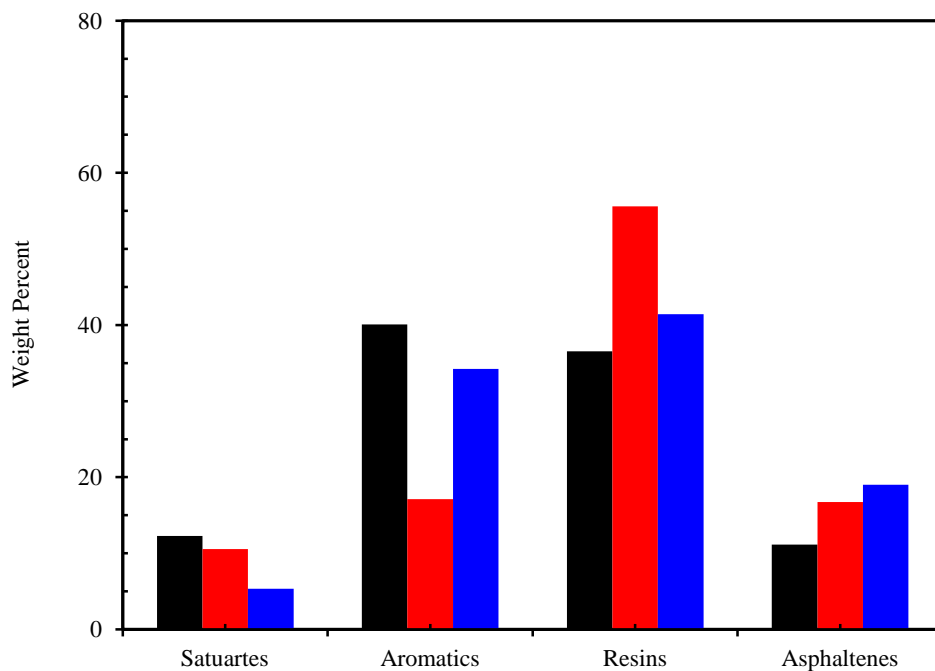


Figure 5–40: SARA compositional analysis of raw bitumen (black) and two residues taken from liquid-liquid equilibrium of Surmont bitumen / propane mixtures at different temperatures and at 8 MPa with an overall propane concentration of 0.4 weight fraction; red, 50°C; blue, 100°C.

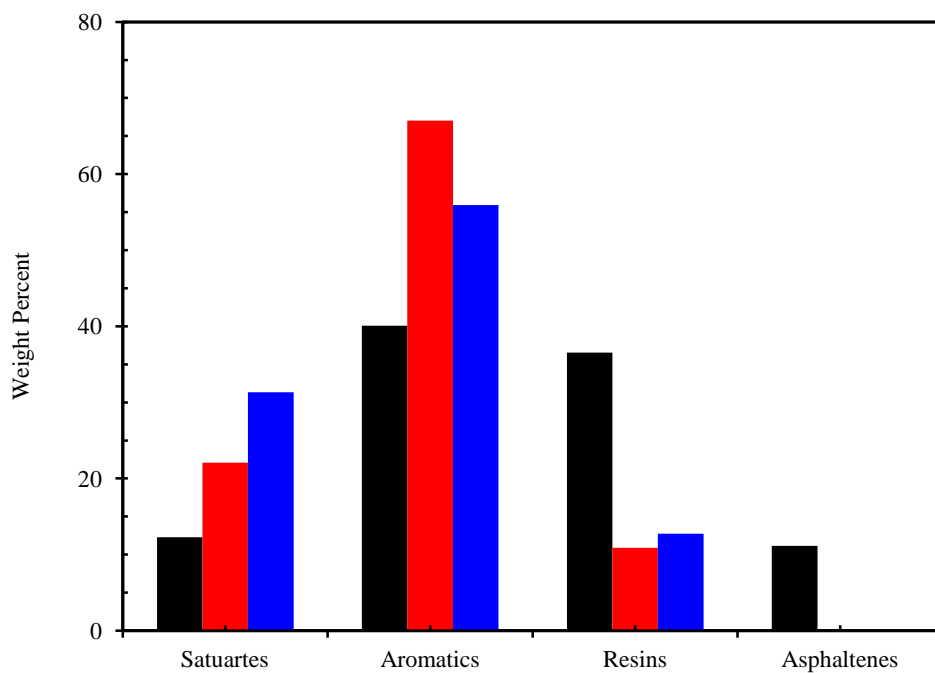


Figure 5–41: SARA compositional analysis of raw bitumen (black) and two extracts taken from liquid-liquid equilibrium of Surmont bitumen / propane mixtures at different temperatures and at 8 MPa with an overall propane concentration of 0.8 weight fraction; red, 50°C; blue, 100°C.

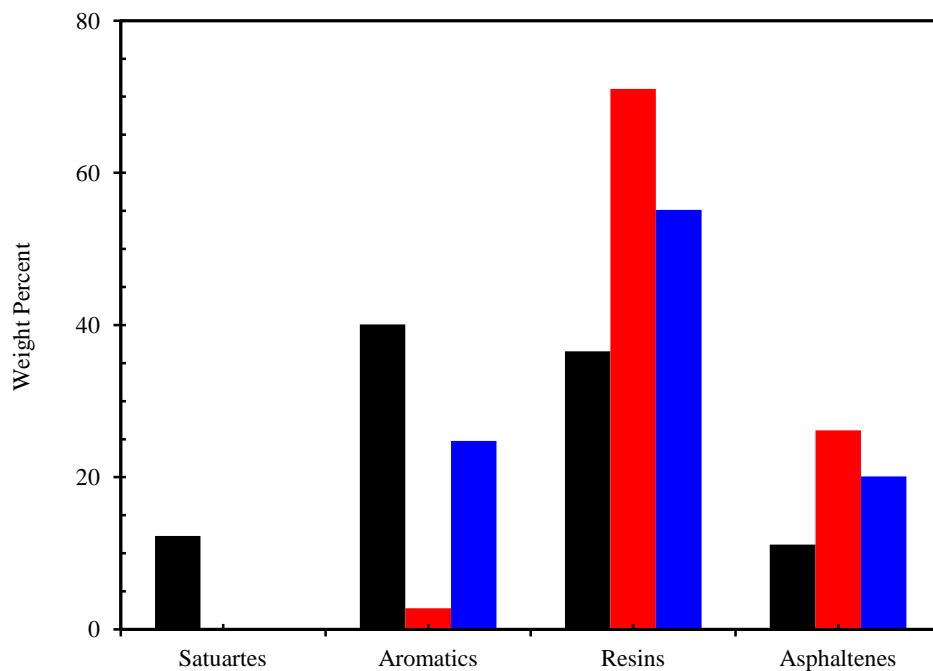


Figure 5–42: SARA compositional analysis of raw bitumen (black) and two residues taken from liquid-liquid equilibrium of Surmont bitumen / propane mixtures at different temperatures and at 8 MPa with an overall propane concentration of 0.8 weight fraction; red, 50°C; blue, 100°C.

Similar variations in the SARA fractions of flashed-off liquid samples are observed at high overall propane concentration, 0.8 weight fraction (Figures 5–41 and 5–42). In this case, the extract produced at the temperature of 50°C contains the total saturate and aromatic fractions of bitumen and it is free from asphaltene molecules. When the temperature increases to 100°C, the aromatic content of sample reduces and a slight change in its resin content is detected. The examination of SARA analysis for residues also shows that propane is more selective towards the saturate and aromatic fractions of the bitumen and as the temperature increases the aromatic content of residues increases.

5.4.4.3. Effect of Overall Propane Concentration

The excess volume of propane in the mixture enhances the precipitation of asphaltene and resin fractions. This is evidence by the comparison of the SARA fractions of the extracts presented in Figures 5–43, 5–45, and 5–47 at different overall propane concentrations. The increase in overall propane concentration increases the saturate and

aromatic contents of the extract and consequently reduces the asphaltene and resin fractions. An opposite trend in SARA fractions of residue is evidence from Figures 5–44, 5–46, and 5–48. The results obtained here is in agreement with the definition of resins as the fraction of oil insoluble in excess liquid propane at room temperature (Firoozabadi, 1999). It can also be concluded that when the resin fraction of bitumen is precipitated into the asphaltene-enriched phase, the asphaltene content of the solvent-enriched phase approaches a zero value. This is in agreement with the colloidal model proposed by Leontarities and Mansoori (1987) that is based on assumption that asphaltene particles are suspended in the oil and stabilized by resins. Swanson (1942) and Witherspoon and Munir (1958) stated that the asphaltene molecules dissolved in the maltene fraction of oil with the help of resins. Dickie and Yen (1967) suggested that resins play an important role to keep asphaltene molecules as polar compounds in the non-polar fractions of oil. Thus, the resin fraction is essential for asphaltene particles to be in mixture (Mansoori 2009).

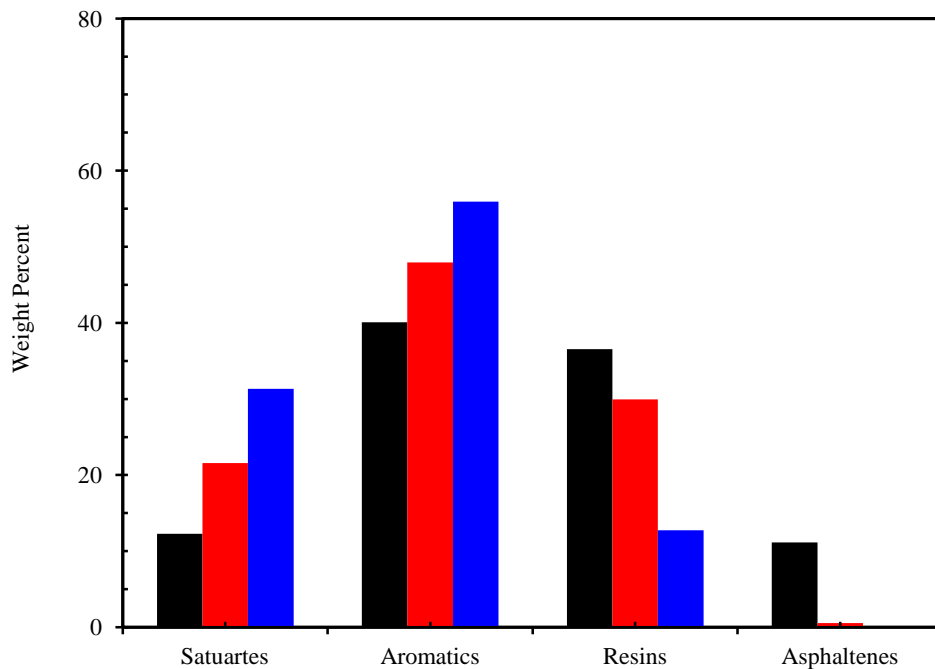


Figure 5–43: SARA compositional analysis of raw bitumen (black) and two extracts taken from liquid-liquid equilibrium of Surmont bitumen / propane mixtures with different overall propane concentrations at 100°C and 8 MPa; red, 0.4 weight fraction; blue, 0.8 weight fraction.

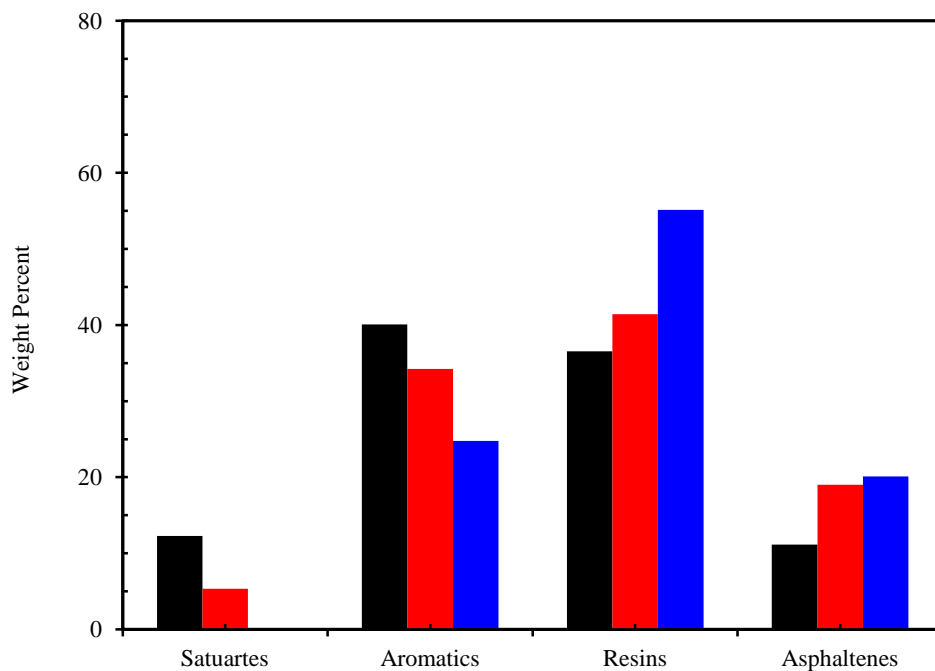


Figure 5-44: SARA compositional analysis of raw bitumen (black) and two residues taken from liquid-liquid equilibrium of Surmont bitumen / propane mixtures with different overall propane concentrations at 100°C and 8 MPa; red, 0.4 weight fraction; blue, 0.8 weight fraction.

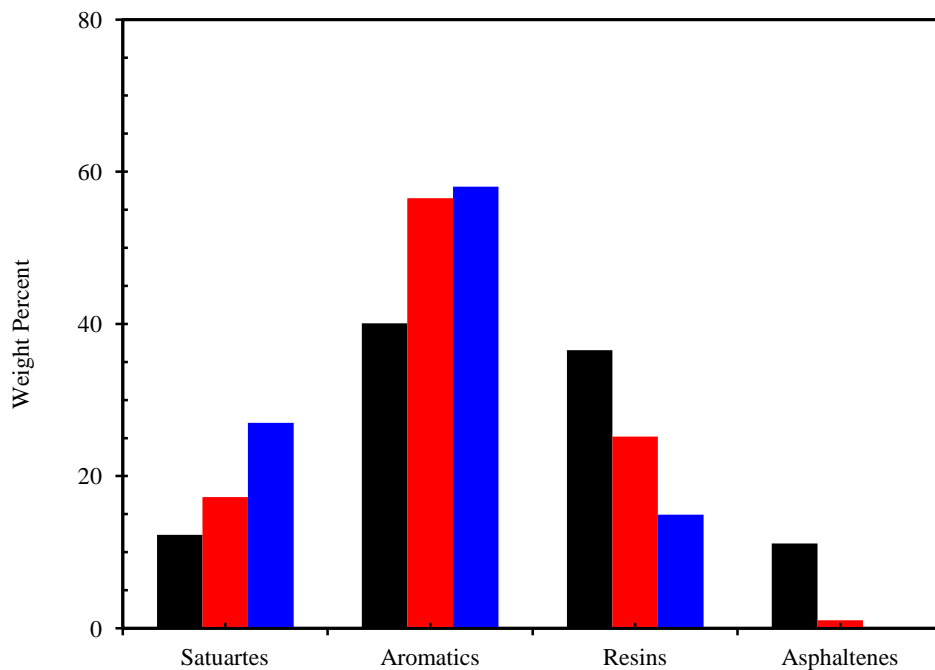


Figure 5-45: SARA compositional analysis of raw bitumen (black) and two extracts taken from liquid-liquid equilibrium of Surmont bitumen / propane mixtures with different overall propane concentrations at 50°C and 2 MPa; red, 0.4 weight fraction; blue, 0.8 weight fraction.

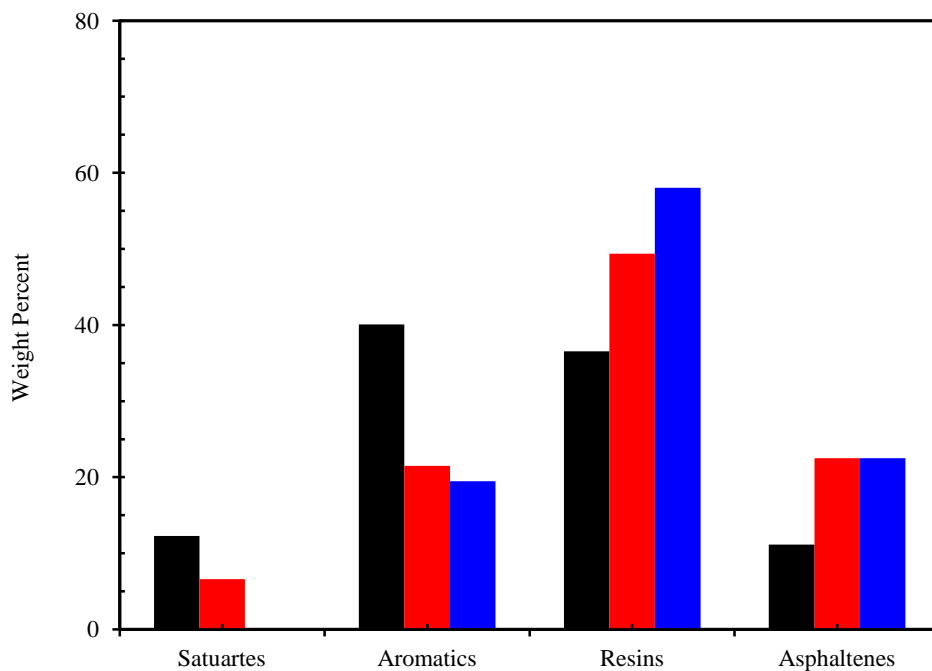


Figure 5-46: SARA compositional analysis of raw bitumen (black) and two residues taken from liquid-liquid equilibrium of Surmont bitumen / propane mixtures with different overall propane concentrations at 50°C and 2 MPa; red, 0.4 weight fraction; blue, 0.8 weight fraction.

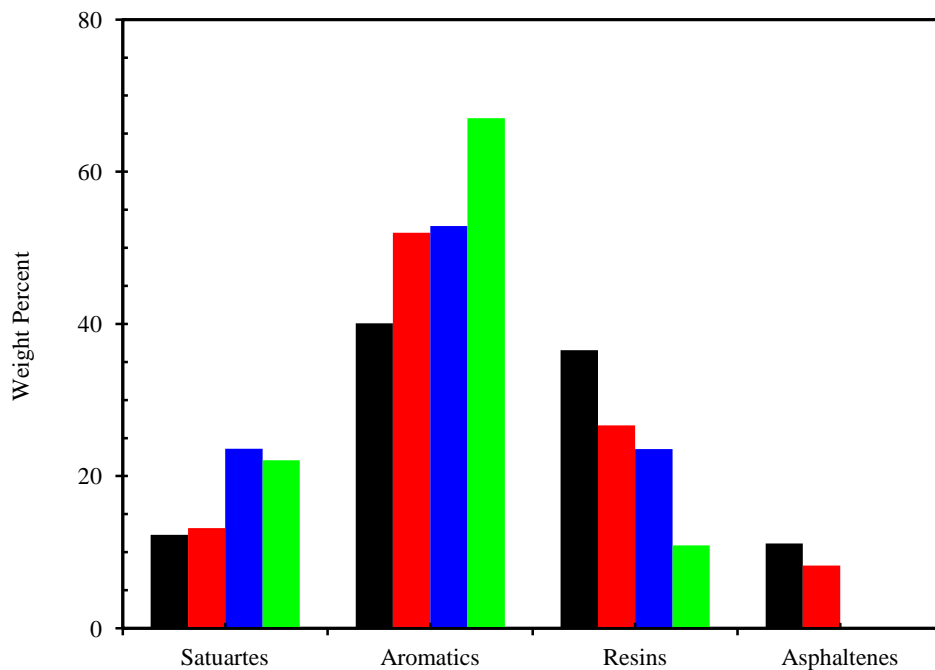


Figure 5-47: SARA compositional analysis of raw bitumen (black) and three extracts taken from liquid-liquid equilibrium of Surmont bitumen / propane mixtures with different overall propane concentrations at 50°C and 8 MPa; red, 0.4 weight fraction; blue, 0.6 weight fraction; green, 0.8 weight fraction.

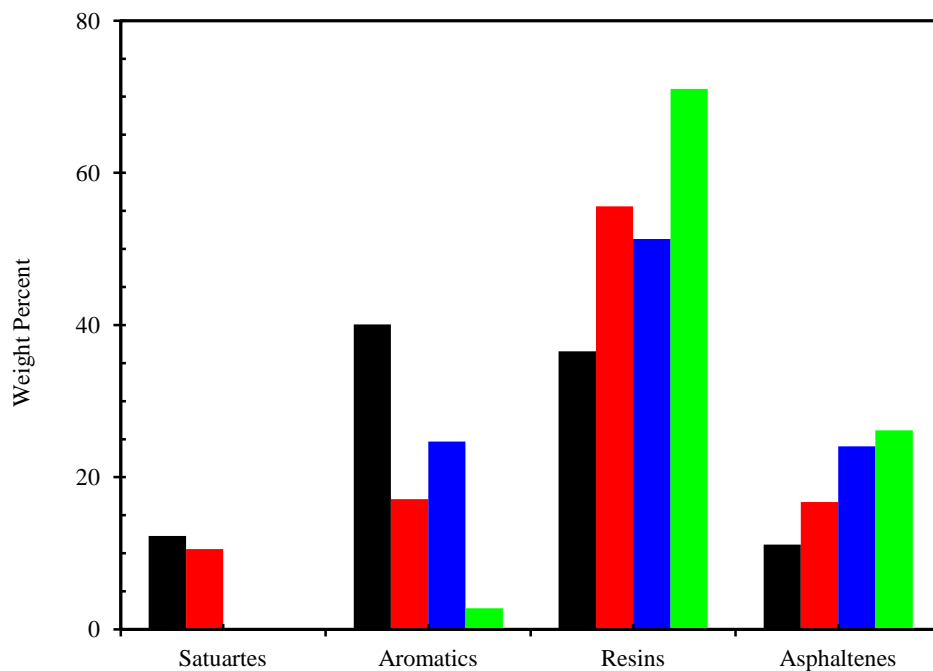


Figure 5–48: SARA compositional analysis of raw bitumen (black) and three residues taken from liquid-liquid equilibrium of Surmont bitumen / propane mixtures with different overall propane concentrations at 50°C and 8 MPa; red, 0.4 weight fraction; blue, 0.6 weight fraction; green, 0.8 weight fraction.

The analysis of the residues pointed out the presence of saturate and aromatic fractions in the asphaltene-enriched phases. However, the addition of propane as a non-polar solvent in excess amount produces a residue free from saturate and aromatic fractions (Figure 5–48). At the same time, the extracts became free from the asphaltene and resin fractions (Figure 5–47).

5.5. Phase Diagrams

In this section, the phase diagrams for bitumen/propane are drawn on the basis of the generated experimental data. Thus, the regions are defined on the basis of the experimental data; the transition zones and the regions between the experimental points may subject to further experimental analysis. The mixtures of propane and Surmont bitumen exhibit liquid-liquid phase partitioning at the temperatures of 50°C (pressure > 1.5 MPa) and 100°C (pressure > 4.5 MPa). On the basis of the experimental observations,

a qualitative pressure-temperature diagram for Surmont bitumen / propane systems is presented in Figure 5–49. The blue symbols correspond to the conducted experiments in which the vapour-liquid equilibrium exists. The red symbols are the experimental conditions which lead to liquid-liquid equilibrium and finally, the green symbols are the experimental data reported in the literature. No asphaltene precipitation was observed during the experiments, and the asphaltenes were separated as a second liquid phase in all experiments.

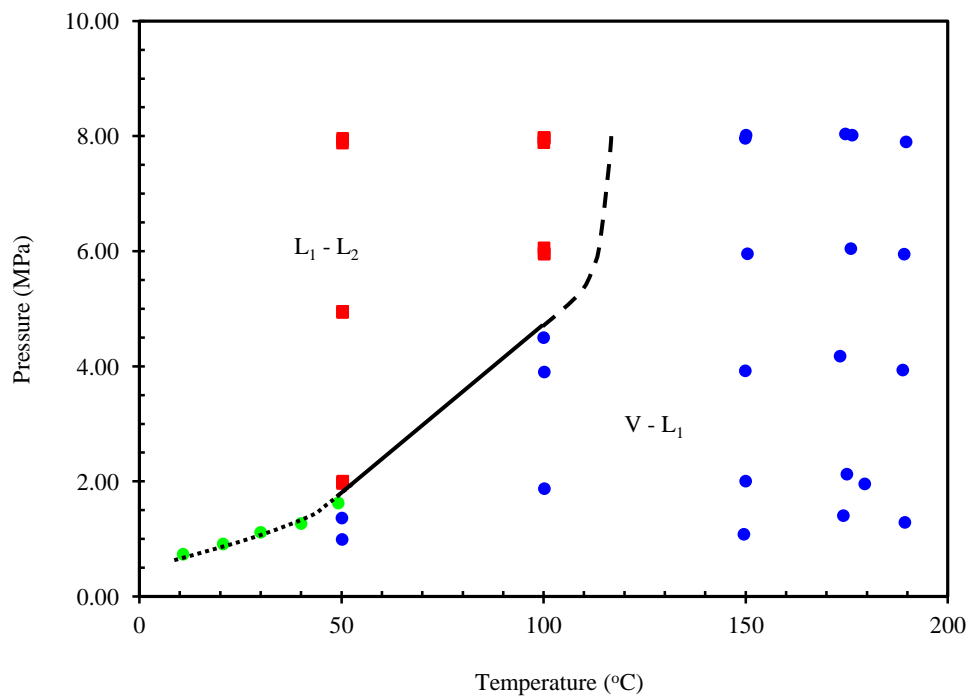


Figure 5–49: Pressure-temperature (P - T) diagram for Surmont bitumen / propane systems; ●, vapour-liquid experimental data; ●, vapour-liquid experimental data for Athabasca bitumen / propane systems taken from Badamchi-Zadeh et al. (2009a); ■, liquid-liquid experimental data.

As the figure indicates, the phase boundary between the V-L and L-L regions is indicated by a line. At lower temperatures, the L-L equilibrium occurs at lower pressures. The transition between the regions is presented by a dashed line and no experimental data confirms the three phase (vapour-liquid-liquid) region so far. The boundary between the vapour-liquid and liquid-liquid regions is clearly determined at the temperatures of (50 and 100)°C where the transition occurs at the pressures around (1.5 and 4.5) MPa,

respectively. At the temperatures higher than 100°C in which propane is at supercritical conditions, the vapour phase may contain the light hydrocarbons extracted from bitumen at high pressures (> 10 MPa).

The pressure-composition diagrams for Surmont bitumen / propane mixtures are presented in Figures 5–50 and 5–51 at constant temperatures (50 and 100°C). Three regions depending on the pressure and overall propane concentration, L_1 , L_1 - L_2 , and L_1 - V , were observed during the experiments. The experimental results show that, if two liquids are present, the less dense phase is enriched in saturates and aromatics, while the more dense phase is enriched in resins and asphaltenes. The selectivity of the component distribution at constant temperature is clearly a function of overall propane concentration and pressure.

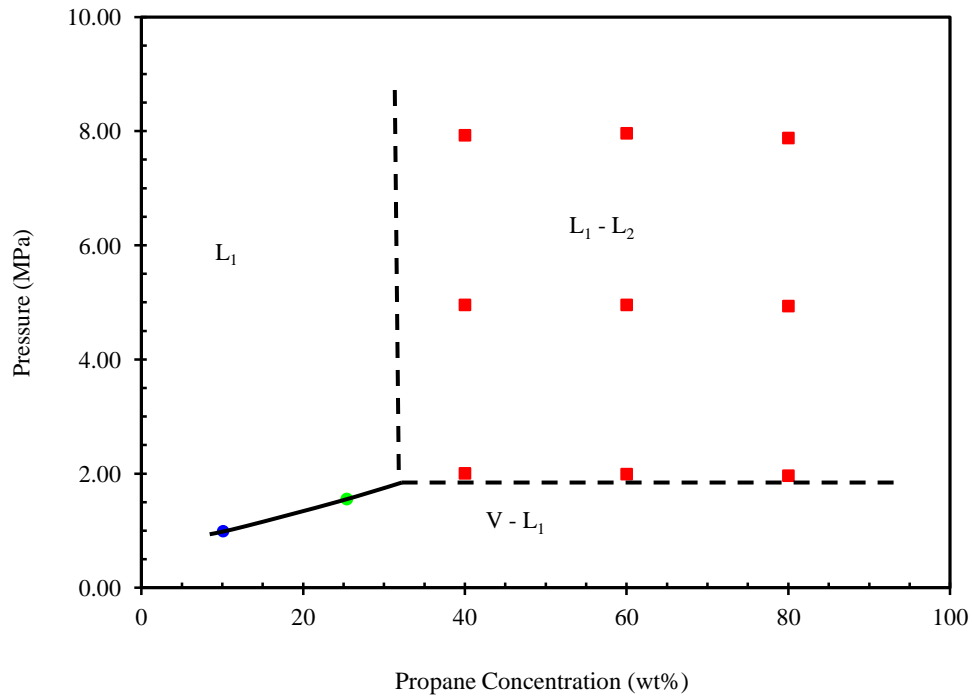


Figure 5–50: Pressure-composition (P - x) diagram for Surmont bitumen / propane systems at 50°C; ●, vapour-liquid experimental data; ●, vapour-liquid experimental data for Athabasca bitumen / propane systems taken from Badamchi-Zadeh et al. (2009a); ■, liquid-liquid experimental data.

At the temperature of 50°C, the vapour phase in the V - L_1 region is virtually pure propane and the composition of liquid phase varies with the pressure. In the L_1 - L_2 region,

as more propane is added to the mixture at this temperature, the physical properties of phases change. The pressure-composition diagram presented in Figure 5–50 indicates that at the pressures greater than about 1.5 MPa, the increase in the overall propane concentration converts the state of system from single liquid phase into L_1 - L_2 equilibrium condition. However, at the pressures less than about 1.5 MPa, the single liquid phase region changes to V - L_1 equilibrium by which the vapour phase is virtually pure propane. The dashed lines in Figure 5–50 are the qualitative transitions boundaries between the L_1 - L_2 and V - L_1 and between L_1 - L_2 and L_1 regions. The boundary between L_1 and V - L_1 regions were experimentally confirmed and thus, it is shown by solid line.

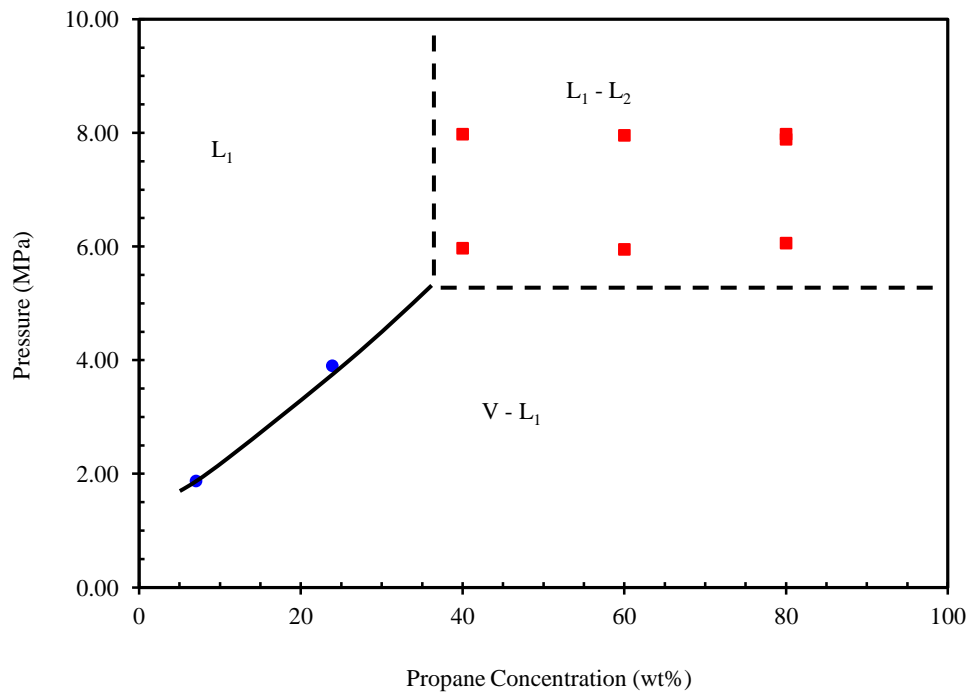


Figure 5–51: Pressure-composition (P - x) diagram for Surmont bitumen / propane systems at 100°C; ●, vapour-liquid experimental data; ■, liquid-liquid experimental data.

Similar to the temperature of 50°C, at higher temperature (i.e. 100°C), the vapour phase in the V - L_1 region is virtually pure propane and the composition of liquid phase varies with the pressure. At this temperature, the V - L_1 region occurs over wider range of pressure. At the pressures greater than about 4.5 MPa, the increase in the overall propane

concentration converts the state of system from single phase into L_1 - L_2 equilibrium condition. However, at the pressures less than about 4.5 MPa, the single phase region changes to V - L_1 equilibrium by which the vapour phase is virtually pure propane.

By combining the phase behaviour observations and the physical properties measurements at a constant overall propane concentration and at a constant temperature, a diagram for the compositions of coexisting phases versus equilibrium pressure; a diagram for the densities of coexisting phases versus equilibrium pressure were plotted. Figures 5–52 and 5–53 show the coexisting phase compositions at a constant temperature and at a constant overall propane concentration. Noted that the plots are shown for the cases where there is excess propane in the system (overall propane concentrations are 0.4 and 0.6 weight fractions). That is, no single phase region can be detected at constant temperature and pressure. The composition of propane in L_1 within V - L_1 region increases with the pressure. This behaviour is expected because the solubility of hydrocarbon gaseous in bitumen increases with the pressure. As the pressure further increases into 4.5 MPa, the V - L_1 region is still observed and the vapour phase is pure propane. However, at the pressures higher than 4.5 MPa, the vapour phase (i.e. solvent-enriched phase) composition is dramatically changes and reduces with the pressure. Here, the V - L_1 equilibrium is changed into L_1 - L_2 equilibrium condition.

In L_1 - L_2 region at the temperature of 50°C, the composition of the solvent-enriched phase (L_1) reduces with the pressure due to the extraction of light hydrocarbons into this phase. On the other hand, the composition of propane in the asphaltene-enriched phase (L_2) remains almost constant with the pressure. The slope of curve for the composition of propane in L_2 is not the same as that of V - L_1 region. That is, the composition is not increased in L_2 with pressure as in L_1 within V - L_1 region. The bitumen components in L_2 become heavier with increasing pressure, due to higher extraction of light components into L_1 at higher pressures; thus, a reduction in the concentration of propane in L_2 is expected (the heavier hydrocarbon component, the lower solubility of ethane at fixed temperature and pressure). In contrast, the solubility of propane in heavy hydrocarbons

increases with pressure. The first factor cancels out the second one and no notable change in the composition is observed.

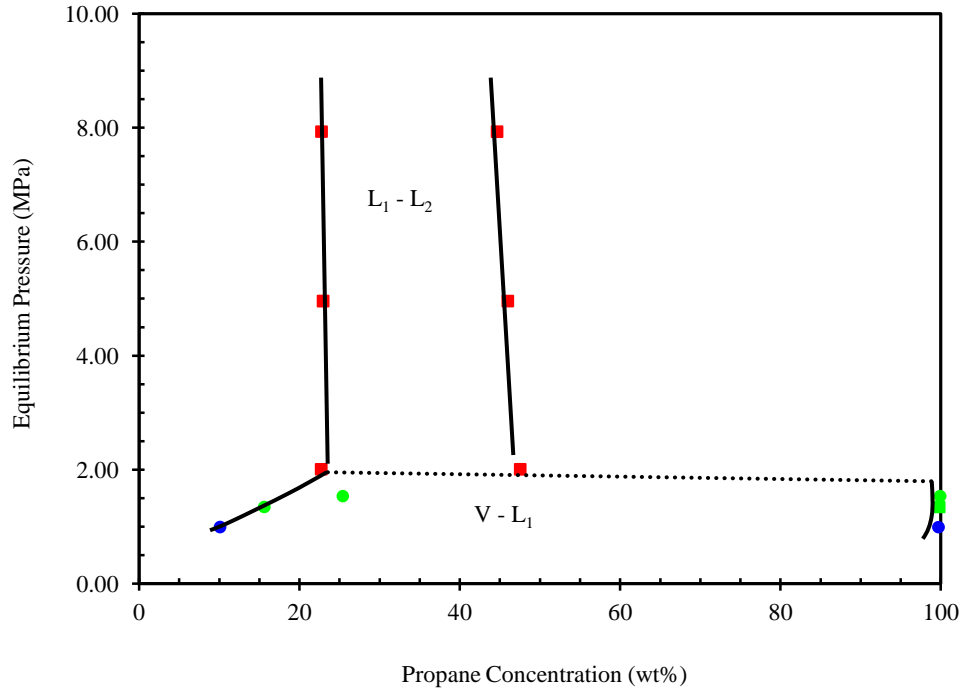


Figure 5-52: Coexisting phase compositions for Surmont bitumen /propane systems at 50°C and at a constant overall propane concentration of 0.4 weight fraction; ●, vapour-liquid experimental data; ●, vapour-liquid experimental data for propane / Athabasca bitumen systems taken from Badamchi-Zadeh et al. (2009a); ■, liquid-liquid experimental data.

The variation of the composition of the solvent-enriched phase (L_1) in L_1 - L_2 region is more significant at the temperature of 100°C compared to 50°C (Figure 5-53). This might be due the nature of propane at high temperatures which behaves like supercritical fluid close to the critical condition. As previously mentioned, the extraction of light hydrocarbons into the solvent-enriched phase causes a reduction in the composition of propane in L_1 with pressure. Although the extraction capability at high temperatures is less than that of liquid propane, the impact of pressure is higher. For instance, at the temperature of 50°C, an increase in the pressure from (5 to 8) MPa at a constant overall propane concentration of 40 weight percent increases the extraction yield about 10 percent while the increase in the pressure (6 to 8) MPa at the temperature of 100°C,

doubles the extraction yield. This clarifies the considerable variation of the composition of propane in L_1 with pressure at the temperature of 100°C which is due to greater change of extraction yield with pressure.

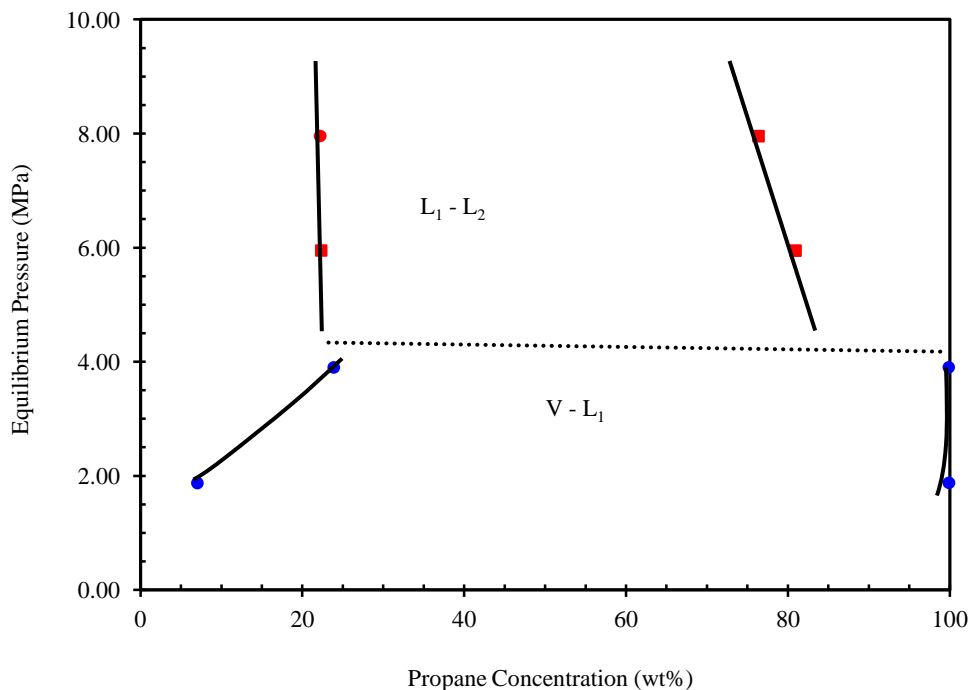


Figure 5-53: Coexisting phase compositions for Surmont bitumen / propane systems at 100°C and at a constant overall propane concentration of 0.6 weight fraction; ●, vapour-liquid experimental data; ■, liquid-liquid experimental data.

Figures 5-54 and 5-55 show the densities of coexisting phase as a function of equilibrium pressure at two different temperatures (50 and 100°C) and a constant overall propane concentration of 0.4 weight fraction. No single phase region was detected in the studied pressure range. As anticipated from the figures, the density of L_1 within $V-L_1$ region reduces with the pressure. This is due to higher dissolution of propane in the bitumen with the increase in pressure. Nevertheless, further increase in the pressure results in change in the state of system from $V-L_1$ equilibrium to L_1-L_2 equilibrium. The dramatic variation in the density of the solvent-enriched phase indicates the phase transition from V into L_1 . The experimental results in liquid-liquid equilibrium study indicated that the density of L_1 in L_1-L_2 region is higher than density of pure propane at

specified pressure. This confirms that the light hydrocarbon components are extracted into the solvent-enriched phase (L_1).

A noticeable change in the density of saturated bitumen occurs at the temperature of 50°C when the pressure increases to 2 MPa. In V- L_1 region, the density of saturated bitumen reduces with pressure whereas further increase in the pressure (L_1 - L_2 region) results in a dramatic increase in the density. Indeed, the system undergoes a change in state from V- L_1 to L_1 - L_2 . The vapour phase is converted into L_1 and the saturated bitumen comes out as L_2 . The increase in the density is directly due to depletion of saturated bitumen from the light components.

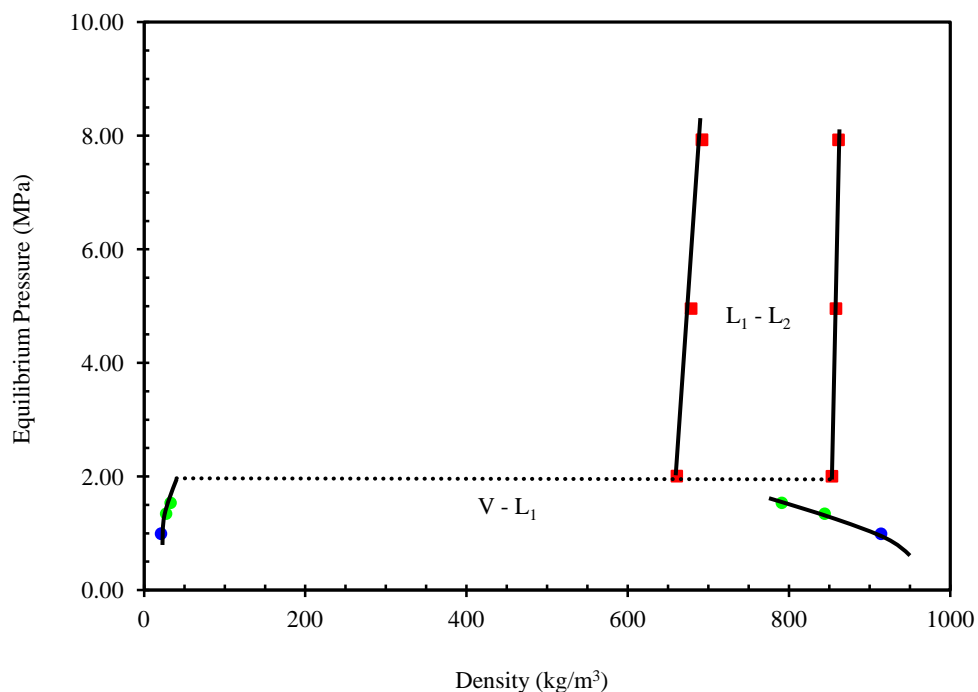


Figure 5-54: Coexisting phase densities for Surmont bitumen / propane systems at 50°C and at a constant overall propane concentration of 0.4 weight fraction; ●, vapour-liquid experimental data; ●, vapour-liquid experimental data for propane / Athabasca bitumen systems taken from Badamchi-Zadeh et al. (2009a); ■, liquid-liquid experimental data.

Further investigation of coexisting phase densities reveals that the pressure affects the densities of both liquid phases at equilibrium condition. The influence of pressure on the density of the phases is an indirect indication of the pressure effect on the extraction yield

which causes an increase in the densities of L_1 and L_2 in L_1 - L_2 region. The variation of the density of L_2 is not as significant as that of L_1 at the temperature of 50°C . This is because of three main factors. First is the increase in propane concentration in L_2 with pressure. Second factor is the direct impact of pressure on the density of liquid; increase in density with pressure. The third factor is that L_2 becomes leaner in light hydrocarbons with the increase in pressure. The density results in Figure 5–54 for L_2 reveal that the first factor is almost balanced with other two factors and a slight increase in the density of L_2 is observed. Whereas, at high temperature condition (i.e. 100°C), the variation of the density of L_2 is more considerable than that of 50°C .

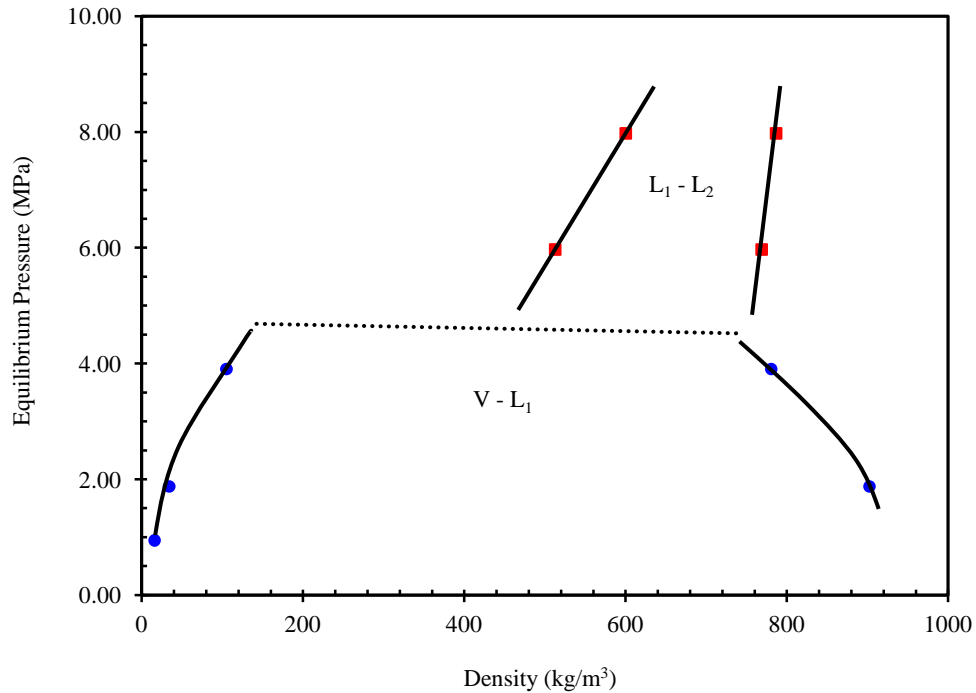


Figure 5–55: Coexisting phase densities for Surmont bitumen / propane systems at 100°C and at a constant overall propane concentration of 0.6 weight fraction; ●, vapour-liquid experimental data; ■, liquid-liquid experimental data.

Although the density of L_2 remains almost constant with pressure at the temperature of 50°C , the density of L_1 is considerably increased with the pressure because the solvent-enriched phase is mainly composed of the liquid propane and light components. That is, the greater extraction of bitumen components and the influence of pressure on the

density of liquid raise the density of L_1 . Thus, as the pressure increases, more components are transferred into L_1 and make this phase much heavier.

5.6. Comparison of Saturated Liquid Properties for Light Hydrocarbons / Bitumen Systems

In previous sections, the solubility and saturated phase properties for Surmont bitumen diluted with ethane and propane were reported in the temperature range (50 to 200)°C and at the pressures up to 8 MPa. The solubility generally increases with pressure at a constant temperature and decreases with the temperature at a constant pressure.

Of particular importance is the saturated bitumen density and viscosity, which determine the fluid flow properties. The application of solvent injection to heavy oil and bitumen recovery processes requires the predictions of performance for a field-scale design. This directly depends on the reduction of oil viscosity by solvent dilution. Thus, the comparison and evaluation of the solvent dissolution effects on the properties are crucial. In this section, comparisons between the measured properties for gas-saturated bitumen are presented.

Experimental measurements for the saturated bitumen density and viscosity were taken: at a constant pressure and at a constant temperature and, at a constant composition and at a constant temperature. In the first approach, the system temperature and pressure were kept constant, and the solvent was dissolved into bitumen. In fact, the solvent is available in an excess amount. Different solvents have different solubilities; and, using this approach, we could investigate the maximum solubility of different solvents in bitumen. For instance, we concluded that heavier hydrocarbon solvents have higher solubility than lighter ones, leading to higher viscosity reduction.

In the second approach, the main objective was the investigation of the effect of different solvents on the properties of saturated bitumen. In this case, the compositions of different solvents were kept constant in the saturated mixture, and the saturated properties

were then measured. Specific amount of solvent at a constant temperature was added to a specific amount of bitumen; and, at a constant pressure, the solvent was dissolved into bitumen, resulting in a single liquid phase. The properties of saturated liquid phase for different solvents were measured; and, based on these measurements; we can investigate the effects of solvent type on saturated properties.

The amount of solvent that needs to be dissolved into bitumen was selected on the basis of the lighter solvent, as it has the lower solubility. The solubility of lightest solvent at desired temperature and pressure could be selected; however, to ensure that all solvent dissolved in the bitumen and single phase was obtained, lower values were considered.

5.6.1. Constant Pressure and Constant Temperature

The vapour-liquid equilibrium data reported in previous sections fall into the category of solubility and physical property measurements at constant temperature and at constant pressure. In this case, the maximum solubility of a specific solvent in bitumen at a constant pressure and at a constant temperature was measured. In addition, the density and viscosity of the saturated liquid phase at maximum solubility were reported. Figure 5–56 illustrates the measured maximum solubility of four different solvents – methane, ethane, propane, and butane – in Surmont bitumen at the temperatures of 150 and 190°C. As depicted in the figure, the solubility of solvent (in weight fraction) in the bitumen at a constant temperature and at a constant pressure was decreased in the following order,

$$n\text{-butane} > \text{propane} > \text{ethane} > \text{methane}$$

The difference between the solubilities at two isotherms became significant as the solvent became heavier. The corresponding saturated phase properties – density and viscosity – are plotted in Figures 5–57 and 5–58, respectively. Only the temperatures of 150 and 190°C were considered here, because at lower temperatures (e.g. 100°C), the liquid-liquid equilibrium existed for bitumen/propane and bitumen/butane mixtures at studied pressures.

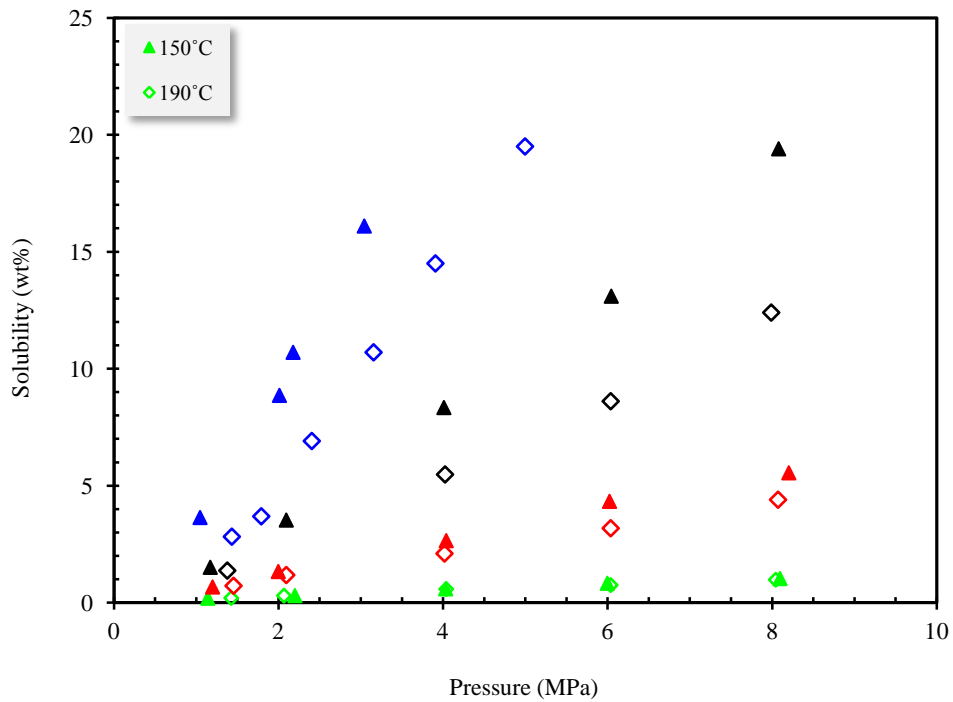


Figure 5-56: The maximum solubility of light hydrocarbon gases in Surmont bitumen at the temperatures of 150 and 190°C; blue, butane; black, propane; red, ethane; green, methane.

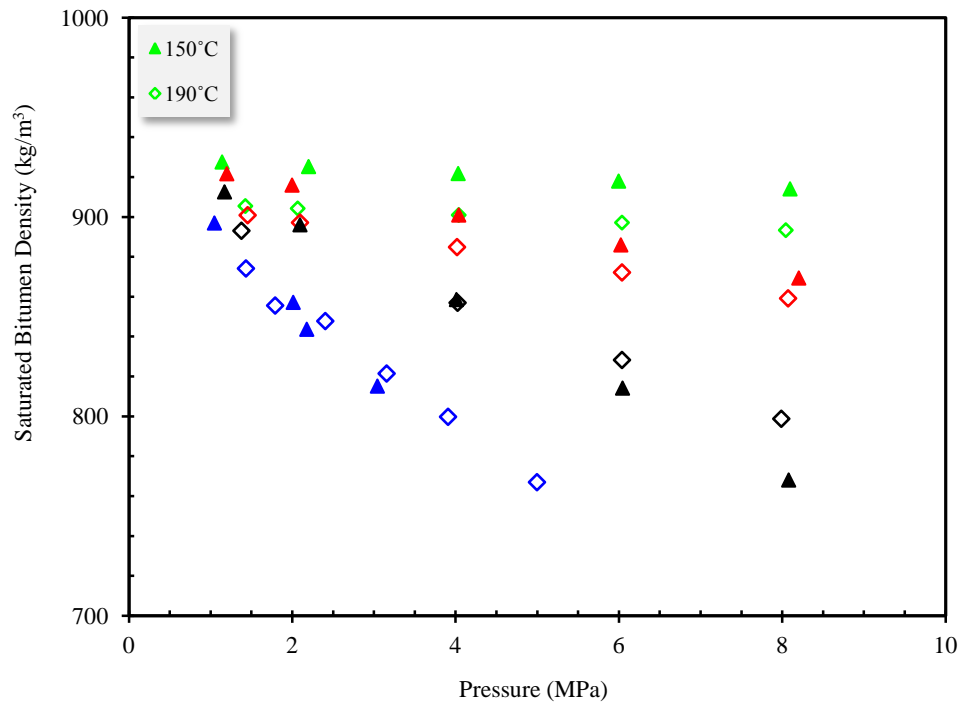


Figure 5-57: Comparison of the measured saturated bitumen density of Surmont bitumen and different light hydrocarbon gases at the temperatures of 150 and 190°C; blue, butane; black, propane; red, ethane; green, methane.

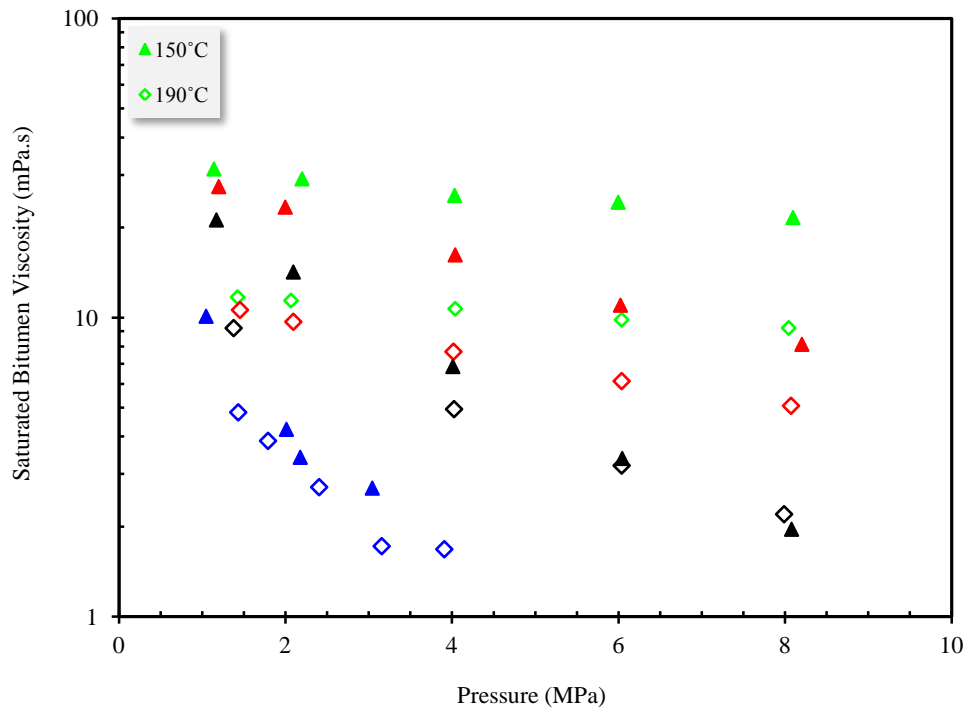


Figure 5–58: Comparison of the measured saturated bitumen viscosity of Surmont bitumen and different light hydrocarbon gases at the temperatures of 150 and 190°C; blue, butane; black, propane; red, ethane; green, methane.

As depicted in Figures 5–57 and 5–58, the heavier solvent (butane) is more effective in the reduction of bitumen density and viscosity. For all temperatures, linear relationships existed for the saturated bitumen viscosities and densities with pressure. At high temperatures, the viscosity reduction was less significant than at low temperatures. These experimental data can be used for optimization of recovery processes in the field and as guide for reservoir engineers to select an appropriate solvent on the basis of the operational conditions.

The experimental results shown in Figures 5–57 and 5–58 also indicate that the butane (or heavier hydrocarbon solvent) had a greater effect on the viscosity reduction. Figure 5–56 illustrates that butane had the highest solubility at a constant pressure and a constant temperature. Thus, due to the higher solvent fraction in the liquid phase, the saturated viscosity and density were lower, i.e. increasing the pressure resulted in higher dissolution of heavier hydrocarbon gas and lower saturated viscosity and density.

Considering the above results, one can conclude that at a constant temperature and a constant pressure, the solubility determines the saturated phase properties. Higher solubility corresponded to higher viscosity reduction. Therefore, the heavier solvent is more effective, due to higher solubility. However, at a constant solvent fraction, the solvent (methane, ethane or propane) may lead to different viscosity reductions. In the next section, we evaluate this behaviour.

5.6.2. Constant Solvent Weight Fraction and Constant Temperature

The experimental measurements for the phase behaviour of bitumen saturated with light hydrocarbon gases have confirmed that, at a constant pressure, the heavier hydrocarbon gas had more viscosity reduction, due to higher dissolution of the solvent. However, in some cases, such as the injection of a gas mixture, the available solvent in the injected gas may not exceed the maximum solubility of the desired hydrocarbon. In this case, the total amount of desired hydrocarbon gas in the injected fluid may dissolve in the oil *in-situ*. Thus, at a constant temperature, a specific amount of solvent might be dissolved in the bitumen.

Luo et al. (2007b) studied the phase behaviour of Lloydminster heavy oil saturated with a gas mixture at ambient temperature. The gas mixture composed of 70 mol% methane, 25 mol% propane, 3.5 mol% *n*-butane, and 1.5 mol% *iso*-butane. The authors found that the heavy oil and gas mixture formed a homogenous phase at 0.551 and 2.068 MPa while two liquid phases were observed at 3.202 and 5.048 MPa. At two low pressures, it was found that the major component dissolved in the heavy oil was methane (>75 mol%). As expected, the solubility of heavier hydrocarbon gases in heavy oil is much higher than that of methane at the same condition. The authors gave the lack of enough propane and butane in the solvent mixture as the reason for the observed behaviour.

To evaluate the impact of dissolving a specific amount of solvent in the bitumen and the corresponding saturated phase properties, four different operational conditions were

considered. The selection of the operating conditions depended on the solubility measurements conducted in the previous section. For example, at 150°C and 8 MPa, the maximum solubility of ethane in Surmont bitumen was 5.55 wt%, which was lower than that of propane and butane at the same conditions. Thus, the composition of 4 wt% was selected as the constant composition at this condition, which was smaller than maximum solubility for a single liquid phase. At a constant temperature of 150°C and a constant solvent fraction of 4 wt%, the saturated phase properties for Surmont bitumen / solvent systems were measured. Table 5–10 summarizes all four operating conditions for the measurements.

Table 5–10: Operational conditions for constant temperature and constant solvent weight fraction experiments; T , temperature; w_s , solvent weight fraction.

T (°C)	$10^2 w_s$	Maximum solubility (ethane) (wt%)
50	10	14.2
100	6	8.5
150	4	5.6
190	2.5	4.4

The experimental saturated phase densities and viscosities for a constant temperature and a constant solvent weight fraction with different hydrocarbon gases are summarized in Tables 5–11 and 5–12 and are plotted in Figures 5–59 and 5–60. The experiments for Surmont bitumen / methane was not considered here because the measured maximum solubility of methane at 150°C and 8 MPa was reported as 1.03 wt% by Kariznovi (2013) which is much lower than the values reported in Table 5–10.

As depicted in Figures 5–59 and 5–60, at a constant solvent weight fraction, the lighter hydrocarbon was more effective than the heavier hydrocarbon. These results were in contradiction with the results obtained at a constant pressure, where the heavier solvent was more effective. At lower temperatures, the impact of the dissolution of a specific amount of solvent on the saturated phase properties was more significant.

Table 5–11: Experimental saturated liquid densities for Surmont bitumen saturated with different solvents; T , temperature; ρ_s , saturated liquid density; w_s , weight percent of solvent in saturated liquid phase.

T (°C)	w_s	ρ_s (kg/m ³)		
		Ethane-Saturated	Propane-Saturated	Butane-Saturated
50	10	894.6	919.4	934.3
100	6	903.2	916.0	926.6
150	4	892.6	901.9	908.3
190	2.5	881.3	888.9	890.1

Table 5–12: Experimental saturated liquid viscosities for Surmont bitumen saturated with different solvents; T , temperature; μ_s , saturated liquid viscosity; w_s , weight percent of solvent in saturated liquid phase.

T (°C)	w_s	μ_s (mPa.s)		
		Ethane-Saturated	Propane-Saturated	Butane-Saturated
50	10	56.7	117	207
100	6	29.5	38.3	47.1
150	4	11.6	14.2	15.6
190	2.5	6.46	7.07	7.89

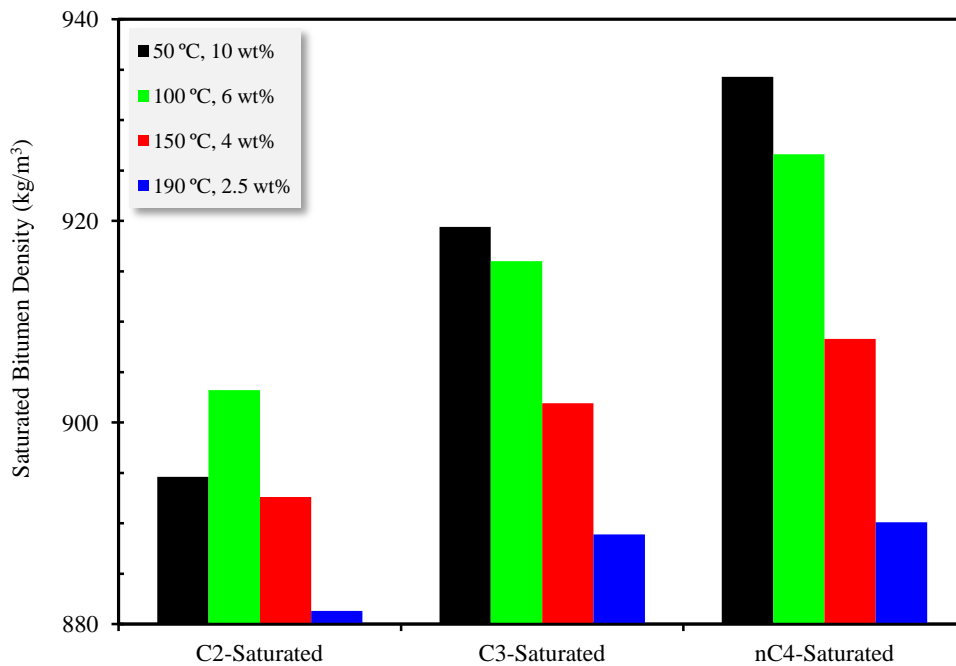


Figure 5–59: The comparison of the saturated liquid densities for Surmont bitumen saturated with different solvents at different temperatures and a constant solvent weight fraction.

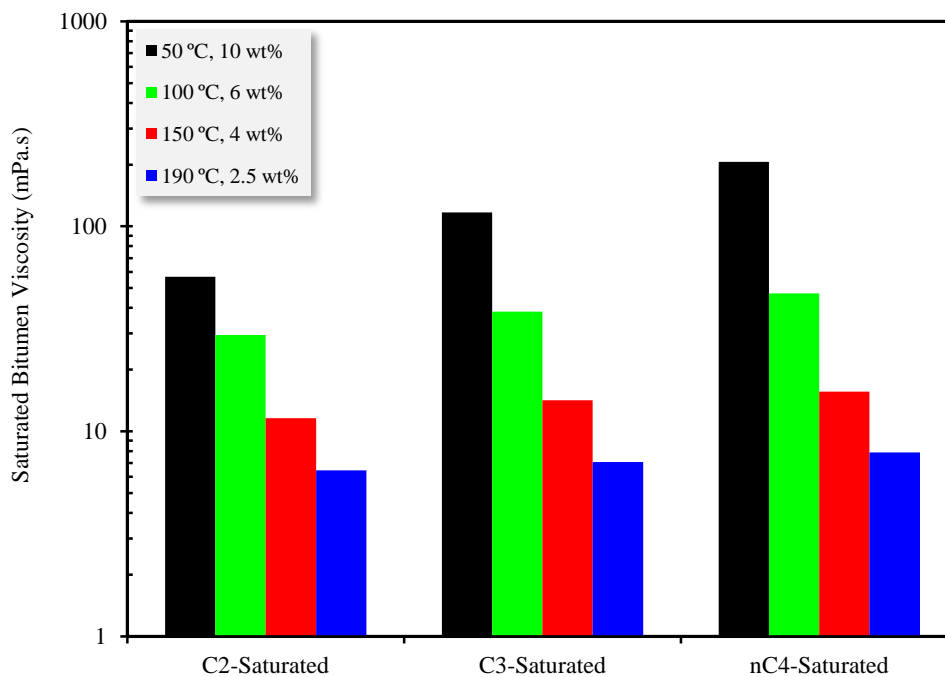


Figure 5–60: The comparison of the saturated liquid viscosities for Surmont bitumen saturated with different solvents at different temperatures and a constant solvent weight fraction.

Generally speaking, lighter hydrocarbons have smaller molecules; and, at a constant composition (wt%), lighter hydrocarbons contain a higher number of molecules, which are distributed among the oil molecules. Thus, the dissolution of lighter hydrocarbons is more effective than heavier ones. These results are valuable for designing the composition of the gas mixture in which the carrier gas would be methane or nitrogen. The addition of a light hydrocarbon into the carrier gas can result in higher viscosity reduction.

The results presented in Section 5.6.2, along with the solubility measurements in Section 5.6.1, can be used as a comprehensive set of experimental data for the design and evaluation of gas mixture composition. The solubility measurements determine the operational conditions, while the results in Section 5.6.2 indicate the selection of an appropriate hydrocarbon gas for the desired viscosity reduction.

Chapter 6: Thermo-physical Properties of Bitumen/Hexane Mixtures

This chapter considers the phase behaviour of bitumen/*n*-hexane mixtures and the application of *n*-hexane for heavy oil and bitumen *in situ* recovery methods. The measurements for the density and viscosity of bitumen diluted with *n*-hexane were reported at different temperatures, pressures, and solvent weight fractions. The data for the mixtures were also evaluated with predictive schemes as well as with correlation models representing certain mixing rules proposed in the literature. The influences of pressure, temperature, and solvent weight fraction on the density and viscosity of mixtures are considered in the models and evaluated from the experimental results.

6.1. Introduction

As outlined in Chapter 1, the benefits of steam-solvent co-injection over steam or solvent-based processes are higher viscosity reduction, higher oil production rate, less amount of water consumption, and lower GHG emissions. During the co-injection process, the bitumen viscosity is reduced by two different mechanisms, the temperature increase provided by steam and the dilution by solvent dissolution. The addition of solvent improves the performance of the process and reduces the steam requirement. The advantages of solvent co-injection processes have been investigated by many researchers (Nasr et al. 2002; Nasr and Ayodele 2006; Ayodele et al. 2009; Ardali et al. 2011; Mohammadzadeh et al. 2012). Different solvents including light solvents, such as propane; to heavier ones, such as *n*-pentane to *n*-octane; field solvents, such as condensate and naphtha; and aromatic solvents, such as xylene and toluene have been tested. The experimental conditions varied from low pressures of 60 kPa (Li and Mamora 2010) to medium pressures of 550 kPa (Ardali et al. 2012) and 1500 kPa (Ivory et al. 2008) and even higher pressures of 2200 kPa (Zhao et al. 2005). The experimental results

confirm that co-injection improves the production rate and recovery of oil with less energy and water consumption and reduces greenhouse gas (GHG) emissions.

To have beneficial effect of solvent additive to SAGD process, the hydrocarbon steam additive should reach the bitumen surface; that is, it must remain in the gaseous state when traveling with steam in the chamber. Thus, the success of ES-SAGD process highly depends on the selection of a suitable solvent. Nasr et al. (2002) proposed that the best solvent is the one which has the closest properties as those of the water at the temperature and pressure conditions in the steam chamber. Hexane or diluent, which contain mostly higher carbon numbers than 6, was proposed by Nasr et al. (2002) and considered as ideal hydrocarbon additives for ES-SAGD process. Hexane has the closest vaporization temperature to the injected steam for the operational condition of SAGD process in Alberta. For instance, considering an operating temperature of 215°C; the saturation pressure of water is 2.11 MPa while this value is 2.27 MPa for hexane which is very close to the water saturation pressure.

The lab-scale experiments by Nasr et al. (2002) showed that the drainage rates with the co-injection of hexane (1% mass fraction) and steam were approximately double compared to pure steam injection. The authors considered hydrocarbon solvents from C₁ up to C₈ and commercial diluents. The results indicated that the co-injection of steam and hexane produced the highest drainage rates among the solvents tested. McCormack (2009) did a numerical investigation for the implications of hexane addition to steam in SAGD process. The study showed lower energy requirements and the improvement in the SOR by the addition of hexane to steam compared to conventional SAGD process. Mohebati et al. (2013) conducted extensive numerical studies in a three-dimensional model to evaluate the benefit of hexane additive to steam in SAGD process. The results indicated that hexane co-injection reduces the SOR and improves the process performance and is more advantageous in Athabasca reservoir than in Cold Lake and Lloydminster.

Although the potential advantage of hydrocarbon solvents has been confirmed by many researchers as discussed in the text, the application of these new recovery processes

is challenging. Hydrocarbon solvents, such as hexane, are more expensive than the produced oil and the success of process depends on how much solvent can be recovered during and at the end of the process. Prediction and optimization of solvent-assisted processes are challenging task because the existence of solvent in the solvent-based process or the introduction of a solvent into steam-based processes leads to complex phase behaviour system. For any given heavy oil and solvent mixture, it may be necessary to predict the phase boundaries, amounts and compositions of solvent in the bitumen and asphaltene precipitation regions. It is necessary to know how solvent additive affects oil properties at elevated temperatures before all the potential benefits can be determined. The quantitative effects of hexane dissolution on bitumen viscosity, density, and phase behaviour are not well understood especially at elevated temperature in which the steam-based processes are applied. Thus, in this chapter, the phase behaviour and physical properties of bitumen/hexane systems are investigated.

6.2. Literature Background

The phase behaviour of bitumen diluted with hexane has gained less attention and few experimental data for the thermo-physical properties as well as phase equilibrium information have been reported. Park et al. (2000) has reported the experimental data on the extraction behaviour and fractionation of an aromatic heavy oil using *n*-hexane as the extraction solvent. They found that the total amount of extracted oil increases with increasing temperature while a reduction in the density of solvent is obtained with increase in temperature. No asphaltene fraction in the extracted oil was found when the extraction was conducted under vapour-liquid condition.

Alboudwarej (2003) reported the fractional asphaltene yield from Lloyminster heavy oil and Cold Lake and Athabasca bitumens diluted with *n*-hexane. In another study, Akbarzadeh et al. (2005) used regular solution theory to model the asphaltene precipitation of different oils diluted with *n*-alkanes. For Athabasca bitumen / *n*-hexane

mixtures, the authors found that the yield of precipitation increases as the solvent mass fraction in the solution increases and the fractional yield is higher at the temperature of 0°C compared to 25°C.

In this chapter, the aim is to measure the thermo-physical properties of Athabasca bitumen / hexane mixtures. This information is crucial for the understanding of the recovery processes that include hexane as a solvent. Thus, the density and viscosity of Surmont bitumen diluted with *n*-hexane were reported at different temperatures, pressures, and solvent weight fractions. The aim was to evaluate the impact of variations in the above-mentioned parameters on the viscosity and density of mixture. Some liquid solvents such as benzene and toluene are known to be miscible with bitumens in all proportions without asphaltene instability. This is not the case for paraffinic solvents such as *n*-alkanes. There is a critical concentration in which the asphaltene fraction of oil starts to separate from the liquid mixture (Mousavi-Dehghani et al. 2004). The separation of asphaltene from mixture leads to significant change in the properties of the mixture (Escobedo and Mansoori 1995, 1997). Wiehe et al. (2005) determined the onset of asphaltene precipitation for Athabasca bitumen / *n*-hexane mixtures at room temperature. The volume fraction of *n*-hexane at the onset of asphaltene precipitation was reported as 0.669. The corresponding weight fraction of *n*-hexane (critical concentration) is 0.568 for the asphaltene separation.

After the density and viscosity measurements for the Surmont bitumen / *n*-hexane mixtures at a constant solvent concentration, the equilibrium cell was opened to check the possible asphaltene precipitation from the mixture. The results showed that the asphaltene precipitation only occurred at a concentration of 0.6 *n*-hexane weight fraction. Figure 6–1 shows a picture of the precipitated asphaltenes from the mixture at a temperature of 100°C and a solvent concentration of 0.6 weight fraction. At the equilibrium condition, the asphaltene enriched phase was semi-solid and highly viscous with a small amount of *n*-hexane as presented in Figure 6–1a. After the evaporation of *n*-hexane, the asphaltenes became more solid-like and converted into bright and black powders (Figure 6–1b).

In this study, to avoid the asphaltene precipitation, the maximum *n*-hexane weight fraction was considered to be less than the critical value. Thus, the mixtures with (0.05, 0.1, 0.2, 0.3, 0.4, and 0.5) weight fractions of *n*-hexane were considered.



Figure 6–1: Digital photographs of the precipitated asphaltene from the mixture of Surmont bitumen / *n*-hexane at the temperature of 100°C and at a concentration of 0.6 *n*-hexane weight fraction; a) immediately after experiment; b) after evaporation of *n*-hexane.

6.3. Density of Mixtures

Tables 6–1 to 6–3 summarize the measured density values for pseudo-binary mixtures of Surmont bitumen and *n*-hexane at different temperatures, pressures, and solvent weight fractions. As the tables show, the density of binary mixture is reduced with temperature and is increased with pressure. The density of pure *n*-hexane and of raw Surmont bitumen shows similar trends as their binary mixtures with temperature and pressure. The density of the pseudo-binary mixture is significantly decreased with increasing *n*-hexane weight fraction. The impact of pressure on the density of pure *n*-hexane is more pronounced at high temperature conditions (150 and 190°C). The critical temperature of *n*-hexane is 235°C and as the temperature increased toward the critical point, the variation of *n*-hexane density with the pressure becomes more significant. The same trend was also observed for the raw bitumen. That is, at high temperatures (150 and 190°C), the impact of pressure on the density of bitumen was more significant compared to low temperatures (23°C). The temperature considerably changes the density of *n*-

hexane over the studied pressure (NIST). Although the density of bitumen is also reduced with temperature, its variation is not as significant as pure *n*-hexane.

Table 6–1: Experimental liquid densities of Surmont bitumen / *n*-hexane mixtures at 0.05 and 0.1 weight fractions of hexane; *T*, temperature; *P*, pressure; ρ_m , density of mixture.

<i>w</i> = 0.05			<i>w</i> = 0.1		
<i>T</i> (°C)	<i>P</i> (MPa)	ρ_m (kg/m³)	<i>T</i> (°C)	<i>P</i> (MPa)	ρ_m (kg/m³)
189.7	2.05	877.8	189.7	2.09	849.9
189.7	4.10	880.7	189.7	4.09	852.9
189.7	6.06	882.7	189.7	6.08	855.2
189.7	8.08	884.7	189.7	8.07	857.5
189.7	10.05	886.6	189.7	10.02	859.7
150.2	2.11	903.5	150.0	2.07	876.1
150.2	4.05	905.6	150.0	4.10	879.2
150.2	6.12	907.5	150.0	6.08	881.1
150.2	8.09	909.2	150.0	8.10	883.0
150.2	10.11	910.9	150.0	10.06	884.8
100.7	2.04	934.9	100.5	2.04	909.3
100.7	4.09	936.5	100.5	4.08	910.9
100.7	6.09	937.9	100.5	6.10	912.4
100.7	8.12	939.0	100.5	8.08	913.9
100.7	10.07	940.7	100.5	10.11	915.5
50.0	2.06	966.2	50.0	2.09	941.5
50.0	4.14	967.5	50.0	4.16	942.9
50.0	6.12	968.6	50.0	6.09	944.1
50.0	8.06	969.7	50.0	8.10	945.3
50.0	10.11	970.9	50.0	10.09	946.6
23.2	2.04	982.4	23.6	2.05	958.0
23.2	4.07	980.4	23.6	4.15	959.8
23.2	6.17	984.9	23.6	6.09	960.9
23.2	8.11	986.0	23.6	8.09	962.1
23.2	10.09	987.0	23.6	10.08	963.2

Table 6–2: Experimental liquid densities of Surmont bitumen / *n*-hexane mixtures at 0.2 and 0.3 weight fractions of hexane; *T*, temperature; *P*, pressure; ρ_m , density of mixture.

<i>w</i> = 0.2			<i>w</i> = 0.3		
<i>T</i> (°C)	<i>P</i> (MPa)	ρ_m (kg/m ³)	<i>T</i> (°C)	<i>P</i> (MPa)	ρ_m (kg/m ³)
189.5	2.13	798.1	189.0	2.13	749.7
189.5	4.11	801.1	189.0	4.12	753.7
189.5	6.06	804.3	189.0	6.09	757.1
189.5	8.05	807.1	189.0	8.08	760.5
189.5	10.08	809.8	189.0	10.09	763.8
150.2	2.08	826.9	149.4	2.09	782.2
150.2	4.09	829.4	149.4	4.09	785.6
150.2	6.10	831.8	149.4	6.09	788.3
150.2	8.08	834.0	149.4	8.08	790.9
150.2	10.08	836.3	149.4	10.07	793.4
100.6	2.06	861.9	100.5	2.09	819.9
100.6	4.10	863.9	100.5	4.09	822.0
100.6	6.10	865.6	100.5	6.09	824.0
100.6	8.10	867.0	100.5	8.12	826.0
100.6	10.08	868.7	100.5	10.11	827.9
50.0	2.03	897.6	50.0	2.11	856.4
50.0	4.09	898.9	50.0	4.11	858.0
50.0	6.08	900.1	50.0	6.07	859.5
50.0	8.08	901.4	50.0	8.09	861.0
50.0	10.11	902.8	50.0	10.09	862.5
23.8	2.05	913.7	23.4	2.09	875.0
23.8	4.10	915.8	23.4	4.09	876.6
23.8	6.09	917.2	23.4	6.11	878.1
23.8	8.08	918.6	23.4	8.08	879.5
23.8	10.14	919.9	23.4	10.13	880.9

Table 6–3: Experimental liquid densities of Surmont bitumen / *n*-hexane mixtures at 0.4 and 0.5 weight fractions of hexane; *T*, temperature; *P*, pressure; ρ_m , density of mixture.

<i>w</i> = 0.4			<i>w</i> = 0.5		
<i>T</i> (°C)	<i>P</i> (MPa)	ρ_m (kg/m ³)	<i>T</i> (°C)	<i>P</i> (MPa)	ρ_m (kg/m ³)
188.9	2.12	698.7	189.2	2.11	657.2
188.9	4.12	705.7	189.2	4.09	663.3
188.9	6.10	710.4	189.2	6.10	669.0
188.9	8.09	714.0	189.2	8.11	674.1
188.9	10.12	718.1	189.2	10.05	678.7
150.1	2.09	735.6	149.6	2.11	695.1
150.1	4.09	739.5	149.6	4.08	700.3
150.1	6.10	743.0	149.6	6.10	704.0
150.1	8.08	746.1	149.6	8.10	707.6
150.1	10.08	749.1	149.6	10.14	711.1
100.6	2.09	775.5	100.5	2.11	739.1
100.6	4.09	778.1	100.5	4.10	741.9
100.6	6.09	780.4	100.5	6.09	744.5
100.6	8.10	782.8	100.5	8.13	747.1
100.6	10.08	785.0	100.5	10.10	749.6
50.2	2.06	815.0	49.9	2.09	779.3
50.2	4.12	816.8	49.9	4.11	781.4
50.2	6.04	818.7	49.9	6.09	783.2
50.2	8.08	820.5	49.9	8.09	785.0
50.2	10.09	822.2	49.9	10.09	786.8
22.7	2.09	835.1	23.1	2.10	800.2
22.7	4.09	836.5	23.1	4.11	801.8
22.7	6.08	838.0	23.1	6.10	803.4
22.7	8.10	839.4	23.1	8.09	804.9
22.7	10.10	840.9	23.1	10.10	806.5

The variation of the mixture density with temperature and pressure is highly dependent on the *n*-hexane weight fraction. At low solvent concentrations (i.e. 0.05 weight fraction), the mixture behaves similar to bitumen whereas at a high *n*-hexane weight fraction (i.e. 0.5), the mixture behaviour is more similar to the pure solvent. Thus, the variation of density with pressure is not considerable at *n*-hexane weight fraction of 0.05.

6.3.1. Prediction of Mixture Density

The measured density data of Surmont bitumen / *n*-hexane mixtures are predicted with the following equation,

$$\rho_m = \frac{1}{\frac{w_s}{\rho_s} + \frac{1-w_s}{\rho_B}} \quad 6-1$$

where w_s is the weight fraction of *n*-hexane, ρ_s and ρ_B are the densities of *n*-hexane and bitumen, respectively. This equation was developed on the assumption that no volume change occurs upon mixing. The density of pure *n*-hexane at each temperature and pressure was taken from NIST database and that of raw bitumen taken from Chapter 3 were used for the calculations. The density values were predicted using the above equation, and the results were in agreement with the measured data, within 1.36% AARD.

Figures 6–2 and 6–3 display the measured density data for the mixtures of Surmont bitumen / *n*-hexane along with the predicted values. In these figures, the density is plotted as a function of *n*-hexane weight fraction at different temperatures and at a constant pressure. Figure 6–2 shows the results at the lowest pressure, 2 MPa, and Figure 6–3 illustrates the same measurements at the highest pressure, 10 MPa. The symbols are the experimental data and lines are the predictions using equation 6-1. The predictions agree with the measured data. An examination of Figures 6–2 and 6–3 demonstrates that the mixture densities are significantly varied with the *n*-hexane weight fraction over the

studied concentrations. The predictions are in good agreement with the measured data at lowest temperature (23°C). As the temperature increases, the deviation between the predicted densities and the measured values becomes more. The same trends are also observed at other pressures.

Figures 6–4 and 6–5 illustrate the impact of pressure on the mixture density at different solvent weight fractions and at the temperatures of 23 and 190°C, respectively. As depicted in these figures, the mixture density is linearly changed with the pressure at a constant solvent weight fraction and the pressure effect is greater at higher temperature (i.e. 190°C). A closer examination of Figures 6–4 and 6–5 reveals that the predictions at highest temperature and highest solvent concentrations deviate significantly from the experimental data.

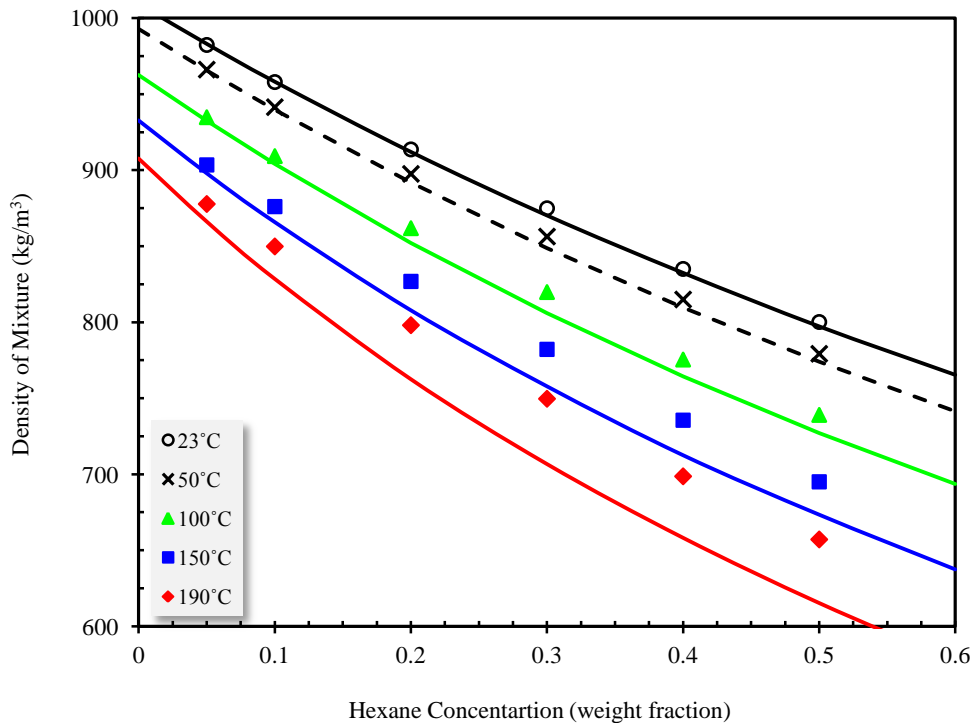


Figure 6–2: Density of Surmont bitumen / *n*-hexane mixtures as a function of the weight fraction of *n*-hexane at different temperatures and at a constant pressure of 2 MPa; ■,▲,○,◆,×, experimental data; ----, predicted values.

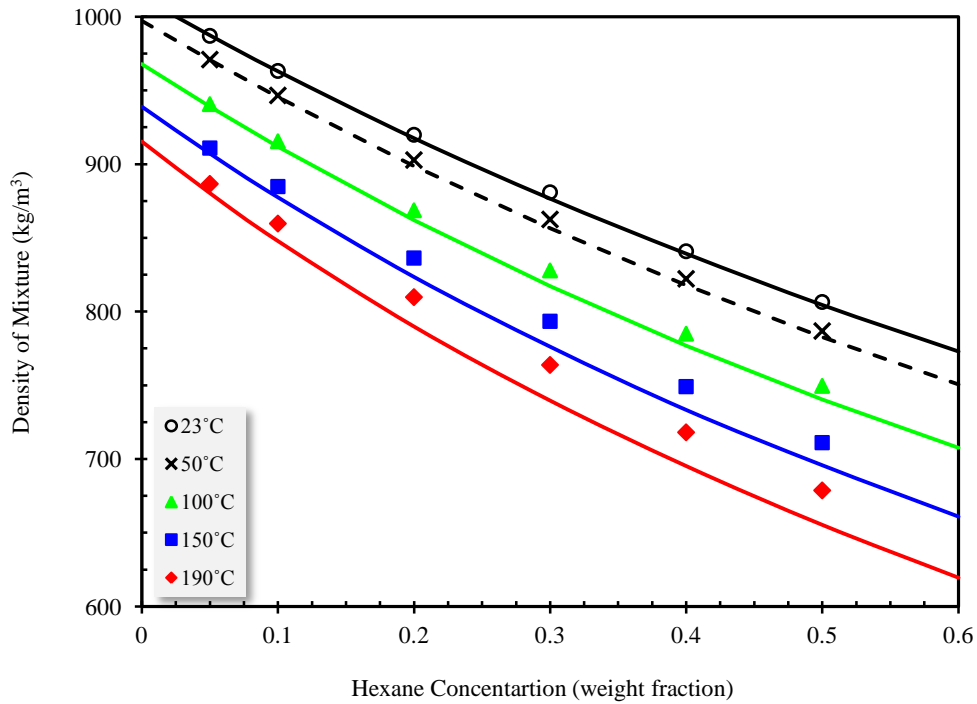


Figure 6-3: Density of Surmont bitumen / *n*-hexane mixtures as a function of the weight fraction of *n*-hexane at different temperatures and at a constant pressure of 10 MPa; ■, ▲, ○, ◆, ×, experimental data; ----, predicted values.

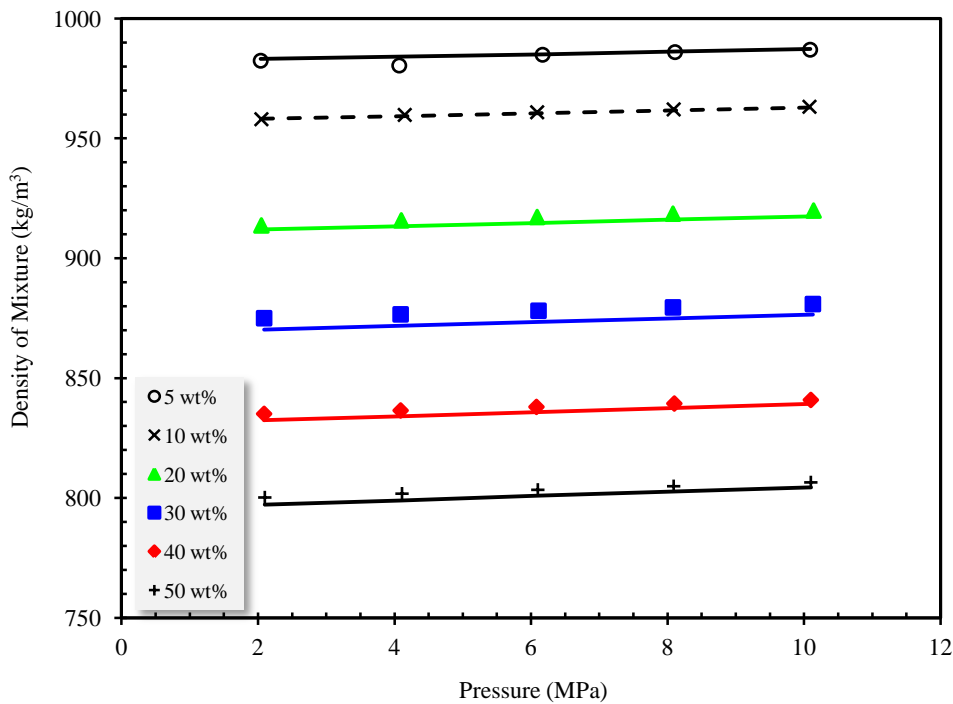


Figure 6-4: Density of Surmont bitumen / *n*-hexane mixtures as a function of pressure at different *n*-hexane weight fractions and at the lowest temperature (23°C); ○, ×, ▲, ■, ◆, +, experimental data; ----, predicted values.

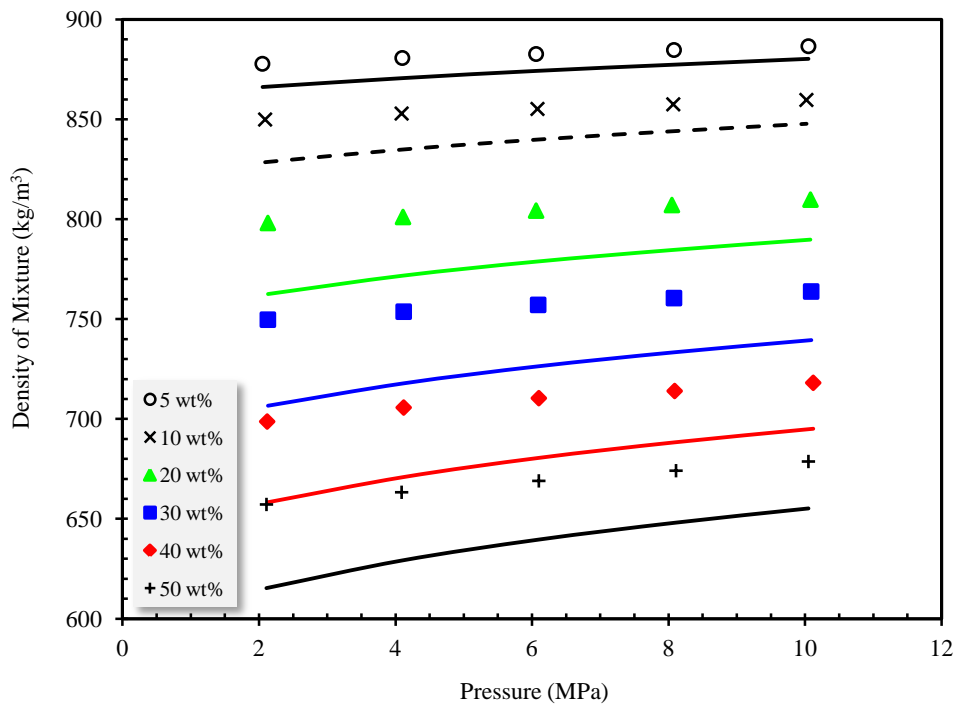


Figure 6–5: Density of Surmont bitumen / *n*-hexane mixtures as a function of pressure at different *n*-hexane weight fractions and at the highest temperature (190°C); ○, ×, ▲, ■, ◆, +, experimental data; ----, predicted values.

The variation of mixture density with pressure at other temperatures (i.e. 50, 100, and 150°C), as it is shown in Figures 6–6 and 6–7, is linear over the studied pressure, and the linear increase of the mixture density with the pressure occurs at all measured concentrations. Figure 6–6 shows the variation of the mixture density with the pressure at the lowest *n*-hexane weight fraction (i.e. 0.05) while Figure 6–7 displays the same results at the highest *n*-hexane weight fraction (i.e. 0.5). As depicted in these figures, the mixture density is linearly increased with the pressure at different temperatures.

A comparison of Figures 6–6 and 6–7 reveals that equation 6-1 predicts the experimental data better at higher pressures. That is, the deviation between the predictions and measured data is more significant at lower pressures. It is also worth to mention that at higher *n*-hexane concentrations or at higher temperatures, equation 6-1 under-predicts the measured values. Thus, it can be concluded that the volume change on mixing is significant for the mixtures of Surmont bitumen and *n*-hexane. The volume

change on mixing is more pronounced at high temperatures or at high solvent weight fractions because larger deviations from the measured data were obtained.

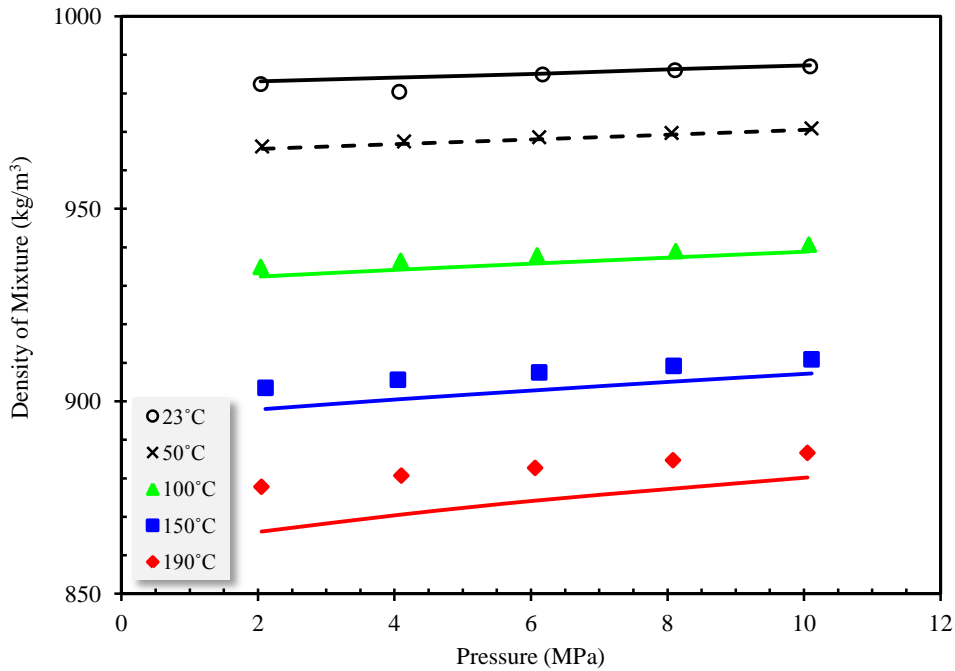


Figure 6–6: Density of Surmont bitumen / *n*-hexane mixtures as a function of pressure at different temperatures and at the lowest solvent weight fraction (0.05); \circ , \times , \blacktriangle , \blacksquare , \blacklozenge , experimental data; ----, predicted values.

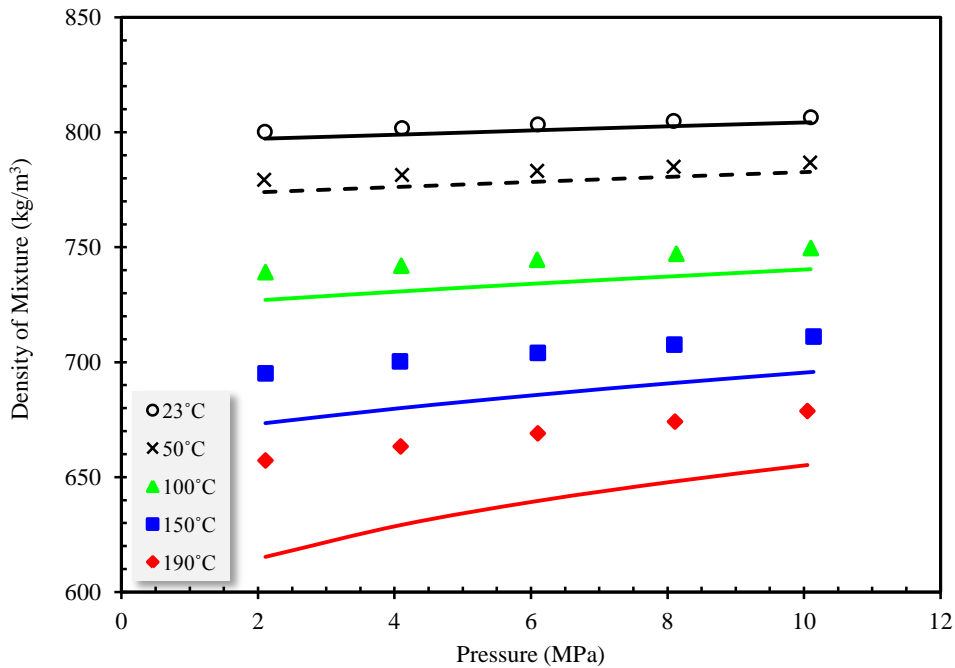


Figure 6–7: Density of Surmont bitumen / *n*-hexane mixtures as a function of pressure at different temperatures and at the highest solvent weight fraction (0.5); \circ , \times , \blacktriangle , \blacksquare , \blacklozenge , experimental data; ----, predicted values.

As previously explained in Chapter 3, the density of raw bitumen is linearly varied with temperature at a constant pressure. The variations of mixture density with temperature at two different pressures, (2 and 10) MPa, are shown in Figures 6–8 and 6–9. As depicted in these two figures, all prepared mixtures somehow follow a linear decrease in density with temperature. The comparison of Figures 6–8 and 6–9 confirmed that the linear decrease of the mixture density with temperature was observed for all measured pressures. The density data at the highest *n*-hexane weight fraction (0.5) slightly deviate from the linear trend and it is due to the non-linear trend of the density with temperature for *n*-hexane at a constant pressure. As depicted in Figure 6–8, the deviation between the predictions by equation 6-1 and experimental data becomes significant at high temperatures.

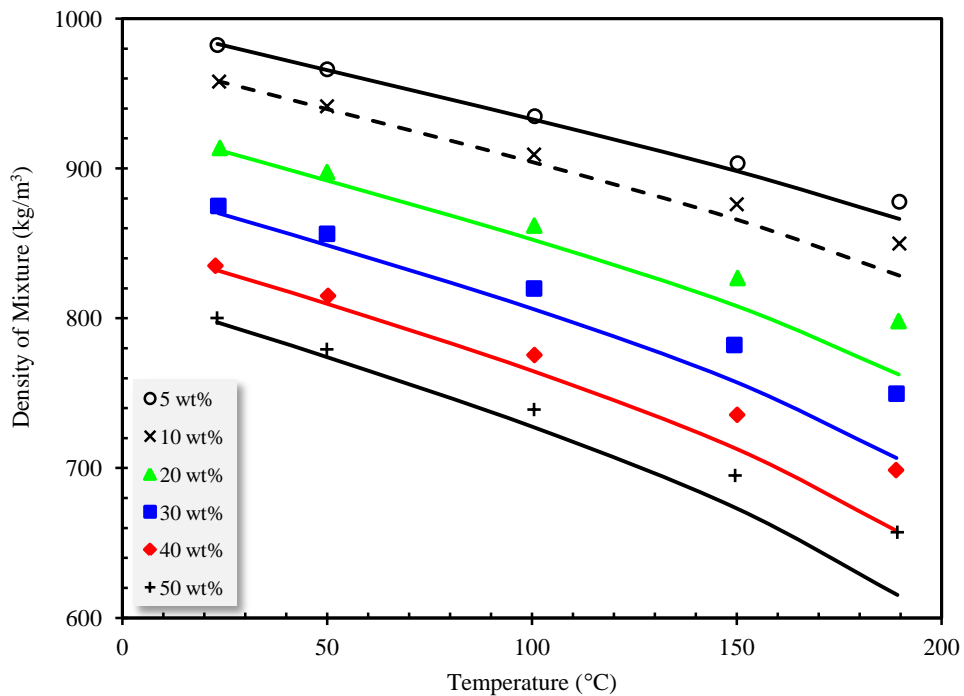


Figure 6–8: Density of Surmont bitumen / *n*-hexane mixtures as a function of temperature at different *n*-hexane weight fractions and at the lowest pressure (2 MPa); \circ , \times , \blacktriangle , \blacksquare , \blacklozenge , experimental data; ----, predicted values.

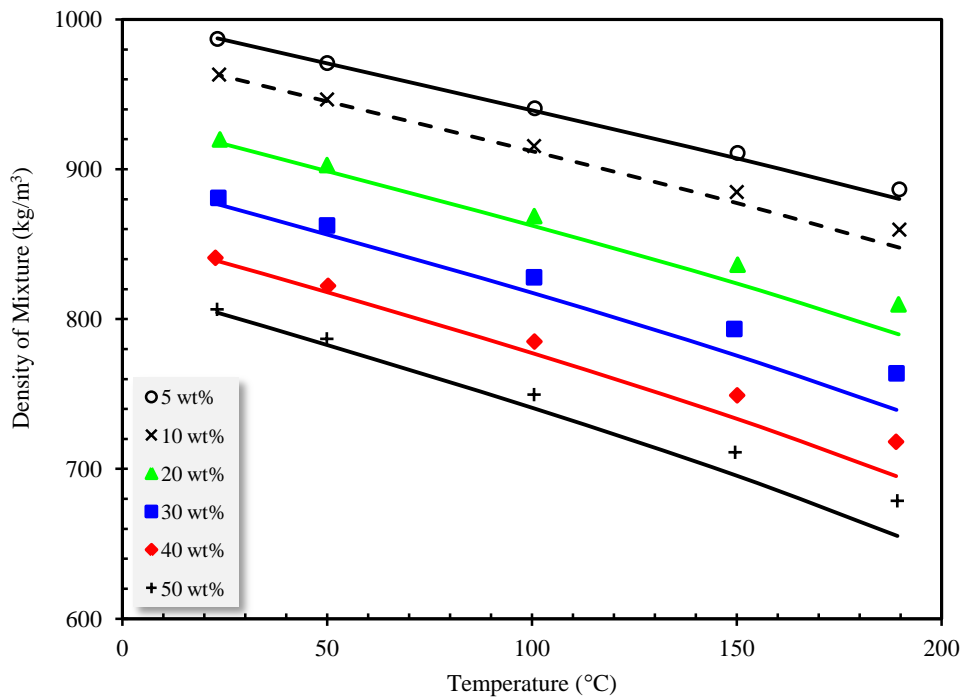


Figure 6-9: Density of Surmont bitumen / *n*-hexane mixtures as a function of temperature at different *n*-hexane weight fractions and at the highest pressure (10 MPa); \circ , \times , \blacktriangle , \blacksquare , \blacklozenge , $+$, experimental data; ----, predicted values.

6.3.2. Volume Change on Mixing

The properties of mixtures can often be relatively different than the species comprising the mixtures. When two species or components are mixed, the volume of the mixture can be different than the summation of the volumes of each component. That is, the total volume may increase or decrease when the mixing occurs. For chemically similar components such as toluene and benzene, the volume change upon mixing is negligible whereas for unlike components such as alcohols and water, a significant change in the volume during the mixing process was observed. Thus, the structure of materials and the co-operative accommodation of the molecules affect the volume change on mixing.

The petroleum fluids contain molecules with different sizes and structures and different densities; thus, the mixture of two separate compounds rarely shows no volume change upon mixing. The mixtures of Surmont bitumen and *n*-hexane were subjected to

the volume change on the mixing. Although the volume change on the mixing is not significant for moderate temperature and pressure changes, its value was changed with the operating parameters and solvent concentration. As the modelling results in previous section show, the assumption of no volume change for the calculation of the mixture densities resulted in the under-prediction of the measured data. This indicates that the mixtures of Surmont bitumen / *n*-hexane undergo a negative volume change on the mixing. That is, the total volume of the mixture reduces during the mixing process and reaching to the equilibrium state. The negative volume change on the mixing was observed for all measured data at different temperatures, pressures, solvent weight fractions.

The volume change upon mixing is calculated by

$$\Delta V_{\text{mixing}} = V_{\text{final,m}} - V_{\text{initial,B}} - V_{\text{initial,s}} \quad 6-2$$

The summation of the volumes of each component before mixing is called ideal volume and if the volume change on mixing be zero, the solution is known as ideal solution, thus,

$$V_{\text{ideal,mix}} = V_{\text{initial,B}} + V_{\text{initial,s}} \quad 6-3$$

As presented earlier, the value of volume change on the mixing was varied with the operating parameters. In order to evaluate the impact of different parameters on the volume change on mixing, the following dimensionless parameter is used,

$$\frac{\Delta V_{\text{mixing}}}{V_{\text{ideal,mix}}} = \frac{\frac{1}{\rho_{\text{m,exp}}} - \left(\frac{w_s}{\rho_s} + \frac{1-w_s}{\rho_B} \right)}{\frac{w_s}{\rho_s} + \frac{1-w_s}{\rho_B}} \quad 6-4$$

where w_s is the weight fraction of *n*-hexane, ρ_s and ρ_B are the densities of *n*-hexane and bitumen, respectively, and $\rho_{\text{m,exp}}$ is the measured density of mixture.

The predicted densities in previous section showed that at a constant pressure and a constant solvent weight fraction, the deviation between the measured data and the calculated values became significant with the increase in temperature. This is an indirect

representation of the increase in the volume change on the mixing with the temperature. However, if the calculated values from equation 6-4 is plotted with respect to the temperature at a constant pressure and a constant solvent weight fraction, it is found that the volume change upon mixing directly affected by the temperature. Figures 6–10 and 6–11 illustrate the dimensionless volume change as a function of temperature at a constant pressure. As depicted in these figures, volume change on mixing increases with the temperature. Although the extent of increase in volume change on mixing is not the same at different pressures, the increasing trend was observed for all measured pressures.

The effect of solvent weight fraction on the volume change on the mixing is also noticeable from Figures 6–10 and 6–11. The increase in the solvent weight fraction enhanced the volume change on the mixing for the mixtures. This trend was expected because the mixture of two components reaches to lower values of the volume change on the mixing at infinite dilution of each component.

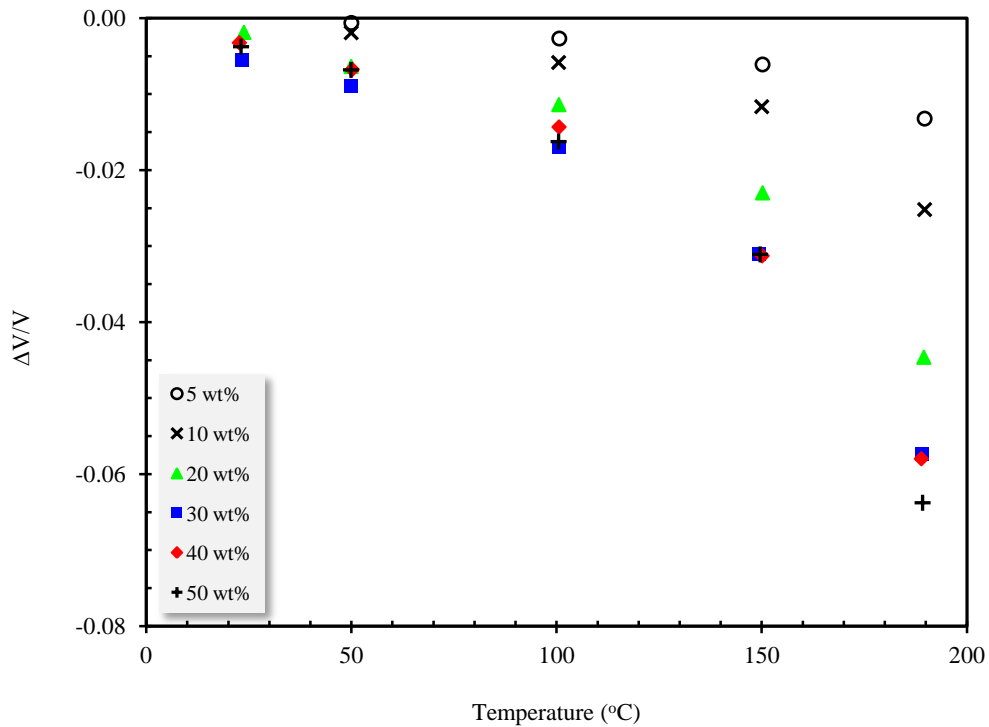


Figure 6–10: Effect of temperature on the volume change on mixing for Surmont bitumen / *n*-hexane mixtures with different solvent weight fractions at a constant pressure of 2 MPa.

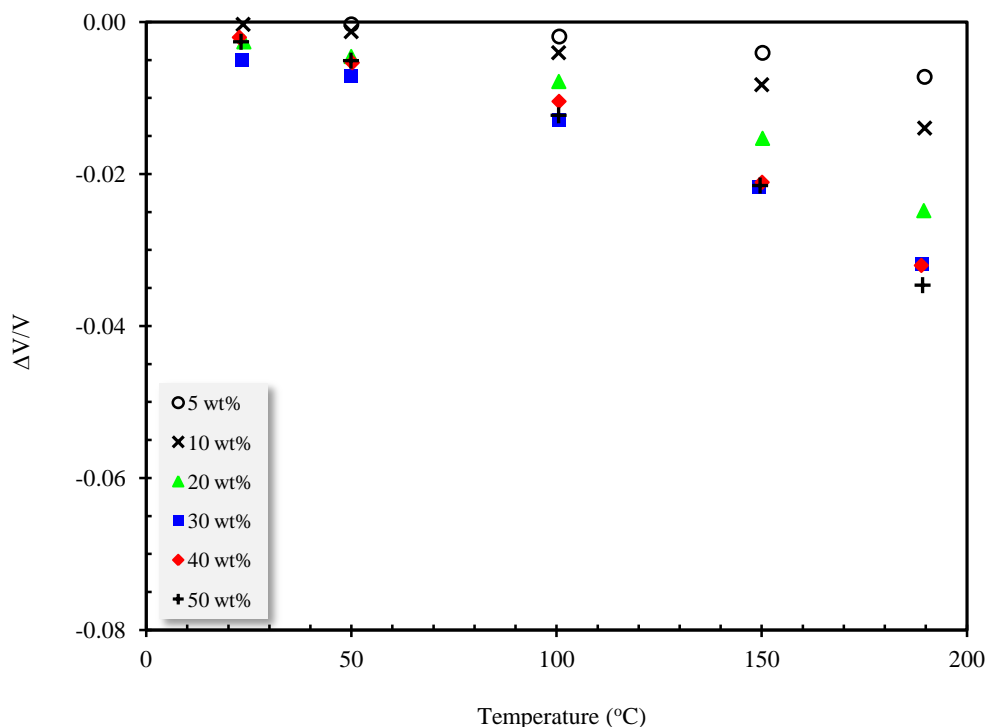


Figure 6–11: Effect of temperature on the volume change on mixing for Surmont bitumen / *n*-hexane mixtures with different solvent weight fractions at a constant pressure of 10 MPa.

The density of raw bitumen and pure *n*-hexane is a function of temperature and pressure. Thus, the volume of the components and its molecular behaviour was changed with the change in the operating conditions. The measured volume change on mixing reduced with the increase in the pressure at a constant temperature. This is due to a better arrangement of the *n*-hexane molecules in the bitumen molecules. As the pressure increases at a constant temperature, the density of raw bitumen as well as pure *n*-hexane was increased. The molecules of each component are made to come closer together with the increase in the pressure and consequently reduction in the occupied volume. At high pressure, less void space between bitumen and hexane molecules exists; thus, less number of molecules can occupy the void spaces during the mixing process.

The effect of pressure on the volume change on mixing at the lowest temperature (i.e. 23°C) is negligible and this behaviour was observed for all solvent weight fractions. As the temperature increases, the variation of the volume change on mixing with pressure

becomes significant. At two high temperatures (150 and 190°C), the volume change on mixing is noticeably observed for the mixtures. The variations are a non-linear function of pressure. Figure 6–12 illustrates the change in the volume during mixing process for Surmont bitumen / *n*-hexane mixtures at the highest temperature (190°C). The decreasing trend of the volume change on mixing with the pressure was observed at five different temperatures and six *n*-hexane weight fractions. The mixture of Surmont bitumen / *n*-hexane with 0.05 weight fraction of solvent exhibits a smaller pressure dependence than that of 0.5 weight fraction of solvent where a large decrease in the volume change on mixing is measured for a given pressure change at high *n*-hexane weight fraction.

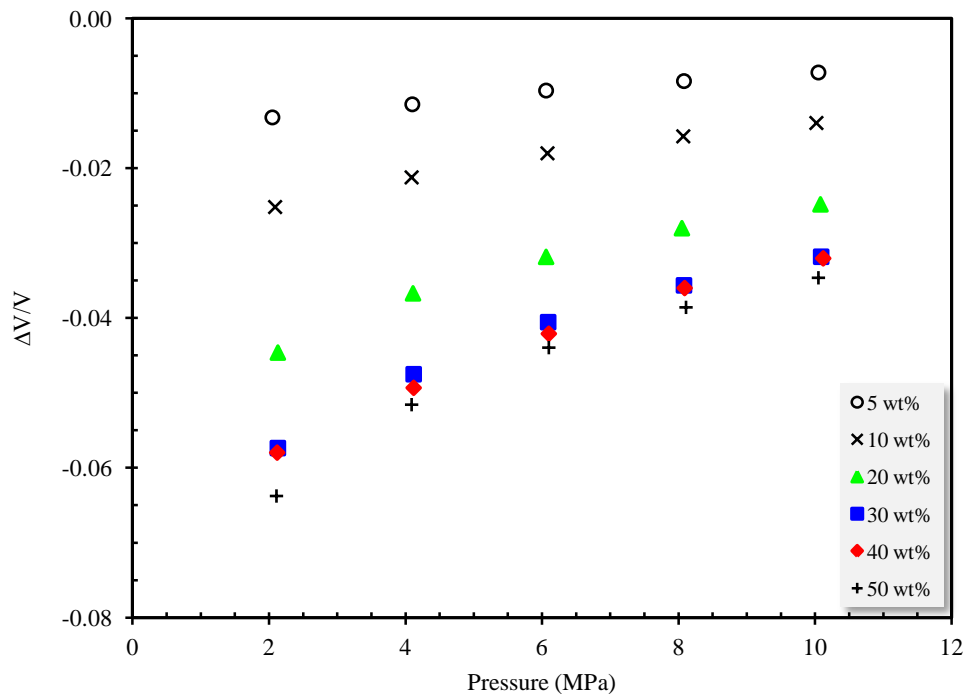


Figure 6–12: Effect of pressure on the volume change on mixing for Surmont bitumen / *n*-hexane mixtures with different solvent weight fractions at 190°C.

To evaluate the impact of temperature and pressure on the volume change on mixing, the volume change can be plotted as a function of pressure at different temperatures and at a constant weight fraction of hexane. It was observed that at hexane weight fraction of 0.05, the impact of pressure is not significant. However, increasing the solvent weight

fraction into 0.1 or 0.2, the variation of volume change on mixing with pressure becomes substantially important. Figure 6–13 demonstrates the volume change on mixing as a function of pressure at highest solvent weight fraction (0.5). As anticipated from the figure, the volume change on mixing at the ambient temperature (23°C) even at high solvent weight fractions is negligible. Thus, it can be concluded that at ambient temperature, the volume change on mixing for the mixtures of Surmont bitumen / *n*-hexane over the entire concentration range is insignificant and equation 6-1 can adequately predict the density of mixture.

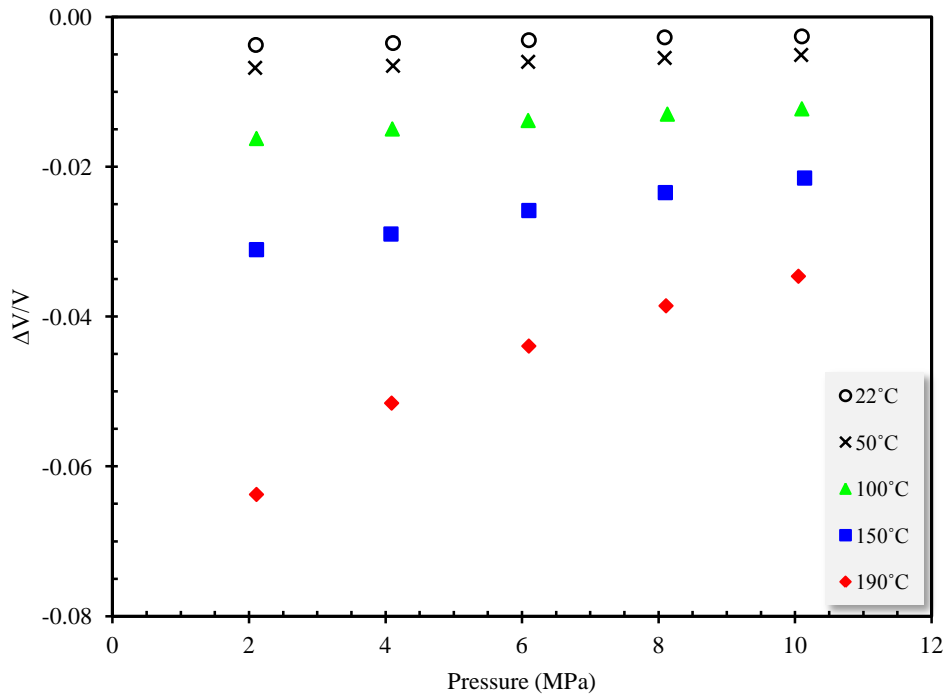


Figure 6–13: Effect of pressure on the volume change on mixing for Surmont bitumen / *n*-hexane mixtures at a constant solvent weight fraction of 0.5 and at different temperatures.

The volume change on mixing increases as the solvent weight fraction in the mixture increased. For some binary systems such as (*n*-hexane + *n*-decane), the volume change on mixing reaches to a minimum or maximum value at a specific concentration (Asfour et al. 1990). For the Surmont bitumen / *n*-hexane mixtures, the volume change on mixing increases with increasing the *n*-hexane weight fraction over the studied conditions. As it

was also previously mentioned, the mixtures show a negative volume change on the mixing. A negative value of volume change on mixing in the entire concentration range indicates the formation of more compact structure compared to the pure species. Figures 6–14 and 6–15 illustrate the volume change on mixing for the Surmont bitumen / *n*-hexane mixture as a function of solvent weight fraction at a constant pressure. Figure 6–14 shows the results at the pressure of 2 MPa and Figure 6–15 demonstrates the same measurements at the pressure of 10 MPa.

As depicted in the figures, the increase in the solvent weight fraction resulted in a larger value for the volume change on the mixing. The pressure reduces the volume change on the mixing at a constant temperature. Similar to the binary hydrocarbon systems, the pressure reduced the maximum value of the volume change on the mixing and forced the concave curve toward a zero value. As it was expected from the binary hydrocarbon mixtures, the volume change on mixing should be increased with the solvent weight fraction to a maximum and starts decreasing toward a zero value. However, as depicted in Figure 6–14 for the bitumen / *n*-hexane mixtures, the volume change on mixing flatten off after the *n*-hexane weight fraction of 0.3. It might be due to the asphaltene instability in the mixtures beyond this concentration. Escobedo and Mansoori (1995, 1997) observed a dramatic change on the viscosity of oil and *n*-alkane mixtures when the *n*-alkane concentration in the mixture increased stepwise without any observed asphaltene precipitation. They corresponded this behaviour to the flocculation of asphaltene particles in the mixture at a specific solvent concentration.

As the results of the measurements at 0.6 *n*-hexane weight fraction confirmed the visual observation of the asphaltene precipitation from the mixture, the observed behaviour in the plot of the volume change on the mixing with respect to the solvent weight fraction might be due to the flocculation of the asphaltene particles within the mixtures.

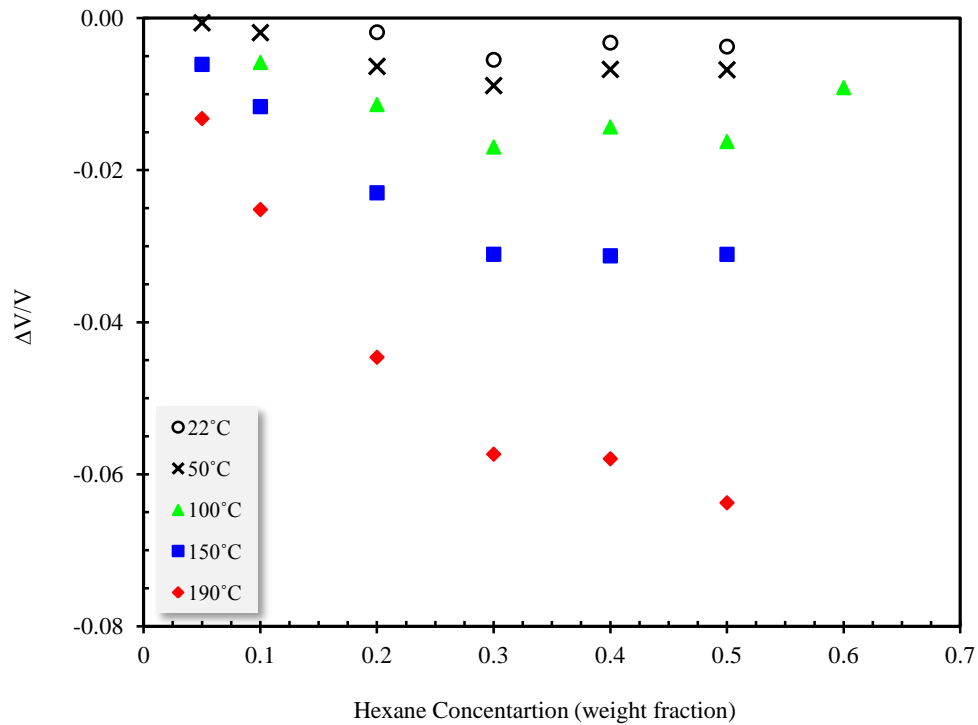


Figure 6-14: Volume change on mixing for Surmont bitumen / *n*-hexane mixtures as a function of the weight fraction of hexane at different temperatures and at a constant pressure of 2 MPa.

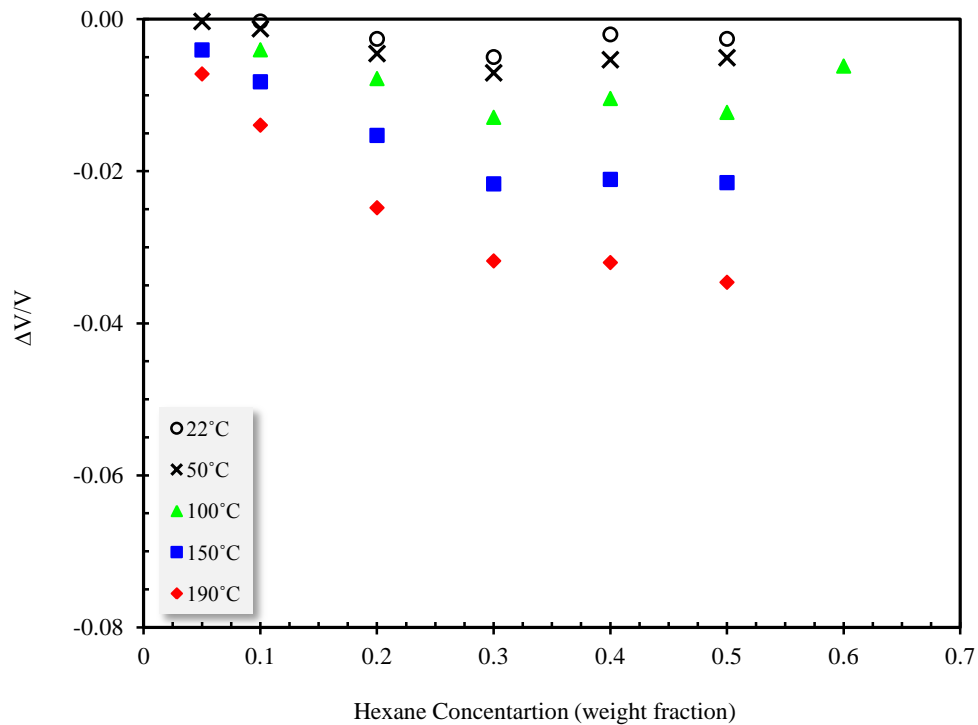


Figure 6-15: Volume change on mixing for Surmont bitumen / *n*-hexane mixtures as a function of the weight fraction of hexane at different temperatures and at a constant pressure of 10 MPa.

6.3.3. Improvement in Calculation of Mixture Density

The predicted densities from equation 6-1 resulted in an under-prediction of the measured data. As discussed earlier, the volume change on mixing for the Surmont bitumen / *n*-hexane mixtures is significant. In this section, two approaches to improve the calculation of the densities are presented. The first approach considers the excess volume in the prediction of the densities and the second approach applied the concept of effective liquid densities to represent the measured densities.

6.3.3.1. Excess Volume Mixing Rule

The measured density data of Surmont bitumen / *n*-hexane mixtures are correlated with the following equation (Saryazdi 2012),

$$\frac{1}{\rho_m} = \frac{w_s}{\rho_s} + \frac{1-w_s}{\rho_B} - w_s(1-w_s) \left[\frac{1}{\rho_s} + \frac{1}{\rho_B} \right] \beta_{ij} \quad 6-5$$

where w_s is the weight fraction of *n*-hexane, ρ_s and ρ_B are the densities of *n*-hexane and bitumen, respectively. The last term accounts for the volume change on mixing and β_{ij} is the binary interaction parameter between *n*-hexane and bitumen which is obtained by the regression of the measured data. The densities were correlated using the above equation, and the results were in agreement with measured data. The best fitted binary interaction parameter (β_{ij}) was 0.0265 which gave lowest AARD.

6.3.3.2. Effective Liquid Densities

The density of the mixtures with a dissolved gas can be predicted with equation 6-1 but using the effective liquid density for the gas. Tharanivasan et al. (2011) proposed a method based on the extrapolation of the molar volume of liquid normal alkanes to obtain the effective liquid molar volumes of light normal alkanes present in gaseous state in pure form. The authors plotted the molar volume of liquid normal alkanes with respect to the molecular weight and extrapolated the curve to determine the effective liquid molar

volumes of light normal alkanes. Tharanivasan et al. (2011) reported the effective liquid densities for normal alkanes at the pressures above 10 MPa.

Recently, Saryazdi (2012) found that the proposed correlation by Tharanivasan et al. (2011) resulted in larger values for the molar volumes of the *n*-alkanes when it was extrapolated to lightest hydrocarbons. Saryazdi (2012) explained this over-prediction by closeness of the *n*-alkanes to critical points and proposed to plot the molar volumes of only the higher *n*-alkanes with respect to molar mass. Saryazdi (2012) found that the molar volume trend in this case is linear and the author redeveloped the new effective density correlation using the molar volumes of the higher liquid *n*-alkanes whose molar volumes were linearly related to their molecular weight. Thus, the higher *n*-alkane molar volumes at fixed temperatures and pressures were extrapolated linearly to determine new effective molar volumes for the lighter *n*-alkanes (Saryazdi, 2012). The effective molar volumes were then converted to density and plotted versus pressure at fixed temperatures. Saryazdi (2012) proposed the following equation for the effective densities of *n*-hexane,

$$\rho = 901.512 - 0.80985T + (-0.142 + 2.6846 \times 10^{-3}T)P \quad 6-6$$

where ρ is density in kg/m^3 , T is temperature in Kelvin and P is pressure in MPa.

The measured densities of the Surmont bitumen / *n*-hexane were predicted using equation 6-1 along with the effective densities of *n*-hexane obtained using equation 6-6 and the results are quite well represented with this approach. The density of raw bitumen at each temperature and pressure given in Chapter 3 were used for the calculations. Table 6-4 summarizes the calculated deviations of the models for the prediction of mixture densities. As the deviations show, the best results are obtained with the effective liquid densities followed by excess volume mixing rule, and no volume change assumption.

Table 6-4: The deviations of different models for the calculation of Surmont bitumen / *n*-hexane mixture densities.

Calculation Method	AARD (%)	AAD (kg/m^3)	MAD (kg/m^3)
No volume change	1.36	10.5	43.0
Excess volume	0.92	7.2	33.9
Effective density	0.31	2.5	11.5

Figures 6–16 to 6–18 illustrate the dispersion plots of the calculated densities versus the measured values for the mixtures of Surmont bitumen / *n*-hexane using three different approaches. The excess volume mixing rule slightly improves the predictions compared to the method with the assumption of no volume change on mixing. Considering effective liquid densities for *n*-hexane significantly improve the predictions.

Figures 6–19 and 6–20 display the measured densities for the mixtures of Surmont bitumen / *n*-hexane along with the calculated values. In Figure 6–19, the density is plotted as a function of *n*-hexane weight fraction at different temperatures and at a constant pressure (2 MPa). Figure 6–20 illustrates the impact of pressure on the mixture density at different solvent weight fractions and at the temperature of 190°C. As anticipated from the figures, the application of effective liquid densities for the prediction of mixture densities resulted in a close agreement between the measured data and calculated ones. Although the excess volume mixing rule with one adjustable parameter slightly improve the correlations, the calculated values at high temperature and high solvent weight fractions still far from the experimental data.

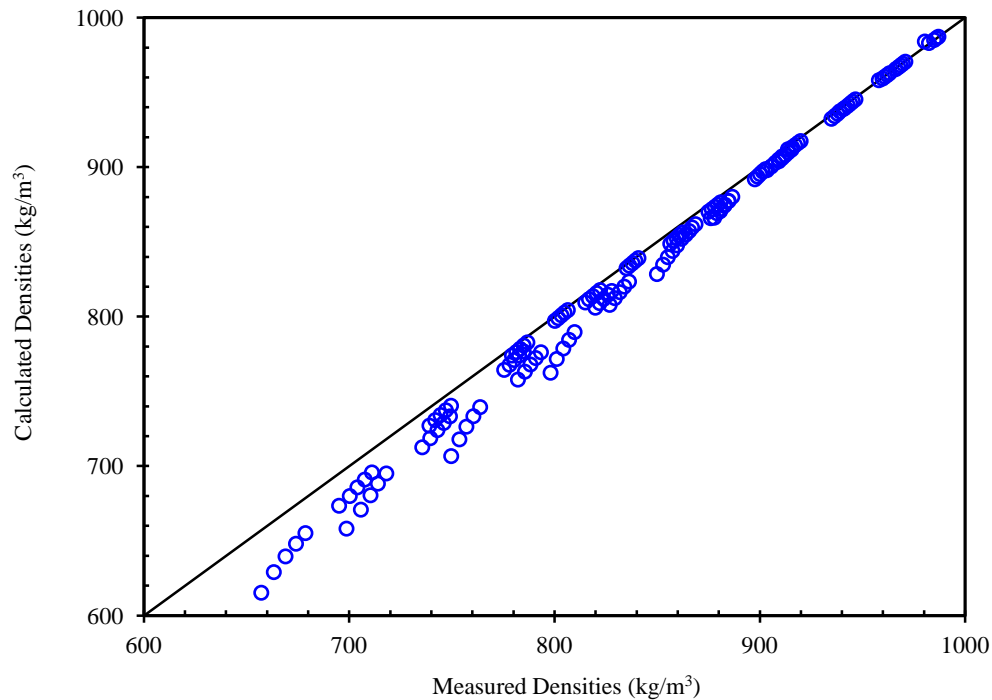


Figure 6–16: Calculated densities of Surmont bitumen / *n*-hexane mixtures using no volume change on mixing assumption versus the measured values.

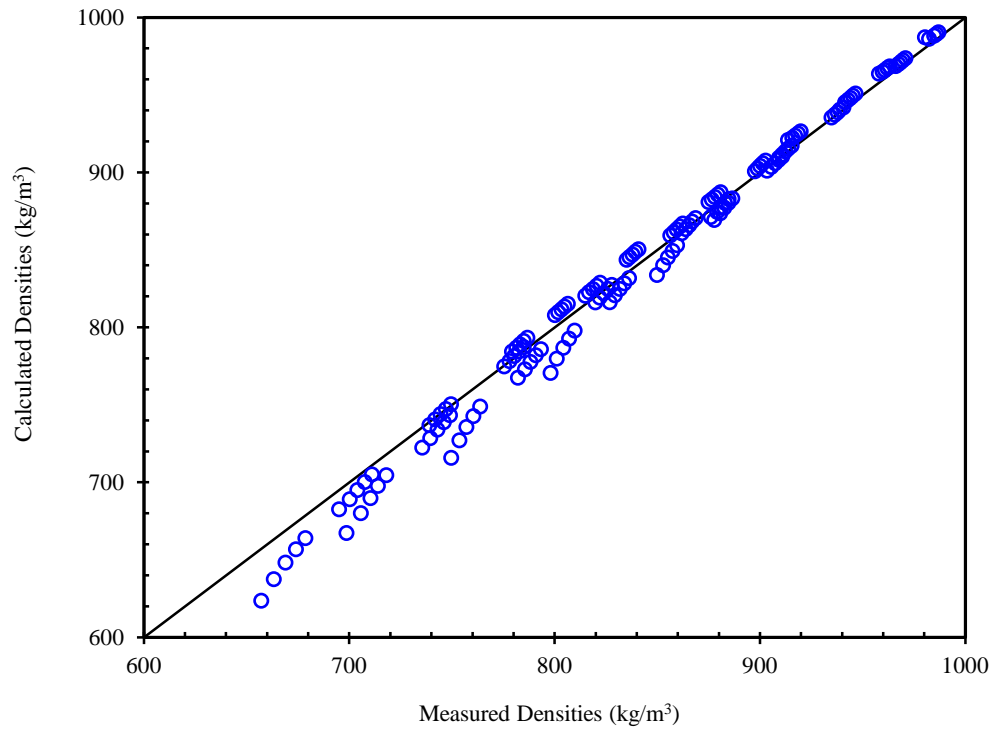


Figure 6–17: Calculated densities of Surmont bitumen / *n*-hexane mixtures using excess volume mixing rule versus the measured values.

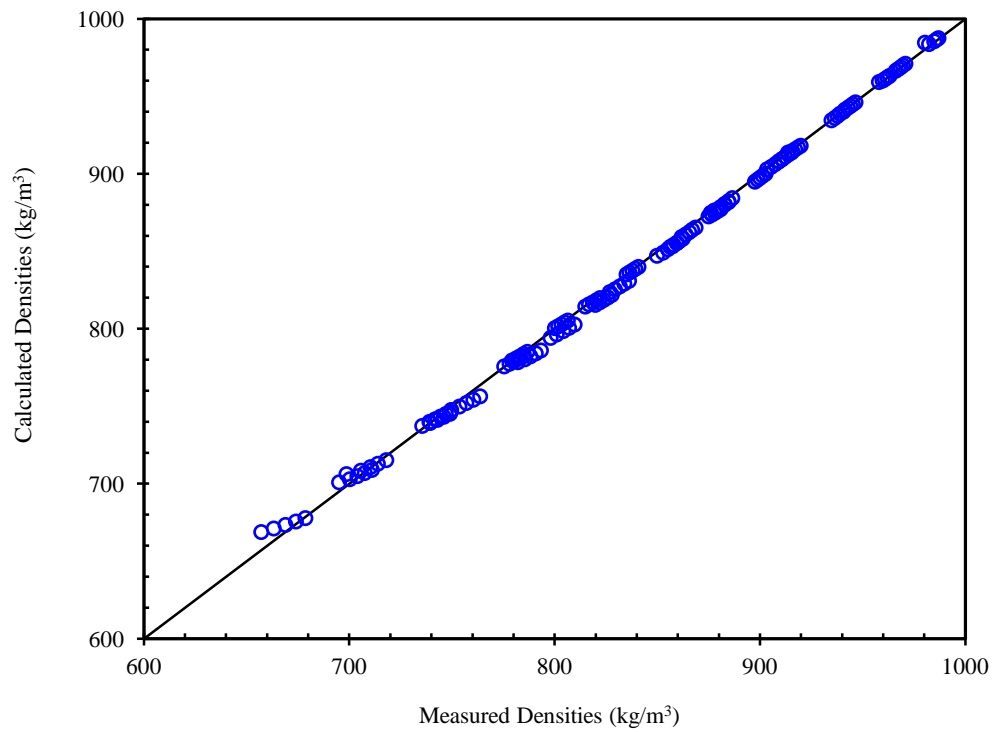


Figure 6–18: Calculated densities of Surmont bitumen / *n*-hexane mixtures using effective liquid densities versus the measured values.

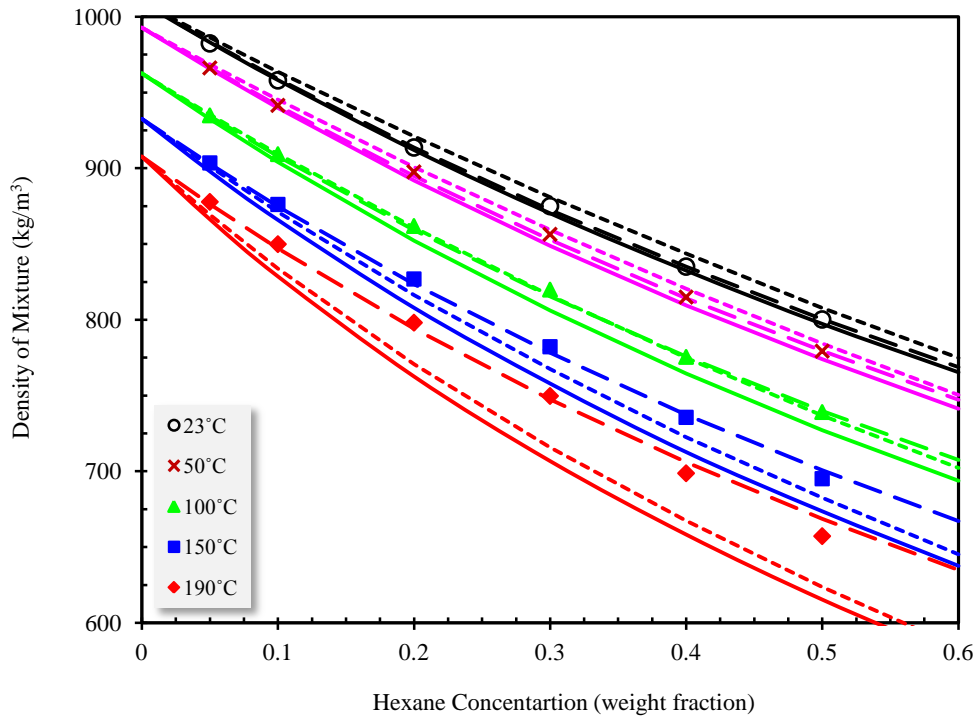


Figure 6-19: Density of Surmont bitumen / *n*-hexane mixtures as a function of the weight fraction of *n*-hexane at different temperatures and at a constant pressure of 2 MPa; ■, ▲, ○, ◆, ×, experimental data; —, no volume change on mixing; ----, excess volume mixing rule; — · —, effective liquid densities.

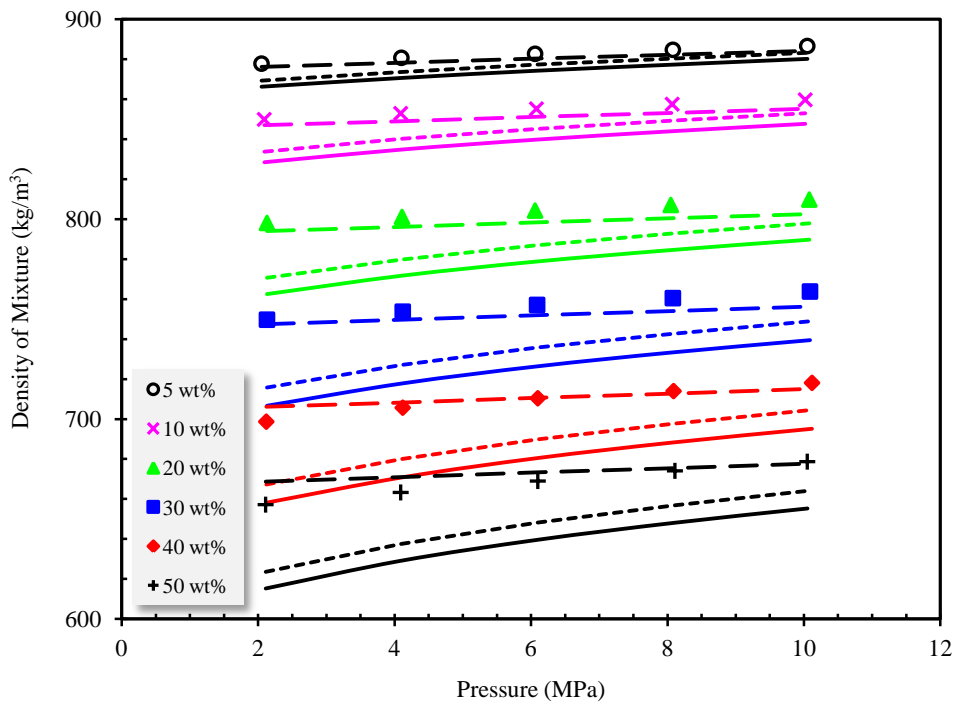


Figure 6-20: Density of Surmont bitumen / *n*-hexane mixtures as a function of pressure at different *n*-hexane weight fractions and at the highest temperature (190°C); ○, ×, ▲, ■, ◆, +, experimental data; —, no volume change on mixing; ----, excess volume mixing rule; — · —, effective liquid densities.

6.4. Viscosity of Mixtures

Tables 6–5 to 6–7 summarize the experimental viscosity values of the pseudo-binary mixture, Surmont bitumen / *n*-hexane, at different temperatures, pressures, and solvent weight fractions. The viscosity of the mixture is reduced with temperature and increased with the pressure. The solvent weight fraction significantly decreases the viscosity of the mixture. The viscosity of pure *n*-hexane and raw bitumen is also reduced with the temperature and increased with the pressure.

The impact of pressure on the mixture viscosity is more pronounced at lower *n*-hexane weight fractions. This behaviour is expected; because, as the weight fraction of solvent increases, the behaviour of mixture is more similar to pure *n*-hexane. The data on the viscosity of pure *n*-hexane (NIST database) indicate that the viscosity of *n*-hexane is not significantly affected by the pressure due to simple structure of *n*-hexane compared to bitumen. However, a stronger functionality between bitumen viscosity and pressure exists. Thus, any mixture prepared from the species of bitumen and *n*-hexane shows a behaviour similar to bitumen at low *n*-hexane weight fraction. The impact of pressure on the mixture viscosity is also dependent on the temperature. That is, at lower temperatures, the pressure results in higher viscosity variations.

It is worth to mention that the impact of pressure on the viscosity of pure *n*-hexane is more pronounced at high temperature conditions (i.e. 150 and 190°C). The critical temperature of *n*-hexane is 235°C and as the experimental temperature increased toward the critical point, the variation of *n*-hexane viscosity with the pressure becomes more significant.

Table 6–5: Experimental liquid viscosities of Surmont bitumen / *n*-hexane mixtures at 0.05 and 0.1 weight fractions of hexane; *T*, temperature; *P*, pressure; μ_m , viscosity of mixture.

<i>w</i> = 0.05			<i>w</i> = 0.1		
<i>T</i> (°C)	<i>P</i> (MPa)	μ_m (mPa.s)	<i>T</i> (°C)	<i>P</i> (MPa)	μ_m (mPa.s)
190.5	2.05	5.29	189.5	2.09	3.36
190.5	4.10	5.45	190.0	4.09	3.44
190.6	6.06	5.64	190.0	6.08	3.52
190.6	8.08	5.83	190.0	8.07	3.65
190.7	10.05	6.04	190.0	10.02	3.83
151.7	2.11	12.5	151.0	2.07	6.89
151.7	4.05	13.1	151.0	4.10	6.91
151.6	6.12	13.9	151.0	6.08	7.21
151.7	8.09	14.1	151.3	8.10	7.43
151.7	10.11	14.6	151.0	10.06	7.52
102.5	2.04	63.9	102.5	2.04	26.4
102.5	4.09	66.4	102.5	4.08	27.7
102.5	6.09	69	102.5	6.10	28.8
102.6	8.12	71.4	102.5	8.08	29.8
102.7	10.07	74.3	102.6	10.11	30.8
53.5	2.06	927	53.0	2.09	231
53.5	4.14	990	53.0	4.16	244
53.2	6.12	1064	53.0	6.09	260
53.3	8.06	1129	53.0	8.10	266
53.5	10.11	1197	53.0	10.09	280
27.7	2.04	6618	27.5	2.05	1570
27.0	4.07	9931	27.5	4.15	1811
27.5	6.17	11070	27.5	6.09	1943
27.7	8.11	11910	27.5	8.09	2047
27.9	10.09	12920	27.8	10.08	2205

Table 6–6: Experimental liquid viscosities of Surmont bitumen / *n*-hexane mixtures at 0.2 and 0.3 weight fractions of hexane; *T*, temperature; *P*, pressure; μ_m , viscosity of mixture.

<i>w</i> = 0.2			<i>w</i> = 0.3		
<i>T</i> (°C)	<i>P</i> (MPa)	μ_m (mPa.s)	<i>T</i> (°C)	<i>P</i> (MPa)	μ_m (mPa.s)
190.0	2.13	1.81	190.0	2.13	0.931
190.0	4.11	1.89	190.0	4.12	0.969
190.0	6.06	1.93	190.0	6.09	1.01
190.1	8.05	1.96	190.0	8.08	1.04
190.2	10.08	2.00	190.0	10.09	1.06
151.5	2.08	2.81	150.5	2.09	1.36
151.5	4.09	2.87	150.5	4.09	1.40
151.5	6.10	2.96	150.5	6.09	1.45
151.5	8.08	3.04	150.5	8.08	1.49
151.5	10.08	3.12	150.5	10.07	1.54
102.5	2.06	6.94	102.7	2.09	3.00
102.5	4.10	7.06	102.7	4.09	3.07
102.5	6.10	7.30	102.7	6.09	3.16
102.5	8.10	7.37	102.7	8.12	3.25
102.5	10.08	7.64	102.7	10.11	3.36
52.5	2.03	36.4	52.4	2.11	10.7
52.5	4.09	38.4	52.5	4.11	11.0
52.5	6.08	39.5	52.5	6.07	11.3
52.5	8.08	41.3	52.5	8.09	11.7
52.5	10.11	42.5	52.5	10.09	12.0
28.5	2.05	98.8	27.7	2.09	24.7
28.5	4.10	113	27.7	4.09	26.3
28.5	6.09	121	27.7	6.11	27.4
28.5	8.08	128	27.7	8.08	28.4
28.5	10.14	134	27.7	10.13	29.4

Table 6–7: Experimental liquid viscosities of Surmont bitumen / *n*-hexane mixtures at 0.4 and 0.5 weight fractions of hexane; *T*, temperature; *P*, pressure; μ_m , viscosity of mixture.

<i>w</i> = 0.4			<i>w</i> = 0.5		
<i>T</i> (°C)	<i>P</i> (MPa)	μ_m (mPa.s)	<i>T</i> (°C)	<i>P</i> (MPa)	μ_m (mPa.s)
189.5	2.12	0.423	190.0	2.11	0.318
188.0	4.12	0.483	190.0	4.09	0.325
189.5	6.10	0.490	190.0	6.10	0.334
189.5	8.09	0.504	190.0	8.11	0.345
189.5	10.12	0.514	190.0	10.05	0.351
151.7	2.09	0.718	149.6	2.11	0.496
151.3	4.09	0.770	150.1	4.08	0.52
151.6	6.10	0.780	150.5	6.10	0.518
151.7	8.08	0.790	151.0	8.10	0.522
151.7	10.08	0.841	151.3	10.14	0.507
103.0	2.09	1.37	102.4	2.11	0.845
103.0	4.09	1.42	102.7	4.10	0.867
103.0	6.09	1.44	102.9	6.09	0.892
103.0	8.10	1.47	102.9	8.13	0.853
103.0	10.08	1.52	103.0	10.10	0.864
53.3	2.06	3.57	52.6	2.09	1.79
53.3	4.12	3.65	53.0	4.11	1.78
53.3	6.04	3.80	53.0	6.09	1.82
53.3	8.08	3.80	53.0	8.09	1.88
53.3	10.09	3.90	53.0	10.09	1.92
26.5	2.09	8.01	28.7	2.10	2.97
27.0	4.09	8.24	28.7	4.11	3.03
27.3	6.08	8.75	28.7	6.10	3.11
27.8	8.10	7.92	28.7	8.09	3.14
28.0	10.10	7.84	28.7	10.10	3.22

6.4.1. Correlation and Prediction of Mixture Viscosity

The measured viscosity data of *n*-hexane and Surmont bitumen mixtures were also evaluated with relationships developed for the mixtures. These relationships were mostly developed for light and medium oils diluted with solvents. Centeno et al. (2011) summarized a total of 26 mixing rules and classified them according to the number and type of parameters and the information required for each relationship. In this study, we have evaluated four prediction schemes, Arrhenius', Cragoe's, Shu's, and Lobe's models, and two correlations, Lederer's and power law models. These models were commonly used for heavy oil / solvent mixtures.

Arrhenius' model (Arrhenius 1887) or log-type mixing rule is commonly used in the reservoir simulators to predict the viscosity of oil-blended mixtures and the equation is,

$$\mu_m = \mu_s^{x_s} \times \mu_B^{(1-x_s)} \quad 6-7$$

or in the log-form,

$$\ln \mu_m = x_s \ln \mu_s + (1 - x_s) \ln \mu_B \quad 6-8$$

where, x_s is mole fraction of solvent, μ_s and μ_B are the viscosities of solvent and bitumen, respectively.

The power law model is based on the Kendall model, in which the viscosity of mixture is directly dependent on the concentration,

$$\mu_m = \left[x_s \mu_s^n + (1 - x_s) \mu_B^n \right]^{\frac{1}{n}} \quad 6-9$$

where the exponent n is the adjustable parameter in this correlation, x_s is the mole fraction of solvent, and μ_s and μ_B are the viscosities of solvent and bitumen, respectively. In the Kendall-Monroe model (Kendall and Monroe 1917), a value of 1/3 was considered for the exponent n while the Bingham model (Bingham 1918) represent the mixture viscosity data with $n = -1$.

Cragoe (1933) developed a linear mixing rule for the mixture of petroleum oils as,

$$\frac{1}{\ln(2000\mu_m)} = \frac{w_s}{\ln(2000\mu_s)} + \frac{1-w_s}{\ln(2000\mu_B)} \quad 6-10$$

where, w_s is the weight fraction of solvent, μ_s and μ_B are the viscosities of solvent and bitumen, respectively.

Lederer (1933) proposed a modified version of classic log-type viscosity mixing rule as,

$$\ln \mu_m = \left(1 - \frac{\theta\varphi_B}{\theta\varphi_B + \varphi_s}\right) \ln \mu_s + \left(\frac{\theta\varphi_B}{\theta\varphi_B + \varphi_s}\right) \ln \mu_B \quad 6-11$$

where θ is an adjustable parameter having values between 0 and 1, and φ_s and φ_B are the volume fractions of solvent and bitumen, respectively. Shu (1984) developed a method to calculate the constant θ as,

$$\theta = \frac{17.04(\rho_B - \rho_s)^{0.5237} \rho_B^{3.2745} \rho_s^{1.6316}}{\ln\left(\frac{\mu_B}{\mu_s}\right)} \quad 6-12$$

where ρ_s and ρ_B are the densities of solvent and bitumen, respectively. Shu (1984) showed that the model could determine the viscosity of heavy oils, bitumen and petroleum fractions. The model has been shown to provide good viscosity estimations over a wide range of data. However, the equation requires density values which create further computational work and introduce more experimental error. In this study, the densities of solvent and bitumen were also measured, thus there is no restriction for applying Shu's prediction scheme.

Lobe (1973) proposed a correlation for prediction of kinematic viscosities of a binary mixture composed of a solvent and oil as,

$$\nu_m = \varphi_s \nu_s \exp(\eta_B \varphi_B) + \varphi_B \nu_B \exp(\eta_s \varphi_s) \quad 6-13$$

where φ_s and φ_B are the volume fractions of solvent and bitumen, and ν_s and ν_B are the kinematic viscosities of solvent and bitumen, respectively. Lobe proposed the following expressions for the η_s and η_B ,

$$\eta_s = -1.7 \ln \left[\frac{\nu_B}{\nu_s} \right] \quad 6-14$$

$$\eta_B = 0.27 \ln \left[\frac{\nu_B}{\nu_s} \right] + \left(1.3 \ln \left[\frac{\nu_B}{\nu_s} \right] \right)^{\frac{1}{2}} \quad 6-15$$

These equations were obtained using the experimental data for many binary mixtures.

Table 6–8 summarizes the AARDs of the calculated viscosity values using six aforementioned models for the Surmont bitumen / *n*-hexane mixtures. In this study, the fraction of solvent was considered as mole, weight, and volume fractions in Arrhenius', power law, and Cragoe's models. Arrhenius' model results in better predictions when the mole fraction is considered in the models. Cragoe's and power law models give the best results with the volume fraction. The adjustable parameters in the models were obtained by minimizing the AARD of the calculated values and measured ones. Although the minimization of the sum of squared residuals (SSR) resulted in less scattered data, the AARDs are bigger than the case that the AARDs are minimized.

Table 6–8: Calculated AARDs of different models for the correlation and prediction of the viscosity for Surmont bitumen / *n*-hexane mixtures.

Model	AARD (%)		
	Mole fraction	Weight fraction	Volume fraction
Arrhenius	46.6	4388	1329
Power Law	43.6 ^a	28.8 ^b	12.3 ^c
Cragoe	82.9	189	30.3
Lederer	----	----	44.5 ($\theta = 0.2869$)
Shu	----	----	60.4
Lobe	----	----	107

^a $n = 0.0186$; ^b $n = -0.3365$; ^c $n = -0.2049$

Nourozieh et al. (2013) reported the experimental viscosity of Athabasca bitumen / *n*-decane mixtures and represented the data with different models. They found that the Arrhenius' and power law models led to better results when the mole fraction was considered. Cragoe's model gave best results with the volume fractions. Barrufet and Setiadarma (2003) also found that the use of mole fractions in Arrhenius' and power law

models provides the lowest absolute errors for the entire composition range in their study of heavy oil and *n*-decane mixtures.

Figure 6–21 shows the comparison between the Arrhenius’ model and the measured viscosity data using three different solvent fractions (i.e. mole, weight, and volume). The best predictions are obtained with considering the mole fraction in the model. When the viscosities are calculated on the basis of the weight and volume fraction, the predicted values are basically greater than the experimental data. When the viscosities of the mixture is less than 1000 mPa.s, the Arrhenius’ model (mole basis) under-predicts the experimental data while for the viscosities greater than 1000 mPa.s, the calculated values are slightly over-predicted.

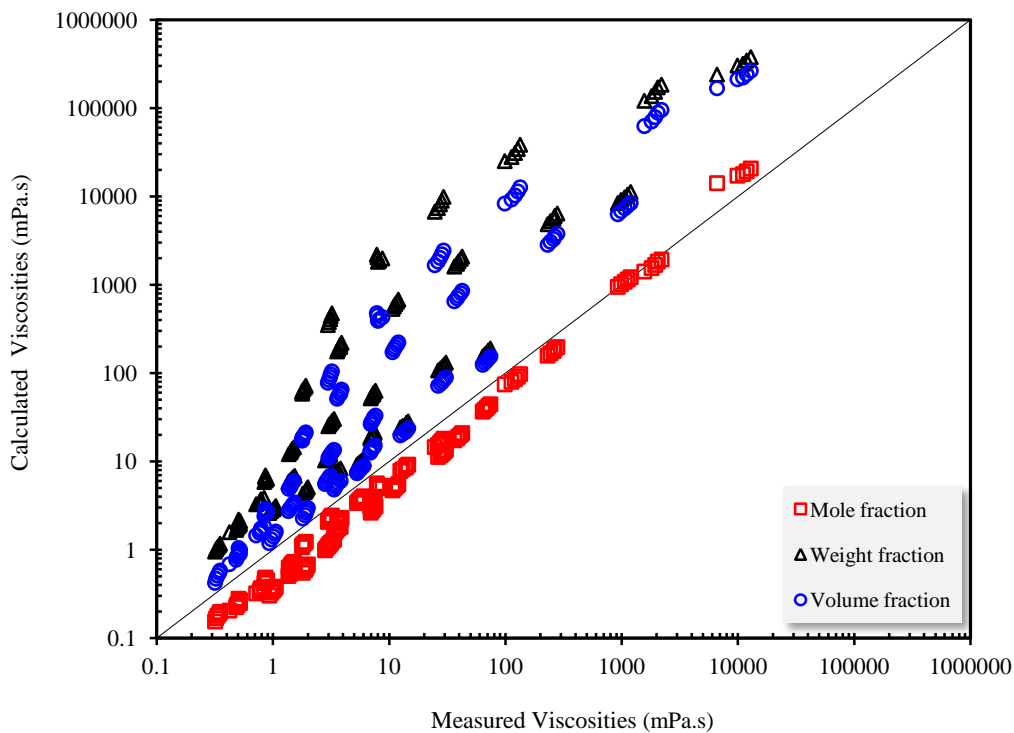


Figure 6–21: The comparison between the calculated viscosities with Arrhenius’ model and experimental data for Surmont bitumen / *n*-hexane mixtures.

Figure 6–22 illustrates the comparison between the power law model and the measured data using different fraction basis. In this model, the parameter (*n*) was adjusted for each fraction basis and the best fitted parameter is listed in Table 6–8. Although the

predictions using weight and mole fractions are reasonable, the best predictions are obtained with considering the volume fraction in the model. A comparison shows that AARD of power law model with the volume fraction is 12.3% while AARDs are 43.6% and 28.8% for mole and weight fractions basis, respectively.

Similar to the Arrhenius model, the power law model (with mole fraction) under-predicts the viscosities in the range (0.1 to 1000) mPa.s and over-predicts the data when the viscosities of the mixtures are greater than about 1000 mPa.s. Opposite to the Arrhenius model, the power law model with the weight fraction mostly under-predicts the viscosities over the entire range.

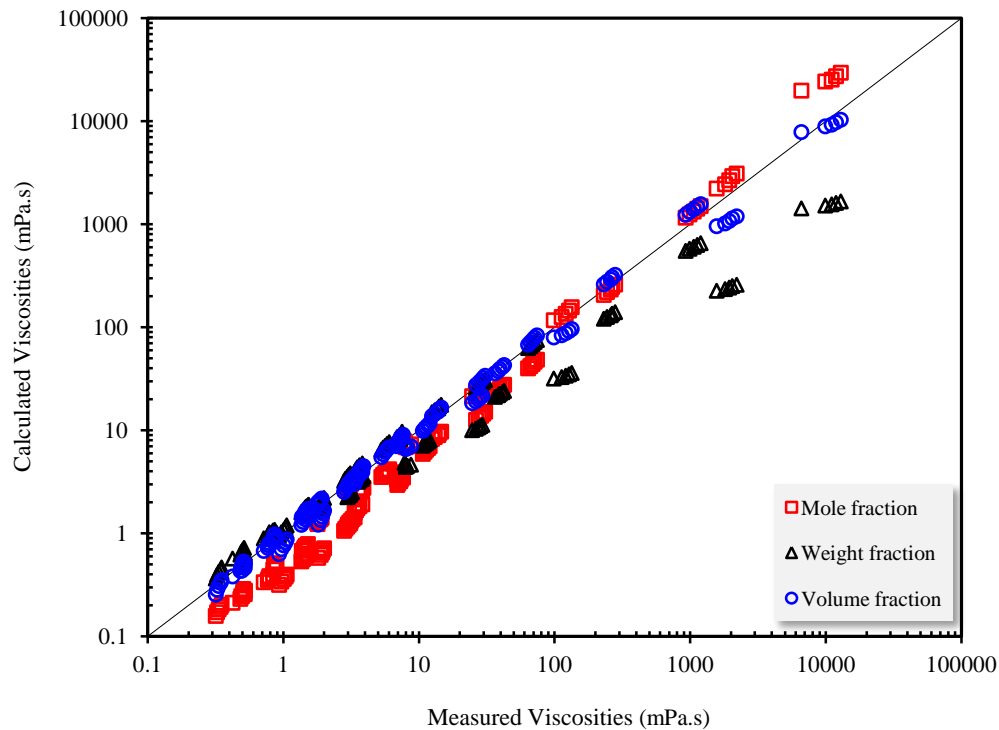


Figure 6–22: The comparison between the calculated viscosities with power law model and experimental data for Surmont bitumen / *n*-hexane mixtures.

The comparison between the Cragoe’s model and the measured viscosity data is shown in Figure 6–23. Similar to the power law model, the best predictions are obtained with considering the volume fraction in the model. The calculated values with the Cragoe’s model with the mole fraction are generally smaller than the experimental

viscosity data whereas the calculated results with the weight fraction are greater than the measured data. The errors for both cases are too big; a comparison shows that AARD of Cragoe's model with the volume fraction is 30.3% while AARDs are 82.9% and 189% for mole and weight fractions basis, respectively.

The calculated viscosities of the Cragoe's model with the volume fraction are slightly greater than the experimental data when the viscosities of the mixture are greater than 100 mPa.s. In the viscosity range of (0.1 to 100) mPa.s, the model adequately predicts the experimental viscosity data.

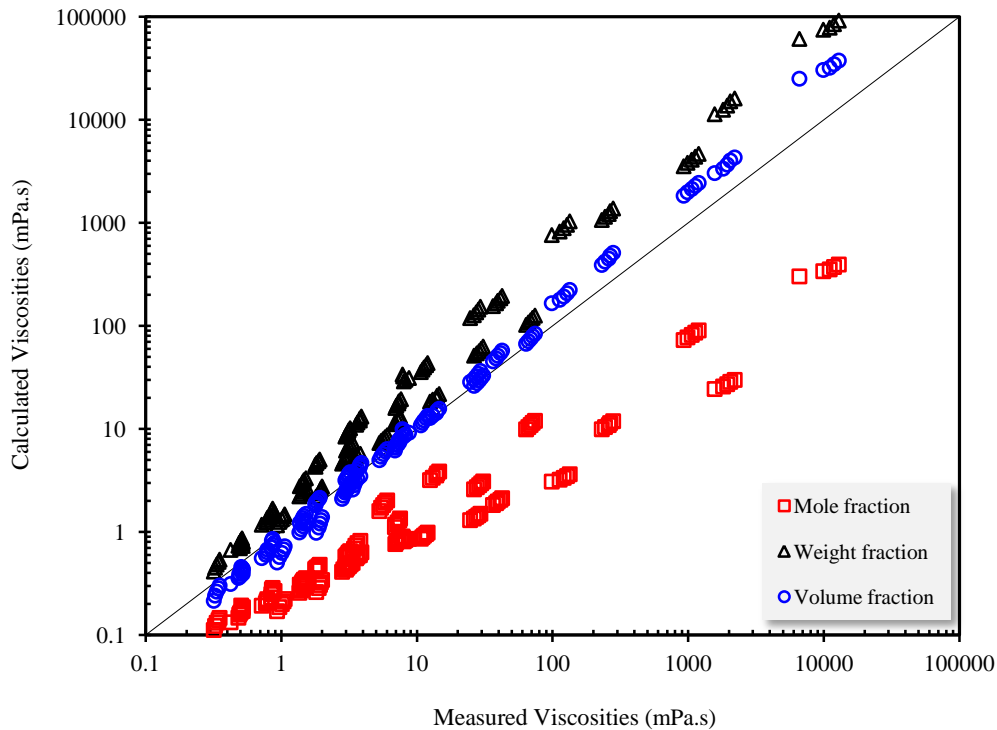


Figure 6–23: The comparison between the calculated viscosities with Cragoe's model and experimental data for Surmont bitumen / *n*-hexane mixtures.

Figures 6–24 to 6–26 illustrate the calculated results using Lederer's, Shu's, and Lobe's models compared to experimental viscosity data, respectively. The adjustable parameter for Lederer's model was obtained by regression of all data as $\alpha = 0.2869$ (coefficient in Lederer's model). As depicted in the figures, the Lederer's model could not predict the results well over wide range of viscosity data; the model under-predicts

the data for the viscosities less than 100 mPa.s and over-predicts the measured values for the viscosities greater than 100 mPa.s. Shu's and Lobe's models provide good predictions for the viscosities less than 100 mPa.s while the results show large deviations for the viscosities greater than 100 mPa.s.

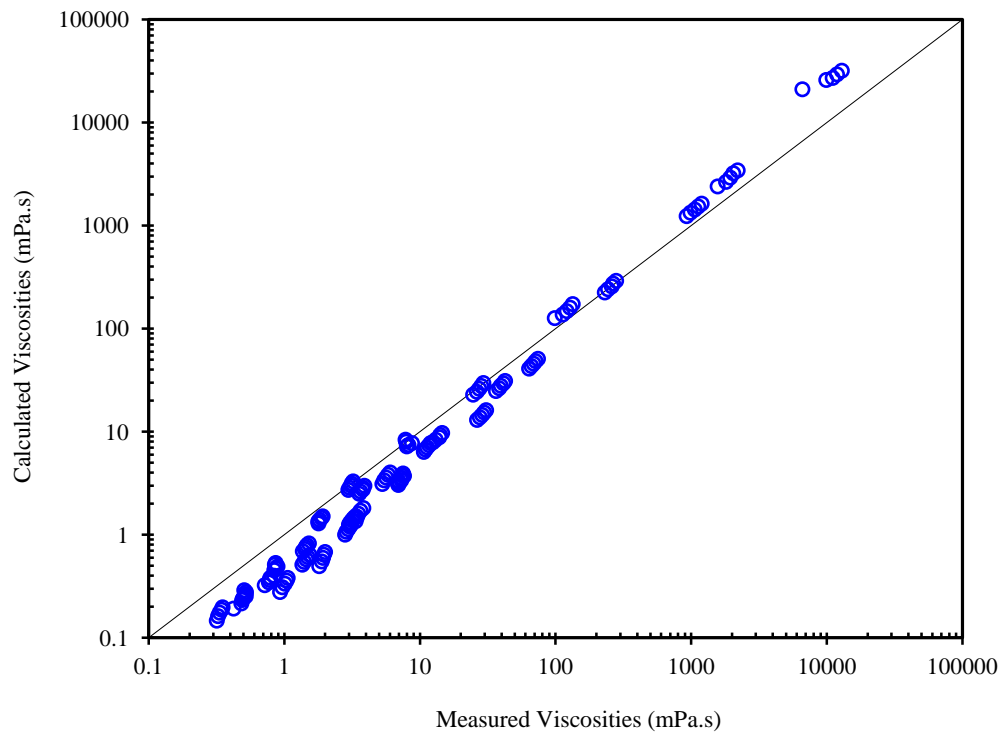


Figure 6–24: The comparison between the calculated viscosities with Lederer's model and experimental data for Surmont bitumen / *n*-hexane mixtures.

As it is difficult to distinguish the results of the models, the comparison was confined to the AARDs. A comparison on the basis of AARDs shows that Lederer's model provided better correlations and could fit the data better than Shu's, and Lobe's models. The AARD of Lederer's model is 44.5% while the AARDs are 60.4% and 107% for Shu's and Lobe's models, respectively.

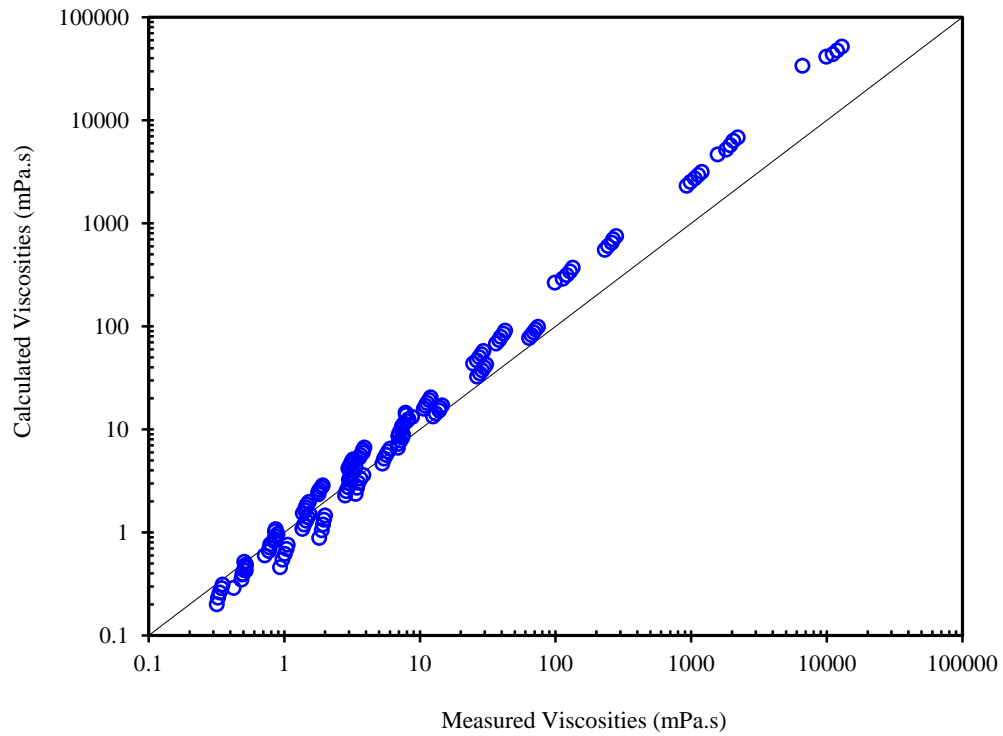


Figure 6–25: The comparison between the calculated viscosities with Shu’s model and experimental data for Surmont bitumen / *n*-hexane mixtures.

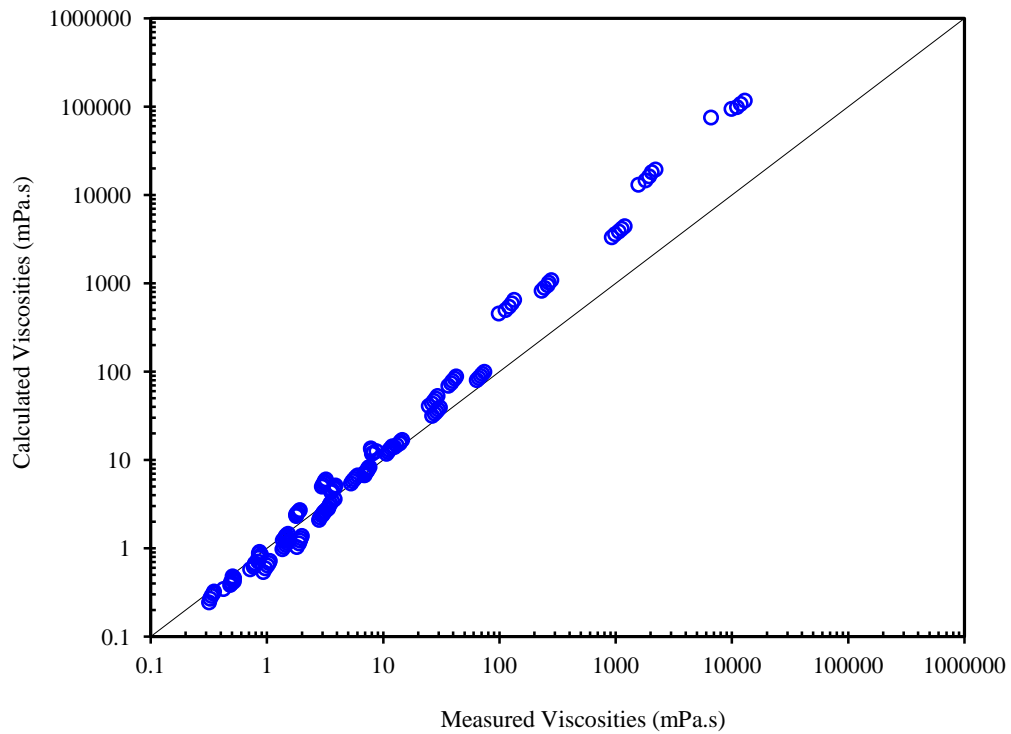


Figure 6–26: The comparison between the calculated viscosities with Lobe’s model and experimental data for Surmont bitumen / *n*-hexane mixtures.

From the calculated AARDs in Table 6–8, it can be concluded that the models predict the experimental viscosity data of Surmont bitumen / *n*-hexane mixtures well over the entire range in the following order,

1. power law (volume)
2. power law (weight)
3. Cragoe (volume)
4. power law (mole)
5. Lederer
6. Arrhenius (mole)
7. Shu
8. Cragoe (mole)
9. Lobe

Due to better correlations of the results with power law and Cragoe’ models using the volume fraction, these two models were compared with experimental data to analyze the data and find the trends. The results obtained by the power law model are shown by solid lines in the figures and the dashed lines represent the results of Cragoe’ model. The temperature values reported in each figure are the average values.

Figures 6–27 and 6–28 illustrate the effect of increasing *n*-hexane weight fraction on the mixture viscosity at different temperatures in semi-log scale. Figure 6–27 shows the results at the lowest pressure (2 MPa) and Figure 6–28 displays the same data at the highest pressure (10 MPa). As presented in these figures, the viscosity of mixture shows a non-linear trend with respect to solvent weight fraction. The impact of temperature on the viscosity of mixture was less pronounced at higher *n*-hexane concentrations. It could be due to the temperature dependency of bitumen and *n*-hexane viscosities. At low *n*-hexane concentrations, the mixtures behave more similar to the bitumen; thus, the mixture shows higher temperature dependency.

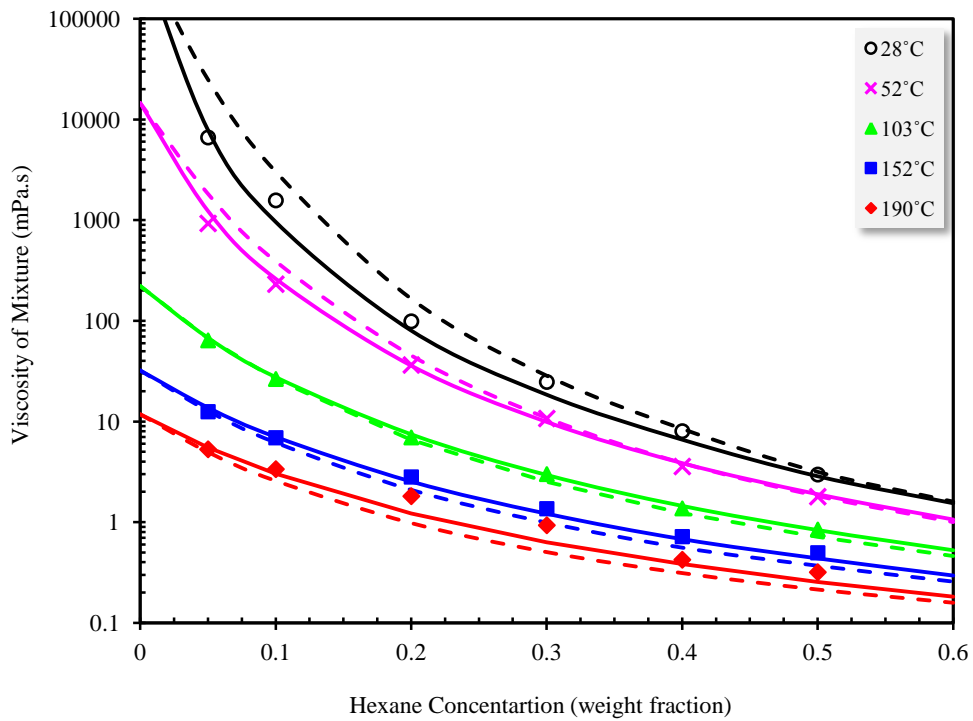


Figure 6–27: Viscosity of Surmont bitumen / *n*-hexane mixtures as a function of the weight fraction of *n*-hexane at different temperatures and at a constant pressure of 2 MPa; ○, ×, ▲, ■, ◆, measured viscosities; calculated values: —, power law model; - - -, Cragoe's model.

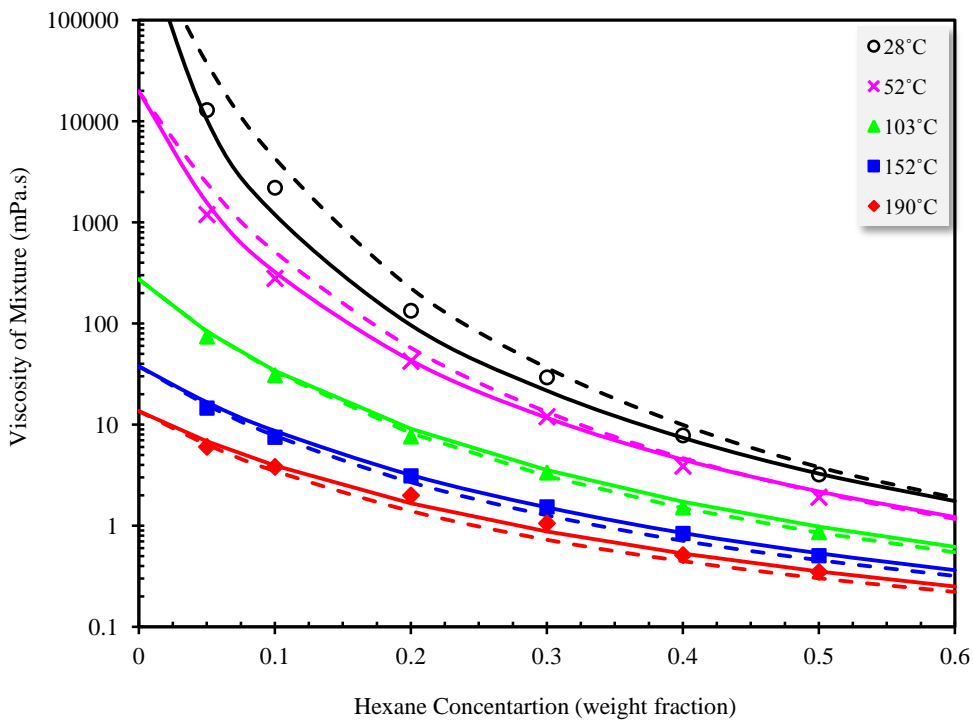


Figure 6–28: Viscosity of Surmont bitumen / *n*-hexane mixtures as a function of the weight fraction of *n*-hexane at different temperatures and at a constant pressure of 10 MPa; ○, ×, ▲, ■, ◆, measured viscosities; calculated values: —, power law model; - - -, Cragoe's model.

The experimental viscosity data are well correlated using the power law model. Despite no significant difference in the results of two models, power law model predicted the experimental data better than the Cragoe's model. The Cragoe's model over-predicts the data at the lower temperatures (i.e. 28 and 52°C) and under-predicts at the higher temperatures (i.e. 150 and 190°C) while the power law model slightly under-predicts all measured data.

An examination of Figures 6–27 and 6–28 demonstrates that the mixture viscosity shows a curvilinear trend with *n*-hexane concentration when log (viscosity) is plotted versus solvent weight fraction. This behaviour was observed when the concentration was reported in weight fraction. However, by converting the concentration into mole fraction, a linear trend for the mixture viscosities with concentration was observed.

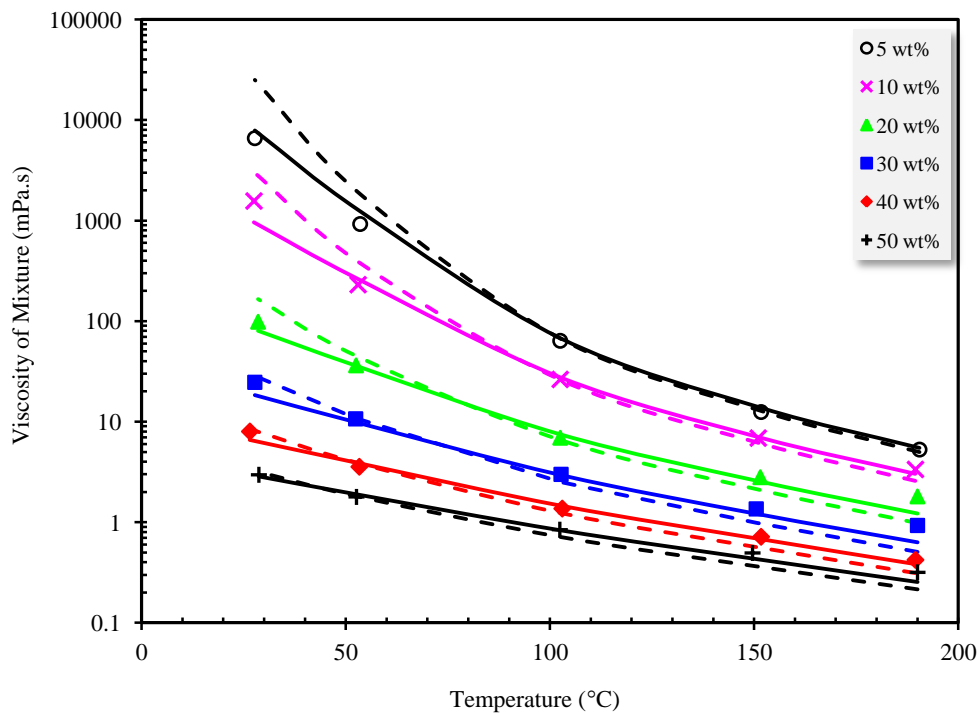


Figure 6–29: Viscosity of Surmont bitumen / *n*-hexane mixtures as a function of temperature at different weight fractions of *n*-hexane and at a constant pressure of 2 MPa; \circ , \times , \blacktriangle , \blacksquare , \blacklozenge , $+$, measured viscosities; calculated values: —, power law model; - · - ·, Cragoe's model.

The temperature reduces the viscosity of heavy oil and bitumen. As it was presented in Section 3.2.2, the viscosity of raw bitumen was considerably changed with the

temperature. The diluted bitumen also showed significant viscosity variations with the temperature. Figures 6–29 and 6–30 illustrate the variation of mixture viscosities with temperature at two pressures (2 and 10) MPa, respectively. These figures illustrate that the viscosity data, when plotted in semi-log scale, follow a linear trend at high *n*-hexane weight fractions and a non-linear trends at low *n*-hexane weight fractions. At higher *n*-hexane weight fractions, the mixtures behave similar to *n*-hexane and the viscosity of *n*-hexane shows linear trend with temperature (in semi-log plot). However, at lower *n*-hexane concentrations, the mixture is enriched in bitumen and its viscosity, as stated in equation 3-7, is not linearly changed with the temperature.

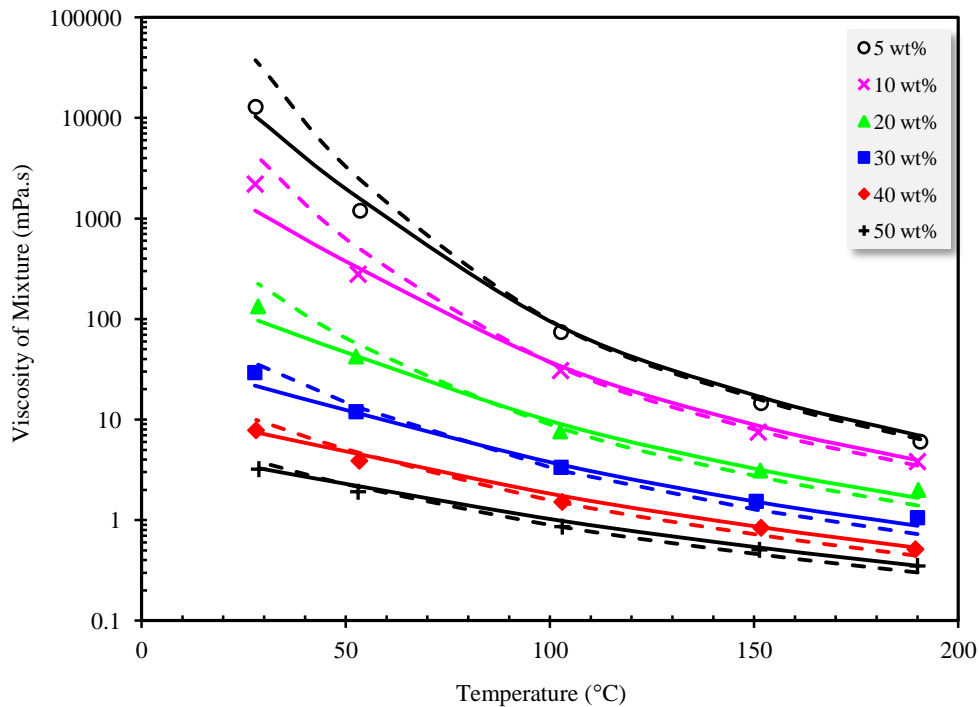


Figure 6–30: Viscosity of Surmont bitumen / *n*-hexane mixtures as a function of temperature at different weight fractions of *n*-hexane and at a constant pressure of 10 MPa; \circ , \times , \blacktriangle , \blacksquare , \blacklozenge , $+$, measured viscosities; calculated values: —, power law model; - - -, Cragoe's model.

To have a better representation of data and comparison with the models, the viscosity data at different *n*-hexane weight fractions were plotted versus pressure. Figure 6–31 shows the impact of pressure on the viscosity of Surmont bitumen / *n*-hexane mixtures at a constant temperature (28°C). Cragoe's model over-predicted the viscosity values of

mixtures at different solvent weight fractions while power law model under-predicts the data. When the temperature is increased to the highest measured value (190°C), an opposite behaviour was observed for two models (Figure 6–32). That is, Cragoe’s model under-predicted the viscosity values of mixtures at different solvent weight fractions while power law model slightly over-predicts the data.

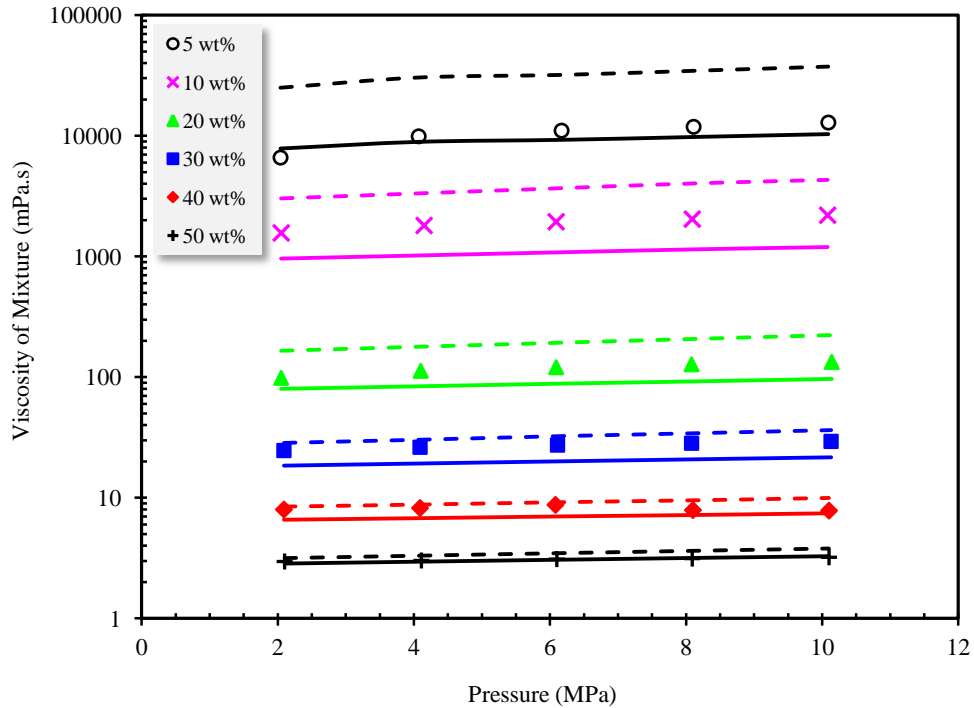


Figure 6–31: Effect of *n*-hexane concentration w_s and pressure P on the viscosity of Surmont bitumen / *n*-hexane mixtures at the lowest temperature (28°C); \circ , \times , \blacktriangle , \blacksquare , \blacklozenge , $+$, measured viscosities; calculated values: —, power law model; - - -, Cragoe’s model.

As it was not presented here, the best match between the experimental data and Cragoe’s model was obtained at the temperature of 103°C. However, at the temperature of 28°C, the calculated viscosities with Cragoe’s model show largest deviation. Power law model represents the viscosity data more accurately at the temperature of 190°C and the model cannot correlate the data at the lowest temperature (28°C) as good as other temperatures.

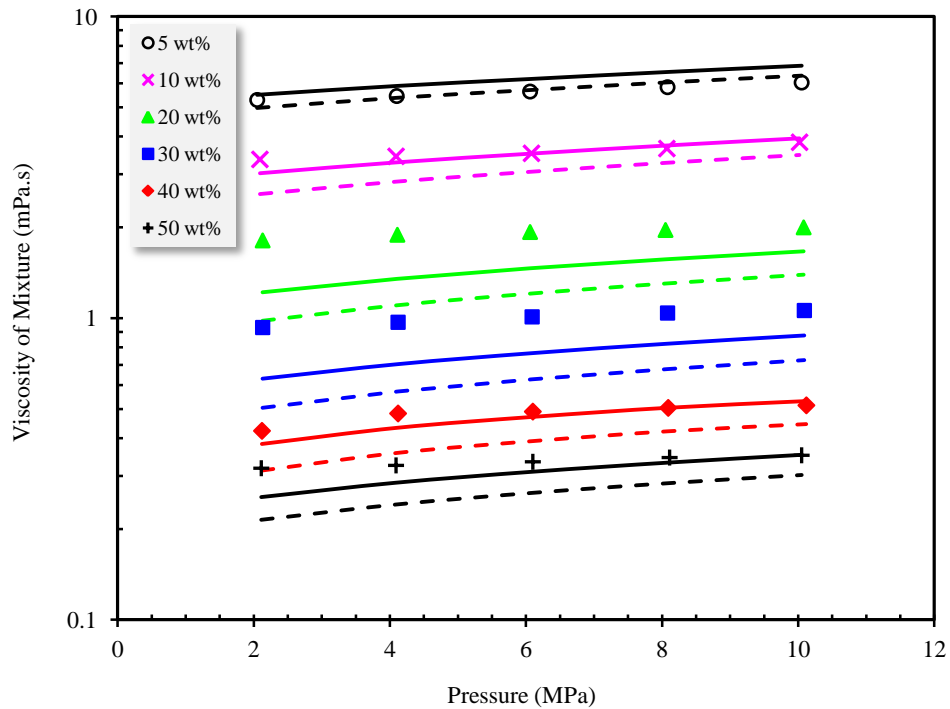


Figure 6–32: Effect of *n*-hexane concentration w_s and pressure P on the viscosity of Surmont bitumen / *n*-hexane mixtures at the highest temperature (190°C); \circ , \times , \blacktriangle , \blacksquare , \blacklozenge , $+$, measured viscosities; calculated values: —, power law model; ---, Cragoe’s model.

To determine the effect of pressure and *n*-hexane concentration on the mixture viscosity, the viscosity data are plotted as a function pressure at 0.05 and 0.5 weight fractions of *n*-hexane in Figures 6–33 and 6–34, respectively. The symbols with the same color indicate a constant temperature in these plots. These figures show that the mixture viscosity is linearly increased with the pressure at each isotherm, and this effect is greater at lower *n*-hexane weight fraction (i.e. 0.05).

Comparing Figures 6–33 and 6–34 indicate that the slope of viscosity-pressure plots is higher at a lower solvent weight fraction. In fact, the impact of pressure on the viscosity of bitumen and *n*-hexane is different. The viscosity of *n*-hexane is not affected by moderate pressure increment; therefore, the viscosity of bitumen/*n*-hexane mixtures at high *n*-hexane concentrations follows the same trend. At low solvent weight fractions, the pressure has more significant effect on the mixture viscosity due to higher bitumen concentration in the mixture.

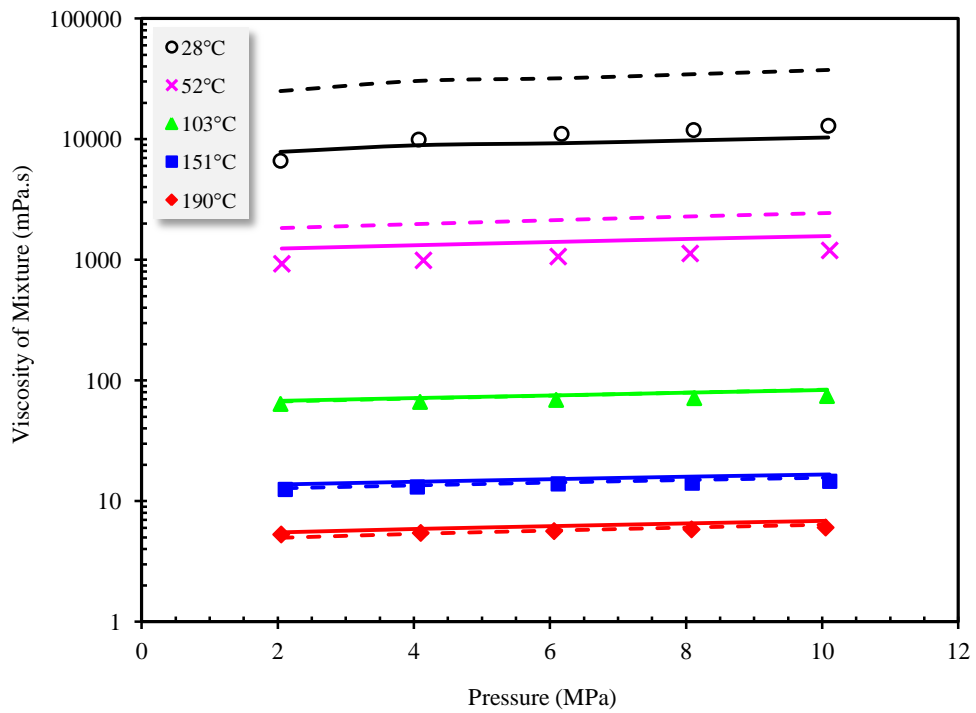


Figure 6–33: Effect of pressure P on the viscosity of Surmont bitumen / n -hexane mixtures at the lowest n -hexane weight fraction (0.05); \circ , \times , \blacktriangle , \blacksquare , \blacklozenge , $+$, measured viscosities; calculated values: —, power law model; - - -, Cragoe's model.

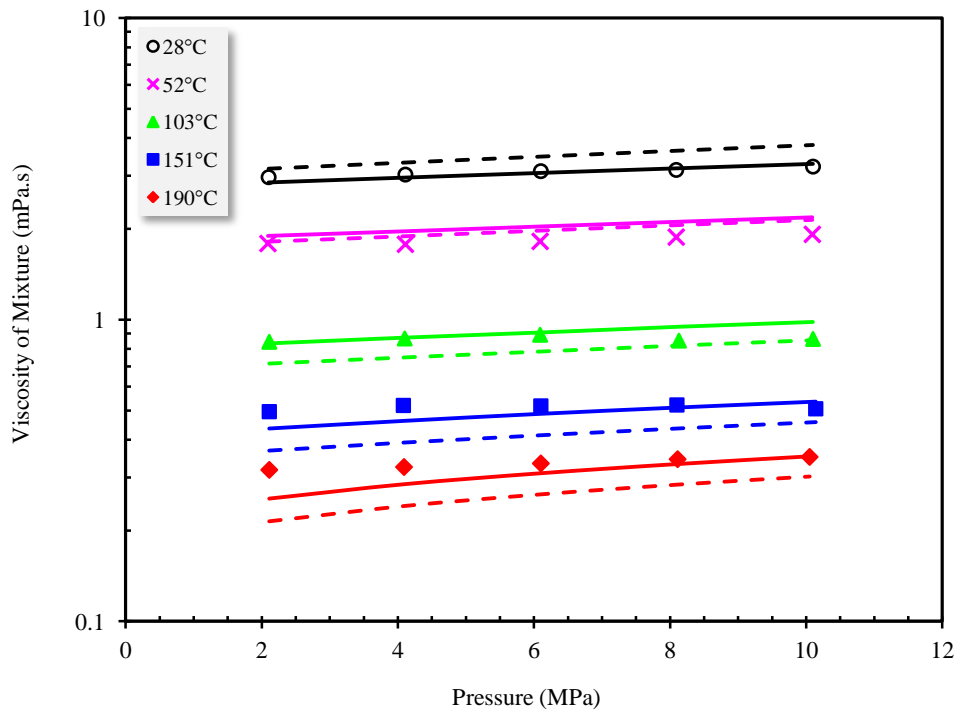


Figure 6–34: Effect of pressure P on the viscosity of Surmont bitumen / n -hexane mixtures at the highest n -hexane weight fraction (0.5); \circ , \times , \blacktriangle , \blacksquare , \blacklozenge , $+$, measured viscosities; calculated values: —, power law model; - - -, Cragoe's model.

The examination of the results reveals that the maximum deviation between the measured viscosity data and the calculated values was obtained at the lowest solvent weight fraction (0.05). As the weight fraction of *n*-hexane in the mixture increased, the deviation of the models from the experimental results reduced.

Chapter 7: Thermo-physical Properties of Bitumen/Condensate Mixture

This chapter presents the phase behaviour of bitumen/condensate mixtures and the application of condensate for *in situ* bitumen recovery methods and pipeline transportation. As with bitumen/*n*-hexane mixtures, the measurements for the density and viscosity of bitumen diluted with condensate were reported at different temperatures, pressures, and solvent weight fractions. The data for the mixtures were also evaluated with predictive schemes as well as with correlation models representing certain mixing rules proposed in the literature.

7.1. Introduction

Bitumen is extremely viscous at reservoir conditions; therefore, it is essential to reduce its viscosity for enhanced oil recovery and pipeline transportation. This viscosity reduction is commonly attained by increasing the temperature and/or the dilution with gaseous solvents or liquid diluents. The dilution of bitumen with a solvent breaks down or weakens the intermolecular forces and dramatically reduces the viscosity (Miadonye et al. 2001). The effect is significant and the addition of a small amount of solvent leads to considerable reduction in the viscosity.

The phase behaviour experiments and solubility measurements reported in the previous sections were for pure solvents. However, in field applications, a complex mixture of hydrocarbon molecules is used as the solvent (injection fluid). This mixture, usually called naphtha or condensate, is the fraction of hydrocarbons in petroleum that boil between 30 and 200°C. It consists of a complex mixture of hydrocarbon molecules, generally having between 5 and 12 carbon atoms. Naphtha is similar to condensate but it is slightly heavier and contains components with higher boiling points.

The commercial application of liquid solvents to reduce bitumen viscosity in *in-situ* processes has been investigated by several authors. Hernandez and Farouq-Ali (1972) experimentally studied the oil recovery from Athabasca oil sand using a number of solvents (tetrachloride, toluene, benzene, and naphtha) with and without steam. In another study, Farouq-Ali and Snyder (1973) evaluated oil recovery from Athabasca oil sands using a two-dimensional vertical model with the injection of naphtha, steam, or a combination of both. Farouq-Ali and Abad (1976) also investigated oil recovery from Athabasca oil sands using naphtha in conjunction with steam in a vertical tar sand pack and in a large three-dimensional model.

Although different hydrocarbon additives can be co-injected with steam in ES-SAGD processes, the inventors of the ES-SAGD process (Nasr et al. 1991; Nasr and Isaacs 2001; Nasr et al. 2002; Nasr and Ayodele 2005) found it preferable to use a solvent with a saturation temperature close to the saturation temperature of steam at operating pressure. In optimal conditions, the evaporation temperature of the additive should be within $\pm 15^{\circ}\text{C}$ of the steam saturation temperature. Considering this criteria, the condensate is a good candidate for the ES-SAGD process.

Several field and pilot tests have tried condensate and naphtha-steam co-injection. Nexen conducted a pilot test of the ES-SAGD process in Long Lake over a two-month period from February 13th to April 16th, 2006. They ran the ES-SAGD in a well pair, which had the most stable rating condition with the lowest SOR. They used heavy hydrocarbon fractions (C_7 to C_{12}) with steam. The solvent concentration was 10% when they started the co-injection and was then reduced to 5% to maintain the solvent at the concentration of 5%. The test was stopped after two months because no increase in bitumen production rate was observed. Suncor implemented an ES-SAGD project using naphtha as the solvent but the results were not encouraging and they did not observe any increase in the oil production rate (Orr 2009). Despite the lack of encouraging results in the field implementation of condensate and naphtha, it can still be considered as a

recovery method for bitumen reservoirs. Further investigation and studies are required to fully understand the phenomenon and make it practical for bitumen recovery.

Shu and Hartman (1988) did a simulation study to investigate the effect of steam slug in the presence of solvent. They considered three classes of solvents based on solvent volatility (light, medium and heavy) and solvent concentration (no more than 10%). Based on these categories, condensate belongs to the medium class. The simulation found that, the lighter solvents resulted in earlier oil recovery and the highest recovery was obtained using medium solvent. The heavy solvents did not improve the oil recovery.

Palmgren and Edmunds (1995) proposed naphtha-assisted gravity drainage (NAGD) process. In this process, hot naphtha vapour was replaced with water vapour in order to combine the effective thermal process with the dilution mechanism of the naphtha. Their study showed that higher oil recovery and oil rate could be obtained using the NAGD process but the process economy was highly dependent on the naphtha recovery at the end of the process.

Nasr et al. (2002) modified the SAGD process by co-injecting a small concentration of condensable hydrocarbon additive with steam phase through a conventional SAGD pattern. They did an initial screening and considered propane to octane (C_3 - C_8) and diluent as the solvent. The diluent used in their study was a gas condensate with the majority of its hydrocarbon fractions between C_4 to C_{10} . Their experimental results showed improved bitumen recovery but the improvement was more significant for hexane and diluent.

Boak and Palmgren (2007) did a simulation study of solvent-steam co-injection using a pseudo-compositional thermal reservoir simulator. They studied the effects of co-injection of naphtha as a multi-component mixture and propane and pentane as pure components. Their simulation showed that the co-injection of all solvents studied (propane, pentane, and naphtha) resulted in an improvement in SOR proportional to the solvent concentration. Higher solvent concentration resulted in greater improvement. However, the oil production rate was only improved using naphtha. The oil production

rate decreased when the solvent concentration exceeded 5 mole percent due to accumulation of solvent gas at the front of the vapour chamber.

Deng et al. (2010) conducted an ES-SAGD lab test with the co-injection of steam and diluent using Athabasca bitumen. Their study showed that the co-injected solvent transports with steam and mixes with the bitumen in the boundary of the chamber and thus the oil production is enhanced due to further viscosity reduction of the solvent bitumen mixture. They concluded that the solubility of solvent in bitumen is important for ES-SAGD process and needs to be determined.

The above discussion highlights the potential advantages of condensate for bitumen extraction, transportation, and *in-situ* recovery that have been confirmed by many researchers. However, the application and optimization of condensate for recovery and extraction processes are challenging. The condensate is relatively expensive and the process should be conducted under optimum conditions to make it economically practical. Predicting and optimizing the performance of solvent-based processes are challenging task because the addition of solvent creates a complex phase behaviour system. We must determine how solvent additives affect the properties of oil at elevated temperatures in order to determine all of the potential benefits.

7.2. Literature Background

Knowledge of diluent-bitumen interactions and their thermo-physical properties is becoming increasingly important for technical people in the industry. This information improves project economic and lessens the environmental impact through the reduction of greenhouse gas (GHG) emissions and water used in bitumen recovery. In addition, the knowledge of the properties of diluent-bitumen mixtures is necessary to design *in-situ* recovery and surface processes. The time and cost involved in obtaining experimental data necessitates the development of a method to predict the transport properties of bitumen and solvent mixtures.

The phase behaviour study of condensate/bitumen systems in the literature is limited to a study by Motahhari et al. (2011) which reported the viscosities of a condensate, two bitumen samples from Peace River field, and bitumen/condensate mixtures. They correlated the mixture data using an expanded fluid viscosity model.

Wen et al. (2005) conducted viscosity measurements for mixtures of heavy oil and solvents. They added solvents at different ratios to each oil and used NMR spectra to measure the viscosity of the mixture. They used four oils (Peace River, Cold Lake, Edam, and Atlee Buffalo) and six solvents (kerosene, toluene, naphtha, heptane, hexane, and pentane). Measurements were conducted at the temperature of 25°C and at atmospheric pressure. They modelled the viscosity data using Shu's and Cragoe's models.

In this chapter, the experiments for Surmont bitumen / condensate mixtures were conducted to measure the density and viscosity of condensate-saturated Surmont bitumen at different fractions of condensate (0.05 to 0.5 weight fractions). Five different temperatures (ambient, 50, 100, 150, and 190°C) were used in the experiments. In addition, the separation of asphaltene fractions from the mixture was confirmed by visual observation of the solid particles.

7.3. Condensate Properties

The condensate used in the experiments was provided by Nexen Inc. Prior to any experiments, the density and viscosity of the condensate was measured over the temperature and pressure ranges, 22 to 190°C and 2 to 10 MPa. The pure solvent density and viscosity data were used to predict the properties of the mixture. The compositional analyses for the condensate were also completed using two standard methods, ASTM D2887 and ASTM D7169. The first method is applicable for light mixtures including petroleum products and fractions with a final boiling point of 538°C. The second test method, ASTM D7169, provides useful information on the amount of residue by determining the boiling point distribution of crude oils, vacuum residues, and other

petroleum fractions through a temperature of 720°C, which corresponds to the elution of *n*-C₁₀₀. The compositional analysis was used to obtain the molecular weight of the condensate and to characterize the condensate for equation of state modelling.

7.3.1. Compositional Analysis

The compositional analysis of the condensate (boiling point versus percent distilled) was obtained with two ASTM methods, D2887 and D7169, and is summarized in Table 7-1. The initial boiling point found using two methods was 33.5 and 33.8°C which are similar values. The final boiling point obtained was 377°C for ASTM D2887 and 344°C for ASTM D7169. Although ASTM D2887 is more appropriate than ASTM D7169 for condensate, two methods provided similar results. The boiling point curve of the condensate was converted into the carbon number distribution with the built-in software installed in the SimDis apparatus and the results are presented in Table 7-2.

7.3.2. Molecular Weight

As outlined in Chapter 3, the molecular weight of the condensate can be measured with two different methods, vapour pressure osmometry and cryoscopy method. The former is based on the change in the boiling point of a solvent when a solute is added and the latter is based on the freezing point depression. The molecular weight of the condensate can also be estimated from the compositional analysis. The carbon number distribution presented in Table 7-2 along with the molecular weight of the components was used to obtain the molecular weight of the condensate. The correlation (shown in equation 4-7) was applied to obtain the molecular weight of components C_n , where $n \geq 10$. For components with $n \leq 10$, the molecular weight is taken from Riazi (2005). The fraction of components in the condensate determined from ASTM methods was converted into a mole fraction. The molecular weight of condensate was then calculated from,

$$MW = \sum_i x_i MW_i \quad 7-1$$

The calculated molecular weights are 85.7 and 86.7 g/mol using the carbon number distributions from ASTM D2887 and D7169, respectively. During the rest of this chapter, the fraction of condensate in the mixture is converted from a weight fraction into a mole fraction using an average molecular value of 86.2 g/mol.

Table 7-1: Boiling point distribution of condensate.

ASTM 2887		ASTM 7169	
% Off	Boiling Point (°C)	% Off	Boiling Point (°C)
IBP	33.5	IBP	33.8
1	33.6	1	34.0
2	33.8	2	34.3
3	34.1	3	34.8
4	34.8	4	35.0
5	34.9	5	35.2
6	34.9	6	35.4
7	35.0	7	35.6
8	35.0	8	35.7
9	35.1	9	35.9
10	35.1	10	36.0
11	35.1	11	36.2
12	35.2	12	36.4
13	35.2	13	36.6
14	35.3	14	36.9
15	35.3	15	37.2
16	35.4	16	37.5
17	35.4	17	37.9
18	35.5	18	38.4
19	35.5	19	38.9
20	35.6	20	39.5
21	35.7	21	40.3
22	35.7	22	41.6
23	35.8	23	43.6
24	35.8	24	46.5
25	35.8	25	49.8
26	35.9	26	53.3
27	35.9	27	56.7
28	35.9	28	60.3
29	36.0	29	63.9
30	36.0	30	65.1
31	36.1	31	66.1
32	36.1	32	67.2
33	36.1	33	70.0
34	36.2	34	73.4
35	36.3	35	76.1
36	36.4	36	78.5
37	41.3	37	80.1
38	44.6	38	81.6
39	47.6	39	83.1
40	50.4	40	84.6
41	53.3	41	86.5
42	56.0	42	88.9

43	58.1	43	91.3
44	59.8	44	93.4
45	61.1	45	95.2
46	62.2	46	97.0
47	63.4	47	98.6
48	64.4	48	99.2
49	65.3	49	99.9
50	65.9	50	100.7
51	66.4	51	101.7
52	66.8	52	102.6
53	67.2	53	103.4
54	67.6	54	104.2
55	67.9	55	105.2
56	68.2	56	107.7
57	68.6	57	110.3
58	68.9	58	111.8
59	69.2	59	113.4
60	69.6	60	116.2
61	70.2	61	118.6
62	71.1	62	122.7
63	72.6	63	127.9
64	74.3	64	130.8
65	77.3	65	136.2
66	85.1	66	140.2
67	87.4	67	148.6
68	88.7	68	158.4
69	89.7	69	172.3
70	90.6	70	193.4
71	91.6	71	231.2
72	92.7	72	343.9
73	93.8		
74	94.9		
75	95.8		
76	96.6		
77	97.2		
78	97.8		
79	98.2		
80	98.7		
81	99.2		
82	100.2		
83	109.4		
84	115.3		
85	118.2		
86	120.1		
87	125.1		
88	126.8		
89	128.4		
90	137.2		
91	145.3		
92	152.8		
93	167.8		
94	188.8		
95	226.6		
96	377.0		

Table 7-2: Component distribution of condensate.

ASTM 2887		ASTM 7169	
Cut	% Off	Cut	% Off
C5	35.73	C5	37.60
(C ₅ , C ₆)	25.29	(C ₅ , C ₆)	22.09
(C ₆ , C ₇)	21.92	(C ₆ , C ₇)	14.36
(C ₇ , C ₈)	8.01	(C ₇ , C ₈)	15.68
(C ₈ , C ₉)	4.39	(C ₈ , C ₉)	4.65
(C ₉ , C ₁₀)	1.57	(C ₉ , C ₁₀)	1.86
(C ₁₀ , C ₁₁)	0.89	(C ₁₀ , C ₁₁)	0.98
(C ₁₁ , C ₁₂)	0.54	(C ₁₁ , C ₁₂)	0.54
(C ₁₂ , C ₁₃)	0.33	(C ₁₂ , C ₁₃)	0.43
(C ₁₃ , C ₁₄)	0.12	(C ₁₃ , C ₁₄)	0.16
(C ₁₄ , C ₁₅)	0.11	(C ₁₄ , C ₁₅)	0.15
(C ₁₅ , C ₁₆)	0.11	(C ₁₅ , C ₁₆)	0.14
(C ₁₆ , C ₁₇)	0.10	(C ₁₆ , C ₁₇)	0.13
(C ₁₇ , C ₁₈)	0.10	(C ₁₇ , C ₁₈)	0.13
(C ₁₈ , C ₁₉)	0.09	(C ₁₈ , C ₁₉)	0.12
(C ₁₉ , C ₂₀)	0.09	(C ₁₉ , C ₂₀)	0.12
(C ₂₀ , C ₂₁)	0.09	(C ₂₀ , C ₂₁)	0.05
(C ₂₁ , C ₂₂)	0.08	(C ₂₁ , C ₂₂)	0.04
(C ₂₂ , C ₂₃)	0.07	(C ₂₂ , C ₂₃)	0.04
(C ₂₃ , C ₂₄)	0.03	(C ₂₃ , C ₂₄)	0.04
(C ₂₄ , C ₂₅)	0.03	(C ₂₄ , C ₂₅)	0.04
(C ₂₅ , C ₂₆)	0.03	(C ₂₅ , C ₂₆)	0.04
(C ₂₆ , C ₂₇)	0.03	(C ₂₆ , C ₂₇)	0.04
(C ₂₇ , C ₂₈)	0.03	(C ₂₇ , C ₂₈)	0.03
(C ₂₈ , C ₂₉)	0.03	(C ₂₈ , C ₂₉)	0.03
(C ₂₉ , C ₃₀)	0.03	(C ₂₉ , C ₃₀)	0.03
(C ₃₀ , C ₃₁)	0.03	(C ₃₀ , C ₃₁)	0.03
(C ₃₁ , C ₃₂)	0.03	(C ₃₁ , C ₃₂)	0.03
(C ₃₂ , C ₃₃)	0.03	(C ₃₂ , C ₃₃)	0.03
(C ₃₃ , C ₃₄)	0.02	(C ₃₃ , C ₃₄)	0.03
(C ₃₄ , C ₃₅)	0.02	(C ₃₄ , C ₃₅)	0.03
(C ₃₅ , C ₃₆)	0.02	(C ₃₅ , C ₃₆)	0.03
(C ₃₆ , C ₃₇)	0.01	(C ₃₆ , C ₃₇)	0.03
(C ₃₇ , C ₃₈)	0.00	(C ₃₇ , C ₃₈)	0.02
(C ₃₈ , C ₃₉)	0.00	(C ₃₈ , C ₃₉)	0.03
(C ₃₉ , C ₄₀)	0.00	(C ₃₉ , C ₄₀)	0.02
(C ₄₀ , C ₄₁)	0.00	(C ₄₀ , C ₄₁)	0.02
(C ₄₁ , C ₄₂)	0.00	(C ₄₁ , C ₄₂)	0.02
(C ₄₂ , C ₄₃)	0.00	(C ₄₂ , C ₄₃)	0.02
(C ₄₃ , C ₄₄)	0.00	(C ₄₃ , C ₄₄)	0.02
(C ₄₄ , FBP)	0.00	(C ₄₄ , C ₄₅)	0.02
		(C ₄₅ , C ₄₆)	0.02
		(C ₄₆ , C ₄₇)	0.02
		(C ₄₇ , C ₄₈)	0.02
		(C ₄₈ , C ₄₉)	0.01
		(C ₄₉ , C ₅₀)	0.02
		(C ₅₀ , C ₅₁)	0.01

7.3.3. Density and Viscosity

To evaluate the correlations for the viscosity and density of bitumen/condensate mixtures, the density and viscosity of the condensate over a wide range of pressures and temperatures are required. Once a correlation for the density or viscosity of condensate as a function of pressure and temperature is developed, the equation can directly be applied in reservoir simulations to calculate the viscosity at the desired temperature and pressure. With a comprehensive set of data, correlations can be developed easily and comparisons of mixture data with condensate can be made. Thus, prior to the measurements for the mixtures, the density and viscosity of condensate were measured for a wide range of temperatures and pressures. The viscosity and density of the condensate was measured using a procedure similar to the one used for bitumen.

The density of the condensate sample was measured over wide range of temperatures by the Anton Paar density measuring cell. The temperature was varied within $\pm 0.1^\circ\text{C}$ and the pressure was controlled with a Quizix pump. The uncertainty of pressure and density measurements was 0.01 MPa and 0.1 kg/m^3 , respectively. The measured density data at different temperatures 23 to 190°C over the pressure range atmospheric pressure to 10 MPa are listed in Table 7–3. As expected, the density of the condensate is reduced as temperature is increased at a constant pressure. This behaviour was observed for all pressures. At a constant temperature, however, the density increases with pressure.

The impact of pressure on the density of condensate is more pronounced at high temperatures (i.e. 150 and 190°C). As the experimental temperature increases toward the critical point, the variation of condensate density with the pressure becomes more significant. The same trend was observed for the raw bitumen. That is, at higher temperatures (i.e. 150 and 190°C), the impact of pressure on the density of bitumen was more significant than the lower temperatures (i.e. 23°C).

The density of the condensate is a value between the densities of *n*-hexane and *n*-heptane at constant pressure and temperature. The variation of condensate density with

pressure at a constant temperature is more pronounced than that of pure components. For example at the temperature of 190°C, a density increment of 19.6 kg/m³ was observed for *n*-hexane over the pressure increase of 4 to 10 MPa whereas this increment is 26.9 kg/m³ for condensate. The data in Table 7–3 also confirmed that the temperature considerably changes the density of condensate over the studied pressure. Although the density of bitumen is also reduced with temperature, its variation is not as significant as that of condensate.

Table 7–3: Measured ρ_{exp} and correlated ρ_{corr} density of condensate at different temperatures T and pressures P ; AD, absolute deviation.

T (°C)	P (MPa)	ρ_{exp} (kg/m ³)	ρ_{corr} (kg/m ³)	AD (kg/m ³)
189.7	4.023	496.8	497.9	1.1
189.7	6.052	505.3	507.5	2.2
189.7	7.992	513.7	517.0	3.3
189.7	10.033	523.7	527.1	3.4
149.6	1.973	541.9	542.6	0.7
149.6	4.024	551.5	549.3	2.2
149.6	6.022	559.9	555.9	4.0
149.6	8.041	567.0	562.7	4.3
149.6	9.982	572.8	569.3	3.5
100.5	2.002	601.3	601.2	0.1
100.5	4.03	605.9	605.4	0.5
100.5	5.982	610.1	609.4	0.7
100.5	8.017	613.9	613.7	0.2
100.5	10.006	617.5	617.8	0.3
50.4	2.024	651.0	651.6	0.6
50.4	4.009	653.3	654.1	0.8
50.4	5.983	655.5	656.6	1.1
50.4	8.004	657.7	659.1	1.4
50.4	9.995	660.2	661.7	1.5
21.5	2.029	676.6	676.3	0.3
21.5	4.022	678.5	678.2	0.3
21.5	6.021	680.5	680.0	0.5
21.5	8.006	682.5	681.9	0.6
21.5	9.997	684.5	683.8	0.7

The measured density values were fitted with the following equation that takes into account the impact of pressure and temperature. The procedure to obtain the coefficients of the equation was explained in Chapter 3.

$$\rho = [691.06 - 0.7299T - 0.002039T^2] \exp\{0.001076 \exp(0.01148T)P\} \quad 7-2$$

where T is temperature in Celsius, P is the pressure in MPa, and ρ is the density in kg/m^3 . The fitted correlation represents the density of condensate within $\pm 4.3 \text{ kg.m}^{-3}$ with an average absolute deviation of 1.4 kg/m^3 . The AARD of the correlated densities from the measured values is 0.25 %. This confirms that the data are well represented by equation 7-2.

The viscosity of the condensate sample was also measured at the temperatures up to 190°C over the pressure range 2 to 10 MPa. The measured data are summarized in Table 7-4. As the data show, the viscosity of the condensate is reduced with the temperature at a constant pressure and increases with the pressure at a constant temperature. It is worth mentioning that the impact of pressure on the viscosity of the condensate is more pronounced at high temperature conditions (i.e. 150 and 190°C) while for the bitumen, the variation of viscosity with pressure is more significant at low temperatures (i.e. 22 and 50°C).

The viscosity of the condensate was fitted with a four-constant correlation,

$$\ln(\mu) = [-0.8759 - 0.00812T] + (0.00182 + 7.05 \times 10^{-5}T)P_g \quad 7-3$$

where T is the temperature in K, μ is the viscosity in mPa.s , and P_g is the gauge pressure in MPa. The AARD between the measured data and correlated values is 3.6%.

7.4. Density of Mixture

Tables 7-5 to 7-7 summarize the experimental density values of the pseudo-binary mixture of Surmont bitumen and condensate at different temperatures, pressures, and solvent weight fractions. As the tables show, the density of the binary mixture is reduced with temperature at a constant pressure and is increased with pressure at a constant

temperature. The density of the pseudo-binary mixture is significantly decreased with increasing condensate weight fraction at constant temperature and pressure. At the temperature of 190°C, the pseudo-binary mixtures form vapour-liquid equilibrium at a constant pressure of 2 MPa. Therefore, no single phase was observed at this condition to report density and viscosity of single liquid phase.

Table 7–4: Measured μ_{exp} and correlated μ_{corr} viscosity of condensate at different temperatures T and pressures P ; ARD, absolute relative deviation.

T (°C)	P (MPa)	μ_{exp} (mPa.s)	μ_{corr} (mPa.s)	ARD (%)
188.5	2.992	0.096	0.094	2.1
189.1	4.023	0.099	0.095	4.0
189.4	6.052	0.102	0.098	3.9
189.7	7.992	0.106	0.101	4.7
189.9	10.033	0.108	0.104	3.7
151.5	1.973	0.122	0.125	2.5
151.7	4.024	0.126	0.128	1.6
151.8	6.022	0.128	0.131	2.3
151.8	8.041	0.132	0.134	1.5
151.8	9.982	0.134	0.137	2.2
100.6	2.002	0.175	0.187	6.9
101.4	4.03	0.177	0.189	6.8
101.9	5.982	0.180	0.192	6.7
102.3	8.017	0.182	0.195	7.1
102.5	10.006	0.184	0.198	7.6
53.2	2.024	0.286	0.273	4.5
53.1	4.009	0.289	0.277	4.2
53.1	5.983	0.294	0.280	4.8
53.0	8.004	0.299	0.283	5.4
53.0	9.995	0.304	0.286	5.9
25.7	2.029	0.342	0.340	0.6
26.1	4.022	0.341	0.342	0.3
26.3	6.021	0.343	0.344	0.3
26.5	8.006	0.345	0.346	0.3
26.6	9.997	0.348	0.348	0.0

Table 7–5: Experimental liquid densities of the pseudo-binary mixtures of Surmont bitumen / condensate at 0.05 and 0.1 weight fractions of condensate; w , weight fraction of condensate in the mixture; T , temperature; P , pressure; ρ_m , density of mixture.

$w = 0.05$			$w = 0.1$		
T (°C)	P (MPa)	ρ_m (kg/m ³)	T (°C)	P (MPa)	ρ_m (kg/m ³)
189.8	2.01	----	190.0	2.01	----
189.8	4.02	885.3	190.0	4.04	858.3
189.8	6.02	887.7	190.0	6.01	860.7
189.8	8.01	888.8	190.0	7.98	862.9
189.8	9.99	892.1	190.0	10.00	865.1
150.5	1.98	908.9	150.3	2.03	883.5
150.5	4.00	911.2	150.3	3.99	885.6
150.5	6.05	912.6	150.3	6.01	887.5
150.5	8.04	914.5	150.3	8.00	889.3
150.5	10.03	916.2	150.3	10.03	891.1
100.7	1.99	939.4	100.8	2.01	915.0
100.7	3.98	941.1	100.8	4.02	916.9
100.7	6.01	942.5	100.8	6.03	918.4
100.7	8.05	943.9	100.8	7.99	919.9
100.7	10.05	945.2	100.8	10.05	921.5
50.2	2.03	970.4	49.9	2.00	947.5
50.2	4.04	971.5	49.9	4.03	948.9
50.2	6.05	972.6	49.9	6.01	950.2
50.2	8.02	973.8	49.9	8.00	951.4
50.2	10.03	974.9	49.9	10.00	952.6
22.7	2.05	986.7	23.1	2.01	964.4
22.7	4.01	987.6	23.1	4.01	965.5
22.7	5.98	988.7	23.1	6.01	966.6
22.7	7.98	989.7	23.1	8.02	967.7
22.7	10.03	990.7	23.1	9.99	968.8

Table 7–6: Experimental liquid densities of the pseudo-binary mixtures of Surmont bitumen / condensate at 0.2 and 0.3 weight fractions of condensate; w , weight fraction of condensate in the mixture; T , temperature; P , pressure; ρ_m , density of mixture.

w = 0.2			w = 0.3		
T (°C)	P (MPa)	ρ_m (kg/m ³)	T (°C)	P (MPa)	ρ_m (kg/m ³)
189.6	2.01	----	189.6	2.01	----
189.6	4.00	809.8	189.6	4.03	762.8
189.6	6.03	812.9	189.6	6.00	766.6
189.6	7.99	815.4	189.6	8.02	769.9
189.6	9.96	818.0	189.6	10.03	773.1
150.8	2.01	836.6	150.6	2.00	791.4
150.8	4.00	838.9	150.6	4.02	794.3
150.8	6.01	841.5	150.6	6.02	797.2
150.8	7.99	843.7	150.6	8.03	799.9
150.8	10.00	845.9	150.6	10.01	802.5
100.2	2.02	871.9	101.0	2.02	829.1
100.2	4.01	873.7	101.0	4.04	831.4
100.2	5.99	875.4	101.0	6.03	833.5
100.2	8.01	877.1	101.0	8.03	835.5
100.2	9.98	878.8	101.0	10.01	837.5
50.0	2.04	905.6	49.9	2.02	865.6
50.0	4.02	906.9	49.9	4.04	867.3
50.0	5.99	908.3	49.9	6.04	868.9
50.0	8.01	909.7	49.9	8.00	870.4
50.0	10.01	911.0	49.9	10.01	871.9
21.8	2.00	924.3	22.1	2.00	886.0
21.8	4.00	925.6	22.1	4.02	886.9
21.8	5.99	926.8	22.1	5.99	888.1
21.8	8.04	928.1	22.1	8.00	889.4
21.8	10.03	929.3	22.1	10.00	890.8

Table 7–7: Experimental liquid densities of the pseudo-binary mixtures of Surmont bitumen / condensate at 0.4 and 0.5 weight fractions of condensate; w , weight fraction of condensate in the mixture; T , temperature; P , pressure; ρ_m , density of mixture.

w = 0.4			w = 0.5		
T (°C)	P (MPa)	ρ_m (kg/m ³)	T (°C)	P (MPa)	ρ_m (kg/m ³)
189.8	2.01	----	189.5	2.01	----
189.8	4.03	718.5	189.5	4.01	677.5
189.8	5.99	723.2	189.5	6.00	682.9
189.8	7.98	727.1	189.5	8.01	687.5
189.8	9.99	731.1	189.5	10.01	692.2
150.3	2.03	749.5	150.5	2.02	709.9
150.3	4.04	752.8	150.5	3.98	714.1
150.3	6.07	756.3	150.5	6.00	718.0
150.3	8.00	759.4	150.5	8.01	721.6
150.3	10.00	762.4	150.5	9.99	725.1
100.6	1.99	790.4	100.8	1.98	753.7
100.6	3.99	792.6	100.8	4.05	756.7
100.6	5.98	794.9	100.8	6.03	759.2
100.6	8.03	797.3	100.8	7.99	761.7
100.6	10.05	799.5	100.8	10.00	764.2
50.3	2.01	828.0	50.3	1.99	793.9
50.3	3.99	829.9	50.3	3.99	796.0
50.3	6.02	831.6	50.3	6.06	798.0
50.3	8.05	833.4	50.3	8.00	799.8
50.3	9.98	835.1	50.3	10.00	801.7
22.5	1.99	848.6	22.7	2.00	815.2
22.5	3.99	850.2	22.7	4.02	816.7
22.5	6.00	851.7	22.7	6.03	818.3
22.5	8.02	853.0	22.7	8.00	819.9
22.5	9.96	854.4	22.7	9.95	821.4

The impact of pressure on the density of the condensate and raw bitumen is more pronounced at high temperature conditions (i.e. 150 and 190°C). The data on the density of the condensate confirm that the temperature changes the density considerably over the studied pressure range. Although the density of bitumen is also reduced with temperature, the variation is not as significant as that of condensate. The variation of the mixture density with temperature and pressure is highly dependent on the condensate weight fraction. At low solvent concentrations (i.e. 0.05 weight fraction), the mixture behaves similarly to bitumen whereas at a high weight fraction (i.e. 0.5), the mixture behaviour is more similar to that of the condensate. For this reason, the variation of mixture density with pressure is not considerable at a condensate weight fraction of 0.05 while it is significant at condensate weight fraction of 0.5.

7.4.1. Prediction of Mixture Density

The measured density data of Surmont bitumen / condensate mixtures were predicted by equation 6-1 which was developed on the assumption that no volume change occurs upon mixing. The density of the condensate at each temperature and pressure was calculated from the developed correlations and those of raw bitumen were taken from Chapter 3. The mixture density values were predicted using equation 6-1, and the results were in agreement with the measured data, within 1.43% AARD. The density of the mixture can also be predicted by,

$$\rho_m = \frac{1}{\sum_i \frac{w_i}{\rho_i}} \quad 7-4$$

where w_i and ρ_i are the weight fraction and density of components in the mixture, respectively. Although SimDis data and the component distribution for the condensate are available, this equation requires the density of each component at each temperature and pressure, which is not available. For this reason, equation 7-2 was used throughout this section to represent the density of condensate.

Figures 7-1 and 7-2 display the measured density data and the predicted values for the mixtures of Surmont bitumen and condensate. In these figures, the density is plotted as a function of the condensate weight fraction at different temperatures and constant pressure. Figure 7-1 shows the results at the lowest pressure, 2 MPa, and Figure 7-2 illustrates the data at the highest pressure, 10 MPa. The symbols are the experimental data and the lines are the predictions using equation 6-1. At a constant temperature of 190°C, no single phase was observed over the studied concentrations. Despite a lack of measured data, the predictions are shown in the figure.

The predictions can be interpreted to agree with the measured data. An examination of Figures 7-1 and 7-2 demonstrates that the mixture densities are significantly varied with the condensate weight fraction over the studied concentrations. The predictions are in good agreement with the measured data at the lowest temperature (23°C). As the temperature increases, the deviation between the predicted densities and the measured values increases. The same trends were also observed at other pressures.

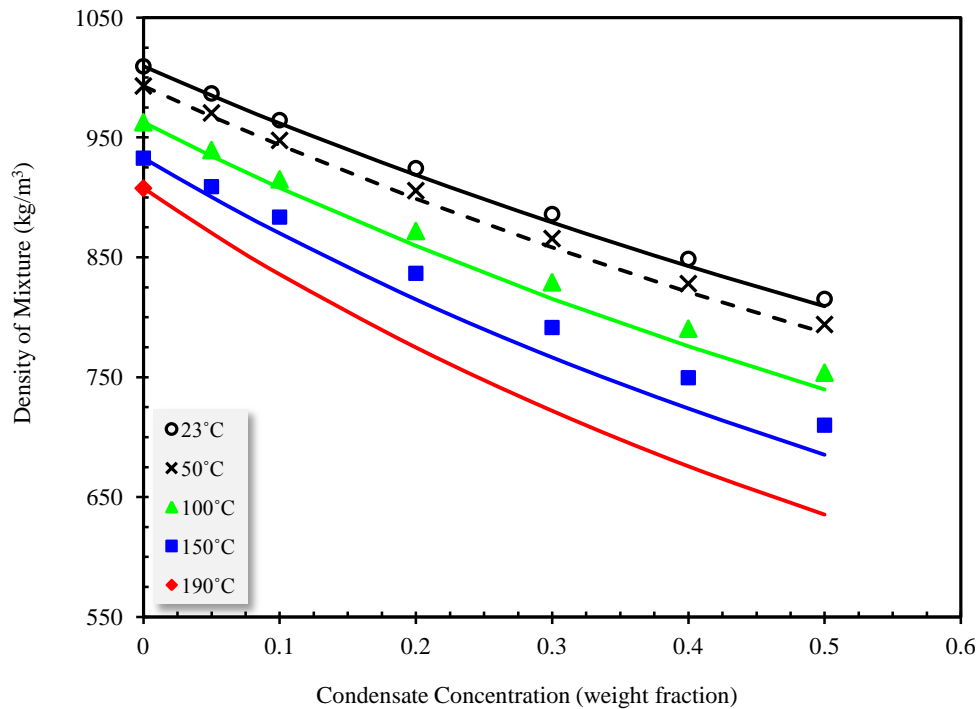


Figure 7-1: Density of Surmont bitumen / condensate mixtures as a function of the weight fraction of condensate at different temperatures and at a constant pressure of 2 MPa; ■,▲,○,◆,×, experimental data; ----, predicted values.

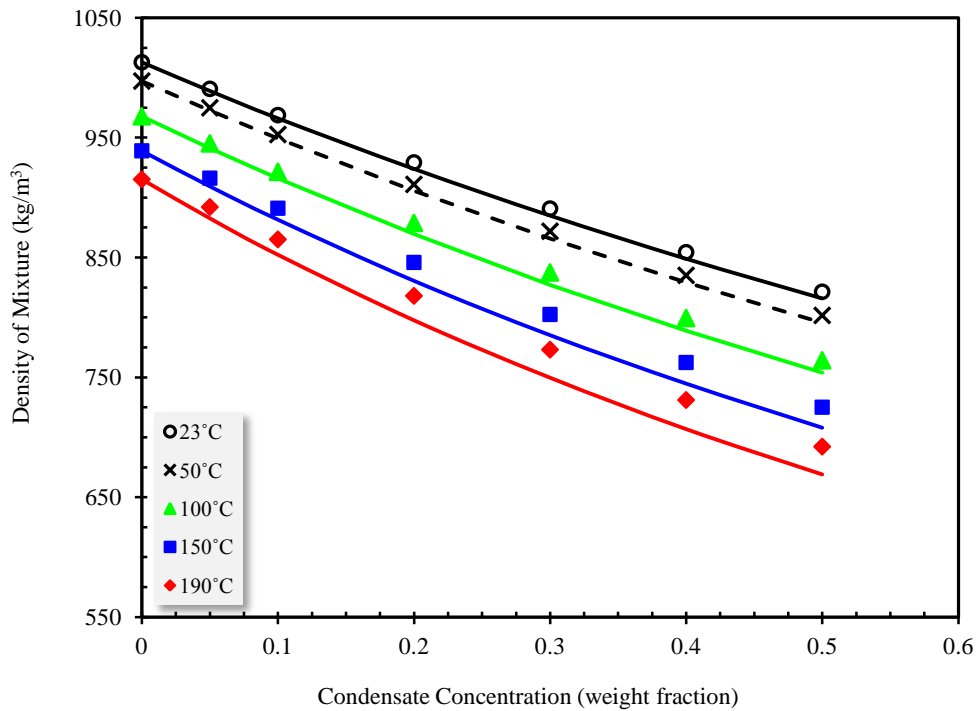


Figure 7-2: Density of Surmont bitumen / condensate mixtures as a function of the weight fraction of condensate at different temperatures and at a constant pressure of 10 MPa; $\blacksquare, \blacktriangle, \circ, \blacklozenge, \times$, experimental data; ---, predicted values.

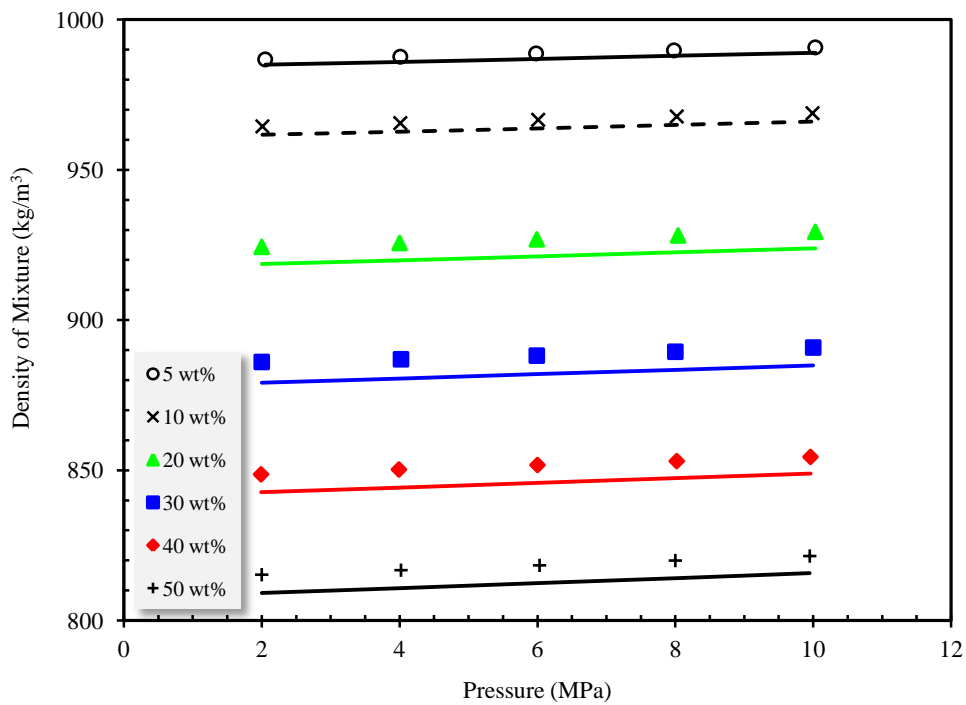


Figure 7-3: Density of Surmont bitumen / condensate mixtures as a function of pressure at different condensate weight fractions and at the lowest temperature (23°C); $\circ, \times, \blacktriangle, \blacksquare, \blacklozenge, +$, experimental data; ---, predicted values.

Figures 7–3 and 7–4 illustrate the impact of pressure on the mixture density at different solvent weight fractions and at temperatures of 23 and 190°C. As depicted in the figures, the mixture density shows a linear relationship to the pressure at a constant solvent weight fraction and this effect is more significant at higher temperatures (i.e. 190°C). A closer examination of Figures 7–3 and 7–4 reveals that the predictions at the highest temperature and the highest solvent concentrations deviate from the experimental data and the increase in temperature results in a higher deviation between the predictions and the measured values.

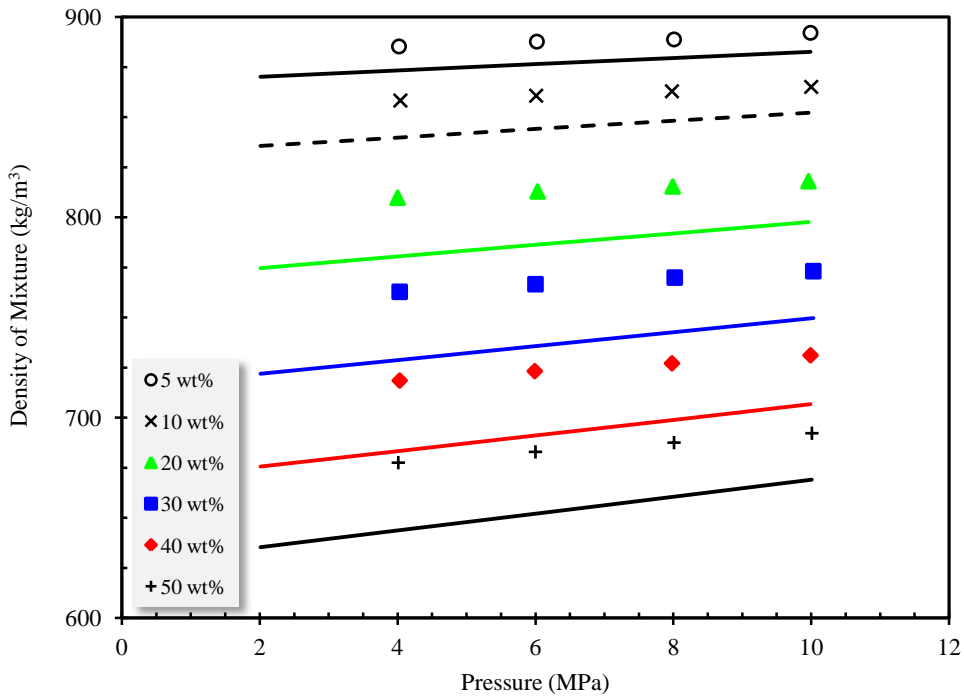


Figure 7–4: Density of Surmont bitumen / condensate mixtures as a function of pressure at different condensate weight fractions and at the highest temperature (190°C); \circ , \times , \blacktriangle , \blacksquare , \blacklozenge , $+$, experimental data; ----, predicted values.

The variation of mixture density with pressure at other temperatures (i.e. 50, 100, and 150°C), shown in Figures 7–5 and 7–6, is linear over the studied pressure. The linear increase of the mixture density with the pressure occurs at all measured concentrations. Figure 7–5 shows the variation of the mixture density with the pressure at the lowest condensate weight fraction (0.05) while Figure 7–6 displays the same results at the

highest condensate weight fraction (0.5). As depicted in these figures, the mixture density increases linearly with the pressure at different temperatures. The effect of pressure on the mixture density is more pronounced at higher temperatures and at higher concentrations.

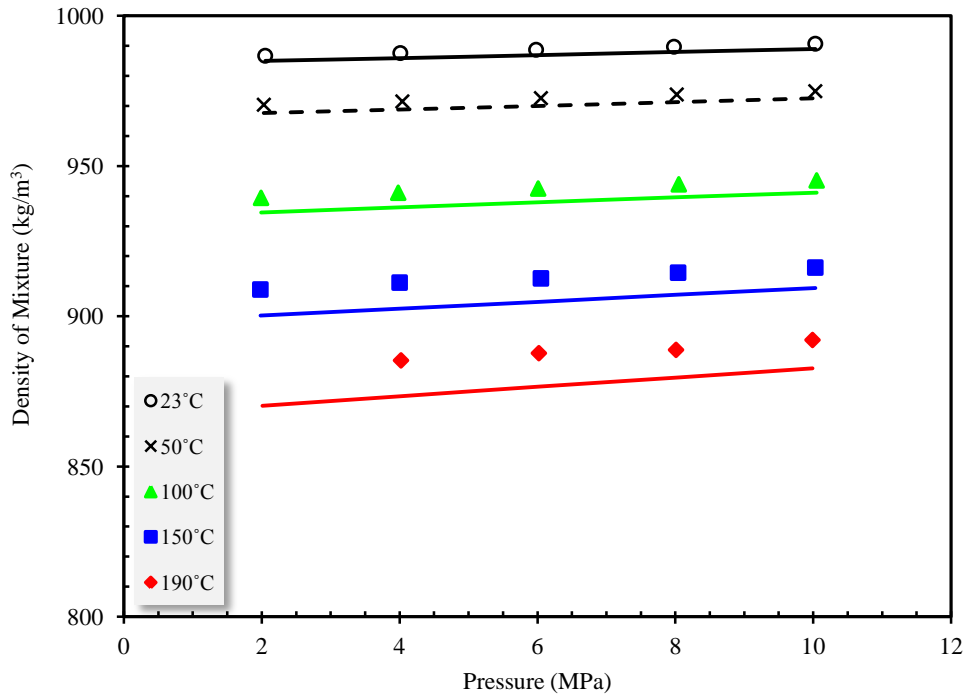


Figure 7-5: Density of Surmont bitumen / condensate mixtures as a function of pressure at different temperatures and at the lowest solvent weight fraction (0.05); \circ , \times , \blacktriangle , \blacksquare , \blacklozenge , experimental data; ----, predicted values.

A comparison of Figures 7-5 and 7-6 reveals that equation 6-1 provides better predictions at higher pressures and the deviation between the predictions and the measured data is more significant at lower pressures. It is also worth mentioning that at higher condensate concentrations or higher temperatures, equation 6-1 under-predicts the measured values. We conclude that the volume change on mixing is significant for the mixtures of Surmont bitumen and condensate. The volume change on mixing is more pronounced at high temperatures or at large solvent weight fractions where larger deviations from the measured data were obtained.

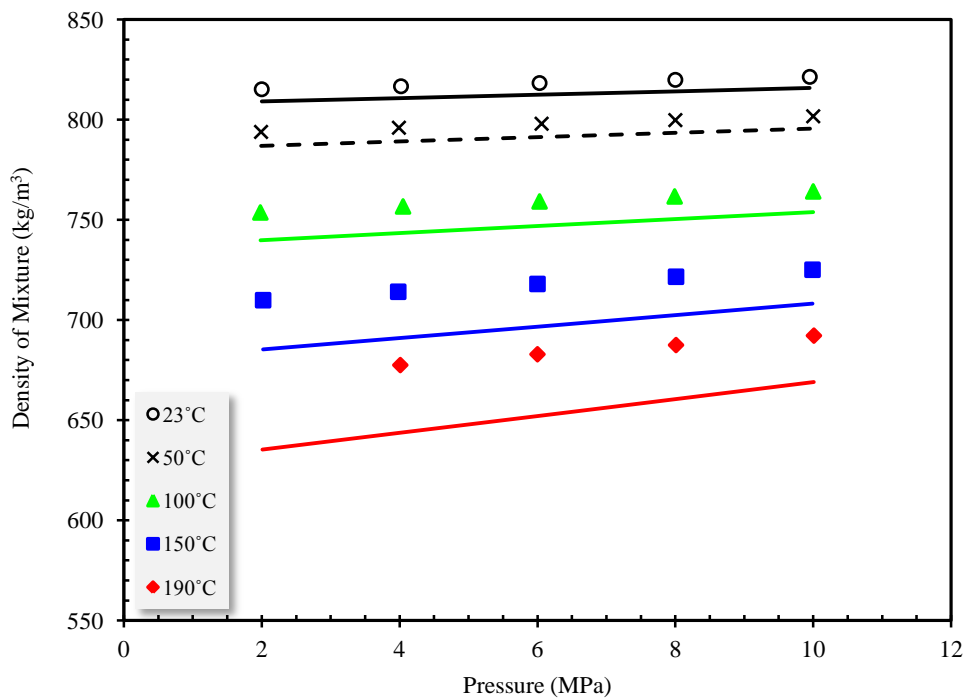


Figure 7-6: Density of Surmont bitumen / condensate mixtures as a function of pressure at different temperatures and at the highest solvent weight fraction (0.5); \circ , \times , \blacktriangle , \blacksquare , \blacklozenge , experimental data; ----, predicted values.

As outlined in Chapter 3, the density of the raw bitumen is linearly decreased with temperature at a constant pressure. The variations of mixture density with temperature at two different pressures (2 and 10 MPa) are shown in Figures 7-7 and 7-8. As depicted in the figures, all prepared mixtures follow a linear decrease in density with temperature. Comparison of Figures 7-7 and 7-8 confirms that the linear decrease of the mixture density with temperature is consistent for all measured pressures. The density data at the highest condensate weight fraction (0.5) deviate slightly from the linear trend because of the non-linear trend of the density with temperature for the condensate at a constant pressure. A comparison of the mixture densities for Surmont bitumen / condensate and Surmont bitumen / hexane reveals that the hexane-diluted bitumen shows greater non-linear variations with temperature.

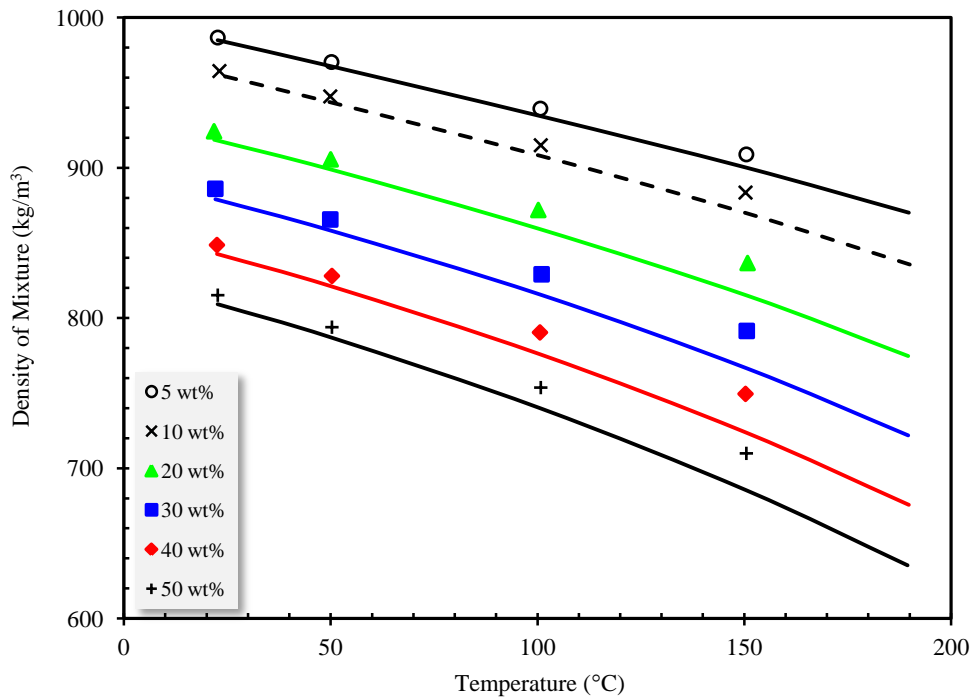


Figure 7-7: Density of Surmont bitumen / condensate mixtures as a function of temperature at different condensate weight fractions and at the lowest pressure (2 MPa); \circ , \times , \blacktriangle , \blacksquare , \blacklozenge , experimental data; ----, predicted values.

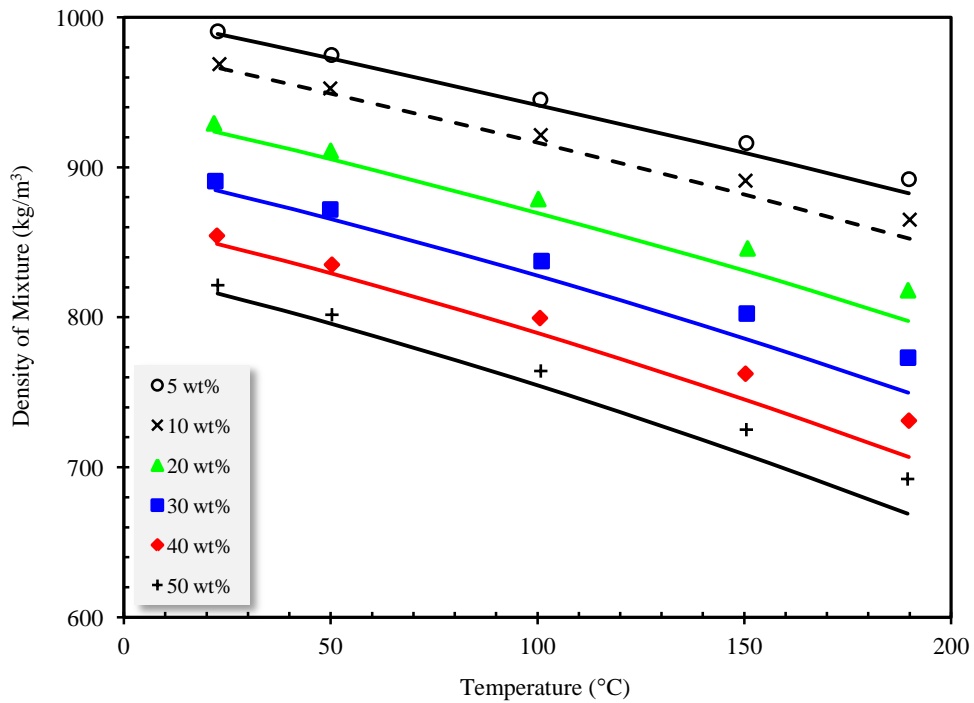


Figure 7-8: Density of Surmont bitumen / condensate mixtures as a function of temperature at different condensate weight fractions and at the highest pressure (10 MPa); \circ , \times , \blacktriangle , \blacksquare , \blacklozenge , experimental data; ----, predicted values.

7.4.2. Volume Change on Mixing

The predicted densities in the previous section show that at a constant pressure and constant solvent weight fraction, the deviation between the measured data and the calculated values became significant when the temperature was increased. This is an indirect representation of the increase in the volume change on the mixing with the temperature. However, when the values calculated with equation 6-4 are plotted with respect to the temperature at a constant pressure and a constant solvent weight fraction, the volume change upon mixing is directly affected by the temperature. Figures 7–9 and 7–10 illustrate the dimensionless volume change (equation 6-4) as a function of temperature at a constant pressure. As depicted in these two figures, the volume change on mixing increases with the temperature. Although the extent of increase in volume change on mixing is not the same at different pressures, the increasing trend was observed for all of the pressures that were measured. The effect of the solvent weight fraction on the volume change on mixing is also evident in Figures 7–9 and 7–10. The increase in the solvent weight fraction enhanced the volume change on mixing for the mixtures.

The densities of raw bitumen and condensate are a function of temperature and pressure. The volume of the components and their molecular behaviour changed as the operating conditions were manipulated. The measured volume change on mixing was reduced as the pressure was increased at a constant temperature. As the pressure increases at a constant temperature, the density of the raw bitumen and the condensate was increased. The molecules of each component are pushed closer together by increasing pressure and resulting in a reduction of the occupied volume. Due to less void space between molecules at high pressures, limited number of molecules can occupy the void spaces and thus volume shrinkage is less at high pressures.

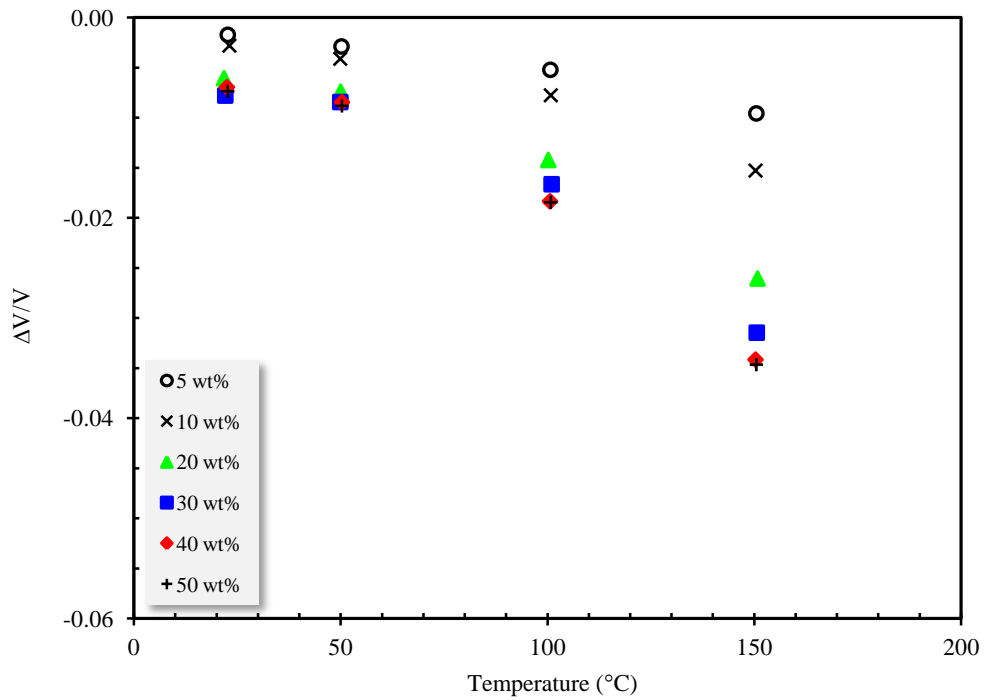


Figure 7-9: Effect of temperature on the volume change on mixing for Surmont bitumen / condensate mixtures with different solvent weight fractions at a constant pressure of 2 MPa.

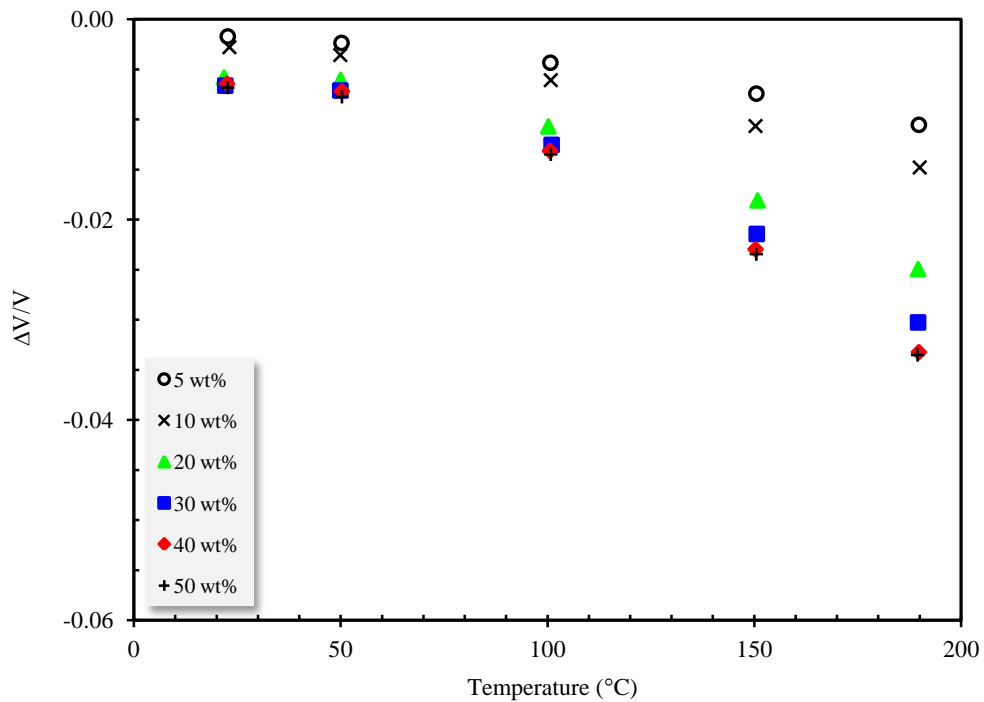


Figure 7-10: Effect of temperature on the volume change on mixing for Surmont bitumen / condensate mixtures with different solvent weight fractions at a constant pressure of 10 MPa.

The effect of pressure on the volume change on mixing at the lowest temperature (23°C) is negligible (less than 1 %) for all solvent weight fractions. As the temperature increases, the variation of the volume change on mixing with pressure becomes significant. At two high temperature conditions (150 and 190°C), significant volume change on mixing is observed for the mixtures. The variations are a non-linear function of pressure. Figure 7–11 illustrates the change in the volume during the mixing process for Surmont bitumen / condensate mixtures at the highest temperature (190°C). The decreasing trend of the volume change on mixing with the pressure was observed at five different temperatures and six condensate weight fractions. The mixture of Surmont bitumen / condensate with 0.05 weight fraction of solvent exhibits a smaller pressure dependence than that of 0.5 weight fraction of solvent where a large decrease in the volume change on mixing is measured for a given pressure.

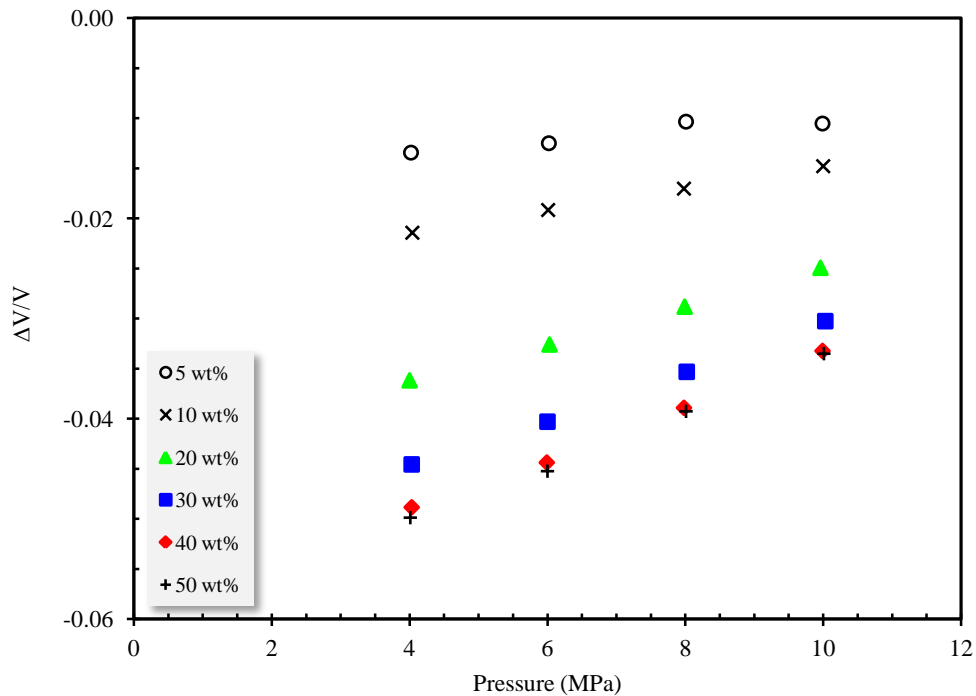


Figure 7–11: Effect of pressure on the volume change on mixing for Surmont bitumen / condensate mixtures with different solvent weight fractions at 190°C.

To evaluate the impact of temperature and pressure on the volume change on mixing, volume change can be plotted as a function of pressure at different temperatures and at a constant weight fraction of condensate. It was observed that at the condensate weight fraction of 0.05, the impact of pressure is insignificant. However, when the solvent weight fraction increased to 0.1 or 0.2, the variation of volume change on mixing with pressure becomes significant. Figure 7–12 demonstrates the volume change on mixing as a function of pressure at the highest solvent weight fraction (0.5). As anticipated from the figure, the volume change on mixing at the ambient temperature (23°C) is negligible even at high solvent weight fractions. It can be concluded that at ambient temperature, the volume change on mixing for the mixtures of Surmont bitumen / condensate over the entire concentration range is insignificant and equation 6-1 can adequately predict the density of mixture.

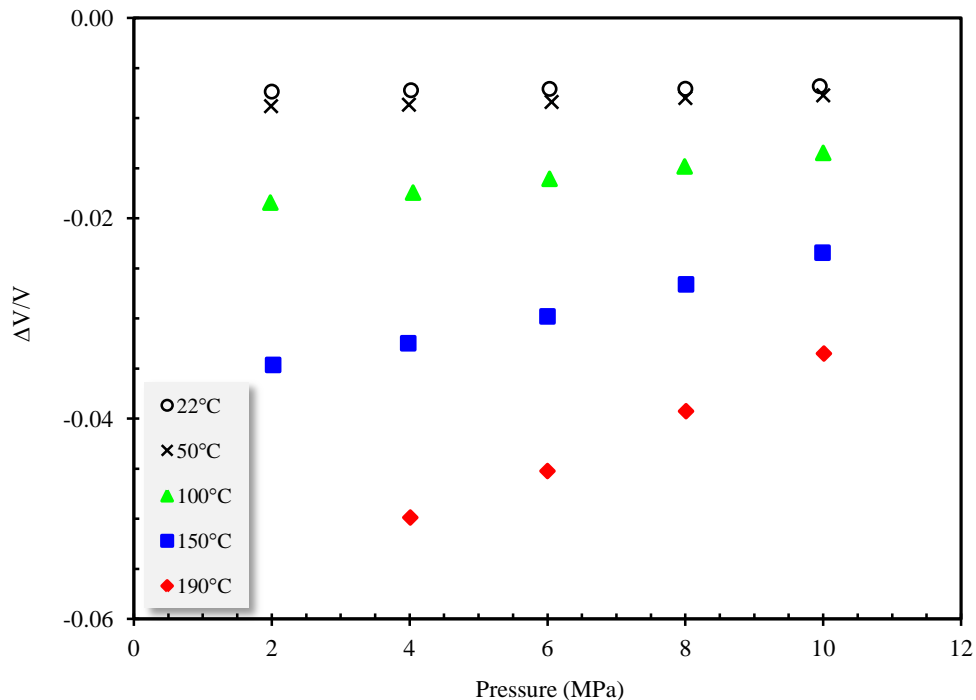


Figure 7–12: Effect of pressure on the volume change on mixing for Surmont bitumen / condensate mixtures at a constant solvent weight fraction of 0.5 and at different temperatures.

The volume change on mixing increases as the solvent weight fraction in the mixture is increased. For some binary systems, such as (*n*-hexane + *n*-decane), the volume change on mixing reaches a minimum or maximum value at a specific concentration (Asfour et al. 1990). For the Surmont bitumen / condensate mixtures, the volume change on mixing increases as the condensate weight fraction is increased. As previously mentioned, the mixtures show a negative volume change on the mixing indicating the formation of a more compact structure compared to the pure species.

Figures 7–13 and 7–14 illustrate the volume change on mixing for the Surmont bitumen / condensate mixture as a function of the solvent weight fraction at a constant pressure. Figure 7–13 shows the results at the pressure of 2 MPa and Figure 7–14 details the measurements at the pressure of 10 MPa.

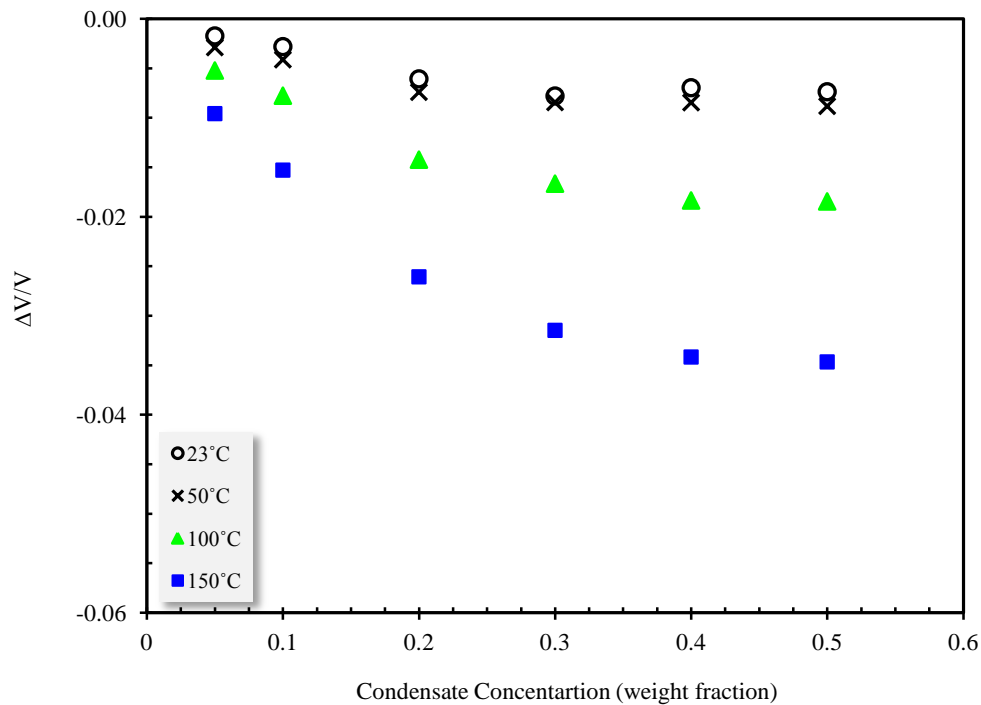


Figure 7–13: Volume change on mixing for Surmont bitumen / condensate mixtures as a function of the weight fraction of pentane at different temperatures and at a constant pressure of 2 MPa.

As depicted in the figures, increasing the solvent weight fraction results in a larger value for the volume change on the mixing. Similar to the binary hydrocarbon systems,

the pressure reduced the maximum value of the volume change on the mixing and forced the concave curve toward zero. As expected from the binary hydrocarbon mixture results, the volume change on mixing should increase as the solvent weight fraction increases, reaches a maximum values, and starts decreasing towards zero. However, as depicted in Figure 7–13 for the bitumen / condensate mixtures, the volume change on mixing flattens off after the condensate weight fraction of 0.3.

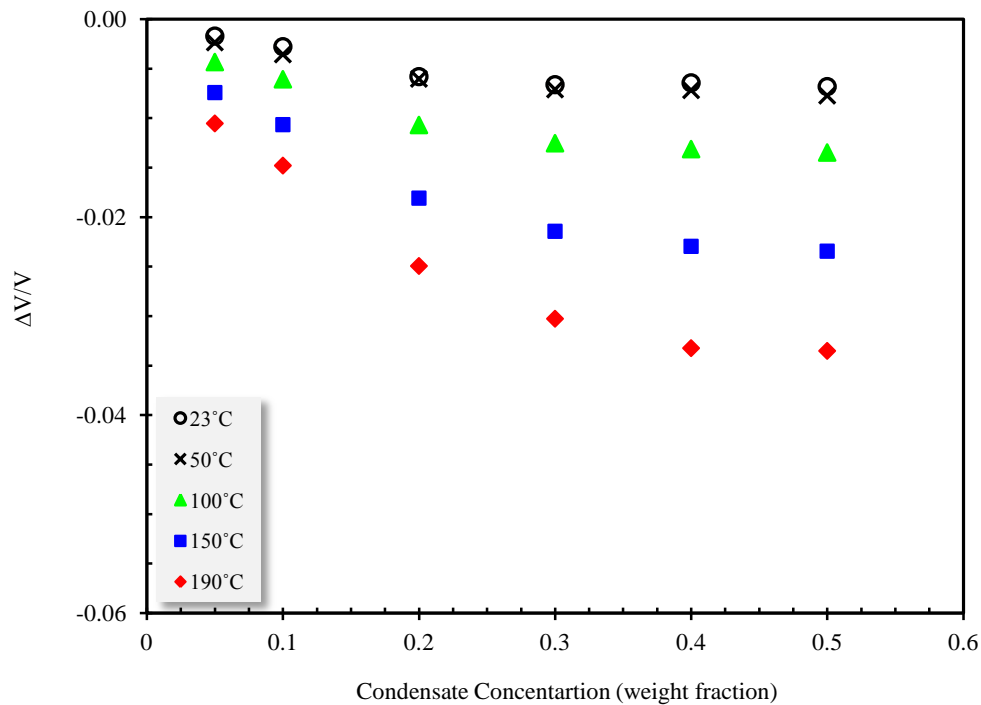


Figure 7–14: Volume change on mixing for Surmont bitumen / condensate mixtures as a function of the weight fraction of pentane at different temperatures and at a constant pressure of 10 MPa.

7.4.3. Improvement in Calculation of Mixture Density

As discussed earlier, there is significant volume change on mixing for the Surmont bitumen / condensate mixtures. Accordingly, the excess volume mixing rule is applied in this section to improve the accuracy of density calculations. The measured density data of the Surmont bitumen / condensate mixtures are correlated with equation 6-5. The last term in this equation accounts for the volume change on mixing and β_{ij} is the binary interaction parameter between the condensate and bitumen obtained by the regression of

the measured densities. The density of the condensate at each temperature and pressure was calculated from the developed correlation and that of raw bitumen was taken from Chapter 3. The best fitted binary interaction parameter (β_{ij}) was 0.0313, which gave the lowest average absolute relative deviation. Table 7–8 summarizes the calculated deviations of the models for prediction of the mixture densities. As the deviations show, the calculated results using the excess volume mixing rule are slightly better those calculated with the assumption of no volume change on mixing.

Table 7–8: Deviations of different models for calculation of Surmont bitumen / condensate mixture density

Calculation Method	AARD (%)	AAD (kg/m ³)	MAD (kg/m ³)
No volume change	1.43	11.5	35.1
Excess volume	0.78	6.3	24.0

Figures 7–15 and 7–16 are dispersion plots illustrating the calculated densities versus the measured values for the mixtures of Surmont bitumen / condensate using two different approaches. The excess volume mixing rule slightly improves the predictions compared to the method with the assumption of no volume change on mixing. The models show a larger deviation from the experimental data in the lower density values. This indicates that the calculated results at high temperature and/or high concentrations cannot be well predicted with these two models.

Figures 7–17 and 7–18 display the measured densities for the mixtures of Surmont bitumen / condensate along with the calculated values. In Figure 7–17, the density is plotted as a function of the condensate weight fraction at different temperatures and at a constant pressure (2 MPa). Figure 7–18 illustrates the impact of pressure on the mixture density at different solvent weight fractions and at the temperature of 190°C. As shown in the figures, the application of the excess volume mixing rule for the prediction of densities resulted in a better agreement between measured and calculated data.

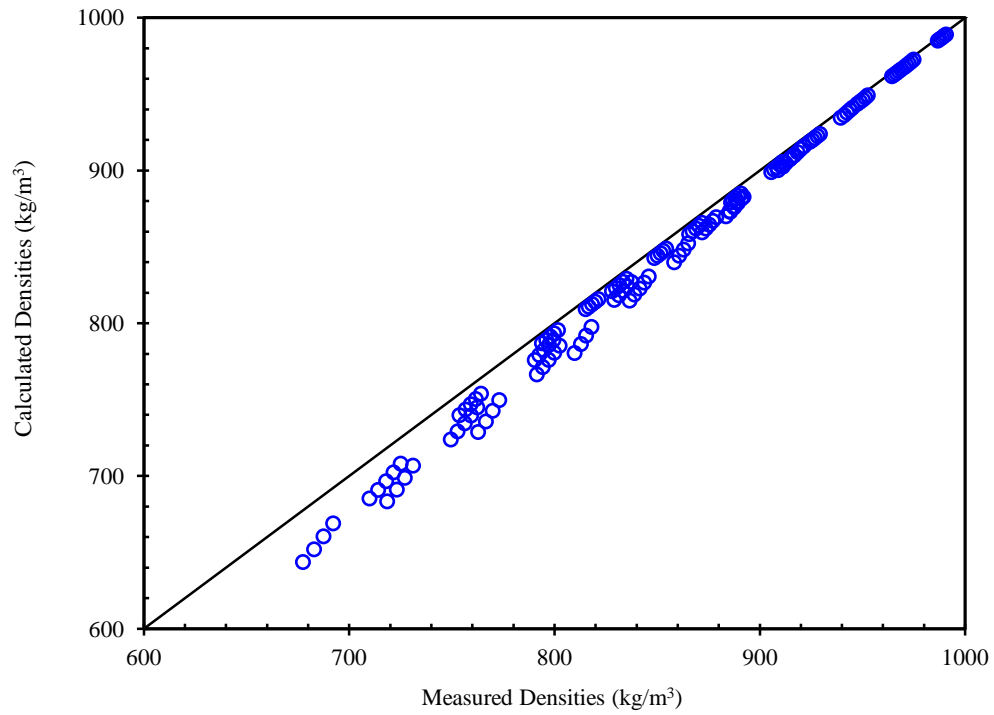


Figure 7–15: Calculated densities of Surmont bitumen / condensate mixtures using no volume change on mixing assumption versus the measured values.

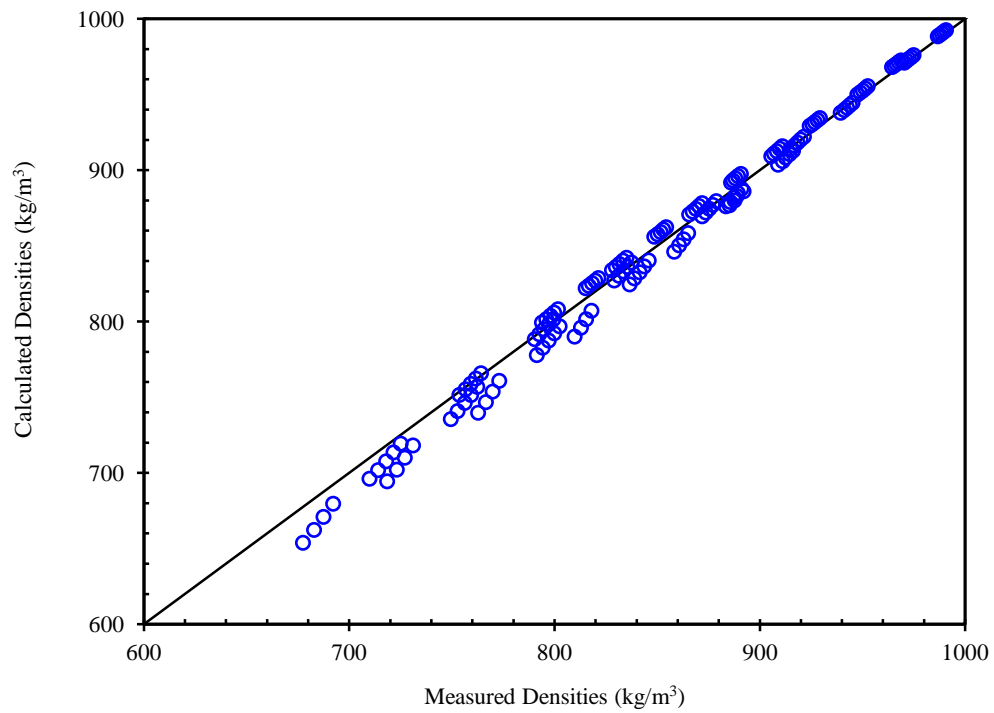


Figure 7–16: Calculated densities of Surmont bitumen / condensate mixtures using excess volume mixing rule versus the measured values.

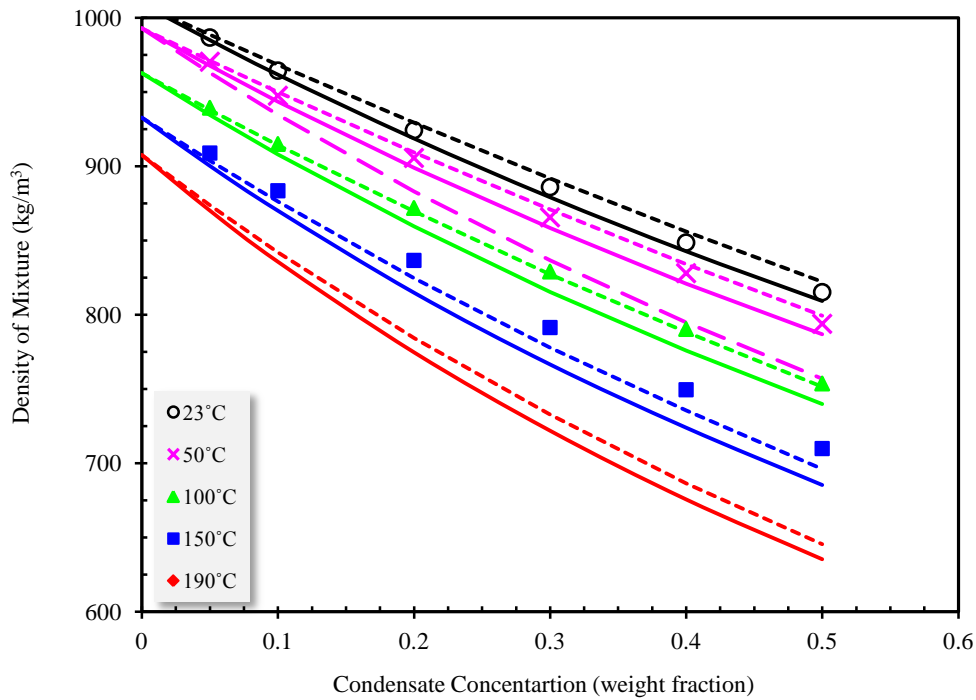


Figure 7-17: Density of Surmont bitumen / condensate mixtures as a function of the weight fraction of condensate at different temperatures and at a constant pressure of 2 MPa; ■, ▲, ○, ◆, ×, experimental data; —, no volume change on mixing; ----, excess volume mixing rule.

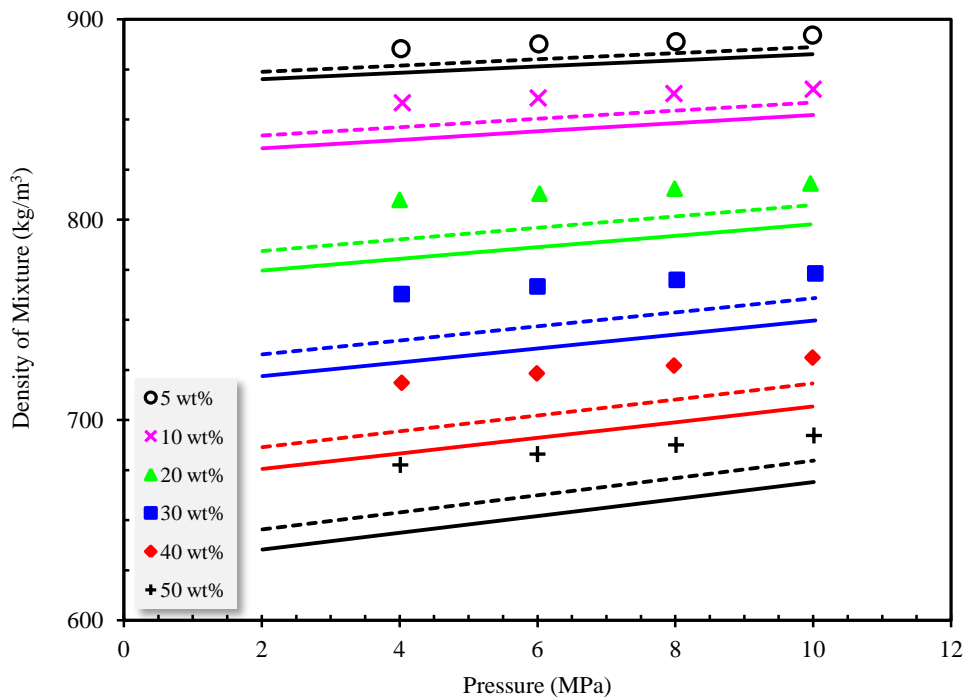


Figure 7-18: Density of Surmont bitumen / condensate mixtures as a function of pressure at different condensate weight fractions and at the highest temperature (190°C); ○, ×, ▲, ■, ◆, +, experimental data; —, no volume change on mixing; ----, excess volume mixing rule.

7.5. Viscosity of Mixtures

Tables 7–9 to 7–11 summarize the experimental viscosity values of the pseudo-binary mixture, Surmont bitumen / condensate, at different temperatures, pressures, and solvent weight fractions. At the temperature of 190°C, the pseudo-binary mixtures form a vapour-liquid equilibrium at a constant pressure of 2 MPa. Under these conditions, no single liquid phase was observed and so the viscosity could not be reported.

The viscosities of the condensate and the raw bitumen are reduced with the temperature at a constant pressure and increased with the pressure at a constant temperature. Similarly, the viscosity of the mixture at a constant solvent weight fraction is reduced as the temperature decreases at a constant pressure and increased as the pressure rises at a constant temperature. Under conditions of constant temperature and pressure, the solvent weight fraction significantly decreases the viscosity of the mixture.

The impact of pressure on the viscosity of the mixture is more pronounced at the lower condensate weight fractions. This behaviour is expected because as the weight fraction of solvent becomes higher, the behaviour of mixture becomes increasingly similar to that of the condensate.

The data on the viscosity of the condensate indicate that the viscosity is not significantly affected by changes in pressure. However, bitumen viscosity is more pressure dependent than the condensate. We have determined that any mixture prepared from bitumen and condensate shows behaviour similar to bitumen at low condensate weight fractions. The impact of pressure on the mixture viscosity is also dependent on the temperature. That is, at low temperatures, changes in the pressure result in higher viscosity variations.

Table 7–9: Experimental liquid viscosities of the pseudo-binary mixtures of Surmont bitumen / condensate at 0.05 and 0.1 weight fractions of condensate; w , weight fraction of condensate in the mixture; T , temperature; P , pressure; μ_m , density of mixture.

$w = 0.05$			$w = 0.1$		
T (°C)	P (MPa)	μ_m (mPa.s)	T (°C)	P (MPa)	μ_m (mPa.s)
189.6	2.01	----	190.0	2.01	----
189.6	4.02	5.78	190.0	4.04	3.65
189.9	6.02	6.02	190.2	6.01	3.86
190.0	8.01	6.11	190.3	7.98	4.13
190.2	9.99	6.41	190.3	10.00	4.18
151.5	1.98	13.2	150.9	2.03	7.68
151.5	4.00	14.0	151.2	3.99	7.92
151.6	6.05	14.6	151.3	6.01	8.03
151.7	8.04	15.6	151.4	8.00	8.23
151.7	10.03	15.6	151.5	10.03	8.48
101.5	1.99	70.3	102.1	2.01	30.1
101.5	3.98	72.7	102.4	4.02	30.6
101.2	6.01	78.4	102.6	6.03	31.5
101.5	8.05	82.3	102.7	7.99	32.5
101.7	10.05	84.8	102.8	10.05	33.6
53.9	2.03	1039	52.0	2.00	253
53.1	4.04	1194	52.2	4.03	279
52.9	6.05	1307	52.3	6.01	297
52.8	8.02	1390	52.4	8.00	316
52.7	10.03	1464	52.4	10.00	335
24.4	2.05	20780	27.1	2.01	2056
25.5	4.01	21980	27.2	4.01	2404
26.6	5.98	23080	27.2	6.01	2637
26.6	7.98	----	27.3	8.02	2873
26.6	10.03	----	27.3	9.99	3109

Table 7–10: Experimental liquid viscosities of the pseudo-binary mixtures of Surmont bitumen / condensate at 0.2 and 0.3 weight fractions of condensate; w , weight fraction of condensate in the mixture; T , temperature; P , pressure; μ_m , density of mixture.

$w = 0.2$			$w = 0.3$		
T (°C)	P (MPa)	μ_m (mPa.s)	T (°C)	P (MPa)	μ_m (mPa.s)
190.0	2.01	----	190.0	2.01	----
190.0	4.00	1.83	190.0	4.03	0.902
190.0	6.03	1.86	190.0	6.00	0.931
189.4	7.99	1.92	190.0	8.02	0.955
189.7	9.96	1.97	190.0	10.03	0.979
149.1	2.01	3.13	151.4	2.00	1.459
149.9	4.00	3.24	151.3	4.02	1.510
150.5	6.01	3.28	151.5	6.02	1.541
150.7	7.99	3.33	151.5	8.03	1.588
151.0	10.00	3.39	151.6	10.01	1.636
101.5	2.02	8.00	102.4	2.02	3.34
101.5	4.01	8.61	102.7	4.04	3.48
101.5	5.99	9.04	102.8	6.03	3.53
101.5	8.01	9.42	102.8	8.03	3.63
101.5	9.98	9.79	102.8	10.01	3.73
53.0	2.04	42.6	52.3	2.02	11.8
53.0	4.02	44.6	52.4	4.04	12.2
53.0	5.99	46.0	52.5	6.04	12.6
53.0	8.01	47.9	52.6	8.00	12.8
53.0	10.01	49.8	52.7	10.01	13.3
26.0	2.00	170	26.5	2.00	29.4
26.0	4.00	180	26.8	4.02	31.3
26.1	5.99	186	27.0	5.99	32.4
26.5	8.04	188	27.1	8.00	33.5
26.8	10.03	194	27.2	10.00	34.5

Table 7–11: Experimental liquid viscosities of the pseudo-binary mixtures of Surmont bitumen / condensate at 0.4 and 0.5 weight fractions of condensate; w , weight fraction of condensate in the mixture; T , temperature; P , pressure; μ_m , density of mixture.

$w = 0.4$			$w = 0.5$		
T (°C)	P (MPa)	μ_m (mPa.s)	T (°C)	P (MPa)	μ_m (mPa.s)
190.0	2.01	----	190.0	2.01	----
189.6	4.03	0.502	190.0	4.01	0.328
189.8	5.99	0.520	190.0	6.00	0.339
189.9	7.98	0.535	190.0	8.01	0.344
190.0	9.99	0.543	190.0	10.01	0.361
151.5	2.03	0.748	150.8	2.02	0.472
151.5	4.04	0.762	151.2	3.98	0.480
151.3	6.07	0.789	151.4	6.00	0.491
151.4	8.00	0.807	151.5	8.01	0.502
151.5	10.00	0.826	151.6	9.99	0.512
101.0	1.99	1.539	101.6	1.98	0.867
101.0	3.99	1.586	102.2	4.05	0.882
101.0	5.98	1.608	102.4	6.03	0.892
101.0	8.03	1.647	102.6	7.99	0.905
101.0	10.05	1.679	102.7	10.00	0.919
51.5	2.01	4.19	51.9	1.99	2.04
51.5	3.99	4.34	52.1	3.99	2.03
51.5	6.02	4.49	52.3	6.06	2.06
51.5	8.05	4.55	52.5	8.00	2.11
51.5	9.98	4.66	52.6	10.00	2.15
28.2	1.99	8.02	27.9	2.00	3.16
28.2	3.99	8.32	27.7	4.02	3.31
28.2	6.00	8.54	27.7	6.03	3.41
28.4	8.02	8.72	27.7	8.00	3.48
28.3	9.96	8.96	27.9	9.95	3.53

7.5.1. Correlation and Prediction of Mixture Viscosity

Few correlations for the calculation of the viscosity for bitumen/diluents mixtures have been documented in the literature. Miadonye et al. (1995) developed a viscosity correlation to predict the viscosity-temperature relationship of bitumen mixed with various proportions of diluents such as GCOS synthetic crude, Mobil solvent and naphtha. Miadonye et al. (2000) proposed an equation for predicting the kinematic viscosity of bitumens and heavy oils mixed with diluents. This correlation requires the knowledge of the viscosities of raw bitumen and pure solvent at any given temperature. Miadonye et al. (2001) extended a correlation to predict the viscosity of bitumen-diluent mixtures, as well as the mass fraction required to reduce the bitumen viscosity to pumping viscosity. Motahhari et al. (2011) correlated the viscosity of a condensate, two bitumen samples from the Peace River field, and bitumen/condensate mixtures using an expanded fluid viscosity model.

The measured viscosity data of the Surmont bitumen / condensate mixtures were evaluated with relationships developed for the mixtures (Section 6.4.1). Table 7-12 summarizes the AARDs of the calculated viscosity values using six aforementioned models for the Surmont bitumen / condensate mixtures. In the models, the viscosity of the condensate was calculated from the developed equation (equation 7-1) at the desired temperature and pressure and the measured viscosities of bitumen reported in Chapter 3. In this study, the fraction of solvent was considered as mole, weight, and volume fractions in Arrhenius', power law, and Cragoe's models. Arrhenius' model results in better predictions when the mole fraction is considered in the models. Cragoe's and power law models give the best results with the volume fraction. The adjustment of the parameters in the models was obtained by minimizing the AARD of the calculated and measured values.

Table 7–12: Calculated AARDs of different models for the correlation and prediction of the viscosity for Surmont bitumen / condensate mixtures.

Model	AARD (%)		
	Mole fraction	Weight fraction	Volume fraction
Arrhenius	46.5	4180	1320
Power Law	37.2 ^a	31.1 ^b	12.5 ^c
Cragoe	82.4	169	22.4
Lederer	----	----	36.6 ($\theta = 0.2895$)
Shu	----	----	55.8
Lobe	----	----	81.6

^a $n = 0.0257$; ^b $n = -0.3334$; ^c $n = -0.2112$

Figure 7–19 shows a comparison between the Arrhenius’ model and the measured viscosity data using three different solvent fractions (mole, weight, and volume). The best prediction is obtained using the mole fraction in the model. When the viscosities are calculated on the basis of the weight and volume fraction, the predicted values are greater than the experimental data.

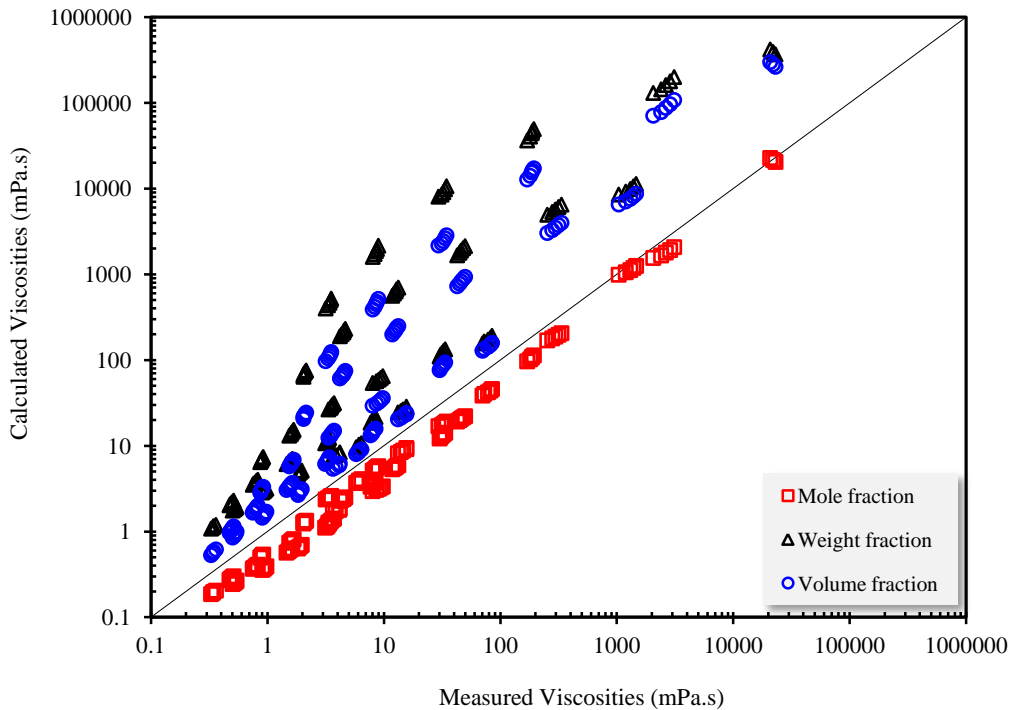


Figure 7–19: The comparison between the calculated viscosities with Arrhenius’ model and experimental data for Surmont bitumen / condensate mixtures.

Figure 7–20 illustrates the comparison between the power law model and the measured data using different fractions. In this model, the parameter (n) was adjusted for each fraction and the best fitted parameter is listed in Table 7–12. Although the predictions using weight and mole fractions are reasonable, the best predictions are obtained using the volume fraction in the model. A comparison shows that the AARD of the power law model with the volume fraction is 12.5% while the AARDs are 37.2% and 31.1% for mole and weight fractions, respectively.

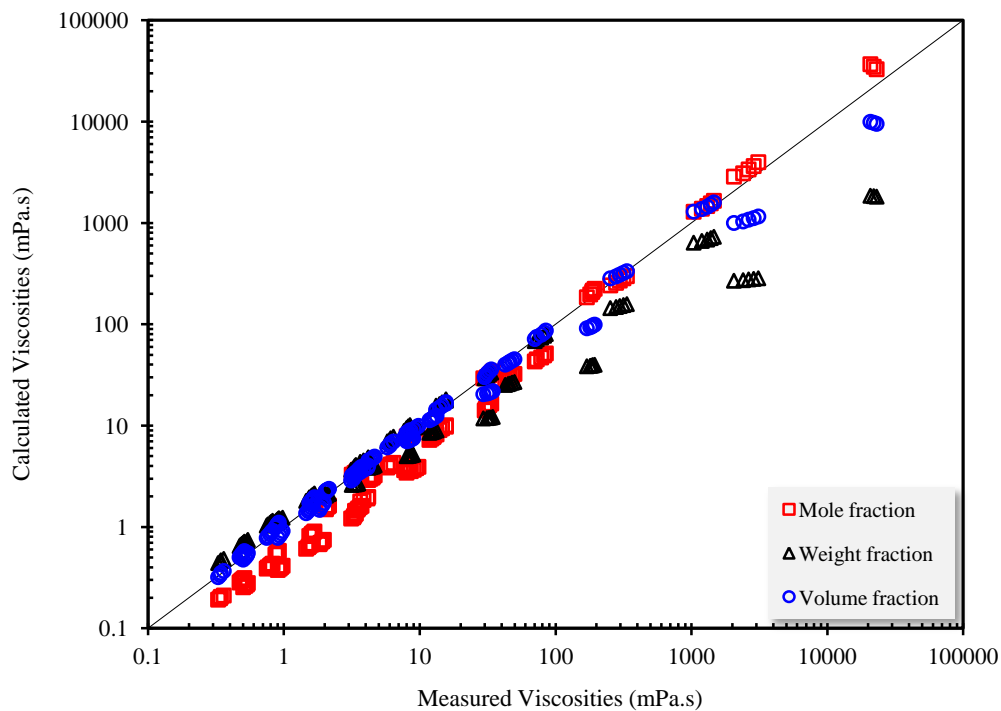


Figure 7–20: The comparison between the calculated viscosities with power law model and experimental data for Surmont bitumen / condensate mixtures.

The power law model (with mole fraction) under-predicts the viscosities in the range 0.1 to 1000 mPa.s and over-predicts the data when the viscosities of the mixtures are greater than about 1000 mPa.s. In contrast to the Arrhenius model, the power law model using the weight fraction generally under-predicts the viscosities over the entire range.

The comparison between the Cragoe's model and the measured viscosity data is shown in Figure 7–21. Similar to the power law model, the best predictions are obtained by considering the volume fraction in the model. The values calculated with the Cragoe's model using the mole fraction are generally smaller than the experimental viscosity data whereas the results calculated using the weight fraction are greater than the measured data. The errors for both cases are too large. A comparison shows that the AARD of Cragoe's model with the volume fraction is 22.4% while the AARDs are 82.4% and 169% for mole and weight fractions, respectively. The viscosities calculated by the Cragoe's model with the volume fraction show higher deviations at the viscosities greater than 100 mPa.s. In the viscosity range of 0.1 to 100 mPa.s, the model adequately predicts the experimental viscosity data.

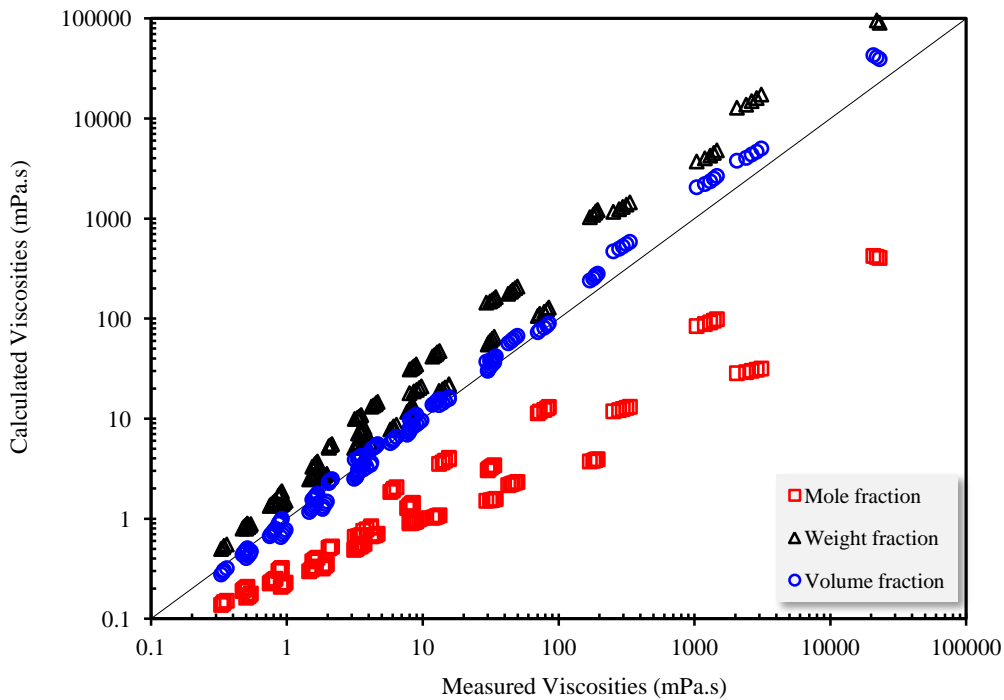


Figure 7–21: The comparison between the calculated viscosities with Cragoe's model and experimental data for Surmont bitumen / condensate mixtures.

Figures 7–22 to 7–24 illustrate the calculated results using Lederer's, Shu's, and Lobe's models compared to experimental viscosity data, respectively. The adjustable

parameter for Lederer’s model was obtained by regression of all of the data where $\alpha = 0.2895$ (coefficient in Lederer’s model). As depicted in the figures, the Lederer’s model could not accurately predict the results over a wide range of viscosity data. The model under-predicts the data for the viscosities that are less than 100 mPa.s. Shu’s and Lobe’s models provide good predictions for the viscosities less than 100 mPa.s but the results show large deviations for the viscosities greater than 100 mPa.s.

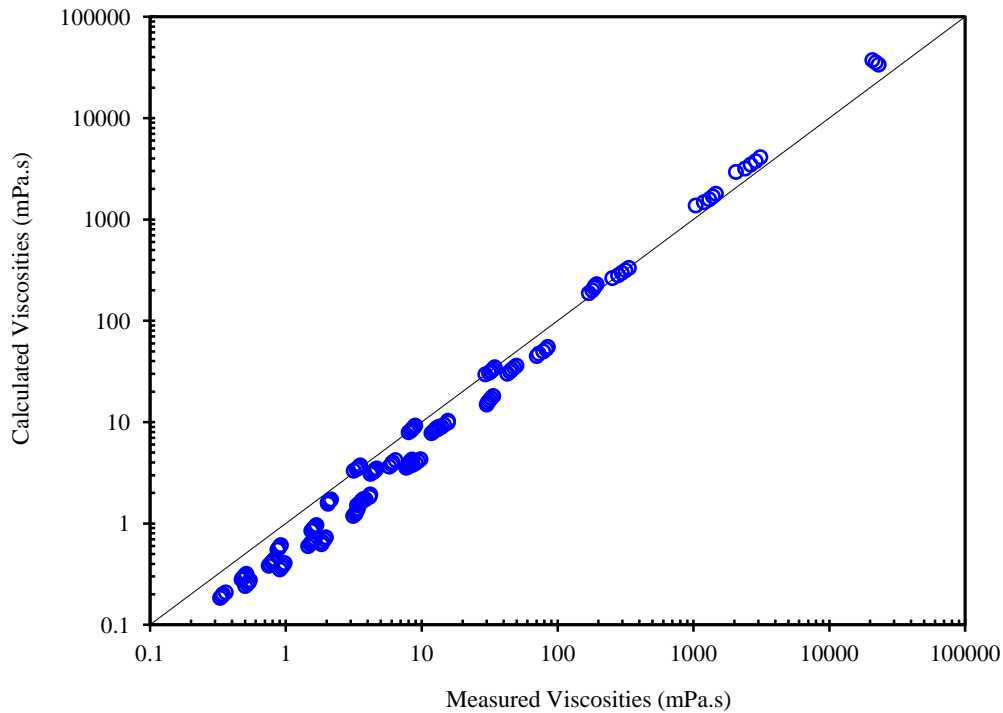


Figure 7–22: The comparison between the calculated viscosities with Lederer’s model and experimental data for Surmont bitumen / condensate mixtures.

As it is difficult to distinguish the results of the models, the comparison was confined to the AARDs. A comparison on the basis of AARDs shows that Lederer’s model provided better correlations and fit the data better than either of Shu’s or Lobe’s models. The AARD of Lederer’s model is 36.6% while the AARDs of Shu’s and Lobe’s models are 55.8% and 81.6%, respectively.

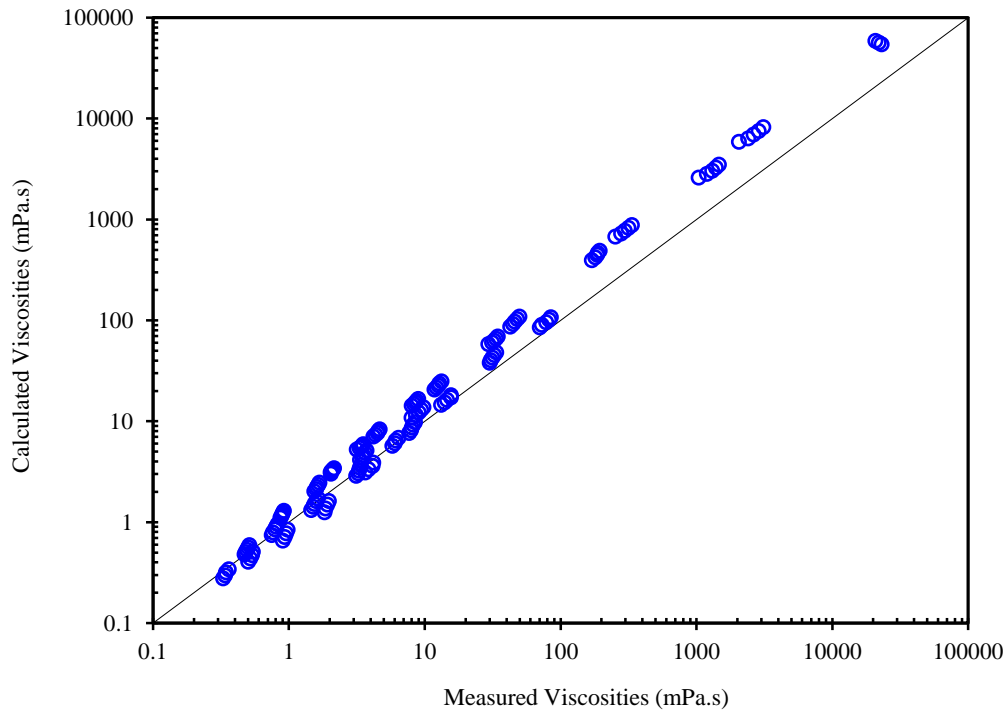


Figure 7–23: The comparison between the calculated viscosities with Shu's model and experimental data for Surmont bitumen / condensate mixtures.

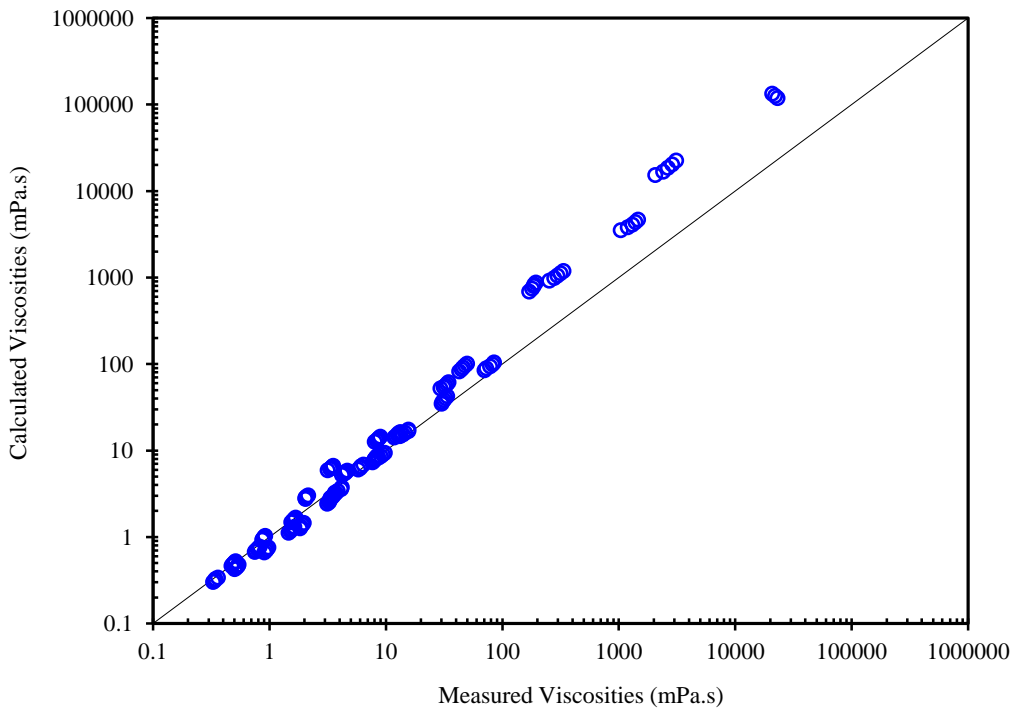


Figure 7–24: The comparison between the calculated viscosities with Lobe's model and experimental data for Surmont bitumen / condensate mixtures.

From the calculated AARDs in Table 7–12, we can conclude that the models predict the experimental viscosity data of Surmont bitumen / condensate mixtures over the entire range in the following order, from most accurate to least accurate,

1. power law (volume)
2. Cragoe (volume)
3. power law (weight)
4. Lederer
5. power law (mole)
6. Arrhenius (mole)
7. Shu
8. Lobe
9. Cragoe (mole)

The power law and Cragoe’s models using the volume fraction were selected for further comparison with the experimental data because they showed a better representation of measured data. The results obtained by the power law model are shown in the figures by solid lines and the dashed lines represent the results of the Cragoe’s model. The temperature values reported in each figure are the average values.

Figures 7–25 and 7–26 illustrate the effect of increasing the condensate weight fraction on the mixture viscosity at different temperatures in a semi-log scale. Figure 7–25 shows the results at the lowest pressure (2 MPa) and Figure 7–26 displays the data at the highest pressure (10 MPa). As presented in these figures, the viscosity of the mixture shows a non-linear trend with respect to the solvent weight fraction. The impact of change in temperature on the viscosity of the mixture is less pronounced at higher condensate concentrations. This could be a result of the temperature dependency of bitumen and condensate viscosities. At low condensate concentrations, the behaviour of the mixtures is more similar to that of the bitumen; therefore, the mixture shows higher temperature dependency.

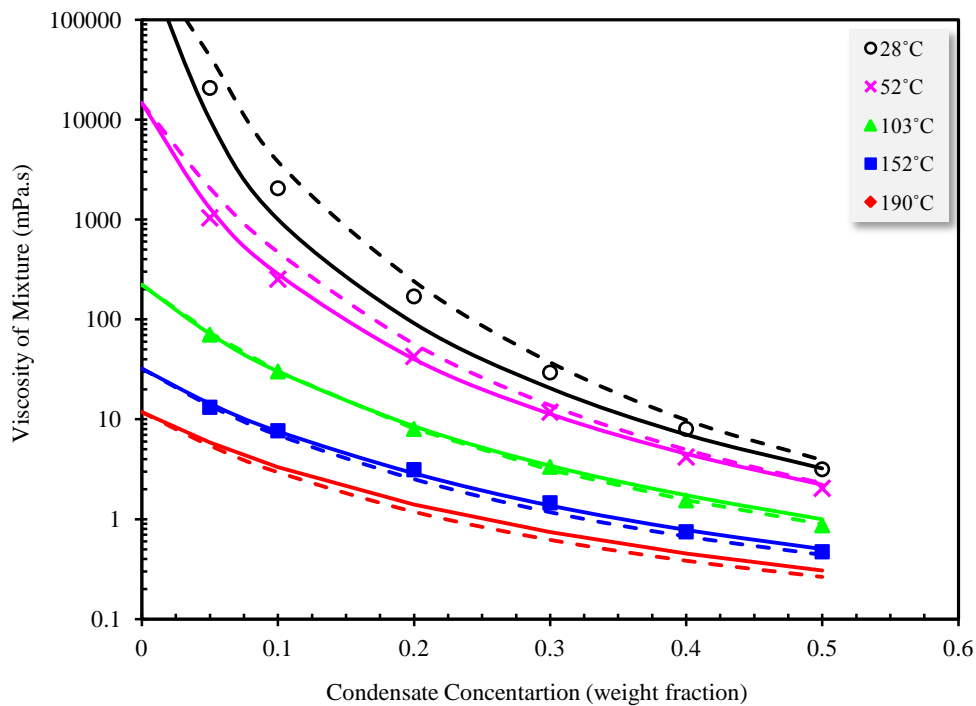


Figure 7–25: Viscosity of Surmont bitumen / condensate mixtures as a function of the weight fraction of condensate at different temperatures and at a constant pressure of 2 MPa; \circ , \times , \blacktriangle , \blacksquare , \blacklozenge , measured viscosities; calculated values: —, power law model; - - -, Cragoe's model.

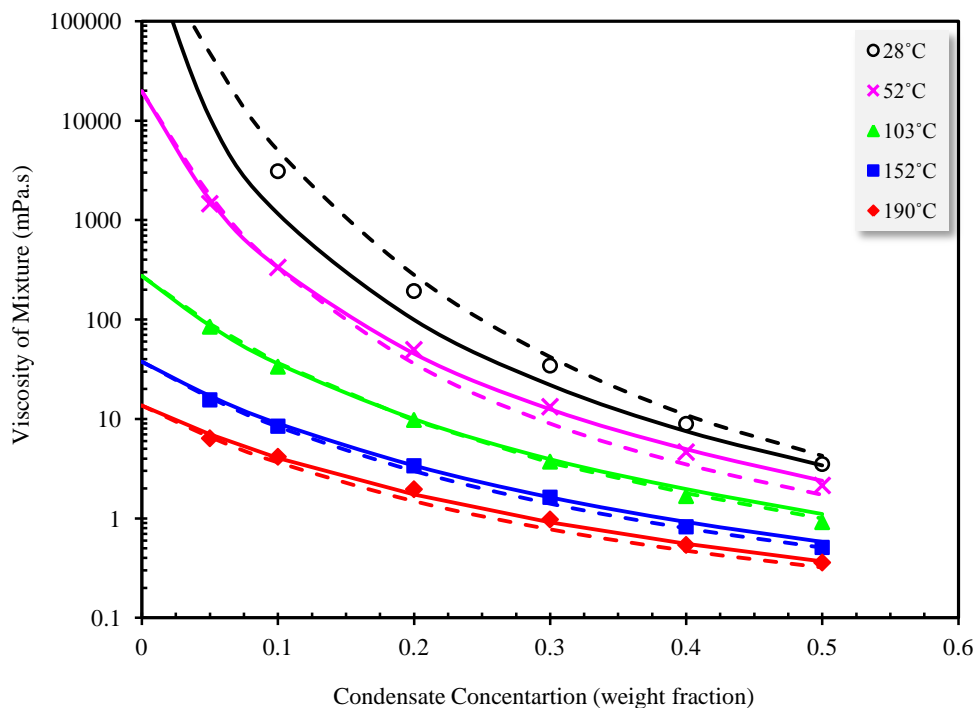


Figure 7–26: Viscosity of Surmont bitumen / condensate mixtures as a function of the weight fraction of condensate at different temperatures and at a constant pressure of 10 MPa; \circ , \times , \blacktriangle , \blacksquare , \blacklozenge , measured viscosities; calculated values: —, power law model; - - -, Cragoe's model.

The viscosity data are well correlated using the power law model. Although there was no significant difference in the results of two models, the power law model predicted the experimental data slightly better than Cragoe's model. Cragoe's model over-predicts the data at the lower temperatures (i.e. 28 and 52°C) and under-predicts at the higher temperatures (i.e. 190°C) while the power law model slightly under-predicts all of data.

Increasing the temperature significantly reduced the viscosity of heavy oil and bitumen (Section 3.2.2). The diluted bitumen also showed significant viscosity variations with the temperature. Figures 7-27 and 7-28 illustrate the variation of mixture viscosities with temperature at two pressures (2 and 10 MPa). These figures illustrate that the viscosity data, when plotted in semi-log scale, obey linear trend at higher condensate weight fractions and a non-linear trend at lower condensate weight fractions. At higher condensate weight fractions, the mixtures behave similar to condensate and the viscosity of condensate shows a linear trend with temperature (in semi-log plot). However, at lower condensate concentrations, the mixture is enriched in bitumen and its viscosity, as stated in equation 3-7, does not change linearly with the temperature.

To provide a better representation of the data and allow comparison with the models, the viscosity data at different condensate weight fractions were plotted versus pressure. Figure 7-29 shows the impact of pressure on the viscosity of Surmont bitumen / condensate mixtures at a constant temperature (28°C). Cragoe's model over-predicted the viscosity values for mixtures at different solvent weight fractions while the power law model under-predicted the data. When the temperature increased to the highest measured value (190°C), the same behaviour was observed for both models (Figure 7-30). That is, both Cragoe's and the power law models under-predicted the viscosity values of mixtures at different solvent fractions. The best match between the experimental data and Cragoe's model was obtained at 103°C. However, at the temperature of 28°C, the viscosities calculated with Cragoe's model show the largest deviation. The power law model represents the data more accurately at the temperature of 103°C but the model cannot correlate the data at the lowest temperature (i.e. 28°C) as well as other temperatures.

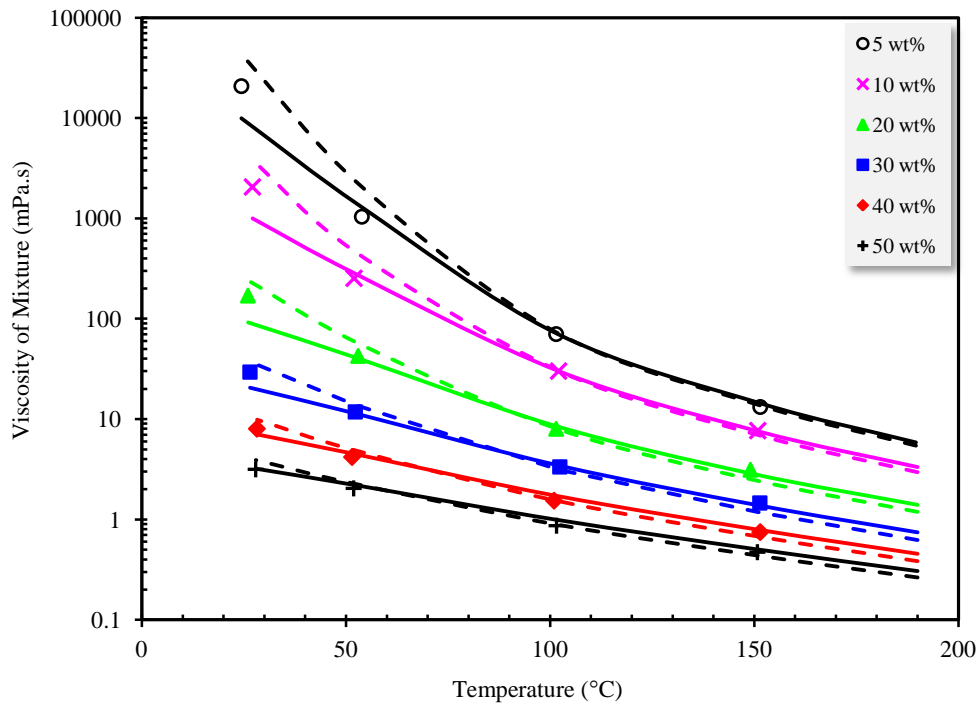


Figure 7-27: Viscosity of Surmont bitumen / condensate mixtures as a function of temperature at different weight fractions of condensate and at a constant pressure of 2 MPa; \circ , \times , \blacktriangle , \blacksquare , \blacklozenge , $+$, measured viscosities; calculated values: —, power law model; ---, Cragoe's model.

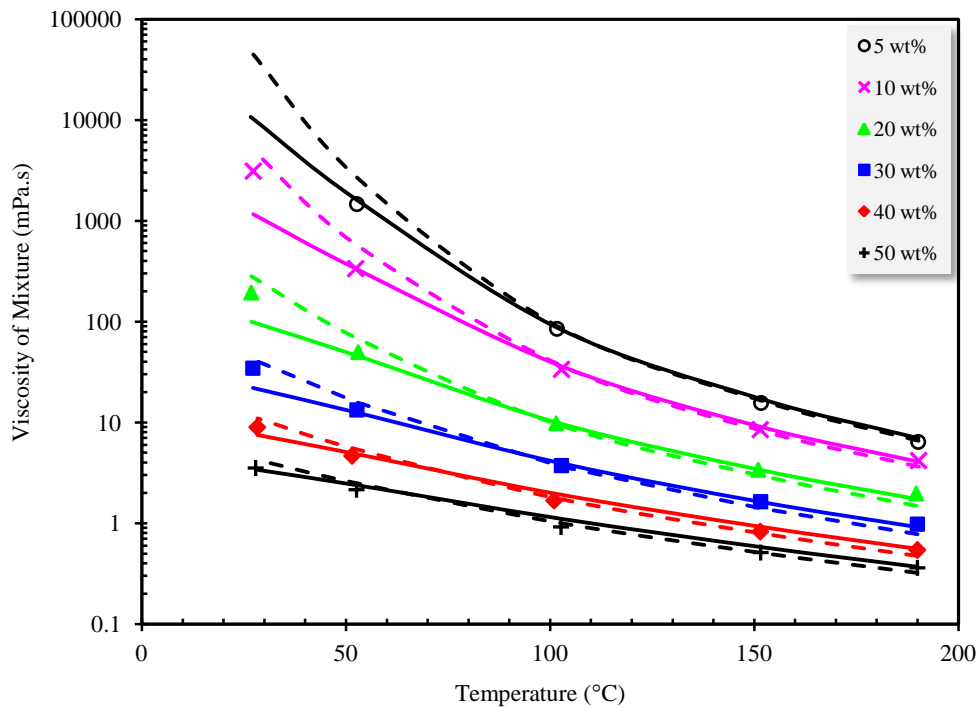


Figure 7-28: Viscosity of Surmont bitumen / condensate mixtures as a function of temperature at different weight fractions of condensate and at a constant pressure of 10 MPa; \circ , \times , \blacktriangle , \blacksquare , \blacklozenge , $+$, measured viscosities; calculated values: —, power law model; ---, Cragoe's model.

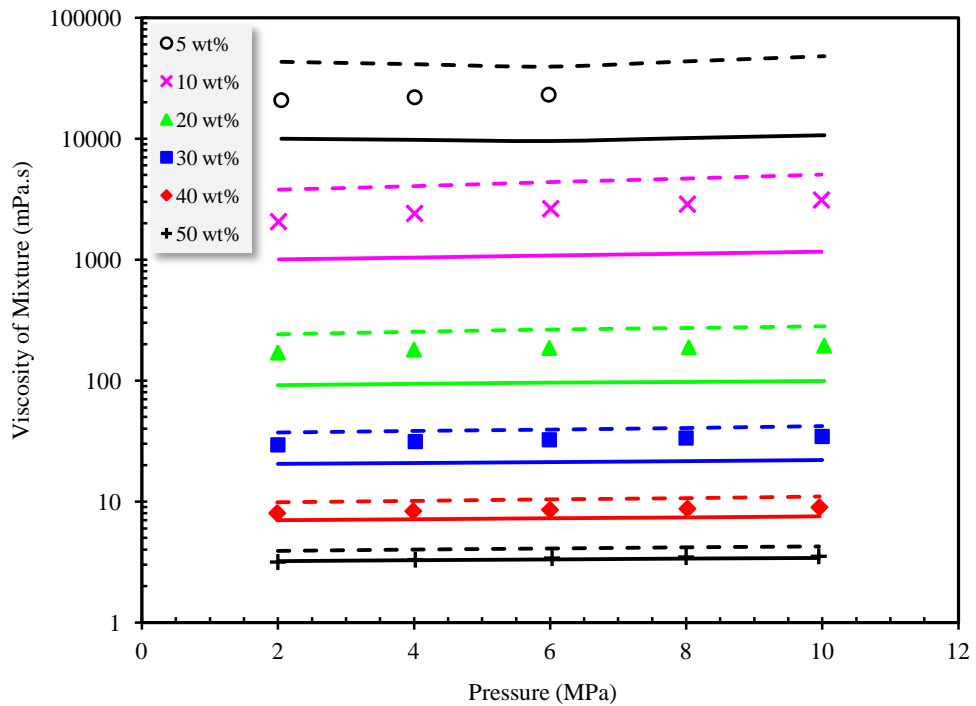


Figure 7–29: Effect of condensate concentration w_s and pressure P on the viscosity of Surmont bitumen / condensate mixtures at the lowest temperature (28°C); \circ , \times , \blacktriangle , \blacksquare , \blacklozenge , $+$, measured viscosities; calculated values: —, power law model; - - -, Cragoe's model.

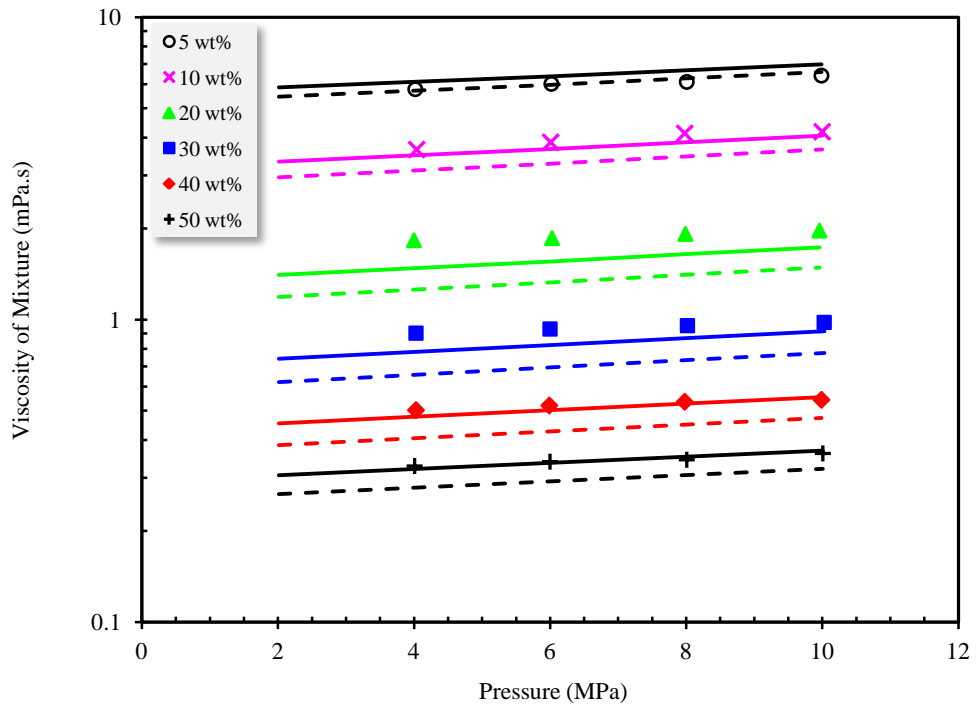


Figure 7–30: Effect of condensate concentration w_s and pressure P on the viscosity of Surmont bitumen / condensate mixtures at the highest temperature (190°C); \circ , \times , \blacktriangle , \blacksquare , \blacklozenge , $+$, measured viscosities; calculated values: —, power law model; - - -, Cragoe's model.

To determine the effects of pressure and dilution of the mixture with condensate on viscosity, the viscosity data were plotted as a function pressure at 0.05 and 0.5 weight fractions of condensate (Figures 7–31 and 7–32). The symbols with the same color indicate a constant temperature in these plots. Figures 7–31 and 7–32 show that the mixture viscosity has a linear relationship with the pressure at each isotherm, and this effect is greater at lower condensate weight fractions (0.05). Comparing the figures indicates that the slope of the viscosity-pressure plots is higher at lower solvent weight fractions. In fact, the impact of pressure on the viscosity of bitumen and condensate is different. The viscosity of condensate is not affected by moderate pressure increments; therefore, the viscosity of bitumen/condensate mixtures at high condensate concentrations follows the same trend. At low solvent weight fractions, the pressure has a more significant effect on the mixture viscosity due to the higher concentration of bitumen in the mixture.

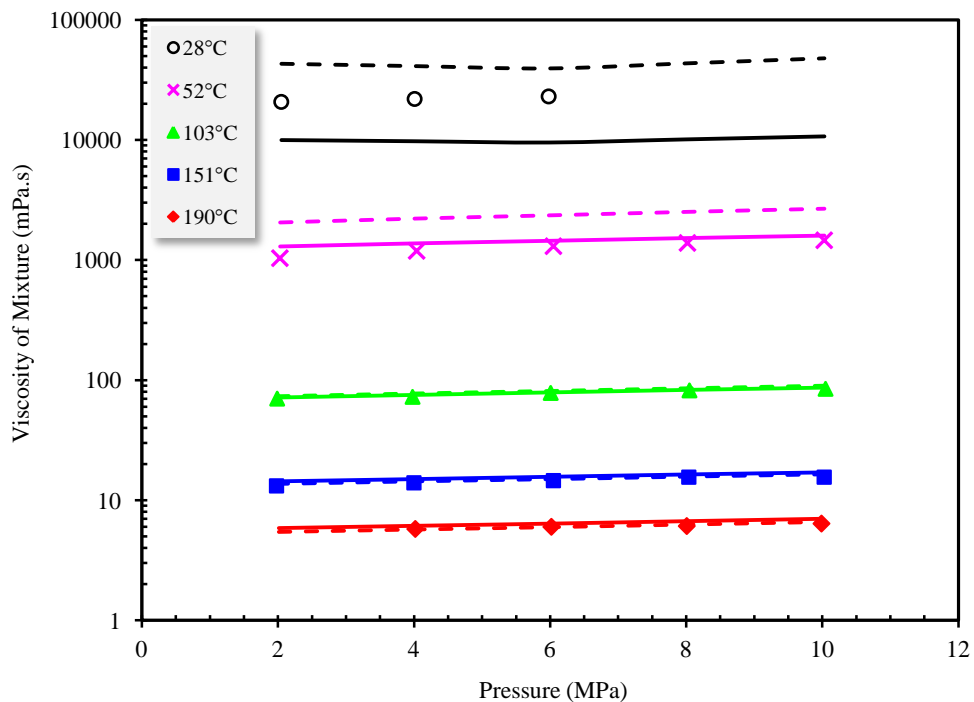


Figure 7–31: Effect of pressure P on the viscosity of Surmont bitumen / condensate mixtures at the lowest condensate weight fraction (0.05); \circ , \times , \blacktriangle , \blacksquare , \blacklozenge , $+$, measured viscosities; calculated values: —, power law model; - - -, Cragoe's model.

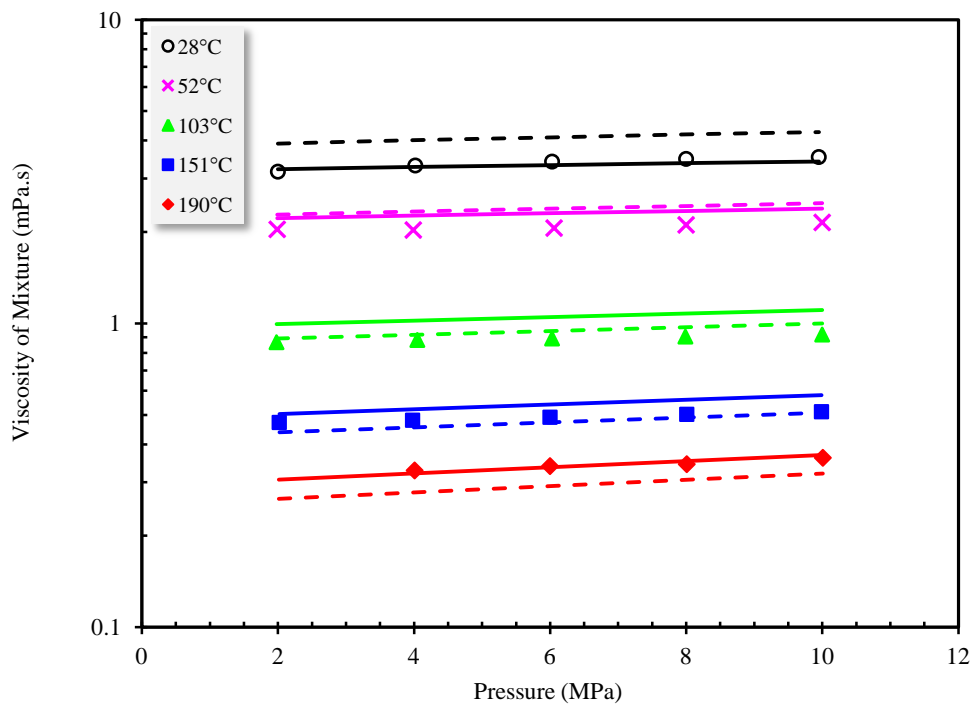


Figure 7–32: Effect of pressure P on the viscosity of Surmont bitumen / condensate mixtures at the highest condensate weight fraction (0.5); \circ , \times , \blacktriangle , \blacksquare , \blacklozenge , $+$, measured viscosities; calculated values: —, power law model; - - -, Cragoe's model.

Examination of the results reveals that the maximum deviation between the measured viscosity data and the calculated values was obtained at the lowest solvent weight fraction (0.05). As the weight fraction of the condensate in the mixture increases, the deviation of the models from the experimental results is reduced.

7.6. Repeatability of Data

Although it was not possible to repeat all of the measurements for the density and viscosity of the Surmont bitumen / condensate mixtures, the experiments at some temperatures, pressures, and solvent weight fractions were repeated. This was done to verify the repeatability of the data and results. The data for repeated experiments are presented in Table 7–13. As the table shows, the maximum deviation for saturated phase densities was 2.9 kg/m^3 and the average deviation for the measured densities is 1.9 kg/m^3 .

The maximum deviation for saturated liquid viscosities was 5.0 % with an average deviation of 2.7%.

Table 7–13: Repeated experiments for density and viscosity of Surmont bitumen / condensate mixtures at temperature T ; P , pressure; ρ_s , saturated liquid density; μ_s , saturated liquid viscosity; w_s , weight fraction of condensate in mixture.

100 w_s	T (°C)	P (MPa)	ρ_s (kg/m³)	μ_s (mPa.s)	Deviation (kg/m³)	Deviation (%)
10	49.9	2.00	----	253	----	±4.3
	50.1	2.10	----	232		
	99.5	4.14	907.0	----	±0.4	----
	100.5	4.03	906.2	----		
20	21.8	2.00	924.3	170	±2.0	±0.3
	21.7	2.18	920.2	169		
	100.2	2.02	871.9	8.00	±2.8	±4.4
	99.6	2.10	866.3	7.32		
30	22.1	2.00	886.0	29.4	±2.9	±1.2
	21.2	2.13	880.3	28.7		
	49.9	2.02	----	11.8	----	±0.4
	50.1	2.12	----	11.7		
	101.0	2.02	829.1	3.34	±2.1	±4.9
	100.5	2.10	825.0	3.03		
	150.6	2.00	791.4	1.46	±2.9	±5.0
	149.4	2.21	785.6	1.32		
40	100.6	1.99	790.4	1.54	±0.6	±4.9
	99.6	2.12	791.6	1.70		
50	50.3	1.99	----	2.04	----	±0.7
	50.1	2.12	----	2.01		
	100.8	1.98	753.7	0.867	±1.9	±0.7
	100.3	2.09	750.0	0.880		
	150.5	2.02	709.9	0.472	±2.0	±3.0
	149.4	2.16	705.9	0.501		

7.7. Asphaltene Precipitation

The density and viscosity of Surmont bitumen diluted with condensate were measured at different temperatures, pressures, and solvent weight fractions in previous sections. The impact of variations in the above-mentioned parameters on the viscosity and density of the mixture was evaluated. Some liquid solvents such as benzene and toluene are known to be miscible with bitumens in all proportions without asphaltene precipitation. This is not the case for paraffinic solvents such as *n*-alkanes. At a specific solvent concentration, the asphaltenes become unstable in the solution. Wiehe et al. (2005) determined the onset of asphaltene precipitation for Athabasca bitumen / *n*-alkane mixtures at room temperature.

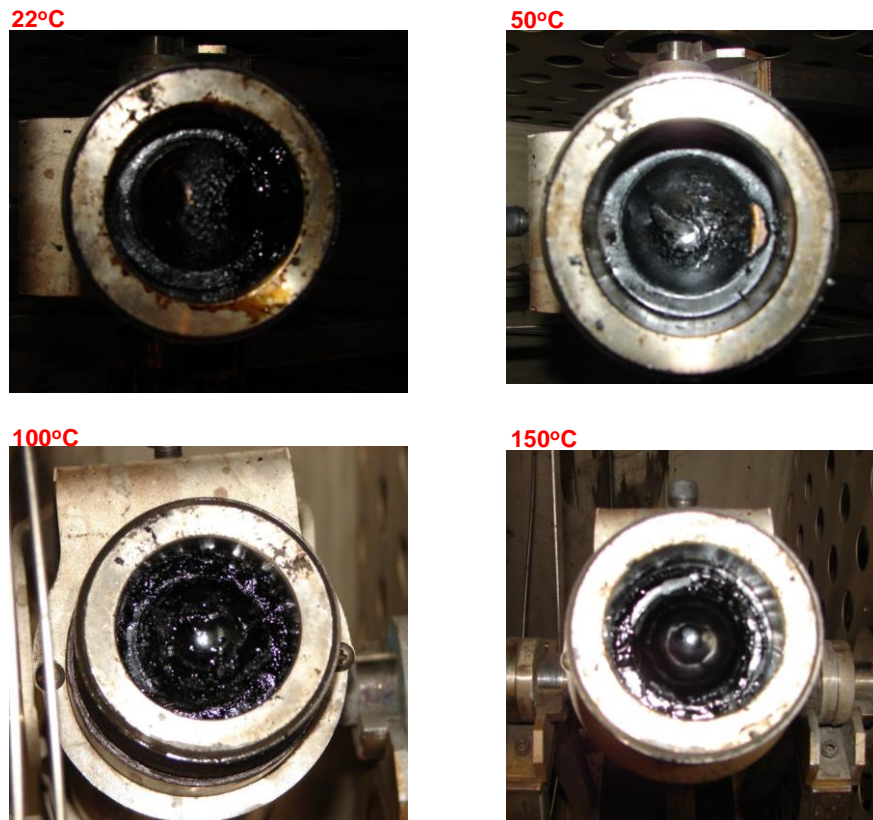


Figure 7–33: Digital photographs of the precipitated asphaltene for the mixture of Surmont bitumen / condensate at different temperatures and at concentrations higher than 0.5 condensate weight fractions.

After the density and viscosity measurements for the Surmont bitumen / condensate mixtures at a constant solvent concentration, the equilibrium cell was opened to check for possible asphaltene precipitation from the mixture. The results showed that the asphaltene precipitation occurred at concentrations higher than 0.5 condensate weight fraction. Further measurements on the concentrations of 0.6 and 0.7 were conducted to ensure that the asphaltene had separated from the mixture. In the case of solid formations, such as asphaltenes, the solid particles precipitate around the rocking ball. When the cell is placed in an upward position, the precipitated particles settle to the bottom of the equilibrium cell. Figure 7–33 shows the asphaltene precipitation in the equilibrium cell at different temperatures.

Chapter 8: Equation of State Modelling

Chapter 8 presents the phase behaviour modelling study of bitumen/solvent systems using the equation of state. The modelling study starts with bitumen characterization using the compositional analysis, density and molecular weight of the bitumen presented in Chapter 3. The characterized bitumen was then introduced into Peng-Robinson equation of state model. Finally, the equation of state was tuned to match the generated vapour-liquid and liquid-liquid equilibrium data in Chapters 4 and 5.

8.1. Introduction

Phase behaviour modelling is a thermodynamic calculation which determines the formation and composition of different phases (vapour, liquid, and solid) as a function of the overall composition, pressure and temperature. It has a wide range of applications in the chemical and petroleum industries. Different methods, such as molecular simulation, activity coefficient, and equation of state, can be used to model the phase behaviour of crude oil systems.

The equation of state approach is the most common and practical method among the above-mentioned techniques, and the cubic form is the most common type of equation of state used in chemical and petroleum industries, due to their simplicity and accuracy. The first cubic equation of state was van der Waals equation of state. Several forms were then proposed; however, a significant improvement was obtained by Redlich and Kwong (1949). They introduced a temperature dependence attractive term to van der Waals equation of state.

Soave (1972) proposed a more general temperature dependent term that results in a significant improvement for the Redlich-Kwong equation of state. Peng and Robinson (1976) improved equation of state prediction by considering Soave's improvement and proposed a volume dependency term of the attractive term.

Equation of state modelling is considered as a robust method for phase behaviour modelling of well-defined systems. However, the modelling of complex or ill-defined fluids and systems, such as bitumen/solvent mixtures, presents significant challenges. The component properties (critical properties, acentric factor and molecular weight) and interaction parameters of the components should be defined. Indeed, these properties are used to characterize the fluid.

The phase behaviour and thermodynamic properties of heavy oil and bitumen are important for production, pipeline transportation, upgrading, and refining. From a reservoir/production engineering point of view, the equilibrium properties of bitumen-containing mixtures at *in-situ* conditions are important for recovery of bitumen from oil sands, the development of numerical simulators, and the application of various flooding processes in enhanced oil recovery. However, only limited experimental data for these systems have been reported in the literature, because these experimental measurements are time-consuming and expensive. This problem is more pronounced in the case of heavier solvents, such as propane or when a liquid-liquid system forms at equilibrium condition. Modelling can, therefore, be considered as an alternative to study the interaction of a bitumen/solvent system. The phase behaviour of bitumen/solvent systems is limited compared to conventional oil and simple hydrocarbon systems.

Mehrotra et al. (1985) conducted a phase behaviour modelling study using Peng-Robinson equation of state to estimate bitumen density and the solubilities of carbon dioxide and ethane in Athabasca and Peace River bitumens. They used five pseudo-component characterizations of Bishnoi et al. (1977) in their study for Athabasca bitumen. The critical properties obtained from Kesler-Lee (1976) correlation for pseudo components predicted the experimental solubility data well. They also extended the equation of state multiphase flash calculation of low temperature and high pressure conditions to capture the liquid-liquid and vapour-liquid-liquid equilibrium.

Fu and Puttagunta (1986) developed a correlation for the binary interaction coefficients of the modified Soave-Redlich-Kwong equation of state for representing the

vapour-liquid data of bitumen/solvent systems. They considered a temperature dependent binary interaction coefficient to improve the prediction.

Fu et al. (1988) measured the vapour-liquid equilibrium data for the mixtures of Cold Lake bitumen, methane, and ethane. They used Soave-Redlich-Kwong and Peng-Robinson equations of state to model the experimental data and proposed that both models could model the experimental data if an appropriate bitumen characterization and interaction parameters were used. They considered temperature dependent binary interaction parameters in both models.

Mehrotra and Svrcek (1988b, 1988c) and Mehrotra et al. (1989b) used Peng-Robinson equation of state to predict the solubility of light gases (nitrogen, carbon dioxide, carbon monoxide, methane, and ethane) in Cold Lake, Athabasca, and Wabasca bitumens over the temperature range 20 to 110°C and at pressures up to 10 MPa. They characterized the bitumen as three pseudo-components, which were representative of distillable maltene, undistillable maltene, and asphaltene. They used Kesler-Lee (1976) correlation for calculating critical properties. The results showed that three pseudo-components could adequately match the experimental data.

Wu (1996) applied Peng-Robinson equation of state to model the vapour-liquid phase behaviour of the mixtures of methane, carbon dioxide, and heavy oil. The modelling study showed that Peng-Robinson equation of state could match most literature data with an accuracy of 5 % when properly tuned. Frauenfeld et al. (2002) modelled the solubility of methane, ethane, propane, and carbon dioxide in a blended Cold Lake/Lloydminster oil and in Lloydminster Aberfeldy oil using Peng-Robinson equation of state. The model was tuned through the adjustment of the interaction coefficients. The equation of state model was then used to generate K-values for the gas-oil systems. They claimed that the developed model could be used for generating K-value tables for other conditions.

Badamchi-Zadeh et al. (2009a) experimentally measured the saturation pressure, solubility and corresponding liquid phase densities and viscosities of Athabasca bitumen / propane mixtures at temperatures from 10 to 50°C. They used van Laar activity

coefficient model to predict the saturation pressure for the Athabasca bitumen / propane system. In a subsequent study, Badamchi-Zadeh et al. (2009b) performed the same study for carbon dioxide and mixture of carbon dioxide and propane.

Kariznovi et al. (2010) did a phase behaviour modelling study for four bitumens (Athabasca, Wabasca, Peace River, and Cold Lake) with four different solvents (nitrogen, methane, ethane, and carbon dioxide) using experimental data from Mehrotra and Svrcek (1985a, 1985b, 1985c, 1988a) and Svrcek and Mehrotra (1982 and 1989). They used Peng-Robinson equation of state considering different number of pseudo-components (Three, five and six). They proposed a set of pseudo-components that could be applied for phase behaviour modelling study of different Alberta bitumens.

Kariznovi et al. (2011b) measured the solubility of propane in Athabasca bitumen and corresponding saturated phase densities and viscosities for the temperatures up to 200°C and the pressures up to 8 MPa. The experimental data was then modelled using Peng-Robinson equation of state which closely matched the experimental results. The volume shift and interaction parameters were adjusted to fit density and solubility data.

Diaz et al. (2011) evaluated the capabilities of different characterization methods for equation of state phase behaviour modelling study of mixtures of bitumen, propane, and carbon dioxide. They characterized Athabasca bitumen using SimDis data using six different approaches. Based on the experimental saturation pressure data of pseudo-binary mixtures, they optimized the interaction parameters and then predicted the liquid-liquid phase boundaries and saturation pressures of pseudo-ternary systems.

Nourozieh et al. (2012d) predicted and estimated the solubility of propane in different bitumens using Peng-Robinson equation of state and two activity coefficient models. For equation of state modelling, the bitumen was characterized as four and six pseudo-components and the uncertain parameters were correlated based on the available experimental data. To apply the activity coefficient model, the bitumen was treated as a single component, and the solubility was predicted by assuming sufficiently low pressure

conditions. They used van Laar and non-random two liquids (NRTL) models for activity coefficient approaches.

Agrawal et al. (2012) measured the saturation pressure of live Peace River bitumen at different condensate concentrations at temperatures from 20 to 180°C. The data were modelled with Peng-Robinson equation of state through the adjustment of binary interaction parameters to fit the saturation pressure and asphaltene onset. A correlation was developed for binary interaction parameters as a function of temperature.

Li and Yang (2013) did a phase behaviour experimental study for propane/*n*-butane/heavy-oil systems at the pressures up to 5030.0 kPa and the temperatures up to 123°C. They modelled the experimental data using a volume-translated Peng-Robinson equation of state with a modified alpha function. They tuned the binary-interaction-parameter to match the experimental data. They claimed that the binary interaction correlations together with the volume-translated Peng-Robinson equation of state systems could accurately match the experimental data, while prediction accuracy was reduced at temperatures close to the critical temperature of a pure solvent.

Badamchi-Zadeh et al. (2013) developed an oil characterization and equation of state model for the mixtures of carbon dioxide, propane, and Athabasca bitumen. They used the solubility data for carbon dioxide and Athabasca bitumen reported by Svrcek and Mehrotra (1982) and applied a volume-shift parameter to match the liquid density. In their study, the SimDist analysis of asphaltene free fraction of Athabasca bitumen was converted to a normal boiling point distribution of bitumen. The binary interaction parameters were adjusted to match the saturation pressure.

Yang et al. (2013) did an experimental and modelling study for methane/propane/heavy-oil (Lloydminster) mixture under reservoir conditions (temperature range of 22 to 50°C and the pressures up to 10 MPa). They used the volume-translated Peng-Robinson equation of state along with a modified alpha function for the phase behaviour modelling study. They proposed a new binary interaction parameter correlation to fit the data of saturation pressures and swelling factors.

Ghasemi and Whitson (2013) proposed a systematic approach for the phase behaviour modelling study of the mixtures containing Athabasca bitumen and light solvents (nitrogen, carbon dioxide, carbon monoxide, methane, and ethane) using cubic equations of state. They used experimental data from Svrcek and Mehrotra (1982) and Mehrotra and Svrcek (1985a) which included the gas solubility, density, and viscosity of gas-saturated Athabasca bitumen for the temperature range of 25 to 118°C and at the pressures up to 10 MPa. A gamma molar distribution model was used to fit the bitumen data. Single-carbon-number (SCN) fractions were then defined and Twu correlation was used to estimate the SCN critical properties. They lumped SCN fractions into five pseudo-fractions.

In this chapter, the phase behaviour of Athabasca bitumen / ethane and Athabasca bitumen / propane mixtures predicted with Peng-Robinson equation of state is discussed. The aim was to capture both vapour-liquid and liquid-liquid equilibrium compositions as well as the phase boundaries. The SimDis data along with bitumen properties, such as molecular weight and density, were used to define single carbon number fraction and the available correlations were used to calculate the critical properties of single carbon fractions. The defined factions were introduced into Peng-Robinson equation of state to model the phase behaviour of bitumen/solvent systems. To improve the equation of state predictions, the binary interaction parameters were tuned based on the measured data.

8.2. Equilibrium Calculation

The obtained experimental data were modelled with a conventional equation of state. The equilibrium condition of component i in phase I and phase II is shown as follows:

$$f_i^I = f_i^{II} \quad 8-1$$

In terms of fugacity coefficients,

$$y_i \hat{\phi}_i^I P = x_i \hat{\phi}_i^{II} P \quad 8-2$$

where the partial fugacity coefficients are calculated from

$$\ln \hat{\phi}_i = \frac{1}{RT} \int_v^\infty \left(\left[\frac{\partial P}{\partial n_i} \right]_{T,v,n_{j \neq i}} - \frac{RT}{v} \right) dv - \ln Z \quad 8-3$$

The relation between the pressure and volume is expressed by the equation of state. For this study, Peng-Robinson (Robinson and Peng 1978) equation of state was employed to calculate the saturation pressure for the primary characterization of bitumen.

$$P = \frac{RT}{v-b} - \frac{a\lambda(T)}{v(v+b)+b(v-b)} \quad 8-4$$

where

$$a = \frac{0.45724R^2T_c^2}{P_c} \quad 8-5$$

$$b = \frac{0.07780RT_c}{P_c} \quad 8-6$$

$$\lambda(T) = [1 + \kappa(1 - T_r^{1/2})]^2 \quad 8-7$$

$$\kappa = 0.379642 + 1.48503\omega - 0.164423\omega^2 + 0.016666\omega^3 \quad 8-8$$

The van der Waals mixing rules were used in this work to obtain the equation of state parameters for the multicomponent mixtures:

$$a_m = \sum_i x_i D_i \quad 8-9$$

$$b_m = \sum_i x_i b_i \quad 8-10$$

with

$$D_i = \sqrt{a_i} \sum_j x_j (1 - \delta_{ij}) \sqrt{a_j} \quad 8-11$$

where δ_{ij} is the interaction coefficient for the binary pairs within the mixture. The interaction coefficients are adjusted to fit the experimental equilibrium data. The binary interaction parameters can be considered as constant values or defined based on the critical properties. These parameters can be related to critical volume of components through the following equation:

$$\delta_{ij} = 1 - \left(\frac{2v_{ci}^{1/6} v_{cj}^{1/6}}{v_{ci}^{1/3} + v_{cj}^{1/3}} \right)^n \quad 8-12$$

Oellrich et al. (1981) showed that a value of 1.2 for n provided a good match for paraffin-paraffin interaction coefficients. However, in this study, n was considered as a matching parameter to fit the equilibrium data.

In order to apply the equation of state for heavy and bitumen phase behaviour study, the fluid should be characterized. Characterization of heavy oils for the estimation of the critical properties is generally done based on boiling point distribution from atmospheric and vacuum distillation. Crude oils and distillate fractions are complex mixtures of thousands of components that have a continuous boiling point distribution.

Two approaches are commonly used for oil characterization. The first is the characterization of the crude oil or crude oil fractions in terms of pseudo-components defined by an average boiling point or hydrocarbon type (e.g. paraffinic, olefinic, naphthenic or aromatics). Correlations, such as those based on boiling point and specific gravity, can be used to calculate the critical properties.

The second approach is the continuous mixture approach where the oil is described by a continuous distribution function with respect to molecular mass, boiling point, or some other measurable property. This approach is appropriate when the oil consists of one type of hydrocarbon, such as paraffins; however, bitumen is a complex mixture of different hydrocarbons types, such as saturates, aromatics, resins and asphaltenes; thus, the second approach cannot be applied to bitumen

The pseudo-component approach should, therefore, be used for bitumen characterization. Once the pseudo-components are defined, their critical properties and compositions are applied into the Peng-Robinson equation of state. The multi-phase equilibrium is then determined by a flash calculation combined with a phase stability test. In this study, WinProp software from Computer Modelling Group (CMG) was used to model the phase behaviour of the bitumen/solvent mixtures. The tangent-plane criterion

of stability analysis of a phase based on the method developed by Nghiem and Li (1984) was used in WinProp software. The equilibrium equation is solved with Quasi-Newton Successive Substitution (QNSS) (Nghiem and Heidemann 1982).

8.3. Characterization

The SimDis data available for the bitumen samples were used for the phase behaviour study. Therefore, the characterization was based on the distillation data. The first step was the characterization of the crude oil or crude oil fractions in terms of pseudo-components defined by an average boiling point or hydrocarbon type (e.g. paraffinic, olefinic, naphthenic or aromatics). On the basis of the distillation data, ninety-four hydrocarbon components were assigned to the distillable fraction (C_{100}). The boiling point of each component is related to carbon number through the following equation,

$$T_b = 1090 - \exp(6.9955 - 0.11193N_c^{2/3}) \quad 8-13$$

where T_b is the boiling point in Kelvin. This equation represents the Katz-Firoozabadi (1978) data with an AAD of 0.2% and it can be extended into C_{100} (Riazi 2005). The physical properties of C_6 to C_{22} were used to obtain similar equations for the molecular weight and specific gravity (Riazi 2005). Thus, the molecular weight and specific gravity of each component can be obtained by,

$$MW = \left[\frac{6.97996 - \ln(1080 - T_b)}{0.01964} \right]^{3/2} \quad 8-14$$

$$SG = 1.07 - \exp[3.56073 - 2.93886MW^{0.1}] \quad 8-15$$

The boiling points of the defined components along with their compositions accurately represent the distillation curve of bitumen samples. An average molecular weight of 2000 g/mol was assigned to the heavy fraction of bitumen based on a study by Diaz et al. (2011). The specific gravity of this fraction was obtained from the correlation developed by Alboudwarej et al. (2003),

$$SG = 670MW^{0.0629} \quad 8-16$$

Based on this characterization scheme, ninety-four pseudo-components (SCN fraction) were defined for the distillable fraction of bitumen and one pseudo-component was considered for the non-distillable fraction. The boiling points, molecular weights, and specific gravities of SCN groups were calculated from equations 8-14 to 8-16. The molecular weight and specific gravity of each SCN group are multiplied by a multiplier to match the molecular weight and density of raw bitumen obtained from equations 7-1 and 7-4, respectively. Diaz et al. (2011) tested different correlations for critical properties and acentric factor to find which one could make acceptable predictions when they applied to non-distillable fractions. They found that the Lee-Kesler correlation provided a better fit of the phase boundaries. Thus, in this study, the critical properties and eccentric factor were obtained from the correlation proposed by Kesler and Lee (1976),

$$T_c = \left(341.7 + 811SG + [0.76392 + 0.21132SG]T_b + \frac{(0.25939 - 1.81239SG) \times 10^5}{T_b} \right) / 1.8 \quad 8-17$$

$$P_c = \exp \left[8.3634 - \frac{0.0566}{SG} - \left(0.24244 + \frac{2.2898}{SG} + \frac{0.11857}{SG^2} \right) \times 10^{-3} (1.8 \times T_b) + \left(1.4685 + \frac{3.648}{SG} + \frac{0.47227}{SG^2} \right) \times 10^{-7} (1.8 \times T_b)^2 - \left(0.42019 + \frac{1.6977}{SG^2} \right) \times 10^{-10} (1.8 \times T_b)^3 \right] / 14.7 \quad 8-18$$

$$\omega = \frac{\left(\ln P_{cr} - 5.92714 + \frac{6.09648}{T_{br}} + 1.28862 \ln T_{br} - 0.169347 T_{br}^6 \right)}{\left(15.2518 - \frac{15.6875}{T_{br}} - 13.4721 \ln T_{br} + 0.43577 T_{br}^6 \right)} \quad \text{for } T_{br} \leq 0.8 \quad 8-19$$

$$\omega = -7.904 + 0.1352 K_w - 0.007465 K_w^2 + 8.359 T_{br} + \frac{(1.408 - 0.01063 K_w)}{T_{br}} \quad \text{for } T_{br} > 0.8 \quad 8-20$$

$$K_w = \frac{(1.8 T_b)^{1/3}}{SG} \quad 8-21$$

where T is temperature in K, P is pressure in atm, T_{br} and P_{cr} are reduced boiling point temperature and reduced critical pressure, respectively. The critical volumes of components were calculated from Twu (1984)'s correlation.

8.4. MacKay River Bitumen / Ethane Mixtures

As previously mentioned, the SimDis data were used to characterize the bitumen. The components' boiling point and composition accurately represent the distillation curve of MacKay River bitumen as presented in Figure 8–1. The properties and compositions of components were applied in Peng-Robinson equation of state. Two different cases were considered to fit the experimental data. In the first case, the measured K-values from vapour-liquid equilibrium experiments were used to obtain the exponent of equation 8-12 for binary interaction parameters. Although this approach provided a lower value for calculated AARD, it failed to model the liquid-liquid regions and phase boundaries. In additions, the solubilities were over-predicted at lower temperatures (50 and 100°C). Thus, in the second case, the measured K-values for liquid-liquid equilibrium conditions were also used to obtain the binary interaction parameters. This method resulted in a higher value for the calculated AARD; however, the liquid-liquid phase compositions and boundaries were reasonably predicted with the equation of state.

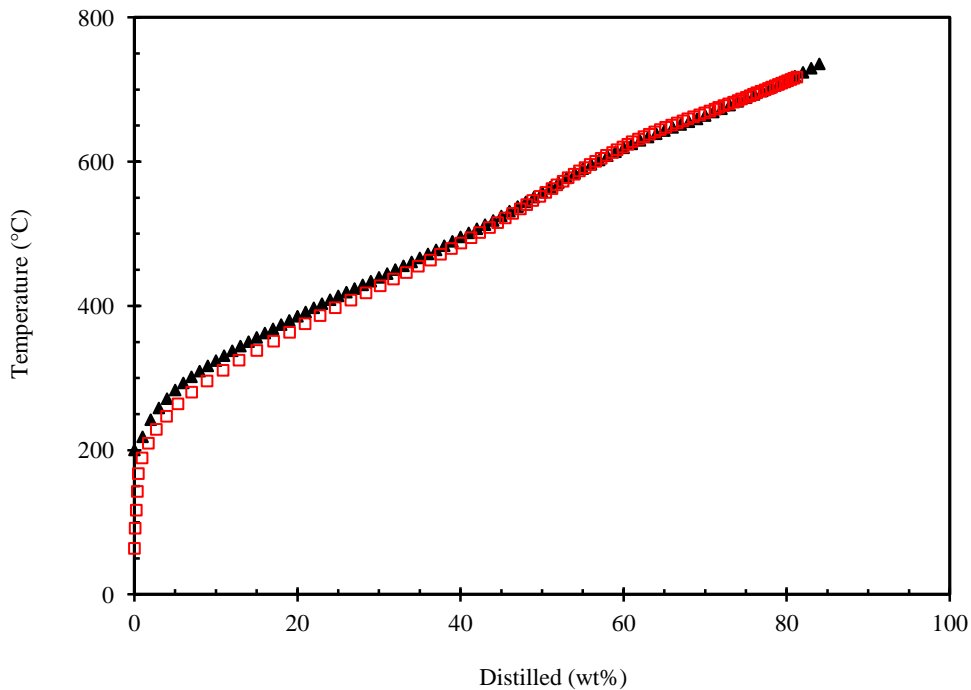


Figure 8–1: Boiling point curves (temperature versus weight percent distilled) for raw MacKay River bitumen (▲) and developed characterization method (□).

Figure 8–2 illustrates the predicted and measured solubilities of ethane in MacKay River bitumen as a function of pressure at different temperatures. In this figure, the symbols represent the measured data, and the lines are predictions by equation of state using two approaches. As anticipated from the figure, the tuning of binary interaction parameters using vapour-liquid data provides a better fit for high temperature conditions, while using liquid-liquid and vapour-liquid data result in better predictions at lower temperatures. Further investigation of two approaches shows that the first approach could not model the phase boundaries and led to a single phase region for liquid-liquid equilibrium conditions, even at high overall ethane concentrations (e.g. 0.4 ethane weight fraction). Although limited K-values for liquid-liquid equilibrium condition were introduced into the equation of state model for tuning, it significantly improved the predictions for phase transition region. The best fitted coefficient for the calculation of binary interaction parameters along with calculated AARD of solubilities are summarized in Table 8–1. As the table shows the second approach provides a larger AARD value for vapour-liquid equilibrium data than the first approach.

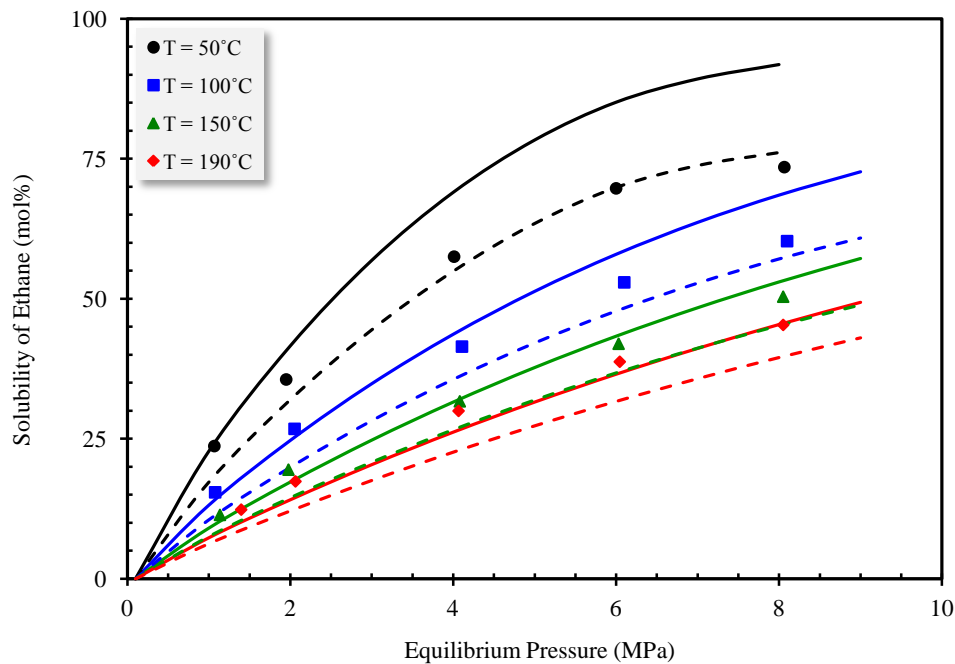


Figure 8–2: Comparison of measured (symbols) and predicted solubilities of ethane in MacKay River bitumen as a function of equilibrium pressure at different temperatures; —, first approach; - - -, second approach.

Table 8–1: Coefficient of the correlation equation for the binary interaction parameters and calculated AARDs of ethane solubilities in MacKay River bitumen using two approaches.

	First Approach	Second Approach
n (equation 8-12)	-0.2968	0.4969
AARD (%)	10.2	16.2

Figure 8–3 shows a complete phase diagram for the second approach for MacKay River bitumen / ethane pseudo-binary mixtures at ambient temperature. The liquid-liquid separation occurs at concentrations higher than 0.19 ethane weight fraction. The vapour-liquid and liquid-liquid regions are well predicted with the equation of state. The mixture forms single liquid phase at ethane concentrations lower than 0.2 weight fraction at pressures higher than 4 MPa.

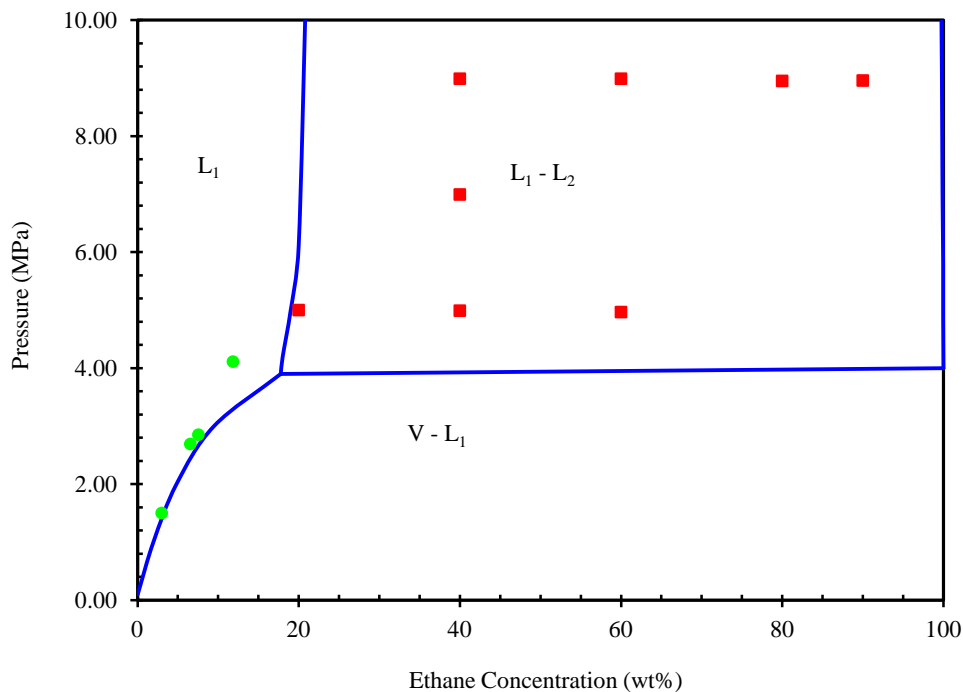


Figure 8–3: Comparison of experimental and modelling results for pressure-composition (P-x) diagram for the mixture of Mackay River bitumen / ethane at ambient temperature; •, the experimental data of Athabasca bitumen / ethane systems by Mehrotra and Svrcek (1985a); ■, liquid-liquid experimental data; lines, predictions by Peng-Robinson equation of state using second approach.

Figure 8–4 demonstrates the compositions of co-existing phases at equilibrium conditions at a temperature of 21.6°C and an overall ethane concentration of 0.4 weight

fraction. As depicted in the figure, the compositions of liquid phases are reasonably predicted with the second approach. Although the predictions for the solvent-enriched phase (liquid 1) is not as good as the other phase, there is a good agreement between the measured data and predicted ones.

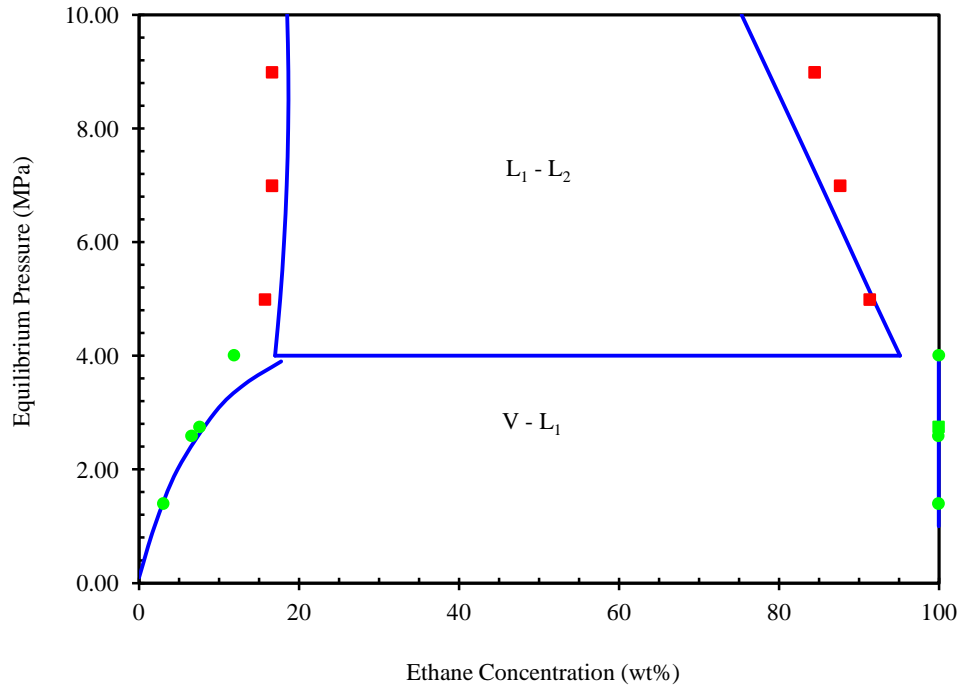


Figure 8–4: Comparison of experimental and modelling results for coexisting phase compositions for the mixture of Mackay River bitumen / ethane at ambient temperature and at a constant overall ethane concentration of 0.4 weight fraction; ●, the experimental data of Athabasca bitumen / ethane systems by Mehrotra and Svrcek (1985a); ■, liquid-liquid experimental data; lines, predictions by Peng-Robinson equation of state using second approach.

Figure 8–5 presents the Peng-Robinson equation of state predictions for the impact of changes in the overall ethane concentration on the composition of equilibrium liquid phases. The composition of ethane in the solvent-enriched phase is slightly under-predicted while the respective value in asphaltene-enriched phase is reasonably well modelled. Figure 8–6 shows the distribution of components in two equilibrium liquid phases at the pressure of 9 MPa with a constant overall ethane concentration of 0.4 weight fraction after evolving ethane. As indicated in the figure, the compositions of extract and residue are well represented by the equation of state. The predicted non-

distilled fractions of extract and residue are 0.006 and 0.214, respectively, which are in close agreement with the experimental values of 0.005 and 0.207.

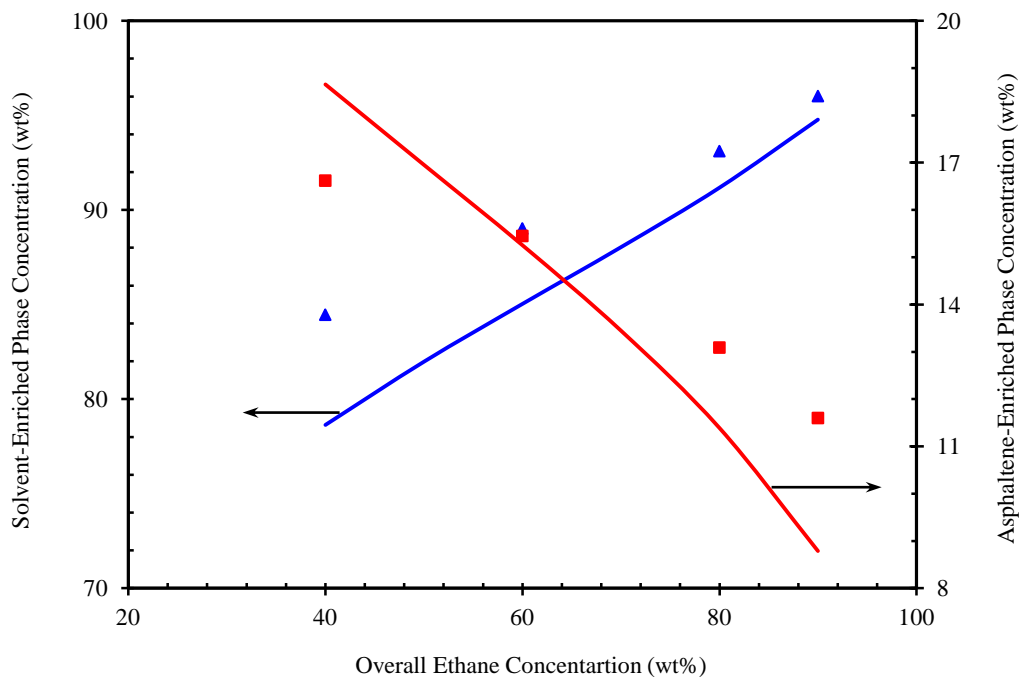


Figure 8-5: A comparison of measured and predicted composition of equilibrium phases in liquid-liquid equilibrium study of MacKay River bitumen / ethane mixtures at ambient temperature and a constant pressure of 9 MPa; \blacktriangle , solvent-enriched phase; \blacksquare , asphaltene-enriched phase; lines, predictions by Peng-Robinson equation of state using second approach.

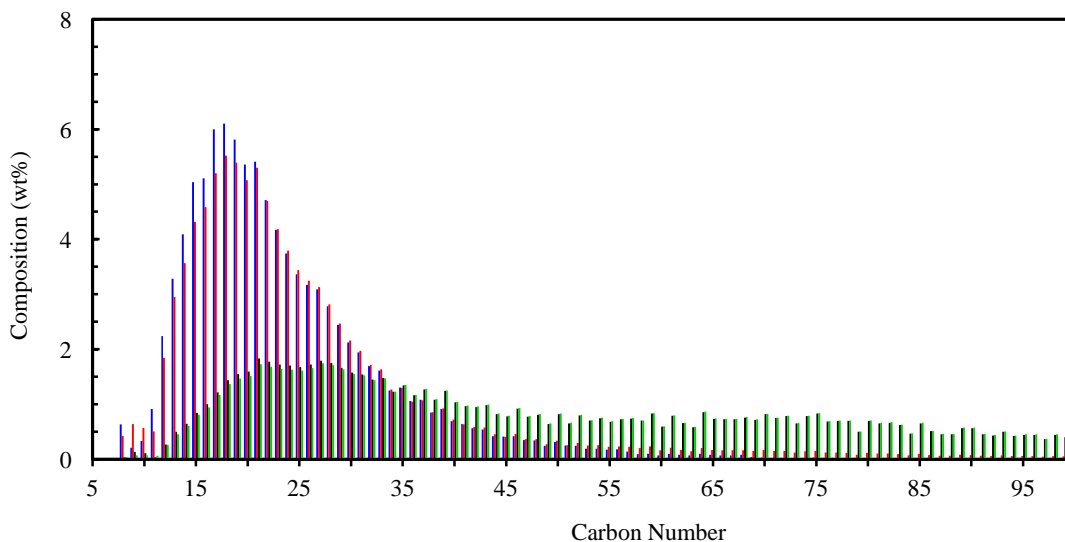


Figure 8-6: A comparison of measured and predicted compositional analysis (component weight percent) for extract (blue and red) and residue (black and green) taken from liquid-liquid equilibrium of MacKay River / ethane mixtures at a constant temperature of 22°C, a constant pressure of 9 MPa, and an overall ethane concentration of 0.4 weight fraction; blue and black, experimental data; red and green, predictions by Peng-Robinson equation of state using second approach.

8.5. Surmont Bitumen / Ethane Mixtures

Similar to MacKay River bitumen, the characterization of Surmont bitumen was done based on the SimDis data. Figure 8–7 illustrates the distillation curve of Surmont bitumen obtained from the components' boiling points and compositions. The properties and compositions of components were applied in Peng-Robinson equation of state. For Surmont bitumen / ethane mixtures, no liquid-liquid equilibrium data were measured, and the measured K-values from vapour-liquid equilibrium experiments were used to obtain the coefficient of equation for binary interaction parameters. The best fitted exponent was 0.0207 which gives an AARD value of 9.5 %. Figure 8–8 illustrates the predicted and measured solubilities of ethane in Surmont bitumen as a function of pressure at different temperatures. In this figure, the symbols represent the measured data, and the lines are predictions by equation of state. As depicted in the figure, the measured solubilities are adequately modelled with Peng-Robinson equation of state and developed characterization method.

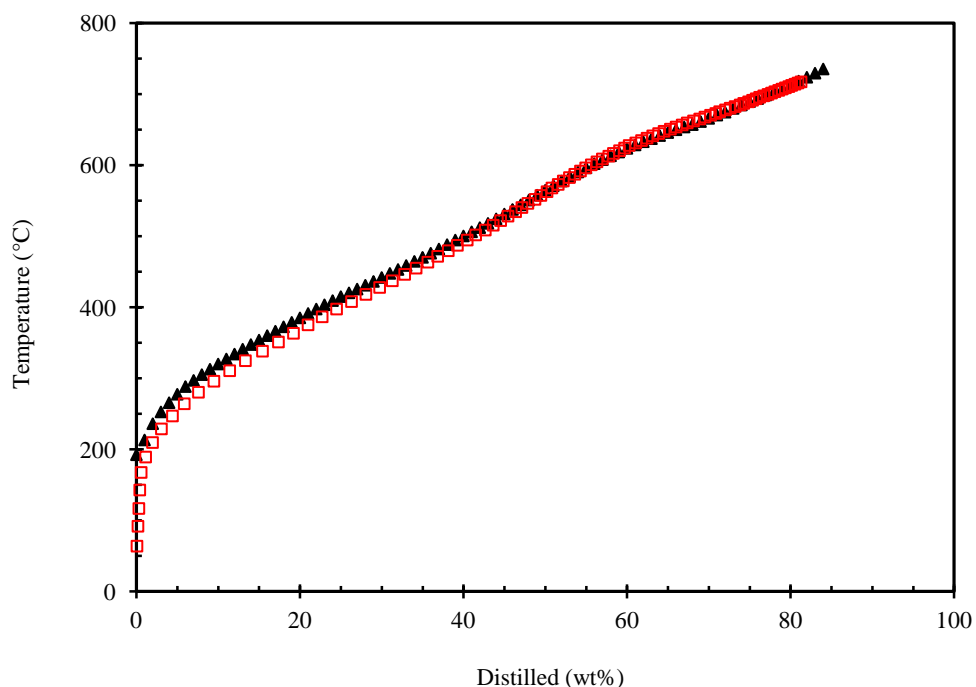


Figure 8–7: Boiling point curves (temperature versus weight percent distilled) for raw Surmont bitumen (▲) and developed characterization method (◻).

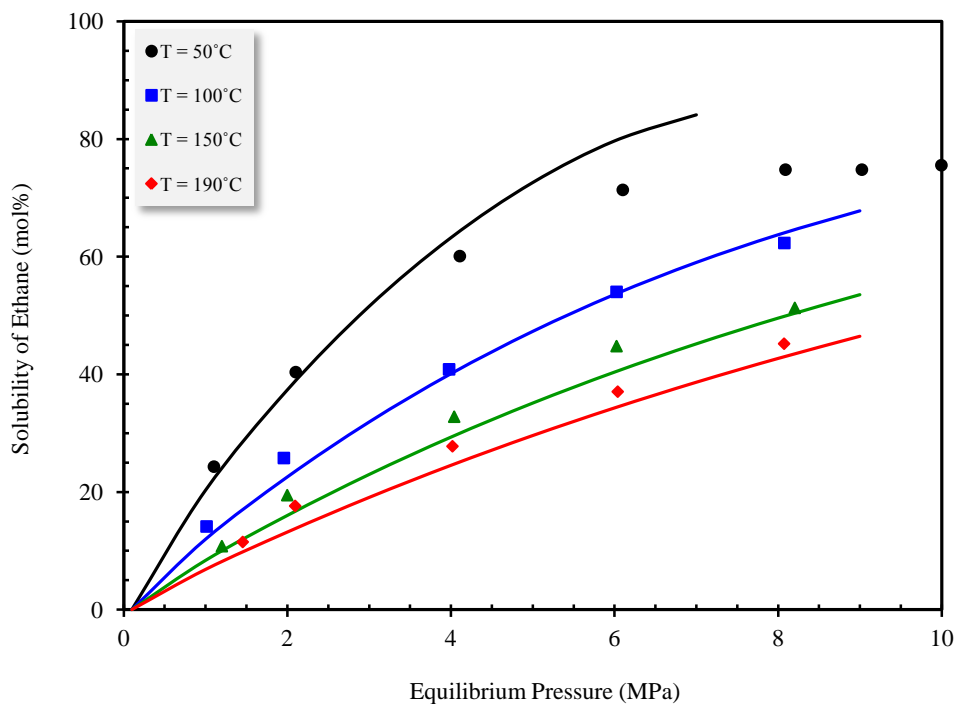


Figure 8–8: Comparison of measured (symbols) and predicted solubilities of ethane in Surmont bitumen as a function of equilibrium pressure at different temperatures; —, predictions by Peng-Robinson equation of state.

8.6. Surmont Bitumen / Propane Mixtures

In order to model the phase behaviour of Surmont bitumen / propane mixtures, the characterization method presented in Figure 8–7 was applied. Three different cases were defined to match the experimental data. In cases 1 and 2, the measured K-values from the vapour-liquid equilibrium experiments were used to obtain the coefficient of equation for binary interaction parameters. Case 1 considered equation 8-12 for the interactions between ethane/pseudo-component and pseudo-component/pseudo-component, whereas case 2 assumed a zero value for pseudo-component/pseudo-component interactions. In case 3 which was similar to Case 1, the measured K-values for liquid-liquid equilibrium conditions were also included to obtain the binary interaction parameters.

The calculated AARDs for cases 1 and 2 demonstrate that there is no quantifiable difference in accuracy of solubility predictions when the interaction of pseudo-

component/pseudo-component is assumed zero. This is because the prediction of solubilities is dominated with the interaction of propane/pseudo-component.

Figure 8–9 illustrates the predicted and measured solubilities of propane in Surmont bitumen as a function of pressure at different temperatures for case 1. In this figure, the symbols represent the measured data, and the lines are predictions by equation of state. As depicted in the figure, the measured solubilities are well predicted with Peng-Robinson equation of state. The sharp change in the solubility at a temperature of 100°C around a pressure of 4 MPa is due to the occurrence of liquid-liquid phase partitioning in the system. Both cases 1 and 2 give an AARD of 3.5 % for the measured solubilities; however, the plotting of the pressure-composition diagram indicates that case 2 could not predict the liquid-liquid region. This is expected; because, the liquid-liquid phase equilibrium is sensitive to pseudo-component and pseudo-component interactions rather than propane and pseudo-component interactions. The best fitted exponents (equation 8-12) for cases 1 and 2 are 0.4033 and 0.3718, respectively.

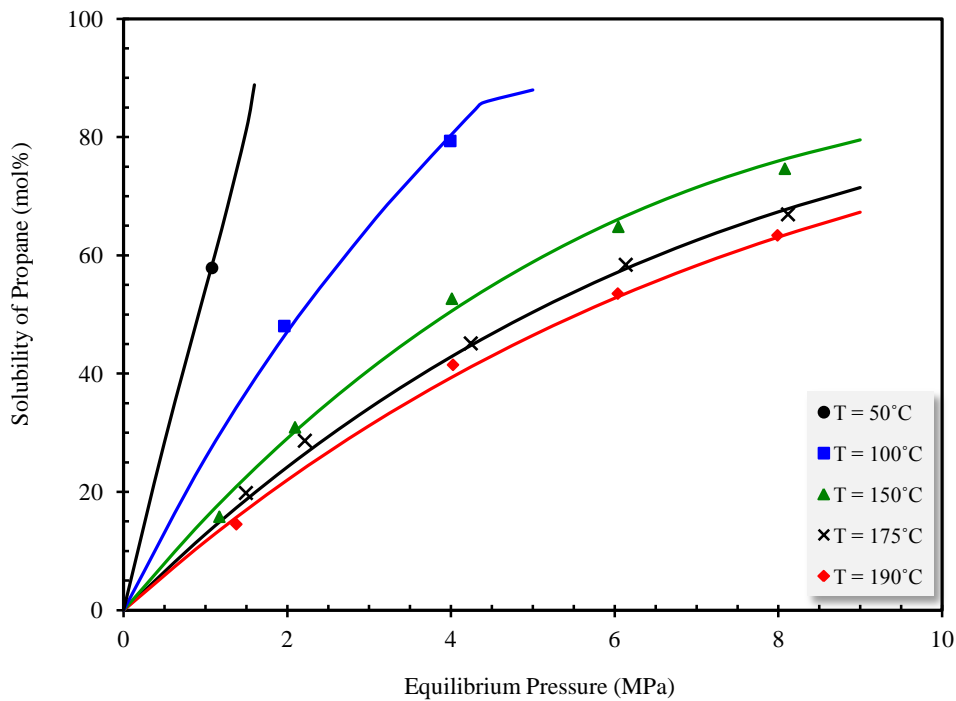


Figure 8–9: Comparison of measured (symbols) and predicted solubilities of propane in Surmont bitumen as a function of equilibrium pressure at different temperatures; —, predictions by Peng-Robinson equation of state (case 1).

Figure 8–10 shows a complete phase diagram for three cases of Surmont bitumen / propane pseudo-binary mixtures at a temperature of 50°C and Figure 8–11 illustrates the same results at a temperature of 100°C. As presented in Figure 8–10, case 2 does not show any liquid-liquid separation at a temperature of 50°C over the concentration range. A single phase region is predicted instead of a liquid-liquid region, inconsistent with the experimental data. However, at a temperature of 100°C, the liquid-liquid phase separation is observed in case 2. Indeed, cases 1 and 2 have similar pressure-composition diagram at this temperature.

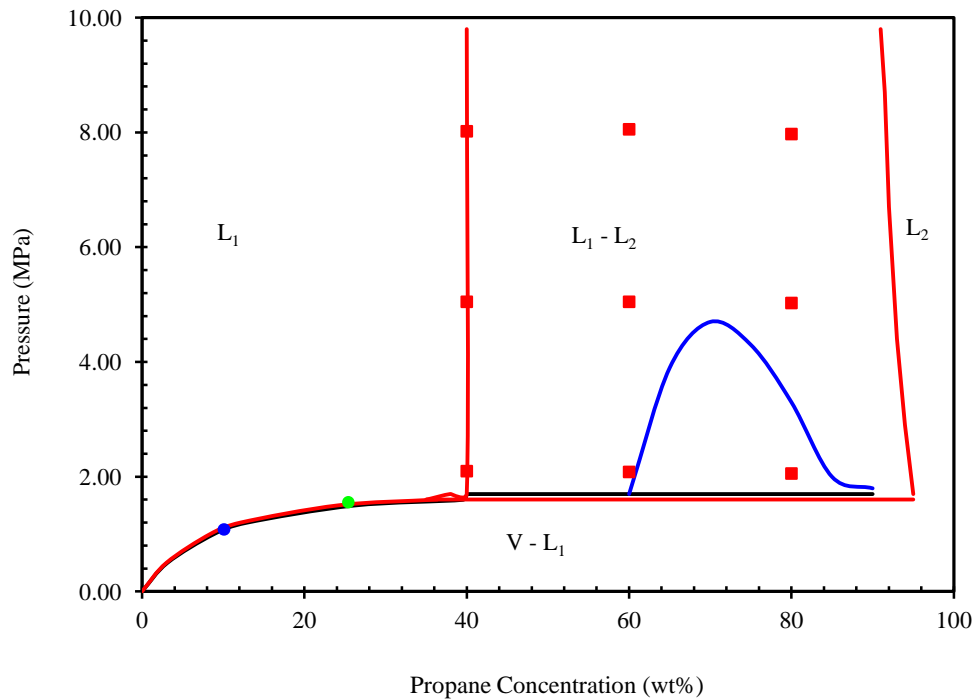


Figure 8–10: Comparison of experimental (symbols) and equation of state modelling results (lines) for pressure-composition (P - x) diagram for Surmont bitumen / propane systems at 50°C; •, vapour-liquid experimental data; •, vapour-liquid experimental data for propane / Athabasca bitumen systems taken from Badamchi-Zadeh et al. (2009a); ■, liquid-liquid experimental data; blue line, case 1; black line, case 2; red line, case 3.

Although the liquid-liquid equilibrium was observed in case 1, the concentration range is narrow and the region is not in agreement with the experimental measurements. This indicates that the equation of state that was tuned with the vapour-liquid data could not adequately predict the liquid-liquid region. Thus, in case 3, K-values from liquid-

liquid equilibrium data were considered in the equation of state tuning. Red lines in Figures 8-10 and 8-11 shows the results for this case. The incorporation of liquid-liquid K-values significantly improves the predictions for liquid-liquid regions. At a temperature of 50°C, the liquid-liquid region is entirely captured in case 3. Even if the liquid-liquid region is not well modelled at a temperature of 100°C and the results are not completely in agreement with the measurements, the improvements in the predictions are noticeable. The best-fitted exponent (equation 8-12) for case 3 is 0.4850.

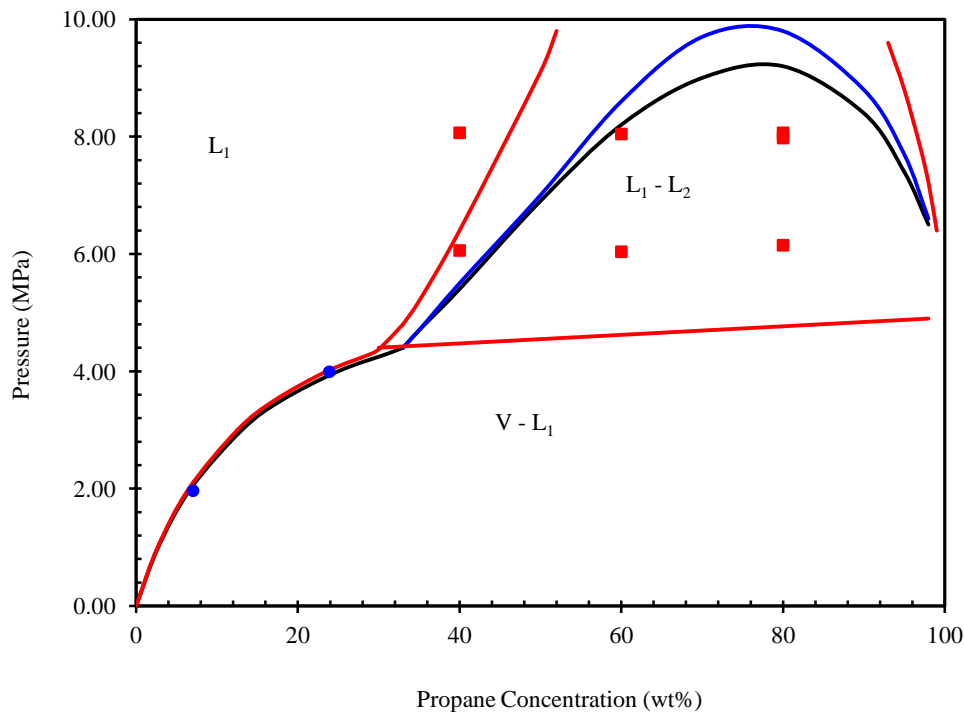


Figure 8–11: Comparison of experimental (symbols) and equation of state modelling results (lines) for pressure-composition (P - x) diagram for the mixture of Surmont bitumen / propane at 100°C; ●, vapour-liquid experimental data; ■, liquid-liquid experimental data; blue line, case 1; black line, case 2; red line, case 3.

Figure 8–12 demonstrates the compositions of co-existing equilibrium phases at the temperature of 50°C and overall propane concentration of 0.4 weight fraction and Figure 8–13 shows the same results at a temperature of 100°C and overall propane concentration of 0.6 weight fraction. As depicted in the figures, the compositions of the liquid phases are reasonably predicted by case 3. Although the predictions for both phases are slightly

under-predicted at a temperature of 50°C, the phase transition boundaries are well represented. At a temperature of 100°C, the equation of state shows more considerable variation of propane composition in solvent-enriched phase with pressure than experimental measurements.

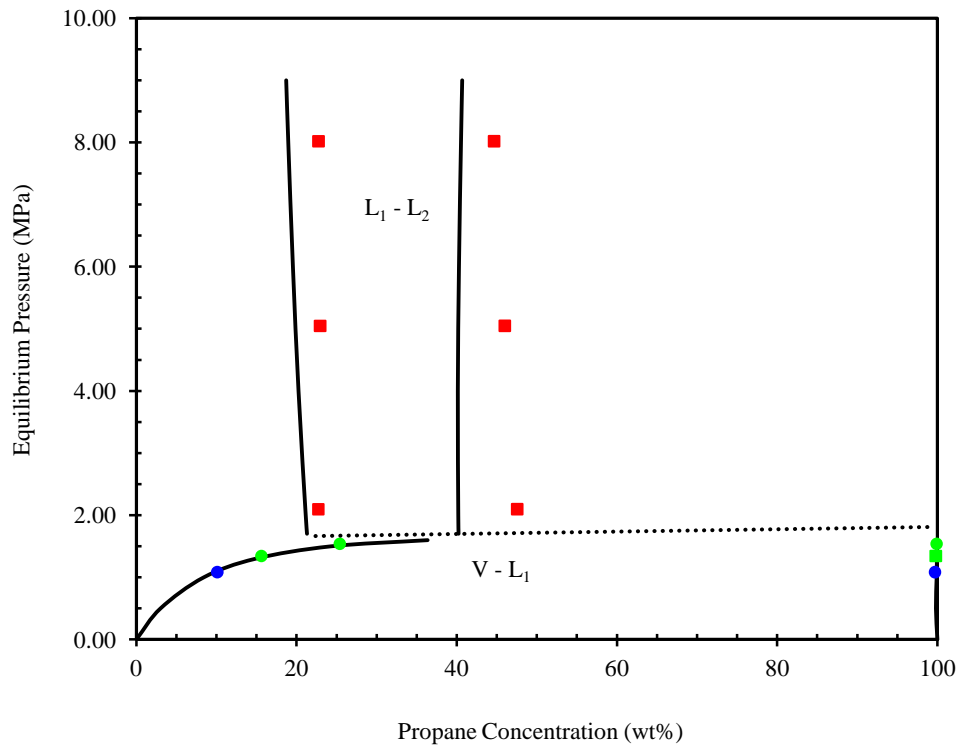


Figure 8-12: Comparison of experimental and modelling results for coexisting phase compositions for Surmont bitumen /propane systems at 50°C and at a constant overall propane concentration of 0.4 weight fraction; ●, vapour-liquid experimental data; ●, vapour-liquid experimental data for propane / Athabasca bitumen systems taken from Badamchi-Zadeh et al. (2009a); ■, liquid-liquid experimental data; lines, predictions by Peng-Robinson equation of state (case 3).

Further investigation of three cases and equation of state results indicates that the inclusion of liquid-liquid equilibrium data in equation of state tuning improves the predictions of phase boundaries and transition regions. The representation of phase compositions in a liquid-liquid region is challenging, because the phase boundaries and compositions in this region should be fitted to the experimental data. In other words, further adjustment of binary interaction parameters may result in better predictions for phase compositions; however, the transition boundaries are inadequately modelled.

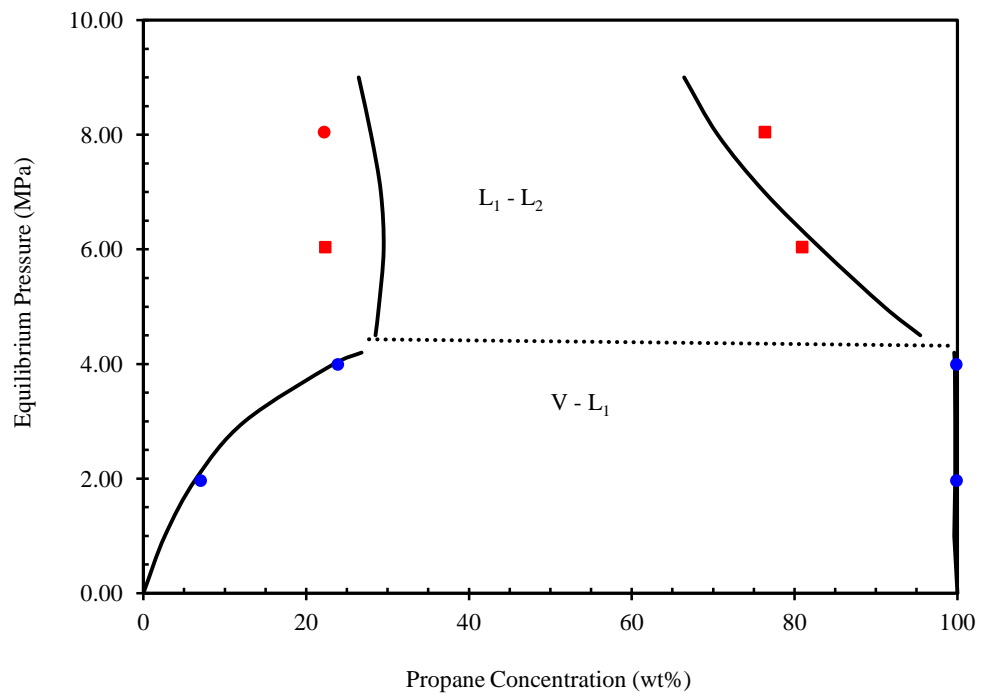


Figure 8-13: Comparison of experimental and modelling results for coexisting phase compositions for Surmont bitumen / propane systems at 100°C and at a constant overall propane concentration of 0.6 weight fraction; ●, vapour-liquid experimental data; ■, liquid-liquid experimental data; lines, predictions by Peng-Robinson equation of state (case 3).

Chapter 9: Conclusions and Recommendations

9.1. Conclusions

A new experimental apparatus for the phase behaviour study of the mixtures bitumen and solvent has been designed and tested for the vapour-liquid and liquid-liquid equilibria. The apparatus has also the capability for detection of solid-liquid equilibria. The phase detection was developed based on the density measurement coupled with the viscosity measurement; it provides a reliable method for phase behaviour study. The feature of the designed apparatus in measuring the accurate volume of feeding fluids and equilibrium phases provided the capability to not only acquire the volumetric data for equilibrium phases, but also obtain the effect of the solvent-to-bitumen feeding ratio on the composition and volume of the phases and other properties.

The density and viscosity of Athabasca bitumen samples taken from different locations were reported over a wide range of temperatures and pressures. A new procedure was developed to obtain the coefficients of the density correlation as a function of temperature and pressure in which the solution is unique and no convergence problem was observed. The viscosity data indicated that as the temperature increased, the pressure dependence of viscosity reduced.

The vapour-liquid equilibrium data for bitumen/ethane mixtures indicated a negligible difference between the solubility of ethane in different bitumens. The saturated viscosity and density data for bitumen/ethane mixtures showed linear variations with pressure for the temperatures of 100, 150, and 190°C. The ethane-saturated bitumen density at 50°C crossover other temperatures and reached to a value even lower than the one at 190°C. It was found that at the temperature of 50°C, the solubility values flatten beyond a pressure of about 6 MPa. In other words, the density and viscosity of ethane-saturated bitumen was not further decreased with the equilibrium pressure. The analysis

of the vapour phase at these conditions showed the formation of a second liquid phase at equilibrium condition.

The liquid-liquid equilibrium for bitumen/ethane mixtures showed that, two phases (solvent-enriched and asphaltene-enriched) exist at equilibrium condition. The former is mostly composed of solvent and light components extracted from the bitumen phase. The latter mainly consists of heavy components of bitumen, such as asphaltenes and resins, which cannot be extracted by solvent. The extraction yields of the bitumen were found to increase with increasing solvent-to-bitumen ratio and pressure at a constant temperature. The solubility data, as well as the compositional analysis of phases, confirmed that asphaltene-enriched phase became heavier as the pressure and solvent-to-bitumen ratio increased. Thus, the lighter components mostly partition into the solvent-enriched phase and an infinity value for equilibrium K-value of light components are obtained.

The liquid-liquid phase separation for the bitumen/propane mixtures was observed at the temperature of 100°C and the pressures greater than 4 MPa and at the temperature of 50°C and the pressures greater than 1.5 MPa. The chemical analysis of the degassed saturated liquids showed the asphaltene-enriched phase has a much higher asphaltene content than raw bitumen, whereas the solvent-enriched phase mainly contains saturate and aromatic fractions of bitumen. Indeed, the partitioning of the bitumen/propane mixtures into two liquid phases could be considered as a asphaltene precipitation process in which the properties of the precipitated asphaltene is different from those of pentane or heptane. It was found that the yield of precipitation for propane is much higher than pentane and heptane, and generally, the precipitation yield reduces with the carbon number of normal alkanes. The extraction yield generally increased with pressure and reduced with temperature. The changes in extraction yield were due to the variation of solvent density.

A comparison of the dissolution of different hydrocarbon gases in bitumen showed that the heavier hydrocarbon gas was more effective on the reduction of bitumen viscosity due to its higher solubility at a constant temperature and pressure. However, this

behaviour was completely different when a constant weight fraction of solvent was dissolved in bitumen. In other words, the lighter hydrocarbon solvent resulted in lower saturated phase viscosity at all temperatures.

The density and viscosity measurements for Athabasca bitumen / hexane and Athabasca bitumen / condensate mixtures showed that the mixture density and viscosity were reproducible within $\pm 3 \text{ kg/m}^3$ and 5 % and the asphaltene precipitation occurred at a concentration of 0.6 weight fraction for two systems. The densities of mixtures revealed linear variations with respect to the pressure and the temperature at all concentrations. Further investigation of the mixture volumes showed that the volume change on mixing increases with increasing the temperature and solvent concentration and reduces with increasing the pressure. The viscosity of the mixtures showed a curvilinear trend with respect to the solvent weight fraction and temperature. The impact of pressure on the mixture viscosity is more pronounced at lower solvent weight fractions and lower temperatures. The evaluation of different models for mixture viscosity indicated that the power law and Cragoe's models represent the data better than other models.

The equation of state modelling indicated that if the measured K-values from vapour-liquid equilibrium experiments are used to obtain the binary interaction parameters, a lower AARD is obtained. However, the tuned model fails to simulate the liquid-liquid regions and phase boundaries. By introducing the measured K-values for liquid-liquid equilibrium conditions, although a higher AARD was obtained, the liquid-liquid phase compositions and boundaries are reasonably predicted with the equation of state.

9.2. Recommendations

Although this study provided the experimental data for the mixtures containing Athabasca bitumen and different solvents over a wide range of pressures and temperatures, the prediction and optimization of solvent-heat assisted recovery processes also require the data on the phase behaviour of pseudo-ternary mixtures

(bitumen/solvent/water). Therefore, further experimental efforts would be required to determine the interactions of bitumen/water and solvent/water in the pseudo-ternary mixtures as the addition of the solvent into steam-based processes leads to complex phase behaviour system.

In this study, the phase behaviour of Athabasca bitumen saturated with pure hydrocarbon gases was investigated. A comparison of dissolution of different hydrocarbon gases in bitumen showed that the viscosity reduction is dependent on the availability of solvent. Further experimental work would be required to determine how the properties of gas-saturated bitumen change when the pure gas in contact with bitumen is replaced with a gas mixture.

The measured data indicated that the precipitated phase (or flashed-off asphaltene-enriched phase) had different chemical properties for various solvents. An investigation of the chemical analysis of the precipitated phase using different precipitants would be valuable for the design of supercritical extraction processes.

References

- Agrawal, P., Schoeggl, F.F., Satyro, M.A., Taylor, S.D., and Yarranton, H.W. 2012. Measurement and modeling of the phase behavior of solvent diluted bitumens. *Fluid Phase Equilibria* 334: 51-64.
- Akbarzadeh, K., Alboudwarej, H., Svrcek, W.Y., and Yarranton, H.W. 2005. A generalized regular solution model for asphaltene precipitation from *n*-alkane diluted heavy oils and bitumens. *Fluid Phase Equilibria* 232 (1-2): 159-170.
- Akbarzadeh, K., Sabbagh, O., Beck, J., Svrcek, W.Y., and Yarranton, H.W. 2004. Asphaltene precipitation from bitumen diluted with *n*-alkanes. Paper SPE 2004-024 presented at Canadian International Petroleum Conference, Calgary, Alberta, Canada, 8-10 June.
- Alboudwarej, H., Akbarzadeh, K., Beck, J., Svrcek, W.Y., and Yarranton, H.W. 2003. Regular solution model for asphaltene precipitation from bitumens and solvents. *AIChE Journal* 49 (11): 2948-2956.
- Al-Murayri, M.T., Harding, T.G., and Maini, B.B. 2011. Impact of non-condensable gas on performance of steam-assisted gravity drainage. *Journal of Canadian Petroleum Technology* 50(7): 46-54.
- Ardali, M., Barrufet, M., and Mamora, D.D. 2012. Laboratory testing of addition of solvents to steam to improve SAGD process. Paper SPE 146993-MS presented at the SPE Heavy Oil Conference, Calgary, Alberta, Canada, 12-14 June.
- Ardali, M., Mamora, D.D., and Barrufet, M. 2011. Experimental study of co-injection of potential solvents with steam to enhance SAGD process. Paper SPE 144598-MS presented at the SPE Western North American Region Meeting, Anchorage, Alaska, USA, 7-11 May.
- Arrhenius, S.A. 1887. *Über die Dissociation der in Wasser gelösten Stoffe. Zeitschrift für Physikalische Chemie* 1: 631-648.
- Asfour, A.F.A., Siddique, M.H., and Vavanellos, T.D. 1990. Density-composition data for eight binary systems containing toluene or ethylbenzene and C₈-C₁₆ n-alkanes at

293.15, 298.15, 308.15, and 313.15 K. *Journal of Chemical & Engineering Data* 35 (2): 192-198.

ASTM, ASTM D2007. Standard test method for characteristic groups in rubber extender and processing oils and other petroleum-derived oils by the clay-gel absorption chromatographic method.

ASTM, ASTM D2887. Standard test method for boiling range distribution of petroleum fractions by gas chromatography.

ASTM, ASTM D7169. Standard test method for boiling point distribution of samples with residues such as crude oils and atmospheric and vacuum residues by high temperature gas chromatography.

Ayodele, O.R., Nasr, T.N., Beaulieu, G., and Heck, G. 2009. Laboratory experimental testing and development of an efficient low-pressure ES-SAGD process. *Journal of Canadian Petroleum Technology* 48 (9): 54-61.

Badamchi-Zadeh, A., Yarranton, H.W., and Maini, B.B. 2013. Phase behavior and physical property modeling for vapex solvents: propane, carbon dioxide, and Athabasca bitumen. Paper SPE 165505 presented at SPE Heavy Oil Conference, Calgary, Alberta, Canada, 11-13 June.

Badamchi-Zadeh, A., Yarranton, H.W., Svrcek, W.Y., and Maini, B.B. 2009a. Phase behaviour and physical property measurement for VAPEX solvents: Part I. Propane and Athabasca bitumen. *Journal of Canadian Petroleum Technology* 48 (1): 54-61.

Badamchi-Zadeh, A., Yarranton, H.W., Maini, B.B., and Satyro, M.A. 2009b. Phase behaviour and physical property measurements for VAPEX solvents: Part II. Propane, carbon dioxide and Athabasca bitumen. *Journal of Canadian Petroleum Technology* 48 (3): 57-65.

Bagci A.S. and Gumrah, F. 2004. Effects of CO₂ and CH₄ addition to steam on recovery of West Kozluca heavy oil. Paper SPE 86953 presented at the SPE International Thermal Operations and Heavy Oil Symposium and Western Regional Meeting held in Bakersfield, California, USA, 16-18 March.

- Barrufet, M.A. and Setiadarma, A. 2003. Reliable heavy oil–solvent viscosity mixing rules for viscosities up to 450 K, oil–solvent viscosity ratios up to 4×10^5 , and any solvent proportion. *Fluid Phase Equilibria* 213 (1-2): 65-79.
- Bingham, E.C. 1918. The variable pressure method for the measurement of viscosity. *Proceeding of American Society for Testing Materials* 18 (Part II): 10.
- Bishnoi, P.R., Heidemann R.A., and Shah, M.K. 1977. Calculation of the thermodynamic properties of bitumen system. In: *The oil sands of Canada - Venezuela 1977*, editors, David A. Redford and Alvin G. Winestock, *Proceedings of the Canada-Venezuela Oil Sands Symposium*, Edmonton, Alberta, Canada, 248-254.
- Boak, J. and Palmgren, C. 2007. Preliminary numerical analysis for a naphtha co-injection test during SAGD. *Journal of Canadian Petroleum Technology* 46 (1): 13-19.
- Butler, R.M. 1985. A new approach to the modelling of steam-assisted gravity drainage. *Journal of Canadian Petroleum Technology* 24 (3): 42-51.
- Butler, R.M. 1999. The steam and gas push (SAGP). *Journal of Canadian Petroleum Technology* 38 (3): 54-61.
- Butler, R.M. and Mokrys, I.J. 1991. A new process (VAPEX) for recovering heavy oils using hot water and hydrocarbon vapour. *Journal of Canadian Petroleum Technology* 30 (1): 97-106.
- Butler, R.M. and Mokrys, I.J. 1993a. Recovery of heavy oils using vapourized hydrocarbon solvents: Further development of the vapex process. *Journal of Canadian Petroleum Technology* 32 (6): 56-62.
- Butler, R.M. and Mokrys, I.J. 1993b. Closed-loop extraction method for the recovery of heavy oils and bitumens underlain by aquifers: The vapex process. *Journal of Canadian Petroleum Technology* 37 (4): 41-50.
- Butler, R.M. and Stephens, D.J. 1981. The gravity drainage of steam-heated oil to parallel horizontal wells. *Journal of Canadian Petroleum Technology* 20 (2): 90-96.

- Butler, R.M., Jiang, Q., and Yee, C.T. 2000. The steam and gas push (SAGP) –3. Recent theoretical developments and laboratory results. *Journal of Canadian Petroleum Technology* 39 (8): 51-60.
- Centeno, G., Sánchez-Reyna, G., Ancheyta, J., Muñoz, J.A.D., and Cardona, N. 2011. Testing various mixing rules for calculation of viscosity of petroleum blends. *Fuel* 90 (12): 3561-3570.
- Chang, C.J., Chiu, K.L., and Day, C.Y. 1998. A new apparatus for the determination of P - x - y diagrams and Henry's constants in high pressure alcohols with critical carbon dioxide. *Journal of Supercritical Fluids* 12 (3): 223-237.
- Chen, H.I., Chang, H.Y., Huang, E.T.S., and Huang, T.C. 2000. A new phase behavior apparatus for supercritical fluid extraction study. *Industrial & Engineering Chemistry Research* 39 (12): 4849-4852.
- Chiu, H.Y., Lee, M.J., and Lin, H. 2008. Vapor–liquid phase boundaries of binary mixtures of carbon dioxide with ethanol and acetone. *Journal of Chemical & Engineering Data* 53 (10): 2393-2402.
- Chung, K.E., Anderson, L.L., and Wiser, W.H. 1979. New procedure for molecular-weight determination by vapour-phase osmometry. *Fuel* 58 (12): 847-852.
- Cragoe, C.S. 1933. Changes in the viscosity of liquids with temperature, pressure and composition. *Proc World Pet Cong London* 2: 529-541.
- Cryette, W.R. 1994. Model 5009 Wide Range Cryoscope – Instruction Manual Precision Systems Inc., Natick, MA.
- Dalmolin, I., Skovroinski, E., Biasi, A., Corazza, M.L., Dariva, C., and Oliveira, J.V. 2006. Solubility of carbon dioxide in binary and ternary mixtures with ethanol and water. *Fluid Phase Equilibria* 245 (2): 193-200.
- Das, S.K. and Butler, R.M. 1998. Mechanism of the vapor extraction process for heavy oil and bitumen. *Journal Petroleum Science Engineering* 21 (1-2): 43-59.

- Day, C.Y., Chang, C.J., and Chen, C.Y. 1996. Phase equilibrium of ethanol + CO₂ and acetone + CO₂ at elevated pressures. *Journal of Chemical & Engineering Data* 41 (4): 839-343.
- Deng, X. 2005. Recovery performance and economics of steam/propane hybrid process. Paper SPE 97760 presented at SPE/PS-CIM/CHOA International Thermal Operations and Heavy Oil Symposium, Calgary, Alberta, Canada, 1-3 November.
- Deng, X., Huang, H., Zhao, L., Law, D.S., and Nasr, T.N. 2010. Simulating the ES-SAGD process with solvent mixture in Athabasca reservoirs. *Journal of Canadian Petroleum Technology* 49 (1): 38-46.
- Deo, M.D., Hwang, J., and Hanson, F.V. 1992. Supercritical fluid extraction of a crude oil, bitumen-derived liquid and bitumen by carbon dioxide and propane. *Fuel* 71 (12): 1519-1526.
- Deo, M.D., Hwang, J., and Hanson, F.V. 1993. The effect of cosolubilizing lighter components on the asphaltene content of heavy oils. *Fuel Processing Technology* 34 (3): 217-228.
- Diaz, O.C, Modaresghazani, J., Satyro, M.A., and Yarranton, H.W. 2011. Modeling the phase behavior of heavy oil and solvent mixtures. *Fluid Phase Equilibria* 304 (1-2): 74-85.
- Dickie, J.P. and Yen, T.F. 1967. Macrostructures of the asphaltic fractions by various instrumental methods. *Analytical Chemistry* 39 (14): 1847-1852.
- Eastick, R.R. and Mehrotra, A.K. 1990. Viscosity data and correlation for mixtures of bitumen fractions. *Fuel Processing Technology* 26: 25-37.
- Edmunds, N.R., Kovalsky, J.A., Gittins, S.D., and Pennacchioli, E.D. 1994. Review of the Phase A steam-assisted gravity drainage test. *SPE Reservoir Engineering* 9 (2): 119-124.
- Escobedo, J. and Mansoori, G.A. 1995. Viscometric determination of the onset of asphaltene flocculation: a novel method. *SPE Production & Facilities* 10 (2): 115-118.

- Escobedo, J. and Mansoori, G.A. 1997. Viscometric principles of onsets of colloidal asphaltene flocculation in paraffinic oils and asphaltene micellization in aromatics. *SPE Production & Facilities* 12 (2): 116-122.
- Escojido, D.M., Urribarri, O., and González, J. 1991. Part 1: Transportation of heavy crude oil and natural bitumen. Paper SPE 24203 presented at 13th World Petroleum Congress, Buenos Aires, Brazil, 20-25 October.
- Farouq-Ali, S.M. and Abad, B. 1976. Bitumen recovery from oil sands, using solvents in conjunction with steam. *Journal of Canadian Petroleum Technology* 15 (3): 80-90.
- Farouq-Ali, S.M. and Snyder, S.G. 1973. Miscible thermal methods applied to a two-dimensional, vertical tar sand pack, with restricted fluid entry. *Journal of Canadian Petroleum Technology* 12 (4): 20-26.
- Ferguson, M.A. Mamora, D.D., and Goite, J.G. 2001. Steam-propane injection for production enhancement of heavy Morichal oil. Paper SPE 69689 presented at SPE International Thermal Operations and Heavy Oil Symposium, Porlamar, Margarita Island, Venezuela, 12-14 March.
- Firoozabadi, A. 1999. Thermodynamics of wax and asphaltene precipitation. In *Thermodynamics of Hydrocarbon Reservoirs*, 1st Edition, A. Firoozabadi, Chapter 5, 295. McGraw-Hill Professional.
- Fraunfeld, T.W.J, Jossy, C., Jossy, E., Bleile, J., and Pierce, G. 2005. Evaluation of the N-Solv process-experimental operation and results, Report prepared for Hatch Ltd. and Nenniger Engineering Inc., Alberta Research Council Inc., Canada.
- Fraunfeld, T.W.J., Kissel, G., and Zhou, S. 2002. PVT and viscosity measurements for Lloydminster-Aberfeldy and Cold Lake blended oil systems. Paper SPE 2002-110 presented at Canadian International Petroleum Conference, Calgary, Alberta, Canada, 11-13 June.
- Freitag, N.P., Sayegh, S.G., and Exelby R. 2005. A new semiautomatic PVT apparatus for characterizing vapex systems. Paper SPE 97783 presented at SPE/PS-CIM/CHOA International Thermal Operations and Heavy Oil Symposium, Calgary, Alberta, Canada, 1-3 November.

- Fu, C. and Puttagunta, R. 1986. Binary interaction coefficients of the modified Soave-Redlich-Kwong equation of state for bitumen-containing systems at in-situ conditions. *Journal of Canadian Petroleum Technology* 25 (5): 38-43.
- Fu, C.T., Puttagunta, V.R., and Vilcsak, G. 1988. Gas solubility of methane and ethane in Cold Lake bitumen at in situ conditions. *Journal of Canadian Petroleum Technology* 27(4):79-85.
- Gao, Z.H., Wu, Q., and He, F. 2002. Studies on vapor-liquid phase equilibria for SCF CO₂+CH₃OH and SCF CO₂+C₂H₅OH systems. *Chemical Journal of Chinese Universities* 23 (8): 1588-1591.
- Ghasemi, M. and Whitson, C.H. 2013. Phase behavior and viscosity modeling of Athabasca bitumen and light solvent mixtures. Paper SPE 165416 presented at SPE Heavy Oil Conference, Calgary, Alberta, Canada, 11-13 June.
- Goite, J.G., Mamora, D.D., and Ferguson, M.A. 2001. Experimental study of Morichal heavy oil recovery using combined steam and propane injection. Paper SPE 69566 presented at SPE Latin American and Caribbean Petroleum engineering Conference, Buenos Aires, Argentina, 25-28 March.
- Gray, M.R. 1994. Upgrading petroleum residues and heavy oils. CRC Press, 1st Edition.
- Guan, J., Kariznovi, M., Nourozieh, H., and Abedi, J. 2013. Density and viscosity for mixtures of Athabasca bitumen and aromatic solvents. *Journal of Chemical & Engineering Data* 58 (3): 611-624.
- Han, B., Peng, D.Y., Fu, C.T., and Vilcsak, G. 1992. An apparatus for phase equilibrium studies of carbon dioxide + heavy hydrocarbon systems. *Canadian Journal of Chemical Engineering* 70 (6): 1164-1171.
- Han, B., Yang, G., Ke, J., Mao, C., and Yan, H. 1998. Phase equilibria of supercritical propane–Fengcheng bitumen system and the density and viscosity of the liquid phase. *Fluid Phase Equilibria* 143 (1-2): 205-211.
- Hernandez, O.E. and Farouq-Ali, S.M. 1972. Oil recovery from Athabasca tar sands by miscible-thermal methods. Paper SPE 7249 presented at Annual Technical Meeting of the Petroleum Society of CIM, Calgary, Alberta, Canada, 16-19 May.

- Hill, A.E. and Malisoff, W.M. 1926. The mutual solubility of liquids. III. the mutual solubility of phenol and water. IV. The mutual solubility of normal butyl alcohol and water. *Journal of American Chemical Society* 48 (4): 918-927.
- Ishihara, K., Tanaka, H., and Kato, M. 1998. Phase equilibrium properties of ethane + methanol system at 298.15 K. *Fluid Phase Equilibria* 144 (1-2): 131-136.
- Ivory, J., Zheng, R., Nasr, T.N., Deng, X., Beaulieu, G., and Heck, G. 2008. Investigation of low pressure ES-SAGD. Paper SPE 117759 presented at the International Thermal Operations and Heavy Oil Symposium, Calgary, Alberta, Canada, 20-23 October.
- Jacoby, R.H. 1987. Phase behavior of light hydrocarbon-heavy oil or tar systems, and its application to recovery processes. *In Situ* 11 (2-3): 145-167.
- Janish, A. 1979. Oil sands and heavy oil: Can they ease the energy shortage? Paper presented at the 1st UNISTAR International Conference on Heavy Crude and Tar Sands, Edmonton, Alberta, Canada, 4-12 June.
- Jennings, D.W., Lee, R.J., and Teja, A.S. 1991. Vapor-liquid equilibria in the carbon dioxide + ethanol and carbon dioxide + 1-butanol systems. *Journal of Chemical & Engineering Data* 36 (3): 303-307.
- Jiang, Q. 1997. Recovery of heavy oil and bitumen using Vapex process in homogeneous and heterogeneous reservoirs. PhD thesis, University of Calgary, Calgary, Alberta, Canada.
- Jiang, Q., Butler, R.M., and Yee, C.T. 2000. The steam and gas push (SAGP) – 2. mechanism analysis and physical model testing. *Journal of Canadian Petroleum Technology* 39 (4): 52-61.
- Johnston, K.P., Ziger, D.H., and Eckert, C.A. 1992. Solubilities of hydrocarbon solids in supercritical fluids. The augmented van der Waals treatment. *Industrial & Engineering Chemistry Fundamentals* 21 (3): 191-197.
- Jossy, C., Frauenfeld, T., and Rajan, V. 2009. Partitioning of bitumen-solvent systems into multiple liquid phases. *Journal of Canadian Petroleum Technology* 48 (11): 16-20.

- Joung, S.N., Yoo, C.W., Shin, H.Y., Kim, S.Y., Yoo, K.P., Lee, C.S., and Huh, W.S. 2001. Measurements and correlation of high-pressure VLE of binary CO₂-alcohol systems (methanol, ethanol, 2-methoxyethanol and 2-ethoxyethanol). *Fluid Phase Equilibria* 185 (1-2): 219-230.
- Kariznovi, M. 2013. Phase behaviour study and physical properties measurement for Athabasca bitumen / solvent systems applicable for thermal and hybrid solvent recovery processes. PhD thesis, University of Calgary, Calgary, Alberta, Canada.
- Kariznovi, M., Nourozieh, H., and Abedi, J. 2010. Bitumen characterization and pseudocomponents determination for equation of state modeling. *Energy & Fuels* 24 (1): 624-633.
- Kariznovi, M., Nourozieh, H., and Abedi, J. 2011a. Experimental apparatus for phase behavior study of solvent-bitumen systems: A critical review and design of a new apparatus. *Fuel* 90 (2): 536-546.
- Kariznovi, M., Nourozieh, H., and Abedi, J. 2011b. Experimental and modeling study of vapor-liquid equilibrium for propane/heavy crude systems at high temperature conditions. Paper SPE 146796 presented at SPE Annual Technical Conference and Exhibition, Denver, Colorado, USA, 30 October-02 November.
- Kariznovi, M., Nourozieh, H., and Abedi, J. 2012a. Phase behavior and viscosity measurements of heavy crude oil with methane and ethane at high-temperature conditions. Paper SPE 152321 presented at SPE Western Regional Meeting, Bakersfield, California, USA, 21-23 March.
- Kariznovi, M., Nourozieh, H., and Abedi, J. 2012b. Liquid-liquid upgrading and separation of heavy components for Athabasca bitumen saturated with light hydrocarbons. Presented at the 62th Canadian Chemical Engineering Conference (CSCHE2012), Vancouver, British Columbia, Canada, 14-17 October.
- Kariznovi, M., Nourozieh, H., and Abedi, J. 2013a. Experimental measurements and predictions of density, viscosity, and carbon dioxide solubility in methanol, ethanol, and 1-propanol. *The Journal of Chemical Thermodynamics* 57: 408-415.

- Kariznovi, M., Nourozieh, H., Guan, J.G., and Abedi, J. 2013b. Measurement and modeling of density and viscosity for mixtures of Athabasca bitumen and heavy *n*-alkane. *Fuel* 112: 83-95.
- Kariznovi, M., Nourozieh, H., and Abedi, J. 2013c. Experimental determination of *k*-values and compositional analysis of liquid phases in the liquid-liquid equilibrium study of (Athabasca bitumen + ethane) systems. *Journal of Chemical & Engineering Data* 58 (6): 1772-1780.
- Katz, D.L. and Firoozabadi, A. 1978. Predicting phase behavior of condensate crude/oil systems using methane interaction coefficients. *Journal of Petroleum Technology* 30 (11): 1649-1655.
- Kawanaka, S., Leontaritis, K.J., Park, S.J., and Mansoori, G.A. 1989. Thermodynamic and colloidal models of asphaltene flocculation. In oil-field chemistry and enhanced recovery and production stimulation. American Chemical Society Symposium Series 396, Chapter 24, 443-458.
- Kendall, J. and Monroe, K. 1917. The viscosity of liquids II. The viscosity-composition curve for ideal liquid mixtures. *Journal of American Chemical Society* 39 (9): 1787-1802.
- Kesler, M.G. and Lee, B.I. 1976. Improve prediction of enthalpy of fractions. *Hydrocarbon Processing* 55 (3): 153-158.
- Khan, M.A.B., Mehrotra, A.K., and Svrcek, W.Y. 1984. Viscosity models for gas-free Athabasca bitumen. *Journal of Canadian Petroleum Technology* 23: 47-53.
- Lederer, E.L. 1933. Viscosity of mixtures with and without diluents. *Proc World Pet Cong Lond* 2: 526-528.
- Leontaritis, K.J. and Mansoori, G.A. 1987. Asphaltene flocculation during oil production and processing: A thermodynamic colloidal model. Paper SPE 16258 presented at SPE International Symposium on Oilfield Chemistry, San Antonio, Texas, USA, 4-6 February.

- Li, H. and Yan, D. 2013. Phase behaviour of C₃H₈/n-C₄H₁₀/heavy-oil systems at high pressures and elevated temperatures. *Journal of Canadian Petroleum Technology* 52 (1): 30-40.
- Li, W. and Mamora, D.D. 2010. Experimental investigation of solvent co-injection in vapor and liquid phase to enhance SAGD performance. Paper SPE 133277 presented at the SPE Annual Technical Conference and Exhibition, Florence, Italy, 19-22 September.
- Lim, G.B., Kry, R.P., Harker, B.C., and Jha, K.N. 1995. Cyclic stimulation of Cold Lake oil sand with supercritical ethane. Paper SPE 30298 presented at SPE International Heavy Oil Symposium, Calgary, Alberta, Canada, 19-21 June.
- Lobe, V.M. 1973. MSc. Thesis, University of Rochester, Rochester, New York, USA.
- Luo, P., Yang, C., and Gu, Y. 2007a. Enhanced solvent dissolution into in-situ upgraded heavy oil under different pressures. *Fluid Phase Equilibria* 252 (1-2): 143-151.
- Luo, P., Yang, C., Tharanivasan, A.K., and Gu, Y. 2007b. In situ upgrading of heavy oil in a solvent-based heavy oil recovery process. *Journal of Canadian Petroleum Technology* 46 (9): 37-43.
- Mannistu, K.D., Yarranton, H.W., and Masliyah, J.H. 1997. Solubility modeling of asphaltenes in organic solvents. *Energy & Fuels* 11 (3): 615-622.
- Mansoori, G.A. 1996. Asphaltene, resin, and wax deposition from petroleum fluids: Mechanisms and modeling. *Arabian Journal for Science and Engineering* 21 (4 B): 707-723.
- Mansoori, G.A. 2002. Cause and effect of deposition and fouling of heavy organics and other compounds in fuel and petrochemical processes. *KU International Journal of Science and Technology*, Transaction B,1-17.
- Mansoori, G.A. 2009. A unified perspective on the phase behaviour of petroleum fluids. *International Journal of Oil, Gas and Coal Technology* 2 (2): 141-167.
- Mccormack, M.E. 2009. Design of steam-hexane injection wells for gravity drainage systems. *Journal of Canadian Petroleum Technology* 48 (1): 22-28.

- Mehl, A., Nascimento, F.P., Falcao, P.W., Pessoa, F.L.P., and Cardozo-Filho, L. 2011. Vapor-liquid equilibrium of carbon dioxide + ethanol: experimental measurements with acoustic method and thermodynamic modeling. *Journal of Thermodynamics* 2011: 1-11.
- Mehrotra, A.K. 1991. A generalized viscosity equation for pure heavy hydrocarbons. *Industrial & Engineering Chemistry Research* 30: 420-427.
- Mehrotra, A.K. 1992a. A generalized viscosity equation for liquid hydrocarbons: Application to oil-sand. *Fluid Phase Equilibria* 75: 257-268.
- Mehrotra, A.K. 1992b. A model for the viscosity of bitumen/ bitumen fractions-diluent blends. *Journal of Canadian Petroleum Technology* 31: 28-32.
- Mehrotra, A.K. 1992c. Mixing rules for predicting the viscosity of bitumens saturated with pure gases. *Canadian Journal of Chemical Engineering* 70: 165-172.
- Mehrotra, A.K. and Svrcek, W.Y. 1984. Measurement and correlation of viscosity, density and gas solubility for Marguerite Lake bitumen saturated with carbon dioxide. *AOSTRA Journal of Research* 1 (1): 51-62.
- Mehrotra, A.K. and Svrcek, W.Y. 1985a. Viscosity, density and gas solubility data for oil sand bitumens. part I: Athabasca bitumen saturated with CO and C₂H₆. *AOSTRA Journal of Research* 1 (4): 263-268.
- Mehrotra, A.K. and Svrcek, W.Y. 1985b. Viscosity, density and gas solubility data for oil sand bitumens. part II: Peace River bitumen saturated with N₂, CO, CH₄, CO₂ and C₂H₆. *AOSTRA Journal of Research* 1 (4): 269-279.
- Mehrotra, A.K. and Svrcek, W.Y. 1985c. Viscosity, density and gas solubility data for oil sand bitumens. part III: Wabasca bitumen saturated with N₂, CO, CH₄, CO₂ and C₂H₆. *AOSTRA Journal of Research* 2 (2): 83-93.
- Mehrotra, A.K. and Svrcek, W.Y. 1986. Viscosity of compressed Athabasca bitumen. *Canadian Journal of Chemical Engineering* 64: 844-847.
- Mehrotra, A.K. and Svrcek, W.Y. 1987a. Viscosity of compressed Cold Lake bitumen. *Canadian Journal of Chemical Engineering* 65: 672-675.

- Mehrotra, A.K. and Svrcek, W.Y. 1987b. Corresponding states method for calculating bitumen viscosity. *Journal of Canadian Petroleum Technology* 26: 60-66.
- Mehrotra, A.K. and Svrcek, W.Y. 1988a. Properties of Cold Lake bitumen saturated with pure gases and gas mixtures. *Canadian Journal of Chemical Engineering* 66 (4): 656-665.
- Mehrotra, A.K. and Svrcek, W.Y. 1988b. Characterization of Athabasca bitumen for gas solubility calculations. *Journal of Canadian Petroleum Technology* 27 (6): 107-110.
- Mehrotra, A.K. and Svrcek, W.Y. 1988c. Correlation and prediction of gas solubility in Cold Lake bitumen. *Canadian Journal of Chemical Engineering* 66 (4): 666-670.
- Mehrotra, A.K., Eastick, R.R., and Svrcek, W.Y. 1989a. Viscosity of cold lake bitumen and its fractions. *Canadian Journal of Chemical Engineering* 67: 1004-1009.
- Mehrotra, A.K., Patience, G.S., and Svrcek, W.Y. 1989b. Calculation of gas solubility in Wabasca bitumen. *Journal of Canadian Petroleum Technology* 28 (3): 81-83.
- Mehrotra, A.K., Sarkar, M., and Svrcek, W.Y. 1985. Bitumen density and gas solubility predictions using the Peng Robinson equation of state. *AOSTRA Journal of Research* 1 (4): 215-229.
- Meldau, R.F., Shipley, R.G., and Coats, K.H. 1981. Cyclic gas/steam stimulation of heavy-oil wells. *Journal of Petroleum Technology* 33 (10): 1990-1998.
- Miadonye, A., Doyle, N., Britten, A., Latour, N., and Puttagunta, V.R. 2001. Modelling viscosity and mass fraction of bitumen-diluent mixtures. *Journal of Canadian Petroleum Technology* 40: 52-57.
- Miadonye, A., Latour, N., and Puttagunta, V.R. 2000. A correlation for viscosity and solvent mass fraction of bitumen-diluent mixtures. *Petroleum Science and Technology* 18: 1-14.
- Miadonye, A., Singh, B., and Puttagunta, V.R. 1994. Modeling the viscosity-temperature relationship of Alberta bitumen. *Fuel Science & Technology International* 12: 335-350.

- Miadonye, A., Singh, B., and Puttagunta, V.R. 1995. Viscosity estimation for bitumen-diluent mixtures. *Fuel Science & Technology International* 13: 681-698.
- Mohammadzadeh, O., Rezaei, N., and Chatzis, I. 2012. More Insight into the pore-level physics of the solvent-aided SAGD (SA-SAGD) process for heavy oil and bitumen recovery. Paper SPE 157776-MS presented at the SPE Heavy Oil Conference, Calgary, Alberta, Canada, 12-14 June.
- Mohebati, M.H., Maini, B.B., and Harding, T.G. 2013. Numerical-simulation investigation of the effect of heavy-oil viscosity on the performance of hydrocarbon additives in SAGD. *SPE Reservoir Engineering and Evaluation* 15 (2): 165-181.
- Mokrys, I.J. and Butler, R.M. 1993. In-situ upgrading of heavy oils and bitumen by propane deasphalting: The vapex process. Paper SPE 25452 presented at SPE Production Operations Symposium, Oklahoma City, Oklahoma, USA, 21-23 March.
- Moradina, I. and Teja, A.S. 1987. Solubilities of five solid n-alkanes in supercritical ethane. *Supercritical Fluids: Chemical and Engineering Principles and Applications*. Squires TG, Paulaitis ME (Editors). American Chemical Society, Washington, DC.
- Motahhari, H., Schoeggl, F.F., Satyro, M.A., and Yarranton, H.W. 2011. Prediction of the viscosity of solvent diluted live bitumen at temperatures up to 175°C. Paper SPE 149405 presented at Canadian Unconventional Resources Conference, Calgary, Alberta, Canada, 15-17 November.
- Mousavi-Dehghani, S.A., Riazi, M.R., Vafaie-Sefti, M., and Mansoori, G.A. 2004. An analysis of methods for determination of onsets of asphaltene phase separations. *Journal of Petroleum Science and Engineering* 42 (2-4): 145-156.
- Nasr, T.N. and Ayodele, O.R. 2005. Thermal techniques for the recovery of heavy oil and bitumen. Paper SPE 97488 presented at the SPE International Improved Oil Recovery Conference in Asia Pacific, Kuala Lumpur, Malaysia, 5-6 December.

- Nasr, T.N. and Ayodele, O.R. 2006. New hybrid steam-solvent processes for the recovery of heavy oil and bitumen. Paper SPE 101717 presented at Abu Dhabi International Petroleum Exhibition and Conference, Abu Dhabi, UAE, 5-8 November.
- Nasr, T.N. and Isaacs, E.E. 2001. Process for enhancing hydrocarbon mobility using a steam additive. US Patent 6, 230, 814, 15 May.
- Nasr, T.N., Beaulieu, G., Golbeck, H., and Heck, G. 2002. Novel expanding solvent-SAGD process (ES-SAGD). Paper SPE 2002-072 presented at the Petroleum Society's Canadian International Petroleum Conference, Calgary, Alberta, Canada, 11-13 June.
- Nasr, T.N., Kimber, K.D., Vendrinsky, D.A., and Jha, K.N. 1991. Process enhancement in horizontal wells through the use of vertical drainage channels and hydrocarbon additives. Paper SPE 21794 presented at the SPE Western Regional Meeting, Long Beach, California, USA, 20-22 March.
- Nellesteyn, F.J. 1938. The colloidal structure of bitumen. In: *The Science of Petroleum*, Oxford University Press, London, 4, 2760.
- Nghiem, L.X. and Heidemann, R.A. 1982. General acceleration procedure for multiphase flash calculation with application to oil-gas-water systems. Paper presented at the 2nd European Symposium on Enhanced Oil Recovery, Paris, France, 8-10 November.
- Nghiem, L.X. and Li, Y.K. 1984. Computation of multiphase equilibrium phenomena of reservoir fluid. *Fluid Phase Equilibria* 17 (1): 77-95.
- Nourozieh, H., Kariznovi, M., and Abedi, J. 2010. Phase behavior study of liquid-liquid equilibria in bitumen-solvent mixtures. Presented at 60th Canadian Chemical Engineering Conference (CSCHE2010), Saskatoon, Saskatchewan, Canada, 24-27 October.
- Nourozieh, H., Kariznovi, M., and Abedi, J. 2011a. Physical properties and extraction measurements for Athabasca bitumen + light hydrocarbon system: Evaluation of pressure effect, solvent-to-bitumen ratio, and solvent type. *Journal of Chemical & Engineering Data* 56 (11): 4261-4267.

- Nourozieh, H., Kariznovi, M., Abedi, J., and Chen, Z. 2011b. A new approach to simulate the boundary layer in the vapor extraction process. *Journal of Canadian Petroleum Technology* 50 (11): 11-18.
- Nourozieh, H., Kariznovi, M., and Abedi, J. 2012a. Development and evaluation of a modified experimental apparatus for phase behavior study of solvent-heavy crude systems. *Fuel Processing Technology* 102: 116-123.
- Nourozieh, H., Kariznovi, M., and Abedi, J. 2012b. Compositional analysis of liquid phases and component distribution in liquid-liquid equilibrium of Athabasca bitumen / ethane systems applicable for heavy oil recovery and upgrading methods. Presented at the 62th Canadian Chemical Engineering Conference (CSCHE2012), Vancouver, British Columbia, Canada, 14-17 October.
- Nourozieh, H., Kariznovi, M., and Abedi, J. 2012c. Liquid-liquid equilibria of solvent/heavy crude systems: in situ upgrading and measurements of physical properties. Paper SPE 152319 Presented at SPE Western Regional Meeting, Bakersfield, California, USA, 21-23 March.
- Nourozieh, H., Kariznovi, M., and Abedi, J. 2012d. Investigation of different models for thermodynamic modeling of bitumen/propane mixture. *Canadian Energy & Technology Innovation (CETI) Journal* 1 (1): 33-40.
- Nourozieh, H., Kariznovi, M., Guan, J., and Abedi, J. 2013. Measurement of thermo-physical properties and modeling for pseudo-binary mixtures of *n*-decane and Athabasca bitumen. *Fluid Phase Equilibria* 347: 62-75.
- Oellrich, L., Ploecker, U., Prausnitz, J.M., and Knapp, H. 1981. Equation-of-state methods for computing phase equilibria and enthalpies. *International Chemical Engineering* 21 (1): 1-15.
- Orr, B. 2009. ES-SAGD: past, present and future. Paper SPE 129518 presented at SPE Annual Technical Conference and Exhibition, New Orleans, USA, 4-7 October.
- Oyekunle, L. 2000. A two-parameter correlation for petroleum bitumens. *Petroleum Science and Technology* 18: 63-79.

- Palmgren, C. and Edmunds, N. 1995. High temperature naphtha to replace steam in the SAGD process. Paper SPE 30294 presented at the SPE International Heavy Oil Symposium, Calgary, Alberta, Canada, 19-21 June.
- Pang, T. and McLaughlin, E. 1985. Supercritical extraction of aromatic hydrocarbon solids and tar sand bitumens. *Industrial & Engineering Chemistry Process Design and Development* 24 (4): 1027-1032.
- Park, S.J., Kim, C.J., and Rhee, B.S. 2000. Fractionation of aromatic heavy oil by dynamic supercritical fluid extraction. *Industrial & Engineering Chemistry Research* 39 (12): 4897-4900.
- Parkinson, G. and Johnson, E. 1989. Supercritical processes win CPI acceptance. *Chemical Engineering* 96 (7): 35-39.
- Peng, D.Y. and Robinson, D.B. 1976. A new two-constant equation of state. *Industrial & Engineering Chemistry Fundamentals* 15 (1): 59-64.
- Pursley, S.A. 1975. Experimental studies of thermal recovery processes. Paper prepared at the Maracaibo Heavy Oil Symposium, Maracaibo, Venezuela, 04 June.
- Puttagunta, V.R., Singh, B., and Miadonye, A. 1993. Correlation of bitumen viscosity with temperature and pressure. *Canadian Journal of Chemical Engineering* 71: 447-450.
- Radosz, M., Cotterman, R.L., and Prausnitz, J.M. 1987. Phase equilibria in supercritical propane systems for separation of continuous oil mixtures. *Industrial Engineering Chemistry Research* 26 (4): 731-737.
- Reamer, H.H. and Sage, B.H. 1966. Phase equilibria in hydrocarbon systems. volumetric and phase behavior of the propane-*n*-decane system. *Journal of Chemical & Engineering Data* 11 (1): 17-24.
- Redford, D.A. and McKay, A.S. 1980. Hydrocarbon–steam process for recovery of bitumen from oil sands. Paper SPE 8823 presented at the SPE/DOE Enhanced Oil Recovery Symposium, Tulsa, Oklahoma, USA, 20-23 April.

- Redlich, O. and Kwong, J.N.S. 1949. On the thermodynamics of solutions. *Chemical Reviews* 44 (1): 233-244.
- Reid, R.C., Prausnitz, J.M., and Sherwood, T.K. 1977. The properties of gases and liquids, 3rd Edition, McGraw-Hill, 435-436.
- Riazi, M.R. 2005. Characterization and properties of petroleum fractions. 1st Edition, Philadelphia, PA.
- Rivero, J.A. and Mamora, D.D. 2002. Production acceleration and injectivity enhancement using steam-propane injection for Hamaca extra-heavy oil. Paper SPE 75129 presented at SPE/DOE Improved Oil Recovery Symposium, Tulsa, Oklahoma, USA, 13-17 April.
- Robinson, D.B. and Peng, D.Y. 1978. *The Characterization of the Heptanes and Heavier Fractions for the GPA Peng-Robinson Programs*; Gas Processors Association, Research Report RR-28: Tulsa, Oklahoma, USA.
- Rose, J.L. 1999. Extraction of Peace River bitumen using supercritical ethane. PhD thesis, University of Calgary, Calgary, Alberta, Canada.
- Rose, J.L., Monnery, W.D., Chong, K. and Svrcek, W.Y. 2001. Experimental data for the extraction of Peace River bitumen using supercritical ethane. *Fuel* 80 (8): 1101-1110.
- Saryazdi, F. 2012. Density prediction for mixtures of heavy oil and solvents. MSc thesis, University of Calgary, Calgary, Alberta, Canada.
- Schmitt, W.J. and Reid, R.C. 1985. The influence of the solvent gas on solubility and selectivity in Supercritical extraction. *Supercritical Fluid Tech.* Elsevier Science, Publishers, Amsterdam, 123-147.
- Secuianu, C., Feroiu, V., and Geanță, D. 2008. Phase behavior for carbon dioxide + ethanol system: Experimental measurements and modeling with a cubic equation of state. *Journal of Supercritical Fluids* 47 (2): 109-116.
- Shu, W.R. 1984. A viscosity correlation for mixtures of heavy oil, bitumen, and petroleum fractions. *SPE Journal* 24: 277-282.

- Shu, W.R. and Hartman, K.J. 1988. Effect of solvent on steam recovery of heavy oil. *SPE Reservoir Engineering* 3 (2): 457-465.
- Sih, R., Armenti, M., Mammucari, R., Dehghani, F., and Foster, N.R. 2008. Viscosity measurements on saturated gas-expanded liquid systems-ethanol and carbon dioxide. *Journal of Supercritical Fluids* 43 (3): 460-468.
- Sih, R., Dehghani, F., and Foster, N.R. 2007. Viscosity measurements on gas expanded liquid systems-methanol and carbon dioxide. *Journal of Supercritical Fluids* 41 (1): 148-157.
- Soave, G. 1972. Equilibrium constants from a modified Redlich-Kwong equation of state. *Chemical Engineering Science* 27 (6): 1197-1203.
- Speight, J.G. 2007. *The Chemistry and Technology of Petroleum*, 4th Edition, Marcel Dekker Inc., New York.
- Sperry, J.S. 1981. Heavy-oil recovery system completes three field tests in mid-continent region. *Oil & Gas Journal* 79 (30): 225-237.
- Stievano, M. and Elvassore, N. 2005. High-pressure density and vapor-liquid equilibrium for the binary systems carbon dioxide-ethanol, carbon dioxide-acetone and carbon dioxide-dichloromethane. *Journal of Supercritical Fluids* 33 (1): 7-14.
- Subramanian, M. 1996. Supercritical fluid extraction of oil sand bitumen from the Uinta basin, Utah, PhD dissertation, University of Utah, Salt Lake City, Utah (December 1996).
- Subramanian, M. and Hanson, F.V. 1998. Supercritical fluid extraction of bitumens from Utah oil sands. *Fuel Processing Technology* 55 (1): 35-53.
- Suzuki, K., Sue, H., Itou, M., Smith, R.L., Inomata, H., Arai, K., and Saito, S. 1990. Isothermal vapor-liquid equilibrium data for binary systems at high pressures: carbon dioxide-methanol, carbon dioxide-ethanol, carbon dioxide-1-propanol, methane-ethanol, methane-1-propanol, ethane-ethanol, and ethane-1-propanol systems. *Journal of Chemical & Engineering Data* 35 (1): 63-66.

- Svrcek, W.Y. and Mehrotra, A.K. 1982. Gas solubility, viscosity and density measurements for Athabasca bitumen. *Journal of Canadian Petroleum Technology* 21 (4): 31-38.
- Svrcek, W.Y. and Mehrotra, A.K. 1988. One-parameter correlation for bitumen viscosity. *Chemical Engineering Research & Design* 66: 323-327.
- Svrcek, W.Y. and Mehrotra, A.K. 1989. Properties of Peace River bitumen saturated with field gas mixtures. *Journal of Canadian Petroleum Technology* 28 (2): 50-56.
- Swanson, J.M. 1942. A contribution to the physical chemistry of the asphalts. *Journal of Physical Chemistry* 46 (1): 141-150.
- Tharanivasan, A., Yarranton, H., and Taylor, S. 2011. Application of a regular solution-based model to asphaltene precipitation from live oils. *Energy & Fuels* 25 (2): 528-538.
- Tinss, J.C. 2001. Experimental studies of steam-propane injection to enhance recovery of an intermediate crude oil. MSc Thesis, Texas A&M University, College Station, Texas, USA.
- Tipman, R., Long, Y.C., and Shelfantook, W.E. 2001. Solvent process for bitumen separation from oil sands froth. *U.S. Patent No. 6,214,213*. Washington, DC: U.S. Patent and Trademark Office.
- Twu, C.H. 1984. An internally consistent correlation for predicting the critical properties and molecular weights of petroleum and coal-tar liquids. *Fluid Phase Equilibria* 16 (2): 137-150.
- Venturini, G.J. and Mamora, D.D. 2003. Simulation studies of steam-propane injection for the Hamaca heavy oil field. Paper SPE 2003-056 presented at Canadian International Petroleum Conference, Calgary, Alberta, Canada, 10-12 June.
- Weinstein, H.G. 1974. Mathematical models for thermal recovery processes. Presented at Heavy Oil Symposium, University of Zulia, Maracaibo, Venezuela, 23-27 July.
- Wen, Y., Bryan, J., and Kantzas, A. 2005. Evaluation of bitumen-solvent properties using low field NMR. *Journal of Canadian Petroleum Technology* 44 (4): 22-28.

- Wiehe, I.A., Yarranton, H.W., Akbarzadeh, K. Rahimi, P.M., and Teclemariam, A. 2005. The Paradox of Asphaltene Precipitation with Normal Paraffins. *Energy & Fuels* 19 (4): 1261-1267.
- Witherspoon, P.A. and Munir, Z.A. 1958. Size and shape of asphaltic particles in petroleum. Paper SPE 1168 presented at Fall Meeting of the Los Angeles Basin Section, Los Angeles, California, USA, 16-17 October.
- Wu, R. 1996. Three phase equilibrium study for heavy oil by Peng-Robinson equation of state. Paper SPE 96-37 presented at 47th Annual Technical Meeting, Calgary, Alberta, Canada, 10-12 June.
- Yang, P., Li, H., and Yang, D. 2013. Phase behaviour of CH₄-C₃H₈-heavy oil systems under reservoir conditions. Paper SPE 165502 presented at SPE Heavy Oil Conference, Calgary, Alberta, Canada, 11-13 June.
- Yaws, C.L. 1999. *Chemical Properties Handbook*. McGraw-Hill, New York.
- Yu, J.M., Huang, S.H., and Radosz, M. 1989. Phase behavior of reservoir fluids: supercritical carbon dioxide and Cold Lake bitumen. *Fluid Phase Equilibria* 53: 429-438.
- Zhao, L., Nasr, T.N., Huang, H., Beaulieu, G., Heck, G., and Golbeck, H. 2005. Steam alternating solvent process: Lab test and simulation. *Journal of Canadian Petroleum Technology* 44 (9): 13-16.
- Zosel, K. 1978. Separation with supercritical gases: practical applications. *Angewandte Chemie International Edition in English* 17 (10): 702-709.
- Zou, X., Zhang, X., and Shaw, J.M. 2007. Phase behavior of Athabasca vacuum bottoms + *n*-alkane mixtures. *SPE Production & Operations* 22 (2): 265-272.

Appendix A: Copyrights and Permissions



RightsLink®

Home

Account
Info

Help



ACS Publications
High quality. High impact.

Title: Physical Properties and
Extraction Measurements for the
Athabasca Bitumen + Light
Hydrocarbon System: Evaluation
of the Pressure Effect, Solvent-
to-Bitumen Ratio, and Solvent
Type

Logged in as:
Hossein Nourozieh
Account #:
3000686133

LOGOUT

Author: Hossein Nourozieh, Mohammad
Kariznovi, and Jalal Abedi

Publication: Journal of Chemical and
Engineering Data

Publisher: American Chemical Society

Date: Nov 1, 2011

Copyright © 2011, American Chemical Society

PERMISSION/LICENSE IS GRANTED FOR YOUR ORDER AT NO CHARGE

This type of permission/license, instead of the standard Terms & Conditions, is sent to you because no fee is being charged for your order. Please note the following:

- Permission is granted for your request in both print and electronic formats, and translations.
- If figures and/or tables were requested, they may be adapted or used in part.
- Please print this page for your records and send a copy of it to your publisher/graduate school.
- Appropriate credit for the requested material should be given as follows: "Reprinted (adapted) with permission from (COMPLETE REFERENCE CITATION). Copyright (YEAR) American Chemical Society." Insert appropriate information in place of the capitalized words.
- One-time permission is granted only for the use specified in your request. No additional uses are granted (such as derivative works or other editions). For any other uses, please submit a new request.

BACK

CLOSE WINDOW

Copyright © 2013 [Copyright Clearance Center, Inc.](#) All Rights Reserved. [Privacy statement.](#)
Comments? We would like to hear from you. E-mail us at customercare@copyright.com



RightsLink®

Home

Account
Info

Help



ACS Publications Title:
High quality. High impact.

Experimental Determination of
k-Values and Compositional
Analysis of Liquid Phases in the
Liquid-Liquid Equilibrium Study
of (Athabasca Bitumen +
Ethane) Systems

Logged in as:
Hossein Nourozieh
Account #:
3000686133

LOGOUT

Author: Mohammad Kariznovi, Hossein
Nourozieh, and Jalal Abedi

Publication: Journal of Chemical and
Engineering Data

Publisher: American Chemical Society

Date: Jun 1, 2013

Copyright © 2013, American Chemical Society

PERMISSION/LICENSE IS GRANTED FOR YOUR ORDER AT NO CHARGE

This type of permission/license, instead of the standard Terms & Conditions, is sent to you because no fee is being charged for your order. Please note the following:

- Permission is granted for your request in both print and electronic formats, and translations.
- If figures and/or tables were requested, they may be adapted or used in part.
- Please print this page for your records and send a copy of it to your publisher/graduate school.
- Appropriate credit for the requested material should be given as follows: "Reprinted (adapted) with permission from (COMPLETE REFERENCE CITATION). Copyright (YEAR) American Chemical Society." Insert appropriate information in place of the capitalized words.
- One-time permission is granted only for the use specified in your request. No additional uses are granted (such as derivative works or other editions). For any other uses, please submit a new request.

BACK

CLOSE WINDOW

Copyright © 2013 [Copyright Clearance Center, Inc.](#) All Rights Reserved. [Privacy statement.](#)
Comments? We would like to hear from you. E-mail us at customercare@copyright.com

**ELSEVIER LICENSE
TERMS AND CONDITIONS**

Sep 13, 2013

This is a License Agreement between Hossein Nourozieh ("You") and Elsevier ("Elsevier") provided by Copyright Clearance Center ("CCC"). The license consists of your order details, the terms and conditions provided by Elsevier, and the payment terms and conditions.

All payments must be made in full to CCC. For payment instructions, please see information listed at the bottom of this form.

Supplier	Elsevier Limited The Boulevard, Langford Lane Kidlington, Oxford, OX5 1GB, UK
Registered Company Number	1982084
Customer name	Hossein Nourozieh
Customer address	2500 University Dr NW Calgary, AB T2N1N4
License number	3227170243020
License date	Sep 13, 2013
Licensed content publisher	Elsevier
Licensed content publication	Fuel Processing Technology
Licensed content title	Development and evaluation of a modified experimental apparatus for phase behavior study of solvent-heavy crude systems
Licensed content author	Hossein Nourozieh, Mohammad Kariznovi, Jalal Abedi
Licensed content date	October 2012
Licensed content volume number	102
Licensed content issue number	
Number of pages	8
Start Page	116
End Page	123
Type of Use	reuse in a thesis/dissertation
Portion	full article
Format	both print and electronic
Are you the author of this Elsevier article?	Yes
Will you be translating?	No
Order reference number	
Title of your thesis/dissertation	Phase Partitioning and Thermo-physical Properties of Athabasca Bitumen / Solvent Mixtures
Expected completion date	Sep 2013
Estimated size (number of pages)	400
Elsevier VAT number	GB 494 6272 12
Permissions price	0.00 USD
VAT/Local Sales Tax	0.0 USD / 0.0 GBP
Total	0.00 USD
Terms and Conditions	

**ELSEVIER LICENSE
TERMS AND CONDITIONS**

Sep 13, 2013

This is a License Agreement between Hossein Nourozieh ("You") and Elsevier ("Elsevier") provided by Copyright Clearance Center ("CCC"). The license consists of your order details, the terms and conditions provided by Elsevier, and the payment terms and conditions.

All payments must be made in full to CCC. For payment instructions, please see information listed at the bottom of this form.

Supplier	Elsevier Limited The Boulevard, Langford Lane Kidlington, Oxford, OX5 1GB, UK
Registered Company Number	1982084
Customer name	Hossein Nourozieh
Customer address	2500 University Dr NW Calgary, AB T2N1N4
License number	3227170471367
License date	Sep 13, 2013
Licensed content publisher	Elsevier
Licensed content publication	Fuel
Licensed content title	Experimental apparatus for phase behavior study of solvent-bitumen systems: A critical review and design of a new apparatus
Licensed content author	Mohammad Kariznovi, Hossein Nourozieh, Jalal Abedi
Licensed content date	February 2011
Licensed content volume number	90
Licensed content issue number	2
Number of pages	11
Start Page	536
End Page	546
Type of Use	reuse in a thesis/dissertation
Intended publisher of new work	other
Portion	excerpt
Number of excerpts	3
Format	both print and electronic
Are you the author of this Elsevier article?	Yes
Will you be translating?	No
Order reference number	
Title of your thesis/dissertation	Phase Partitioning and Thermo-physical Properties of Athabasca Bitumen / Solvent Mixtures
Expected completion date	Sep 2013
Estimated size (number of pages)	400
Elsevier VAT number	GB 494 6272 12
Permissions price	0.00 USD
VAT/Local Sales Tax	0.0 USD / 0.0 GBP
Total	0.00 USD
Terms and Conditions	

**ELSEVIER LICENSE
TERMS AND CONDITIONS**

Sep 13, 2013

This is a License Agreement between Hossein Nourozieh ("You") and Elsevier ("Elsevier") provided by Copyright Clearance Center ("CCC"). The license consists of your order details, the terms and conditions provided by Elsevier, and the payment terms and conditions.

All payments must be made in full to CCC. For payment instructions, please see information listed at the bottom of this form.

Supplier	Elsevier Limited The Boulevard, Langford Lane Kidlington, Oxford, OX5 1GB, UK
Registered Company Number	1982084
Customer name	Hossein Nourozieh
Customer address	2500 University Dr NW Calgary, AB T2N1N4
License number	3227170807804
License date	Sep 13, 2013
Licensed content publisher	Elsevier
Licensed content publication	Fluid Phase Equilibria
Licensed content title	Measurement of thermophysical properties and modeling for pseudo-binary mixtures of <i>n</i> -decane and Athabasca bitumen
Licensed content author	Hossein Nourozieh, Mohammad Kariznovi, Jian Guo Guan, Jalal Abedi
Licensed content date	15 June 2013
Licensed content volume number	347
Licensed content issue number	
Number of pages	14
Start Page	62
End Page	75
Type of Use	reuse in a thesis/dissertation
Intended publisher of new work	other
Portion	excerpt
Number of excerpts	5
Format	both print and electronic
Are you the author of this Elsevier article?	Yes
Will you be translating?	No
Order reference number	
Title of your thesis/dissertation	Phase Partitioning and Thermo-physical Properties of Athabasca Bitumen / Solvent Mixtures
Expected completion date	Sep 2013
Estimated size (number of pages)	400
Elsevier VAT number	GB 494 6272 12
Permissions price	0.00 USD
VAT/Local Sales Tax	0.0 USD / 0.0 GBP
Total	0.00 USD
Terms and Conditions	

**ELSEVIER LICENSE
TERMS AND CONDITIONS**

Sep 13, 2013

This is a License Agreement between Hossein Nourozieh ("You") and Elsevier ("Elsevier") provided by Copyright Clearance Center ("CCC"). The license consists of your order details, the terms and conditions provided by Elsevier, and the payment terms and conditions.

All payments must be made in full to CCC. For payment instructions, please see information listed at the bottom of this form.

Supplier	Elsevier Limited The Boulevard, Langford Lane Kidlington, Oxford, OX5 1GB, UK
Registered Company Number	1982084
Customer name	Hossein Nourozieh
Customer address	2500 University Dr NW Calgary, AB T2N1N4
License number	3227170672423
License date	Sep 13, 2013
Licensed content publisher	Elsevier
Licensed content publication	The Journal of Chemical Thermodynamics
Licensed content title	Experimental measurements and predictions of density, viscosity, and carbon dioxide solubility in methanol, ethanol, and 1-propanol
Licensed content author	Mohammad Kariznovi, Hossein Nourozieh, Jalal Abedi
Licensed content date	February 2013
Licensed content volume number	57
Licensed content issue number	
Number of pages	8
Start Page	408
End Page	415
Type of Use	reuse in a thesis/dissertation
Intended publisher of new work	other
Portion	figures/tables/illustrations
Number of figures/tables /illustrations	2
Format	both print and electronic
Are you the author of this Elsevier article?	Yes
Will you be translating?	No
Order reference number	
Title of your thesis/dissertation	Phase Partitioning and Thermo-physical Properties of Athabasca Bitumen / Solvent Mixtures
Expected completion date	Sep 2013
Estimated size (number of pages)	400
Elsevier VAT number	GB 494 6272 12
Permissions price	0.00 USD
VAT/Local Sales Tax	0.0 USD / 0.0 GBP
Total	0.00 USD
Terms and Conditions	